8-12-2016

CALCIUM REGULATION OF CELL-CELL COMMUNICATION AND EXTRACELLULAR SIGNALING

Juan Zou

CALCIUM REGULATION OF CELL-CELL COMMUNICATION AND EXTRACELLULAR SIGNALING

by

pro

JUAN ZOU

Under the Direction of Jenny Yang, PhD

ABSTRACT

As a highly versatile signal, Ca^{2+} operates over a wide temporal range to regulate many different cellular processes, impacting nearly every aspect of cellular life including excitability, exocytosis, motility, apoptosis, and transcription. While it has been well recognized that Ca^{2+} acts as both a second messenger to regulate cell-cell communication upon external stimuli and as a first messenger to integrate extracellular with intracellular signaling in various cell types. Molecular bases for such regulation and related human diseases are largely hampered by the challenges related to key membrane proteins. In the present study, we first investigated the regulatory role of intracellular Ca^{2+} ($[Ca^{2+}]_i$) on Connexin45 (Cx45) gap junction through a ubiquitous Ca^{2+} sensor protein-Calmodulin (CaM). Using bioluminescence resonance energy transfer assay, this study

provides the first evidence of direct association of Cx45 and CaM in a Ca^{2+}-dependent manner in cells. Complementary approaches including bioinformatics analysis and various biophysical methods identified a putative CaM-binding site in the intracellular loop of Cx45 with high Ca^{2+}/CaM-binding affinity and Ca^{2+}-dependent binding mode that is different from alpha family of connexins. To understand the role of extracellular calcium in regulation of gap junction hemichannels, we would like to prove a possible Ca^{2+}-binding site predicted by our computational algorithm MUG^{SR} in Connexin 26 (Cx26) through mutagenesis study, metal binding affinity measurement, conformational changes examination of purified Cx26 protein from Sf9; however, we failed to achieve this goal due to either the limitation of available methods or lethal effect of mutating the predicted Ca^{2+}-binding ligand. Additionally, in this study, we identified a putative Ca^{2+}-binding site in metabotropic glutamate receptor 5 (mGluR5) and demonstrated the importance of this Ca^{2+}-binding site in activation of mGluR5 and modulating the actions of other orthosteric ligands on mGluR5. In addition, we successfully solved the first crystal structure of the extracellular domain of Ca^{2+}-sensing receptor (CaSR) bound with Mg^{2+} and an unexpected Trp derivative. The extensive study of mechanism of CaSR function specifically through Mg^{2+}-binding site and the unexpected ligand-binding site was done using several cell-based assays in wild type CaSR and mutants. Studies in this dissertation provides more information on how Ca^{2+} regulates gap junction channels, modulates mGluR5 activities and structural basis for regulation of CaSR by Mg^{2+} and an unexpected Trp derivative co-agonist.

INDEX WORDS: Ca^{2+}; Mg^{2+}; CaM; Cx45; gap junction; mGluR5; CaSR.

CALCIUM REGULATION OF CELL-CELL COMMUNICATION AND EXTRACELLULAR SIGNALING

by

JUAN ZOU

A Dissertation Submitted in Partial Fulfillment of the Requirements for the Degree of

Doctor of Philosophy

in the College of Arts and Sciences

Georgia State University

2016

2016

CALCIUM REGULATION OF CELL-CELL COMMUNICATION AND EXTRACELLULAR SIGNALING

by

JUAN ZOU

Committee Chair: Jenny Yang

Committee: Jun Yin

Ivaylo Ivanov

Electronic Version Approved:

Office of Graduate Studies

College of Arts and Sciences

Georgia State University

May 2016

DEDICATION

I want first of all to thank our previous lab members who paved the path before me and provided support for me to stand to extend the work. Without the method they established in our lab, I could not achieve all these.

This is also a tribute to my loving family and friends who supported me on this journey. Their thoughtfulness and kindness always warms me. Their constant encouragement always ring in my ears. They have never left my side no matter how many mistakes I have made. Their generous tolerance promote me to be grateful.

I would like to extend my gratitude to the Brain and Behavior fellowship from Georgia State Univeristy. Without it, I could not finish my PhD study here. The great seminar classes provided by Brain and Behavior also introduced me to the mysterious and interesting neuron science field.

ACKNOWLEDGEMENTS

First and foremost, I would like to express my sincere gratitude to my advisor Professor Dr. Jenny Yang for the continuous support of my Ph. D study and research. I thank her for introducing me to this wonderful research world. Her immense knowledge, patience guidance, continuous encouragement allows me to grow as a research scientist. Her enthusiasm, strong thirst for knowledge and motivation always inspire me. She has written countless proposals in the past six years in order to obtain continuous support from NIH and to survive in the competitive academic field. I am motivated by the countless sleepless nights she spent on reading and writing papers, numerous times she sat together with us to discuss the experimental plans, joined us to learn from outside experts and she proudly introduced her students to others in conferences. She has set a good example for me. I could not have imagined having a better advisor and mentor for my Ph. D study. Not only in research, but she also has given me lots of unselfish help, motherly love and forgiveness in life. She is always a genuinely caring and helpful person. She is always the first one that I can share my feelings with, the first shoulder I can cry on, and the first one who gets me through my troubles. Her advice on both my research as well as on my life have been invaluable.

Besides my advisor, I would like to thank the rest of my committee members, Dr. Jun Yin and Dr. Ivaylo Ivanov for serving as my committee members. Their insightful comments, brilliant suggestions, and encouragement helped me all the time in my research and writing of this dissertation. Thank you for making my defense an enjoyable experience. The hard questions in the defense sparked new ideas and invigorated me to widen my research.

My sincere gratitude also goes to Drs. Richard Veenstra and Edward M. Brown. Their profound knowledge in gap junction and G-protein coupled receptor field is always like the lighthouse, which gives me hope and guidance when I am floating like the boat on the ocean of knowledge. During my Ph. D study, especially in the first few years, they are my encyclopedia. Discussions with them always help me solve problems and puzzles, and enlightened me. I will never forget their support and inspiration.

I am particularly indebted to our collaborators: Dr. John Helper from Emory, Dr. Jian Hu from Michigan State University, and Dr. Kelly Moremen from University of Georgia. In 2013, my research was at standstill and I could not prove the interaction between calmodulin and Cx45 in the living cell. We received am email from Dr. Helper asking collaboration on their RGS14 project. In the presentation they gave in our lab, I was so excited to realize that their BRET assay can be used in my experiment to monitor protein-protein interaction *in vivo*. Nicole from Dr. Helper's lab sent me the related plasmid and gave me detailed training on performing the BRET assay. They also kindly allowed to culture cells in their lab and use their microplate reader. With their help, we finally could obtained promising result. Without their precious support it would not be possible to conduct the Cx45 project. Furthermore, both Dr. Hu's and Dr. Moremen's group contributed extensively to the CaSR project. Their expertise in membrane protein expression in mammalian cells and crystallization moved our CaSR project a significant step forward. Without them, we would not be successful to solve the CaSR-ECD structure and identified an unexpected CaSR ligand. Words cannot express how grateful I am to all of them.

I am grateful to Drs. Yanyi Chen and Chen Zhang for their patient hands-on teaching and training. Dr. Chen introduced me to the gap junction field when I first joined in Dr. Yang's group

in 2010. I learnt all important biophysical technique from him, applying what I have learned from him into research. His critical thinking and quick learning also impressed me a lot. I am grateful to Dr. Chen for enlightening me with the first glance of research. In my second year of my Ph. D study, I was attracted by the wide application of cell studies in research. Therefore, I turned to Dr. Zhang and asked her to train me. She said "yes" to me without any hesitation and became my second mentor in Dr. Yang's lab. How lucky I am to have them as my mentors. Their training and advice on both research as well as on my career are priceless.

I would also like to thank all of the rest labmates and friends, particularly Jie Jiang, Jinjuan Qiao, Yusheng Jiang, You Zhuo, Jie Feng, Li Zhang, Mani Salarian, Rakshya Gokhali and Cassie Miller, for the stimulating discussions, for the time we were working together to meet deadlines, and for the fun we had together in the past six years. They are also my close friends in my life, who were always aside to support me.

I could not possibly forget to thank Dr. Robert Wohlhueter and Dr. Shunyi Li, who referred me to Georgia State University. Without their recommendation, I could not fulfill my dream of oversea education. Dr. Robert is also my language and American culture teacher, who always encourage me to involve in the American society as a foreign student.

Last but not the least, I would like to thank my family for their supporting me spiritually throughout my PhD study and my life in general.

TABLE OF CONTENTS

ACKNOWLEDGEMENTS ..... **v**

LIST OF TABLES ..... **xvii**

LIST OF FIGURES ..... **xviii**

1 INTRODUCTION **1**

1.1 Ca^{2+} in Biological System **1**

1.1.1 Ca^{2+} and Mg^{2+} Coordination ***1***

1.1.2 Ca^{2+} homeostasis ***3***

1.1.3 Ca^{2+} Signaling network ***3***

1.1.4 Ca^{2+}, CaM, and CaM-binding modes ***7***

1.2 Gap Junction **12**

1.2.1 Gap junction overview ***12***

1.2.2 Gap junction protein family and the distribution of connexins ***13***

1.2.3 The function of gap junction and its associated diseases ***19***

1.2.4 The regulation of gap junction by Ca^{2+} ***20***

1.2.5 Structure characterization of gap junction ***27***

1.2.6 Gap junction regulation by CaM ***34***

1.3 Family C of G-protein Coupled Receptors (cGPCR) and Its Regulation by $[Ca^{2+}]_o$ 38

1.3.1 mGluR and Structure features of mGluR ***38***

1.3.2 Cell signaling pathways through mGluRs 43

1.3.3 Distribution and function of mGluRs 45

1.3.4 Allosteric and orthosteric modulation of mGluRs 48

1.3.5 Extracellular calcium sensitivity of mGluRs 53

1.3.6 (Patho)physiological process related with group I mGluRs and therapeutic potential of group I mGluRs 57

1.4 Ca^{2+}-sensing Receptor 59

1.4.1 Structure and function of Calcium-sensing receptor 59

1.4.2 Calcium-sensing receptor stimuli 63

1.4.3 Calcium-sensing receptor regulated intracellular signaling pathways .. 66

1.4.4 The biological roles of Calcium-sensing receptor 67

1.5 Challenges Associated with Membrane Protein and Weak Ca^{2+}-binding Affinity 68

1.6 Major Questions to Be Addressed in This Dissertation 70

1.7 The Objectives and Overview of This Dissertation 71

2 Matrerials and methods 74

2.1 Direct Visualization of Interaction between Cam and Cx45 74

2.1.1 BRET assay related mouse Cx45 and rat CaM construction 74

2.1.2 CaM and its mutants expression in E.coli 74

2.1.3 Circular dichroism spectroscopy 75

2.1.4 Dansylated CaM fluorescence change induced by peptides derived from connexins 75

2.1.5 Equilibrium Calcium titrations 76

2.1.6 ^{15}N-^{1}H heteronuclear single quantum coherence (HSQC) 76

2.1.7 Pulse-field-gradient diffusion NMR 77

2.1.8 Bioluminescence resonance energy transfer (BRET) assay 77

2.1.9 Surface plasma resonance (SPR) 78

2.2 Cx26 Gap Junction Hemichannel Regulation by Extracellular Ca^{2+} 79

2.2.1 Plasmid construction and protein engineering 79

2.2.2 Protein expression and purification/isolation 80

2.2.3 Mammalian cell culture and transfection 83

2.2.4 Permeability measurement of Cx26 hemichannel using dye loading assay 83

2.2.5 Liposome preparation 84

2.2.6 Proteo-liposome preparation 84

2.2.7 Oocyte preparation 84

2.2.8 Proteo-liposome injection 85

2.2.9 Two electrons whole cell recording 85

2.3 Is mGluR5 a Calcium-sensing receptor? 86

2.3.1 mGluR5 and its mutants construction 86

2.3.2 Cell culture and transfection 86

2.3.3 mGluR5 cell surface expression visualization by immunostaining 87

2.3.4 Quantitatively analysis of mGluR5 and its mutants' cell surface expression 87

2.3.5 Measurement of $[Ca^{2+}]_i$ response to $[Ca^{2+}]_o$ in single cells transfected with WT or mutant mGluR5 88

2.3.6 Exploration of $[Ca^{2+}]_o$ effect on mGluR5 response to L-Glu or L-Quis stimulation 88

2.3.7 Determination of $[Ca^{2+}]_o$ effect on ERK1/2 phosphorylation mediated by mGluR5 89

2.3.8 mGluR5-ECD expression in Sf9 89

2.3.9 Trp-Tb^{3+} fluorescence energy transfer 90

2.3.10 Ca^{2+}-Tb^{3+} competition 91

2.4 Structural Basis for Regulation of Human Calcium-Sensing Receptor by Magnesium Ions and an Unexpected Tryptophan Derivative Co-agonist 91

2.4.1 Purification of the extracellular domain of the human CaSR (hCaSR-ECD) secreted from HEK293s GnTI-cells 91

2.4.2 Crystallization, data collection and structure determination 91

2.4.3 High-resolution LC-ESI-MS and identification of CaSRL 92

2.4.4 Monitoring Mg^{2+}- binding to CaSR-ECD by fluorescence spectroscopy 95

2.4.5 CaSRL and Mg^{2+} binding site mutation design 95

2.4.6 Cell culture and transfection 96

2.4.7 Immunostaining 96

2.4.8 Measurement of $[Ca^{2+}]_i$ changes triggered by $[Mg^{2+}]_o$ in single CaSR-transfected cells 96

2.4.9 Determination of the effect of CaSRL on Mg^{2+}-evoked $[Ca^{2+}]_i$ signaling by stimulation of CaSR in cell populations 97

2.4.10 Determination of ERK1/2 phosphorylation 98

3 DIRECT VISUALIZATION OF INTERACTION BETWEEN CALMODULIN AND COONEXIN45 100

3.1 Introduction 100

3.2 Results 102

3.2.1 Establishing a BRET cellular assay to probe CaM and Cx45 direct interaction in cells 102

3.2.2 Ca^{2+}-dependent interaction between Cx45 and CaM 108

3.2.3 Identification of putative CaM binding region in the single cytoplasmic loop of Cx45 110

3.2.4 Fluorometric Measurements with Dansyl-CaM 113

3.2.5 Surface Plasmon Resonance 115

3.2.6 Ca^{2+}-dependent specific interaction between Cx45p and CaM revealed by NMR 117

3.2.7 Calcium equilibrium titration 122

3.2.8 Probing the CaM-Peptide complex state by diffusion NMR 127

3.3 Discussion..... 128

3.3.1 The unique features of Cx45 128

3.3.2 Interaction of CaM with connexins..... 129

3.3.3 Key factors in CaM contributing to interaction with Cx45p$_{164-186}$ 131

3.3.4 CaM uses different action mode to regulate different connexins 135

3.3.5 Effects of Cx45p$_{164-186}$ on calcium binding 135

3.3.6 Implication for regulation of connexins 136

4 Cx26 gap junction hemichannel regulation by extracellular Ca^{2+} 137

4.1 Introduction..... 137

4.2 Result..... 141

4.2.1 Ca^{2+}-binding site prediction and comparison with reported sites 141

4.2.2 Cx26 isolation from pig liver 143

4.2.3 Expression and purification of Cx26 in E.coli 148

4.2.4 Expression and purification of mCx26 in Sf9 153

4.2.5 Tb^{3+} titration..... 158

4.2.6 Ca^{2+}-Tb^{3+} competition and Ca^{2+} induced conformation change..... 160

4.2.7 Dye uptake assay 167

4.2.8 Monitoring Channel Activity of Proteo-liposomes with Cx26 Gap Junction in Single Oocytes..... 174

4.3 Discussion..... 181

5 ELUCIDATION OF A NOVEL EXTRACELLULAR CALCIUM-BINDING SITE ON METABOTROPIC GLUTAMATE RECEPTOR 5..... 186

5.1 Introduction..... 186

5.2 Result..... 190

5.2.1 Prediction of Ca^{2+}-binding site in the extracellular domain (ECD) of mGluR5 190

5.2.2 Monitoring Ca^{2+} binding to mGluR5-ECD by fluorescence..... 192

5.2.3 Immunofluorescence analysis of surface expressed WT and its mutants in HEK293 cell 196

5.2.4 Extracellular Ca^{2+} solely elicits mGluR5-mediated $[Ca^{2+}]_i$ responses.. 198

5.2.5 Effects of mGluR5 mutating proposed Ca^{2+}-binding residues on $[Ca^{2+}]_o$ sensing capability..... 201

5.2.6 ERK1/2 phosphorylation in WT and point mutant of mGluR5 induced by $[Ca^{2+}]_o$ 203

5.2.7 Enhancement of mGluR5 sensitivity and response to L-Glu by extracellular Ca^{2+}..... 205

5.3 Discussion..... 209

5.3.1 The putative Ca^{2+}-binding site is conserved in group I mGluRs..... 209

5.3.2 Ubiquitous actions of extracellular Ca^{2+} on mGluR5..... 210

5.3.3 Possible physiological significance of $[Ca^{2+}]_o$ effects on mGluR5 in neuron system 212

5.3.4 The response of mGluR5 to extracellular Ca^{2+} resemble CaSR more than mGLuR1 213

6 STRUCTURAL BASIS FOR REGULATION OF HUMAN CALCIUM-SENSING RECEPTOR BY MAGNESIUM IONS AND AN UNEXPECTED TRYPTOPHAN DERIVATIVE 216

6.1 Introduction 216

6.2 Results 218

6.2.1 Purified hCaSR-ECD from HEK293 cells forms a homodimer 218

6.2.2 Crystal structure of hCaSR-ECD 219

6.2.3 Identification of a tryptophan derivative tightly bound at the putative ligand binding site of hCaSR-ECD 222

6.2.4 Mg^{2+} elicits CaSR-mediated $[Ca^{2+}]_i$ signaling pathways and ERK1/2 phosphorylation 226

6.2.5 Identification of metal binding sites 231

6.2.6 The unexpected Trp derivative function as a co-activator and potentiates the actions of extracellular divalent cations 235

6.2.7 Determining Mg^{2+} binding capability using hCaSR-ECD 242

6.3 Discussion 243

7 MAJOR CONCLUSIONS AND SIGNIFICANCE 259

Publications 262

Manuscript under review or in preparation 262

REFERENCES 263

APPENDICES 302

Appendix A: Expression of mCx26 using Bac-to-Bac baculovirus expression system 302

Appendix A.1 Introduction 302

Appendix A.2 Methods 305

Appendix A.3 Results 309

LIST OF TABLES

Table 1.1 Connexin gene expression pattern in human...... 17

Table 1.2 Key features of mGluRs...... 45

Table 1.3 Orthosteric and allosteric ligands of mGluR1...... 51

Table 1.4 Orthosteric and allosteric ligands of mGluR5...... 52

Table 3.1 Luminescence of donor Cx45-Rluc...... 106

Table 3.2 Fluorescence of acceptor CaM-Venus...... 107

Table 3.3 Fluorescence of acceptor Venus-CaM...... 107

Table 3.4 Binding kinetics determined by SPR...... 117

Table 3.5 Effects of Cx45p$_{164-186}$ Binding on the Ca^{2+}-binding Properties of CaM...... 127

Table 4.1 Disease mutations in the predicted Ca^{2+}-binding site...... 139

Table 5.1 Summary of EC50s from experiments measuring $[Ca^{2+}]_i$ response and ERK1/2 phosphorylation...... 205

Table 6.1 Crystallographic statistics of hCaSR-ECD and hCaSR-ECD/Gd^{3+}...... 221

Table 6.2 EC50 of $[Mg^{2+}]_o$ for stimulation of $[Ca^{2+}]_i$ signaling in cell population assay. ... 234

Table 6.3 EC_{50} of $[Mg^{2+}]_o$ for elicitation of $[Ca^{2+}]_i$ rise in cell population assay when different concentrations of CaSRL co-applied...... 240

LIST OF FIGURES

Figure 1.1 Ca^{2+} signaling network. 6

Figure 1.2 EF hand (26) 8

Figure 1.3 CaM function as an adaptor protein to interact with various target proteins. .. 11

Figure 1.4 Diverse CaM-binding modes. 11

Figure 1.5 Gap junction on the cell membrane. 13

Figure 1.6 A molecular phylogenetic tree for human connexin protein (HCx) and rat connexin33 (rCx33). 14

Figure 1.7 The life cycle of connexin. 16

Figure 1.8 Scheme presentation of connexin and gap junction channel. 18

Figure 1.9 Illustration of disease phenotypes associated with abnormal gap junctions. 20

Figure 1.10 Comparison of gap junction particles isolated from calf lens fibers in the presence of EDTA (a) or subsequently incubated in the presence of $CaCl_2$ (b). 22

Figure 1.11 Ca^{2+} regulation model from Dr. Unwin. 22

Figure 1.12 Extracellular connexin surface recorded by AFM in a Ca^{2+}-free buffer (left) and a buffer with 0.5 mM Ca^{2+} (right). 23

Figure 1.13 The diameter change of reconstituted Cx43 hemichannel pores in different cations. 24

Figure 1.14 Ca^{2+}-binding site in Cx26 gap junction channel crystal structure. 26

Figure 1.15 Overall structure of Cx26 gap junction channel in ribbon representation. 30

Figure 1.16 Wall-eye stereo view of Cx26 monomer in ribbon representation. 32

Figure 1.17 Structure comparison between new Cx26 crystal structures and the existing 2ZW3. 34

Figure 1.18 Structure organization of mGluRs. mGluRs function as dimer on the cell surface. 40

Figure 1.19 L-Glu- and L-Quis-binding affinity of mutants in predicted L-Glu-binding site. 42

Figure 1.20 Schematic diagram of the mGluR dimer in different activity states. 43

Figure 1.21 Localization of mGluRs in the CNS. 47

Figure 1.22 Orthosteric and allosteric site of mGluRs. 48

Figure 1.23 Conserved L-Glu binding sites in mGluRs. 50

Figure 1.24 The amino acid sequence of human CaSR. 62

Figure 3.1 Bioluminescence resonance energy transfer. 104

Figure 3.2 Probing interaction between Cx45 and CaM in HEK293 cells by BRET. 105

Figure 3.3 Interaction of Cx45 and CaM in live cells as measured by BRET. 109

Figure 3.4 Membrane topology of Cx45 and the putative CaM-binding site. 111

Figure 3.5 Revealing CaM-peptide interaction with CD spectroscopy. 113

Figure 3.6 Steady-state fluorescence studies of interaction between D-CaM and Cx45p164-186. 115

Figure 3.7 SPR analysis of Cx45p$_{164-186}$ and CaM interaction. 116

Figure 3.8 Monitoring CaM-Cx45p$_{164-186}$ complex formation by MS. 118

Figure 3.9 NMR studies characterizing the residues of CaM affected upon Cx45p$_{164-186}$ binding. 121

Figure 3.10 Changes in CaM Phe-fluorescence emission spectra upon addition of Ca^{2+} in the absence (a and b) or presence of Cx45p$_{164-186}$ (c and d). 123

Figure 3.11 Equilibrium calcium titrations of CaM with (solid cycles) or without (open cycles) Cx45p$_{164-186}$ by monitoring Phe fluorescence emission. 124

Figure 3.12 Changes in CaM Tyr-fluorescence emission spectra upon addition of Ca^{2+} in the absence (a and b) or presence of Cx45p$_{164-186}$ (c and d). 125

Figure 3.13 Equilibrium Calcium titrations of CaM with (solid circles) or without (open circles) Cx45p$_{164-186}$ by monitoring Tyr fluorescence emission. 126

Figure 3.14 Determination of hydrodynamic of holo-CaM-Cx45p$_{164-186}$ complex using pulse-field gradient NMR. 128

Figure 3.15 CaM-binding affinity correlated to connexin helicity. 134

Figure 4.1 Hemichannel activity-dependent cell death can be rescued by elevated Ca^{2+}. . 138

Figure 4.2 Prediction of a Ca^{2+}-binding site at the extracellular mouth of Cx26 gap junction channel. 142

Figure 4.3 Sequence alignment of mouse, rat, bovine, sheep and human Cx26. 143

Figure 4.4 Brief procedure describing the isolation of Cx26 from pig liver. 145

Figure 4.5 Sucrose gradient optimization. 146

Figure 4.6 Cx26 isolated from liver had low yield and low purity. 148

Figure 4.7 Optimization of human Cx26 for E.coli expression. 151

Figure 4.8 hCx26 expression in C43(DE3). 153

Figure 4.9 Expression of hCx26 from C43(DE3). 153

Figure 4.10 mCx26 purified from Sf9. 155

Figure 4.11 Cx26 Splitting by Urea. 156

Figure 4.12 SDS-Page gel and western blot for analyzing intact and split junctions. 157

Figure 4.13 Tb^{3+} titration. 159

Figure 4.14 Ca^{2+}-Tb^{3+} competition. 162

Figure 4.15 Secondary structure of mCx26 in the presence or absence of Ca^{2+}. 165

Figure 4.16 Thermal stability of mCx26 in the presence or absence of Ca^{2+}. 166

Figure 4.17 Expression of hCx26-eGFP and its mutants in HeLa cells. 171

Figure 4.18 hCx26 dye uptake in the presence of Ca^{2+} or EGTA. 171

Figure 4.19 Dye uptake comparison between wild type Cx26 and mutant D46N. 173

Figure 4.20 Working model: injection of proteo-liposomes in oocyte 176

Figure 4.21 Effects of lipid compositions on Cx26 channel activity. 178

Figure 4.22 Channel activity of Cx26-liposomes in the oocytes. 180

Figure 4.23 Cx26 channel activity regulated by $CaCl_2$. 181

Figure 5.1 Signal transduction pathways activated by mGluR5 stimulation. 189

Figure 5.2 Putative Ca^{2+}-binding site in mGluR 1 and 5. 191

Figure 5.3 mGluR5-ECD forms a dimer. 193

Figure 5.4 Determining Ca^{2+} binding capability using mGluR5-ECD purified from Sf9 culture. 195

Figure 5.5 Analysis of cell surface expression of mGluR5 and its variants. 197

Figure 5.6 $[Ca^{2+}]_o$-sensing capability of mGluR5. 200

Figure 5.7 Disturbance of the intact Ca^{2+}-binding pocket lead to impaired $[Ca^{2+}]_o$ sensing capability. 202

Figure 5.8 $[Ca^{2+}]_o$-activated ERK signaling in mGluR5-transfected HEK293 cells. 204

Figure 5.9 $[Ca^{2+}]_o$ potentiates L-Glu-activated $[Ca^{2+}]_i$ signaling in mGluR5-transfected HEK293 cells. 207

Figure 5.10 mGluR5 mutants' response to L-Glu in the presence of 1.8 mM Ca^{2+}. 208

Figure 5.11 L-Glu did not influence the $[Ca^{2+}]_o$ sensitivity of mGluR5. 211

Figure 5.12 mGluR5 localization in neural system. 213

Figure 5.13 Impaired L-Glu sensitivity of mGluR5 variants. 215

Figure 6.1 Size exclusion chromatography of purified hCaSR-ECD. 219

Figure 6.2 Crystal structure of hCaSR-ECD. 220

Figure 6.3 Identification and characterization of a tryptophan derivative bound to hCaSR-ECD. 224

Figure 6.4 Identification of CaSRL. 225

Figure 6.5 Mg^{2+} or Ca^{2+} elicited CaSR-mediated intracellular Ca^{2+} response. 228

Figure 6.6 Schematic overview of CaSR effectors. 229

Figure 6.7 Extracellular Mg^{2+} evoked phosphorylation of ERK1/2. 230

Figure 6.8 Structural Basis for Mg^{2+}/Ca^{2+} modulated CaSR activities. 232

Figure 6.9 Metal binding at the "acidic patch". 233

Figure 6.10 Mutations of site 3 coordinating residue (E228I or E228I/E229I double mutant) reduced Mg^{2+}-evoked intracellular Ca^{2+} mobilization. 234

Figure 6.11 CaSRL does not function solely 235

Figure 6.12 CaSRL function as a novel high-affinity co-agonist of CaSR. 237

Figure 6.13 CaSRL potentiate CaSR mediated ERK1/2 activation. 237

Figure 6.14 Monitoring CaSRL binding to hCaSR-ECD by SPR. 239

Figure 6.15 Indirectly measuring EC_{50} of CaSRL. 240

Figure 6.16 Replacement of CaSRL by phenylalanine. 241

Figure 6.17 Determining Mg2+ binding capability using hCaSR-ECD. 243

Figure 6.18 Structure-based sequence alignment of CaSRs and mGluRs (by PROMALS3D) (439)). 245

Figure 6.19 Comparison of CaSR and mGluR2 structures. 245

Figure 6.20 Structural comparison of CaSR ligand binding site with that of mGluR1. 247

Figure 6.21 Disease related mutations on CaSR ECD. 249

Figure 6.22 Replacement of TNCA by phenylalanine. 250

Figure 6.23 Structure of the proposed calcium binding "Site 1". 251

Figure 6.24 Identification of a bicarbonate anion near the ligand binding site. 252

Figure 6.25 Identification of a potential Mg^{2+} binding site at the hinge region. 254

Figure 6.26 A positively charged pocket for loop 1 association. 255

Figure 6.27 Key determinants for the molecular basis of disease-associated mutations and regulation. 258

1 INTRODUCTION

1.1 Ca^{2+} in Biological System

1.1.1 Ca^{2+} and Mg^{2+} Coordination

Depending on the fact that Ca^{2+} is a hard metal ion, this divalent cation Ca^{2+} prefers coordination by oxygen atom, although, nitrogen and sulfur from sidechain groups are also considered as potential Ca^{2+}-binding ligand based on observation in small molecule interactions (1-3). Those oxygen atoms are from side chain carboxyl groups (Asp, Glu), carboxamide groups (Asn, Gln), hydroxyl groups (Ser, Thr), and main-chain carboxyl oxygen atoms from most amino acid residues, cofactors, and water molecules. The coordination of Ca^{2+} usually utilizes binding ligands from turn/loop regions rather than α-helix or β-sheet (4,5). Typically, the coordination number of oxygen atoms around Ca^{2+} is 3-8 (6-9), however, the coordination number varies, depending on classes of Ca^{2+}-binding sites (7). Class I Ca^{2+}-binding site supply Ca^{2+}-binding ligand from a continuous short sequence of amino acids. In class II Ca^{2+}-binding site, one ligand originates from the amino acid sequence far away from the continuous fragment which provide the rest of Ca^{2+}-binding ligands. The smallest class III Ca^{2+}-binding site is composed of amino acid far away from each other in the sequence, but close in the tertiary structure (10). Ca^{2+} ions in proteins is coordinated by an inner sphere of hydrophilic groups and embedded in an outer sphere composed by hydrophobic groups, exhibiting a pentagonal bipyramide geometry. The average Ca-O ligand binding distance is within the range of 2.01-3.15 Å as reported previously (11-14). Ca^{2+}-binding sites were recently classified by Kirberger *et al*. based on geometric properties (6).

By analyzing the Ca^{2+}-binding pocket in more than 40 crystal structures deposited in the protein data bank (PDB), our lab established computational algorithm named MUG to predict the putative Ca^{2+}-binding site in proteins (15). Utilizing MUG, we are able to identify know the Ca^{2+}-

binding pockets in holo-protein structures. However, possible Ca^{2+}-induced conformational change is ignored. Later on, we further improved MUG algorithm to MUG^{SR} which allows minor backbone conformational changes and side chain rotations upon Ca^{2+}-binding. This algorithm was verified by successful prediction of 44 Ca^{2+}-binding sites out of 49 sites in documented X-ray crystal structures.

Another abundant intracellular divalent cation is $Mg^{2+,}$ which is also characterized as a "hard" metal (16). Through binding with proteins or nucleotides, Mg^{2+} also exert influence on many biological processes (17-19). By analyzing of over thousand Mg^{2+}-binding site, we summarized several major similarities and differences between Ca^{2+}- and Mg^{2+}-binding sites. First, as "hard" metals, they both prefer oxygen ligand atoms, such as Asp/Glu carboxylate oxygen and backbone carbonyl oxygen. However, Mg^{2+} also prefers other "hard" oxygen atom providers such as water and phosphates in addition to oxygens from protein (18,20). Second, water molecules have been identified as coordinating ligand in both Mg^{2+}- and Ca^{2+}-biding sites. However, the protein ligand over water ligand ratio is quite different (3:3 and 2:2 for Mg^{2+}; 6:1 and 5:2 for Ca^{2+}). In 63% of Mg^{2+}-binding site, water ligand number exceeds or equals protein ligands; while 76% of Ca^{2+}-binding site has more protein ligands than water ligand. Third, the coordination ligand number for Mg^{2+} and Ca^{2+} are approximately balanced at 6. However, more than 99% Mg^{2+}-binding sites display 6 or less ligands; while 50% Ca^{2+}-binding site has more than 6 ligands. Fourth, the Ca^{2+}-O and Mg^{2+}-O distances are distinct. About 53% of Mg^{2+}-O distance is in the range of 2.0-2.2 Å with an average of 2.1 Å. Those differences may contribute to the different roles of Mg^{2+} and Ca^{2+} in biological systems.

1.1.2 Ca^{2+} homeostasis

The cellular function of calcium (Ca^{2+}) was firstly reported by Sydney Ringer in 1883 (21). He found that the contraction of isolated frog hearts could be maintained in the saline solution prepared using London tap water which contained calcium, while not in the saline solution made up using distilled water without calcium. Later, Ca^{2+} induced contraction of frog muscle was further demonstrated to occur only when it was applied to their cut ends. Since then, especially after 1940s, the calcium signaling saga started and numerous subsequent works identified series of cellular processes including cell motility, gene transcription, muscle contraction, and exocytosis, are regulated by Ca^{2+}.

The extracellular Ca^{2+} concentration ($[Ca^{2+}]_o$) is about 20,000-fold higher than the intracellular Ca^{2+} concentration ($[Ca^{2+}]_i$). This huge difference across the plasma membrane creates the Ca^{2+} gradient from mM (extracellular) to nM (intracellular). However, the concentration of Mg^{2+}, another common physiological divalent ion, is reported to have only very small gradients (2 or less) across the plasma or intracellular membranes (22). One important reason why cells reduce Ca^{2+} concentration in cytosol is that Ca^{2+} can precipitate intracellular phosphate and exhibit its toxic properties in cell. In the long evolutionary history, cells adapted different ways to exclude high $[Ca^{2+}]_{i,}$ meanwhile utilize its concentration difference in signal transduction. In addition to extrude or compartmentalize Ca^{2+}, another way to control Ca^{2+} concentration is through thousands of Ca^{2+}-binding proteins with a broad range of binding affinities from nM to mM. Those protein could be receptors, buffer proteins, pumps or channels.

1.1.3 Ca^{2+} Signaling network

The Ca^{2+} homeostasis is tightly regulated by parathyroid hormones (PTH). When the concentration of Ca^{2+} in the extracellular fluid is too low, PTH synthesis and secretion from

parathyroid gland will significantly increase to directly act on bone and kidney by stimulating Ca^{2+} release and resorption, or indirectly work on intestine by stimulating Ca^{2+} absorption, respectively. Once the Ca^{2+} concentration in the extracellular fluid decrease below certain value, the PTH secretion will be decreased to reduce the bone Ca^{2+} release, kidney Ca^{2+} absorption and intestine Ca^{2+} absorption. The other effect of PTH secretion is to stimulate the production of 1, $25(OH)_2D$, which is the active form of vitamin D. This precursor of vitamin D could enhance the Ca^{2+} absorption in small intestine.

The Ca^{2+} signaling network is complex (**Fig. 1.1**) where cell plasma membrane establishes the simplest Ca^{2+} compartmentalization. The extracellular Ca^{2+} ($[Ca^{2+}]_o$) concentration in mammalian cells ranges from 1.5 to 2 mM. $[Ca^{2+}]_o$ could act as a first messenger through receptors on the cell membrane such as Ca^{2+}-sensing receptors (CaSR). Activation of those receptors by $[Ca^{2+}]_o$ leads to the transduction of extracellular signal into cytosol of cells through downstream signaling pathways. $[Ca^{2+}]_o$-binding to CaSR, for example, elicits complex intracellular signaling through activation of various downstream signaling proteins including G protein and protein lipase C (PLC), which in turn result in production of second messengers like inositol trisphosphate (IP_3) and DAG, through decomposition of phosphatidylinositol 4,5-bisphosphate (PIP_2). Subsequently, those second messenger further target on cytosolic molecules, leading to downstream signal changes, including Ca^{2+} release from endoplasmic reticulum (ER). Extracellular electrical, hormonal, and mechanical stimuli can also produce Ca^{2+} signals by causing influx of Ca^{2+} ion across the plasma membrane or release from intracellular Ca^{2+} store ER.

The intracellular Ca^{2+} concentration is tightly and precisely controlled at around 100-200 nM by proteins which can transport it in or out of the cytosol, or bind with it to limit its free concentration in the cytosol. Those proteins are divided into two broad categories, one of which

interact to regulate its free concentration, such as Ca^{2+}-buffering and Ca^{2+}-transporting proteins. The other group function as Ca^{2+} sensor by binding with Ca^{2+} to decode its signal. Residing in the cytosol or organelles, Ca^{2+}-buffering proteins usually has low Ca^{2+}-binding affinity, allowing large amount of Ca^{2+} storage. Ca^{2+}-transporting proteins are usually channels, pumps or exchangers on the plasma or organelle membrane. For example, plasma membrane Ca^{2+} ATPase (PMCA), voltage-gated channel, Na^{2+}/Ca^{2+} exchangers on the plasma membrane are pumps, channels and exchangers, respectively, mediating Ca^{2+} entry or exit through cell membrane. By transporting Ca^{2+} across the membranes, Ca^{2+}-transporting proteins usually produce sharp Ca^{2+} signal.

Both Ca^{2+}-buffering protein and Ca^{2+} triggering proteins can bind with Ca^{2+}. The difference between them is that Ca^{2+} triggering proteins process Ca^{2+} signals upon binding to Ca^{2+} while Ca^{2+}-buffering proteins do not. Ca^{2+}-sensing proteins firstly decode the Ca^{2+} signal via Ca^{2+}-dependent conformational change and then pass those information to targets that receive messages and translate them into function. The well-known Ca^{2+} sensor is the EF hand protein Calmodulin (CaM). There are one pair of EF hands with different Ca^{2+}-binding affinity in each domain of CaM. Upon Ca^{2+} binding, CaM undergoes changes from a “closed” to an “open” conformation. This change result in exposing more hydrophobic surface, which provides binding sites for a large number of target proteins. As a multifunctional intermediate, CaM integrates different signaling through interaction with numerous targets and associated with them reversibly. How CaM is able to interact with various target proteins is not well understood. This question will be addressed in Chapter 3.

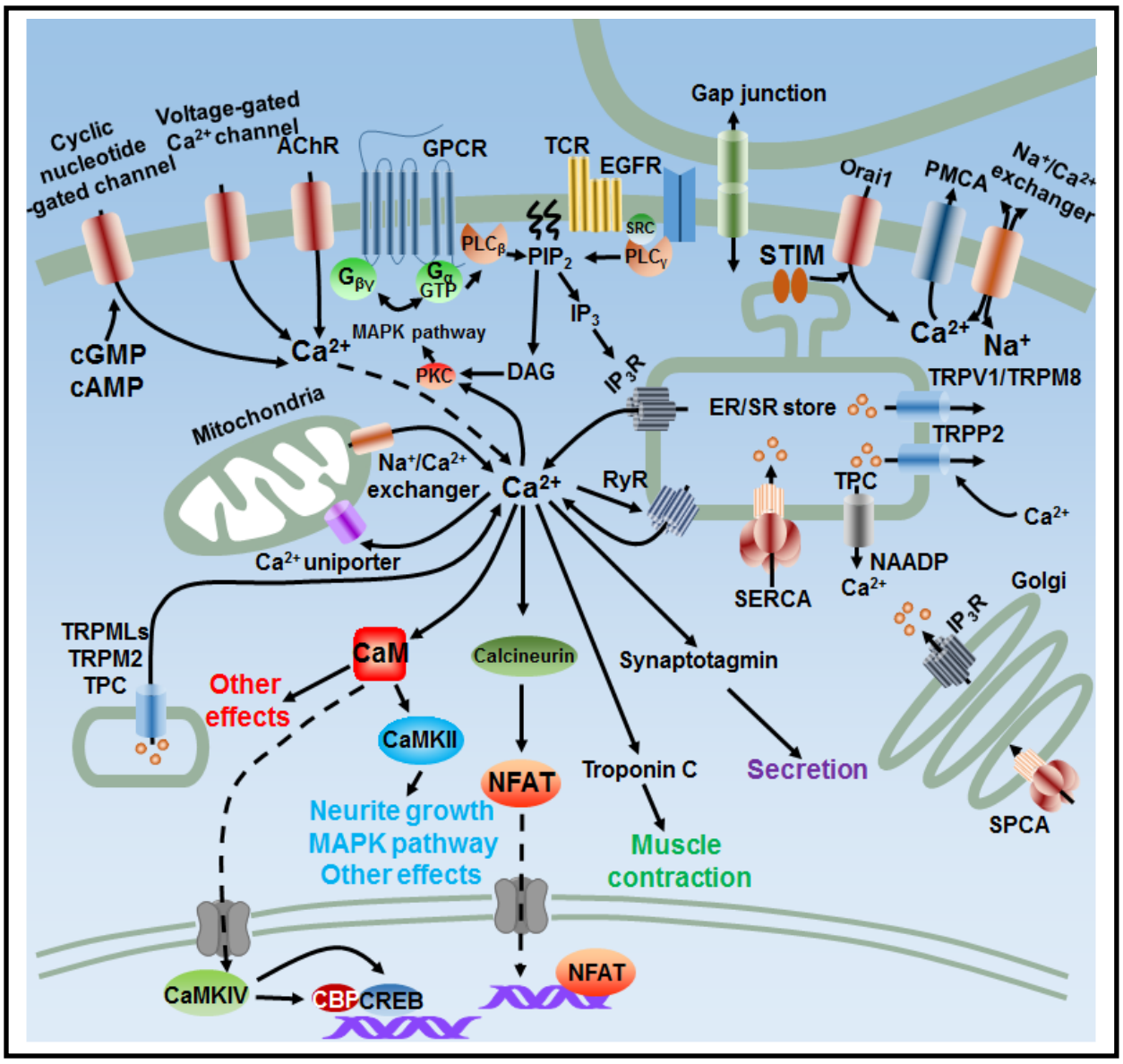

Figure 1.1 Ca^{2+} signaling network.

Extracellular stimuli firstly activate receptors on the plasma membrane, leading to the production of second messengers from numerous downstream signaling pathways and resulting in $[Ca^{2+}]_i$ elevation. In turn, elevated $[Ca^{2+}]_i$ leads to activation of various Ca^{2+} sensor proteins such as CaM and triggers downstream events such as activation of Ca^{2+}-dependent protein kinase. Ca^{2+}-permeable channels, pumps or exchangers on the membrane

including plasma, and organelle membranes can also be activated to allow Ca^{2+} mobilization through membrane (23).

1.1.4 Ca^{2+}, CaM, and CaM-binding modes

CaM is a small (17 kDa) Ca^{2+}-binding protein with ubiquitous express in eukaryotic cells. It is one of the famous Ca^{2+} sensor and adaptor protein, which contributes tremendously in understanding about processing of Ca^{2+} signals by EF-hand proteins. The crystal structure of parvalbumin is a historical landmark in Ca^{2+} signaling leading to the EF-hand-protein concept. Through the interaction with numerous targets, CaM transfers Ca^{2+} signals to regulate multitudes of intracellular processes such as cell growth, proliferation, motility, and apoptosis. The concept of EF-hand was first devised in 1973 when the parvalbumin crystal structure was solved (24). The canonical EF-hand in CaM is characterized by a 29-residue helix-loop-helix motif as shown in figure 1.2. Ca^{2+} in the EF-hand is coordinated by oxygens from sidechain carboxyl of amino acids at position 1, 3, 5 and 12, from main chain carboxyl of amino acid at position 7, and a bridged water at position 9. The topology of EF-hand resembles the spread thumb and forefinger of our hand. The EF-hands in two globular domains of CaM display different binding affinities for metal ions. The Ca^{2+}-binding affinity of C domain is 3-fold higher than that of N domain. Four sites from two globular domains function cooperatively to bind Ca^{2+}. In the absence of Ca^{2+}, CaM is in a "closed conformation" with antiparallel EF-hand helices from two domains. Upon Ca^{2+}-binding, CaM adapts to an "open conformation" in which helices are more perpendicular to each other, exposing more hydrophobic surface for a wide range of targets binding (25) .

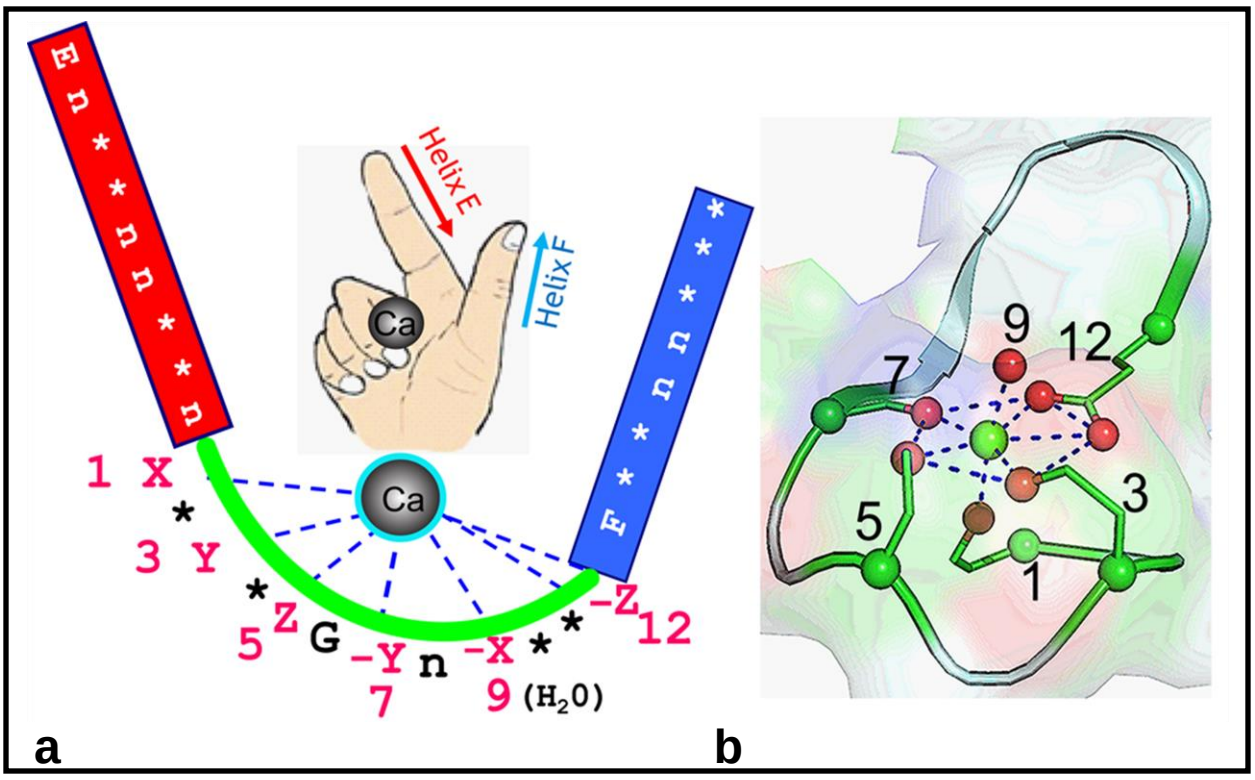

Figure 1.2 EF hand (26)

(a) Cartoon representation of EF hand. The canonical EF hand is formed by helix-loop-helix. Ca^{2+} ion in the EF hand is coordinated by ligands inside of this 12-residue loop region. Oxygen coordinating Ca^{2+} ions are from side chain of amino acids at position 1, 3, 5 and 12, main chain of amino acid at position 7, and water at position 9. (b) Crystal structure of EF in CaM.

Recent work involving crystallization, nuclear magnetic resonance (NMR), and mutagenesis studies have revealed how CaM interact with and regulate its targets in various different ways. Typically, before binding with its targets reversibly or irreversibly, CaM needs to be activated by Ca^{2+}. However, apo-CaM can also bind to the targets in many cases. CaM-binding

proteins possess specific regions characterized with a net positive charge, moderate hydrophilicity, and moderate to high helical hydrophobic moment (27,28). Many target sequence are intrinsically disordered and undergo a disorder-to-order conformational transition as reported (29-31). Those CaM-binding motifs are generally divided into IQ motif which is Ca^{2+}-independent CaM binding motif and Ca^{2+}-dependent CaM binding motifs. Ca^{2+}-dependent motifs can be further grouped based on the distance between hydrophobic anchor residues (28,30,32-36).

IQ motif represents a large group of CaM-binding sequences. One of the well-known characteristics of IQ motif is its Ca^{2+}-independence in CaM binding. However, recently, more and more work found that some IQ motifs also bind with Ca^{2+}-loaded CaM (37,38). Studies of CaM interaction with unconventional myosin provide primary elucidation of characteristics of IQ motif. IQ refers to the first two amino acids isoleucine and glutamine in the consensus sequence (IQXXXRGXXXR) of IQ motifs. The first residue isoleucine can be replaced by other hydrophobic amino acids such as leucine and valine. Glycine at position 7 is also ambiguous in some CaM-binding proteins like PEP19 and some myosin protein (39). Position 11 can be either arginine or lysine. A more generalized IQ motif can be presented as [I, L, V]QxxxRxxx[R, K]. Currently more IQ motif-containing proteins have been reported. Some of them called IQ-like motifs ([FILV]Qxxx[RK]xxxxxxxx) which does not strictly follow the generalized IQ motif sequence listed above. They are incomplete IQ motifs with only the first half of the IQ motif. Studies of the essential and regulatory light chain of conventional myosin revealed that C-domain of apo-CaM interacts with the first half of IQ motif (IQxxxR), while N-domain of apo-CaM binds with the second half without inducing significant conformation change of N-domain. The binding affinity of IQ motifs to CaM varies among different IQ motifs and Ca^{2+} concentrations.

How CaM interacts with its targets and regulates its binding partners varies. Through analyzing the CaM complex structures deposited in protein data bank (PDB), CaM-binding could be grouped into two general categories: extended and collapsed (Fig. 1.3). In extended mode, two domains of CaM interacts with different site of targets. The distance between two domains of CaM is not significantly influenced. The collapsed mode is also called canonical wrap-around mode, in which two domains of CaM bind to the hydrophobic anchor residues in the binding motif and form a hydrophobic pocket which wraps the helical target inside. The distance between two domains could be largely shortened by the flexible linker from 50 Å to less than 10 Å. Figure 1.4 shows that CaM regulates various cytosolic and membrane proteins including gap junctions. How Ca^{2+}/CaM regulates connexins especially Cx45 for cell-cell communication will be addressed in Chapter 3.

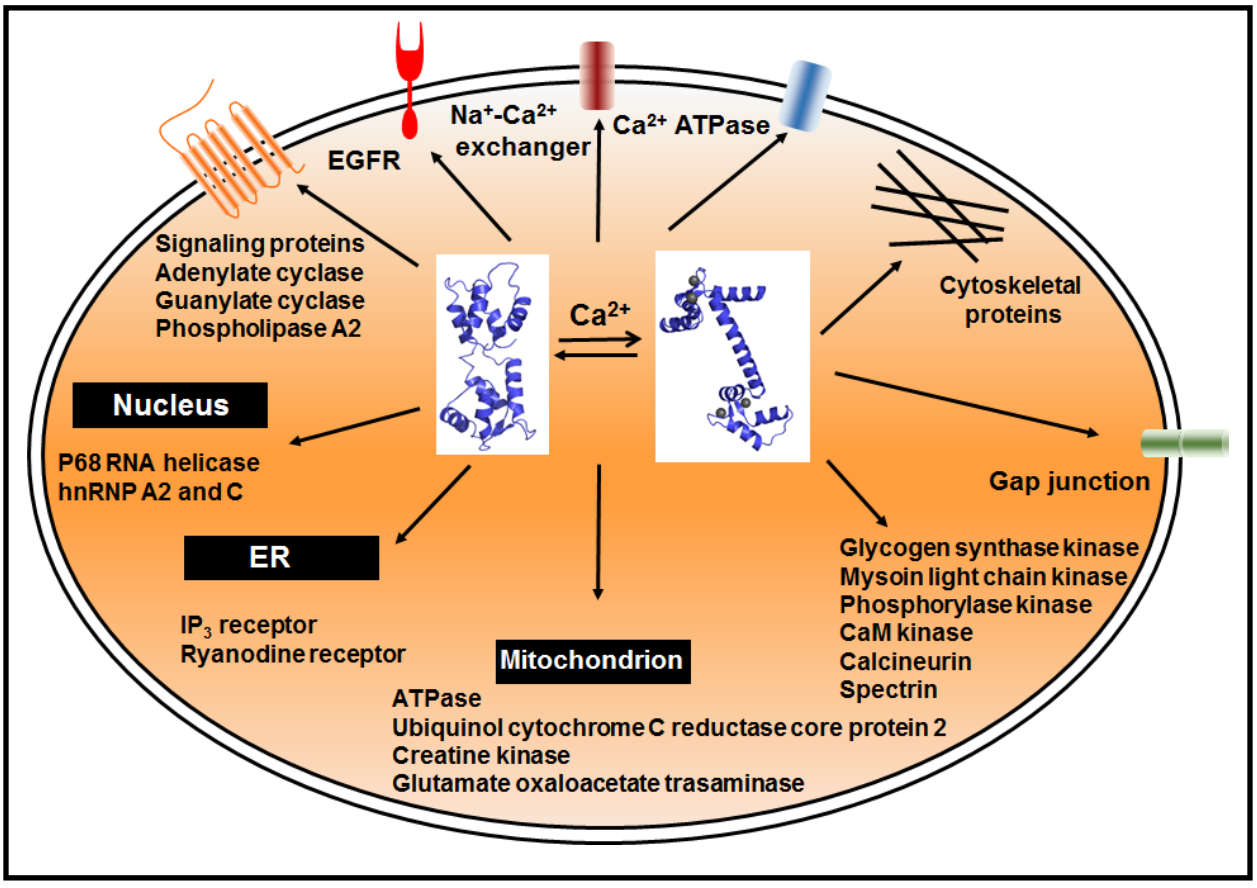

Figure 1.3 CaM function as an adaptor protein to interact with various target proteins.

Ca^{2+}-free and Ca^{2+}-load CaM are able to bind with a wide range of targets including soluble cytosolic proteins and membrane proteins.

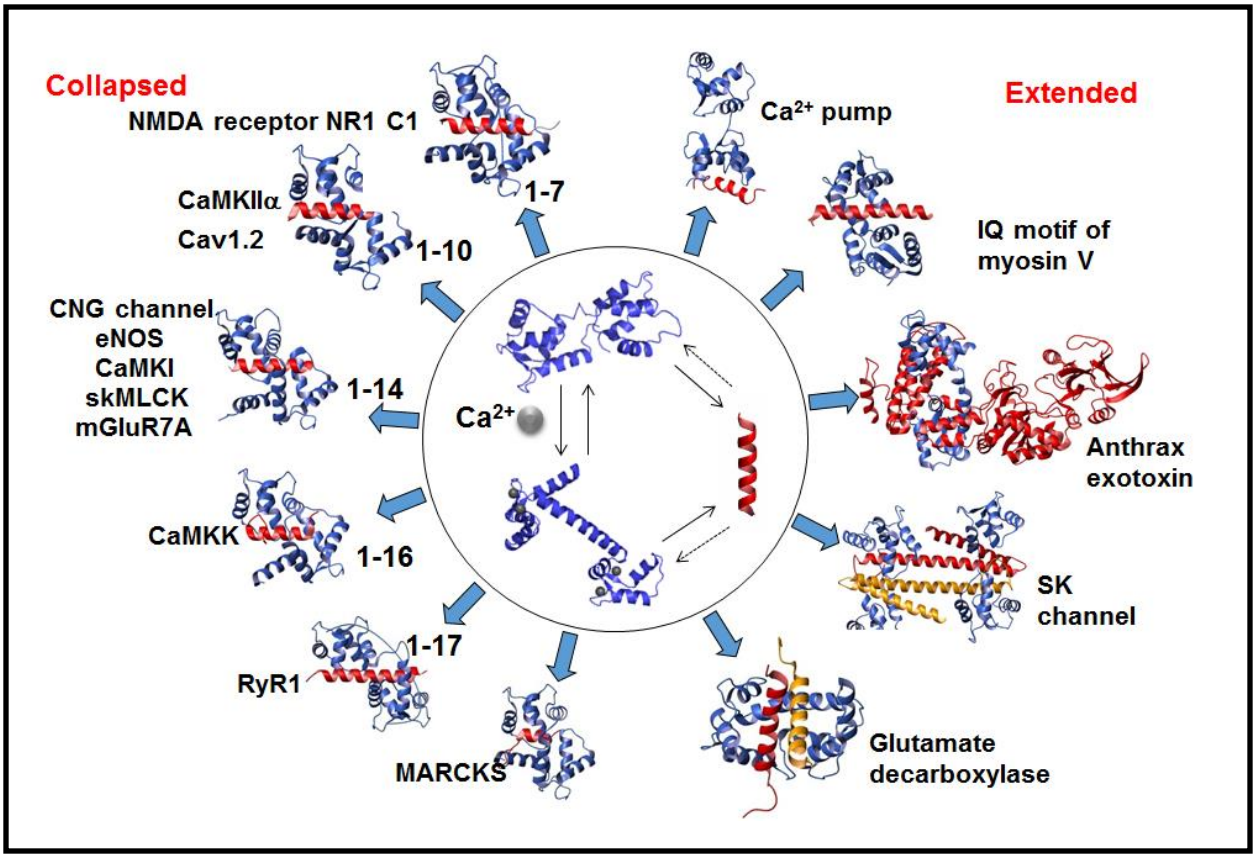

Figure 1.4 Diverse CaM-binding modes.

CaM interact with various target proteins in different binding modes. These modes can be divided into two groups-collapsed and extended, based on whether the distance between N- and C-domain of CaM is influenced or not.

1.2 Gap Junction

1.2.1 Gap junction overview

Gap Junction is a specialized membrane structure, which is spanning the membrane of two neighboring cells, leaving a 2-3nm characteristic gap between them (40)(**Fig. 1.5**). It forms a channel between two adjacent cells and provides a direct pathway for intercellular communication. Molecules up to 1kD (41), like second messenger, metabolites and so on, can pass through this channel. Not only the chemical coupling, but gap junction also allows the electrical coupling between two neighboring cells. Residing on the membrane, it offers an accurate tuning of several biological processes including cell differentiation, growth and development. So far, about 21 genes coding gap junction proteins have been discovered in human (42). Each of them has distinct physiological properties and regulation responses. This diversity is further amplified by expression of multiple gap junction protein in one cell to enable the heterologous interactions between different members (43). Gap junctions integrate the cellular functions of essentially every tissue in the body with a few notable exceptions (e.g. blood, skeletal muscle). The functional loss of gap junction may result in embryonic lethality (e.g. Cx45) (44,45), perinatal death due to congenital malformations (e.g. Cx43-/-) (46), and to disease pathologies (e.g. CMTX, Cx32; ODDD, Cx43; DFNA/B, Cx26, Cx30, Cx43; cataracts, Cx46, Cx50) (47). However, the molecular basis of dysfunction or loss of function is unclear. Connexin mutations may interfere the gene expression, affect the protein or DNA stability, impede protein trafficking, translocation and assembly or alter the regulation of gap junction.

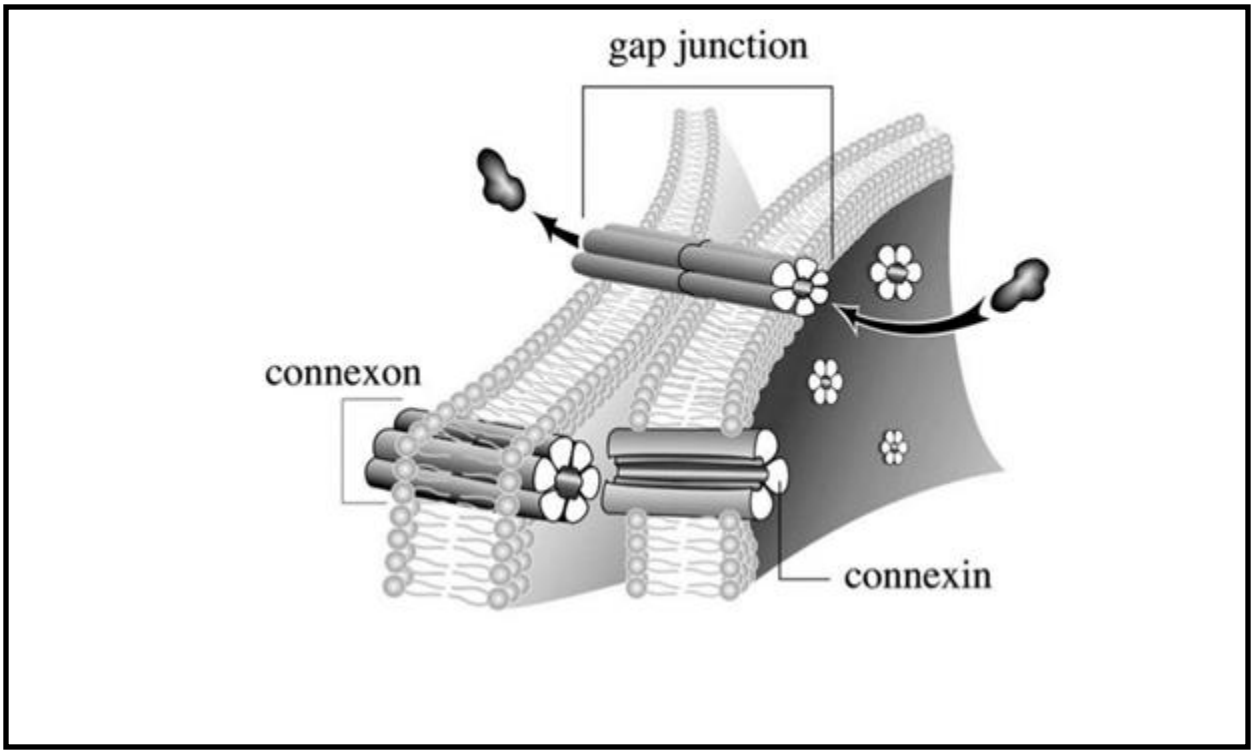

Figure 1.5 Gap junction on the cell membrane.

Hemichannels in apposed plasma membranes of neighboring cells can dock to each other and form gap junction channels, which enable the information and nutrients exchange between two adjacent cells. Hemichannel can also exist independently on the membrane and serves as the bridge connecting the extracellular environment and internal environment of cell.

1.2.2 Gap junction protein family and the distribution of connexins

Gap junctions were initially believed to be constituted by the same connexin until gap junction- enriched sample from different tissues displayed different bands on SDS-PAGE (48-51). Subsequently, more and more evidence came out to indicate that gap junction proteins harbor a big family. Until now, 19 connexin genes in the mouse genome and 21 connexin genes in the

human genome have been deposited in the mouse and human genomic databases. The widest acceptance of nomenclature used to distinguish connexin is word connexin abbreviation connexin followed by the predicted molecular mass of connexins in kilodaltons (52,53). Additionally, a prefix is added to label the species that connexins originate from. An alternative nomenclature was created to clarify some confusion met when homologous connexins have completely different molecular masses in distinct species (e.g., hCx46, bCx44 and cCx56). Connexins are sorted into subgroups (α, β and γ) based on amino acid sequence homology and evolutionary relationships.

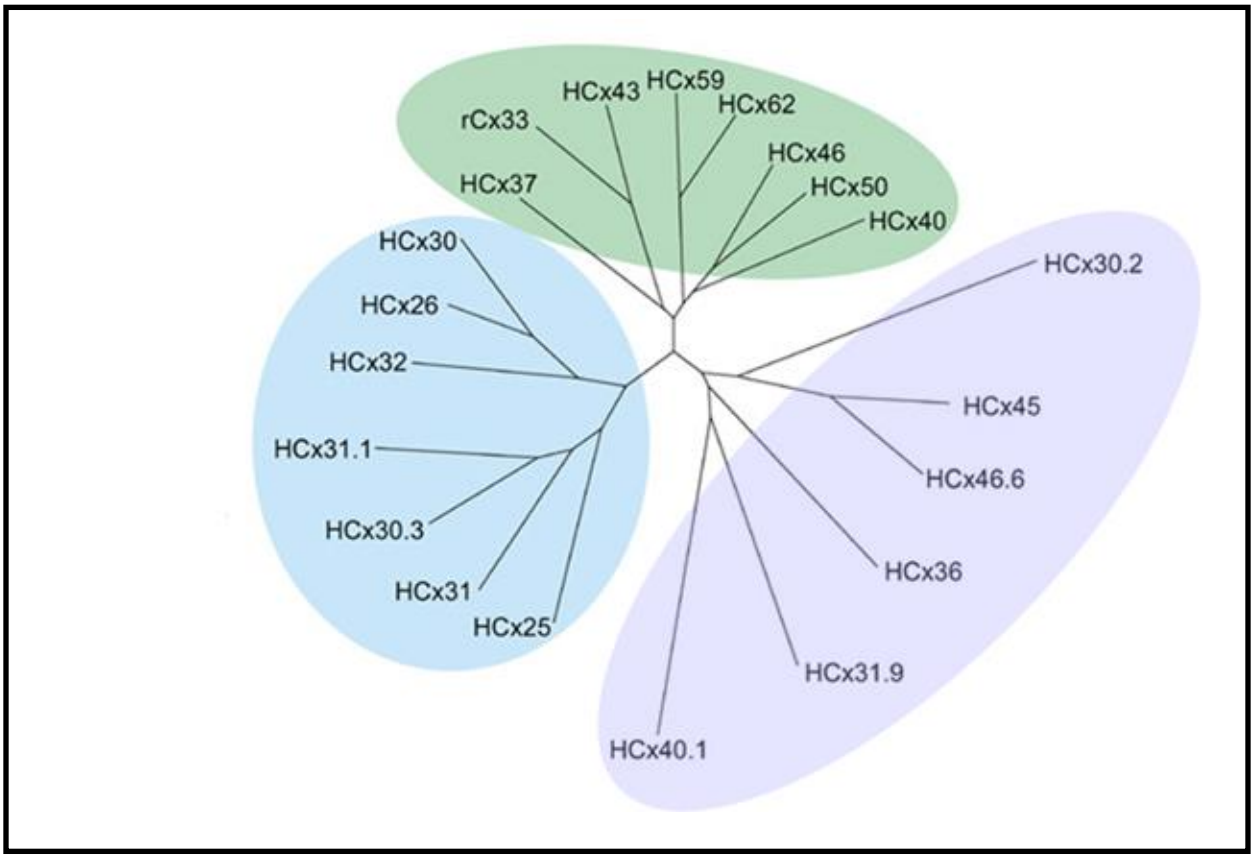

Figure 1.6 A molecular phylogenetic tree for human connexin protein (HCx) and rat connexin33 (rCx33).

The divergent sequence portions (the intracellular loop and the carboxyl-terminal domain) were removed from the multiple alignments. The connexin family can be broadly separated into three main subgroups, the historical, α (green) and β (blue) and a more divergent γ branch (54).

Compared with α and β family, γ family is well known and widely divergent. On the above phylogenetic tree (**Fig. 1.6**), connexins in the γ family show larger evolutionary distances. Sequence alignment of hCx45, hCx26 and hCx50 result indicates that γ family Cx45 does not have the "MDW" amino acid at the beginning of N-termini. Besides, the CL is much longer in Cx45 than that of Cx26 and Cx50. Compared with the β-type connexins, the α-type connexins have a larger M2–M3 cytoplasmic loops and a larger cytoplasmic C-terminal tails. Besides, the second amino acid "G" is absent in beta family amino acid. Finally, the initiation of assembly occurs in distinct cellular organelles (Figure 5); one of the beta family members Cx32 assembly occurs in the ER/ERGIC (55). In contrast, Cx43 (56)and Cx46 (57) which belong to the alpha family start to assemble in the trans-Golgi network (**Fig. 1.7**).

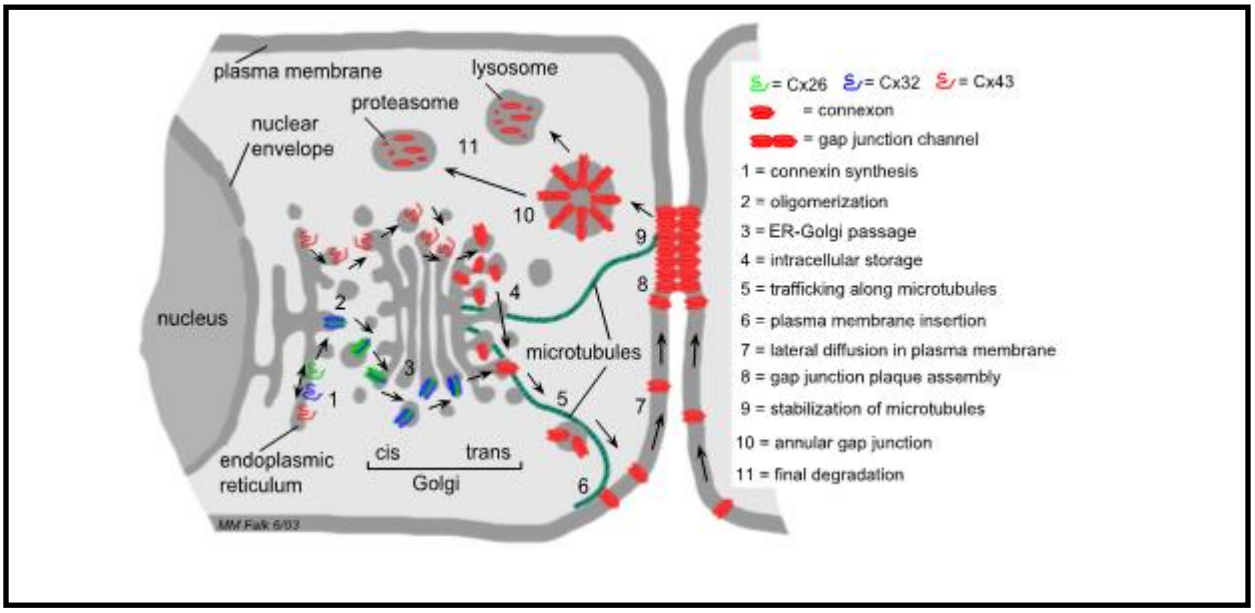

Figure 1.7 The life cycle of connexin.

Connexins were synthesized in the ER first, following by oligomerization in different intracellular department. The initiation of assembly of Cx32 and Cx43 are from ER and trans-Golgi network, respectively. The hexamers were transported along the microtubules to the cell surface, where plasma membrane insertion occurred. Hemichannels could undergo lateral diffusion in plasma membrane and form gap junction plaque eventually by docking with hemichannels from the other cell. Microtubes participated in the stabilization of gap junction plaque. The degradation of gap junction protein were achieved in lysosome or proteasome (55).

Connexins universally distribute in vertebrate tissues with the exception of several highly differentiated cell types: red blood cell, mature skeletal muscle cell and spermatocytes. The connexin expression pattern is complicated in tissues. One or even more connexins may express in a given tissue and a given connexin can be present in more than one tissues. The cDNA probes significantly contribute to the screening of connexins in different tissues. A list of connexins

expressed in various tissue types are listed below (**Table 1.1**). Cx26 can be observed in liver, skin, liver and cochlea, but Cx46 and Cx50 expression is exclusively in the eye. Furthermore, in the different stages of one given tissue, the types of connexins vary and the expression amount displays a great variety. Take Cx43 as an example, abundant mRNA of Cx43 and Cx38 had been identified in Xenopus Oocytes before ovulation and meiotic maturation, while Cx43 gradually disappears during the maturation of oocytes. Then Cx38 is replaced with Cx30 by the early gastrula stage (58,59). In summary, the regulation of connexin expression is both temporal and spatial.

Table 1.1 Connexin gene expression pattern in human.

Gene	Expression Patterns
GJB2(Cx26)	**Cochlea, skin, liver, placenta, breast**
GJB1(Cx32)	**Liver, oligodendrocytes, chawann cells**
GJA1(Cx43)	**Heart, lens, brain, adrenal gland, etc.**
GJCa(Cx45)	**Heart and brain**
GJA3(Cx46)	**lens**
GJA8(Cx50)	**lens**

Among all these characterized connexins, it is worthwhile to note that Cx26 usually expresses in conjunction with other connexins in the same family (60). The co-existence of different connexins in one cell dramatically increases the structure combinations of both connexon and GJ channels (**Fig. 1.8**). Homomeric or heteromeric connexons can be formed by six identical connexins or different connexins, respectively. Another complexity is generated during the docking of connexons from two adjacent cells. GJ channels can be either formed by two identical or different hemichannels, leading the formation of homotypic or heterotypic GJ.

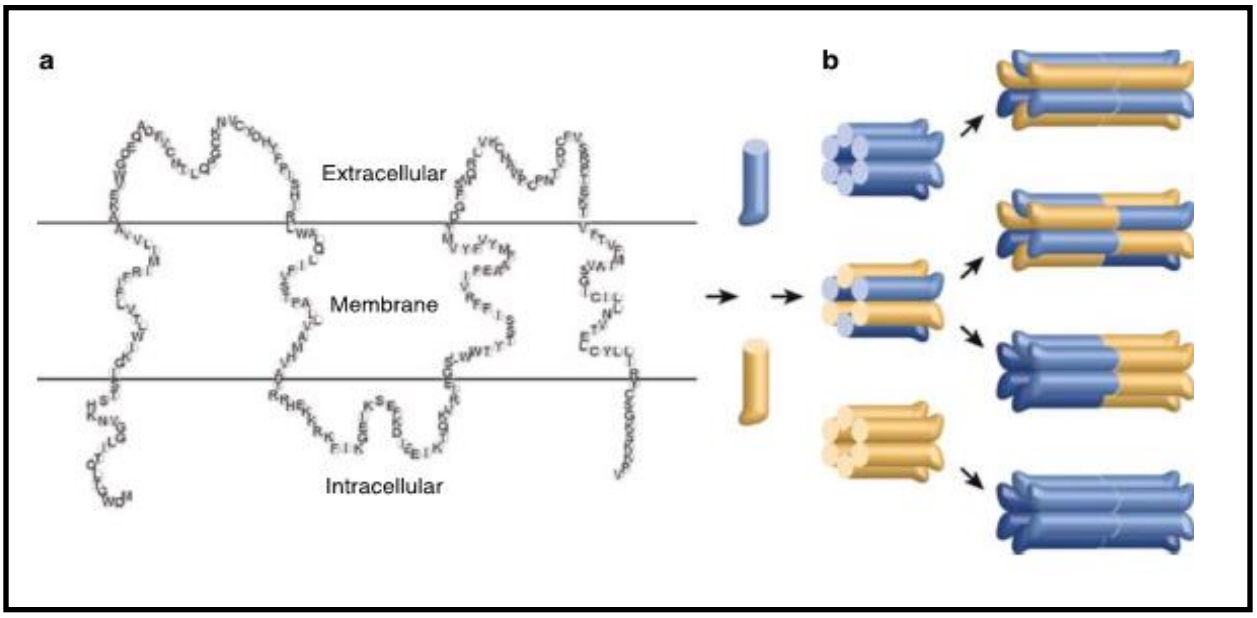

Figure 1.8 Scheme presentation of connexin and gap junction channel.

(a) Connexin is compromised by four transmembrane helices, two extracellular loops, one cytoplasmic loop, N- and C-domains. (b) Six connexins oligomerize to form hemichannels called "connexons", which then align in the extracellular space to complete the formation of gap junction channels. Different connexins can selectively interact with each other to form homomeric, heteromeric, and heterotypic channels, which differ in their content and spatial arrangement of connexins subunits (61).

It is not certain to what extent the formation of heterotypic gap junction channels will alter the cell communication. The heterogeneous gap junction channels are conducive to cells from the following aspects: 1) expand the diversity of molecules exchanged between cells since different gap junctions exhibit unique permeability; 2) increase the options for fine regulation of gap junctions; 3) provide control over the assembly of hemichannels and gap junction channels (62). It is notable that a given connexin is only compatible to certain connexins. The heterogeneous gap

junction communication had been assessed using the *xenopus* oocyte expression system (63,64). So far, the compatibility of connexins has been depicted. Bruzzone and his colleagues fused one fragment from the N-terminus to the second transmembrane of Cx32 to Cx43 from the cytoplasmic loop to the C-terminus and overexpressed this mutant in *xenopus* oocytes. By measuring the gap junction conductance, they found that this mutant only paired functionally with Cx43, but not Cx32. The result indicates that the middle cytoplasmic loop and the C-terminus are portions influence the interaction between different connexins (65).

1.2.3 The function of gap junction and its associated diseases

Gap junctions play an indispensable role in direct electrical and chemical communication between cells, through the transmission of current and molecules less than 1kD, such as inositol triphosphate (IP3) and calcium Ca^{2+}. It is involved in many biological processes, including development, differentiation, cell synchronization, neuronal activity and the immune response (66,67).

This protein family is related with many diseases, like skin disease, tooth disease, and heart diseases (**Fig. 1.9**). The first inherited abnormality of a gap junction protein was reported in 1993 with mutations in Cx32 in individuals with X-linked charcot-marie-tooth disease (68). Then in 1997, mutations in Cx26 were identified in case of deafness (69), a finding that led to the significant discovery that mutations in Cx26 are in fact a common cause for several forms of deafness. Later, mutations were discovered in seven connexins: Cx30, 30.3, 31, 40 43, 46 and 50 to be related with different diseases. Among them, four connexins were associated with skin

diseases: Cx26, Cx30, Cx30.3, Cx31. Cx46 and 50 have been shown to underlie cases of cataract (70,71).

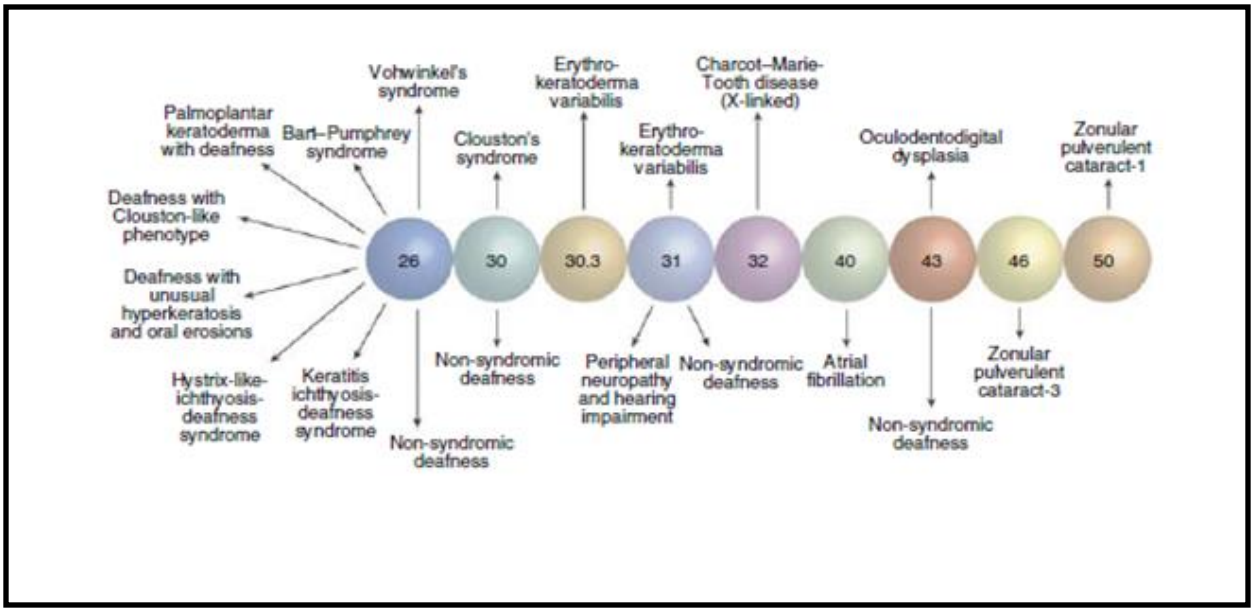

Figure 1.9 Illustration of disease phenotypes associated with abnormal gap junctions. **Mutations in connexins lead to abnormal function of gap junction channels or hemichannels, resulting different diseases (47).**

1.2.4 The regulation of gap junction by Ca^{2+}

Since communication between neighboring cells is regulated at multiple levels, the gap junction gating displays several different ways, like voltage gating and chemical gating, which are the faster regulations involved in changing the unitary conductance of single channels or altering their permeability of opening. The slower regulation is achieved through slowing the synthesis and assembly rates, thus reducing the number of gap junction present in the membrane. The slow and rapid regulation may overlap, for example, the rate of trafficking the connexon to the membrane

may be slowed down or degradation is accelerated, meanwhile, the conductance of gap junction channels is altered. In this dissertation, I will focus on the chemical gating, especially Ca^{2+} and CaM regulation of GAP JUNCTION channels.

The discovery of Ca^{2+} in gap junction regulation can be traced back to 1970s when a plentiful of articles reported that extracellular calcium was required for the heart muscle "healing-over" (72-76). When the cardiac muscle is damaged in injury, the resting membrane potential first depolarizes, followed by a recovery to normal. This process is called "healing-over", which is initiated as a self-protection mechanism to prevent the spread of damage to neighboring cells. It is concluded that extracellular Ca^{2+} ions in the bath solution is essential for the healing over of mammalian heart muscle and cell uncoupling mediated through gap junction (77-83). Later on, structural changes induced by $[Ca^{2+}]_o$ were observed in gap junctions isolated from calf lens fiber (84). As shown in figure 1.10, loosely packed junctional regions were captured in Freeze-fracture experiment when calf lens were incubated in EDTA solution in which Ca^{2+} concentration was buffered within a range of 10^{-8} to 10^{-6} M. The random center to center distance between each particles were ranging from 8 to 11 nm. In the contrast, gap junction particles were induced to form condensed crystalline array with a center-to-center distance of 6.5-7 nm by Ca^{2+}.

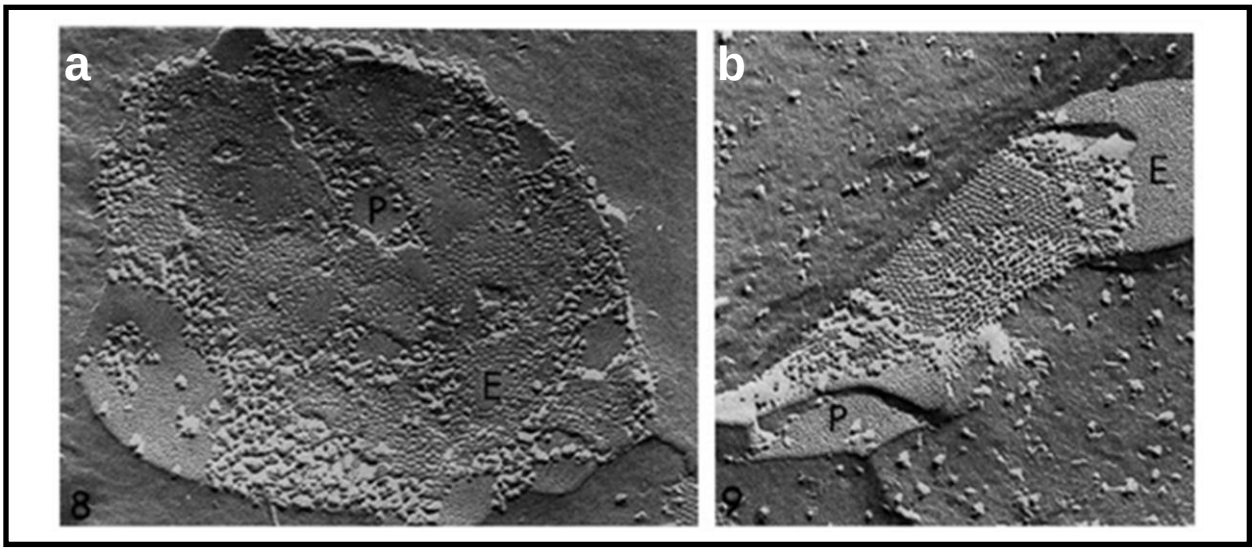

Figure 1.10 Comparison of gap junction particles isolated from calf lens fibers in the presence of EDTA (a) or subsequently incubated in the presence of $CaCl_2$ (b).

Images were obtained from freeze-fracture replica experiments. The distribution pattern of gap junction particles in EDTA buffer is random and loose, on the contrary, condensed crystalline pattern were detected when gap junction particles were immersed in Ca^{2+} buffer. E: E face; P: P face.

In 1980, Dr. Unwin proposed a Ca^{2+} gating model (**Fig. 1.11**): the helices of gap junction protein twist to close the channel in the presence of Ca^{2+} (85). Large conformation changes are required in this proposed model. But until now, no evidence support this model.

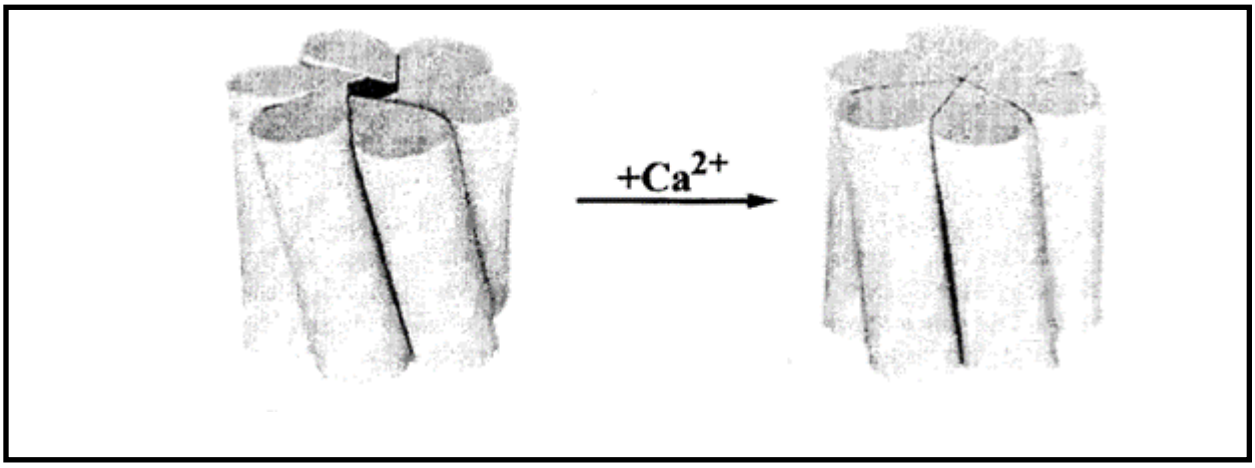

Figure 1.11 Ca^{2+} regulation model from Dr. Unwin.

Six cylinders stand for the six gap junction protein connexin. The helices of six cylinders twist a little to close the channel in the presence of Ca^{2+} (85).

The rapid development in the atomic force microscopy facilitated the progress of visualization of conformations of gap junction channels. Back to 2002, Daniel imaged the Ca^{2+}

induced conformational change of gap junction channel (**Fig. 1.12**) using AFM (86). Before the injection of Ca^{2+} solution, gap junction channels display 1.5 nm diameter entrances, while the injection of 0.5 mM Ca^{2+} reduces the diameter of entrance to 0.6 nm. Besides, the plaque heights also increased from 0.6 nm to 18 nm, which suggests that Ca^{2+} not only alters the conformation of the surface of connexon (hemi-channel), but also affects the structure of intact channel.

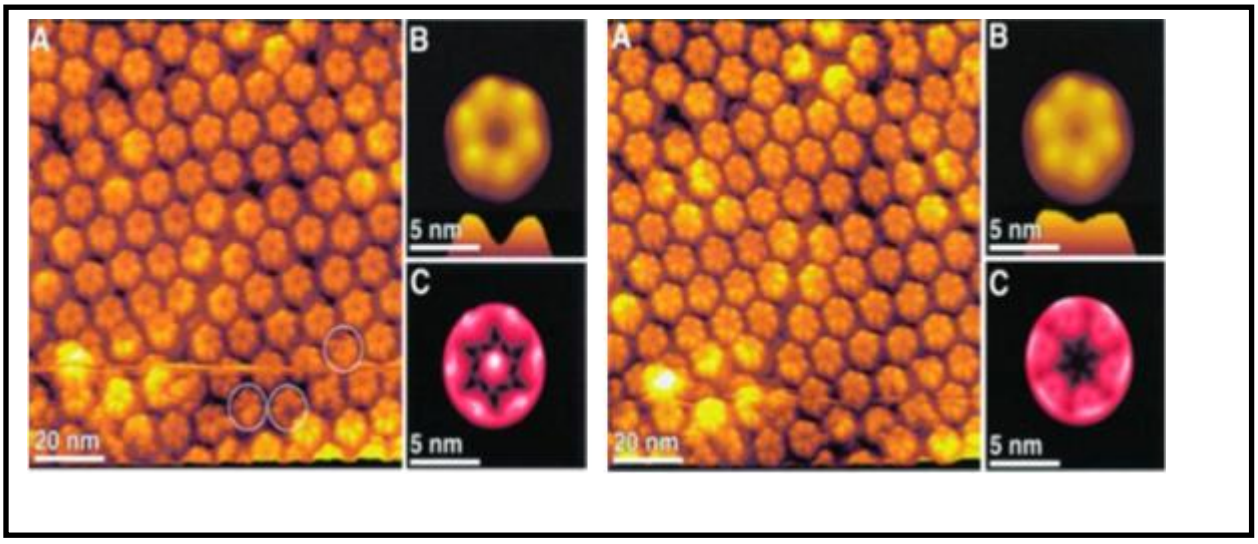

Figure 1.12 Extracellular connexin surface recorded by AFM in a Ca^{2+}-free buffer (left) and a buffer with 0.5 mM Ca^{2+} (right).

A is the AFM image showing single connexons. Circles in the image pointed out some connexons with defects. B is the average of all connexons captured in image A. The connexin arrangement in connexon are depicted, as well as the side view of the channel pore. C is the average standard deviation map calculated from connexons in image A.

Recently, Julian *et al*. studied the effect of different divalent cations on the pore size of Cx43 (**Fig. 1.13**) (87). When there was no Ca^{2+} in the buffer, the addition of Mg^{2+} or Ni^{3+} could not close the pores. While 1 mM Ca^{2+} triggered the decrease of pore size and 1.4 mM Ca^{2+} could

even make some channels close. At 1.8 mM Ca^{2+}, the pores completely closed. Figure 1.14H and I clearly showed the extracellular surface of the channel in Ca^{2+} free buffer and 1.8 mM Ca^{2+} buffer. The size distribution of Cx43 hemichannel pore analysis also clearly indicated that the average pore inner diameter of Cx43 hemichannels in 1.8 mM Ca^{2+} buffer was approximately 1nm smaller than that in Ca^{2+} free buffer. With the increase of Ca^{2+} concentration in the buffer, the population of open pores dramatically reduced from 100% to less than 5%.

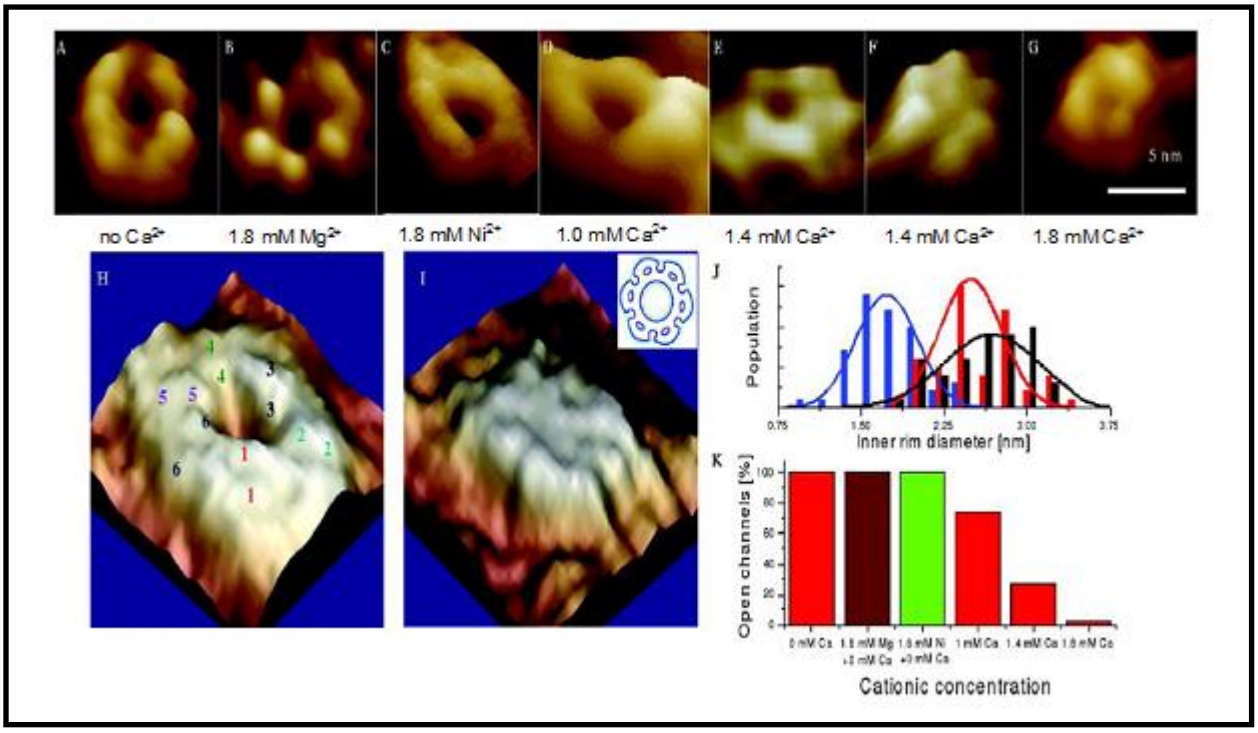

Figure 1.13 The diameter change of reconstituted Cx43 hemichannel pores in different cations. **A-G shows the surface of the pore mouth in different cation concentrations. H and I are two zoomed connexons presented as open (H) and closed (I) hemichannels. Connexin monomers were numbered as 1 to 6. J is the inner pore diameter distribution graph in the absence of Ca^{2+} (black), or in the presence of 1.8 mM Ca^{2+} (blue) or 1.8 mM Ni^{2+} (red). The percentages**

of open channels in different concentration of bath Ca^{2+} concentrations are plotted in the figure K.

All the above results suggests that Ca^{2+} plays a crucial role in channel gating. But the exact mechanism is still unknown. What is the Ca^{2+} binding sequence? Does it directly bind with the gap junction or not? How does the Ca^{2+} regulate the opening of gap junction channel? Until this year, the first Ca^{2+}-loaded crystal structure of Cx26 was published, uncovering the binding site of Ca^{2+} and its mechanism of channel closure induction (88). In this dodecamer structure, 12 Ca^{2+} ions were coordinated by 5 oxygens from residues E47, G45, and E42. Among the three binding ligand, G45 and E47 are from one monomer, while E42 is provided by another adjacent monomer (**Fig. 1.14**). The Ca^{2+}-bound and Ca^{2+}-free structures are similar. The threshold diameter of both pores are around 15 Å. Those two structures directly revised the old model in which Ca^{2+}-binding induces major rearrangement of six helices to close the gap junction channel proposed by Unwin *et al* earlier. The comparison between Ca^{2+}-bound and Ca^{2+}-free structures revealed that the arrangement of six helices are nearly identical. The bound Ca^{2+} was still exposed to the aqueous environment and no occlusion was formed in the Ca^{2+}-bound structure. Even though no major difference between Ca^{2+}-bound and Ca^{2+}-free structures were seen, minor deviations were identified. In the absence of Ca^{2+}, the side chains of both E42 and E47 rotated $\geq 90^{o}$ and formed intrasubunit hydrogen bond with R75 and K188, respectively. The carbonyl of Cx45 moved closer to E42 to result in additional interactions between subunits when Ca^{2+} is absent.

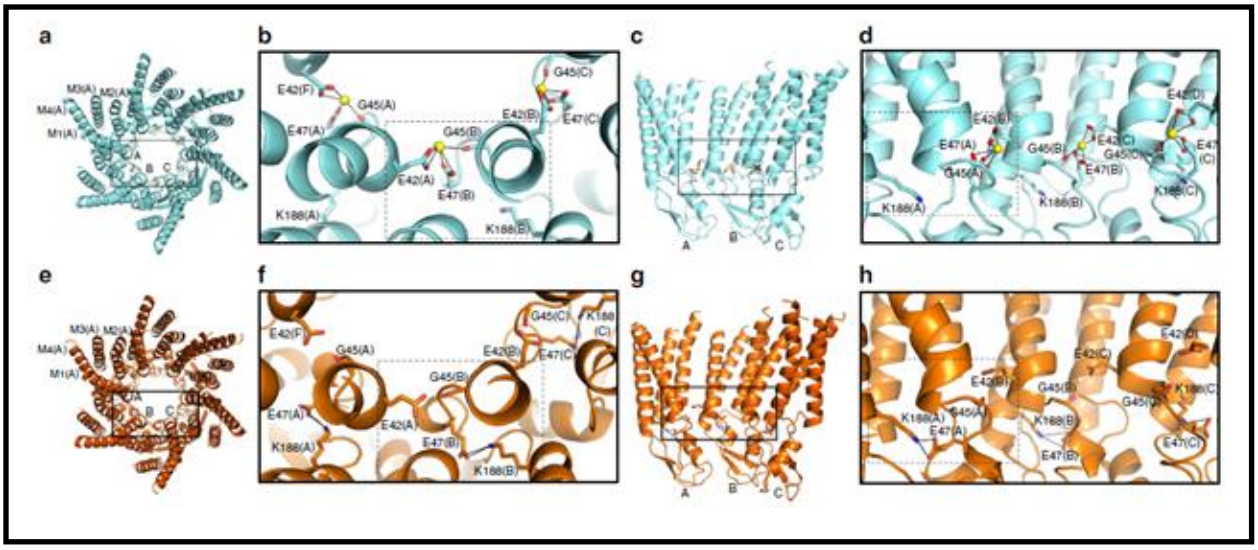

Figure 1.14 Ca^{2+}-binding site in Cx26 gap junction channel crystal structure.

The helices arrangement are very similar in Ca^{2+}-bound (a, cyan) and Ca^{2+}-free structures (e, orange). In the Ca^{2+}-bound structure , Ca^{2+} is positioned at the interface between two adjacent monomers , coordinated by five oxygens from residues E42 (from monomer F), G45 (from monomer A), and E47 (from monomer A) (b) In the Ca^{2+}-free structure, the side chain of three Ca^{2+}-binding ligands rotated and build interactions with other surrounding residues. Side view of Ca^{2+}-bound hemichannel (c) or Ca^{2+}-free hemichannel (g) with three monomers close to the viewer been removed. (d) Side view of the Ca^{2+} coordination sites in Ca^{2+}-bound structure (d) or Ca^{2+}-free structure (h).

The new Ca^{2+}-bound structure did not form steric occlusion of the pore, but it did change the electrostatic potential of the pore. Molecular dynamics (MD) simulations of the Ca^{2+}-free and Ca^{2+}-bound structures found that K^+ permeabilization was severely impeded by Ca^{2+}-binding. A positive pore surface potential is created which determines the pore selectivity when Ca^{2+} binds. Ca^{2+}-free gap junction channels with a negative surface potential prefers the passage of anions or

molecule with negative charges. Based on the above evidence, Bennett *et al.* proposed that an electrostatic barrier of the pore is formed when the Ca^{2+} binding sites are occupied, resulting in significantly reduced permeability of positively charged molecules and cations.

1.2.5 Structure characterization of gap junction

The long history of gap junction structure characterization can be traced back to 1960s, which was several years prior to the time that gap junction protein was been identified. The sectional disk-like structures were visualized in cardiomyocyte plasma membrane (89), striated and smooth muscle cells (90,91), and synaptic membrane complex (92,93) by electron micrograph (EM) in the late 1960s and early 1970s. In the early EM images, gap junction was delineated as hexagonal nexus structures, while Stoeckenius *et al.* found that lipid micelles can also array to hexagonal structure when temperature is elevated (94). Therefore it is hard to say which one (gap junction or lipid) forms the hexagonal structure, but here is a possibility that the hexagonal nexus structure was an artefact of temperature. Until 1967, gap junction was distinguished from tight junction when Revel and Karnovsky observed the dense spot in the center of gap junction by EM (95). The dense spot indicated that gap junction had hollow and hydrophilic center, which possibly enable molecules to pass through. Later Payton and his colleagues (96) proved that a membrane impermeable dye Procion yellow M4RS can be transferred between adjacent cells via cytoplasm-to-cytoplasm exchange. Subsequent freeze-fracture revealed GJs spanning plasma membrane of two neighboring cells as hexagonal subunits called “connexon”. Specimen prepared for freeze-fracture was intact gap junctions purified using a bulk purification protocol created by Goodenough et al (97).

From then on to 1999, medium resolution structure of gap junctions was achieved. X-ray diffraction data further confirmed gap junctions' hexagonal array structure (98). In the later study by Unwin et al, left-handed twist of connexons triggered by Ca^{2+} was observed. This rotation contributed to a wider extracellular surface and narrower cytoplasmic mouth. The advent of Edman degradation speeded up the identification of gap junction proteins. Nicholson first reported that liver and heart gap junction proteins were different but also related (99). A 32 kDa protein was identified in rat and human liver (100). Other gap junction proteins like 43 (52) have since been discovered. Considering multiple connexins expressed in one specific tissue, the molecular weight (52) of isoforms was used to name connexins and replaced the previous nomenclature system built on tissue expression (59). Later on, connexins were described as consisting of 4 helical transmembrane domain (TM1, TM2, TM3 and TM4), two extracellular loops (EL1 and EL2), one cytoplasmic loop (CL) by prediction, circular dichroism (CD), proteolysis susceptibility and site-directed antibody localization studies.

High resolution gap junction structure was published in 1999 (101), in which a 7.5Å crystallographic structure of CT-truncated Cx43 turned over a new chapter of gap junction structure study. Truncation of Cx43 at residue 263 removed the most flexible part of Cx43 and increased the diffraction resolution. The crystal structure depicted a widening cytoplasmic surface with a diameter of 70 Å and a narrowing cytoplasmic surface with a diameter of 50 Å. Additionally, the crystal structure suggested that each connexin has four helical TM domains (two right-handed and two left-handed), which supported the hydropathy plots prediction. Atomic force microscopy (AFM) played significant role in visualizing conformational change induced by Ca^{2+} and pH. Muller et al clearly captured the pore diameter drop from 1.5 nm in Ca^{2+} free buffer to 0.6 nm when 0.5 mM Ca^{2+} was injected into the buffer (86). In 2005, the decrease of central pore

of 73 % Cx43 connexon from 2.5 nm to 1.8 nm upon the addition of 1.4 mM Ca^{2+} to the buffer was again published (87). Later, pH-mediated pore closure of Cx26 was identified by AFM too (102). The channel entrance size narrowed down from 1.7 nm to 0.6 nm when buffer pH dropped from 7.6 to 6.0. But Cx26 only responded to acidification in aminosulfonate buffer. In the same year, a 10 electron crystallographic structure of Cx26M34A was reported by Sosinsky lab (103). This structure is quite similar to the truncated Cx43 gap junction reported by Thimm in 2005. The astonishingly similarity hinted that the most distinct cytoplasmic parts may function as a regulator. But the flexibility of these cytoplasmic domains makes them to be invisible in this crystal structure. The new discovery from the projection maps of Cx26M34A is the plug-like density in the pore of Cx26M34A channel. One year later, the same group compared the Cx26M34A and Cx26M34Adel2-7 electron cryo-crystallography at the same resolution and found a significantly decreased plug density in the pore of Cx26M34Adel2-7 (104). Cx26M34Adel2-7 is derived from Cx26 M34A by deleting amino acids 2 to 7 at the N-terminus. The difference indicates that N-domain of Cx26 contributes to the plug revealed in the Cx26M34A projection map. A higher resolution (5 Å) further proved that N-terminus is the most reasonable candidate of forming the plug. Besides, N-domain may function as stabilizing the open state of Cx26 channel since N-domain deletion mutation displayed no electrical activity in paired Xenopus oocytes and reduced dye transferring capability in Hela cells (105). The conclusion based on the 3.5 Å crystal structure reported by Maeda group (106) further enriched our understanding on the gap junction structure. The traditional Japanese drum shape channel (**Fig. 1.15**) shared similar size and shape with C-terminal truncated Cx43 channel.

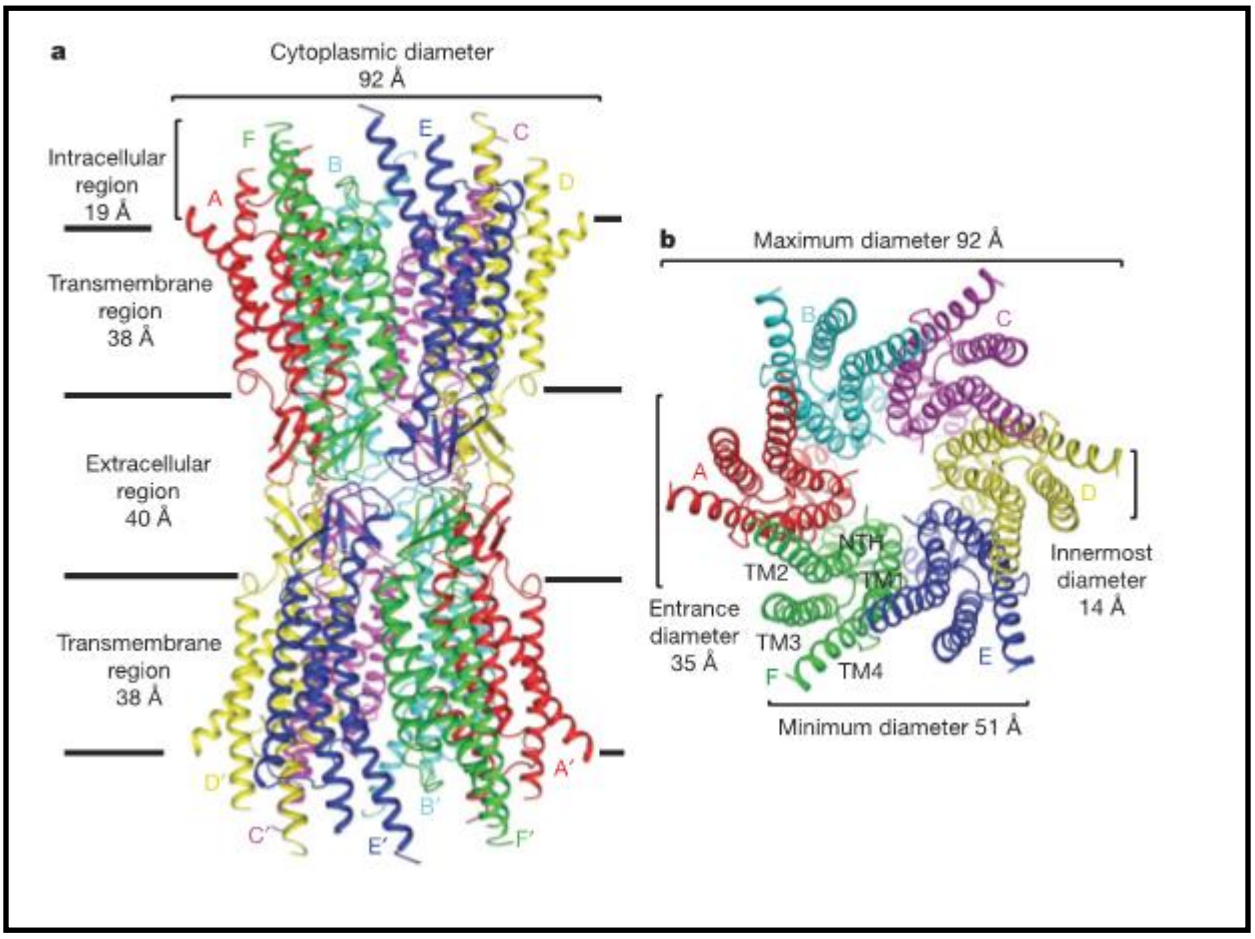

Figure 1.15 Overall structure of Cx26 gap junction channel in ribbon representation.

The corresponding protomers in the two hemichannels, which are related by a two-fold axis, are shown in the same color. (a) Side view of the Cx26 gap junction channel. (b) Top view of the Cx26 gap junction channel showing the arrangement of the transmembrane helices TM1 to TM4. The pore has an inner diameter of 35 Å at the cytoplasmic entrance, and the smallest diameter of the pore is 14Å (106).

Due to the high flexibility of cytoplasmic domains, the cytoplasmic domains were not resolved in the crystal structure. The height of Cx26 channel is about 155 Å without accounting the disordered cytoplasmic loop and C-terminus. The maximum diameter (92 Å) of Connexon

exists at the cytoplasmic side and the minimum at the extracellular side (51 Å). The pore diameter decreased from 40 Å at the cytoplasmic side to 14 Å at the extracellular membrane surface, followed by a widening to 25 Å at the extracellular space. The heights of intracellular, transmembrane and extracellular regions are 19 Å, 38 Å and 40 Å respectively. Four transmembrane domains of Cx26 forms the typical helical bundle structure, in which two adjacent helix are antiparallel. The debate here is about which membrane segment are pore-lining helix. Previous work (107,108) demonstrated that TM1 is the likeliest candidate, while other data (109,110) were inclined to TM3. In this crystal structure, TM1 was believed as the major pore-lining domain and contribute to narrowing the pore at the extracellular side of the membrane (**Fig. 1.16**). The extracellular loop E1 starts with a 310 helix and ends with a short α–helix. E2 has a short antiparallel β-sheet and a flexible N-terminal half. The C-terminal half of E2 begins with a 310 turn. Six highly conserved Cys residues on E1 and E2 form intramolecular disulfide bonds to stabilize themselves. It is reported that mutations in any of them cause the formation of nonfunctional gap junction channels (111,112). The previous functional studies also indicate that a number of diseases related Cx26 mutations are the ones which involve in the interactions to stabilize the monomer or hexamer structures (113-115). Roberto Bruzzone and his colleagues also proved that EL2 can influence the interactions between connexins expressed in adjacent cells using the expression of chimeric connexins in Xenopus Oocytes (65). No apparent obstacle was detected

along the pore, thus the author considered it as an open channel. But recently Zonta *et al*. argued that this channel is more unlikely to be a fully open channel (116).

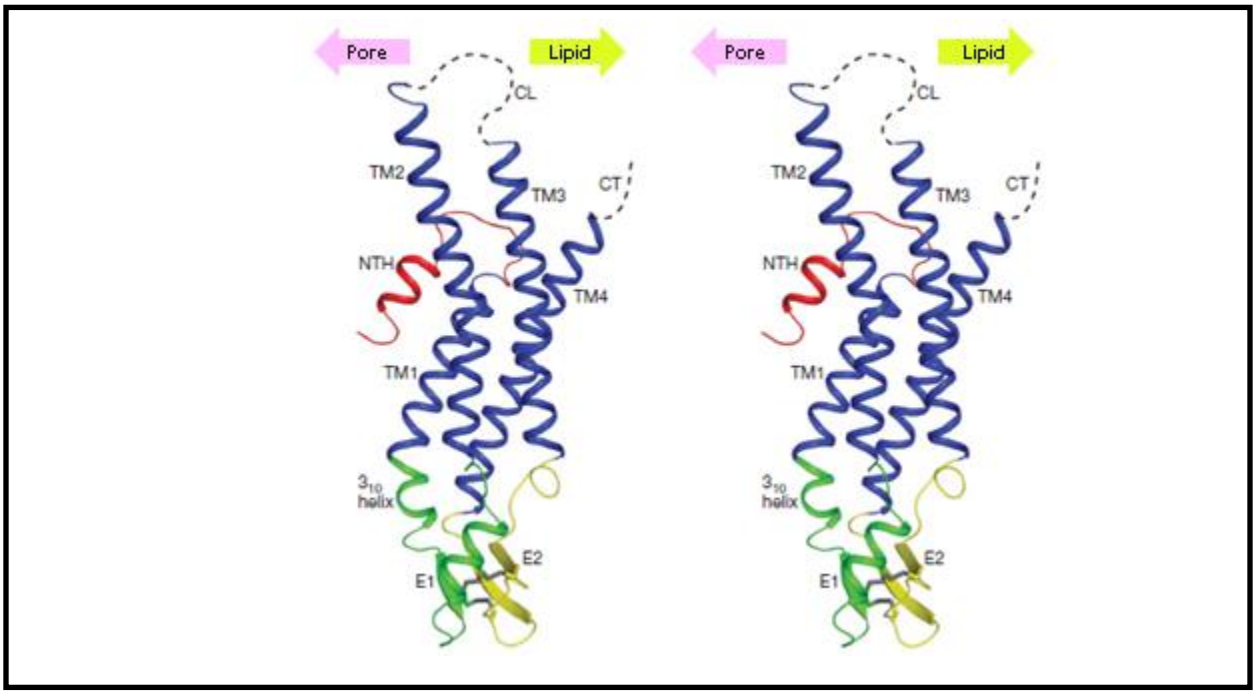

Figure 1.16 Wall-eye stereo view of Cx26 monomer in ribbon representation.

Each region is colored differently, and the upper arrows indicate the pore side and the lipid side. Three disulfide bonds in the extracellular region are shown in stick representation. Unobserved regions in the cytoplasmic loop and the C-terminal tail are represented by dashed lines (117).

Recently, another two X-ray structures of Cx26 grown in the presence or absence of Ca^{2+} were solved with a resolution of 3.3 Å and 3.8 Å, respectively (88). The overall structure of those two structure are very similar to the existing Cx26 structure (2ZW3) though the two structures were solved independently of 2ZW3 (**Fig. 1.17a**). The new structure is also a dodecameric channel with two hemichannels docked together. Cytoplasmic loop, N- and C-termini are still missing in the new determined structures due to their high flexibility. The channel dimensions of the new defined structures are all similar to 2ZW3 (**Figs. 1.17a, 1.17d and 1.17e**). The significant backbone divergence between the new structure and 2ZW3 occurs only at residues 42-46 and 56-59 regions (**Figs. 1.17b and 1.17c**).

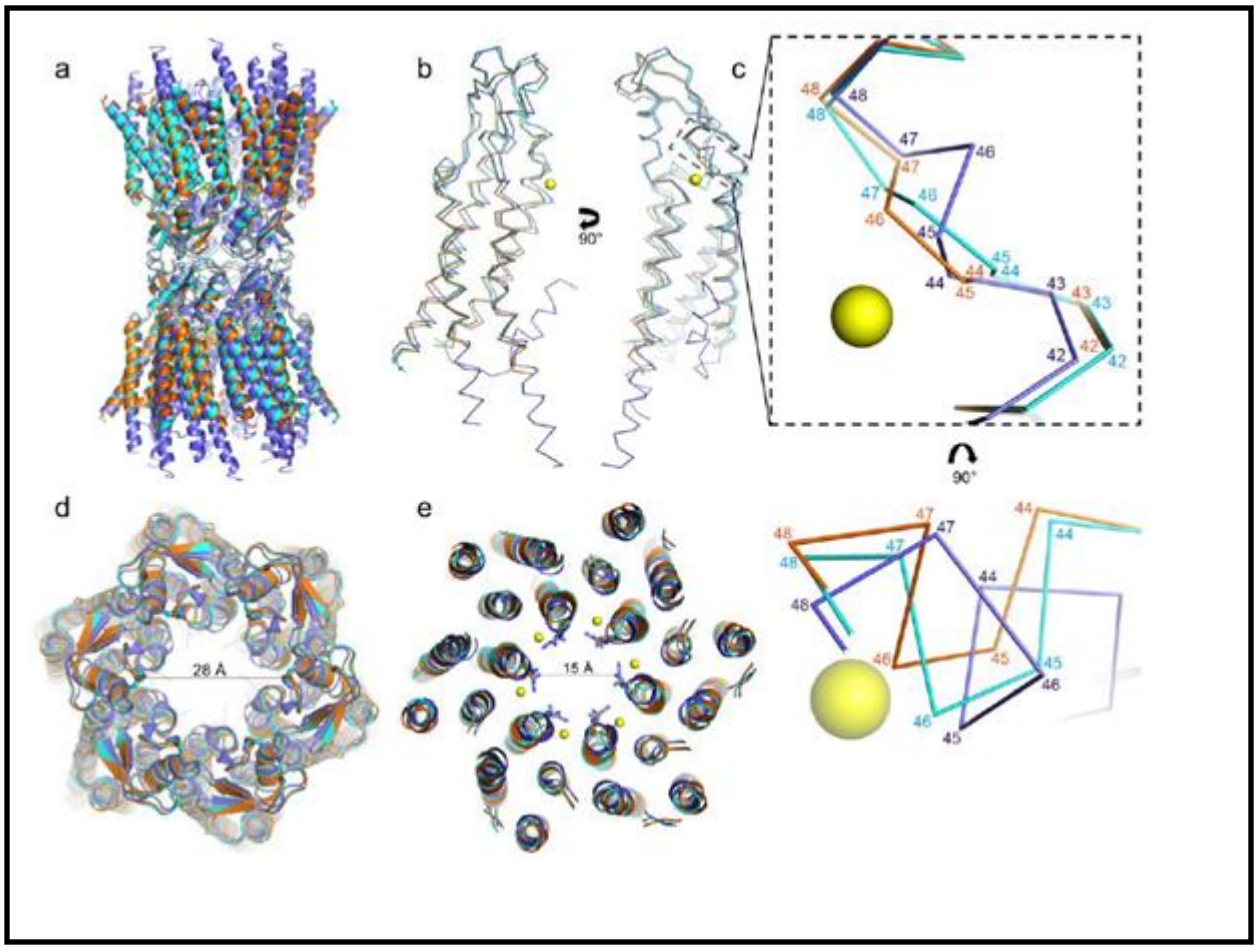

Figure 1.17 Structure comparison between new Cx26 crystal structures and the existing 2ZW3.

(a) Overlay of the Ca^{2+}-free (orange), Ca^{2+}-bound (cyan), and 2ZW3 (purple) structures. (b) Overlay of a single connexin in the above three Cx26 crystal structures. (c) A close up view of Ca^{2+}-binding region. This region is where one of the major backbond deviations happens between 2ZW3 and new structures. (d) Overlay of bottom view of three Cx26 structures. The pore has an inner diameter of 28 Å at the cytoplasmic entrance. (e) Overlay of top view of three Cx26 structures. The smallest diameter of the pore is 14 Å (88).

To date, the mysterious veil of gap junction structure was uncovered by researchers' earnest effort, though many details are still waiting for the exposure. Take the localization of NT as an example, the proposed topology (118,119) believes that NT resides in the cytoplasmic region while the resistance to both protease and antibodies suggests it inserts into the lumen of the channel (120). Besides, electrophysiological studies and NMR studies suggest the involvement of NT in the pore lining. The most variable regions of connexins are the cytoplasmic loop (CL) and the C-termini, both of which are not resolved in the available crystal structures due to their high flexibility. The CL region is suggested to be involved in CaM binding, which plays crucial role in gap junction regulation (121).

1.2.6 Gap junction regulation by CaM

Modulation of the cytoplasmic Ca^{2+} concentration ($[Ca^{2+}]_i$) is a ubiquitous mechanism by which cells transduce external signals into biological responses. The signaling cascade initiated by the rise in $[Ca^{2+}]_i$ is often mediated via Ca^{2+}-binding proteins such as calmodulin (CaM) (122,123).

CaM, a key multifunctional transducer of Ca^{2+} signals in eukaryotes, has four EF-hand Ca^{2+} binding motifs in two globular N- and C-domains that are separated by a flexible linker. Upon Ca^{2+} binding, CaM undergoes a large conformational change, exposing hydrophobic patches that are important in its binding to more than 300 target proteins in multiple cellular processes (124-126). CaM uses either its N- or C-domains with different Ca^{2+} binding affinities to differentiate between local and global $[Ca^{2+}]_i$ changes, and to regulate a diverse group of membrane channels/pumps that include cyclic nucleotide-gated (CNG) channels(127), N-methyl-D-aspartate receptor (NMDA receptor) (128), ryanodine receptors (RyR) (129), Ca^{2+}-activated K^+ channels of small or intermediate conductance (SK or IK) (130,131), Trp family channels (132), Ca^{2+} channels, and gap junction channels (133-137).

Over the years, a significant body of data supports the involvement of CaM in the regulation of gap junctions comprised of the three connexin subfamilies. Délèze (138) first showed that Ca^{2+} is essential for the healing process in mammalian heart muscle by preventing longitudinal diffusion of molecules in cardiac fibers. Subsequently, Rose et al. (139) showed that in salivary gland cells, inhibition of cell-to-cell coupling occurs when the intracellular concentration of Ca^{2+} was increased from 0.1 μM to 50 μM. Recognizing that most Ca^{2+}-induced phenomena are mediated by CaM (140), Peracchia and colleagues (141) first tested the hypothesis that gap junctions were regulated by CaM by examining the effect of the CaM inhibitor trifluoperazine (TFP) on the electrical coupling of amphibian embryonic cells exposed to CO_2 to lower intracellular pH. While the role of CaM in mediating the action of Ca^{2+} on enzyme activation was well known in the 1980s, gap junctions represented the first membrane channels shown to be modulated by CaM; only a decade later was the next CaM regulated channel identified (127). Peracchia and colleagues demonstrated that TFP reversibly inhibits the CO_2-induced electrical

uncoupling in amphibian embryo cells by interfering with the mechanism which closes the cell-to-cell channels. Subsequently, more specific CaM blockers (calmidazolium and W7) were shown to prevent uncoupling of Xenopus embryonic cells (142) and crayfish axons (143,144), indicating the generalized nature of this role for CaM in regulating gap junctions. This hypothesis was strengthened by evidence that the gap junction protein Cx32 bound CaM in gel overlays (145-147) suppression of CaM expression in oocytes can also inhibit CO_2 induced electrical uncoupling and injection of CaM into oocytes can recover it (148). Cx32 was also shown to colocalize with CaM using immunofluorescence microscopy (149). Later, Blodow *et al*. reported that CaM antagonists suppress gap junction coupling of Cx26 in isolated Hensen cells of the guinea pig cochlea (150). Louis and Lurtz first showed that the gap junction mediated cell-to-cell transfer of dye between lens epithelial cells was inhibited by Ca^{2+}-CaM (151). The rapid onset of this inhibition (within seconds) suggested that this inhibition was mediated by the direct interaction of CaM with one or more of the lens connexins rather than by the action of a CaM-dependent protein kinase. They subsequently demonstrated in Cx43-transfected HeLa cells that cell-to-cell dye transfer was inhibited by Ca^{2+}-CaM (152). Cell-to-cell communication was half-maximally inhibited at ~ 300 nM $[Ca^{2+}]_i$ (153), and this inhibition was prevented by pre-incubation of lens cultures with CaM antagonists (151). In HeLa cells transiently expressing the CaM-binding-deficient mutants (Cx43K146E, R148E-EYFP and Cx43M147Q, L151E, I156E-EYFP), elevated $[Ca^{2+}]_i$ was unable to inhibit cell-cell dye transfer, confirming that residues 136–158 in the intracellular loop of Cx43 contain the CaM-binding site that mediates the Ca^{2+}-dependent regulation of Cx43 gap junctions (154). Direct gap junction conductance (Gj) measurements confirmed that increases in $[Ca^{2+}]_i$ and decreases in Cx43 Gj were temporally correlated and inhibited by CaM antagonists like calmidazolium, CaMKII CaMi peptide, or the $Cx43p_{136–158}$ peptide (155). We have further shown

that inhibition of gap junction conductance by intracellular Ca^{2+} and CaM can be reversed by 90% with the addition of 10 mM EGTA and removal of external $CaCl_2$ from the bath saline solution, but only if Ca^{2+}-chelation commenced prior to complete uncoupling (155). On the other hand, Cx40-transfected N2a neuroblastoma cell pairs were not uncoupled by intracellular Ca^{2+}, such lack of intracellular Ca^{2+} regulation of Cx40 was consistent with the observation that Cx40 does not contain the putative CaM binding site in the same cytosolic loop region (155). The inhibition of Cx44-mediated cell-to-cell dye transfer by Ca^{2+} was also shown to be regulated by CaM as this inhibition was prevented by prior incubation of Cx44-transfected cells with a CaM antagonist (156). Cx50 was also shown to colocalize with CaM (157), and by measuring gap junctional conductance of Cx50-transfected N2a neuroblastoma cells, the reduction of Cx50-mediated junctional coupling was shown to be Ca^{2+}-dependent. Junctional coupling mediated by either Cx50 or Cx43 was prevented by pre-incubation of transfected cells with a CaM inhibitor, indicating that the $[Ca^{2+}]_i$ -dependent inhibition of Cx50 and Cx43 was CaM mediated. Furthermore, the Ca^{2+}-dependent inhibition of gap junction permeability in Cx50-transfected cells was prevented by intracellular injection of a synthetic peptide encompassing the CaM binding domain of Cx50, while the scrambled peptide was without effect (121). CaM regulation of the γ-connexin Cx45 was reported by Peracchia and coworkers by monitoring the sensitivity of Cx45 channels to CO_2, and inhibiting CaM expression in oocytes (158). Mouse Cx36, perch Cx35 and Cx34.7 that form electrical synapses have also been reported to bind CaM in a Ca^{2+}-dependent manner using surface plasmon resonance assays and GST fusion proteins harboring the carboxyl-domain of these connexins (159,160).

In Chapter 3, we are going to address several key questions, such as how CaM regulates different families of connexins. Through the same binding mode? What is the binding affinity? Where is the interaction site?

1.3 Family C of G-protein Coupled Receptors (cGPCR) and Its Regulation by $[Ca^{2+}]_o$

GPCR is the largest cell surface receptor family and can be classified into five families, A, B, C, D and E according to their sequence homology of the seven transmembrane domain. cGPCR represents a unique group which process an exceptionally large ECD and function as constitutive dimers on the cell membrane (161). cGPCR is composed of Ca^{2+}-sending receptors (CaSR), metabotropic glutamate receptor (mGluR), γ-aminobutyric $acid_B$ receptors ($GABA_B$), and a small group of olfactory , taste (sweet and amino acid taste receptors) and pheromone receptors (162).

1.3.1 mGluR and Structure features of mGluR

As mentioned above, cGPCR possess a large ECD which is also called as the Venus flytrap domain (VFT) (**Fig. 1.18**). Until 2000, Kunishima *et al.* solved the ECD crystal structure of mGluR1 in the presence or absence of its orthosteric ligand L-Glu and for the first time demonstrated the ECD structure of cGPCR (163). Since then multitudes of resolved crystal structure of mGluR ECD came out (164,165), together revealing that mGluRs containing two globular lobes separated by a cleft in which orthosteric ligand is bound. Both lobes are typical α/β folds where the central parallel β-strands are sandwiched by α-helices. Constitutive dimers formed through the interaction between VFT from two protomers. A pair of disulfide bond formed between two protomers were suggested to stabilize the dimer (166-168). Ligand binding to VFD

can induce tremendous conformational change, resulting in the formation of active or inactive receptors.

Except $GABA_B$ receptor, most cGPCR contain a Cysteine rich domain (CRD) inside of the ECD. The unique feature of CRD is reflected in 9 highly conserved cysteines. The crystal structure of mGluR3 solved in 2003 showed that the CRD with a length of 40 Å is an independent domain which connects the VFT and the transmembrane domain (165). The function of CRD is not clear yet. Earlier mutagenesis and chimera approaches revealed that RCD is involved in signal transduction from the VFT to the transmembrane domain when CaSR was activated by $[Ca^{2+}]_o$ (169). Replacing the third conserved Cys residue in the CRD abolished intracellular signaling induced by agonist (170).

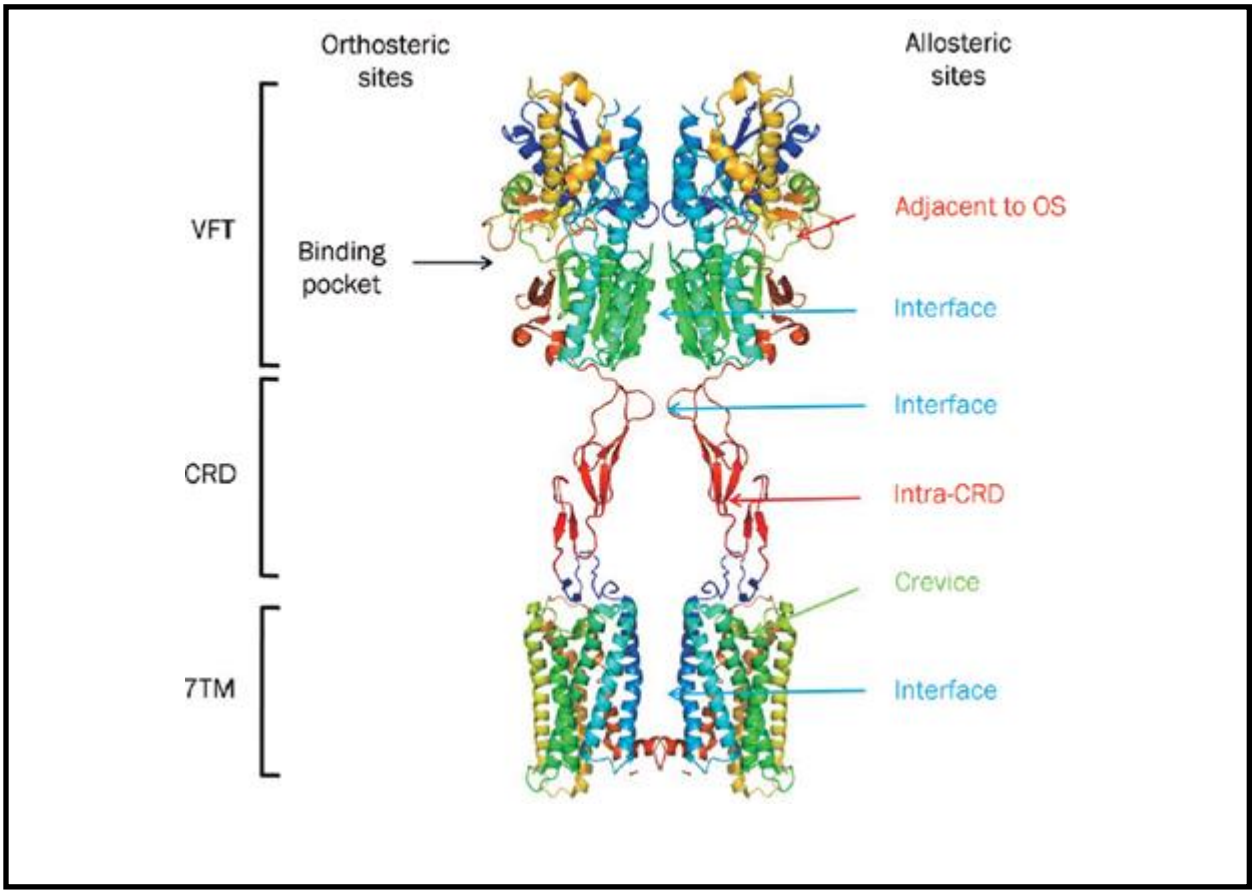

Figure 1.18 Structure organization of mGluRs. mGluRs function as dimer on the cell surface. **The dimerization is fulfilled by VFT interaction and stabilized by a pair of disulfide bond formed between two Cys residues in the VFT. mGluRs have a common structure composed by VFT with two lobes, CRD and TMD. The two lobes of VFT form a cleft where orthosteric ligand can bind.**

mGluRs have the similar heptahelical transmembrane helices termed as seven-transmembrane domain (TMD) to other family C GPCRs, even though the TMD of mGluR shares a very low sequence similarity to other cGPCRs. Those transmembrane helices are connected by several short intracellular and extracellular loops. Allosteric modulators were reported to regulate mGluR function through binding to the TMD (171,172). Despite the importance of TMD in drug discovery, the TMD structure of mGluR has remained unclear until 2014, in which the first crystal structure of the TMD of mGluR was determined (173). The allosteric modulator NAM mavoglurant (AFQ056) (174), which is in phase III clinical trials for fragile X syndrome treatment, was co-crystallized with TMD of mGluR5. The extracellular loop 2 (ECL2) is on the top of the receptor and interacting with both N end of transmembrane domain 1 (TM1) and C end of transmembrane domain 3 (TM3). The helical bundles of the transmembrane regions and the ECL2 restrict the narrow ligand entrance to be around 7 Å.

Compared with the ECD, the C-terminus is very small (around 300 amino acids) and this domain is of particular importance for G protein coupling (175-178). The H8 helix in the C-terminus show particular importance for efficient G protein coupling (179). Direct binding of H8 with βγ dimer of the heterotrimeric G-protein has also been observed by pulldown approach (180). However, deletion of H8 retained the G-protein coupling capability of mGluR7 and GABAB receptor (181,182), which suggest other area instead of the H8 of C-terminus is involved in G-

protein binding. The C-terminus is highly divergent and subjected to splice in many mGluRs and the function of alternative splicing remains elusive. The C-terminus also serves as the target for other intercellular protein partner binding, such as Homer protein (183,184) and the PDZ domain clustering protein PICK1 (185-188).

Since mGluRs are the target of L-Glu and mediate excitatory synaptic transmission in CNS, extensive efforts have devoted into identification of L-Glu-binding site. By chimeric receptor construction, Katsu *et al* found that replacing half of the mGluR1 ECD with the corresponding amino acids in mGluR2 ECD altered the agonist selectivity from mGluR1 to a pattern more like mGluR2 (189). This result suggested that the ECD is involved in ligand binding. The glutamate binding site was first predicted by Patrick *et al* in 1993 using a ECD structure model built based on the sequence homology observed between mGluR1 and bacterial periplasmic binding protein (PBP) (181). In this initial prediction, they reported that Ser165, Ser164, Ser186 and Thr188 may be involved in glutamate binding. Replacing putative binding residues Ser165 and Thr188 to A significantly reduced the L-Glu and L-Quis binding affinity (**Fig. 1.19**). Later on more direct evidence also pointed out that the ECD domain is responsible for ligand binding. The first evidence came from a soluble mGluR1 ECD expressed and purified from Sf9 (190). This protein was secreted and presented in the culture medium as dimer which retained the similar ligand binding affinity and selectivity to the full-length mGluR1. Another example is provided by Hampson's group (191). They also examined the ligand binding affinity of a soluble ECD domain of mGluR4. Compared with full-length mGluR4, the truncated receptor displayed higher binding affinity to agonist and lower binding affinity to antagonist. They concluded that the first amino acid fragment covering residues 1 to 548 played dominant role in determining ligand binding, and other amino acid following this area may also be involved in ligand binding. Mutagenesis studies in mGluR4

proposed that several conserved residues (Arg78, Ser159 and Thr182) are part of the fundamental recognition motif for agonist binding (192). Mutating those residues severely altered the agonist binding capability while without affecting the surface expression. The first crystal structure of ECD of mGluR1 shed a new light on structure basis of ligand binding (163). The complex form of ECD was crystalized in the presence of 1 mM L-Glu. L-Glu was found in the cleft formed between lobe 1 and lobe 2 of ECD. Several putative binding residues (R78, S164, S165, S186 and T188) proposed in the previous studies through mutagenesis directly formed hydrogen bond with glutamate or water-mediated hydrogen bonds to anchor L-Glu in the crevice. In the open complex form, L-Glu were exclusively coordinated by residues from the lobe 1 and residues from lobe 2 involved in and contributed additional stabilization force in the closed complex form. Glutamate binding was proposed to change the equilibrium of open and closed conformation and to stabilize the closed conformation to activate the receptor (**Fig. 1.20**)(162).

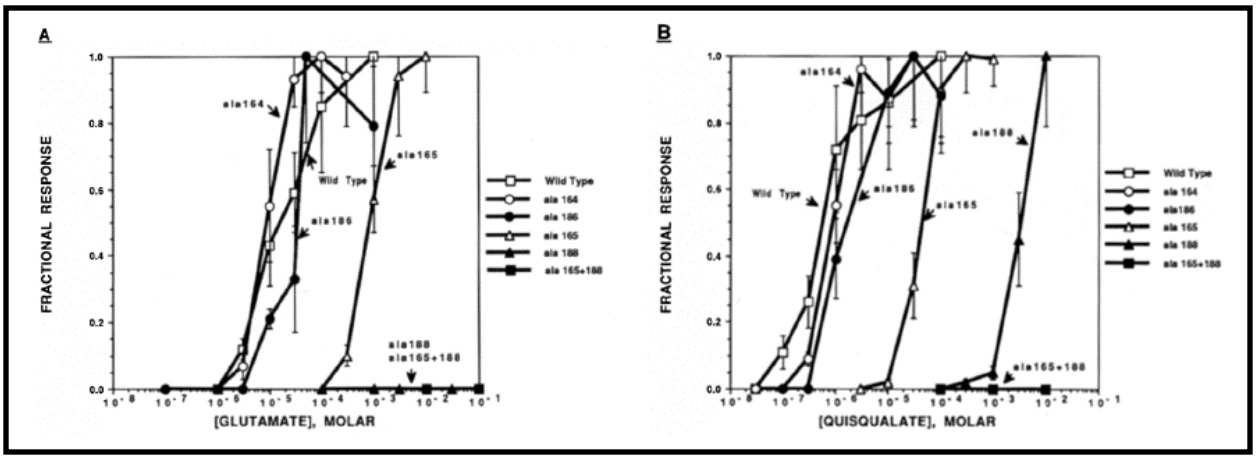

Figure 1.19 L-Glu- and L-Quis-binding affinity of mutants in predicted L-Glu-binding site.

Cells were transfected with wild type mGluR1 or L-Glu-binding site mutants. The IP_1 accumulation inside of cells were examined after 30-minute stimulation with either L-Glu or L-Quis.

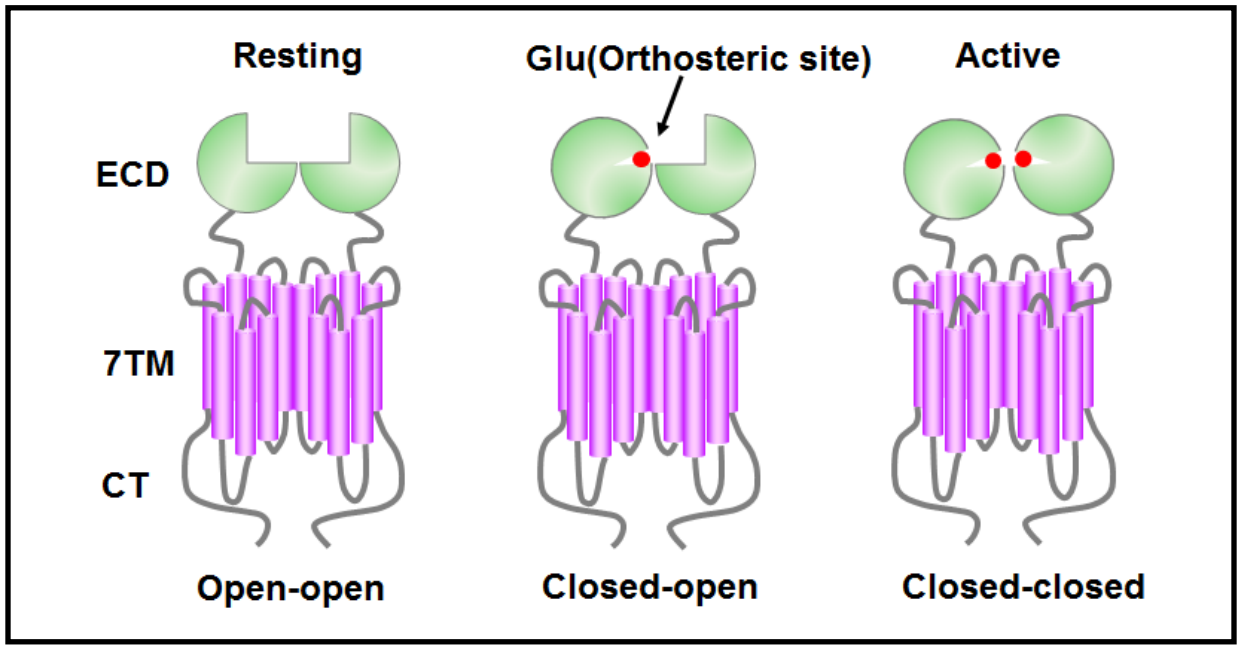

Figure 1.20 Schematic diagram of the mGluR dimer in different activity states.

mGluRs function as dimer on the cell surface. The cleft formed by two lobes of VFT is the orthosteric binding site. The inactive Open-open state without any L-Glu binding can be stabilized by ligand binding. When one of the orthosteric ligand binding sites are occupied by L-Glu, mGluRs change its Open-open state to a Closed-open conformation and further binding of L-Glu to another protomer can achieve a fully active Closed-closed state (193).

1.3.2 Cell signaling pathways through mGluRs

The conventional downstream signaling pathway mediated through mGluRs are G-protein-dependent. Group I mGluRs are coupled to G_q, which in turn activates the cell membrane-bound enzyme phospholipase C (PLC) to decompose PIP2 into IP3 and DAG, both of which are second messengers. IP3 further activates the IP3 receptor on the endoplasmic reticulum (ER) by direct binding, opening the intracellular Ca^{2+} store and releasing Ca^{2+} into the cytosol. The increase in

$[Ca^{2+}]_o$ can work with DAG together to activate protein kinase C, resulting in the phosphorylation of many proteins and altering many cellular activities. Elevated intracellular Ca^{2+} can also activate calmodulin (CaM), which in turn activates Ca^{2+}/CaM-dependent kinases (CAMKs). It is reported that active CaM can bind to the C-terminus of mGluR5 and increase the receptor cell surface expression (194). However, in other reported cases, group I mGluRs can mediate dual signal transduction pathways, PIP2 hydrolysis and cAMP accumulation, through different G-protein coupling in some systems (193,195-200). Group II and III mGluRs are negatively coupled to G_i, resulting in the inhibition of adenylate cyclase (AC) activity. Depression of AC further leads to a reduction of cyclic adenosine monophosphate(cAMP) production (201). cAMP is an allosteric activator of protein kinase A (PKA). Earlier studies revealed that activation of group II and III mGluRs inhibited the cAMP accumulation while activating AC when applying forskolin (202-207), an AC activator, to activate AC.

Although the G-protein-coupled signaling pathways mediated through mGluR are predominant, other alternative signaling pathways have been extensively reviewed (208-212)(**Table 1.2**). Over the past decades, several reports have appeared in the literature reporting metabotropic responses that, surprisingly, do not involve G-proteins (213). The first evidence that mGluRs also function in a G-protein-independent signaling manner came from experiments showing that inhibition of G-proteins by a general G-protein inhibitor did not affect the slow excitatory postsynaptic currents (EPSCs) mediated through mGluR1 in CA3 pyramidal cells (214). In hippocampal pyramidal neurons derived from $G\alpha_q$- and $G\alpha_{11}$-deficient mice, mGluR agonists were still able to evoke the inward, depolarizing current mediated by mGluRs (215). Inhibition of G protein by intracellular GDPβs with or without sodium channel blocker QX-314 had shown to prevent mGluR-mediated cationic current, while this can be rescued by elevation of $[Ca^{2+}]_i$,

suggesting an alternative G-protein-independent signaling pathway mediated by group I mGluRs was activated (216). A few studies have been documented showing activation of mGluRs lead to activation of Src tyrosine kinase and downstream messengers such as ERK (211,214,217). The components involved in G-protein-independent signaling pathway mediated through mGluRs are unclear yet. It is also not conclusive which neuronal responses preferentially utilize G-protein-independent pathways.

Table 1.2 Key features of mGluRs.

Group	Receptor	Synaptic localization	Coupled G protein	Signaling pathways
Group I	mGluR1	Predominantly postsynaptic	Predominantly $G\alpha_{q/s}$	PLC stimulation MAP kinase phosphorylation AC stimulation (some cases)
	mGluR5			
Group II	mGluR2	Presynaptic and postsynaptic	Predominantly $G\alpha_i$	AC inhibition Activation of K^+ channel Inhibition of Ca^{2+} channel
	mGluR3			
Group III	mGluR4	Predominantly presynaptic	Predominantly $G\alpha_i$	AC inhibition Activation of K^+ channel Inhibition of Ca^{2+} channel Stimulation of cGMP (some cases)
	mGluR6	Postsynaptic		
	mGluR7	Presynaptic		
	MGluR8	Predominantly presynaptic		

1.3.3 Distribution and function of mGluRs

cDNA of mGluR1 was successfully cloned from rat brain and expressed in Xenopus oocytes with the proper function in 1991 as the first metabotropic glutamate receptor that been directly proved to be existed (218,219), though the existence of mGluR was hypothesized in 1985 based on the phenomenon that L-Glu could induce the accumulation of IP3 in the CNS (220,221). Following the discovery of mGluR1, to date, 8 different mGluR subtypes have been identified (218,219,222-229). Although they all are widely spread in the neuron and glial cells, they exhibit

different expression patterns and different localization in the CNS. Those differences even exist between mGluRs from the same group and correlate to their various physiological roles in the CNS. As shown in figure 1.21, in general group I mGluRs (mGluR1 and mGluR5) are mainly localized in the postsynaptic area, and the other two groups of mGluRs are predominantly localized in presynaptic locations (193). However, there are many exceptions. For example, group I mGluRs also show presynaptically distribution and expression of mGluR2/3 in postsynaptic locations was also identified. In addition to neurons, mGluR5 and mGluR3 also express on glial cells to regulate synaptic activity. Table 1.2 summarizes the key features including the synaptic locations, coupled G proteins, and downstream signaling pathways of different mGluRs.

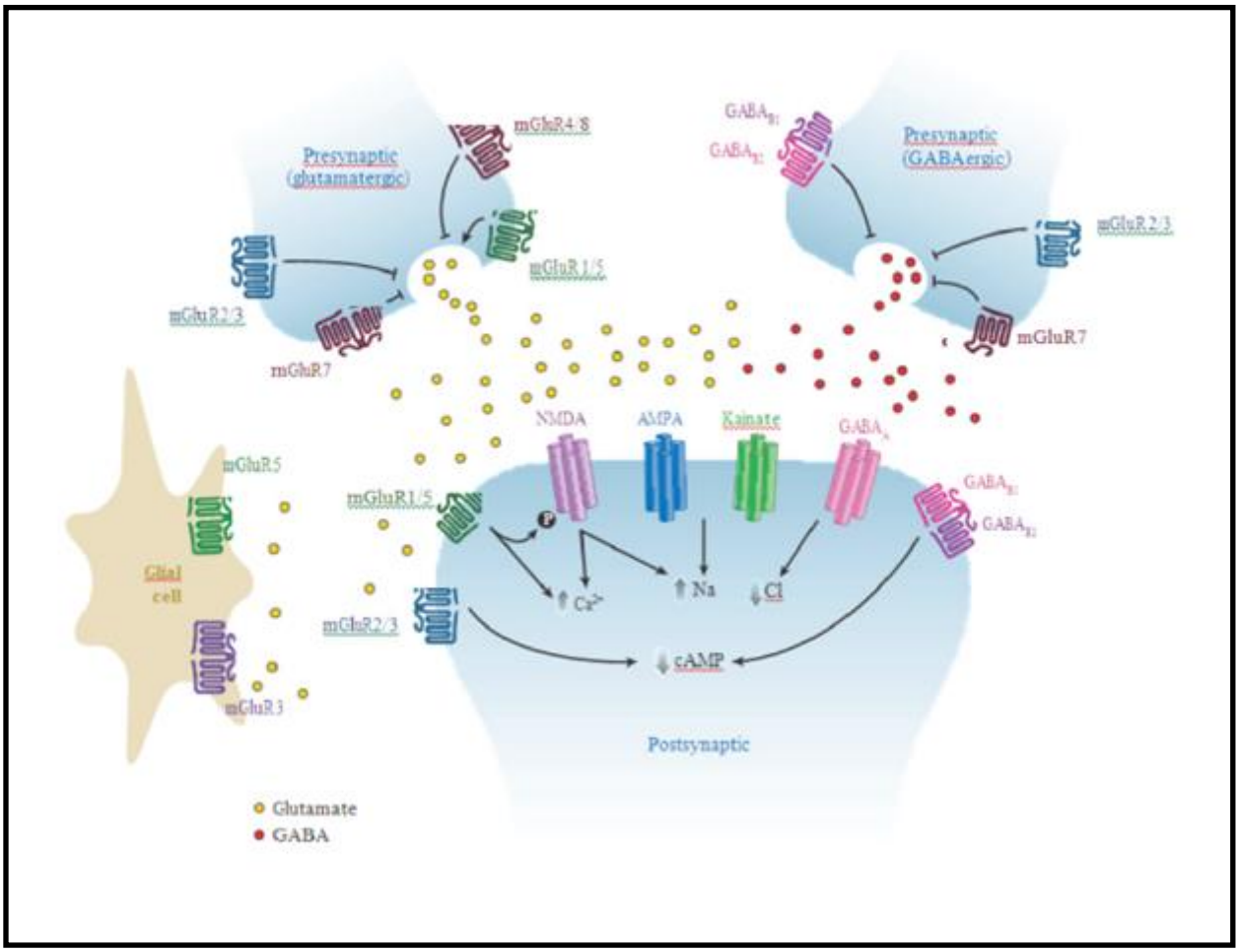

Figure 1.21 Localization of mGluRs in the CNS.

The expression of mGluRs in the CNS have some overlapping, but generally, group I mGluRs mainly distribute in the postsynaptic area, targeted by L-glutamate. Majority of group II and III mGluRs express in presynaptic locations, inhibiting the release of L-Glu (yellow dots) or GABA (red dots). However, group I mGluRs also have been found in the presynaptic locations, promoting the release of L-Glu. L-Glu or GABA released from the presynapses target to the mGluRs, NMDA, Kainate and AMPA on the postsynapses or on the glial cells (mGluR3 and mGluR5), initiating the downstream signaling pathways mediated through them (193).

The functional roles of mGluRs are diverse and complicated due to their widespread distribution, specific subcellular localization, and connection to broad downstream signaling pathways. Detailed discussion of the physiological roles of mGluRs are published in plentiful of reviews (210,230-234). The common roles of three subgroup of mGluRs can be summarized as: the short-term effects of activation of group I mGluRs are cell depolarization and neuronal excitability increase (235-237). Group I mGluRs also involve in long-term depression (LTD) and long-term potentiation (LTP) of transmission, and induction of long-term neuronal excitability (238-240). The general role of group II and III mGluRs is inhibiting the release of neuro transmitters. As mentioned above, in addition to the common role of each group, each subtype of mGluRs are highly specific, even mGluRs in the same group have different physiological functions in a single neuron. The individual role of each mGluR were extensively studied in knockout mice (241-266) and reviewed in multiple papers (193,201).

1.3.4 Allosteric and orthosteric modulation of mGluRs

The ligand binding sites in cGPCRs are divided into two categories: orthosteric and allosteric binding sites (**Fig. 1.22**). The former sites reside in the extracellular domain of cGPCR where the endogenous ligand binds. The later sites are distinct binding sites which exist in either 7TM, or the sites adjacent to the orthosteric site or the interface between VFT, CRD and 7TM.

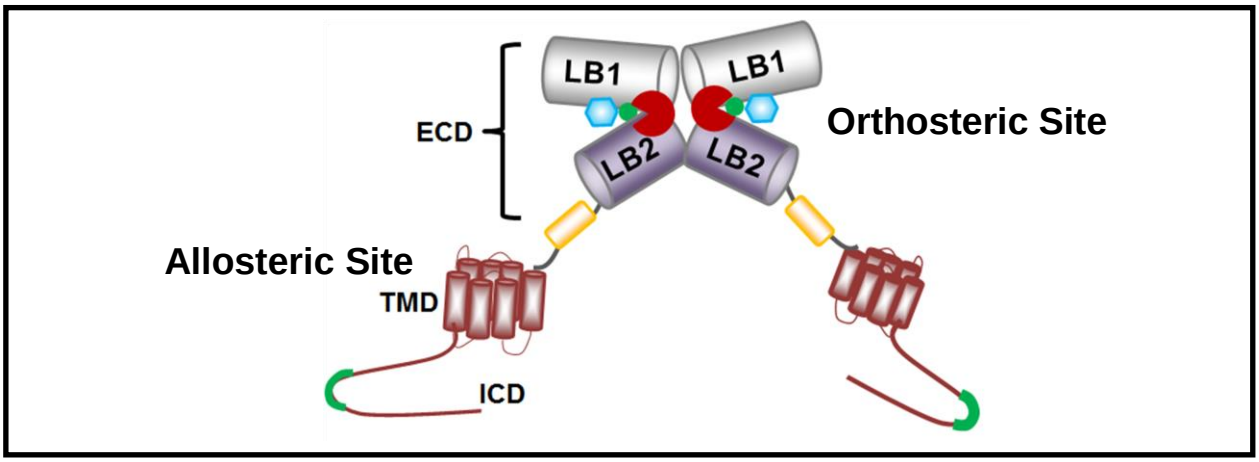

Figure 1.22 Orthosteric and allosteric site of mGluRs.

The endogenous ligand L-Glu binds to the hinge region made by two globular lobes 1 and 2. Orthosteric ligands compete the same site with L-Glu, while allosteric ligands bind to another distinct sites other than the orthosteric site.

The orthosteric agonist or antagonist binds to the same site as the endogenous ligand and can compete with them. The first selective agonist of mGluR receptor trans-ACPD was discover in 1989. Since then, numerous of orthosteric agonists and antagonists emerged due to the extensive effort made in the drug discovery field. Lots of orthosteric ligand resemble the glutamate structure, but showing different potency and efficacy. Significant conformational changes in VFT can be induced by orthosteric ligand binding (**Fig. 1.20**). A closed conformation or an open conformation

can be stabilized by binding of a full agonist or antagonist, respectively (163-165,267). Partial agonists binding lead to a partial or a complete, but unstable, closed structure of the VFT (267,268). Earlier identified orthosteric agonist or antagonists displayed activity across all mGluR subtypes, with few exception. For example, trans-ACPD showed similar potency on all mGluR subtypes except for mGluR7, on which no agonist activity was observed at concentrations up to 1 mM (269). However, more selective agonist or antagonist that act on specific subtypes of mGluRs have now been discovered, providing valuable insights into the function of those receptors *in vivo* or *in vitro*. To date, most of the mGluR-selective orthosteric ligands are amino acids derivatives, which fail to be actively transported across the cell membrane and blood-brain barrier, leading to poor bioavailability. The potency of group I mGluR agonist display the following rank order: quisqualic acid > ABH x D-I > 3,5-DHPG = S-Glu >DHPMP > 1S, 3R-ACPD > L-CCG-1 > 3-HPG > CHPG > t-ADA (210,270). Quisqualic acid has the strongest potency on group I mGluR though it is a non-selective agonist. 3,5-DHPG, 3-HPG and t-ADA are group I mGluR-specific agonists which is inactive on ionotropic receptors or on mGluR2 and mGluR4, but the efficacy and potency are much lower than quisqualic acid. To date, LY393675 is the most potent and selective orthosteric antagonist despite of the intense efforts have been made.

The highly conserved endogenous ligand sites (**Fig. 1.23**) of mGluRs contributes to the difficulty in discovery of highly mGluR subtype selective orthosteric ligand since orthosteric ligands also bind to the endogenous ligand binding site. The development of selective allosteric modulator brings new dawn to the treatment of CNS disorders caused by different type of mGluRs. Allosteric ligands target at a distinct site other than the endogenous ligand binding sites. The ones possessing the intrinsic efficacy without the orthosteric ligand are named as allosteric agonists or antagonists, while those which fail to show effects on mGluRs in the absence of orthosteric ligands

are allosteric modulators, either potentiating (positive modulator) or inhibiting (negative modulator) the effects of orthosteric ligands. Besides, most of them are small non-amino acid derivatives, which can enter through the blood-brain barrier and are orally bioavailable (271-273). The first allosteric modulator CPCCOEt of mGluR1 was reported in 1996. This compound does not have the Glu pharmacophore and acts like a non-competitive antagonist with moderate potency (274). Later on, it is found that this compound binds to an allosteric site in the 7TM (275,276). The emergence of this compound lead to the high-throughput screening of allosteric ligands. SIB-1893 and mpep were reported as the first non-competitive mGluR5 antagonists in 1999 (277,278). To date, more and more high potent and specific allosteric modulators of group I mGluRs have been reported as summarized in the following tables (**Tables. 1.3 and 1.4**).

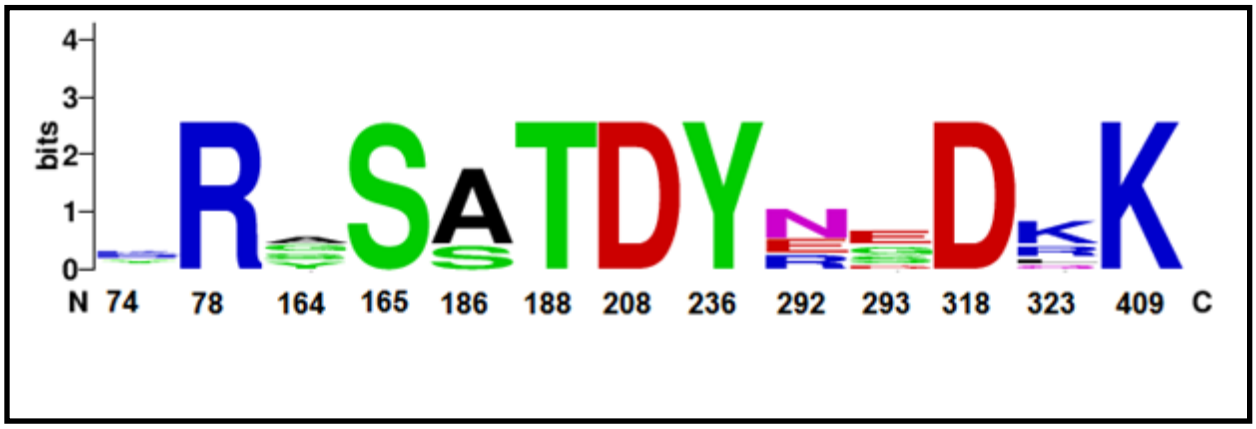

Figure 1.23 Conserved L-Glu binding sites in mGluRs.

Amino acids numbering at bottom row refers to mGluR1. Sequence alignment of amino acids in the hinge region of all mGluRs interacting with L-Glu based on the closed mGluR1 crystal structure with L-Glu binding. Half of the residues are highly conserved among 8 different mGluR subtypes.

Table 1.3 Orthosteric and allosteric ligands of mGluR1.

Agonists				
Ligand	Sp.	Action	Affinity	Units
[^{3}H]quisqualate	Rn	Full agonist	7.5 – 7.7	pKd
quisqualate	Rn	Full agonist	7.5 – 8.0	pKi
L-glutamic acid	Rn	Full agonist	6.4 – 6.5	pKi
ibotenate	Rn	Full agonist	5.9 – 6.4	pKi
(1S,3R)-ACPD	Rn	Full agonist	5.5 – 6.1	pKi
3,5-DHPG	Rn	Full agonist	5.8	pKi
L-CCG-I	Rn	Full agonist	5.6	pKi
(S)-3HPG	Rn	Partial agonist	4.9	pIC50
Antagonists				
Ligand	Sp.	Action	Affinity	Units
AIDA	Hs	Antagonist	4.2	pA2
LY341495	Hs	Antagonist	7.8	pKi
(S)-4C3HPG	Hs	Antagonist	5.8 – 6.0	pKi
LY367385	Rn	Antagonist	5.9	pKi
(S)-4CPG	Rn	Antagonist	5.4	pKi
DCG-IV	Rn	Antagonist	4.1	pKi
AIDA	Rn	Antagonist	4	pKi
(+)-MCPG	Rn	Antagonist	3.8	pKi
3-MATIDA	Rn	Antagonist	5.2	pIC50
LY367385	Hs	Antagonist	5.1	pIC50
(S)-(+)-CBPG	Rn	Antagonist	4.2	pIC50
(S)-TBPG	Rn	Antagonist	4.2	pIC50
Allosteric Regulators				
Ligand	Sp.	Action	Affinity	Units
[3H]R214127	Hs	Negative	9	pKd
[3H]EM-TBPC	Rn	Positive	8.2	pKd
NPS2390	Rn	Negative	8.9	pKi
R214127	Rn	Negative	8.9	pKi
9-dimethylamino-3-(4-ethylphenyl)-3H-5-thia-1,3,6-triazafluoren-4-one	Hs	Negative	8.3	pKi
Ro67-7476	Rn	Positive	7.5 – 7.9	pKi
Ro01-6128	Rn	Positive	7.5 – 7.7	pKi

CPCCOEt	Rn	Negative	5.3	pKi
Ro67-4853	Rn	Positive	5.1	pKi
R214127	Hs	Negative	8.9	pIC50
A841720	Hs	Negative	8	pIC50
3,5-dimethyl PPP	Rn	Negative	7.8	pIC50
DM-PPP	Rn	Negative	7.8	pIC50
YM298198	Rn	Negative	7.8	pIC50
BAY 367620	Rn	Negative	6.8 – 8.0	pIC50
EM-TBPC	Rn	Negative	6.9	pIC50
LY456236	Hs	Negative	6.9	pIC50
CPCCOEt	Hs	Negative	5.2	pIC50

Table 1.4 Orthosteric and allosteric ligands of mGluR5.

Agonists				
Ligand	Sp.	Action	Affinity	Units
quisqualate	Rn	Full agonist	7.5	pIC50
L-glutamic acid	Rn	Full agonist	6.1	pIC50
L-CCG-I	Rn	Full agonist	5.8	pIC50
(1S,3R)-ACPD	Rn	Full agonist	5.7	pIC50
ibotenate	Rn	Full agonist	5.7	pIC50
3,5-DHPG	Rn	Partial agonist	5.4	pIC50
(S)-3HPG	Rn	Partial agonist	5	pIC50
CHPG	Hs	Full agonist	3.4	pIC50
Antagonists				
Ligand	Sp.	Action	Affinity	Units
ACDPP	Hs	Antagonist	6.9	pIC50
(S)-4C3HPG	Rn	Antagonist	5.6	pIC50
LY341495	Hs	Antagonist	5.1	pIC50
DCG-IV	Rn	Antagonist	4.7	pIC50
(S)-4CPG	Rn	Antagonist	4.6	pIC50
(+)-MCPG	Rn	Antagonist	3.7	pIC50
Allosteric Regulators				
Ligand	Sp.	Action	Affinity	Units
[3H]fenobam	Hs	Negative	7.5	pKd

[3H]fenobam	Rn	Negative	7.3	pKd
BOMA	Hs	Negative	8.5	pKi
MTEP	Hs	Negative	7.8	pKi
5-MPEP	Rn	Neutral	6.4	pKi
VU-1545	Hs	Positive	8	pEC50
CDPPB	Hs	Positive	7.6 – 8.0	pEC50
CDPPB	Rn	Positive	7.7	pEC50
MTEB	Hs	Negative	8.7	pIC50
[3H]M-MPEP	Hs	Negative	8.4	pIC50
[3H]M-MPEP	Hs	Negative	8.3	pIC50
[14C]MTEP	Rn	Negative	7.7	pIC50
MPEP	Hs	Negative	7.4 – 7.7	pIC50
fenobam	Hs	Negative	7.2	pIC50
PTeB	Hs	Negative	7.2	pIC50
DFB	Hs	Positive	5.6 – 8.5	pIC50
ADX-47273	Rn	Positive	6.5	pIC50
CPPHA	Hs	Positive	6.3	pIC50
SIB-1757	Hs	Negative	6.0 – 6.4	pIC50
SIB-1893	Hs	Negative	5.9 – 6.5	pIC50

1.3.5 Extracellular calcium sensitivity of mGluRs

In 1993, Brown *et al*., successfully cloned Ca^{2+}-sensing receptor with an apparent Ca^{2+}-binding affinity of 3 mM from bovine parathyroid and proposed two putative Ca^{2+}-binding regions with plenty of acidic residues in this Ca^{2+}-sensing receptor (279). The Ca^{2+}-sensing receptor shared significant overall similarity with mGluRs, especially with mGluR1 (218,219) and mGluR5 (223). However, whether mGluR have the Ca^{2+} sensing capability was unknown at that time. Later on, in 1996, another family member of cGPCR was cloned from salmon brain and expressed in *Xenopus* oocytes (280). Both $[Ca^{2+}]_o$ and L-Glu in the bath solution could evoke the Ca^{2+}-Cl^- current in oocytes without addition of external agonists. Interestingly, this bifunctional metabotropic glutamate receptor shared very high similarity with mGluRs, especially to mGluR1α (around 69 % amino acids are identical), and a slightly lower similarity to CaSR (around 24 %

amino acids are identical). Other polyvalent cations like Gd^{3+} and Mg^{2+} could also induce the Ca^{2+}-Cl^- current which suggested that the activation of Ca^{2+}-Cl^- channels are not due to extracellular Ca^{2+} influx. The above phenomenon attracted researchers' attention and started to raise the question of whether mGluRs can function as Ca^{2+}-sensing receptor with extracellular Ca^{2+} sensing property.

By monitoring the activity of Ca^{2+}-Cl^- channels in oocytes expressed mGluR1 or mGluR5, Kubo et al., first reported that mGluR1/mGluR5 displayed similar response to CaSR with the application of extracellular Ca^{2+} (281). Gd^{3+} and Mg^{2+} were also examined and turned out that Gd^{3+} was more effective and Mg^{2+} was less effective than Ca^{2+} in activating mGluR1 and mGluR5. This is also consistent with that of CaSR. A lower activation effect was also detected in oocytes expressing mGluR3, but not mGluR2. By replacing the entire N-terminal domain of mGluR1 with that of mGluR2 or mGluR3, those chimeric receptors did not change their sensitivity to L-Glu, but activation of chimeric mGluR2 by extracellular Ca^{2+} was detected. Although, the EC50 of it was still much higher than chimeric mGluR3 and mGluR1. The result suggested that the Ca^{2+}-sensing capability relies on the N-terminal of mGluRs. In this paper, they proposed that Ser166 in mGluR1 was the key residue determine the Ca^{2+}-sensitivity of mGluR1. The corresponding residues in mGluR3 and mGluR5 are Ser, while in mGluR2 is Asp. Replacing Ser with Asp in chimeric mGluR3 and wild type mGluR1 significantly increased the EC50 to $[Ca^{2+}]_o$, while mutation D146S in chimeric mGluR2 significantly decreased the EC50 value to extracellular Ca^{2+}. Though several crystal structures of mGluRs are deposited in the protein data bank. None of them has Ca^{2+} bound in the ECD, though Gd^{3+} was identified located in the dimer interface (164). Later functional studies of Gd^{3+}-binding site revealed that residue Glu238 is functionally involved in activation of mGluR1 and modulation of agonist effect on mGluR1. Mutating this residue abolished the Gd^{3+}

sensing property while preserving the Ca^{2+}- and L-Glu-binding ability (282). On the contrary, consistent with the previous report, replacing S166 with D abolished Ca^{2+} activation of mGluR1 while maintaining the Gd^{3+}- and L-Glu stimulation.

In addition to direct activation of several cGPCRs by extracellular Ca^{2+}, a number of studies have shown that extracellular Ca^{2+} has modulatory effect on the signaling mediated through some cGPCRs. Back in 1998, the [^{3}H]-InsP1 accumulation evoked by mGluR1 agonist was significantly facilitated by increasing $[Ca^{2+}]_o$ in baby hamster kidney cells (283). This modulation was also observed in another receptor $GABA_B$ in 2000 (284). The affinity of GABA and 3-aminopropylphosphinic acid binding to $GABA_B$ receptors were dramatically dropped about 10-fold when Ca^{2+} was removed. However, extracellular Ca^{2+} had little effect on another agonist baclofen and antagonists CGP64213 and CGP56999A. Mutagenesis studies in this paper also showed that replacing Ser269 to Ala abolished the Ca^{2+} effect on the $GABA_B$ receptor.

Both the directive activation and modulatory effect have been observed in cells with native mGluR expression (285,286). In Purkinje cells, mGluR1 is predominant amongst the mGluR subtypes (218). $[Ca^{2+}]_i$ rise in Purkinje cells were detected in responses to extracellular Ca^{2+} exposure (285,286). No such significant $[Ca^{2+}]_i$ occurred in Purkinje cells coming from mGluR1 knockout mice and such response to extracellular Ca^{2+} was recovered in Purkinje cells isolated from mGluR1 rescue mice. Application of mGluR antagonist (R,S)-α-methyl-4-carboxyphenyl-glycine (MCPG) dramatically decreased this $[Ca^{2+}]_i$ rise. Blocking the receptor-operated or P-type Ca^{2+} channels by antagonist SKF-96365 and ω-agatoxin IVA did not significantly affect the $[Ca^{2+}]_i$ responses to extracellular calcium, which suggests that the increase of $[Ca^{2+}]_i$ is not a result of Ca^{2+} influx through Ca^{2+} channels. In addition to this direct activation, extracellular Ca^{2+} also augmented the cellular responses evoked by L-Glu or its analog.

On the contrary, there are opposite results reporting that extracellular Ca^{2+} did not evoke the receptor activation. The basal phospholipase C activity was not altered by increase of $[Ca^{2+}]_o$ from 1.3 to 4 mM in baby hamster kidney cells stably expressing mGluR1 (283). However, no result was shown in the paper to support this claim. In another paper published in 1998, Shigeki *et al*., analyzed the $[Ca^{2+}]_i$ increase attributed by mGluR1 activation and found that the initial $[Ca^{2+}]_i$ rise was resulted by Ca^{2+} mobilization from the intracellular Ca^{2+} stores induced by receptor activation, while the sustained phase of $[Ca^{2+}]_i$ increase was related to the extracellular Ca^{2+} flux through receptor-operated Ca^{2+} channels. The experiment they designed to prove the above statement was applying Ca^{2+} channel blockers. A receptor-operated Ca^{2+} channel blocker SK & F96365 abolished the oscillatory Ca^{2+} response in the sustained phase of L-Glu activation. This result is opposite to the same experiment performed in Purkinje cells by Tabata *et al*. in 2002. Nash *et al*., concluded that mGluR1 did not function as a Ca^{2+}-sensing receptor based on their observation that Ca^{2+} solely did not stimulate any $[Ca^{2+}]_i$ increase and IP3 accumulation in CHO-lac-mGluR1 cells (287). They believed that extracellular Ca^{2+} could prolong the activation of mGluR1 instead of affect the initiation of mGluR1 activation. With or without extracellular Ca^{2+}, agonist L-Quis induced the similar initial response peak of IP_3 accumulation, accompanied with $[Ca^{2+}]_i$ due to Ca^{2+} release from cytosolic Ca^{2+} store. But in this paper, only the IP1 accumulation as a response to extracellular Ca^{2+} was shown. The $[Ca^{2+}]_i$ response to extracellular Ca^{2+} was not presented, as well as any application of Ca^{2+} channel blockers. The author also argued mGluR1 could not function as Ca^{2+} sensing receptor since the synaptic Ca^{2+} would always occupied the possible Ca^{2+} binding site if there is any. However, the Ca^{2+}-binding site could be a weak binding site with low Ca^{2+}-binding affinity. Besides, the synaptic Ca^{2+} concentration is actually fluctuating after periods of neuronal activity (288-297).

In addition to the above studies, extracellular Ca^{2+} was also suggested to play a role in mediating postsynaptic efficacy through its actions on mGluRs (13).

1.3.6 (Patho)physiological process related with group I mGluRs and therapeutic potential of group I mGluRs

The widespread expression of mGluRs and close correlation to variety of signaling pathways in the CNS contribute to its involvement in multitudes of physiological (learning, memory, anxiety, fear and mood) and pathological processes. Due to the rapid development of pharmacological agonists and antagonists, more roles of mGluRs in physiological processes and neurological disorders have been elucidated. In the following paragraphs, I will focus on summarizing the main roles of group I mGluRs in physiological processes.

The high expression of mGluR1 in the hippocampus indicates that mGluR1 may play important role in memory and learning. This hypothesis was proved by studies in mGluR1 knockout mice. Deletion of mGluR1 resulted in disability in learning an associative task and induction of LTP in mGluR1 knockout mice (241,298,299). mGluR5 knockout mice also had a poor performance in a memory-based water maze experiment. In addition, pharmacological evidence also proved the indispensable role of group I mGluRs in learning and memory. Application of MCPG (an antagonist of mGluR1 and mGluR5) to rat's amygadala led to the inhibition of LTP (300-302), which is a learning mechanism (303). Injection of MCPG into the rat lateral ventricles, rats failed in a spatial learning version of the water maze task which indicates group I mGluRs are essential for spatial learning (304,305). On the other hand, the group I mGluR agonist trans-azetidine-2, 4-dicarboxylic acid (tADA) could prolong the maintenance of LTP (306). The important role of group I mGluRs in cognition provides great opportunity for drug

development in cognitive disorder treatment. Positive modulators which target at group I mGluRs are potential drugs for improving cognition.

More and more people are facing anxiety now because of the stressful fast-paced society. Many experiments also suggest that group I mGluR, particularly mGluR5, has an important role in anxiety. A dose-dependent anxiolytic-like activities were observed in mice with direct hippocampus injection of group I mGluR antagonists in the conflict drinking vogel test (307,308). An mGluR5 specific antagonist 2-methyl-6-(phenylethynyl) pyridine (MPEP) was reported to be more effective in anxiety relief than (4-methoxy-phenyl)-(6-methoxy-quinazolin-4-yl)-amine HCl (LY456236), a mGluR1 antagonist (309). This piece of data indicates that mGluR5 may be more important than mGluR1 in anxiety though both of them are involved in anxiety. In 1982, Pecknold et al reported that non-benzodiazepine fenobam could treat anxiety in a double-blind standard (diazepam) placebo-controlled study (310). This compound later on was proven to be a potent, selective, and noncompetitive mGluR5 receptor antagonist in 2005 (311). While inhibiting group I mGluRs relieved anxiety, agonist of group I mGluRs were proven to induce anxiety. Direct injection of a group I specific agonist trans-azetidine-2,4-dicarboxylic acid (trans-ADA) into the dorsolateral periaqueductal gray led to anxiety-like responses like jumping (312). In summary, data accumulated to date suggest that group I mGluRs could be candidates of drug targets for anxiety treatment, though further studies need to be done to unravel the exact role of group I mGluRs play in anxiety.

A wealth of experimental evidence collected to date from animal model or pharmacological tests demonstrate group I mGluRs' role in diseases, such as stroke, fragile X syndrome, Alzheimer's disease, Parkinson's disease, Huntington's disease, epilepsy, and drug addiction (212). In those diseases, the expression of mGluRs might be abnormal, or the mGluR-mediated

signaling might be altered, or the regulation of mGluRs might be changed. Considering the complexity of mGluR signaling pathways, the molecular basis of mGluRs role in those diseases need to be further elucidated.

1.4 Ca^{2+}-sensing Receptor

Calcium-sensing receptor (CaSR), belonging to the family C of G-protein-coupled receptors, plays vital role in the maintenance of constant blood Ca^{2+} levels and Ca^{2+} homeostasis. This physiological function is a result of its capability of sensing small changes in $[Ca^{2+}]_o$. Ca^{2+} is the primary orthosteric agonist of CaSR. However, there are numerous agonists and modulators which can activate and modulate the activity of CaSR, in addition to Ca^{2+}. CaSR is also regulated by extracellular pH, ionic strength, and hormones. CaSR-activating or CaSR-inactivating mutations are tightly associated with many genetic human diseases, such as familial hypocalciuric hypercalcemia, neonatal severe hyperparathyroidism (FHH), and autosomal dominant hypoparathyroidism (ADH). Loss of CaSR or impaired CaSR expression or abnormal CaSR function also contributes to some acquired diseases, like chronic kidney disease, cancer, Alzheimer's disease, and so on.

1.4.1 Structure and function of Calcium-sensing receptor

Until 1993 CaSR was firstly identified and cloned from a bovine parathyroid gland cDNA library by Brown *et al (279),* though there were compelling evidence pointing out the existence of a cell surface receptor with $[Ca^{2+}]_o$ sensitivity and parathyroid hormones regulation ability before that (313-320). The isolated CaSR gene is around 5276 bp, encoding 1085 amino acids. As a cGPCR, the structure CaSR is characterized by a large extracellular domain which covers more than 600 amino acid. Due to the lack of crystal structure of CaSR, several groups including our lab generated model structure based on the X-ray structure of mGluRs (321,322). Based on the

mGluR1 structure, the ECD of CaSR is a bilobed Venus-fly-trap structure consisting an N-terminal lobe I and C-terminal lobe II connected by three strands (167). There are three pairs of intramolecular disulfide bonds formed between 6 Cys residues: Cys60 and Cys101; Cys358 and Cys395; Cys437 and Cys449. Another pair of Cys residues (Cys129 and Cys131) are proposed to form intermolecular disulfide bond (167). This is consistent with the finding that the corresponding Cys residues in mGluR1 is crucial for mGluR1 dimerization. Majority of naturally occurring mutations associated with disordered calcium homeostatic are identified in the ECD, highlighting the importance of ECD in CaSR function. Crystal structure of mGluR1 with different orthosteric ligand identified the orthosteric ligand binding site in the hinge region linking lobe I and lobe II. Ligand binding to this cleft results in a closed conformation which stabilizes mGluRs. It is proposed that the ECD of CaSR also contains endogenous ligand binding site. However, the identification of those sites are greatly hampered by the lack of crystal structure for the receptor.

An 84-amino acids long region serves as an adaptor region connecting the VFT and transmembrane domains. This region is called Cys-rich domain because there are 9 conserved Cys residues in such a short region. The importance of Cys-rich domain to the function of the CaSR is highlighted by the fact that deletion of Cys-rich domain completely abolished CaSR activation (169). Mutagenesis studies also revealed that the expression and function of CaSR could be severely disrupted by replacement of Cys residues with Ser (323).

There are seven hydrophobic regions named as TM1-TM7 in the transmembrane domain linked by intracellular and extracellular loops. This is one of the signatures shared by all cGPCRs. Results from mutagenesis studies demonstrated that transmembrane domain is critical in the signal transduction from ECD to G-proteins, in dimerization through noncovalent interactions, and in receptor activation by allosteric ligand. Substitution of A843 with E led to a constitutively active

receptor (324). One naturally occurring mutation P747fs, which lacks of the fifth, sixth, and seventh transmembrane domains, the second extracellular loop, and the C terminus, lost its dimerization capability; while another mutant A877stop with TM5 preserved that (325). CaSR allosteric ligands calcilytic NPS 2143 and the calcimimetic NPS R-568 binding sites are reported to be located in the transmembrane domain (326-328). Mutations in the transmembrane helices could reduce the effects of them.

Immediately following the transmembrane domain is the more divergent C terminus, which is around 216 amino acids with very few identified naturally occurring mutations. The function of C terminus had been extensively investigated by several groups through mutagenesis studies. It is concluded that certain mutations including truncation of C terminus could decrease cell surface expression level (329,330), impair CaSR's ability to respond to $[Ca^{2+}]_o$ (331), or alter the cooperativity for $[Ca^{2+}]_o$ (332).

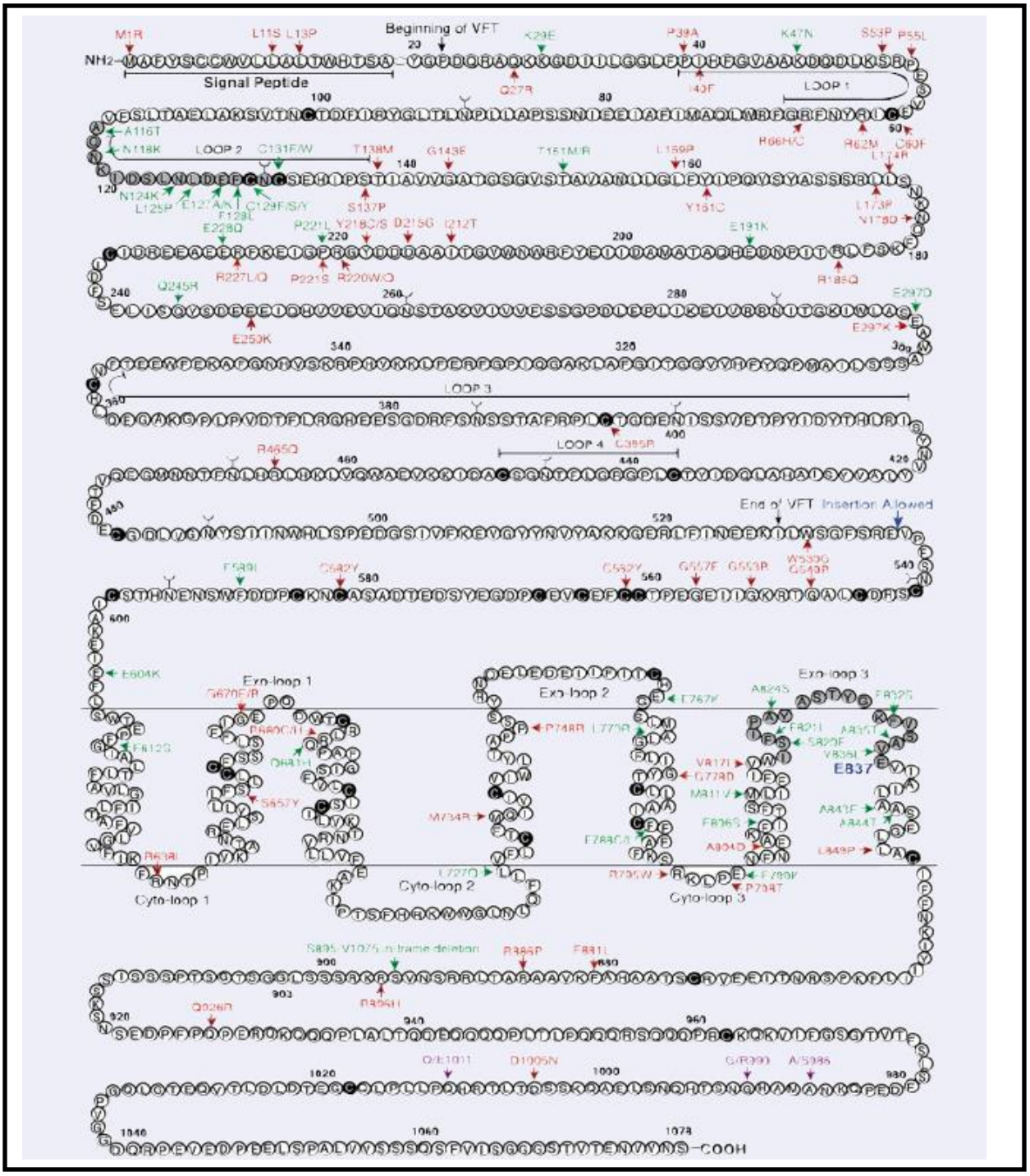

Figure 1.24 The amino acid sequence of human CaSR.

1.4.2 Calcium-sensing receptor stimuli

As a "sensor", CaSR has the ability to respond to diverse stimuli in the extracellular environment. Those stimuli can be divided into two types. Type I refers to those which can directly evoke CaSR activation and type II are called allosteric modulators which can sensitize CaSR to its agonists.

CaSR was found to respond to polyvalent cations, leading to $[Ca^{2+}]_i$ mobilization when firstly cloned and expressed in oocytes (279). In addition to Ca^{2+}, CaSR also respond to a variety of other cations. Their order of potency ranks as $La^{3+} > Gd^{3+} > Be^{2+} > Ca^{2+} = Ba^{2+} > Sr^{2+} > Mg^{2+}$ (333,334). It seems cations with more positive charges showing higher potency. As the primary orthosteric agonist of CaSR, the identification of Ca^{2+}-binding site is greatly hindered by the lack of crystal structures and is available to measure Ca^{2+} binding to CaSR. Using the computational methods, our group generated a modeled structure of CaSR based on the crystal structure of mGluR1. One of the predicted Ca^{2+}-binding site is located in the hinge region of CaSR, coordinated by residues S147, S170, D190, Y218 and E297 (321). This site is also proposed by another group earlier(322). Substitution of Y218 with S or E297 with K dramatically reduced CaSR's response and sensitivity to $[Ca^{2+}]_o$ (321,322). Other mutants including S147A, S170A, and D190A showed a significant drop in maximal response to $[Ca^{2+}]_o$ and increased Ca^{2+} EC_{50} values(322). Our group also identified other four possible Ca^{2+}-binding sites in the ECD of CaSR (321,335). Multiple Ca^{2+}-binding site in ECD may help to explain the high Hill number observed in CaSR activation by $[Ca^{2+}]_o$. Several residues inside of those Ca^{2+}-binding sites are described as either inactivating or activating mutations. For example, both Y218S and E297K are inactivating mutations associated with FHH (336) (337); while E297D plays causative role in ADH (322).

Mg^{2+} and Ca^{2+} are the two physiological cations showing CaSR activation capability, while Ca^{2+} has almost 1-fold higher potency and binding affinity than Mg^{2+} (338). Similar to Ca^{2+}, serum Mg^{2+} concentration was reported to be inversely correlated with PTH levels (339). The function of CaSR as a magnesium sensor is also supported by discoveries in patients with FHH or NSHPT. The elevated serum Mg^{2+} level indicates CaSR's ability to sense extracellular Mg^{2+} ($[Mg^{2+}]_o$) (340). It is also noted that Ca^{2+} and Mg^{2+} may function cooperatively to enhance each other's effect on CaSR (341).

Polyamines are another big group of agonists of CaSR which showed CaSR activation capability. In the presence of 0.5 mM $[Ca^{2+}]_o$, both free $[Ca^{2+}]_o$ concentration and IP_1 production were significantly elevated when polyamines applied (342). A rise of background $[Ca^{2+}]_o$ could shift the response curve of polyamines and lower the EC_{50} values of polyamines. This suggests that polyamine may act as endogenous agonists in physiological conditions through their physiological concentration is much lower than their EC_{50}. The potency of three polyamines were examined and they followed this order: spermine > spermidine >> putrescine (342). This order again proves that agonists with more positive charges are stronger activators of CaSR.

Polypeptides including polyarginine and polylysine were also identified as potential CaSR activators because they could inhibit the PTH release from bovine parathyroid cells (343). Later on, polypeptides were proved to act through CaSR (344). Like the polypeptides, polyvalent aminoglycoside antibiotics also activated CaSR and caused increase in $[Ca^{2+}]_i$ in CaSR transfected HEK293 cells in a dose-dependent manner (345). The EC_{50} values of neomycin, gentamicin, and tobramycin are in the micromolar range, with the rank order gentamicin > tobramycin > neomycin.

Type II stimuli includes both positive and negative allosteric modulators which are demonstrated to modulate the action of other orthosteric agonists on CaSR. GPCR are drug target

for approximately 40% of all drugs on the market. One of the advantages of allosteric modulators over orthosteric ligands is greater selectivity because they do not bind to the conserved orthosteric ligand binding sites (346). Amino acids and pharmacological compounds are two groups of allosteric modulators. L-amino acids particularly aromatic amino acids were reported to enhance the sensitivity of CaSR to its agonists $[Ca^{2+}]_o$ and spermine (347), and enhance $[Ca^{2+}]_o$-stimulated ERK1/2 phosphorylation (348) though in a fine-tuning way. The precise location of L-amino acids binding site is also hindered by the lack of crystal structure. Two mutants (T145A and S170T) in the VFT of CaSR displayed impaired L-amino acid sensing capability while preserved its $[Ca^{2+}]_o$ sensitivity. Later on, our lab identified an L-Phe binding site within the hinge region of ECD, adjacent to our predicted Ca^{2+}-binding site (349). L-Phe occupied binding pocket was shown to enhance the cooperative responses of CaSR to $[Ca^{2+}]_o$.

Two groups of famous synthetic allosteric modulators of CaSR are calcimimetics and calcilytics. Calcimimetics are positive allosteric modulator, shifting the concentration responses curve of $[Ca^{2+}]_o$ to the left, while calcilytics right-shift the concentration response curve of $[Ca^{2+}]_o$, thus known as negative allosteric modulator. Phenylalkylamines, NPS R-467 and NPS R-568 are the first synthetic calcimimetics with potent and stereoselective modulation on CaSR (350). The first synthetic calcilytics is NPS 2143, which function as CaSR antagonist, blocking the elevation of $[Ca^{2+}]_i$ induced by activation of CaSR and stimulating the release of PTH (351). The surface expression level of CaSR could also be changed by those pharmacological agents (352,353).

In addition to the above CaSR ligands, extracellular pH and ionic strength could also alter the sensitivity of CaSR to its agonists (354,355).

1.4.3 Calcium-sensing receptor regulated intracellular signaling pathways

The ECD of CaSR plays major function in sensing extracellular environment changes, whereas the intracellular portion of CaSR mainly functions as a transmitter to modulate and control complex downstream signaling pathways, including PLC signaling, MAPK signaling, inhibition of cAMP, Akt signaling, and Rho signaling. Among them, both the PLC and MAPK signaling pathways were widely applied in CaSR activity studies.

Activation of CaSR leads to activation of PLC, production of IP_3 and DG, Ca^{2+} release from ER, and further activation of PKC. This signaling pathway is mediated by the trimeric G protein, $G\alpha_{q/11}$. Mice without $G\alpha_q$ and $G\alpha_{11}$ showed abnormal high PTH level (356). $[Ca^{2+}]_i$ oscillation induced by CaSR activation have been seen in cells expressing CaSR, such as parathyroid cells and HEK293 transfected with CaSR (357-360). The $[Ca^{2+}]_i$ oscillation with different amplitude and frequency are physiological meaningful in a variety of cell types. Take the human colonic epithelial cells as an example. Two types of CaSR-mediated oscillation have been observed in human colonic epithelial cells. The one with high frequency (around 3 to 4 peak/min) turned to induce inhibition of proliferation, while the one with lower frequency (around 1.5 peak/min) do not have that function (361). Using CaSR-transfected HEK293 cells, McCormick *et al.* found that the dynamic phosphorylation and dephosphorylation of residue T888 by PKC within the C terminus caused sinusoidal oscillations when CaSR is activated by stimuli (362-366). Activated PKC through CaSR-mediated PCL pathway causes phosphorylation of T888, uncoupling the receptor from $G\alpha_{q/11}$. Following this phosphorylation is the dephosphorylation of T888 by protein phosphatases to recover coupling of CaSR to $G\alpha_{q/11}$ and $[Ca^{2+}]_i$ mobilization.

1.4.4 The biological roles of Calcium-sensing receptor

CaSR plays vital role in maintaining systemic Ca^{2+} homeostasis which is balancing the calcium absorption and ingestion. PTH-secreting parathyroid glands, intestines, bone, and kidney are the key homeostatic tissues with CaSR-expressing. Ca^{2+} movement is mainly controlled by PTH secreted by parathyroid gland where CaSR was cloned from. The function of parathyroid gland is affected by CaSR in different ways as reported by different groups. The PTH mRNA level was reduced by increased Ca^{2+} concentration and application of calcimimetic R-568 in the culture medium in bovine parathyroid cells, which indicates that CaSR-mediated signaling could destabilize PTH mRNA and control the PTH synthesis (367). In patient with secondary hyperparathyroidism, the PTH gene expression was elevated and this elevation could be inhibited by positive CaSR allosteric modulator calcimimetic (368). The role of CaSR in regulating parathyroid cell proliferation was suggested by observation that calcimimetic treatment could attenuate the progression of parathyroid hyperplasia and suppress PTH secretion(369). Intestine and kidney are tissues determining how much Ca^{2+} moves into or out of our body, while bone controls how Ca^{2+} moves between the extracellular fluids and bone. Together with CaSR expressed parathyroid glands, CaSR in those tissues is in charge of regulating the levels of $[Ca^{2+}]_o$ by detecting circulating levels of Ca^{2+} in the extracellular fluid. When CaSR senses the drop of $[Ca^{2+}]_o$, it will stimulate the secretion of PTH and suppress the secretion of calcitonin, in turn, elevated PTH promotes bond and kidney resorption. Elevated $[Ca^{2+}]_o$ will further increase the generation of 1,25-dihydroxyvitamin D3 which can increase Ca^{2+} absorption from intestine.

CaSR is also highly expressed in non-homeostatic tissues, like nervous system (370,371), breast (372), heart (373), and skin (374,375), playing important roles in regulating a multitude of cellular processes including secretion (376,377), differentiation (378,379), proliferation (380),

apoptosis (381), and gene expression (367,368). How CaSR contributes to physiology and to some diseases in most cell types remains unclear. However, there are emerging experiment result reporting the function and role of CaSR in specific cell types. This has been extensively reviewed and highlighted in several review papers (382,383).

As a popular and crucial drug target, CaSR also contributes to the treatment of several diseases linked with disorders of Ca^{2+} homeostasis. The generation of CaSR allosteric modulators allows CaSR-based treatment of disorders of Ca^{2+} homeostasis. For example, positive allosteric modulator cinacalcet hydrochloride was the first allosteric modulator of GPCR entering the market, approved by FDA in 2004 for treatment of severe secondary hyperparathyroidism (SHPT) and hypercalcemia.

1.5 Challenges Associated with Membrane Protein and Weak Ca^{2+}-binding Affinity

Challenges encountered in my Ph.D. study, although multifaceted, are mainly associated with membrane protein and the characterization of Ca^{2+}-binding in those membrane proteins.

All three proteins I worked on including gap junction protein, metabotropic glutamate receptor, and Ca^{2+}-sensing receptor are membrane proteins with oligomerization preference. The first challenge associated with eukaryotic membrane protein is expression. There are several factors which may affect the success of expression of eukaryotic membrane protein. To begin with, eukaryotic membrane proteins need different machinery for protein folding, trafficking, translocation, and facilitating disulfide-bond formation, which may be due to lack or difference in other expression systems including *E.coli*, insect cell and yeast. Second, the lipid composition of cell membrane varies in different host. This variation may cause instability of membrane proteins. Third, eukaryotic membrane proteins usually undergo many post-translational modifications including phosphorylation, glycosylation and so on. However, only higher eukaryotes process the

corresponding machinery for those post-translational modifications. Mammalian expression systems resemble the native membrane protein environment best, however, expression cost is not in direct proportion to yield.

Another concern associated with membrane protein is purification and solubilization. Membrane proteins are embedding in the lipids bilayers. Detergent extraction is the standard purification method for membrane proteins. They can cover the hydrophobic surface of membrane protein and solubilize membrane proteins. However, researchers need to test a series of detergents to find out the one which not only have strong solubilization capability and high extraction efficiency but also can provide the most stable membrane protein. There are lots of detergents with high extraction power, but they are too harsh for membrane proteins, while mild detergents usually show low efficiency. Membrane proteins in detergent micelles are not quite stable which will influence the crystallization and further studies. In addition, maintaining the native and functional state of membrane protein in the detergent is of particular difficulty.

Membrane protein crystallization has set another challenge before researchers. In human, around 30% gene codes for membrane proteins, however, only a very low number of full-size membrane protein structures have been solved and deposited in the PDB. This phenomenon reflects how difficult it is to obtain membrane protein crystal structures. Many factors including heavy glycosylation, huge flexibility, high instability, oligomerization, or large molecular size could contribute to the failure of membrane crystallization. The structure and function study of membrane is largely hampered by the lack of crystal structure information.

To study the Ca^{2+}-binding or Ca^{2+}-regulation of those membrane proteins, we are facing another problem regarding the weak Ca^{2+}-binding affinity and invisibility of Ca^{2+}-binding pocket. Due to high on and off rate of Ca^{2+}-binding, it is extremely hard to capture Ca^{2+} in the

crystal. This weak-binding affinity also cause problems in direct measurement of Ca^{2+}-binding affinity in those membrane proteins. Thus, indirect methods has to be established to study Ca^{2+}-binding to study regulation of those receptors and channels.

1.6 Major Questions to Be Addressed in This Dissertation

There are several major questions need to be addressed in each projects:

In project "**Direct Visualization of Interaction between CaM and Cx45"**, the following questions need to be addressed:

1. Can CaM interact with Cx45 in living cells? If yes, is it Ca^{2+}-dependent?
2. Where is the Ca^{2+}/CaM binding site in Cx45?
3. How can we determine the binding of Ca^{2+}/CaM to Cx45 and detect the potential conformational change induced by such interaction?
4. What is the effect of Cx45-binding effect on Ca^{2+}-binding affinity of CaM?

In project "**Cx26 Gap Junction Hemichannel Regulation by Extracellular Ca^{2+}"**, the following questions need to be addressed:

1. Where is the Ca^{2+}-binding site in Cx26?
2. What is the Ca^{2+}-binding affinity of Cx26?
3. What is the effect of mutating predicted Ca^{2+}-binding ligands?
4. How does $[Ca^{2+}]_o$ regulate Cx26 hemichannles?

In project "**Is mGluR5 a Calcium-sensing Receptor?"**, the following questions need to be addressed:

1. Can mGluR5 sense the $[Ca^{2+}]_o$?
2. If mGluR5 has the Ca^{2+}-sensing capability, where is the Ca^{2+}-binding site?
3. What is the Ca^{2+}-binding affinity?

4. How does $[Ca^{2+}]_o$ regulate the activity of mGluR5?
5. What is the effect of $[Ca^{2+}]_o$ on the actions of other agonist of mGluR5?

In project "**Structural Basis for Regulation of Human Calcium-Sensing Receptor by Magnesium Ions and an Unexpected Tryptophan Derivative Co-agonist**", the following questions need to be addressed:

1. What is the function of extracellular Mg^{2+} on CaSR?
2. Where is the Ca^{2+}- and Mg^{2+}-binding sites in CaSR?
3. What is the structure of CaSR-ECD?
4. What is the unexpected tryptophan identified in CaSR-ECD?
5. What is the function of the unexpected ligand?

1.7 The Objectives and Overview of This Dissertation

The objective of this research is to understand how Ca^{2+}/CaM regulate gap junction proteins, to investigate how $[Ca^{2+}]_o$ modulate the activity of metabotropic glutamate receptors, and to probe the structural basis of CaSR-mediated signaling. Specifically, to reach the goals and address the above questions, I will review the background of Ca^{2+} signaling, gap junction, metabotropic glutamate receptor and Ca^{2+}-sensing receptor in **Chapter 1**.

Chapter 2 describes the materials and methods applied in my Ph.D. study to achieve goals described above.

Chapter 3 investigates the interaction of CaM and Cx45 both *in vivo* and *in vitro*.

A1. *Examine the interaction of CaM and Cx45 in living cells.*

In order to visualize the direct interaction between CaM and Cx45 in living cells, bioluminescence resonance energy transfer (BRET) assay will be performed to monitor the

interaction between two proteins. The Ca^{2+}-dependence or CaM-dependence will also be investigated through monitoring BRET signal changes in the presence of BAPTA-AM, $[Ca^{2+}]_o$/ionomycin, or CaM inhibitor W7.

A2. *Predict the CaM-binding site in Cx45 and characterize the interaction between CaM and Cx45 using peptide model.*

To identify the putative CaM-binding site in Cx45, we will analyze the sequence of Cx45 and predict the possible CaM-binding site using the CaM target database. To confirm the binding, peptide derived from the putative CaM-binding site will be synthesized and utilized in series biophysical studies to probe the characteristics of the interaction between CaM and Cx45-derived peptide.

Chapter 4 unravels the $[Ca^{2+}]_o$ regulation of Cx26 gap junction hemichannels.

To identify the putative Ca^{2+}-binding site in Cx26, we will first predict the putative Ca^{2+}-binding site using our computational algorithm MUG^{SR}. We will also purify enough Cx26 protein from insect cell using detergent extraction. The Ca^{2+}-binding characteristics of Cx26 will be examined by biophysical studies. Cx26 regulation by $[Ca^{2+}]_o$ will also be assessed using the oocyte by injection of Cx26 proteo-liposome.

Chapter 5 elucidates the modulatory effect of $[Ca^{2+}]_o$ on mGluR5 and identifies the Ca^{2+}-binding site.

A1. To test the effect of $[Ca^{2+}]_o$-sensing capability of mGluR5, we will monitor the mGluR5 activity by monitoring $[Ca^{2+}]_i$ immobilization and extracellular signal-regulated protein kinases 1 and 2 (ERK1/2) phosphorylation upon $[Ca^{2+}]_o$ stimulation. The modulatory effect of $[Ca^{2+}]_o$ on other mGluR5 agonists will also be examined by monitoring the same phenomenon when eliciting cell presented in various concentrations of $[Ca^{2+}]_o$ using agonist.

A2. To verify the putative Ca^{2+}-binding site, we will firstly mutate the predicted Ca^{2+}-binding residues and then compare the $[Ca^{2+}]_o$ effect on wild type and mutated mGluR5.

Chapter 6 explores the structure basis for regulation of CaSR by divalent cations and other extracellular stimuli.

A1. To solve the structure of CaSR-ECD, we will purify CaSR-ECD from mammalian cells and crystalize CaSR-ECD in different cations.

A2. To probe the function of any CaSR-ECD-bound ligands found in the crystal, we will perform cell experiment to investigate the function of those ligands. We will also mutate the amino acids associated with ligand-binding and compare the effect of ligand on wild type and mutated CaSR.

Chapter 7 summarizes major conclusions and the significance of all discoveries in this dissertation.

2 MATRERIALS AND METHODS

2.1 Direct Visualization of Interaction between Cam and Cx45

2.1.1 BRET assay related mouse Cx45 and rat CaM construction

The yellow fluorescent protein fusion protein expression vector pVenus-N/pVenus-C1 and the Renilla luciferase (RLuc) protein fusion protein expression vectors were received from Dr. Hepler (Emory University, GA) as gifts. The mouse Cx45 plasmid in pcDNA3.1/Hygro (+) was a gift from Dr. Veenstra (SUNY Upstate Medical University, NY). Cx45-pVenus was synthesized by insertion of the PCR product of the mouse Cx45 into vector pVenus-N1 at Nhe I and Xma I enzyme sites upstream of eYFP. Forward and reverse primers were CTA GCT AGC ATG AGT TGG AGC TTC CTG ACT and TCCC CCC GGG AAT CCA GAC GGA GGT CTT CCC. CaM-RLuc8 was generated by insertion of rat CaM gene into vector RLuc8-N1 at Xho I and BamH I. Forward and reverse primers for generation of CaM-RLuc8 were CCG CTC GAG ATG GCT GAC CAG CTG ACC and CGC GGA TCC CTT GCG AGT CAT CAT CTG. All DNA sequences were verified by GENEWIZ.INC (www.genewiz.com).

2.1.2 CaM and its mutants expression in E.coli

Unlabeled or ^{15}N isotopically labeled recombinant rat CaM and CaM half domains (N-CaM: resides from 1 to 75 and C-CaM: resides from 76 to 148) were expressed in *Escherichia* coli and were purified as described elsewhere (154,384). Protein concentrations were determined using the molar absorption coefficients ε_{277} of 3,030 M-1cm-1, ε_{277} of 2,666 M-1cm-1 or ε_{258} of 1,073 M-1cm^{-1} for wild type CaM, C-CaM and N-CaM, respectively.

Dansylated CaM (D-CaM) and CaM half domains (D-N-CaM and D-C-CaM) were synthesized according to the method described previously (385). The dansylation of CaM was

confirmed by ESI-MS. Concentrations of D-CaM, D-N-CaM and D-C-CaM were measured by using the ε335 of 3980 $M^{-1}cm^{-1}$.

^{15}N isotopically labeled recombinant rat CaM and CaM half domains were expressed in a minimum medium consisting of K_2HPO_4, KH_2PO_4, $MgSO_4$ and $(NH_4)_2FeSO_4$ and purified using the same method as unlabeled proteins.

2.1.3 Circular dichroism spectroscopy

CD spectra were recorded on a Jasco-810 spectropolarimeter at ambient temperature using a 0.1 cm path length quartz cuvette, an integration time of 1s and a scan rate of 100 nm/s. The far UV CD spectra of CaM (8 µM) and CaM-peptide complex (8 µM) were obtained in 10 mM Tris, 100 mM KCl, at pH 7.5 with 5 mM $CaCl_2$ or 5 mM EGTA. The far UV CD spectra of the peptide in different percentages of trifluoroethanol (TFE) were obtained using a concentration of 20 µM peptide in the same buffer. Multiple scans (10) were averaged and baselines were subtracted. The secondary structure contents of the peptides were calculated with the online secondary structure prediction server DICHROWEB (http://dichroweb.cryst.bbk.ac.uk/html/home.shtml).

2.1.4 Dansylated CaM fluorescence change induced by peptides derived from connexins

Steady-state fluorescence measurements were carried out in triplicate with a QM1 fluorescence spectrophotometer (PTI) at ambient temperature using a cell path length of 1 cm. Dansylated CaM samples (0.25-1 µM D-CaM or 1 µM D-C-CaM or 1 µM D-N-CaM) were prepared in 10 mM Tris-HCl buffer (pH 7.5) containing 100 mM KCl, 5 mM Ca^{2+} or 5 mM EGTA. Titration was carried out by gradually addition of the peptide stock solution (25-100 µM) prepared in the same buffer. The excitation wavelength was 335 nm, with fluorescence emission intensity recorded between 400-600 nm. The binding constant of the synthetic peptide to modified CaM

was obtained with a 1:1 binding model by fitting normalized florescence data as described previously (154).

2.1.5 Equilibrium Calcium titrations

Equilibrium calcium titrations were performed at room temperature using a QM1 fluorescence spectrophotometer. CaM alone (8 μM) or with Cx45164-186 peptide (molar ratio of 1:1.2) in 50 mM HEPES (pH 7.4), 100 mM KCl, 5 mM (NTA) and 0.05 mM EGTA was titrated with 15 mM or 50 mM calcium solution prepared in the same buffer. The intrinsic fluorescence of tyrosine (λex = 277 nm, λem= 320 nm) or phenylalanine (λex = 250 nm, λem= 280 nm) was used to monitor the calcium binding to C- and N-domain respectively (386). The fluorescent calcium indicator dye (0.2 μM) Oregon Green 488 BAPTA-5N (Oregon Green) was used to determine the free calcium concentration at each titration point using the following equation as previously described. Calcium titrations of CaM samples were repeated at least three times.

2.1.6 ^{15}N-^{1}H heteronuclear single quantum coherence (HSQC)

All ^{15}N-^{1}H HSQC spectra were recorded on either Varian Inova 600 or 800 MHz spectrometer. CaM NMR samples were prepared by diluting protein samples to 250 or 500 μM using buffer with the following composition 10% D2O, 5 mM MES, 10 mM Bis-Tris, 100 mM KCl, 0.02 % NaN3 with 10 mM Ca^{2+} or 10 mM EGTA. The pH values were adjusted to 7.4. NMR spectra were acquired at 37 °C. ^{15}N uniformly-labeled CaM was titrated with different amount of peptides derived from connexins to reach series of peptide/CaM ratios (0, 0.5, 1, 1.5, 2). NMR data were processed using NMRPipe and analyzed using SPARKY software package.

2.1.7 Pulse-field-gradient diffusion NMR

The pulse-field-gradient diffusion NMR was performed on a 600 MHz Varian Inova spectrometer using a modified PG-SLED pulse sequence (387).

2.1.8 Bioluminescence resonance energy transfer (BRET) assay

2.1.8.1 HEK293 cell culture and transfection

HEK 293 cells were cultured at 37 °C in a humidified incubator with 5% CO_2 and fed with colorless DMEM medium (Invitrogen) supplemented with 10 % FBS, 100 units/ml penicillin, 100 mg/ml streptomycin 25 mM glucose and 4 mM glutamine.

Transfection was performed with the aid of reagent polyethylenimine (PEI) (Polyscience. Inc). 8 µl of 1 mg/ml PEI was diluted in 100 µl unsupplemented DMEM medium (Invitrogen). The diluted PEI was incubated at room temperature for 3 minutes. Appropriate amount of DNA was also prepared in another 100 µl of unsupplemented DMEM medium. PEI and DNA were mixed to generate solution T by 3-second vortex, followed by 15-minute incubation at room temperature. Complete DMEM medium was replaced by low serum (5 %) transfection medium and appropriate amount of solution T was added into cell in a drop-wise manner. Cells were allowed to grow for 24 hours.

2.1.8.2 Donor/Acceptor ratio optimization

HEK293 cells were seeded to two 6-well plates in colorless DMEM medium with supplement one day before transfection. Cells in one 6-well plate was transfected with increasing amount (0, 2, 5, 10, 25, 100 ng) of donor plasmid Cx45-Rluc and cells seeded in another plate was transfected with increasing amount (0, 25, 50, 100, 500, 1000 ng) of acceptor pVenus-CaM. Besides, DNA amount in each well was adjusted to 1.5 µg by the addition of empty pc DNA 3.1 plasmid. After 24-hour transfection, the transfection medium was removed and replaced with 750

µl of sterilized BRET buffer (140 mm NaCl, 2.7 mM KCl, 1 mM $CaCl_2$, 1 mM $MgCl_2$, 0.37 mM NaH_2PO_4, 24 mM $NaHCO_3$, 25 mM HEPES, 0.1 % Glucose). Cells were detached from the dish by gently pipetting. 90 µl of the cells in triplicate from each well were placed into white-bottomed 96-well plates. The fluorescence intensity (excitation at 485 nm, emission at 530 nm) of pVenus-CaM was measured by TriStar LB 941 microplate reader. For donor (Cx45-Rluc) luminescence detection, 10 µl of 50 µM benzyl coelenterazine were added into each well and incubated at room temperature for 2 minutes before measuring luminescence at 485±20 nm.

2.1.8.3 BRET assay

Culture medium in each well was replaced by 750 µl sterilized BRET buffer and cells cotransfected with pVenus-CaM/CaM-pVenus and Cx45-Rluc were detached by pipetting. In each well, 90 µl of cells were distributed. Fluorescence measurements were acquired using a TriStar LB 941 Multimode microplate reader. Before measurement, coelenterazine was added to a final concentration of 5 µM and sequential measurements were performed at 460 ± 25 nm and 525 ± 25 nm. The BRET signal was defined as the ratio of light emitted at 525 nm over the light emitted at 460 nm. In some cases, cells were treated either with BAPTA-AM (50 µM) or CaCl2 (5 mM $CaCl_2$ and 10 µM Ionomycin) or N-(6-Aminohexyl)-5-chloro-1-naphthalenesulfonamide hydrochloride (W7, 50 µM) for 20 min, 10 min and 30 min respectively before BRET measurement. The average BRET signals were from three experiments.

2.1.9 Surface plasma resonance (SPR)

2.1.9.1 CM5 chip activation

Using a BIAcore T200 SPR system, we analyzed the interaction of CaM to Cx45 peptide corresponding to CaM-binding site. CM5 chips were activated by injecting a 1:1 ratio mixture of 0.4 M 1-ethyl-3-(3-dimethylaminopropyl)-carbodiimide (EDC) and 0.1 M N-hydroxysuccinimide

(NHS). The injection was lasting about 7 minutes at 10 µl/ min and followed by a wash with HBS-EP buffer (0.01 M HEPES, 0.15 M NaCl, 3 mM EDTA, 0.005 % v/v Surfactant P20).

2.1.9.2 Cx45 peptide immobilization

100 µM Cx45 peptide in water was injected for 1 minute at a speed of 5 µl/min twice to immobilize Cx45 peptide to the CM5 sensor chip by NH_2 coupling with the carboxyl group.

2.1.9.3 Deactivation of the excessive reactive groups

The excessive reactive carboxyl groups were blocked by a 10-minute injection of ethanolamine at a speed of 10 µl/min. A following wash using HBS-EP buffer was applied to remove any remaining ethanolamine.

2.1.9.4 Detection of the interaction between CaM and Cx45 peptide by monitoring the response unit change

Various concentrations of purified full length CaM or CaM half domains in HEPES buffer (10 mM HEPES, 150 mM KCl, 5 mM $CaCl_2$, pH 7.5) were injected for 10 minutes at 15 µl/min and this injection was followed by a 16 minutes buffer wash. The sensor chips were regenerated by 10 times 30-s injection of 30 mM NaOH. The background signal obtained from the reference flow cell was subtracted from the binding curves before data processing.

2.2 Cx26 Gap Junction Hemichannel Regulation by Extracellular Ca^{2+}

2.2.1 Plasmid construction and protein engineering

Mouse Cx26 gene was amplified by PCR using the mouse Cx26 DNA in pcDNA6/V5-His (A) vector (a gift from Dr. Eric Lin, Emory University, GA) as template with Bam H I and Hind III restriction sites added at the 5’ and 3’ ends and ligated into the modified Baculovirus donor plasmid pFastBac HT A vector (with C-terminal his tag). Site-directed mutagenesis was performed

using the QuickChange TM kit (Stratagene, Cedar Creek, TX) by following the manufacturer's instructions. All the DNA sequences were verified by GENEWIZ.INC (www.genewiz.com).

Human Cx26 in pTrcHis 2 A vector was a received as a gift from Dr. James Prestegard (University of Georgia, GA) and was used for bacterial expression. The codon of human Cx26 was optimized by GenScript (www.genscript.com) to replace rare codons.

Human Cx26 in pEGFP-N1 vector was obtained from Dr. Eric Lin (Emory Univeristy, GA) as a gift and was used for mammalian cell expression. Its mutants were generated by using QuickChange TM kit (Stratagene, Cedar Creek, TX) according to the manufacturer's instructions. All the DNA sequencing was done by GENEWIZ.INC.

2.2.2 Protein expression and purification/isolation

2.2.2.1 Cx26 isolation from liver

All the isolation processes were done on ice or in the 4 °C cold box. All the different percentages of sucrose were prepared in Tris-HCl buffer (10 mM Tris-HCl, 1 mM EGTA, 5 mM PMSF, 0.2 % NaN_3, pH 7.5). 150 g of fresh pig liver were chopped into small pieces and washed with Tris-HCl buffer for several times to remove the blood. Then the small pieces of pig liver in 500 ml Tris-HCl buffer were homogenized using the homogenizer and the homogenate was diluted to 2.5 L before filtered through four layers of cheesecloth. Pellet was separated from solution by centrifugation at 7000 rpm for 30 minutes at 4 °C and suspended in 300 ml Tris buffer before repeating the centrifugation. Pellet obtained from last step was suspended in 50 % sucrose. In each ultra-clear ultracentrifugation tubes, 2 ml of sample/50 % sucrose was loaded at the bottom, followed by the 5 ml of 41 % sucrose in the middle and 3 ml of 25 % sucrose on the top. Ultracentrifugation was performed at 27000 rpm for 1.5 hours at 4 °C using SW-28 Ti rotor. No brake was allowed and the lowest acceleration and deceleration rates were used for sucrose

gradient ultracentrifugation to avoid sucrose gradient disturbance. Any materials at the interface of 25 % and 41 % sucrose were collected using a 1 ml pipet and diluted four times with ice-cold Tris-HCl buffer. The diluted sample was applied to centrifugation at 7000 rpm for 30 minutes at 4 °C. After the centrifugation, pellet was suspended in a minimum amount of Tris-HCl buffer and sonicated for 10 minutes using the water bath sonicator. 0.6 % Sarkosyl was added to the mixture, followed by room temperature incubation for 30 minutes. Centrifugation at 7000 rpm was applied again for 30 minutes before re-suspending the pellet using 0.6 % Brij 58. The mixture was subjected to room temperature incubation for 30 minutes again and pellet obtained from the mixture using 30-minute centrifugation at 7000 rpm was suspended in 0.6 % Brji 58.

2.2.2.2 Human Cx26 expression in bacterial system

The bacterial expression was carried out in Escherichia coli C43 (DE3) cells in M9 medium with 100 mg/L of ampicillin at 28 °C. 1 mM Isopropyl-β-D-thiogalacto- pyranoside (IPTG) was added to induce the protein expression for 17 hours when the absorbance at 600 nm arrives at 1. The bacterial pellet was harvested by centrifugation at 7000 rpm for 10 minutes and be lysed in lysis buffer (10 mM HEPES, 500 mM NaCl, 1 mM phenylmethylsulfonyl fluoride (PMSF), pH 8.0) using a cell disruptor.

The supernatant was separated from pellet by ultracentrifugation at 30000rpm for 1 hour at 4 °C. 0.1% n-dodecyl-β-D-maltoside (DDM) was added into the supernatant to increase the solubility of soluble form of Cx26 and the mixture was filtered through a 0.45 μm filter (Millipore, Billerica, MA) before loading to a 16/10 HisPrep HP column (GE Healthcare), which is pre-equilibrated with buffer A (10 mM HEPES, 500 mM NaCl, 40 mM Imidazole, 0.1% DDM, pH 8.0). A linear segmented gradient of 0-100% buffer B (10 mM HEPES, 500 mM NaCl, 500 mM imidazole, 0.1% DDM, pH 7.5) was run using FPLC to elute the protein.

The pellet from the lysate was re-suspended in HEPES buffer (10 mM HEPES, 500 mM NaCl, 1 mM PMSF, 2% DDM, pH 8.0) and the mixture was tumbled overnight at 4 °C. Next day morning the pellet mixture was subjected to ultracentrifugation at 30000 rpm for 1 hour at 4 °C. The supernatant obtained from ultracentrifugation was filtered through a 0.45 0.45 μm filter (Millipore, Billerica, MA) and applied to 2 ml Cobalt resin (Thermo Scientific) pre-equilibrated with buffer A (10 mM HEPES, 500 mM NaCl, 10 mM imidazole, 0.1% DDM, pH 8.0). 20 ml of washing buffer (10 mM HEPES, 500 mM NaCl, 40 mM imidazole, 0.1% DDM, pH 8.0) was utilized to remove any non-specific binding protein on the beads. Elution was fulfilled by the application of elution buffer (10 mM HEPES, 150 mM NaCl, 300 mM imidazole, 0.1% DDM, pH 7.5). Imidazole removal was accomplished by further dialysis in HEPES buffer (10 mM HEPES, 150 mM NaCl, 0.1% DDM, pH 7.5) overnight at 4 °C.

2.2.2.3 Mouse Cx26 expression in insect system

Recombinant baculoviruses were prepared following the instructions of Bac-to Bac Baculovirus Expression System (Invitrogen). Insect Sf9 cells were cultured in the Sf-900™ II SFM media. Sf9 cells were infected at a density of ~ $2x10^6$ cells/ml for expression and harvested 72 h post-infection by centrifugation at 7,000 rpm at 4 °C for 10 min. For purification, cells were washed by phosphate buffered saline (PBS) buffer and lysed by sonication in 1mM bicarbonate and 1mM phenylmethylsulfonyl fluoride (PMSF) buffer. Cell membrane was enriched by ultracentrifugation and was solubilized with 2% n-dodecyl-β-D-maltoside (DDM) in HEPES buffer (10 mM HEPES, 500 mM NaCl, pH 8.0) overnight at 4 °C. Solubilized mCx26 was applied to 2 ml of Cobalt resin (Thermo Scientific). The resin was then wash with 20 ml washing buffer (10 mM HEPES, 500 mM NaCl, 40 mM imidazole and 0.1% DDM, pH 8.0). 300 mM imidazole was added into the washing buffer to elute mCx26. Pure mCx26 protein was verified by

chemiluminescence western blot and mass spectrometry (MS). The oligomers of mCx26 was visualized by both Native PAGE Novex 4-16% Bis-Tris Gel (Invitrogen) and electron microscopy (EM). Protein was dialyzed in dialysis buffer (10 mM HEPES, 150 mM NaCl, 0.1% DDM, pH 7.5) overnight at 4 °C to remove imidazole.

2.2.2.4 Connexin 26 splitting

Pure Connexin26 protein was mixed with buffer (10 mM Tris, 8 M urea, 6 mM EGTA, 10 mM DTT, pH8.0) at 1:1 ratio. The mixture was placed in 37 °C for 1 hour before storing at 4 °C for 5 days. Native gel was run to test the splitting result.

2.2.3 Mammalian cell culture and transfection

To study the Cx26 hemichannel Ca^{2+} permeability, HeLa cells from ATCG (Manassas, VA) were fed on a Dulbecco's Modified Eagle Medium (DMEM) and 10% fetal bovine serum (Invitrogen). The cells were cultured at 37 °C in a humidified incubator with 5% CO_2. One day before transfection, HeLa cells were grown on 13.5 × 20 mm or 22 × 40 mm coverslips based on the experiment design and then were transfected with Cx26-eGFP plasmid with the aid of lipofectamine2000 (Invitrogen).

2.2.4 Permeability measurement of Cx26 hemichannel using dye loading assay

HeLa cells cultured on 22 × 40 mm coverslip were transiently transfected with Cx26-eGFP or its mutants. After 48-hour post-transfection, cells were incubated with 0.5 mg/ml propidium iodide (PI) in the presence of 5 mM Ca^{2+} or EGTA for 20 minutes at 37 °C. The excessive dye was removed and washed away after incubation. The coverslips were mounted in a bathing chamber on the stage of a fluorescence microscope. PI loading was visualized utilizing a Leica DM6000 fluorescence microscope. At least 6 different views were examined to achieve statistical

analysis. Percentage of cells loaded with PI was calculated using this equation: Percentages of cells loaded with PI=Number of cells loaded with PI/ Total cell number in each view.

2.2.5 Liposome preparation

All lipids including synthetic and *E.coli* total lipids extraction were purchased from Avanti Polar Lipids, INC and stored in -20 ^{o}C freezer. When preparing liposome with mixed lipid composition, lipids dissolved in an organic solvent were first mixed before drying. Single lipid or mixed lipid were firstly dried using the lyophilizer at 4 ^{o}C. Then the thin lipid film was resuspended in TAK buffer (50 mM Tris-HCl, 20 mM NH_4Cl, 25 mM KCl, pH 7.5). The suspension was subjected to sonication (Fisher Scientific Sonic Dismembrator Model 500) at the amplitude of 70% in ice cold water bath for proper time with two minute pause until the suspension became light permeable. The liposomes were aliquoted and stored at -80 ^{o}C for future use.

2.2.6 Proteo-liposome preparation

1% DDM was firstly added into liposome prepared above and then the liposome was mixed with purified Cx26 protein at 5:1 ratio. The mixture was dialyzed in buffer (pH 7.5) containing 0.25 M sucrose, 0.4 M KOAC, 20 mM triethanolamine hydrochloride, 1.5 mM $Mg(OAC)_2$, 1 mM EDTA for overnight at 4 ^{o}C to reconstitute the Cx26 proteoliposomes. Second day morning, the mixture were centrifuged at 40000 rpm for 40 minutes at 4 ^{o}C. Supernatant was discarded and the yellowish pellet tightly attached at the bottom of centrifuge tubes was resuspended in TAK buffer. Proteo-liposome must be stored at -80 ^{o}C for future use. The concentration of proteo-liposome was measured by UV at 280 nm.

2.2.7 Oocyte preparation

Frogs were anesthetized by culture in fresh water with 0.3% 3-aminobenzoic acid ethylester for 30-40 minutes until no response when poked using finger. A small abdominal

incision was made by surgery scissors and ovaries were taken out. The oocytes clusters were firstly separated simply by pull. Then smaller oocyte clusters were digested in the OR2 solution (82 mM NaCl, 2 mM KCl, 1 mM $MgCl_2$, and 5 mM HEPES, pH 7.4) supplemented with 2 mg/ml of Type IA collagenase with gentle shaking until 70% of the tissue was digested. Next, the oocytes were subjected to the second time digestion for 5 minutes to achieve 90% digestion after washed with OR2 solution for 3 times. Digestion solution was carefully decanted and remaining collagenase was removed by OR2 solution wash for at least 5 times. Oocytes were then maintained in ND96 buffer (96 mM NaCl, 2 mM KCl, 1 mM $MgCl_2$, 1.8 mM $CaCl_2$, 5 mM HEPES, pH 7.4, 40 mg/L sodium pyruvate, 100 mg/L gentamicin, and 100 mg/L tetracycline) at 16 ^oC for 2 days with gentle shaking.

2.2.8 Proteo-liposome injection

Before injection, oocytes were examined under the microscope and good oocytes with clear separation of two pores and good pigment accumulation were picked up one by one for injection. Good oocytes were placed on a home-made holder with small wells. Then 60 ng of proteo-liposome or same amount of control liposome were injected into the oocytes by a sharp needle. The injected oocytes were incubated with 1.8 mM $CaCl_2$ to suppress budding at 23 °C for 30 mins. Recording bath solution was 90K buffer (90 mM KCl, 5 mM HEPES) with different regulators, such as 5 mM EGTA, or 5 mM Ca^{2+}.

2.2.9 Two electrons whole cell recording

The oocytes were placed in a recording chamber (BSC-HT, Medical System, Greenvale, NY) on a supporting nylon mesh to guarantee both the top and bottom surfaces of oocytes could be immersed in perfusion solution. Two electrode voltage clamping was performed using an amplifier (Geneclamp 500, Axon instruments Inc., Foster City, CA) at room temperature (23-25

°C) as described previously (165). Both the highest and lowest current in each group (30 oocytes) were discarded. The mean value was presented.

2.3 Is mGluR5 a Calcium-sensing receptor?

2.3.1 mGluR5 and its mutants construction

Rat mGluR5 in pRK5 vector received as a gift from Dr. Randy Hall (Emory Univeristy, GA) was used for mammalian cell expression. All mutants were generated using QuickChange TM kit (Stratagene, Cedar Creek, TX) according to the manufacturer's instructions. A flag tag was inserted after signal peptide (1-21) by PCR using rat mGluR5 as template. Forward and reverse primers are GAC GAT GAC AAG CAG TCC AGT GAG AGG AGG and ATC CTT GTA GTC TGC ACT CCC TCG TAC ATC. The extracellular domain gene of rat mGluR5 was amplified by PCR and inserted between BamHI and EcoR I enzyme cleavage site in pFastBac 1 plasmid. Forward and reverse primers are CGC GGA TCC ATG GTC CTT CTG TTG ATC CTG and CGG GAA TTC CTA GTG ATG GTG ATG GTG GTT ATT TTT CTT GGA CCA CAC. The recombinant pFastBac 1 donor plasmid was subsequently transformed into MAX Efficiency DH10Bac competent cell (Invitrogen) to generate the recombinant bacmid. This bacmid was confirmed by sequencing its PCR product.

All mGluR5 single and double mutations were generated using the QuikChange II Site-directed Mutagenesis Kit (Agilent Technologies). All the DNA sequencing was done by GENEWIZ.INC.

2.3.2 Cell culture and transfection

HEK293 cells from ATCG (Manassas, VA) were fed on a Dulbecco's Modified Eagle Medium and 10% fetal bovine serum. The cells were cultured at 37 °C in a humidified incubator

with 5% CO2. Cells were transfected with either mGluR5 WT or mutant using Lipofectamine 2000 (Invitrogen) by follow the manufacturer's instructions.

2.3.3 mGluR5 cell surface expression visualization by immunostaining

mGluR5 constructs contain a flag-tag right after the signal peptide were used in immunostaining experiment. After 48 hour transfection, cells were fixed with 3.7 % formaldehyde for 15 minutes at room temperature, followed by 3 times PBS wash. Mouse anti-flag monoclonal antibody was diluted 3000 times and incubated with cell overnight at 4 °C to stain the cell surface mGluR5. Next day after washing the cell with PBS, cells were stained with goat anti-mouse Alexa488-conjugated secondary antibody for 1 hour at room temperature. Nuclei were stained with DAPI. Fluorescence was visualized using a Zeiss LSM700 confocal microscope.

2.3.4 Quantitatively analysis of mGluR5 and its mutants' cell surface expression

PierceTM Cell surface protein isolation kit (ThermoFisher Scientific) was used to analyze the surface expression of WT and mutated mGluR5. Briefly, WT or mutated mGluR5 transfected HEK293 cells were treated with 30 μg/ml cell-impermeable and cleavable sulfo-NHS-SS-Biotin for 30 min at 4 ºC. The cells were subsequently washed by PBS extensively to remove any unbound biotin before lysis with RIPA buffer containing protease inhibitor. All biotinlysated cell surface protein were mixed with streptavidin agarose beads overnight to be further isolated. Next day, the beads were washed three times in RIPA buffer and the biotinylated surface proteins were eluted with SDS-Page sample buffer (62.5 mM Tris-HCl, 2.5 % SDS, 0.002 % Bromophenol blue, 10 % glycerol and 5 % β-mercaptoethanol, pH 6.8). The elutions were further separated by SDS-Page and transferred to a nitrocellulose membrane. The membranes were probed with anti-FLAG antibody by following the standard western blot protocol. The western blot films were analyzed by Image J. GADPH was used as an internal control.

2.3.5 Measurement of $[Ca^{2+}]_i$ response to $[Ca^{2+}]_o$ in single cells transfected with WT or mutant mGluR5

HEK293 cells grown on coverslip were transiently transfected with mGluR5 WT or mutant for 48 hours. Loading cell with Fura-2 AM was done by incubating with 4 μM Fura-2 AM in HEPES buffer (pH 7.4) with 0.5 mM $CaCl_2$, 140 mM NaCl, 5 mM KCl and 1.0 mM $MgCl_2$. Then the coverslips were mounted in a bath chamber on the stage of a Leica DM600 fluorescence microscope. The ratio of emission fluorescence intensity from both 340 nm and 380 nm was recorded in real time when extracellular Ca^{2+} was added and utilized as an indicator for intracellular Ca^{2+} concentration changes. $[Ca^{2+}]_i$ oscillations in individual cells were defined as three or more successive fluctuations peaks from the baseline after the initial peak. The $[Ca^{2+}]_i$ increase was obtained by subtracting the baseline from the first peak and was an average value from more than 30 cells. When analyzing the $[Ca^{2+}]_i$ oscillation frequency, cells that did not respond to $[Ca^{2+}]$o were excluded.

2.3.6 Exploration of $[Ca^{2+}]_o$ effect on mGluR5 response to L-Glu or L-Quis stimulation

The methods for measuring $[Ca^{2+}]_i$ release were as described above. The concentration of L-Glu or L-Quis was increased stepwise and applied to stimulate mGluR5 in the presence of different concentrations of $[Ca^{2+}]_o$ (0, 0.5 and 1.8 mM). For single cell, the $[Ca^{2+}]_i$ release was reflected by recording the ratiometric change of Fura-2 AM in real time. The $[Ca^{2+}]_i$ oscillation frequency and starting concentration at which cells start to respond was analyzed to determine the effect of $[Ca^{2+}]$o on the sensitivity of mGluR5 to L-Glu or L-Quis.

To compare the mGluR5 and its mutants' response to L-Glu or L-Quis, cells were kept in 1.8 mM $[Ca^{2+}]$o environment during L-Glu or L-Quis stimulation.

2.3.7 Determination of $[Ca^{2+}]_o$ effect on ERK1/2 phosphorylation mediated by mGluR5

Cells transfected with mGluR5 were starved in serum-free high glucose DMEM medium supplemented with 0.2% (W/V) BSA overnight. On the next day, following 10-minute HBSS wash, cells were stimulated by various concentrations of $[Ca^{2+}]_o$ for 5 minutes and subsequently lysed with RIPA lysis buffer. 90 µg of total lysate protein were loaded into 4-20 % gradient gel. Total protein amount for each sample was determined by BSA assay. Anti-phospho-p44/42 ERK and Anti-p44/42 ERK polyclonal antibodies (Cell Signaling Technology, Beverly, MA, USA) were utilized in western blot to detect the phosphorylated and total ERK respectively. Quantitative analysis of the ratio of phosphorylated/total ERK was performed using ImageJ software. The EC50 of $[Ca^{2+}]_o$-dependent response was obtained by fitting the $[Ca^{2+}]_o$ concentration –response curves with the Hill equation.

To investigate the $[Ca^{2+}]_o$ effect on L-Quis/L-Glutamate stimulated ERK phosphorylation, varying levels of L-Quis or L-Glutamate were used to stimulate the cells in the presence of 1.8 mM Ca^{2+} or in the absence of Ca^{2+}.

2.3.8 mGluR5-ECD expression in Sf9

The correct recombinant bacmid containing mGluR5-ECD gene was chosen by white-blue plaque selection and confirmed by sequencing. The pure bacmid was transfected into Sf9 cells at 2 x 10^6 densities by following the manufacturer's instruction of Cellfectin II reagent (Invitrogen). First generation of baculovirus particles were harvest the cell culture medium after 5-day post-transfection by low-speed centrifugation at 1000 rpm for 5 minutes. The titer of the virus was significantly increased by amplifying twice. After determining the titer of the 3rd generation of virus by plaque assay (Protocol xx), Sf9 cells were infected at a density of ~ 2x10^6 cells/ml at MOI of 2 for expression and culture medium was harvested 72 h post-infection by centrifugation at

7,000 rpm at 4 C for 10 min. After pH adjustment and filtration, the culture medium was mixed with Ni sepharose excel beads and stirred for 3-4 hours to allow the protein to bind to beads. 10-fold beads volume of HEPES buffer (10 mM HEPES, 150 mM NaCl, pH 7.5) with 40 mM Imidazole was applied to wash away any non-specific binding. mGluR5-ECD was eluted by HEPES buffer containing 300 mM Imidazole. Gel filtration was further ran to remove the Imidazole in the elution fractions. Protein concentration was determined by UV using a molar absorption coefficient ε_{280} of 74425 $M^{-1}cm^{-1}$.

2.3.9 Trp-Tb^{3+} fluorescence energy transfer

A Photon Technology International (Edison, NJ) Lifetime Fluorimeter was used to record the fluorescence spectra at room temperature using a 1-cm path length cuvette. 2 μM mGluR5-ECD protein sample was prepared in HEPES buffer (10 mM HEPES, 100 mM NaCl, pH 6.8). The emission spectra were recorded from 500 to 600 nm with the excitation at 280 nm. Secondary Rayleigh scattering was circumvented by using a glass filter with a cutoff of 320 nm. The Tb^{3+} titration was performed by adding various volumes of Tb^{3+} stock solution (1 mM) stepwise into the cell. The same amount of Tb^{3+} was also titrated into the same buffer without protein as a buffer control. The fluorescence intensity of buffer control was subtracted from the protein sample and the Tb^{3+} binding affinity of the protein sample was calculated by fitting normalized fluorescence intensity data using the Hill equation,

$$\Delta S = \frac{[M]^n}{K_d{}^n + [M]^n} \qquad \text{Equation 1}$$

Where Δ S is the total signal change of fluorescence intensity, K_d is the apparent binding affinity, n is the Hill coefficient, and [M] is the free metal concentration.

2.3.10 Ca^{2+}-Tb^{3+} competition

The Ca^{2+}-Tb^{3+} competition experiments were performed in solutions containing 30 mM Tb^{3+} and 2 mM protein as the starting point. The stock solution of 100 mM Ca^{2+} with the same concentration of Tb^{3+} was gradually added in to compete with the Tb^{3+}. By assuming that the protein is saturated with Tb^{3+} at the starting point of the competition experiment, the Ca^{2+} binding affinity is further obtained using Equation 2,

$$K_{d,Ca} = K_{app} \frac{K_{d,Tb}}{K_{d,Tb} + [Tb]} \qquad \text{Equation 2}$$

Where $K_{d, ca}$ and $K_{d, Tb}$ are the dissociation constants of Ca^{2+} and Tb^{3+}, respectively. K_{app} is the apparent dissociation constant.

2.4 Structural Basis for Regulation of Human Calcium-Sensing Receptor by Magnesium Ions and an Unexpected Tryptophan Derivative Co-agonist

2.4.1 Purification of the extracellular domain of the human CaSR (hCaSR-ECD) secreted from HEK293s GnTI-cells

hCaSR-ECD (from residue Tyr20 to Phe612) was expressed in suspension culture HEK293S GnTI-cells and purified from the culture medium by Ni^{2+}-NTA chromatography as previously described. To deglycosylate the purified protein, hCaSR-ECD was incubated with recombinant endoglycosidase F1 (Endo F1) at a 1:100 mass ratio of Endo F1 to hCaSR-ECD (388) overnight at 4 °C in 10 mM Tris buffer, pH 7.4. Further separation of hCaSR-ECD from Endo F1 was achieved by size exclusion chromatography (SEC) in 10 mM HEPES (pH 7.3) buffer.

2.4.2 Crystallization, data collection and structure determination

The dimeric hCaSR-ECD was concentrated to 10 mg/mL and crystallized in 10% PEG 8000, 200 mM $MgCl_2$, 10 mM $CaCl_2$ and 100 mM Tris-HCl, pH 7.0, using a sitting drop approach

at 21°C. No crystals were formed in the absence of Ca^{2+} or Mg^{2+}. The plate-shaped crystals were cryo-protected using 25% glycerol and flash-frozen in liquid nitrogen. Dehydration by soaking the crystal in 12% PEG 8000 overnight improved the resolution from 3.5~4 Å to 2-3 Å. The diffraction data of the crystals were collected on the beamline of 21-ID-D at LS-CAT in APS, and indexed, integrated and scaled in *HKL2000* (389). The structure was solved at 2.1 Å by molecular replacement using Auto-MR in *PHENIX* (390). The structure of chain A of mGluR2 with a bound agonist (PDB code: 4XAQ) was used as the search template (391). The electron density map after molecular replacement is clear enough to identify the unique features of hCaSR-ECD, and iterative model building and refinement were performed using *COOT* (392) and Refmac5 in the *CCP4*(393) suite, respectively. The restraints of CaSRL were generated by *JLigand* in *COOT*.

To generate the Gd^{3+} derivative, the native crystals were soaked with a solution containing 12% PEG 8000, 200 mM $MgCl_2$, 10 mM $CaCl_2$, 100 mM Tris-HCl pH 7.0, and 0.5 mM $GdCl_3$ overnight at 21°C. The anomalous signals of a dataset at 2.7 Å collected at the wavelength of 1.6985 Å were used to locate Gd^{3+} in the structure. The structure was solved by molecular replacement using the previously determined structure as the search template. All the figures of protein structures were generated by *PyMOL* v1.3 (Schrodinger LLC).

Using local geometric constraints and electron density intensity as major criteria, Mg^{2+} bound at site 1 and site 2 were unambiguously identified.

2.4.3 High-resolution LC-ESI-MS and identification of CaSRL

There is an unidentified ligand (CaSRL) bound at the putative orthosteric ligand binding site of CaSR-ECD. We examined the known CaSR ligands, including phenylalanine, tryptophan, glutathione (GSH), and polyamines, as well as the reagents used in sample preparation and crystallization, but none of them fit the density well. Among these initial trials, tryptophan

appeared to be the best fit to the electron density of the unknown ligand, but an additional density was unaccounted for when tryptophan was used fit the electron density. The size of the density suggests that CaSRL contains 14-18 heavy atoms (C/N/O/S/P), and the absence of anomalous signal indicates that it does not contain sulfur or phosphate. Accordingly, the M_r of CaSRL must be within the range of ~180-250 Da.

Considering CaSRL is tightly bound with hCaSR-ECD, it is conceivable that hCaSR-ECD has to be denatured to release CaSRL. To extract CaSRL, 50 μL of purified hCaSR-ECD (10 mg/mL) was mixed with 120 μL acetonitrile and vortexed. After high speed centrifugation, 10 μL of the CaSRL extract was injected onto a reverse-phase ACQUITY UPLC BEH C18 column (2.1 mm × 100 mm, 1.7-μm particle size; Waters). Column temperature was maintained at 40°C. The flow rate was 0.3 mL/min with starting conditions at 99% solvent A (water + 0.1% formic acid) and 1% solvent B (acetonitrile). The 15-min gradient profile for elution was as follows: starting at 1% solvent B and hold for 1 min, then ramping to 98% B at 10 min, hold at 98% B to 12 min, at 12.01 min return to 99% A/1% B and maintain until 15 min. The samples were analyzed by using a Waters Xevo G2-XS QToF LC-MS interfaced to a Waters Acquity UPLC system. The MS settings were as follows: electrospray ionization in negative-ion mode, 2.00 kV capillary voltage, 100°C source temperature, 350°C desolvation temperature, 600 liters/h desolvation nitrogen gas flow rate, 35 V cone voltage, and mass range of m/z 50 to 1500 with spectra accumulated at 0.1 seconds/function. Three separate acquisition functions were performed to generate spectra at different collision energies (5, 25, and 60 eV) providing both non-fragmenting and fragmenting conditions. Analyses of samples by electrospray ionization in positive-ion mode were performed under the same conditions as negative-ion mode except the collision energies (5, 20, and 40 eV). Fragmentation, formula, and abundances were analyzed with Waters MassLynx Software.

Using the above approach, we identified a species eluting at ~4.65 min, detected by MS in both positive-ion mode (m/z=217.0990) and negative-ion mode (m/z=215.0824), exclusively present in protein samples from several different batches, but not in sample buffer. The predicted elemental compositions based on mass are $C_{12}H_{13}N_2O_2$ (calculated mass = 217.0977) for positive-ion mode and $C_{12}H_{11}N_2O_2$ (calculated mass = 215.0824 Da) for negative-ion mode. A thorough search in the PubChem database led to a list of candidates containing of up to 200 compounds with the same M_r and formula. By manually fitting the density map with these compounds, only L-1,2,3,4-tetrahydronorharman-3-carboxylic acid (TNCA) fit the density perfectly. The synthetic CaSRL dissolved in the SEC buffer was treated in the same way as the protein samples in the LC-ESI-MS experiment and resulted in a peak detected at the same retention time and having the same mass spectrum. In LC-ESI-MS experiment, we also noticed a minor species eluted at ~4.57 min (Figure S10), which is detectable only in the positive-ion mode (m/z=215.0836) and having a predicted elemental formula of $C_{12}H_{11}N_2O_2$. The 2 Da smaller M_r for this related compound suggests that it is a derivative of CaSRL, likely due to a double bond formation between the backbone N and a neighboring C. As it is also likely to be a tryptophan derivative, we cannot exclude the possibility that it binds hCaSR-ECD with high affinity. This compound may also form during CaSRL extraction. Nevertheless, CaSRL perfectly fits the electron density at 2.1 Å and any extra double bonds in the CaSRL structure would likely be detrimental to fitting the density.

A phenylalanine replacement experiment was carried out by mixing purified hCaSR-ECD protein (0.26 mg/mL) with phenylalanine (final concentrations are 0, 50 and 150 mM, respectively). After overnight incubation at room temperature, hCaSR-ECD in each sample was re-purified with Ni-NTA beads. The protein samples were adjusted to the same concentration using SEC buffer and analyzed by LC-ESI-MS.

2.4.4 Monitoring Mg^{2+}- binding to CaSR-ECD by fluorescence spectroscopy

The imidazole in fractions of hCaSR-ECD eluted from the Ni^{2+}-NTA column was removed by passing the protein through desalting columns in HEPES buffer (10 mM HEPES, pH 7.2). The Trp fluorescence spectra of hCaSR-ECD were recorded on a QM1 fluorescence spectrophotometer (PTI) in a 1-cm-pathlength cell with a xenon short-arc lamp at ambient temperature. The emission between 300-400 nm was acquired during excitation at 282 nm. A solution containing 2 μM hCaSR-ECD in 10 mM HEPES (pH 7.2), 120 mM NaCl, and 10 mM KCl was gradually titrated by addition of Ca^{2+} prepared in the same HEPES buffer. The binding constants of Mg^{2+} to CaSR-ECD were calculated by fitting the titration curve with the Hill equation. The Ca^{2+}-Tb^{3+} competition experiments were performed in solutions containing 35 μM Tb^{3+} and 2 μM hCaSR-ECD as the starting point. $MgCl_2$ was added to the mixture from a 1 M stock solution while maintaining a constant Tb^{3+} concentration in the solution. The Mg^{2+}-binding affinity of the protein was calculated by fitting normalized fluorescence intensity data using the Hill equation:

$$\Delta S = \frac{[M]^n}{K_d{}^n + [M]^n} \qquad \text{(Eq. 1)}$$

Where ΔS is the total signal change in the equation, K_d is the apparent binding affinity, n is the Hill coefficient, and [M] is the free metal concentration.

2.4.5 CaSRL and Mg^{2+} binding site mutation design

All of the full length CaSR mutants were generated by site-directed mutagenesis based on the sequence of the human CaSR in the pcDNA3.1(+) expression vector (provided by Dr. Edward Brown). Site-directed mutagenesis was performed using the QuikChange™ kit (Stratagene, Cedar Creek, TX) according to the manufacturer's instructions. Briefly, a pair of complementary primers of 27–35 bases was designed for generating each mutant with the mutation placed at the middle of the primers. The template human CaSR in pcDNA3.1(+) was amplified using Pfu DNA

polymerase (Stratagene) with these primers for 16 cycles in a PCR instrument (TECHNE). After digestion of the template DNA with DpnI (New England Biolabs), the amplified mutant DNA was transformed into XL10-Gold Ultracompetent cells. All the DNA sequences were verified by Genewiz (www.genewiz.com).

2.4.6 Cell culture and transfection

Monolayer cultures of human embryonic kidney cells (HEK293) were purchased from ATCC (ATCC® CRL-1573™) and maintained in DMEM supplemented with 10% FBS and high glucose (4.5 g/L) at 37 °C. Wild type CaSR or its mutants were transfected into HEK293 cells using Lipofectamine 2000 (Life Technology) by following the manufacturer's instructions.

2.4.7 Immunostaining

Cells transfected with hCaSR-pcDNA3.1(+) were used in the immunostaining experiments, and this construct contains a FLAG-tag between Asp^{371} and Thr^{372}. After 48 h post transfection, cells were fixed with 3.7 % formaldehyde for 15 minutes at room temperature, followed by washing 3 times with PBS. Mouse anti-FLAG monoclonal antibody was diluted 500 times and incubated with cell overnight at 4 °C to stain the cell surface CaSR. The cells were subsequently washed with PBS and stained with goat anti-mouse Alexa488-conjugated secondary antibody for 1 hour at room temperature. Nuclei were stained with DAPI. Fluorescence was visualized using a Zeiss LSM780 confocal microscope.

2.4.8 Measurement of $[Ca^{2+}]_i$ changes triggered by $[Mg^{2+}]_o$ in single CaSR-transfected cells

Measurement of intracellular free Ca^{2+} was assessed as described by Huang, *et al* (394). Briefly, wild type CaSR, or its mutants, were transiently transfected into HEK293 cells grown on coverslips and cultured for 48 h. The cells were subsequently loaded for 15 min using 2 μM Fura-2 AM in 2 mL physiological saline buffer (10 mM HEPES, 140 mM NaCl, 5 mM KCl, 1.0 mM

$MgCl_2$ and pH 7.4). The coverslips were mounted in a bath chamber on the stage of a Leica DM6000 fluorescence microscope. The cells were alternately illuminated with 340 or 380 nm light, and the fluorescence at an emission wavelength 510 nm was recorded in real time as the $[Ca^{2+}]_o$ and/or $[Mg^{2+}]_o$ was increased in a stepwise manner in the presence or absence of 0.25 mM CaSRL in buffer (10 mM HEPES, 155 mM NaCl, 5 mM KCl, 2 mM NaH_2PO_4, 0.5 mM $MgCl_2$ and pH 7.4). The ratio of the emitted fluorescence intensities resulting from excitation at both wavelengths was utilized as a surrogate for changes in $[Ca^{2+}]_i$ and was further plotted and analyzed as a function of $[Ca^{2+}]_o$. All experiments were performed at room temperature. The signals from 20 to 100 single cells were recorded for each measurement. Oscillations were identified as three successive fluctuations in $[Ca^{2+}]_i$ after the initial peak.

2.4.9 Determination of the effect of CaSRL on Mg^{2+}-evoked $[Ca^{2+}]_i$ signaling by stimulation of CaSR in cell populations

Changes in the intracellular Ca^{2+} concentration $[Ca^{2+}]_i$ elicited by extracellular Mg^{2+} ($[Mg^{2+}]_o$) in a population of cells were measured by fluorimetry as described previously(394). A cell line stably expressing CaSR (5001) was seeded on 13.5 x 20-mm coverslips and cultured in DMEM. After reaching 95% confluence, cells were washed three times using loading buffer (20 mM HEPES (pH 7.4), 125 mM NaCl, 5 mM KCl, 1.25 mM $CaCl_2$, 1 mM $MgCl_2$, 1 mM NaH_2PO_4, 1% glucose, and 1% BSA) and subsequently incubated with 4 μM Fura-2 and 4 μM pluronic F127 for 20 minutes at 37 °C to enable sufficient dye loading in the same buffer. After removing the excess Fura-2, coverslips with cells were diagonally positioned in a quartz cuvette filled with 3 ml experimental buffer (125 mM NaCl, 5 mM KCl, 0.5 mM $CaCl_2$, 0.5 mM $MgCl_2$, 1% glucose, and 1% BSA). Measurements of Fura-2 fluorescence at 510 nm when excited at 340 or 380 nm were performed on a QM1 fluorescence spectrophotometer (PTI). The emission ratio of 340/380 was

calculated and used to reflect the changes in $[Ca^{2+}]_i$ when different concentrations of $[Mg^{2+}]_o$ were applied to the cells.

To examine the co-activation of CaSR by CaSRL and $[Mg^{2+}]_o$ or $[Ca^{2+}]_o$, different concentrations of CaSRL were placed in the experimental buffer with a fixed concentration of $[Ca^{2+}]_o$ and varying concentrations of $[Mg^{2+}]_o$, or vice versa, as described in the results section. The effects of other ligands were analyzed by comparing the changes in $[Ca^{2+}]_i$ produced by $[Mg^{2+}]_o$ alone or by co-application of Mg^{2+} with other ligands. The EC_{50} of $[Mg^{2+}]_o$ obtained during incubation with various concentrations of CaSRL is compared with that observed in the presence of $[Mg^{2+}]_o$ alone. The EC_{50} changes were plotted as a function of CaSRL concentration and the curve was fit to the Hill equation. The activation of CaSR by the CaSRL, functioning as a co-agonist with $[Mg^{2+}]_o$, is indicated by the increasingly leftward-shifted EC_{50} for $[Mg^{2+}]_o$ as the concentration of CaSRL increases (Supplementary Table 5).

2.4.10 Determination of ERK1/2 phosphorylation

The 5001 cell line stably expressing hCaSR was starved in serum-free DMEM medium supplemented with 0.2% (w/v) BSA overnight, followed by washing 3-times with HBSS and a subsequent 10 minute HBSS incubation after 12 hours. To induce ERK1/2 phosphorylation, varying concentrations of $[Mg^{2+}]_o$ (0-50 mM) or $[Ca^{2+}]_o$ (0-30 mM) with or without 0.5 mM CaSRL were added to cells and incubated for 10 minutes at 37 °C. The cells were then lysed with Pierce RIPA buffer (ThermoFisher Scientific). Total protein concentration was measured using the BioRad assay. Lysates containing 100 µg of total protein were loaded onto 4-20 % gradient SDS-PAGE gels for separation. After electrophoresis, proteins on the gel were transferred to nitrocellulose membranes and further analyzed by western blotting. Anti-phospho-p44/42 ERK (1:1000 dilution) and anti-p44/42 (1: 2000) polyclonal antibodies were utilized as probes to detect

the phosphorylated ERK1/2 and total ERK1/2 respectively. A chemiluminescent detection method (AP Conjugate Substrate Kit, Bio-Rad) was applied to detect phosphor-ERK1/2 and total-ERK1/2. The respective bands on western blots were evaluated by densitometry. The EC_{50} of $[Mg^{2+}]_o$- or $[Ca^{2+}]_o$-dependent responses were obtained by fitting the $[Mg^{2+}]_o$ or $[Ca^{2+}]_o$ concentration-response curves with the Hill equation (Eq.1).

3 DIRECT VISUALIZATION OF INTERACTION BETWEEN CALMODULIN AND COONEXIN45

3.1 Introduction

As discussed in Chapter 1, gap Junction is a specialized membrane structure, which is spanning the membrane of two neighboring cells and leaving a 2-3nm characteristic gap between them (40). It forms a channel between two adjacent cells and provides a direct pathway for cell communication. Gap junctions integrate the cellular functions of essentially every tissue in the body with a few notable exceptions (e.g. blood, skeletal muscle). It plays an indispensable role in accurately tuning of several biological processes including cell differentiation, growth and development. So far, about 21 genes coding gap junction proteins have been discovered in human (42). Cx45 is a member of this multigene family. Its expression was firstly identified in chick embryos and it is notable that its expression fell 10-fold from the early embryonic heart to the adult (395). Subsequently, Cx45 was reported as one of the main three connexin isoforms found in the heart and it was mainly detected in the sinoatrial node (SAN), the atrioventricular node (AVN), His-bundle and bundle branches (396-400). Cx45 is expressed in other tissues like smooth muscle and brain (396,401,402). Recently, the role of Cx45 in heart has been extensively studied in genetically modified mouse models. Cx45-deficient mice died at around embryonic day 9 and 10 due to heart abnormality (44,45). These observations illustrate that Cx45 is one of the unique necessary component for heart development.

Alteration of regulation of connexins has been shown to be involved in various types of diseases (403-405). Multiple factors including $[Ca^{2+}]_i$, calmodulin (CaM), H^+, voltage, and phosphorylation of the connexin subunits have been reported to regulate intercellular communication mediated by gap junctions (406,407).

Modulation of the cytoplasmic Ca^{2+} concentration ($[Ca^{2+}]_i$) is a ubiquitous mechanism by which cells transduce external signals into biological responses. The signaling cascade initiated by the rise in $[Ca_2^{+}]_i$ is often mediated via Ca^{2+}-binding proteins such as calmodulin (CaM) (122,123,408). CaM is a key multifunctional transducer of Ca^{2+} signals in eukaryotes which has four EF-hand Ca^{2+} binding motifs in two globular N- and C-domains that are separated by a flexible linker. When it binds to Ca^{2+}, CaM undergoes a large conformational change, exposing hydrophobic patches that are essential in its binding to more than 300 target proteins in multiple cellular processes (124-126). CaM can differentiate between local and global $[Ca^{2+}]_i$ changes using its N- or C-domains with different Ca^{2+} binding affinities and kinetic properties. It regulates a diverse group of membrane channels/pumps with different binding modes depending on nature of binding sequences including IQ motifs (133-137). The first intriguing result of Kink et al. reporting that CaM can function as a modulator on Ca^{2+}-dependent Na^+ current or K^+ current (409) opened a Pandora's box of similar regulation on other ion channels (410-415).

The involvement of CaM in the regulation of gap junctions comprised of all three connexin subfamilies has been proposed and reported over the years (416,417). The first evidence of CaM role in regulation of Cx45 was reported by Peracchia and coworkers by monitoring the sensitivity of Cx45 channels to CO_2, and inhibiting CaM expression in oocytes (158). It remains a hot debate for the direct interaction of CaM to connexin due to versatile capability of CaM in regulating various cellular target proteins and limitations of current commonly used pharmacological approaches with CaM inhibitors. To date, there has been no evidence of direct binding between CaM and full length Cx45 and subsequently the mechanism of the regulation remain obscure.

Cx45 shares the same structure topology with other connexins (**Fig. 1.8**). Four α-helical transmembrane domains are connected by two extracellular loops and one intracellular loop. The

transmembrane domains, as well as the extracellular loops and the N-terminal, are conserved among different connexins. On the other hand, as a γ family connexin, Cx45 possesses sequence characteristics which are divergent from that of α or β family connexin isoforms. Sequence alignment of Cx26 (β), Cx50 (α) and Cx45 (γ) indicates Cx45 has a much longer cytoplasmic loop region, which may offer binding sites for other protein partners in the cytosol. Our lab has previously reported a direct role for CaM in regulation of different connexins from α-subfamily such as Cx43, Cx44, and Cx50 and demonstrated (418)such interaction of CaM to these alpha family connexins using peptide models (121,154,156). Largely due to challenges related to intrinsic disorder in cytosolic intracellular loop and carboxyl terminus of connexins, they remain "invisible" even in the determined X-ray structure (106,419).

In the present work, for the first time, we have demonstrated that there is direct interaction between Ca^{2+}/CaM and full-length Cx45 (from γ-subfamily) in HEK293 cells co-transfected with Cx45 and CaM using bioluminescence resonance energy transfer assay. We then revealed the CaM binding site using peptide model and probed the molecular action of such interaction of CaM to Cx45 using various spectroscopic methods including high resolution nuclear magnetic resonance (NMR). We further report here the differential action of Ca^{2+}/CaM on the cytosolic loop of Cx45 with an extended conformation that is different from that of alpha family Connexins, which provide novel insight into CaM regulation of Connexins related to heart development and pathological diseases.

3.2 Results

3.2.1 Establishing a BRET cellular assay to probe CaM and Cx45 direct interaction in cells

Bioluminescence resonance energy transfer has been applied to study protein-protein interaction in both living cells and *in vitro (418).* BRET is based on the energy transfer between

fusion proteins containing GFP mutant (usually is eYFP or Venus) and *Rerilla* luciferase. In BRET, luciferase serves as the donor because its emission spectrum is broad enough to provide good excitation of eYFP. Luciferase does not naturally interact with eYFP. When the substrate of luciferase is provided, luciferase will oxidize the substrate and result in an emission peak at 482 nm. This emission is well overlapping with the excitation spectrum of eYFP, of which the excitation peak is 514 nm. If two fusion proteins are in close proximity, energy generated from the reaction will be transferred to the eYFP and yield yellow fluorescence light with an emission peak of 527 nm. If no interaction between two fusion proteins occurs, luciferase and eYFP will be too far apart for sufficient energy transfer (**Figure 3.1**). In most resonance energy transfer based assays, the typical effective distance between the donor and the acceptor is 10 to 100 angstroms. For BRET, we can expect significant signal between luciferase and eYFP as a result of protein-protein interaction if the distance is less than 10nm. Compared with its homologue FRET (fluorescence resonance energy transfer), BRET is non-destructive because it does require external illumination. In FRET, tissue or cells may be easily damaged by the excitation light. Besides, the external illumination may cause photobleaching, autofluorescence and direct excitation of the acceptor

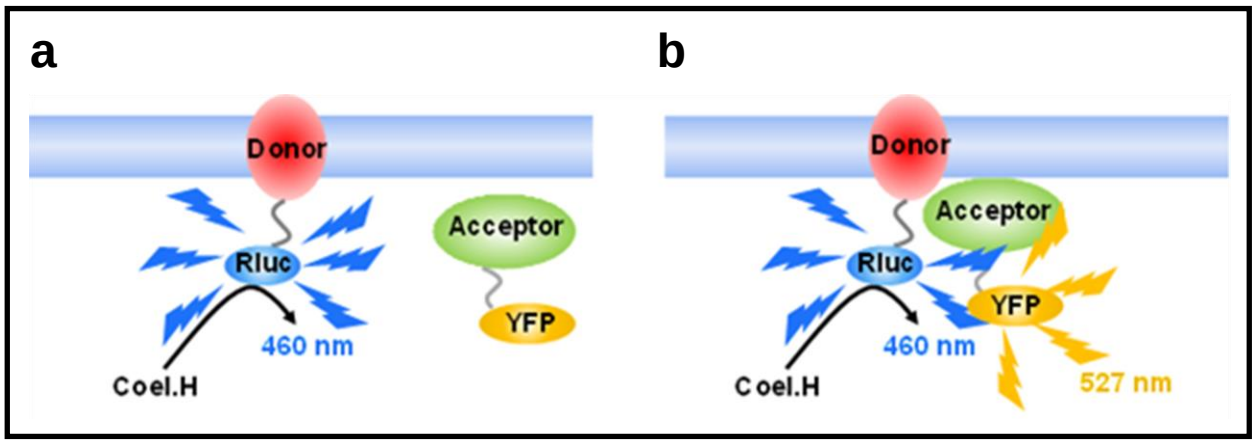

Figure 3.1 Bioluminescence resonance energy transfer.

This widely used technique is based on the resonance energy transfer between the donor luciferase and acceptor YFP. Luciferase can oxidize the membrane permeable substrate Coel.H to produce light emission at 460 nm. If two fusion proteins do not interact with each other in the cell, no energy transfer occurs and the yellow fluorescence protein can't be lighted up (a) However, if two fusion proteins have association in cell, their close proximity can meet the prerequisite for successful energy transfer between donor and acceptor (b) An emission at 527 nm from YFP will display.

We aim to capture the in vivo interaction between Cx45 and CaM in the natural cellular environment instead of in the test tube. Luciferase was fused to the C-terminal of Cx45 and Venus was tagged to either the N- or C-terminal of CaM to form a donor/acceptor pair. If no interaction occurs in the living cell (**Figure 3.2a**), upon the addition of the substrate ctz, only the emission of oxidization product at 482 nm can be detected; on the other hand, if two fusion proteins are close enough (**Figure 3.2b**) to allow the sufficient energy transfer, the neighboring acceptor will be excited and emits yellow fluorescence at 527 nm.

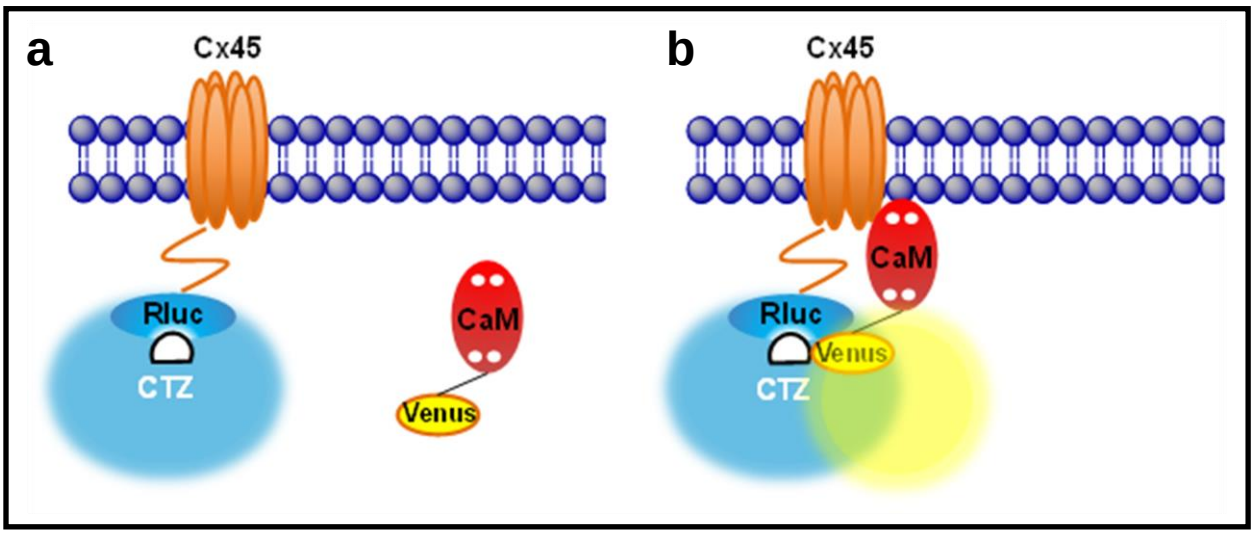

Figure 3.2 Probing interaction between Cx45 and CaM in HEK293 cells by BRET.

Luciferase was tagged to the C-terminal of Cx45 and Venus was fused either to the N- or C-domain of CaM to form the donor/acceptor pair. If no interaction between Cx45 and CaM in co-transfected HEK293 cells, the Venus tagged to CaM will not be illuminated (a); while CaM binding to Cx45 will lead to the sufficient energy transfer from donor Cx45-Rluc to CaM-Venus, resulting in an emission of yellow fluorescence (b).

In our experiment, we used a mutant of eYFP (Venus) as an acceptor. Venus, a novel mutation of eYFP, improves the maturation and brightness at 37 °C of eYFP (420). Because the orientation of the fusion linkage and the composition of the fusion protein may affect the protein expression and activity which in turn significantly affect the signal of BRET, therefore creating two vectors for each protein is necessary to test the orientation of N- or C-terminal fusions. However, previous research reported that N-terminal tags has various of effect on different connexin isoforms, including channel gating, channel conductance and functional channel formation or plaque formation (421-424). So in the BRET assay, we avoided using the Cx45 construct with N-terminal tag. Besides, cells transfected with Cx45 construct tagged with Venus displayed a relatively dim yellow fluorescent emission under the fluorescence microscope when compared with CaM constructs fused with Venus. Therefore, in the following BRET experiments, only three constructs (CaM-Venus, Venus-CaM and Cx45-Rluc) has been utilized. A wrong clone with frame shift of Venus-CaM was initially used for the BRET experiment. The yellow fluorescence was observed under the fluorescent microscope and by fluorimeter. However, no BRET signal was observed when performed the BRET assay.

The best BRET signal is obtained when luciferase fusion protein interacts with Venus fusion protein at 1:1 ratio, because excessive luciferase will result in a decrease of the BRET signal. Therefore, in the experiment design, overexpression of Venus fusion protein is desirable for saturating the luciferase fusion protein. Before performing the BRET assay, the ratio of donor/acceptor needs to be optimized.

Firstly, either a series of donor only or acceptor only DNA were transfected into HEK293 cells. The donor expression was reflecting by the luminescence intensity at 485 nm (**Table 3.1**).The fluorescence intensity of Venus at 530 nm was shown below (**Table 3.2 and 3.3**). Typically, a relative luminescence units (RLU) of 100,000 – 350,000 and a relative fluorescence unit (RFU) of Venus is around 30,000-200,000 are desirable for the micro-plate reader.

Table 3.1 Luminescence of donor Cx45-Rluc.

Cx45-Rluc(ng)	0	2	10	50	100	500
Luminescence	**157**	**37681**	**111827**	**450486**	**608433**	**1239209**
Luminescence	**157**	**28850**	**121639**	**340622**	**617932**	**1176790**
Luminescence	**157**	**34207**	**100051**	**335097**	**669272**	**1208927**
Average	**157**	**33579**	**111172**	**375402**	**631879**	**1208309**

Table 3.2 Fluorescence of acceptor CaM-Venus.

CaM-Venus(ng)	0	25	50	100	250	500
Fluorescence	301106	301675	316178	337462	374692	434393
Fluorescence	296180	301253	311233	335068	376252	433951
Fluorescence	297720	303657	311900	337050	378882	438328
Average	298335	302195	313104	336527	376609	435557

Table 3.3 Fluorescence of acceptor Venus-CaM.

Venus-CaM (ng)	0	25	50	100	500	1000
Fluorescence	295032	389028	475518	702361	1486355	1939991
Fluorescence	297004	396162	500060	710888	1532563	1951511
Fluorescence	297691	394808	511286	714961	1491712	2044762
Average	296576	393332	495621	709403	1503543	1978755

To determine whether CaM associates directly with full-length Cx45 channels inserted into the membrane, we used an energy transfer based technique BRET, in which the energy is transferred between bioluminescent and fluorescent tags. A close proximity of 50 Å between the tags is the essential prerequisite of this energy transfer. The energy transfer is undetectable if the distance between them is larger than 100 Å. In our study, we tagged the bioluminescent donor Renilla reniformis luciferase (Rluc) to the C-tail of Cx45 and the yellow fluorescent acceptor Venus to the N- or C-end of CaM. HEK293 cells were cotransfected with a fixed amount of Cx45-

Rluc and an increasing amount of Venus-CaM or CaM-Venus. Fluorescence intensity of Venus-CaM or CaM-Venus was measured before BRET assay to verify increasing expression of acceptor Venus-CaM/CaM-Venus and western blot was run after experiment to further confirm the same expression level of donor Cx45-Rluc. The BRET signal was determined as the ratio of light emitted at 525 nm over the light emitted at 460 nm. As shown in **Fig. 3.3a**, a significant BRET signal enhancement was observed in cells transfected at an increasing ratio of acceptor/donor in both two constructs. Venus-CaM showed a slightly higher BRET signal compared with CaM-pVenus. Therefore, Venus-CaM was used for future BRET experiments. The application of CaM inhibitor W7 abolished the interaction between Cx45-Rluc and Venus-CaM. Taken together, these data indicate that CaM can physically interact with Cx45 in living cell. The wrong clone with frame shift served as a negative control and no BRET signal was detected for this clone.

3.2.2 Ca^{2+}-dependent interaction between Cx45 and CaM

Next, we reasoned that the interaction between Cx45 and CaM in living cell may need the external Ca^{2+} stimulation. Our in vitro experiments revealed that the interaction between Cx45 and CaM is in a Ca^{2+}-dependent manner. To access the Ca^{2+} effect on the Cx45-CaM association in living cell, 10 μM ionomycin plus 5 mM Ca^{2+} was added to the BRET bath solution and 10-miunte incubation was allowed before BRET measurement. Ionomycin can form the ionomycin calcium salt and act as a motile Ca^{2+} carrier. The enhanced Ca^{2+} influx is expected to activate CaM, and the latter will further associate with Cx45 located on the cytoplasmic membrane. Indeed the enhancive increase of intracellular Ca^{2+} did double the BRET signal in both two construct combinations we tried (**Figure 3.3b**). While, cells treated with BAPTA-AM for 20 minutes before BRET measurement displayed a remarkable BRET ratio decrease. BAPTA with the ester can penetrate the cell membrane and chelates the intracellular Ca^{2+} ions. Without the Ca^{2+} activation,

the interaction between Cx45 and CaM was almost abolished. These data together indicates that intercellular Ca^{2+} is required for the CaM-Cx45 interaction in living cells.

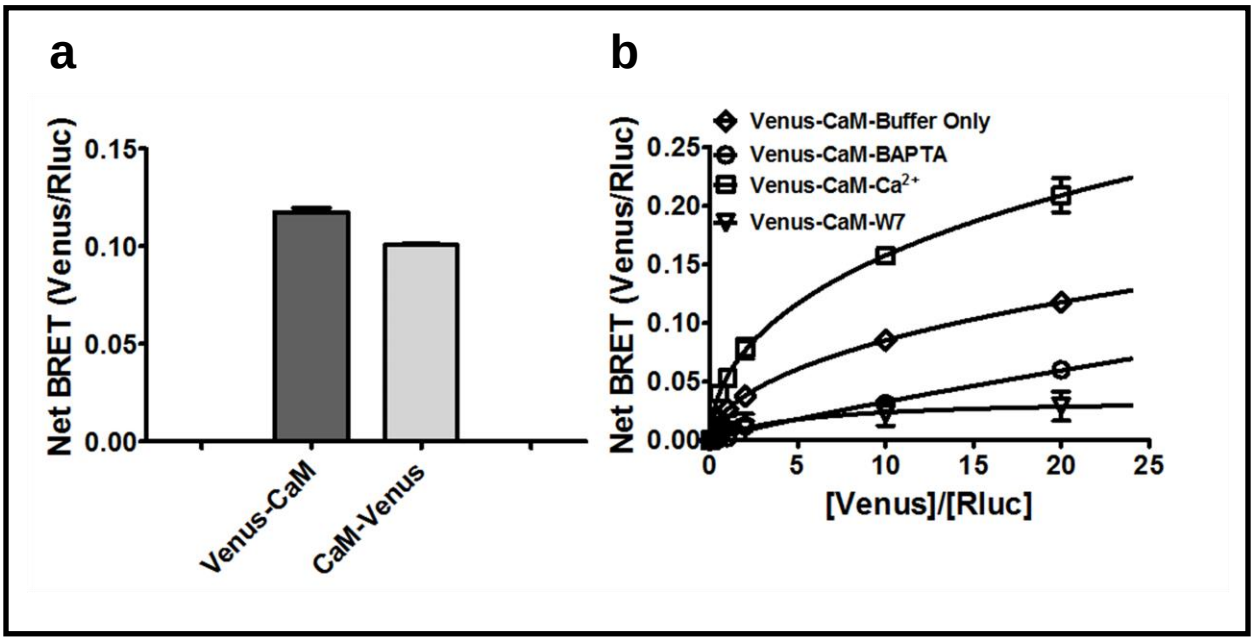

Figure 3.3 Interaction of Cx45 and CaM in live cells as measured by BRET.

(a) Interaction between Cx45-Rluc and CaM-Venus/Venus-CaM was determined by BRET. HEK293 cells were co-transfected with a fixed amount of Cx45-Rluc and with increasing DNA concentrations of Venus-CaM or CaM-Venus (expression level was verified by fluorescence intensity measurement). BRET assays were performed 24 h after transfection. (b) Cells were treated with only BRET buffer, or 5 mM Ca^{2+}, or 50 µM BAPTA-AM for 20 minutes or 50 µM W7 for 30 minutes before BRET measurement. The net BRET ratios comparison is presented as BRET signal saturation curves. The data shown above are the mean ± S.E.

3.2.3 Identification of putative CaM binding region in the single cytoplasmic loop of Cx45

Based on the characteristics including the hydropathy, alpha-helical propensity, residue weight, residue charge, hydrophobic residue content and helical class of Cx45, we predicted a potential CaM binding site within Cx45 using the CaM target database. This site in the intercellular loop covering residues 164-186 was assigned with the highest predictive score.

As a key multifunctional transducer of calcium signals in eukaryotes, CaM is capable to bind with diverse sequences in CaM-regulated proteins through conformation adaptation. These sequences were classified into different motifs (1-14, 1-10, 1-16 and IQ motif) based on the distance between key hydrophobic residues. In Cx45 164-186 region, we predicted a possible CaM-binding motif, GRRRIREDGLMKIYVLQLLARTV, which fits the IQ like motif ((FILV)Qxxx(RK)xxxxxxxx). The IQ like motifs feature that the hydrophobic residue preceding the highly conserved Q residue is mainly I, L and V and the basic residue which is 3 residues away from Q is always residue R or K. The putative CaM-binding motif in Cx45 possesses the characteristics of IQ like motif. In our predicted CaM binding sequence, the residue before Q is the hydrophobic L and the conserved basic residue is R. Further analysis of Cx45 CaM binding region (**Figure 3.4**) revealed that it could be aligned with previously identified IQ like motifs (38,425,426) from other proteins.

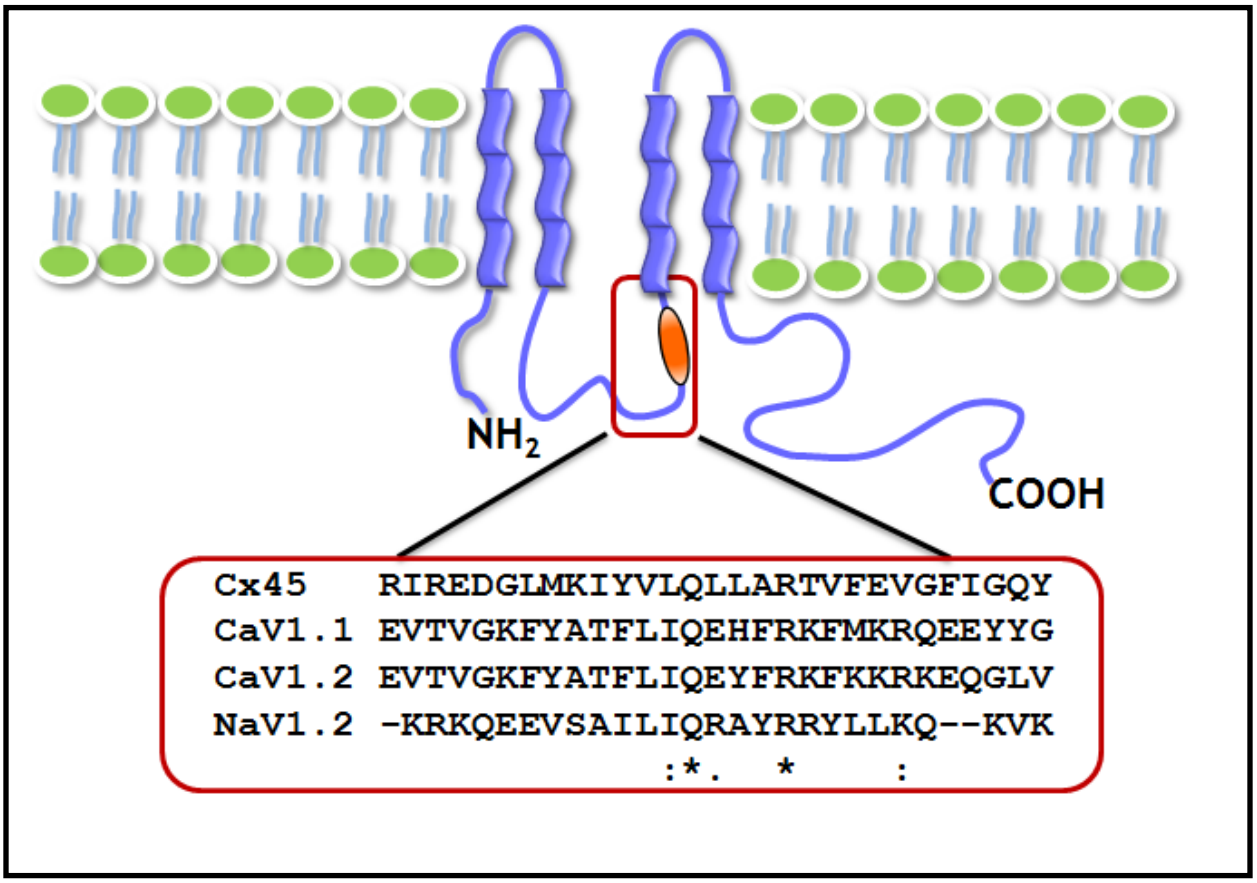

Figure 3.4 Membrane topology of Cx45 and the putative CaM-binding site.

Cx45 has four transmembrane domains connected by two extracellular loop and one intracellular loop, which is longer than α- and β-class of connexins. The CaM-binding site is located in the second half of the intracellular loop. Sequence alignment of the predicted CaM-binding site in Cx45 with other voltage-gated calcium and sodium channels was performed with ClustalW.

3.2.3.1 Revealing CaM-Peptide interactions with CD spectroscopy

Studies revealed that peptides corresponding to the CaM-binding domains has high propensity for helix formation or adopt a helical conformation upon binding to CaM (427-430). The helical formation propensity was evaluated by monitoring its secondary structure using far UV CD in the presence of increasing percentages of tetrafluoroethylene (TFE). TFE has proven useful to induce and stabilize the intrinsic secondary structures of peptides (431-434). In the aqueous environment, Cx45 peptide displayed little ellipticity at 222 nm and 208 nm. However, the alpha helix content dramatically rose from 45% (0 TFE) to 75% when 20% TFE was presenting. The increment was further enhanced by adding more TFE (**Figure 3.5a**). These data suggest Cx45 peptide has high helical propensity.

CD was further used to capture the structure and conformation change in the process of CaM-Cx45p complex formation. A 10.8 % increase of alpha helix was observed after the addition of Cx45 peptide to holo-CaM, while the addition of Cx45 peptide to apo-CaM resulted in a slight decrease (**Figure 3.5b**). One possible explanation for the helix increase of holo-CaM is that the Cx45p-binding pocket of CaM provides the hydrophobic environment needed for the formation of stable helical secondary structure in Cx45 peptide. While in the presence of EGTA, the

hydrophobic surface of CaM disappeared and the hydrophilic environment further decreases the stability of helix structure of Cx45 peptide.

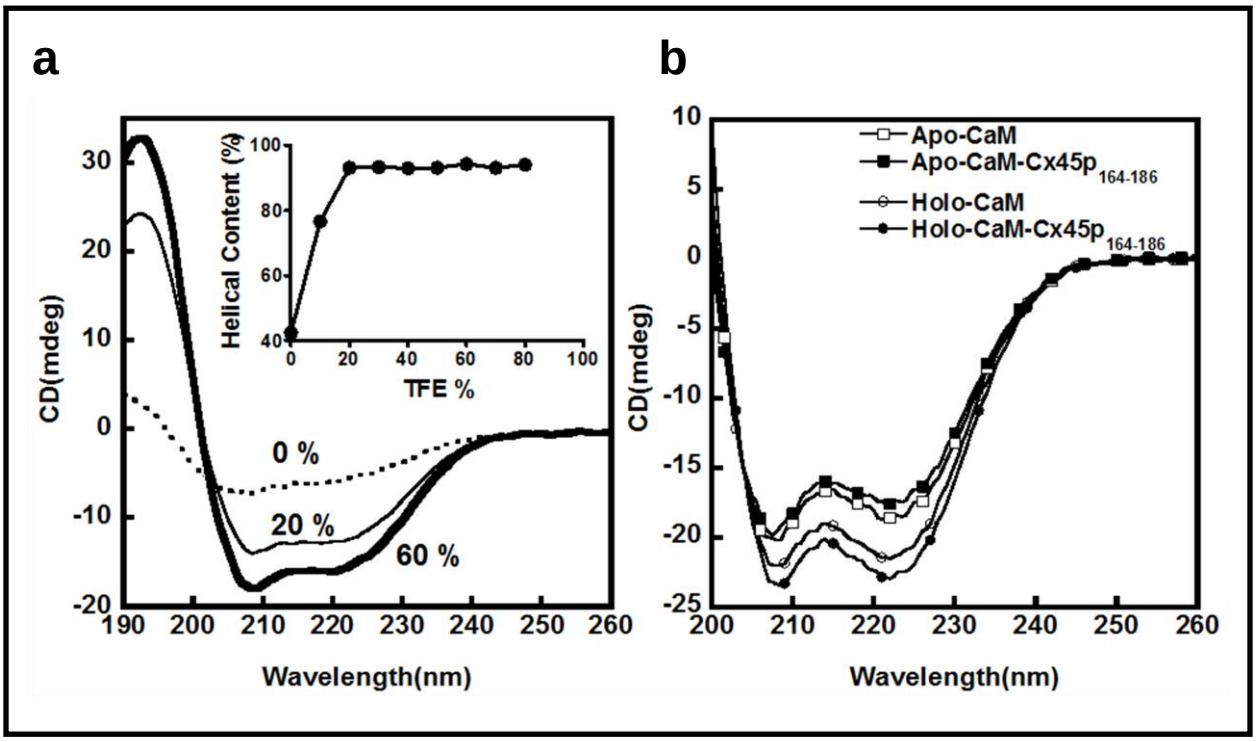

Figure 3.5 Revealing CaM-peptide interaction with CD spectroscopy.

(a) Far UV spectra of Cx45p$_{164-186}$ were obtained in the presence of 0% (dotted line), 20% (thin solid line) and 60% (bold solid line) TFE (v/v). (b) Far UV circular dichroism spectra of CaM in the presence of 5mM EGTA (□) or CaCl2 (○) and a 1:1 CaM/Cx45p$_{164-186}$ complex with 5mM EGTA (■) or CaCl2 (●).

3.2.4 Fluorometric Measurements with Dansyl-CaM

To evaluate the binding affinity of Cx45 peptide with CaM in solution, we measured changes in the fluorescence emission spectrum of dansyl-CaM (D-CaM). The dansyl emission spectrum is greatly sensitive to the local environment. The intensity is enhanced when dansyl is

exposed to a more hydrophobic environment. The maximum emission window of dansyl moiety is around 500 nm, which is far away from the emission of intrinsic aromatic residues. Thus dansyl derivate, with negligible interference from intrinsic aromatic residues, is an ideal tool to detect conformational changes as a result of protein-ligand interactions (385,435,436). The emission of D-CaM shifts from 520 nm to 500 nm when binding with Ca^{2+}. This blue shift can be interpreted as a consequence of Ca^{2+}-induced conformational change of CaM. In the presence of Ca^{2+}, addition of Cx45 peptide further enhanced the intensity of D-CaM and shifted the emission peak to be lower than 500 nm, whereas the peptide was completely ineffective when Ca^{2+} was absent. Together, the data imply that the interaction between D-CaM and Cx45 peptide is in a Ca^{2+}-dependent manner. Figure 4.6 shows the fluorescence emission of D-CaM incubated with increasing amount of Cx45 peptides. The fluorescence enhancement was plotted against the concentration of D-CaM (**Figure 3.6a**). The data points were fit with 1:1 binding model, yielding a *K*d of 5.0 ± 0.6 nM.

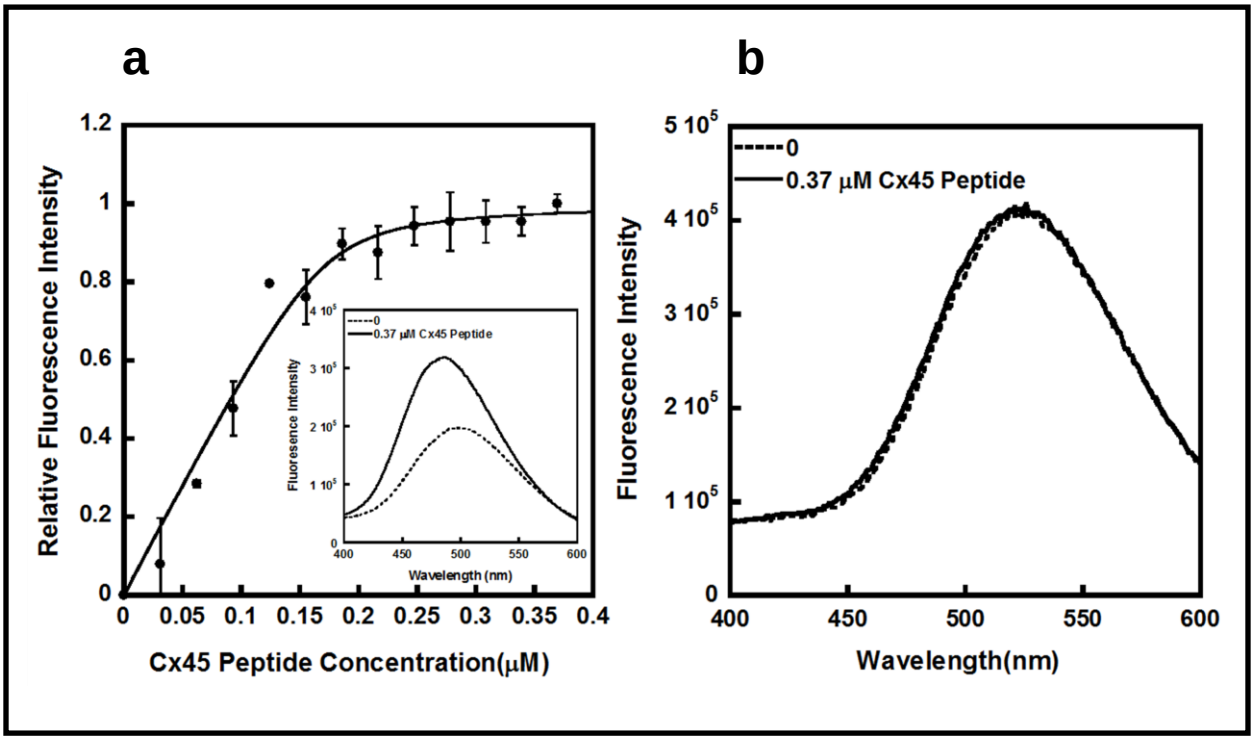

Figure 3.6 Steady-state fluorescence studies of interaction between D-CaM and Cx45p164-186. **(a) The titration curve of D-CaM (0.25μM) with $Cx45p_{164-186}$ in the presence of 5mM Ca^{2+}. The fluorescence spectra of D-CaM with (solid line) or without $Cx45p_{164-186}$ (dotted line) were shown in the inset. (b) The fluorescence spectra of D-CaM (1μM) with varying concentrations of $Cx45p_{164-186}$ in the presence of 5mM EGTA. All experiments were repeated in triplicate.**

To probe which domain of CaM contributes more to the $Cx45p_{164-186}$ binding, we also carried out titrations of $Cx45p_{164-186}$ to dansylated CaM half domains (D-N-CaM and D-C-CaM) with EGTA or Ca^{2+} respectively. Addition of increasing amount of Cx45 peptide to D-N-CaM resulted in fluorescence intensity enhancement accompanied by peak shift in the presence of Ca^{2+}, but not the D-C-CaM. Affinity calculation yielded K_d value of ~2.4 μM, which indicates the binding of Cx45 peptide to the N-domain of CaM is much weaker once C-domain is missing. No Cx45 peptide induced fluorescence change of D-N-CaM was detected when 5 mM EGTA was added. These results are consistent with our NMR studies. No significant fluorescence change of D-C-CaM was detected when incubation with various concentrations of Cx45 peptide. It is tempting to speculate that C-domain of CaM alone may not interact with CaM. However, it is impossible to get rid of the possibility that the fluorescence spectroscopy is not sensitive enough to capture the tiny change caused by interaction.

3.2.5 Surface Plasmon Resonance

The interaction between CaM and the Cx45 peptide was further investigated by surface plasmon resonance (SPR) assay using BIAcore 2000 sensor technology. The Cx45 peptide was immobilized to a CM5 sensor chip. In contrast with the above fluorometric measurement, SPR

allows real-time and label-free detection of biomolecular interactions. In some cases, chemical modification of CaM may hinder its binding to the partners. SPR can reduce the risk that labeling may bring. No significant binding was observed between CaM peptide and the chip surface. Figure 3.7 shows the rapid and reversible association of CaM to Cx45 peptide in the presence of 5 mM Ca^{2+}, but not in the presence of 5 mM EGTA. Rapid dissociation was also observed when using CaM-free buffer to wash the chip. The binding constants for Cx45 peptide are 21μM. The binding constants determination was obtained after subtraction of the reference and the buffer signals. These observations further illustrate that the interaction between CaM and Cx45 is Ca^{2+}-dependent, strong and specific.

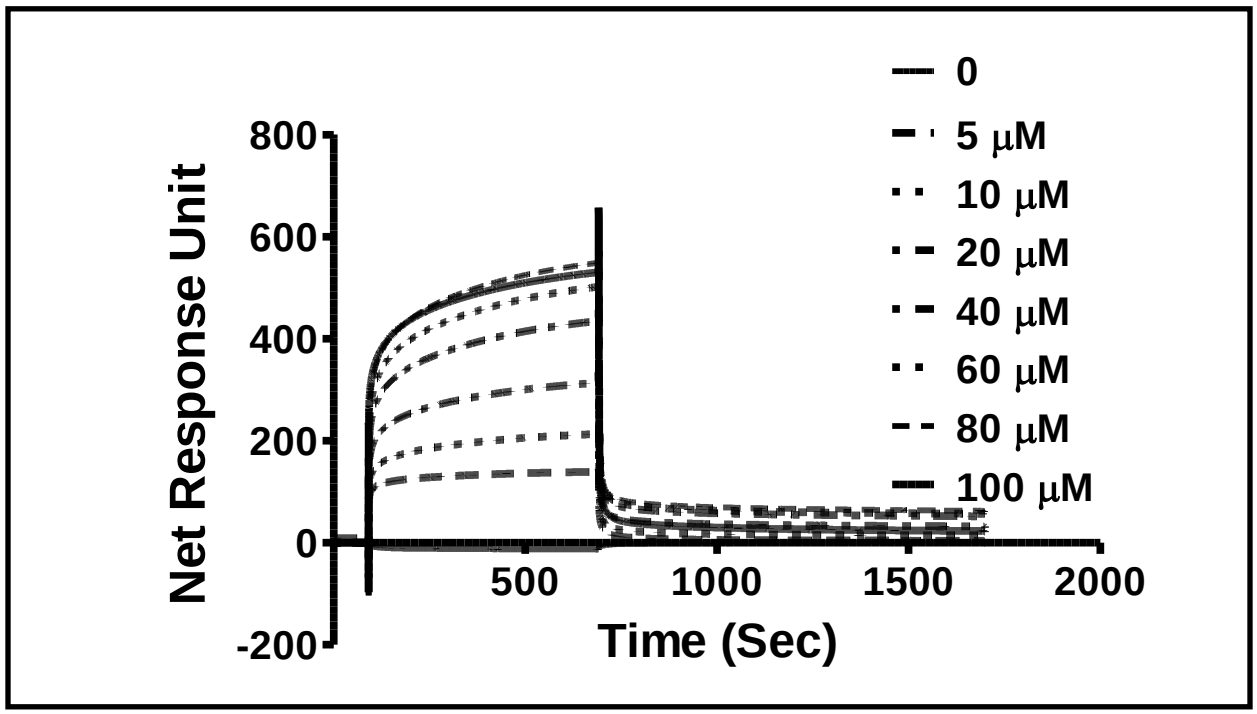

Figure 3.7 SPR analysis of Cx45p$_{164-186}$ and CaM interaction.

The response unit was recorded with Cx45 peptide immobilized on CM5 sensor chip in Ca^{2+}-supplemented condition using a sensitivity enhanced BiAcore T100 SPR system. The concentrations of CaM were 5-100 μM.

Table 3.4 Binding kinetics determined by SPR.

K_{on} ($M^{-1}S^{-1}$)	K_{off} (S^{-1})	K_d (M)
335.4	0.0071	2.117e-05

3.2.6 Ca^{2+}-dependent specific interaction between Cx45p and CaM revealed by NMR

Interaction between CaM and the Cx45 peptide was first examined by mass spectrometry. A 19.69 kDa complex formed by CaM and Cx45 peptide in the presence of 5 mM Ca^{2+} was detected by MALDI (**Figure 3.8a**). The theoretical molecule weight of the CaM-Cx45p complex is around 19.59 kDa, which is extremely close to 19.69 kDa. No such a complex was detected when incubation was in 5 mM EGTA (**Figure 3.8b**).

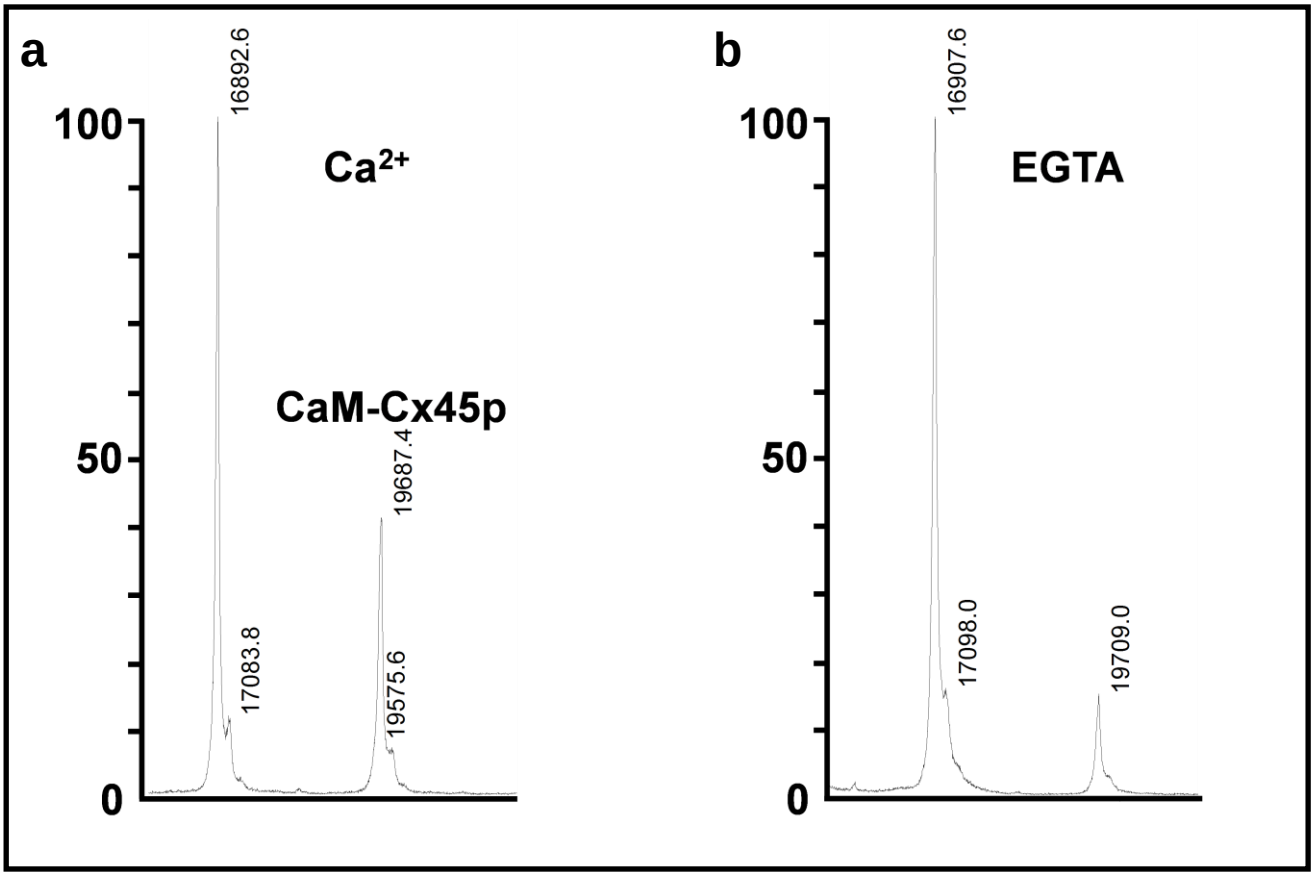

Figure 3.8 Monitoring CaM-Cx45p$_{164-186}$ complex formation by MS.

(a) The MALDI-MS spectrum of the free form of CaM and the CaM-Cx45p$_{164-186}$ complex formed in the presence of Ca^{2+}. (b) In the presence of EGTA, free form of CaM and around 10 % of CaM-Cx45p$_{164-186}$ complex were observed in the MS spectrum.

To further identify the direct Ca^{2+}-dependent interaction and residue-specific alteration, (1H, 15N) HSQC experiment was performed. Unlabeled Cx45p was gradually added into ^{15}N-labeled CaM in the presence of 5mM EGTA or 5mM Ca^{2+}. Significant chemical shift changes were observed in the HSQC spectrum of holo-CaM (**Figure 3.9a**), while spectra of apo-CaM with or without Cx45p were overlapping with each other (**Figure 3.9b**). This further confirmed that the interaction between CaM and Cx45 peptide is in a Ca^{2+} dependent manner.

A global conformation change has been captured by HSQC during the formation of Ca^{2+}/CaM-Cx45p complex (**Figure 3.9c**). Residues at the N- or C-domain or the linker region exhibited chemical shift changes greater than 0.05 ppm. However, the overall change of the N-lobe residues (4.68 ppm) was greater than in the C-lobe residues (2.30 ppm). The weight average chemical shift change was plotted as a function of residue number in Figure 4.8. In the NMR titration spectra, simultaneous appearance of two peaks representing the same residue was observed. This progressive disappearance of the amide signal from a specific amino acid was representing unbound form of CaM, being accompanied by the concomitant emergence of a new set of peaks from the Cx45p-CaM complex. This slow exchange phenomenon can be explained by slow exchange rate of the bound and unbounded status and often appears when this rate is slower than the amide frequency difference, indicating a submicromolar strong protein-peptide interaction (156,437).

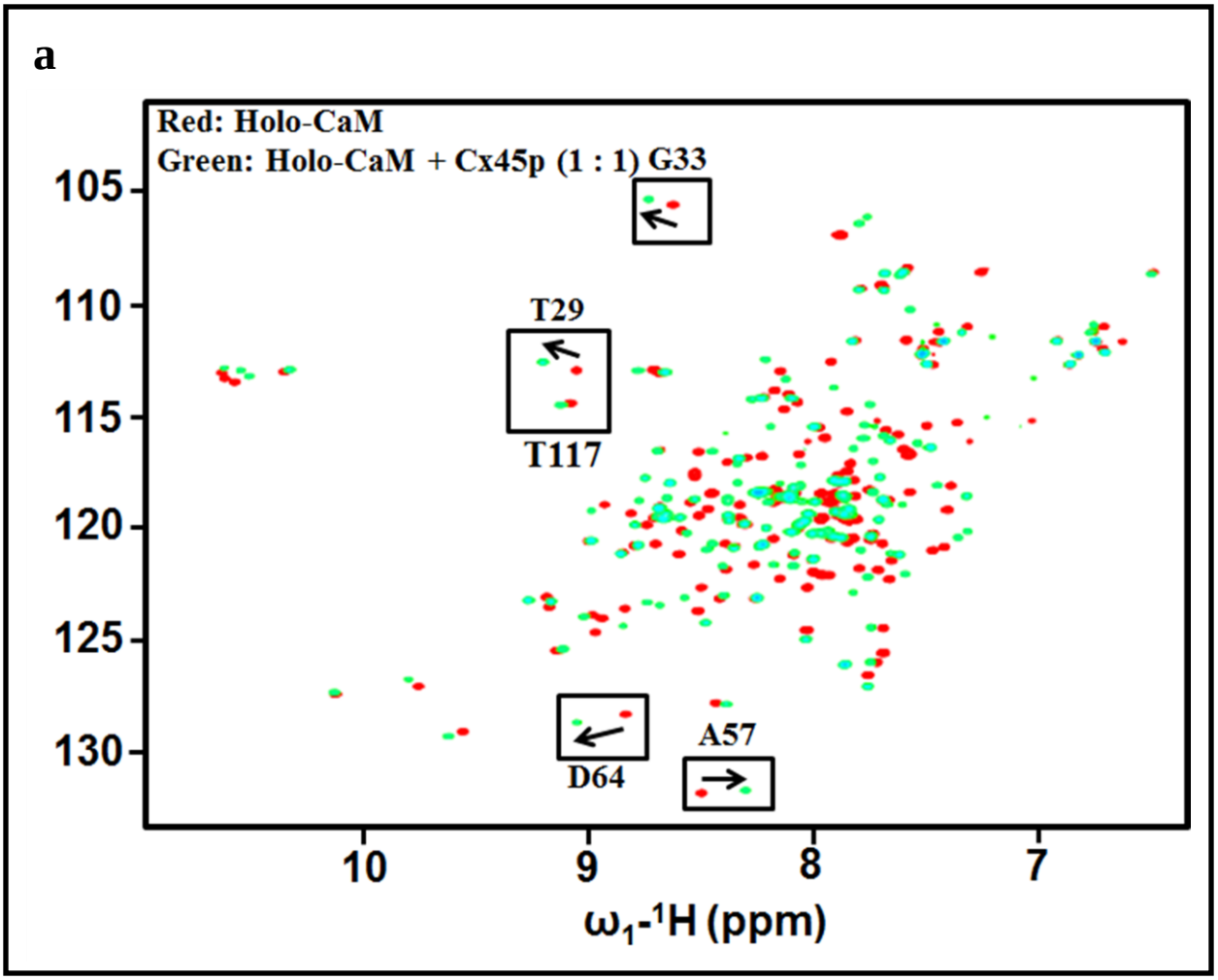
a
Red: Holo-CaM
Green: Holo-CaM + Cx45p (1 : 1)
G33
T29
T117
D64
A57
105
110
115
120
125
130
10
9
8
7
ω1-1H (ppm)

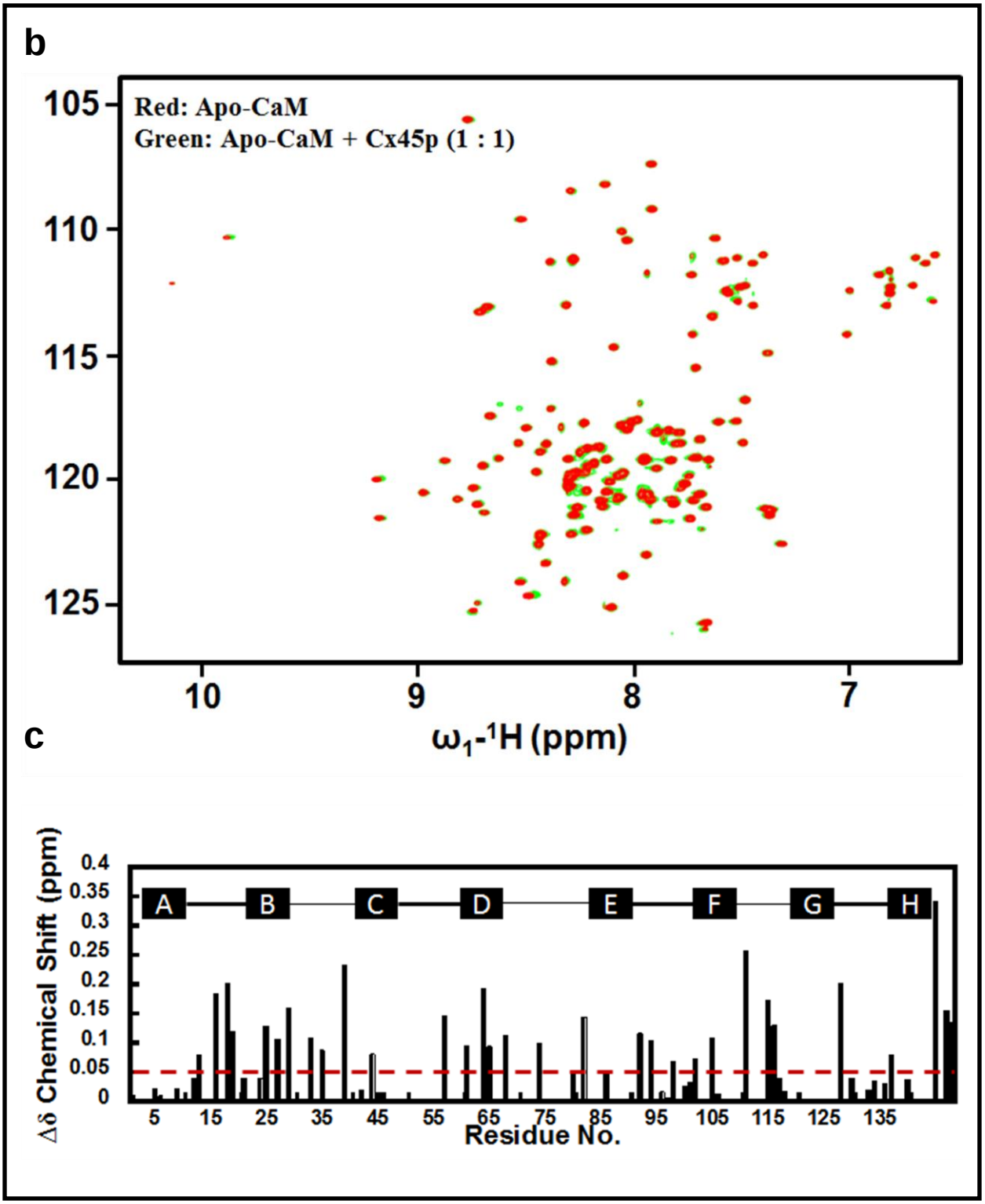

Figure 3.9 NMR studies characterizing the residues of CaM affected upon Cx45p$_{164-186}$ binding.

(a) Overlay of HSQC spectra of holo-CaM (red) with the spectra of holo-CaM-Cx45p$_{164-186}$ complex (green). Framed box highlight residues displaying significant chemical shift changes. (b) Overlay of HSQC spectra of apo-CaM with the spectra of apo-CaM-Cx45p$_{164-186}$ mixture. (c) Chemical shift changes in CaM induced by addition of 2-fold molar excess of Cx45p$_{164-186}$.

3.2.7 Calcium equilibrium titration

To examine whether Cx45p$_{164-186}$ contributes to the calcium binding affinity of CaM, calcium binding affinity of both N- and C-domain of CaM was determined by monitoring the intrinsic fluorescence intensity change of Phe and Tyr respectively. Binding of Ca^{2+} to the N-domain (Site I and II) induced the decrease of Phe fluorescence intensity in the absence of Cx45p$_{164-186}$ (**Figure 3.10**). The Phe fluorescence intensity upon addition of Ca^{2+} was plotted as a function of free calcium concentration determined by calcium indicator Oregon Green 488 BAPTA-5N and fitted by Hill equation. In the presence of Cx45p$_{164-186}$ (molar ratio of CaM: Cx45p$_{164-186}$=1:1.2), the K_d decrease from 11 to 0.7 μM indicated that calcium binding affinity to N-domain of CaM was significantly enhanced (**Figure 3.11 and Table 3.5**).

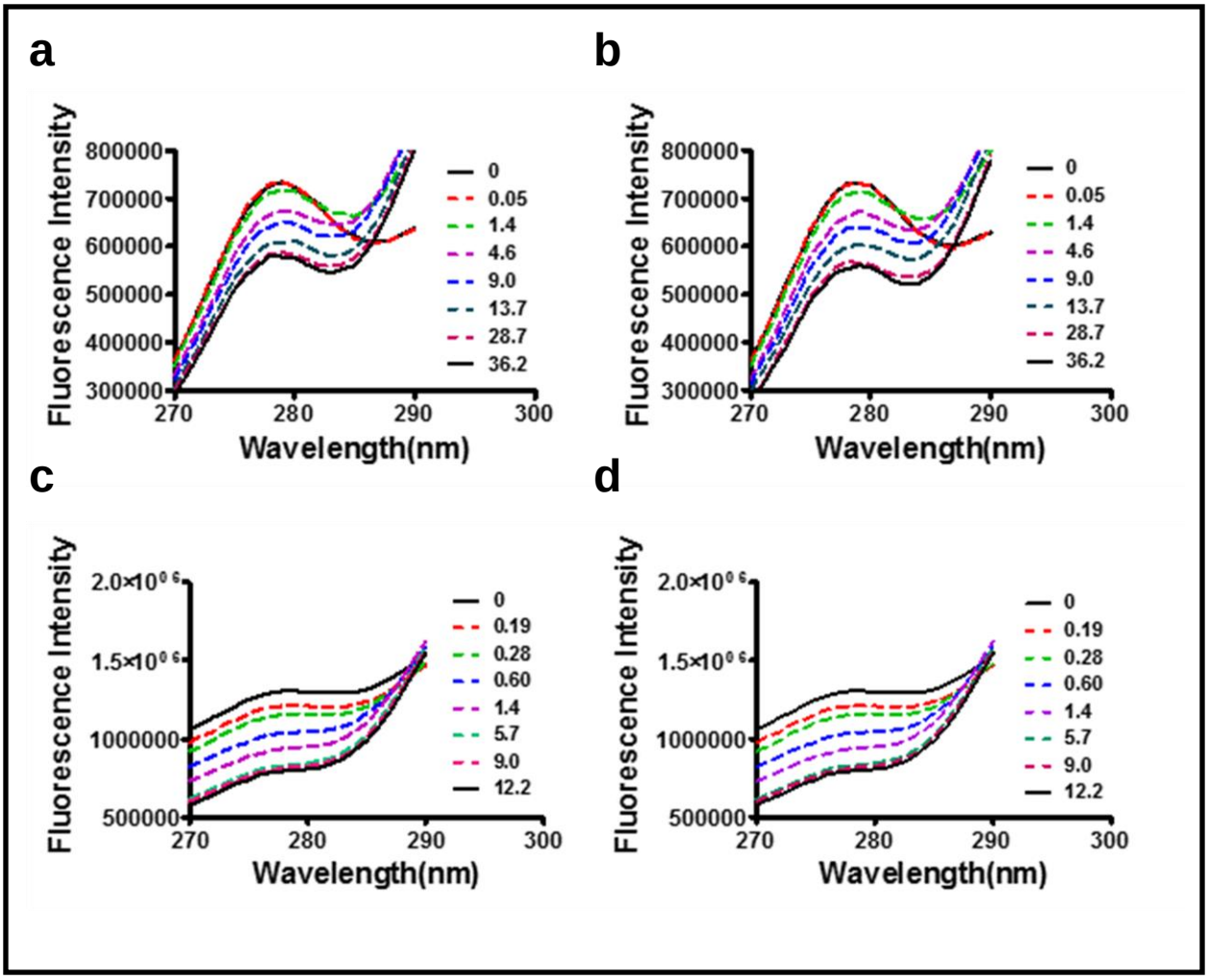

Figure 3.10 Changes in CaM Phe-fluorescence emission spectra upon addition of Ca^{2+} in the absence (a and b) or presence of $Cx45p_{164-186}$ (c and d).

8 µM CaM prepared in 50 mM HEPES, 100 mM KCl, 5 mM NTA and 0.05 mM EGTA was gradually saturated by titrating Ca^{2+} in, with the decrease of Phe fluorescence intensity. Phe fluorescence emission at 279 nm was plotted as a function of wavelength.

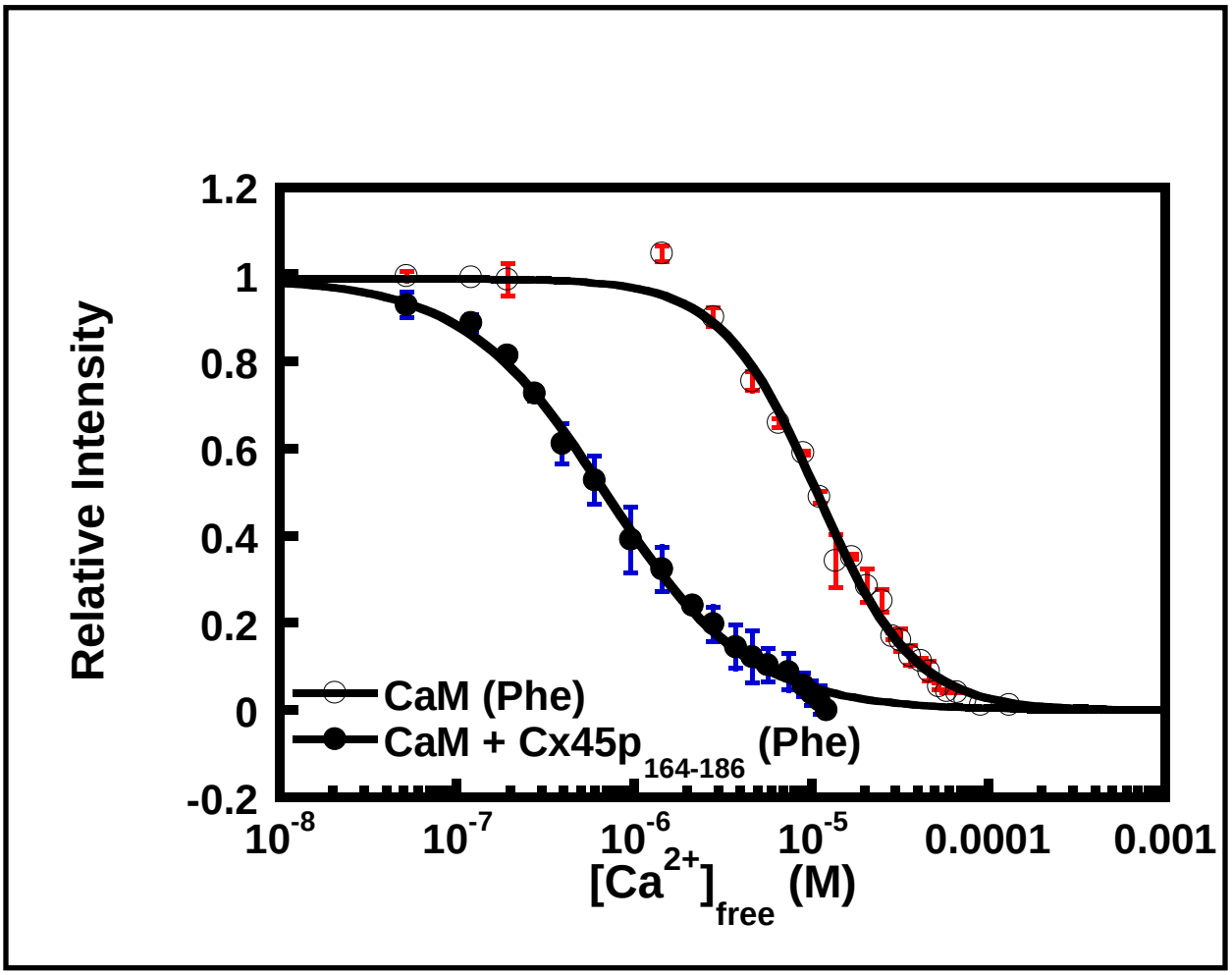

Figure 3.11 Equilibrium calcium titrations of CaM with (solid cycles) or without (open cycles) $Cx45p_{164-186}$ by monitoring Phe fluorescence emission.

Free calcium concentration was determined by calcium indicator Oregon Green.

Enhancement of Tyr fluorescence intensity was used to determine the Ca^{2+}-binding affinity of C-domain of CaM (**Figure 3.12**). The Ca^{2+}-dependent Tyr fluorescence increase was fitted using Hill equation. Addition of excess of $Cx45p_{164-186}$ to the CaM shifted the Ca^{2+} titration saturation curve to the left and the binding affinity was increased by 1 fold (**Figure 3.13 and Table 3.5**).

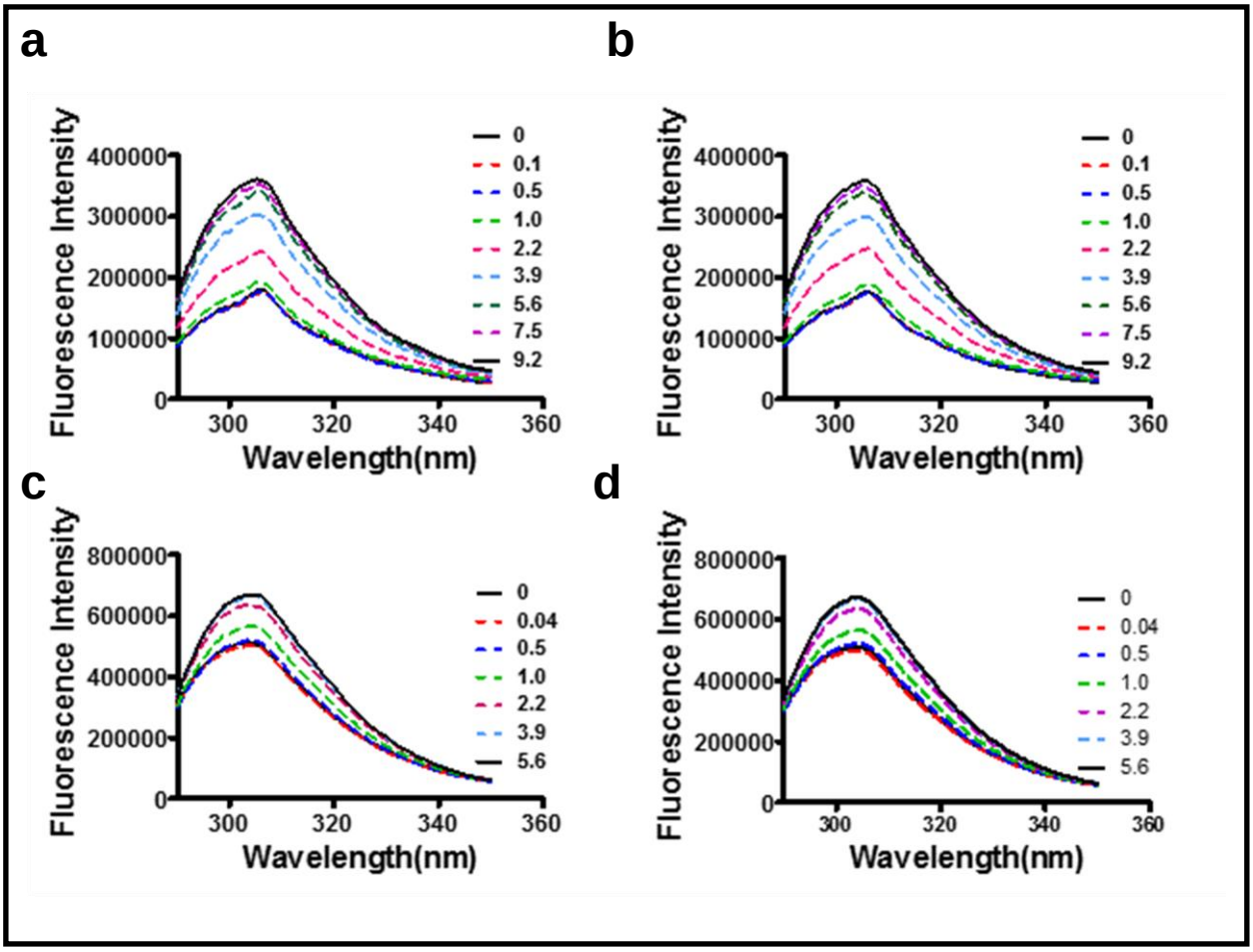

Figure 3.12 Changes in CaM Tyr-fluorescence emission spectra upon addition of Ca^{2+} in the absence (a and b) or presence of $Cx45p_{164-186}$ (c and d).

8 µM CaM prepared in 50 mM HEPES, 100 mM KCl, 5 mM NTA and 0.05 mM EGTA was gradually saturated by titrating Ca^{2+} in, with the increase of Tyr fluorescence intensity. Tyr fluorescence emission at 306 nm was plotted as a function of wavelength.

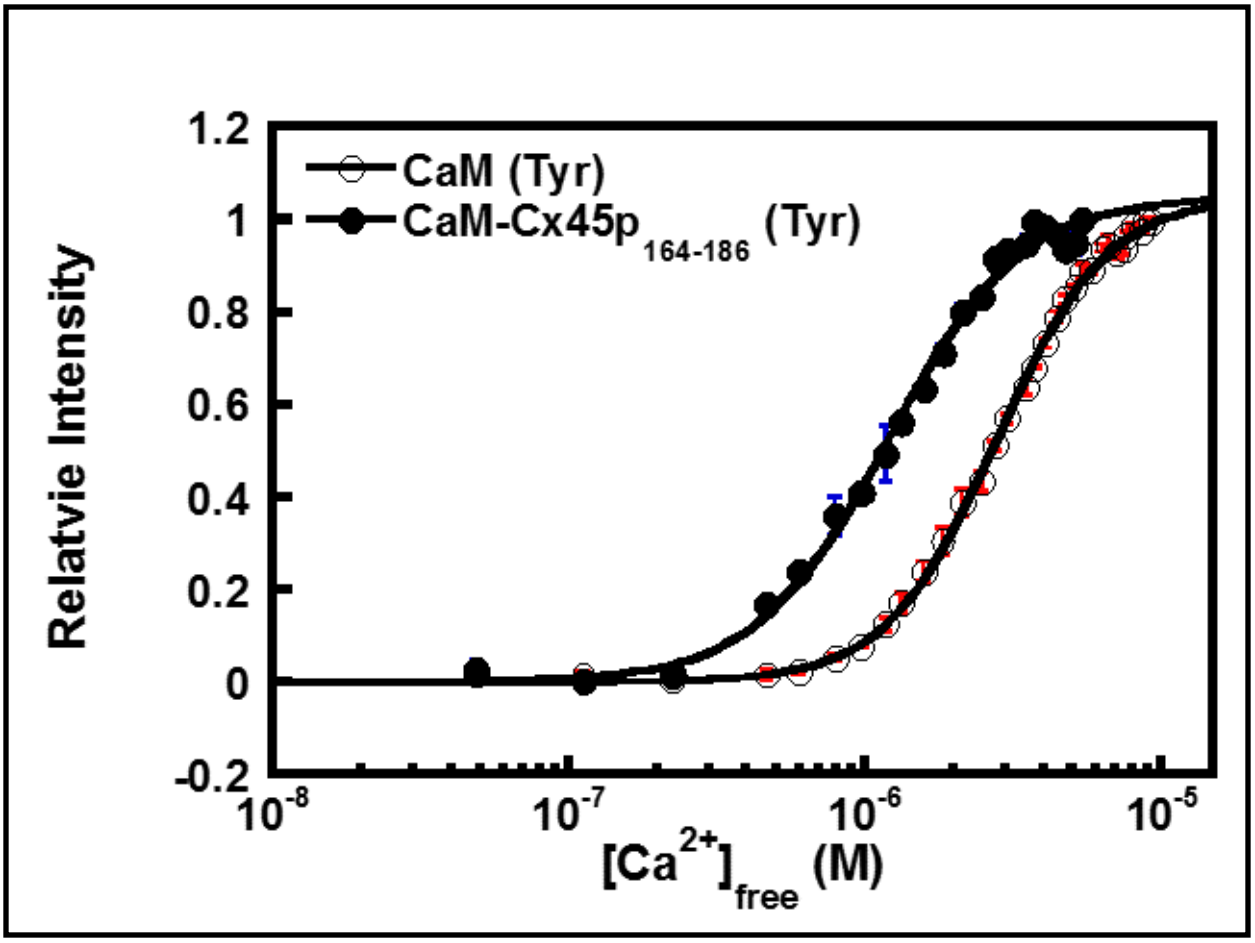

Figure 3.13 Equilibrium Calcium titrations of CaM with (solid circles) or without (open circles) Cx45p$_{164-186}$ by monitoring Tyr fluorescence emission.

Free calcium concentration was determined by calcium indicator Oregon Green.

These data together demonstrate that Cx45p$_{164-186}$ reduced the K_d of Ca^{2+} to both domains of CaM and enhanced the calcium binding affinity of both the N- and C-domain of CaM.

Table 3.5 Effects of $Cx45p_{164-186}$ Binding on the Ca^{2+}-binding Properties of CaM.

	N-domain		C-domain	
	K_d(μM)	Hill	K_d(μM)	Hill
CaM	**11 ± 0.003**	**1.6 ± 0.07**	**2.8 ± 0.002**	**2.3 ± 0.03**
CaM-Cx45p	**0.7 ± 0.002**	**1.0 ± 0.03**	**1.2 ± 0.002**	**1.9 ± 0.06**

3.2.8 Probing the CaM-Peptide complex state by diffusion NMR

Pulse-field gradient NMR was used to measure the self-diffusion rate of CaM or CaM-$Cx45p_{164-186}$ complex. The self-diffusion constant is larger for smaller molecules and less viscous solvents. Therefore, the size of CaM and $Cx45p_{164-186}$ complex can be calculated from the information acquired from self-diffusion rate. The diffusion constant for CaM and CaM-Cx45p was determined to be very close (**Figure 3.10**). The hydrodynamic radius of CaM (22.6 ± 0.6 Å) almost remained the same after formation of the CaM-Cx45p complex. Alpha family connexins previously studied by our lab all showed decrease in term of hydrodynamic radius, because a collapsed complex was formed to embrace the peptide. But in this case, Cx45 binding did not change the size. This result suggests the binding of Cx45p to CaM is different from that of alpha connexins-Cx43, Cx44 and Cx50.

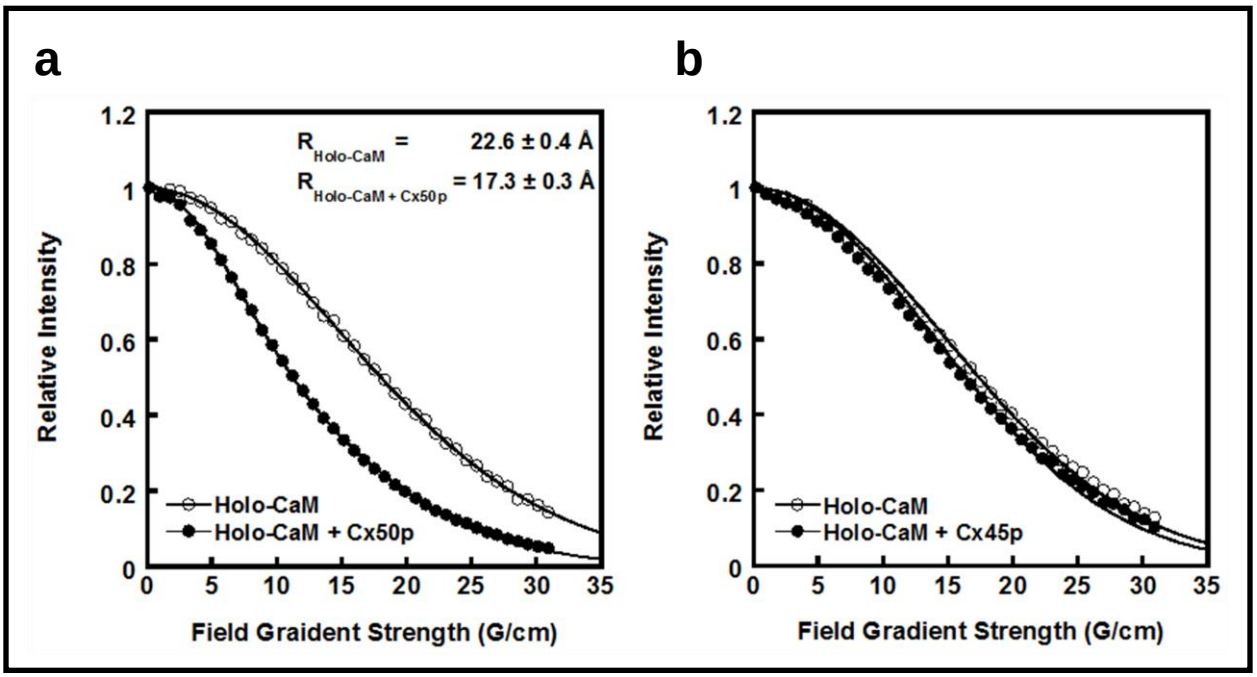

Figure 3.14 Determination of hydrodynamic of holo-CaM-Cx45p$_{164-186}$ complex using pulse-field gradient NMR.

(a) The NMR signal decay of holo-CaM (○) and holo-CaM-Cx50p (●) were plotted as a function of field strength. (b) The holo-CaM (○) NMR signal decay curve did not change upon the addition of Cx45 peptide (●), which indicates the hydrodynamic radius was not altered.

3.3 Discussion

3.3.1 The unique features of Cx45

In addition to the common characteristics shared by all connexins, Cx45 processes some unique features. To begin with, Cx45 has very small pore which only allow small molecules to pass through. The permeability of gap junction channels were examined using dye transfer in oocytes (438). The effective exclusion limits of gap junction channels formed by different

connexins ranks as following: Cx32 ≧ Cx43 >> Cx26 ≧ Cx40 ≈ Cx45≧ Cx37. This limited pore size restraints the application of some dyes in Cx45 formed gap junction channel study. For example, Lucifer yellow, which is widely used to study gap junction channel permeability in the field, showed restricted dye transfer to only 1 or 2 neighboring cells (439). We attempted to perform the dye scrape loading assay to investigate the function of Cx45 gap junction channels in the presence of different regulators, such as CaM inhibitors and Ca^{2+} chelators. However, the dye transfer between cells is hard to be detected. In our dye scrape loading assay, HeLa cells with stable expression of Cx45 were cultured to reach a very high confluence to ensure the formation of gap junction channels between neighboring cells. Different dyes such as Lucifer yellow (LY) (443 g/mol) and propidium iodide (PI) (668 g/mol) were tested and could not successfully pass through Cx45 gap junction channels. In addition to the size limitation, another reason accounting for the failure is that fact that Cx45 prefers positively charged species. Cationic probes such as NBD-m-TMA and ethidium bromide (EthBr) showed slightly higher permeability. Second, the intracellular Ca^{2+}-induced uncoupling of Cx45 gap junction channels are very slow when compared with Cx43 gap junction channels. Besides, only 80% of the conductance of Cx45 gap junction channels dropped when the conductance reached the plateau at the end. The reason behind this remains unclear.

3.3.2 Interaction of CaM with connexins

Our observed interaction of CaM provide the direct evidence to support the long standing hypothesis for the role of CaM in regulation of connexin channels proposed 35 year ago by Peraccia and co-workers (141). To test this hypothesis, they (440) reported the effect of the CaM inhibitor trifluoperazine (TFP) on the electrical coupling of amphibian embryonic cells. They subsequently applied more specific CaM blockers (calmidazolium and W7) to prevent uncoupling

of Xenopus embryonic cells (142) and crayfish axons (441,442), suggesting the generalized nature of CaM's role in regulating gap junctions. The gap junction protein Cx32 bound CaM was later shown in gel overlays (145-147). The suppression of CaM expression in oocytes can also inhibit CO_2 induced electrical uncoupling and injection of CaM into oocytes can recover it (148). Cx32 was also shown to colocalize with CaM using immunofluorescence microscopy (149). Later, Blodow *et al*. reported that CaM antagonists suppress gap junction coupling of Cx26 in isolated Hensen cells of the guinea pig cochlea (150). The effect of inhibiting CaM expression on CO_2-induced electrical uncoupling of Xenopus oocyte pairs expressing Cx45 demonstrated that both chemical and Vj sensitivities of Cx45 channels are reduced predominantly by inhibition of CaM expression oligonucleotides antisense to CaM mRNAs (158). To the best of our knowledge, all in cells experiments concerning the role of CaM in regulation of gap junction channels were collected by applying CaM inhibitors. The possibility in perturbing other multiple targeting processes by CaM inhibitors cannot be excluded due to the nature of such indirect assay. Largely due to challenges associated with membrane proteins and sensitivity of applied methods, the direct visualization of CaM in Connexins and Ca^{2+} dependence of this regulation in cells have yet to be achieved.

In this study for the first time, we report the direct interaction of CaM to Cx45 expressed in the HEK293 cells using BRET-based assay. BRET process, comprised of nonradioactive (dipole-dipole) transfer of energy from a donor enzyme to a suitable acceptor molecule after oxidation of substrate, has been applied to study many proteins in various cellular compartments, from G protein–coupled receptors (GPCRs) (443-445) to nuclear cofactors (446). In BRET, resonance energy transfer efficiency depends on several factors based on the Förster rate equation, such as donor lifetime, distance between donor and acceptor, relative orientation and degree of

spectral overlap (447) and this technique overcomes problems such as photobleaching, autofluorescence and simultaneous excitation of both donor and acceptor fluorophores (447). The advantage of BRET over FRET is that no external excitation is required, thus photobleaching and autofluorescence which are common problems seen in FRET assay. Compared with co-immunoprecipitation experiment, BRET can avoid the detergent solubilization. On the other hand, the disadvantages of BRET assay is also quite clear. Firstly, the fusion donor and acceptor should not severely affect trafficking and function of target proteins. To successfully perform the BRET assay, the interaction site cannot be disrupted by the tags and the ER retention of fusion proteins cannot occur. When generating the fusion protein constructs, the proper location of Venus and luciferase has to be tested. Second, the donor over acceptor ratio need to be optimized. In order to capture all the emission from donor, the acceptor amount needs to over the donor fusion protein to completely statured the donor. However, when expressing those exogenous fusion proteins, the expression level needs to low enough for physiological relevance. All those steps are time-consuming. We have shown that the interaction between CaM and Cx45 can be monitored by tagging YFP (Venus) at either end of CaM. Such BRET ratio can be completely eliminated by either addition of CaM inhibitor W7 or removal of intracellular calcium using BAPTA (~ 0.27 nM). It is interesting to note that the detected BRET ratio for CaM-Cx45 complex in HEK293 cells is about half of the max value in the presence of excess calcium with ionomycin. It is strongly calcium dependent. Such strong calcium dependent result suggests that CaM is well sit at the sensitive status to readily regulate Cx45 upon any changes of cellular conditions.

3.3.3 Key factors in CaM contributing to interaction with Cx45p$_{164-186}$

Using fluorescence spectroscopy, we have demonstrated that Cx45p$_{164-186}$ binds to wild type CaM with the K_d of 5.0 ± 0.6 nM in the presence of Ca^{2+}. Compared to dissociation constants

of different connexins from the same family (γ family) that has been previously reported (160), $Cx45p_{164-186}$ which covers the intercellular loop has stronger binding affinity for CaM than high-affinity sites of C-terminal domains in Cx34.7 (K_d = 29 ± 2 nM), Cx35 (K_d = 72 ± 9 nM), and Cx36 (K_d = 11 ± 3 nM) in the presence of Ca2+. Comparison between $Cx45p_{164-186}$ and connexins from α family also suggest that the binding affinity of this peptide is stronger than $Cx43p_{136–15}$ (860 ± 20 nM) and $Cx44p_{132–153}$ (49 ± 3.0 nM) and similar to $Cx50p_{141-166}$ (4.9 ± 0.6 nM) which is also in the presence of Ca^{2+} (448). In addition, $Cx45p_{164-186}$ binds much stronger to CaM than the N-terminal domain (K_d = 27 nM) and C-terminal region (K_d = 1200 nM) of Cx32 from the β family (160).

The stronger binding affinity of $Cx45p_{164-186}$ compared to other connexins may originate at least in part from the relative helical content of the peptide in solution without formation of complex with CaM as shown by CD spectroscopy (Fig x). Such strong helical content is much greater than connexins from alpha-family Cx50, Cx44 and Cx43. On the other hand Cx50, Cx44 and Cx43 exhibit 94, 55 and 33% helical conformation, respectively in the presence of 30%TFE (121). Cx45 has also demonstrated to have the highest α-helical content induced by TFE and is similar to Cx50 indicating that the intrinsic helicity of the peptide may also contribute to this strong binding affinity of Cx45. Such observation is consistent with previous report that CaM binds to various target proteins whose binding domains have strong α-helical propensity (429). CaM can also bind with high affinity to a relatively small α-helical region of many target proteins (28).

We have identified a CaM-binding motif from residues 164 to 186 (GRRRIREDGLMKIYVLQLLARTV) in Cx45 which follows the IQ motif pattern in a more generalized form ((FILV)Qxxx(RK)xxxxxxxx). To the best of our knowledge, we have reported the first Ca^{2+}-dependent gap junction regulation by CaM via IQ motif. The conventional complete

IQ motifs represented by sequence (IQXXXRGXXXR) primarily associate with CaM in a Ca^{2+}-independent manner. The nature of this Ca^{2+}-independent interaction has been extensively investigated in myosin. One of the important characteristic of the IQ motif is that it binds relatively tightly to CaM at basal levels of intracellular calcium and the interaction changes when calcium levels are increased (449) (39). However, in some instances, IQ motif-containing proteins (including utrophim, Ras GRF1, Nina C myosins and other proteins) have been reported to bind CaM in a Ca^{2+}-dependent manner. In those proteins, CaM can maintain its interaction with the IQ domains both in the presence or absence of Ca^{2+} with dissociation constants ranging from sub-nanomolar to micromolar levels, however, the IQ-motif-binding affinity of CaM varies with the Ca^{2+} concentration and the particular IQ motif in the target protein (28). It is also revealed that Ca^{2+}-free CaM interact with IQ motif through the C lobe (450) while Ca^{2+}-loaded CaM utilizes both N- and C-domain (451). The IQ motif identified in Cx45 cytosolic loop is not a complete IQ motif; instead it has only the first part of an IQ motif (IQXXXR). When bound with a complete IQ motif, the C-terminal lobe of CaM is estimated to be in a semi-open conformation, while the N-terminal lobe is in a closed conformation. In contrast, it is suggested that the N domain of CaM would adopt an open conformation when only the first part of IQ motif is present (452). The $Cx45p_{164\text{-}186}$ binding affinity to CaM is also comparable to other IQ motifs found in channel proteins. For example, the disassociation constant of neuronal voltage-dependent sodium channel type II IQ motif for interaction with CaM is reported to be less than 10 nM.

The CaM-binding affinity of Cx45 is similar to Cx50 and much higher than peptides derived from other α family connexins. The CaM-binding K_d ranks as following: Cx50p (4.9 nM) ≈Cx45p (5.0 nM) < Cx44p (49 nM) < Cx43p (860 nM). This order correlates well with the order of maximum helicity of those peptides formed in the presence of TFE (**Fig. 3.15a**). Many identified CaM target peptide initially are disordered and form α helices upon CaM-binding. Those peptide show high propensity of α helices formation when induced by TFE. In addition to the maximum helicity induced by TFE, it seems that intrinsic helicity also contributes to the CaM-binding affinity. CD result indicated that Cx45 has more intrinsic α helical content than Cx50 (**Fig. 3.15b**). This may explain why Cx45 has similar CaM-binding affinity than Cx50 though Cx50 peptide has higher maximum helicity than Cx45.

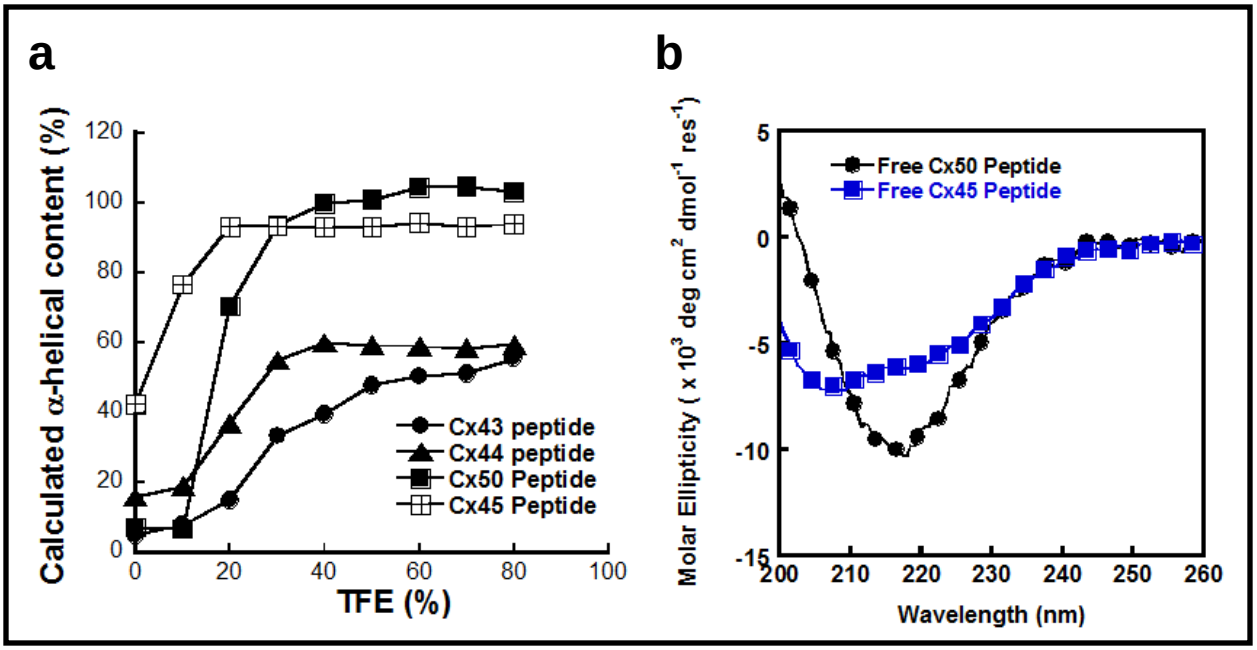

Figure 3.15 CaM-binding affinity correlated to connexin helicity.

(a) Maximum helicity of peptide derived from different connexins. Various percentages of TEF were added into peptide to induce the formation of secondary structure. The α helical content was revealed by CD. (b) The intrinsic helicity of Cx45 and Cx50 were measured by CD.

3.3.4 CaM uses different action mode to regulate different connexins

Structural characterization of CaM by NMR illustrated that in the Ca^{2+}-bound state (holo-CaM), CaM exists in a dynamic equilibrium of two major conformations, extended and semi-compact which it gives enough flexibility for CaM to bind targets in variably extended conformations and to form interdomain connections (453).Various target recognition modes have been attributed to CaM which can be classified into two general binding styles: extended and collapsed (449). Our previous pulsed field gradient NMR results showed that the dynamic radius of holo-CaM decreased significantly upon Cx50-derived peptide binding (121). As α family connexins, the CaM-binding site in Cx43, Cx44, and Cx50 follows the 1-5-10 binding motif, while the Cx45 seems utilize a different CaM-binding motif though the CaM-binding site locates at a similar position in both α and γ family connexins. Addition of Cx45-derived peptide to holo-CaM did not change the dynamic radius of CaM, which suggests CaM interacts with Cx45 in a more extended mode.

We also tried to compare the residues with chemical shift changes with other reported CaM-binding proteins. However, only a small portion of peaks (54 out of 148) can be assigned based on the previous published CaM NMR spectrum. Among them, only partial of them (31 out of 54) showed chemical shift changes. Some residues with significantly changes here also show chemical changes in CaM when interacting with targets with different binding motifs. Thus, more studies need to be perform to come out conclusions based on chemical shift changes.

3.3.5 Effects of $Cx45p_{164-186}$ on calcium binding

The Ca^{2+}-affinity of two domains of CaM can be differentially and dramatically affected by association with various target proteins, either enhanced by some targets (37,454-456) or decreased by other binding partners(426,457). Ca^{2+}-binding data measured in the presence and

absence of Cx45p$_{164-186}$ peptide indicates that addition of Cx45p$_{164-186}$ peptide to CaM increased the Ca^{2+}-binding affinity of both domain of CaM; however, the N-domain of CaM experienced a much greater dissociation constant decrease from 11 to 0.7 μM, a more than 10-fold drop. C-domain of CaM also experienced a relatively smaller dissociation constant change (from 2.8 to 1.2 μM) when Cx45p$_{164-186}$ peptide was applied. This result is well in agreement with the observations in HSQC. As shown in (1H, 15N) HSQC experiment, the overall chemical shift change in the N-lobe residues is greater than in the C-lobe residues which suggest that in the case of an incomplete IQ motif, the conformational change of the N-terminal lobe is higher than the C-lobe upon binding to Cx45p$_{164-186}$. The BRET signal for Venus attached to the N-terminal of CaM (Venus-CaM) slightly higher than CaM-Venus (Venus tagged to the C-terminal) also correlates with the (^{1}H, ^{15}N) HSQC experiment demonstrating higher chemical shift change in the N-lobe residues than in the C-lobe residues.

3.3.6 Implication for regulation of connexins

Based on our current result and previous published results, we hypothesize that Ca^{2+}/CaM binding to Cx45p$_{164-186}$ region induces a gating response that closes the Cx45 gap junctions and follows the gating mechanism of closure proposed by our lab in the past (416). Briefly, elevated $[Ca^{2+}]_i$ is firstly sensed by CaM and promotes interaction between CaM and CL domain of Cx45 to inhibit gap junction mediated intercellular communication. The gating mechanism behind this remains to be fully elucidated. It is possible that Ca^{2+}/CaM together with CL domain of Cx45 function as a “cork” to block the gap junction channel. Another alternative gating mechanism is that Ca^{2+}/CaM association with CL domain of Cx45 induced a conformational change of CL domain which then acts to occlude the cytoplasmic vestibule of Cx45 gap junction channel.

4 CX26 GAP JUNCTION HEMICHANNEL REGULATION BY EXTRACELLULAR CA^{2+}

4.1 Introduction

Human Cx26, coded by gene GJB2, belongs to beta family of gap junction. It widely distributes in human, including cochlea, skin, liver, placenta and breast. Cx26 is co-expressed with Cx30 in the inner ear (458,459), forming homo-or hetero-gap junctions in the cochlea. The gap junction channels in the cochlea play critical role in sound generating. During the sound transduction, the K^+ current flows through the organ of corti to the perilymph, generating the sound. Then this K^+ current is recycled back to the endolymph by gap junction. Mutations in Cx26 and Cx30 are known to be associated with deafness. According to a survey performed by Florida University, about 14% deafness is caused by Cx26 mutations. Now over 100 mutations in Cx26 have been identified to be linked with nonsyndromic sensorineural deafness.

Many of these syndromic deafness mutations localize to the amino-terminal and first extracellular loop (EL) domains. Studies of mutations in the EL using mammalian cells or oocytes revealed altered $[Ca^{2+}]_o$ regulation and permeability in Cx26 hemichannels formed by those mutations. It has been reported that G45E transfection to HeLa cells resulted in cell apoptosis and death within 24 hours of transfection (460). G45E transfection into *Xenopus laevis* oocytes led to huge hemichannel currents and cell lysis (461) (**Fig. 4.1**). Elevated concentration of $[Ca^{2+}]_o$ in the culture medium could rescue those aberrant hemichannels. It was proposed that Cx26

hemichannels formed by mutation G45E could not be properly regulated by $[Ca^{2+}]_o$ and those leaky hemichannel caused cell apoptosis and death. In the EL1, other mutations such as A40V, E47K, and D50N are also reported to show impaired channel permeability, altered $[Ca^{2+}]_o$ sensitivity and disturbed regulation by $[Ca^{2+}]_o$ (460,462,463).

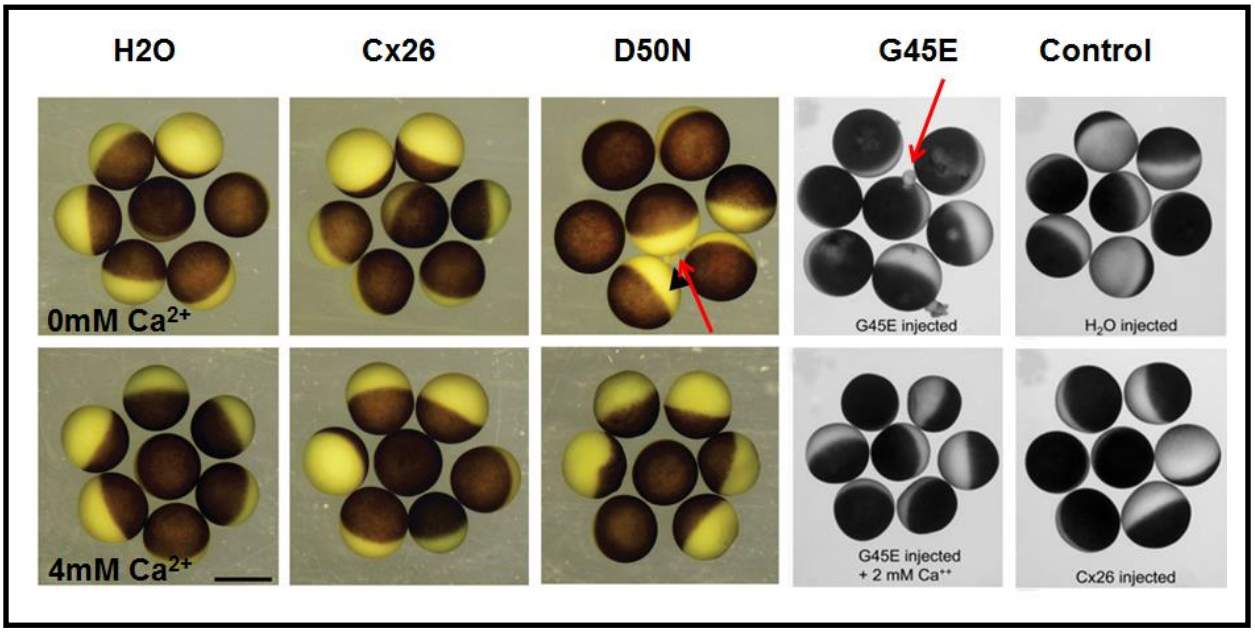

Figure 4.1 Hemichannel activity-dependent cell death can be rescued by elevated Ca^{2+}.

Wild type Cx26 or its mutant RNA was injected into oocyte for hemichannel expression on surface of oocytes. Both D50N and G45 caused early cell lysis as indicated by red arrow. Increase the concentration of $[Ca^{2+}]_o$ in bath solution could prevent oocyte "budding" and successfully rescued oocyte with mutants expression. Water injection was used as negative control.

It is well know that gap junction hemichannels are regulated by $[Ca^{2+}]_o$. However, the mechanism behind it is unclear. The available crystal Cx26 crystal structure when we started this

project is an open structure without any bound Ca^{2+} ions. Using our computational algorithm, we predicted one Ca^{2+} binding site formed by residues from EL1 and EL2. Interestingly, many mutation sites are in our predicted Ca^{2+}-binding site (**Table 4.1**). It is definitely not a coincidence since several functional studies have already revealed abnormal $[Ca^{2+}]_o$ regulation on mutants from the predicted Ca^{2+}-binding site.

Table 4.1 Disease mutations in the predicted Ca^{2+}-binding site.

	Calcium-binding	
	I	II
Possible Function	Hemichannel protection	Plaque formation
Locations	EL1	EL2
Involved Residues	E42, D46, E47, D50	N170, D179, E187
Deafness Mutations	W44C[2]/S[2], G45E[4], D46E[3], E47K[2], D50Y[1]/N[1,4], N54K[5], T55N[1], T55G[5]	P173R[1], D179N[1], W172R[2], P173S[5], K168R[5]

1. Mutations prevent the formation of gap junction channels.

2. Mutations do not affect formation of gap junction channels, but the mutated gap junction channels display null function.

3. Mutations specifically impair the gap junction channel-mediated biochemical coupling.

4. Mutations cause a gain-of-function effect due to abnormal hemichannel opening.

5. Mutations that have not been thoroughly studied in vitro.

Challenges associated with large mammalian membrane protein expression and purification also greatly hampered the study of Ca^{2+} regulation of gap junction channels. The

dodecamer of Cx26 gap junction is a 312 kDa eukaryotic oligomer on the cell surface. Lower host such as *E.coli* and yeast may not harbor the capability of handling the post-translational modification, trafficking, folding, and translocation of it. The extraction of this protein form higher host also brings another challenge for purification. How to preserve the native structure of this protein as much as possible during the detergent extraction and how to prevent aggregation after detergent extraction are all problems need to be addressed. Besides, the physiological extracellular Ca^{2+} concentration remains at mM level, which indicates that the Ca^{2+}-binding site in Cx26 are weak sites with mM Ca^{2+} binding affinity. How to directly monitor the fast on and off rate Ca^{2+} binding with Cx26 at molecular level present another big challenge in front of us. We need to establish direct methods which is sensitive enough to capture the interaction between Ca^{2+} and Cx26 proteins. All these challenges greatly hindered the study to understand the role of Ca^{2+} in Cx26 regulation and the molecular basis for related diseases.

In this chapter, I will report our effort in obtain purified membrane protein Cx26 using three different methods including animal tissue isolation, *E.coli* expression, and baculovirus expression system. After establishing high level expression of Cx26 and developing of purification method, the metal-binding properties of Cx26 and conformation change induced by metal-binding were also investigated using various spectroscopic methods. Cx26 hemichannel regulation by $[Ca^{2+}]_o$ was also probed using dye uptake assay in mammalian cells and using electrophysiological measurement in oocytes. I will summarize all work I have done on this project, and the advantages and limitations of methods used. Then I will report some new discovery about Ca^{2+} regulation in this filed recently in the discussion section.

4.2 Result

4.2.1 Ca^{2+}-binding site prediction and comparison with reported sites

The identification of putative Ca^{2+}-binding sites in Cx26 was performed using MUG^{SR}, a graph theory-based algorithm (464) developed by our laboratory in 2010. The Ca^{2+}-binding site was predicted based on the Cx26 crystal structure solved by Maeda (106). This predicted Ca^{2+}-binding site is located at the mouth of extracellular side of Cx26 gap junction channel (**Fig. 4.2 a**), comprising the carboxyl side chains of E42, D46, and E47 in the flexible extracellular loop 1, and E187 in the extracellular loop 2 (**Fig. 4.2 b**). E42, D46 and E187 are from one monomer, while E47 is from the adjacent monomer. This predicted Ca^{2+}-binding site is highly conserved in both α and β family connexins (**Fig. 4.2c**), suggesting this site plays important structural or functional roles even after the long evolution. A sequence alignment of bovine, sheep, rat, mouse and human Cx26 carried out using the Clustal Omega program (465,466) also reveals the predicted Ca^{2+}-binding site (highlighted in red) is identical in all species (**Fig. 4.3**).

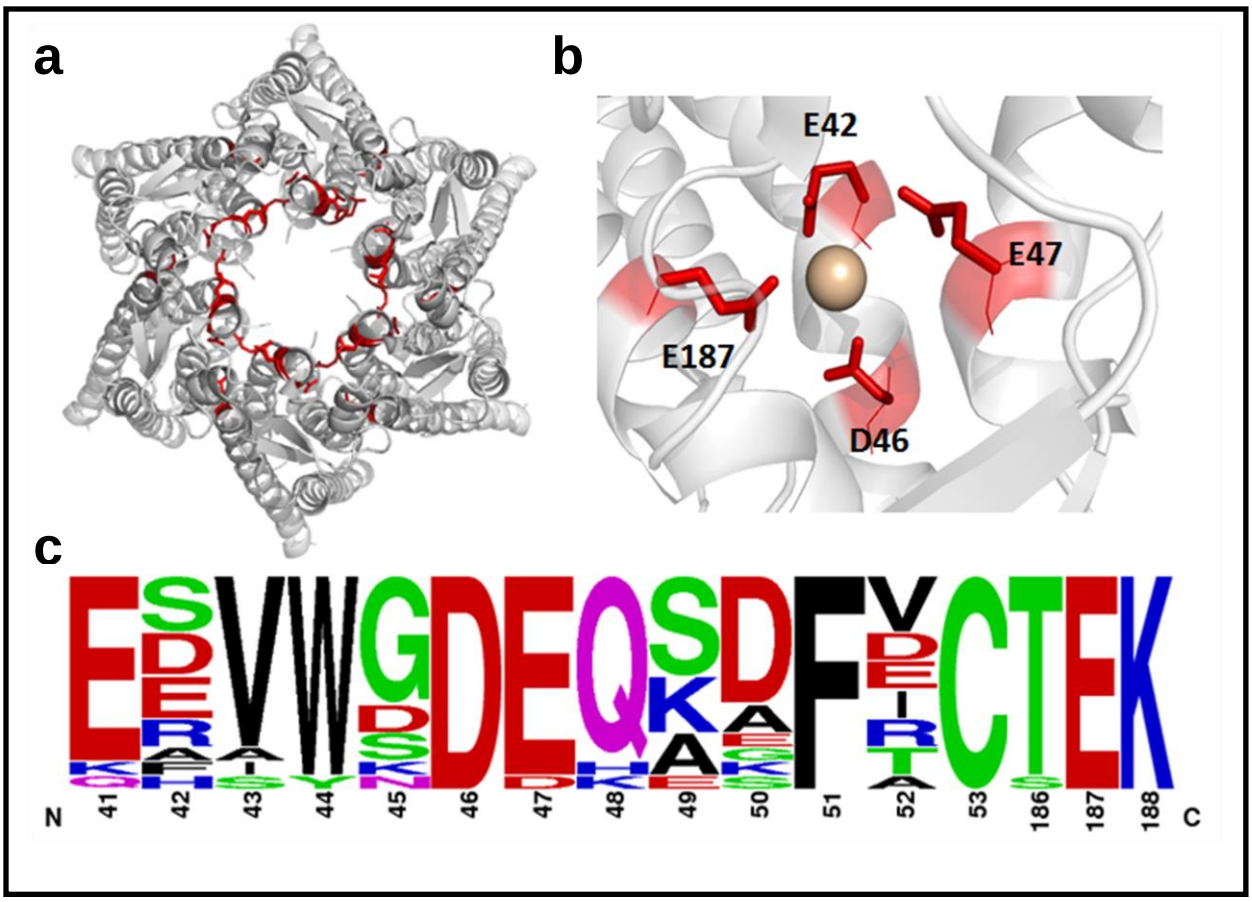

Figure 4.2 Prediction of a Ca^{2+}-binding site at the extracellular mouth of Cx26 gap junction channel.

(a) The putative Ca^{2+}-binding site resides at the extracellular mouth of Cx26 gap junction channel, formed by residues from extracellular loop 1 and loop 2. 6 Ca^{2+}-binding sites were depicted in red in one Cx26 hemichannel. (b) The predicted Ca^{2+}-binding site comprises by E42, D46, and E187 from one protomer, and E47 from the adjacent protomer. (c) Sequence alignment revealed that this predicted Ca^{2+}-binding site in all α and β connexins are very similar, especially D46, E47 and E187.

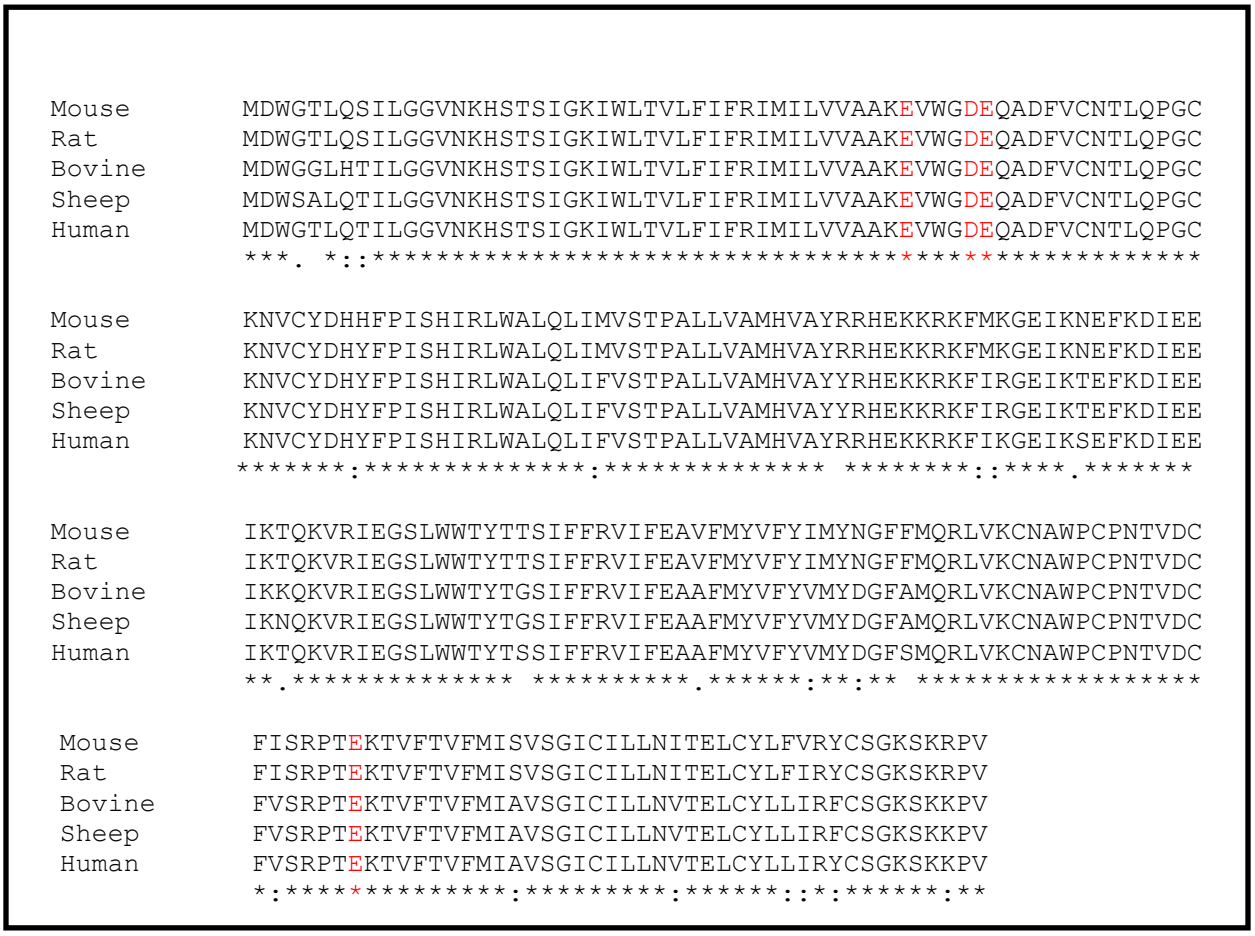

Figure 4.3 Sequence alignment of mouse, rat, bovine, sheep and human Cx26.

Mouse, rat, bovine, sheep and human Cx26 were aligned by Clustal Omega program. The putative Ca^{2+}-binding ligands (highlighted in red) are identical in all five species aligned here.

4.2.2 Cx26 isolation from pig liver

At our initial stage of gap junction study, we attempted to isolate Cx26 from pig liver and simultaneously to set up the insect cell expression system. Fresh pig liver was picked up in the

early morning from university of Georgia meat science technology center and frozen on dry ice. Small pieces of pig liver was homogenized manually by a glass homogenizer and connective tissue was discarded. Further plasma membrane enrichment was achieved by sucrose gradient ultra-centrifugation. Different percentages of sucrose formed sucrose gradient, in which sample with different density re-distributed into the corresponding sucrose layer with the same density. Non-gap junction membrane protein was extracted from the enriched plasma membrane by detergent or strong alkali since connexins have relative resistance to solubilization by nonionic detergents or to extraction with strong alkali. The rest plasma membrane enrichment was further separated by sucrose gradient ultra-centrifugation again. The brief isolation procedure was depicted in figure 4.4.

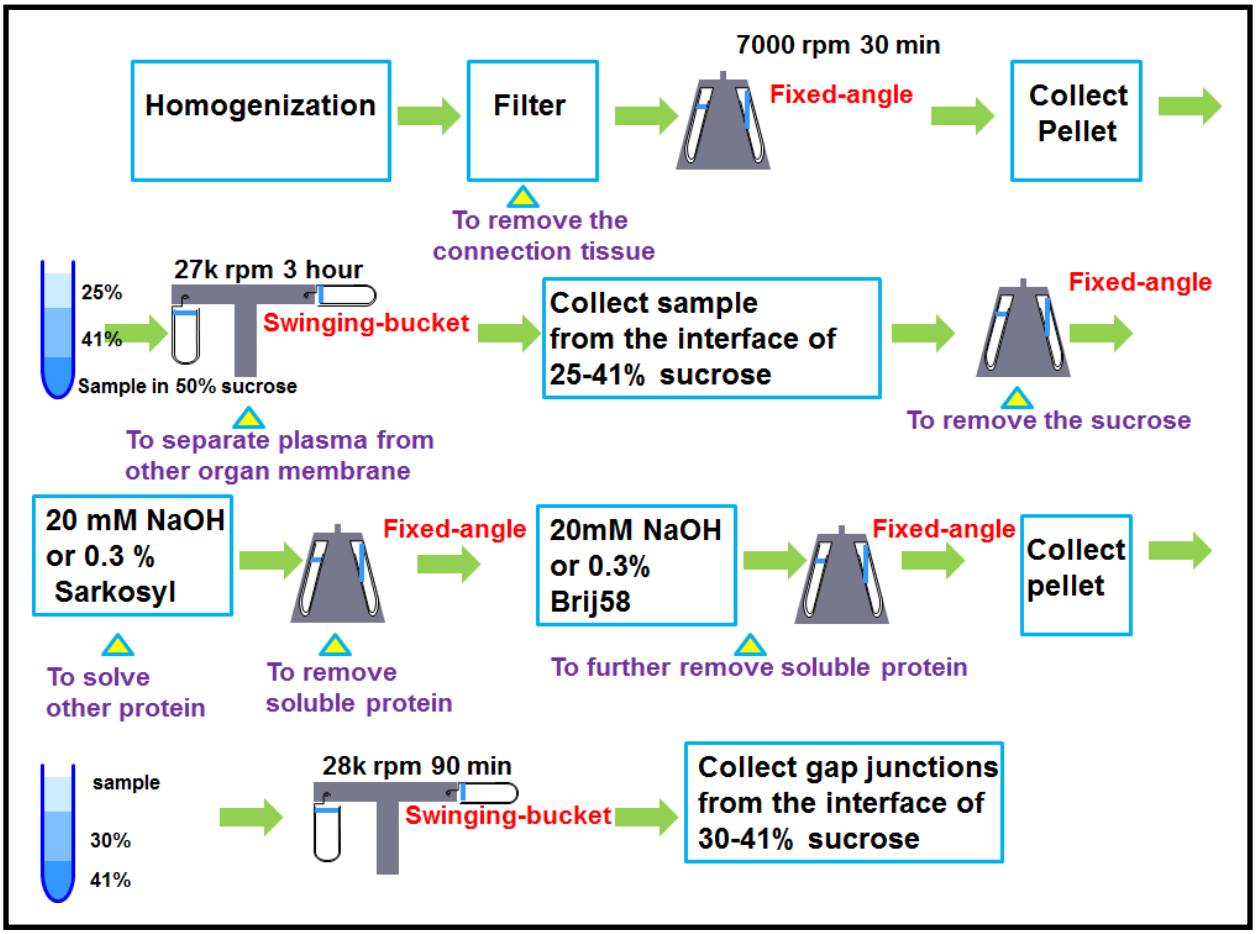

Figure 4.4 Brief procedure describing the isolation of Cx26 from pig liver.

Plasma membrane were enriched from the homogenized pig liver by sucrose gradient ultra-centrifugation. Non-gap junction protein were washed away be either strong alkali or detergent. The rest was further by sucrose gradient centrifugation or FPLC if large amount of liver was used.

To enrich the plasma membrane, we tried two different sucrose gradients (**Fig. 4.5**). In the first sucrose gradient, liver in 8.7 % sucrose sample was placed on the top of the centrifugation tube, followed by 27 % and 50 % sucrose. In the second sucrose gradient, liver sample in 50 % sucrose was placed at the bottom of the centrifuge tube, with 41 % and 25 % sucrose above it. As shown in figure 4.5a, sample collected from the first gradient has less plasma membrane (sample collected at the interface between 27 % and 50 % sucrose were plasma membrane portion). In the corresponding SDS-Page gel, lane 2 was the plasma membrane portion. Besides, sample with different density was not well separated since 90 % of the sample were at the surface between 8.7 % and 27 % sucrose. In the second gradient (**Fig. 4.5b**), liver sample was better separated by the gradient since majority protein were distributed in the different layers of the sucrose instead of concentrate in the surface between 25 % and 41 % sucrose. Besides, much more membrane protein were isolated and enriched in the surface between 41 % and 50 % sucrose. Thus, the second gradient was used in the Cx26 isolation experiment.

Cx26 isolated from 300 g of pig liver could be only clearly detected by western blot, but not SDS-Page (**Fig. 4.6**). In addition to the low yield, it was impossible to separate Cx26 and Cx32,

which co-expressed in the pig liver. In the western blot (**Fig. 4.6b**), an upper band below 34 kDa show up.

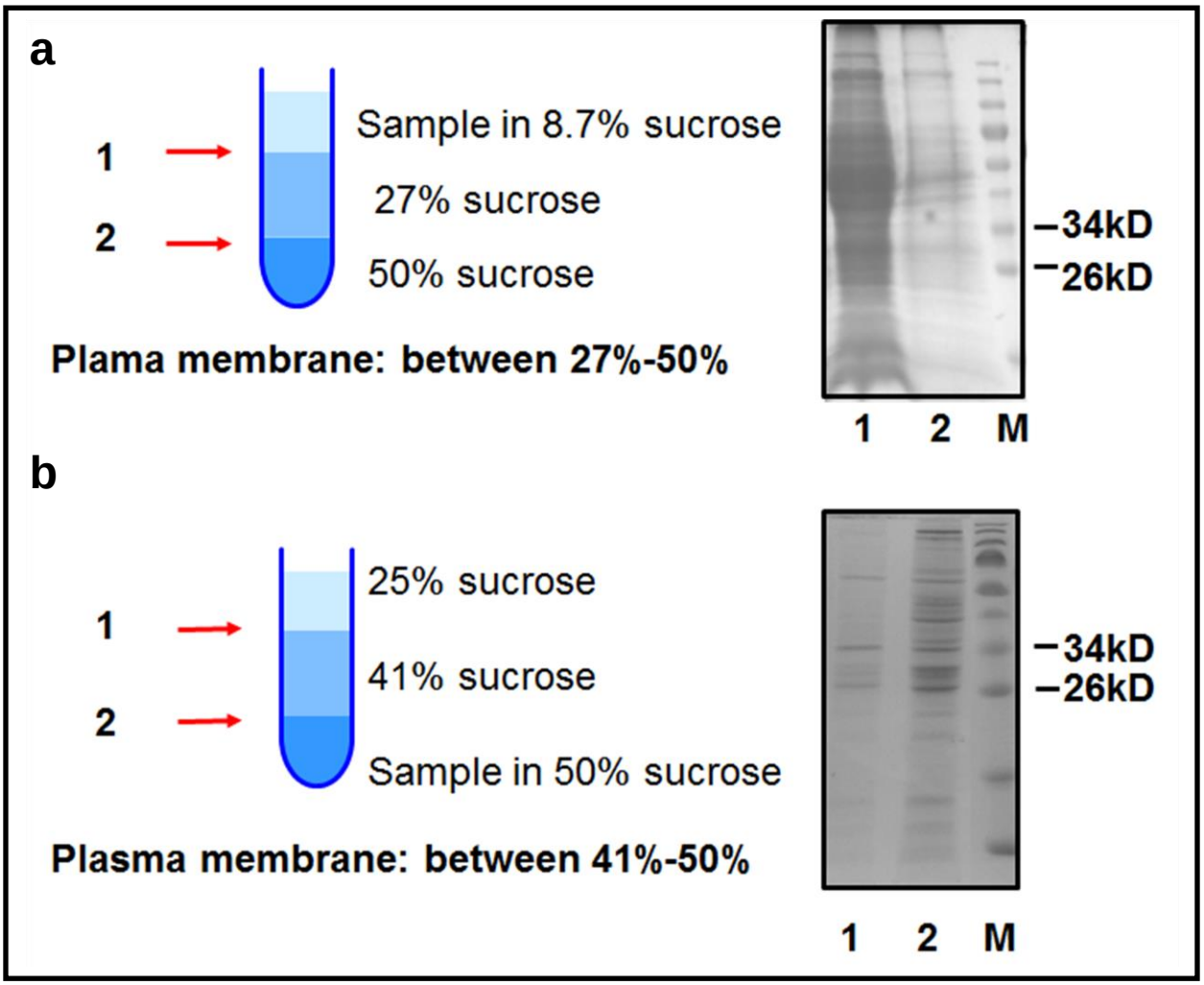

Figure 4.5 Sucrose gradient optimization.

(a) The first sucrose gradient was comprised of 8.7, 27, and 50 % sucrose. Liver sample was mixed with sucrose to obtain 8.7 % sucrose and the mixture was placed on the top of the centrifugation tube. Samples collected from the interface between 8.7 and 27 % (Lane 1) or 27 and 50 % (Lane 2) were loaded to the SDS-Page gel. (b) The second sucrose gradient was comprised of 25, 41, and 50 % sucrose layers. Liver sample was mixed with sucrose to achieve

50 % sucrose and placed underneath the 41 % sucrose layer. Samples collected from interface between 25 and 41 % (Lane 1) or 41 and 50 % (Lane 2) were further separated by SDS-Page gel.

Liver, lens and heart tissue have classically been the organs of choice for isolating gap junctions because the majority of the tissue contains only one or two types of connexins and starting material can be obtained in large quantities. Besides, it is a relative inexpensive way to obtain protein, compared with the cell expression. However, despite these advantages, its unavoidable defects make it not to be adopted widely. The key issues are its impurity and low yield. Take the liver as an example, it contains at least two major connexins: Cx26 and Cx32. Using the isolation methods, we could not successfully get rid of the other one. The estimated gap junctions cover only 0.1 % of the surface area of a hepatocyte. Large amounts of starting material will end up with a tiny quantity of gap junction after miscellaneous and toilsome purification procedures. Moreover, mutated protein cannot be obtained from tissue isolation. This handicap will restrict the application of mutagenesis in gap junction study. Taken together, we decided to move to bacterial expression from liver isolation.

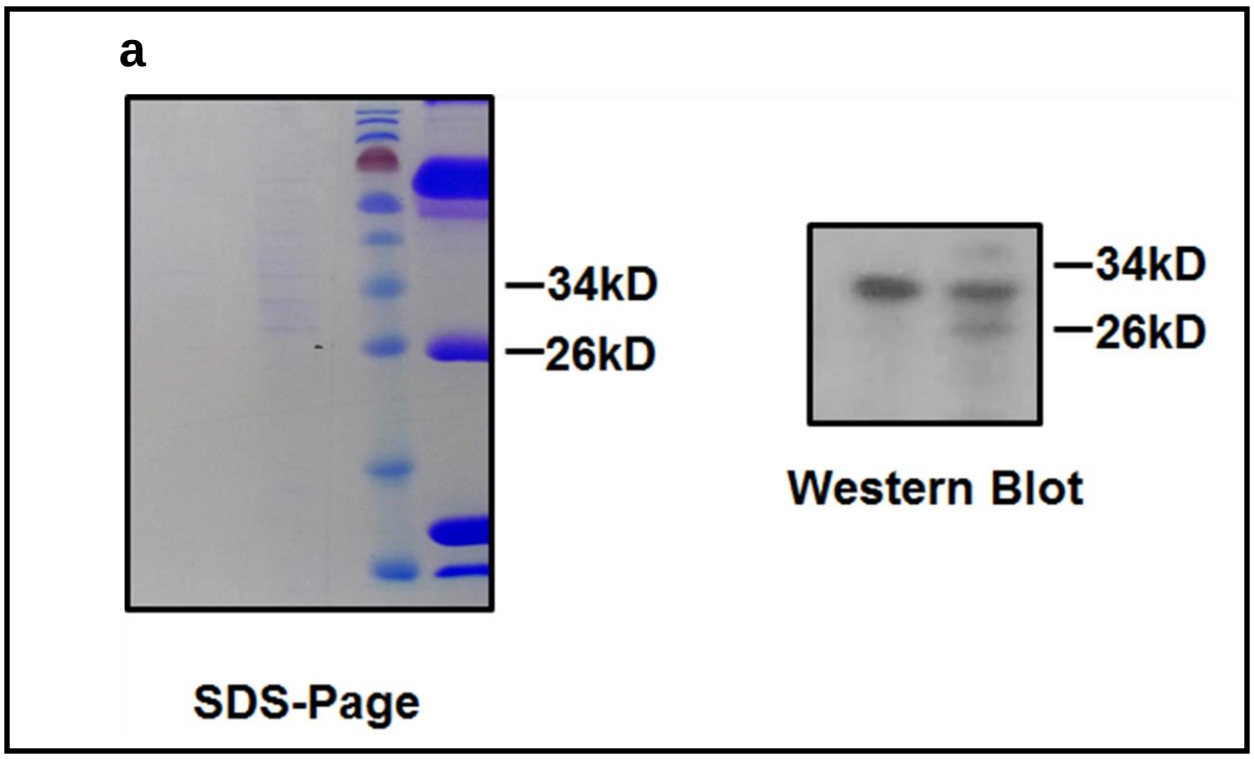

Figure 4.6 Cx26 isolated from liver had low yield and low purity.

(a) Cx26 isolated from 300 g of pig liver were loaded into the SDS-Page gel. (b) Cx26 isolated from pig liver was probed by anti-Cx26 monoclonal antibody using western blot. The upper and darker bands between 26 and 34 kDa were Cx32 co-expressed with Cx26 in liver.

4.2.3 Expression and purification of Cx26 in E.coli

Next, we attempted to express Cx26 in *E.coli* after we failed to isolate pure and large amount of Cx26 from pig liver. Though E.coli is an attractive host for lots of homologous or heterologous protein expression due to its advantages, the lack of one or more tRNAs in *E.coli* caused by rare codons significantly impedes some heterologous gene expression (467,468). Most amino acids are corresponding to multiple codons and each organism has their preference in using

codons. The population of tRNA directly reflects the codon usage preference. Limited tRNA amount and categories lead to translation inhibition, frameshifting, termination and so on (469). Human Cx26 gene contains a large number of rare codons which are much less preferred by *E.coli*. To overcome the codon bias of E.coli for enhanced protein expression, we therefore replaced all rare codons in the human Cx26 gene and purchased a synthetic optimized human Cx26 gene (**Fig. 4.7**) from GeneScript.

```
Original   atggattggggcacgctgcagacgatcctgggggtgtgaacaaacactccaccagcatt
Optimized atggattggggcacCctgcagacCatcctgggTggtgtTaacaaacactccaccTCTatt
           ************** ******** ******** ***** ***************:  ***

Original   ggaaagatctggctcaccgtcctcttcatttttcgcattatgatcctcgttgtggctgca
Optimized  ggCaagatctggctGaccgtActGttcatCtttcgcattatgatcctGgttgtggctgca
           **.************ *****.** ***** ***************** ************

Original   aaggaggtgtggggagatgagcaggccgactttgtctgcaacaccctgcagccaggctgc
Optimized  aaAgaAgtTtggggCgatgagcaggcAgactttgtAtgcaacacTctgcaAccGggctgc
           **.**.** *****.***********.********.******** *****.**.******

Original   aagaacgtgtgctacgatcactacttccccatctcccacatccggctatgggccctgcag
Optimized  aaAaacgtgtgTtacgatcaTtaTttcccGatctcccacatTcgTctTtgggcActgcaG
           **.******** ******** ** ***** ********** ** **:*****.******

Original   ctgatcttcgtgtccacgccagcgctcctagtggccatgcacgtggcctaccggagacat
Optimized  ctgatcttcgtgtcTacCccGgcgctGctCgtggcTatgcaTgtAgcctaTcgTCgCcat
           ************** ** **.***** **.***** ***** **.***** ** .*.***

Original   gagaagaagaggaagttcatcaaggggagataaagagtgaatttaaggacatcgaggag
Optimized  gagaaAaagCgTaaAttcatcaaAggTgaAatTaagTCtgaatttaaAgacatcgaggaA
           *****.***.* **.********.** **.**:***: *********.***********.

Original   atcaaaacccagaaggtccgcatcgaaggctccctgtggtggacctacacaagcagcatc
Optimized  atcaaaacTcagaaggtTcgTatcgaaggctccctgtggtggacctacacTagcTCAatc
           ******** ******** ** ****************************:***: .***

Original   ttcttccgggtcatcttcgaagccgccttcatgtacgtcttctatgtcatgtacgacggc
Optimized  ttcttTcgTgtAatcttcgaagcTgcAttcatgtaTgtTttTtaCgtAatgtaTgacggc
           ***** ** **.*********** **.******** ** ** ** **.***** ******

Original   ttctccatgcagcggctggtgaagtgcaacgcctggccttgtcccaacactgtggactgc
Optimized  ttctccatgcagcgTctggtgaagtgcaacgcctggccGtgtccGaacactgtggactgc
           ************** ********************** ***** ***************

Original   tttgtgtcccggcccacggagaagactgtcttcacagtgttcatgattgcagtgtctgga
Optimized  tttgtTtcccgCccGacCgagaaAactgtTttcacCgtgttcatgattgcagtTtctggT
           ***** ***** ** ** *****.***** *****.***************** *****:

Original   atttgcatcctgctgaatgtcactgaattgtgttatttgctaattagatattgttctggg
Optimized  atttgcatcctgctgaatgtAactgaaCtgtgttatttgctGatCCgCtaCtgttctggT
           ********************.****** *************.** .*.** ********

Original   aagtcaaaaaagccagtttaa
Optimized  aagtcaaaaaaAccagtttaa
           ***********.*********
```

Figure 4.7 Optimization of human Cx26 for E.coli expression.

The original human Cx26 gene was optimized by replacing the rare codons with codons E.coli prefers to use. The changes are highlighted in red and capital letters.

The major issue associated with Cx26 expression in *E.coli* is the low yield. Efforts have been made to optimize the expression conditions using different *E.coli* strains, temperatures, expression vectors, mediums as well as expression time. Some E.coli strains could not grow after hCx26 transformation, some grew very slowly, and some did express this eukaryotic protein at all. Among all *E.coli* strains we tested, C43(DE3) was the best candidate due to its better capability of handling challenge membrane proteins. Finally, optimized hCx26 inserted in pTrcHis2A vector had the best expression in E.coli strain C43(DE3) at 20 °C for 16 hours, however, the expression level was still a problem. As shown in figure 4.8, after IPTG induction, hCx26 expressed in C43(DE3) could only be detected by western blot, while it was hard to be detected in SDS-Page gel since no band was much darker at around 26 kDa after applying IPTG. In addition to the monomer band at around 25 kDa, a dimer band below 55 kDa was also visualized in the western blot, indicating *E.coli* expressed hCx26 has the potential to form oligomers.

To obtain enough hCx26 from E.coli when considering the low expression level, we scaled up our starting material for purification from 2 L to 9 L E.coli. As described in Methods section, E.coli pellet was first sonicated, followed by 3.5 % Empigen solubilization and extraction. The supernatant after solubilization was passed through Ni^{2+} column and protein with his tag was eluted by imidazole. We also tried different detergent in the purification process, like Octyl-beta-Glucoside (OG) and n-Dodecyl-beta-Maltoside (DDM). Both of them were too gentle and Empigen was the most efficient one. The elution factions 1 and 2 (**Fig. 4.9a**) had two bands at

around 25 kDa and only the lower band could be recognized by anti-His tag antibody (**Fig. 4.9b**). The upper bands was too close to the lower band and it is impossible to get rid of it by gel filtration. Besides, anti-hCx26 antibody could not recognize both bands though we tried four different anti-hCx26 antibodies. Mass spectrometry only detected few peptides from the elution fractions with very low coverage (less than 5 %). Most of the protein detected in the elution fractions were other *E.coli* proteins with similar molecular weight. In summary, E.coli was not considered as a good candidate to express this eukaryotic membrane protein.

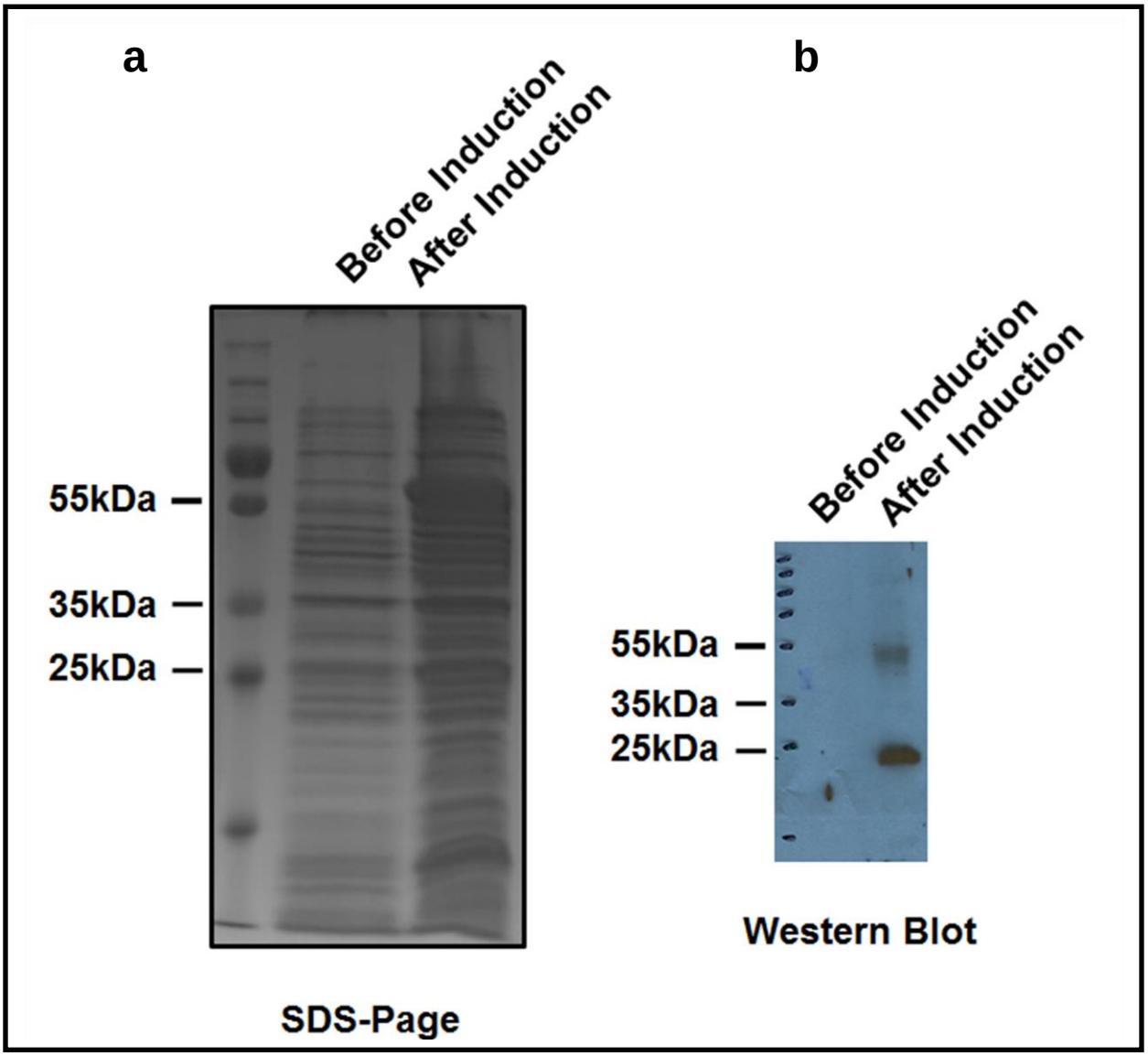

Figure 4.8 hCx26 expression in C43(DE3).

(a) Monitoring hCx26 expression in C43(DE3) before and after IPTG induction. (b) Western blot gel corresponds to the SDS-Page gel.

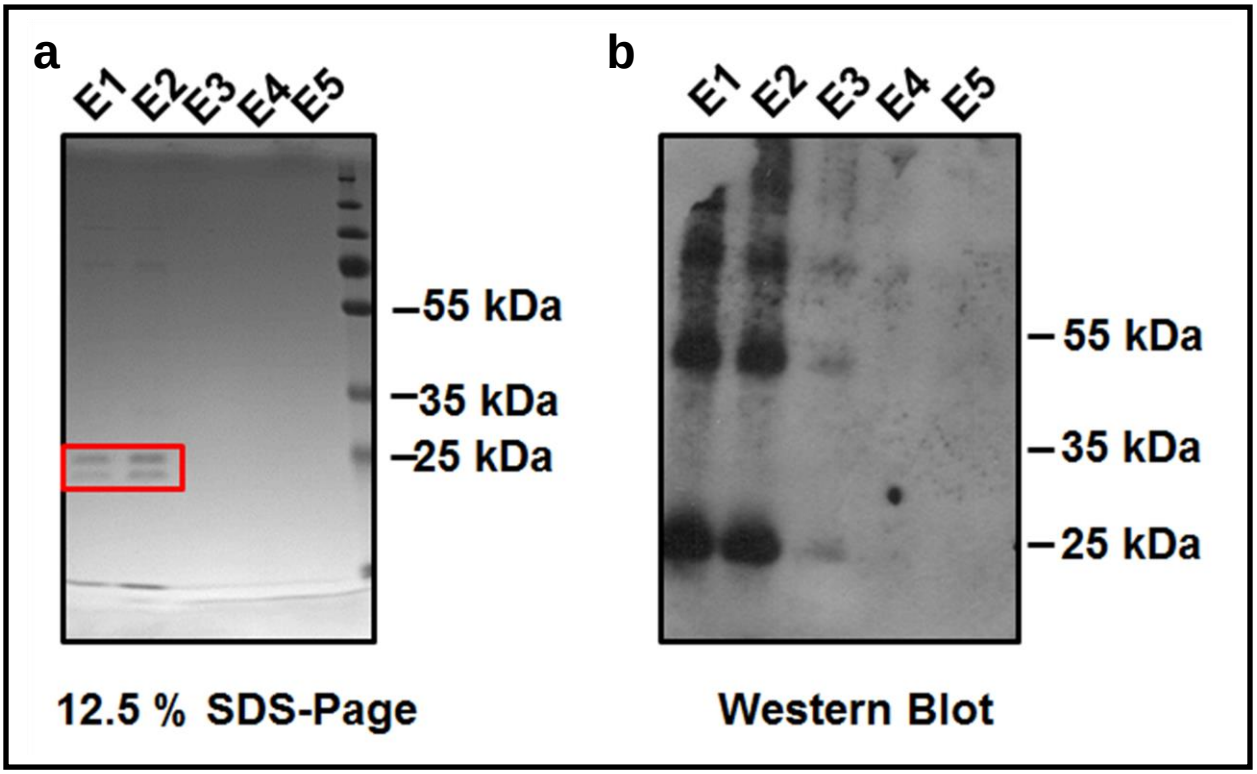

Figure 4.9 Expression of hCx26 from C43(DE3).

(a) Elution fractions were further separated by 12.5 % SDS-Page gel. Two bands at around 25 kDa showed up in elution fraction 1 and 2. The lower bands were recognized by anti-his tag antibody (b) when performed western blot.

4.2.4 Expression and purification of mCx26 in Sf9

The whole procedure for expression and purification of mCx26 in insect cell Sf9 is described in detail in appendix A. mCx26 purified from insect cell Sf9 using his tag column

exhibited typical donut shape under the electron microscope, suggesting the formation of hexamer (**Fig. 4.10a**). However, in the electron microscope image, the sideview of mCx26 was invisible since all of the mCx26 presented their top or bottom view. To check weather mCx26 formed dodecamer, we ran native blue gel in which mCx26 protein mobilized in their native states. As shown in figure 4.10b, without denaturing and reducing reagent, mCx26 purified from Sf9 displayed two bands at around 160 and 247 kDa, corresponding to hexamer and dodecamer, respectively. Anti-mCx26 monoclonal antibody also exhibited immunoreactivity to both bands. The bands with higher molecular weight may be oligomers larger than dodecamer due to the formation of gap junction plaque on the Sf9 membrane.

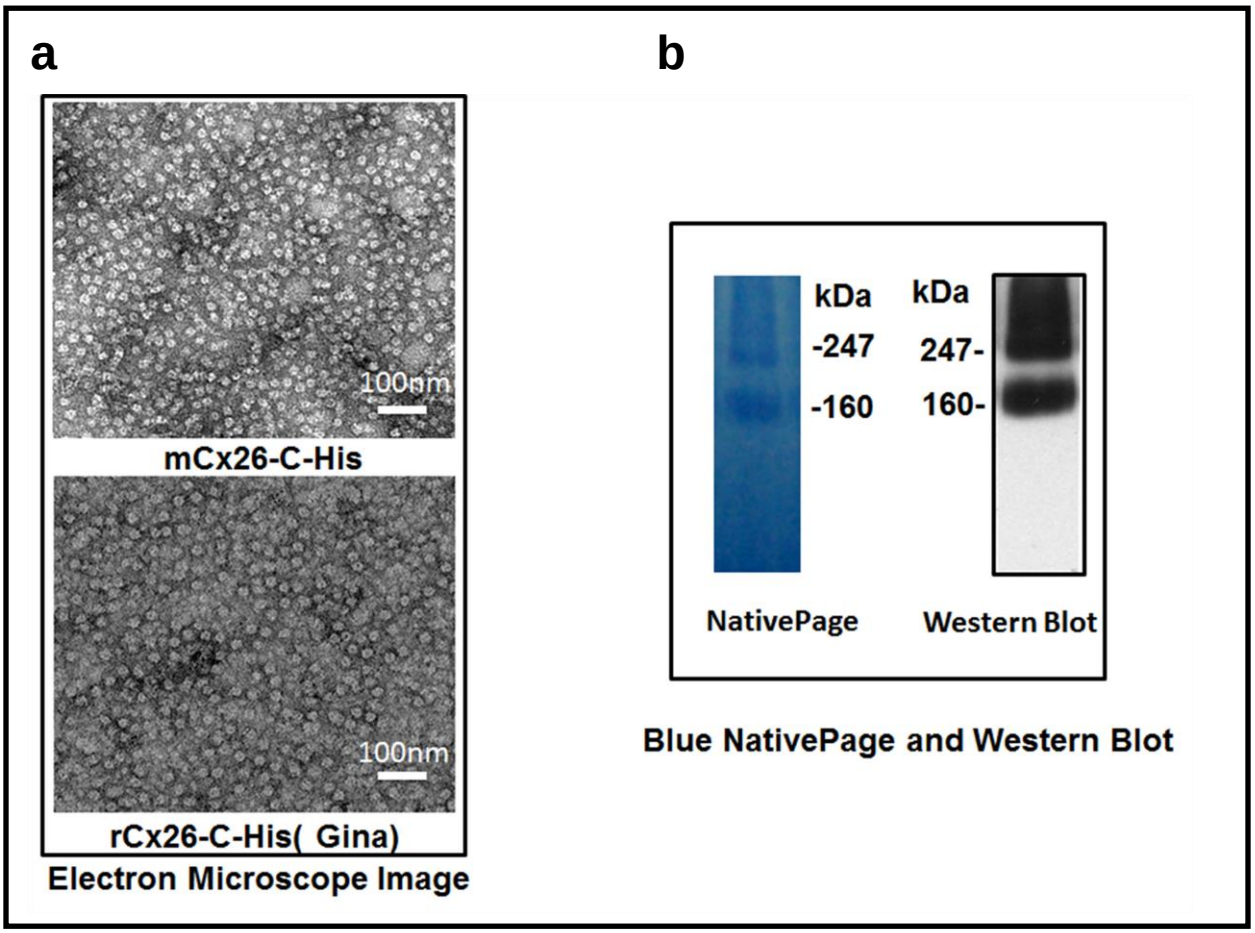

Figure 4.10 mCx26 purified from Sf9.

(a) mCx26 purified from Sf9 showed typical donut shape under the electron microscope, indicating the formation of hemichannels. rCx26 from Dr. Gina Sosinsky's group was used as our golden standard. (b) mCx26 purified from Sf9 formed both hemichannel (hexamer) and gap junction channel (dodecamer) under native conditions as shown in the native page gel and its western blot.

To obtain homogeneous hemichannels which are suitable for biophysical studies, different detergents were tested. However, none of them showed successful splitting. In addition, a various percentages of DDM were also tested and did not give us any promising result. So finally we decided to use more harsh conditions, such as urea. This splitting method was first reported by Gina Sosinsky's to split gap junction plaques formed between adjacent cell mammalian cell membranes. In the present study, we applied the same method to the pure mCx26 and tried to manipulate the population of different oligomers.

After 5 days incubation at 4 °C in 5 mM Tris, 4 M urea, 3 mM EDTA, 5 mM DTT, no significant difference was observed between sample with or without splitting (**Fig. 4.11**). The major bands from two samples appeared at the same locations, which were highlighted by red boxes. However, at location 2, there were two oligomer status existing which can be judged from the two clear separate bands on the native gel. After performing the splitting experiments, only one band showed up at location 2 and the bands at location 1 were much darker. The splitting result indicated that there are one or more strong forces allowing the monomers to form stable and tight oligomers. Once they are formed, it is very difficult to separate them. Apparently, 4 M urea

was not sufficient enough to split. Purified mCx26 was heterogeneous sample containing hexamer, dodecamer or even bigger oligomers.

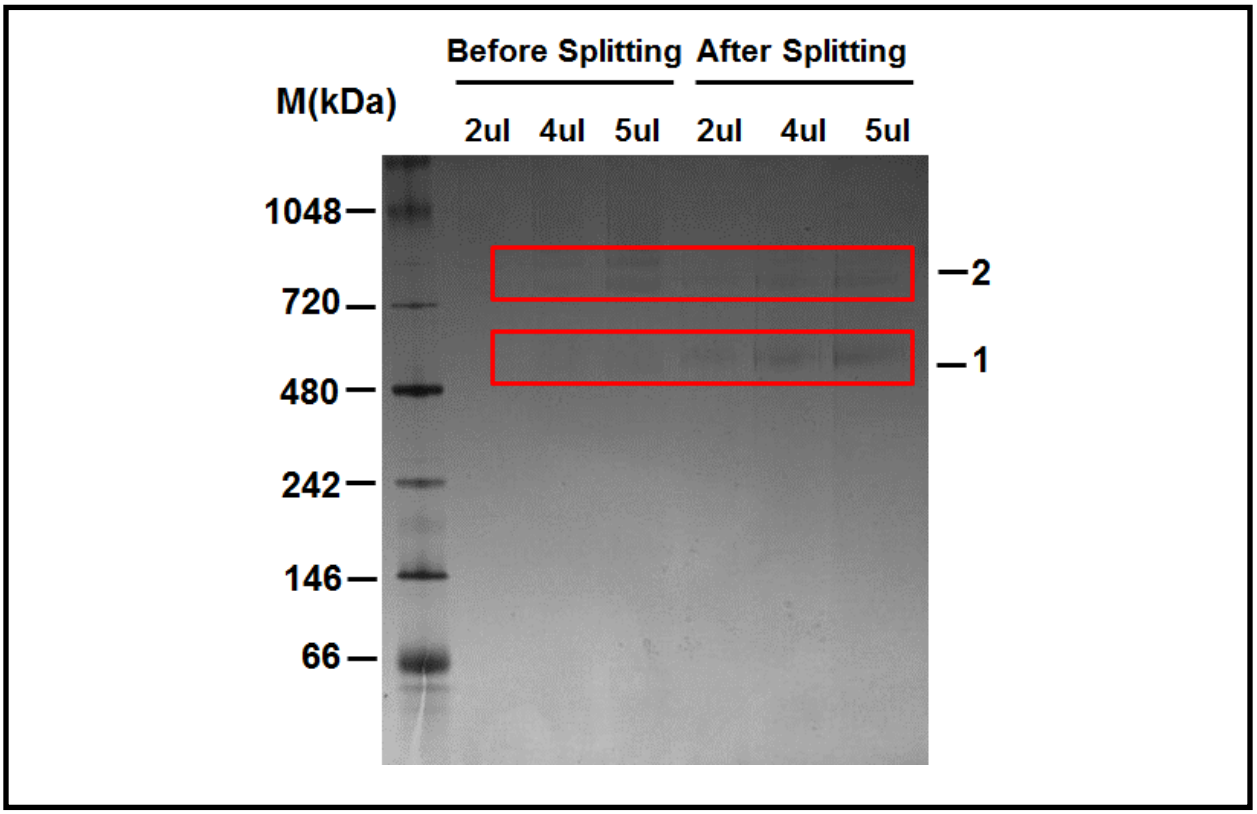

Figure 4.11 Cx26 Splitting by Urea.

mCx26 were incubated with 5 mM Tris buffer (pH 8.0) containing 4 M urea, 3 mM EGTA, and 5 mM DTT for 1 hour at 37 °C first and then for 4 days at 4 °C. Different amount of aqueous was loaded to the native gel. Position 1 and 2 highlighted by red box were the hexamer and dodecamer, respectively.

Gap junction hemichannels from neighboring cells are held together to form gap junction channels spanning the membrane of adjacent cells by hydrophobic forces. Dr. Sosinsky's group

developed a biochemical method to split the gap junction channels using urea and EGTA(470). The function of urea is to destroy the hydrophobic interactions. DTT is added to inhibit the formation of any possible disulfide bond and EGTA is applied to chelate Ca^{2+} ions since Ca^{2+} is also important for the assembly of the membrane pair. This protocol is adapted from a splitting procedure designed earlier by Manjunath *et al* (471). The protocol we used is the same protocol modified by Dr. Sosinsky's group. They reported that the splitting efficiency is as high as 60-90%. However, the starting material they used was not purified gap junction protein, instead it was the membrane fragment with gap junction proteins which could not be dissolved by alkali or detergent Sarkosyl and Brij 58. They stained the membrane sample and used electron microscopy to analyze the efficiency of gap junction splitting by scoring micrographs for numbers of single membranes, double membranes, and partially disrupted membranes. The following SDS-Page gel was showed to compare the protein composition in both intact junctions and split junctions. However, there is no band differences. After splitting, there were still the same amount of oligomer band.

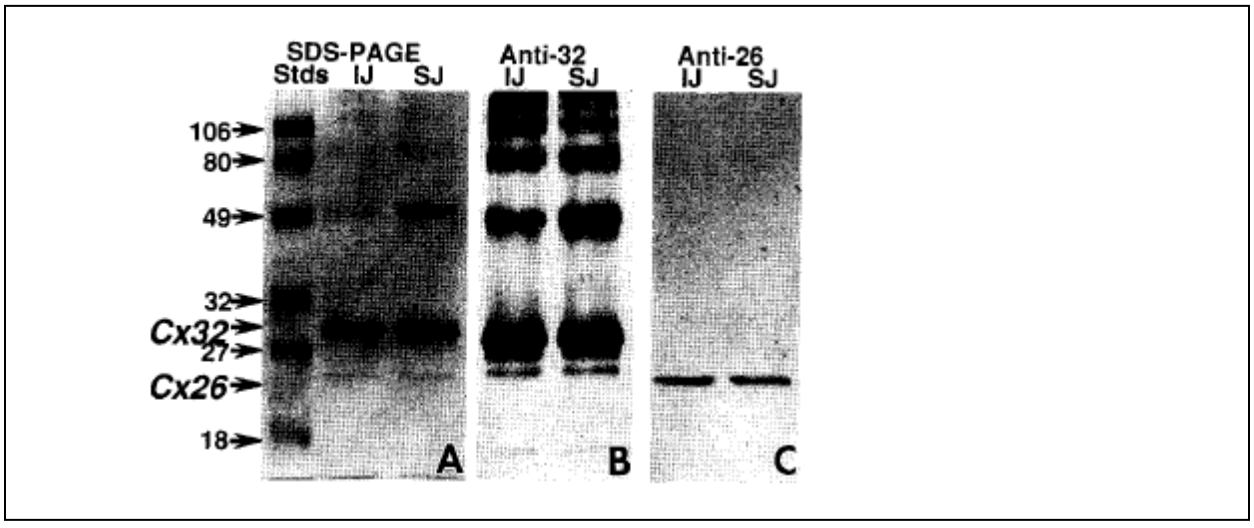

Figure 4.12 SDS-Page gel and western blot for analyzing intact and split junctions.

Cx32 and Cx26 were the two major gap junction proteins in rat heart. IJ represents membrane preparation before splitting and SJ stands for membrane preparation after splitting.

4.2.5 Tb^{3+} titration

Steady-state fluorescence spectrum was recorded using a QM 1 fluorescence spectrophometer at room temperature. For Tb titration, 1-cm-pathlength curvet was used to acquire a 500-600 nm spectrum with an excitation wavelength at 285 nm. The slit widths were set at 1.3mm for excitation and 2.8mm for emission. 2 uM mCx26 in 10 mM HEPES (pH 6.8), 100 mM NaCl and 0.01% DDM was titrated by gradually adding 200 uM Tb^{3+} stock solution in the same buffer. The binding affinity of the Tb^{3+} to mCx26 was obtained by fitting normalized fluorescence data with two separate equations: 1:1 binding equation and hill equation. The equilibrium Tb^{3+} binding constant to mCx26 was determined by monitoring Tb^{3+} fluorescence.

The experiment is designed based on the fluorescence resonance energy transfer, which describes energy transfer between two chromophores. When the initial chromophore is excited, it can transfer its energy to other nearby chromophores. In this experiment, aromatic amino acids, mainly Trp, was excited by a wavelength of 285 nm and its emission wavelength will excite Tb^{3+} close to it. The electronic excited Tb^{3+} will emit fluorescence between 500-600 nm while returning to its ground energy state. The efficiency of this energy transfer depends on the distance between two chromophores, the shorter the higher. The final purpose of this experiment is to obtain the binding affinity of Ca^{2+} to mCx26 indirectly using the competition methods, because Ca^{2+}, unlike Tb^{3+}, cannot be observed directly. So if the protein can bind with Tb^{3+}, Ca^{2+} can be gradually added

to compete with Tb^{3+} for the binding sites. Usually Tb^{3+} and Ca^{2+} share similar binding sites in many proteins.

In figure 4.13, Tb^{3+} fluorescence has the maximum emission peak at 545 nm. The increase of Tb^{3+} concentration contributes to the enhancement of fluorescence intensity. Plateau phase appeared when Tb^{3+} concentration is about 36 uM. Then we plotted the normalized fluorescence intensity as a function of Tb^{3+} concentration (**Fig. 4.13b**) and found that the interaction between Tb^{3+} and mCx26 is a two-phase binding: a stronger one and a weaker one. The dissociation constants are 0.27 ± 0.21 μM and 15.4 ± 0.2 μM respectively. The first binding phase is a 1 to 1 binding model, while the second phase is a cooperative model with a hill number of 4.2. These indicate that the mCx26 purified from Sf9 is more like a hexamer structure.

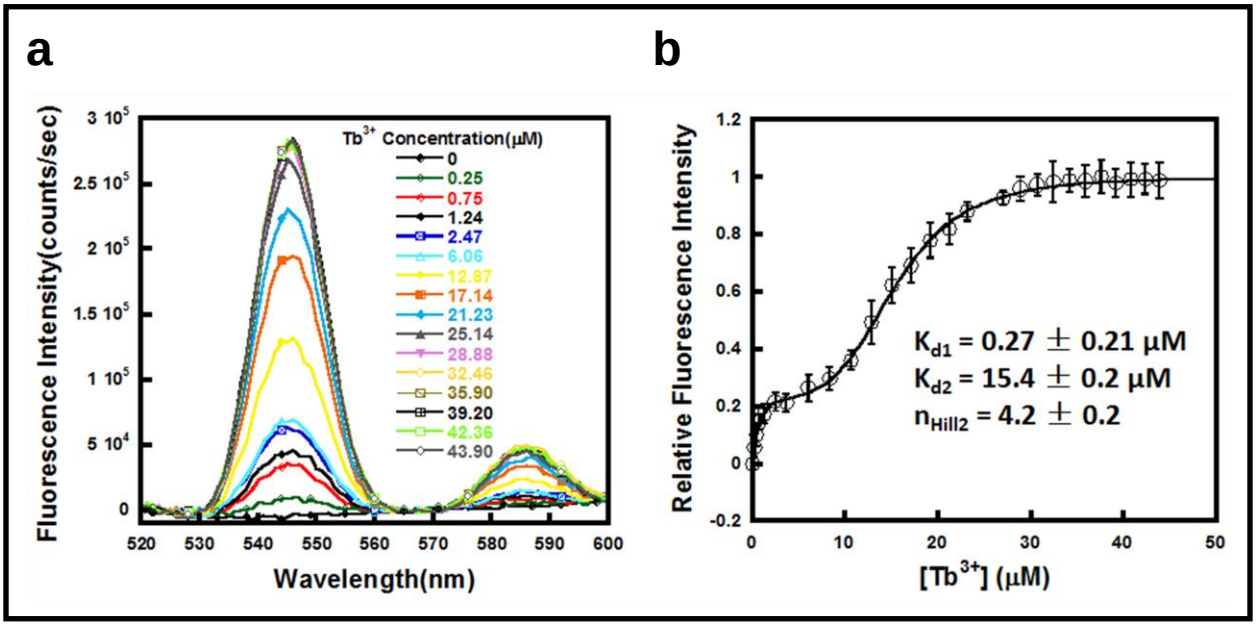

Figure 4.13 Tb^{3+} titration.

(a) mCx26-Tb^{3+} fluorescence spectrum was recorded by fluorometer when free Tb^{3+} was titrated into mCx26. Buffer without any protein was used as control and subtracted from the

mCx26-Tb^{3+} fluorescence spectra. (b) The mCx26-Tb^{3+} fluorescence intensity change at 545 nm were plotted against the concentration of free Tb^{3+} that added in. Two binding phases were observed. The stronger binding site of 2 μM mCx26 was saturated by around 2 μM Tb^{3+}, which suggests the binding model is 1 to 1 binding. Therefore, the first phase of binding was fit to 1 to 1 binding equation as described in the Methods section. The relative weaker binding site of mCx26 is also saturated by Tb^{3+} at a higher concentration, around 20 μM. By fitting the curve with 1 to 1 binding and hill equations, we obtained the two dissociation constants: 0.27 ± 0.21 μM and 15.4 ± 0.2 μM. The Tb^{3+} titration experiment was repeated three times and the data presented here was the average value.

4.2.6 Ca^{2+}-Tb^{3+} competition and Ca^{2+} induced conformation change

To obtain the Ca^{2+}-binding affinity to mCx26, we performed Ca^{2+}-Tb^{3+} competition experiment. The experiment was based on the assumption that Ca^{2+}- and Tb^{3+}-binding sites are the same and Ca^{2+} could kick out Tb^{3+} from the pocket of mCx26. Mouse Cx26 (2 μM) was first mixed with appropriate amount (25 μM) of Tb^{3+}. After 15 minute-incubation, the sample in the quartz cuvette were mixed by inverting cuvette several times before fluorescence measurement. We allowed another 10 minute-incubation before Ca^{2+} (1 M stock) was gradually added into the cuvette. The fluorescence intensity of mCx26-Tb^{3+} was monitored by fluorometer. Duplicate was done in this competition experiment. Ca^{2+} up to ~ 30 mM did not lower the fluorescence intensity of mCx26-Tb^{3+}. Almost no change occurred during the Ca^{2+} titration, though some fluorescence intensity fluctuations (within less than 3% change) happed during titration (**Fig. 4.14**). In summary, the result indicated that Ca^{2+} was unable to compete with Tb^{3+} for the binding site in mCx26.

Possible reasons accounting for this result are that Tb^{3+} binding affinity is much stronger than that of Ca^{2+} or Ca^{2+} and Tb^{3+} do not share the similar binding pocket.

Next, we attempted to investigate the possible conformation changes induced by Ca^{2+}-binding. A large group of Ca^{2+}-binding protein adapt to a different conformation upon Ca^{2+}-binding. The most famous one among them is CaM. Ca^{2+} binding to each globular domain of CaM alters interhelical angles in the EF-hand motifs, leading a conformation change from a "closed" to an "open" state. Thus, we first monitored intrinsic Trp fluorescence change upon Ca^{2+} binding. Interestingly, the intrinsic Trp fluorescence intensity was keeping to decrease while inverting the cuvette even when the protein was gently inverted overnight before we started the experiment. To avoid this decrease, corvette was inverted lots of time until the fluorescence intensity became stable. The instability of Trp fluorescence may be caused by the heterogeneity of the protein sample and the re-assemble of protein-DDM vesicles.

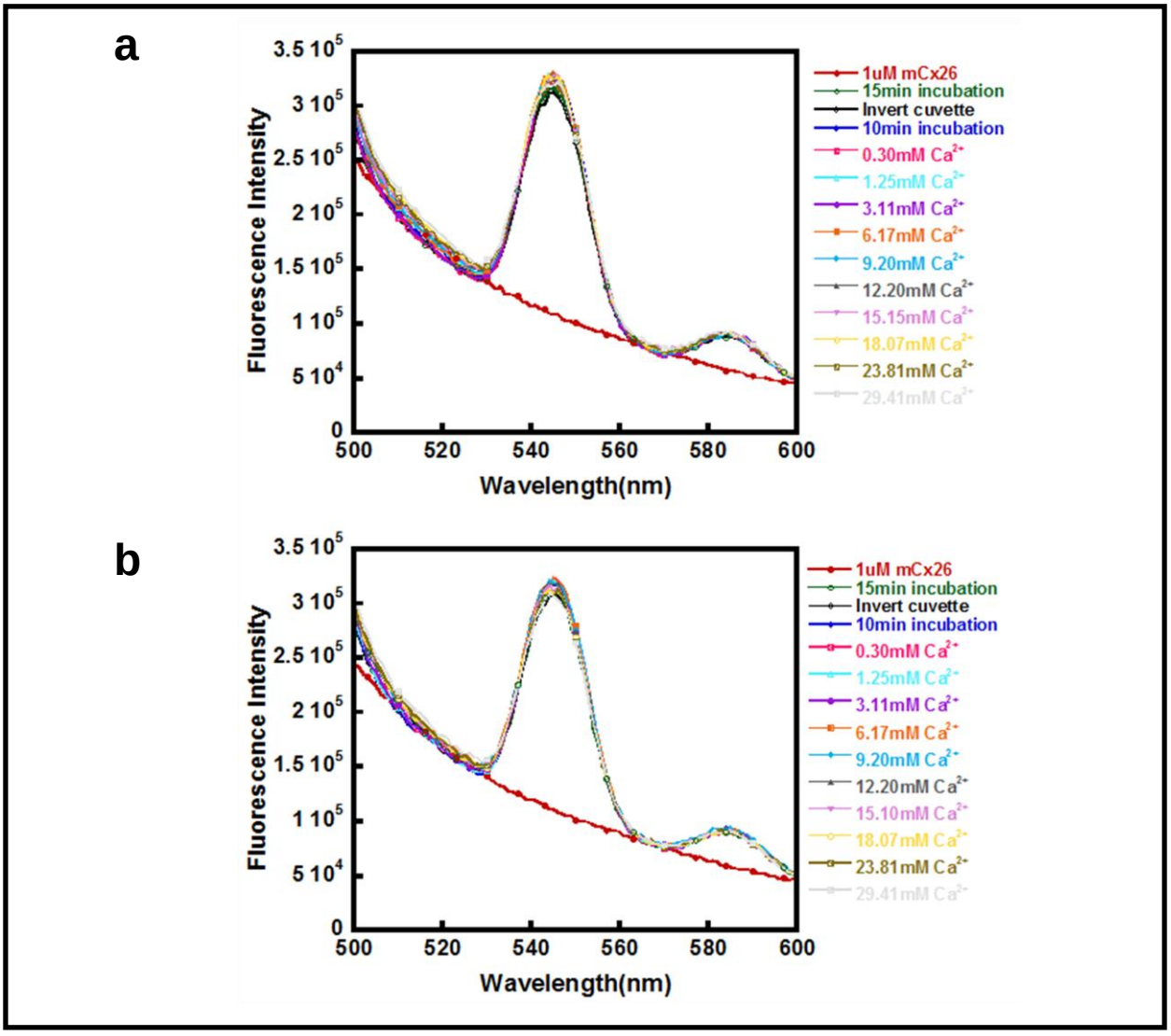

Figure 4.14 Ca^{2+}-Tb^{3+} competition.

(a) and (b) are duplicates. To start with, 1 µM mCx26 was incubated with 25 µM Tb^{3+} for a total of 25 minutes before recording the fluorescence intensity of mCx26-Tb^{3+} at 545 nm. The fluorescence intensity of protein without Tb^{3+} (dark red line) was checked to set up the slit width properly. Titrating Ca^{2+} into the cuvette did not significantly altered the fluorescence intensity of mCx26-Tb^{3+}.

There are several Trp inside or close to the predicted Ca^{2+}-binding site. Significant conformational change usually cause Trp to be more exposed or buried, resulting in the characteristics of Trp fluorescence change. In my Ca^{2+} titration experiment, adding Ca^{2+} into mCx26 did not lead to any fluorescence change that could be detected by fluorometer. In addition to the sensitivity, there are several possibilities. First, Ca^{2+} did not bind to the predicted pocket since purified protein was wrapped by detergent DDM to stay as soluble state. Second, Ca^{2+} did not bind to mCx26. Third, Ca^{2+}-binding did not induce significant conformational change. In 2016, the resolved Ca^{2+}-bound Cx26 crystal structure proved that the third hypothesis was right (88). Ca^{2+} ion indeed bound to the predicted pocket without altering the conformation significantly; only tiny conformation change involving several amino acid was affected.

In addition of monitoring Trp fluorescence, the secondary structure of mCx26 in the presence or absence of Ca^{2+} was recorded in the far UV (190-260nm) on a Jasco-810 spectropolarimeter. The measurements were made in 10 mM HEPES, 100 mM NaCl, 0.01% DDM, at pH 7.5 with 5 mM EGTA or 5 mM Ca^{2+}. The background signals from the corresponding buffer were subtracted from the sample signals. All spectra were an average of at least 8 scans. The far UV CD spectrum can reveal the secondary structure like alpha helix, beta sheet and random coil of proteins or peptides. From the CD spectrum, the percentage of different secondary structures can be estimated by software. To elucidate the influence of Ca^{2+} on the secondary structure of mouse Cx26, we monitored the secondary structure in Ca^{2+} free buffer and in 5 mM Ca^{2+} buffer. As seen in figure 4.15, mCx26 displays the typical alpha helix structure characterized at 222 and 208 nm. When 50 μM EGTA was added to chelate the Ca^{2+} which may bind with the protein during the whole purification process, the residue weighted molar absorption coefficient

becomes less negative, which indicates the extent of helical structure is decreased. The result suggests that there are metals binding with the protein and the release of this metal can change the secondary structure of mCx26. We are not clear about which metal it is. Then 5 mM Ca^{2+} was added to see whether the increased concentration of Ca^{2+} will affect the secondary structure of mCx26 or not. But the CD spectrum is overlapping with the one after adding 50μM EGTA. Our hypothesis deduced from this consequence are that: 1)Other metals instead of Ca^{2+} occupy the binding sites of mCx26 and Ca^{2+} cannot bind with mCx26 to alter its secondary structure; 2)the release of Ca^{2+} from the binding sites of mCx26 by 50 μM EGTA causes the disassemble of hexamers and this process is not a reversible process. Both two cases, adding of Ca^{2+} cannot generate any differences on secondary structures. Considering the secondary structure change may be a slow step, we incubated the protein with 5 mM Ca^{2+} for about 1 hour. But no difference can be observed. 10 mM EGTA was continued to add to the mCx26 and incubated for 1 hour. The secondary structure did not change.

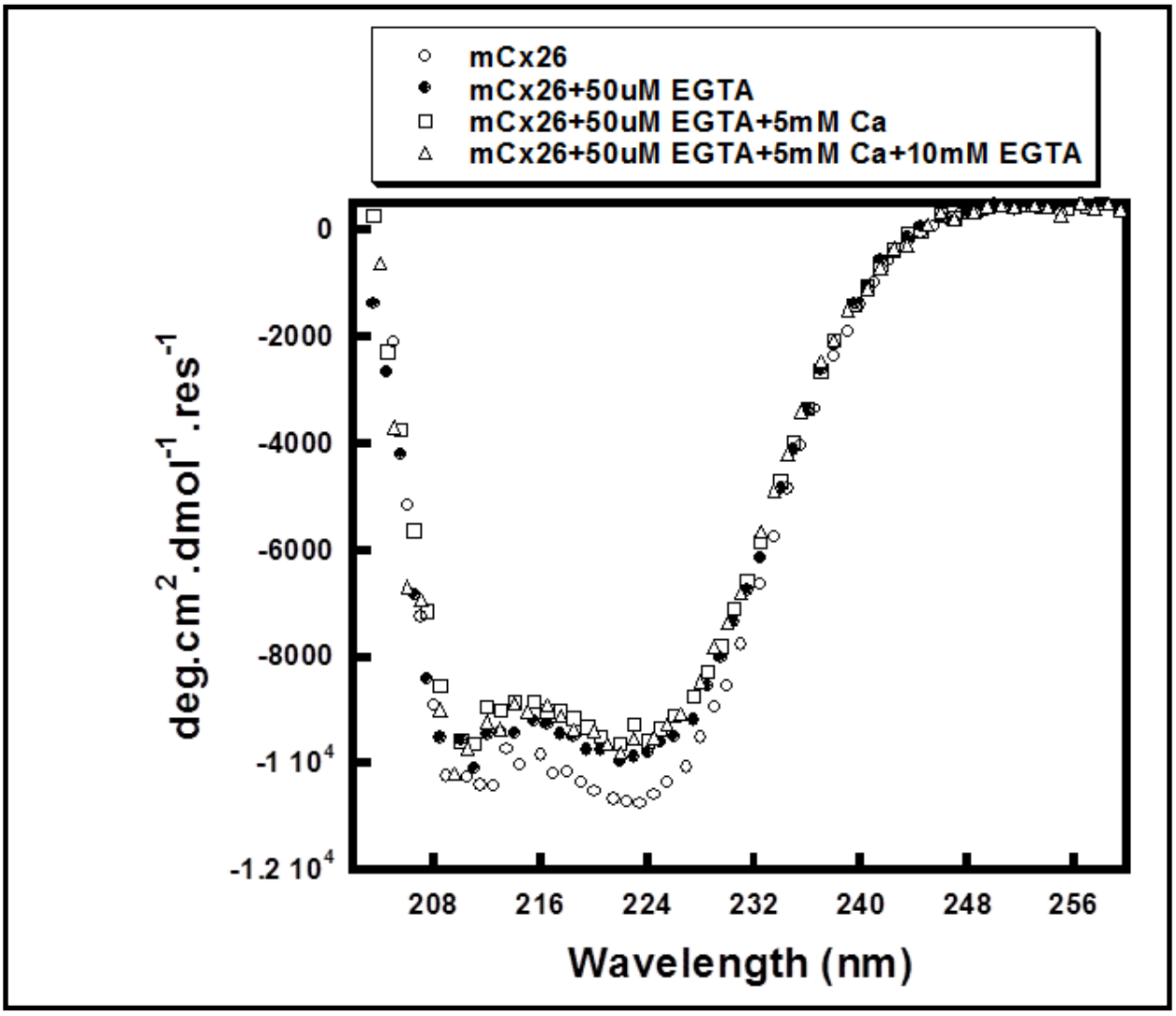

Figure 4.15 Secondary structure of mCx26 in the presence or absence of Ca^{2+}.

The secondary structure of mCx26 in the presence or absence of Ca^{2+} was monitored using CD. The negative peaks at 222 and 208 nm indicate mCx26 is a α-helical protein. Open circle: mCx26 only; closed circle: mCx26 with 50 µM EGTA; open square: mCx26 with 50 µM EGTA and 5 mM Ca^{2+}; open triangular: mCx26 with 5 mM Ca^{2+} and 10 mM EGTA.

Temperature-dependent CD is also performed to compare the melting temperature and stability of mCx26 in Ca^{2+} and EGTA buffer. Temperature gradually increased from 4 to 94 °C and CD signal at 222nm was recorded as in figure 4.16. A more negative CD signal of mCx26 in 5mM Ca^{2+} buffer can be observed when it is compared with mCx26 in 5mM EGTA buffer. It suggests that protein in 5mM Ca^{2+} has higher stability and needs higher temperature to cause the loss of secondary structure. This experiment indirectly proves that Ca^{2+} serves to stabilize the mCx26.

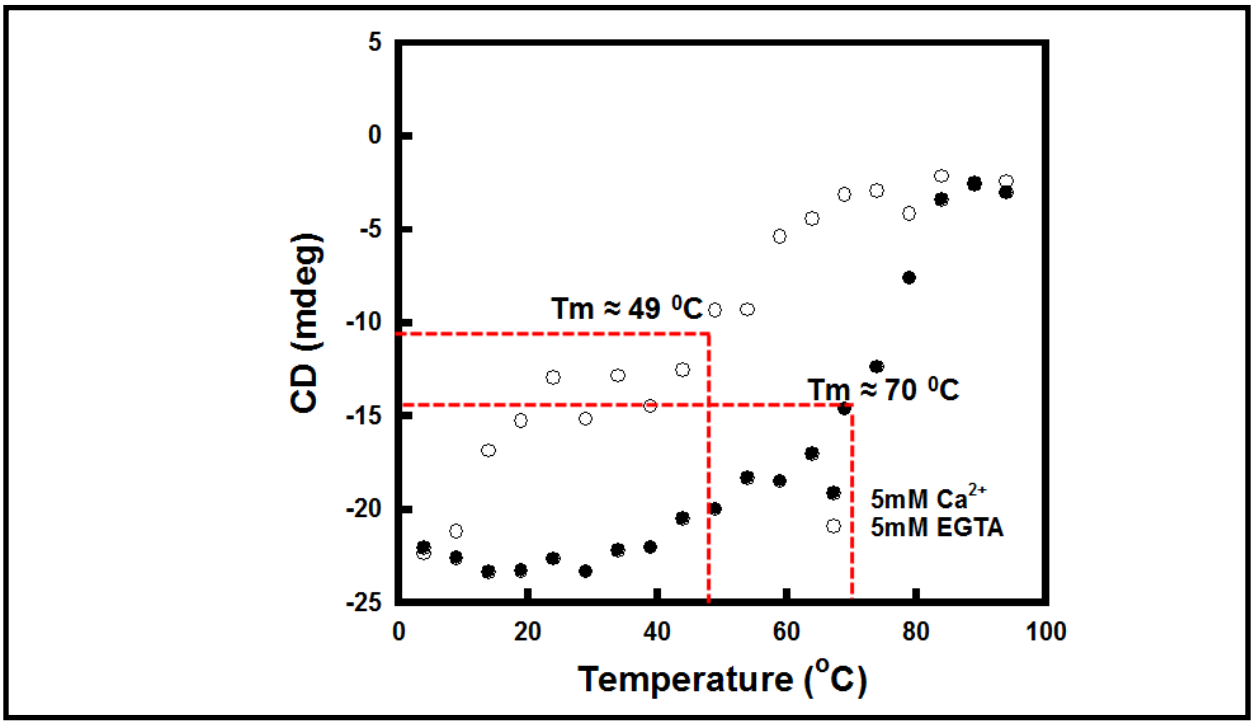

Figure 4.16 Thermal stability of mCx26 in the presence or absence of Ca^{2+}.

The molar ellipticity of mCx26 at 222 nm in the presence or absence of Ca^{2+} was monitored when temperature increased from 4 to 94 °C. At each temperature, mCx26 was scanned for 10 times to obtain the average value. Open circle: with 5 mM EGTA; solid circle: with 5 mM Ca^{2+}.

4.2.7 Dye uptake assay

To study the regulation effects of $[Ca^{2+}]_o$ on wild type Cx26 and predicted Ca^{2+}-binding ligand mutants, we firstly checked the expression of Cx26 and its mutants in HeLa cells. The transfection and expression of exogenous connexins in HeLa cell have been previously described by Dieter Manthey and Klaus Willecke (472). The cell line HeLa used in my study showed minimal levels of endogenous connexins expression. Electrophysiological characterization of human HeLa cells yielded very low electrical conductance (473). Though in the non-transfected Hela cell a major single class of intercellular channel with a conductance of 30 pS which is comparable to the Cx45 channel conductance (473,474) have been identified by Eckert in 1993, no immunofluorescent signal had been detected in non-transfected Hela cell (475). Human Cx26-eGFP showed punctate surface on the plasma membrane surface. Additional green fluorescence signal was also evident in the cytosol, which may be the consequence of overexpression of exogenous connexin 26 (439). Several diseases-related mutants that also reside at our predicted Ca^{2+} binding pocket had been transfected into HeLa cell. Among them, four mutants (A40V, G45E, D50N, and D50Y) cannot be successfully expressed in HeLa cell like the wild type hCx26. Only few dots with green fluorescence could be detected under microscope. Besides, a majority of these round shape dots are dead Hela cells. Previously work done by other group in the *xenopus* oocyte or mammalian cells also reported that cell death or degradation or apoptosis occurred with the expression of these mutants. G45E was reported to induce the apoptosis in HEK 293 cell and higher extracellular Ca^{2+} was required to rescue cells (460,461). A40V (462) was described that it produced leaky hemichannels in *xenopus* oocytes and is less sensitive to extracellular Ca^{2+} compared with wild type hCx26. These altered properties alone or in combination increase the cell death rate. D50N (476) displayed obvious blebbing and an increased rate of cell death compared

to wile type Cx26 cells. The hCx26 utilized in my experiments was tagged with eGFP at the C-end. hCx26 and its mutants expression was checked under the fluorescent microscope by monitoring the green fluorescence emitted by eGFP. As previous reported, A40V, G45E, D50N, and D50Y led to severe cell death. Cells with green fluorescence all displayed as small round dots without normal cell shape. Other two mutants (D46N and D46E) displayed the same expression pattern as the wild type hCx26 in HeLa cell (**Fig. 4.17**).

Dye uptake assay is a convenient and effective way to study the permeability properties of gap junction hemi-channels (460,477,478). No special devices are needed to perform this assay. Besides, extracellular environment can be easily manipulated and controlled. With the aid of different gap junction dyes, the permeability can be reflected under the fluorescent microscope. In my study, PI was chosen because its bright red fluorescence color which can be clearly distinguished with eGFP. Its molecular mass is 668.6 Da and can bind with the nucleic acids. Once excited with its maximum excitation wavelength 535 nm, it will emit the maximum light at 617 nm.

Non-transfected HeLa cell was used as negative control here. To examine the permeability properties of Cx26 hemichannels to larger molecules propidium iodide (PI), non-transfected or transfected Hela cells were incubated in bath solution (with 2mM Ca^{2+}) containing 0.5 mg/ml PI for 10 minutes at 37 ^{0}C. No significant dye uptake was detected in control cell and transfected cells. Then new bath solution (with 2 mM EGTA) containing 0.5 mg/ml PI was added to replace the old bath solution with 2 mM Ca^{2+}. In the same view, no dye uptake occurred in control cells, however, significant dye uptake was observed in hCx26-transfected cells (**Fig. 4.18**). Taken together, PI uptake was through Cx26 gap junction hemichannels expressed on the cell surface and

PI could not pass through Cx26 gap junction hemichannels in the presence of $[Ca^{2+}]_o$ which induced closure of Cx26 hemichannels.

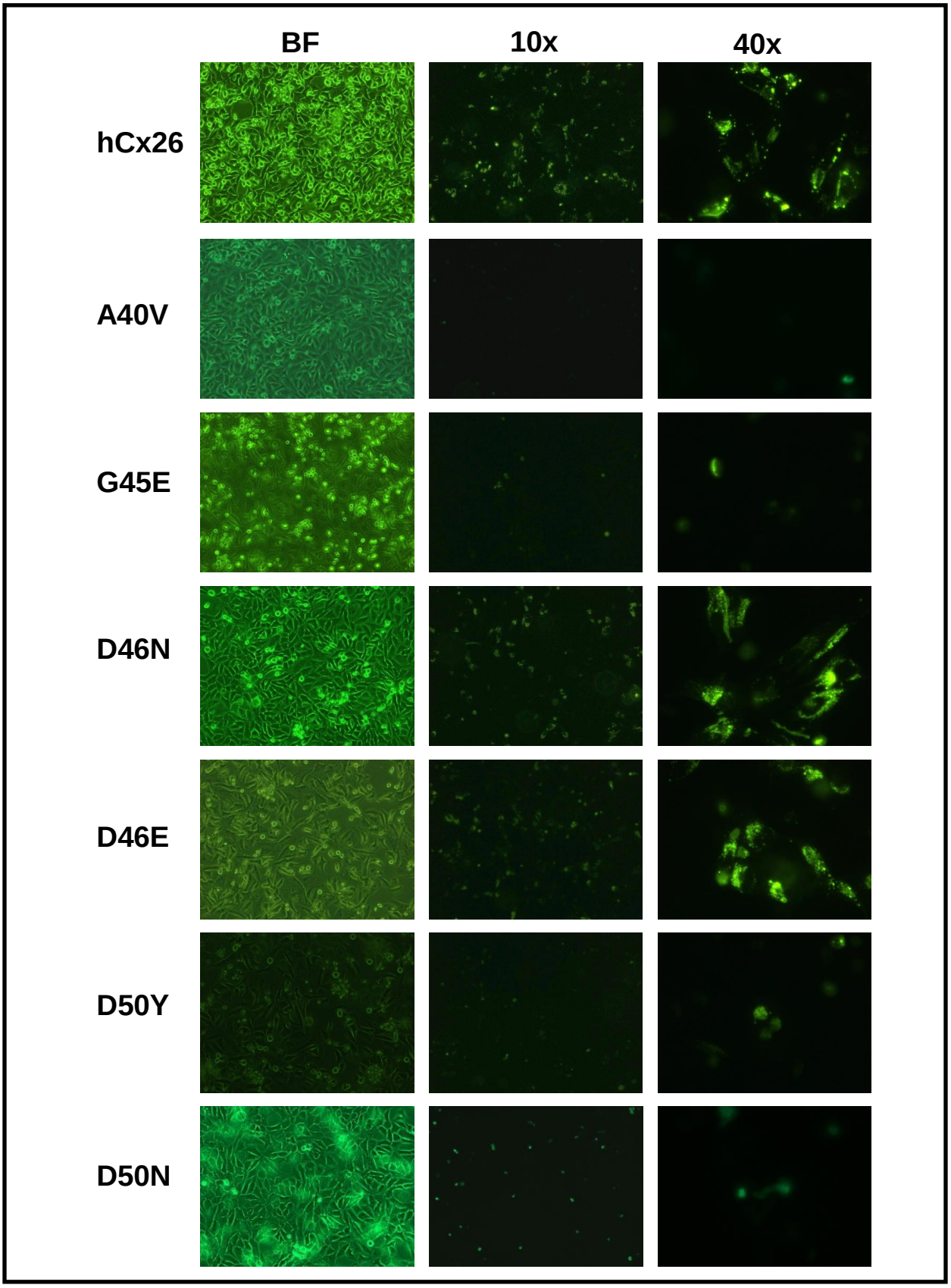
BF
10x
40x
hCx26
A40V
G45E
D46N
D46E
D50Y
D50N

Figure 4.17 Expression of hCx26-eGFP and its mutants in HeLa cells.

Human Cx26 or its mutants were tagged with eGFP at the end of C-terminal and transfected into HeLa cells. After 2-day post-transfection, the fluorescence of eGFP was checked under the fluorescence microscope with different magnifications. BF represents bright filed; 10x represents objective with 10 times magnification; 40x represents objective with 40 times magnification.

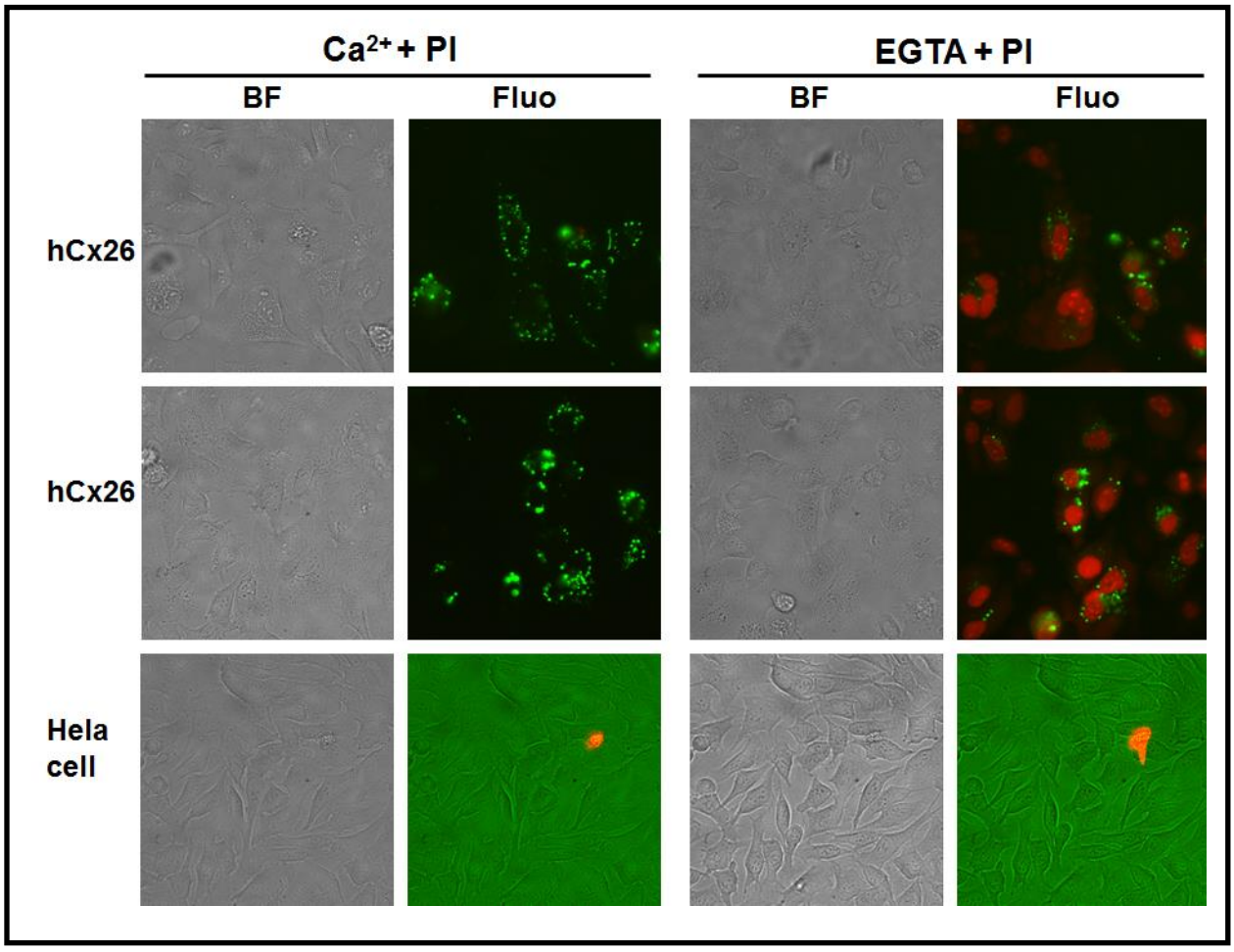

Figure 4.18 hCx26 dye uptake in the presence of Ca^{2+} or EGTA.

hCx26 tagged with eGFP was transfected into HeLa cells and non-transfected cells were negative control. Cells were incubated with bath solution containing 2 mM Ca^{2+} and 0.5 mg/ml PI for 10 minutes and checked under fluorescence microscope. Then the bath solution was replaced by new bath solution with 2 mM EGTA and 0.5 mg/ml PI for another 10 minutes.

We also compared the dye uptake in wild type Cx26 and one mutant D46N (**Fig. 4.19**). In the presence of $[Ca^{2+}]_o$, both wild type Cx26 and D46N could not be loaded with PI dye. Replacement of $[Ca^{2+}]_o$ with EGTA, cells transfected with wild type Cx26 was loaded with PI dye, while no PI dye uptake was observed in cells expressing mutant D46N. There are two possible reasons accounting for this phenomenon: 1) hCx26-D46N cannot be transported to the membrane and cannot assemble to hemichannels on the cell surface. The so-called surface observed in the image with 40 times magnification may not be the true membrane. Besides, even though it is cell surface, no evidence can prove hemichannels are formed. 2) D46N harbors altered channel permeability compared with wild type hCx26. Thus, dye uptake could not be used to study all those Cx26 mutants resided inside of the predicted Ca^{2+}-binding pocket. Most mutants in the predicted Ca^{2+}-binding pocket are lethal. Expression of those mutants led to cell apoptosis and death. Mutants which expressed well in HeLa cells either have disturbed surface expression, or have altered hemichannel permeability, or have impaired hemichannel assemble capability. We could not find a proper way to study those mutants using the instruments we own in our lab.

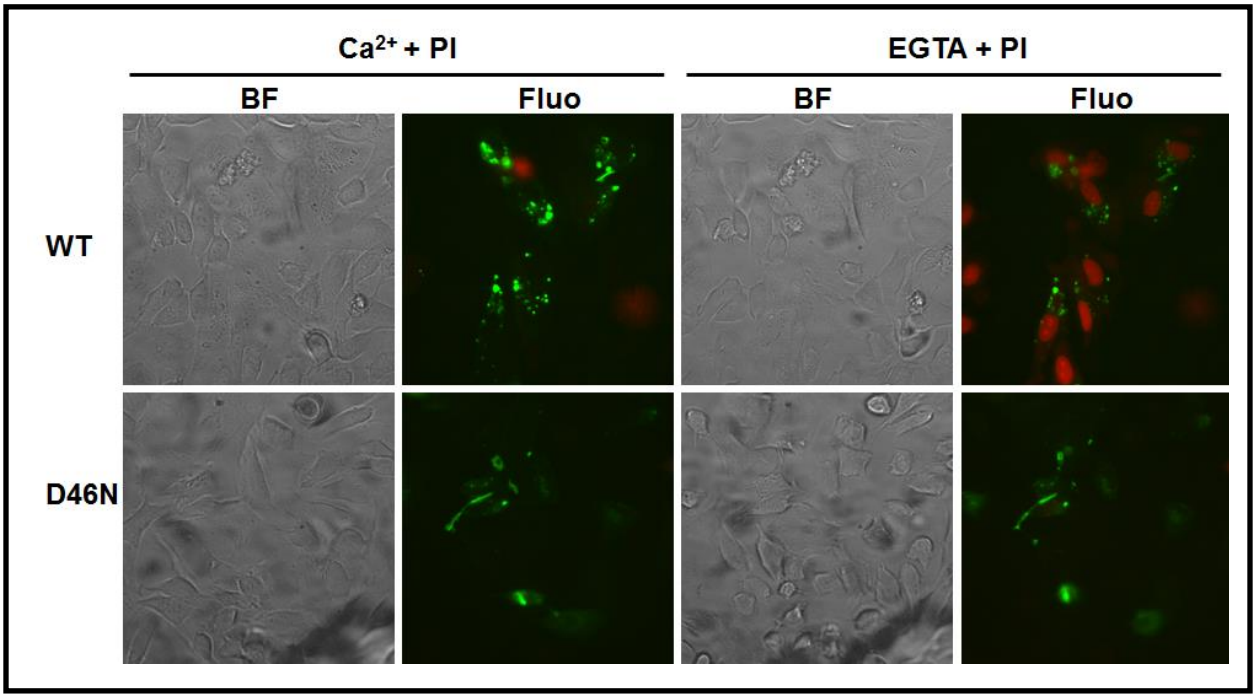

Figure 4.19 Dye uptake comparison between wild type Cx26 and mutant D46N.

Wild type Cx26 and mutant D46N tagged with eGFP were transfected into HeLa cells. After 2-day post-transfection, cells were placed in bath solution with 0.5 mg/ml PI dye and 2 mM Ca^{2+} for 10 minutes and dye uptake was monitored under fluorescence microscope simultaneously. Without moving the view under microscope, bath solution with Ca^{2+} was removed and new bath solution with 2 mM EGTA and PI dye was added. Dye uptake inside of same cells were examined.

In summary, Cx26 hemichannels have high permeability of PI dye in the absence of Ca^{2+}. Addition of 2 mM Ca^{2+} into the dye solution completely blocked the dye permeability through Cx26 hemichannels, which indicates that $[Ca^{2+}]_o$ can induce the closure of Cx26 hemichannels. Mutating the predicted Ca^{2+}-binding coordination ligand or residues in the pocket led to cell

apoptosis which may be caused by abnormal Ca^{2+} regulation. Although D46N mutants did significantly influence the cells death, this mutant was not loaded by PI dye in the absence of Ca^{2+}, which indicated that either the surface expression was severely impaired or this single mutation resulted in closed conformation of Cx26 hemichannels.

4.2.8 Monitoring Channel Activity of Proteo-liposomes with Cx26 Gap Junction in Single Oocytes

To examine the hemi-channel activity of the reconstituted gap junction protein Cx26 and the extracellular Ca^{2+} effects on it, we performed two electrons whole cell voltage clamp experiment to measure the opening of protein conducting channels. Oocytes are considered as a valuable tool for study of external channels since oocytes do not have significant expression of ion channels or receptors (479). The study of exogenous channels will not be affected, though oocytes do express some channels and receptors (480,481), due to the low current of those endogenous channels. The conventional way to study channels in oocytes is through mRNA or cDNA injection. The target channels are firstly expressed and assembled into the oocyte membranes, allowing channel activity measurement by different biochemical or electro-physiological methods when they respond to different intracellular or extracellular stimuli. The cell surface of oocytes is much bigger than mammalian cells, thus they can allow the accommodation of many channel proteins to ensure huge total channel activities.

There are some limitations to perform channel studies in oocytes. To begin with, mRNA or cDNA may be not available in some cases. Second, some eukaryotic membrane proteins cannot successfully expressed in oocyte or inserted on the oocyte membrane due to the different translation machinery or lipid component. Third, if our interest is not a single membrane protein, but a membrane complex with multiple membrane proteins, simply by injecting mRNA or cDNA

of different membrane proteins into oocytes, we cannot guarantee the formation of complex inside of oocytes. On the other hand, by injecting proteo-liposomes into oocytes, we can overcome some challenges that faced by the conventional method. Firstly we can reconstituted membrane protein or membrane protein complex into the liposome to form proteo-liposomes, which is subjected into oocyte injection. If we want to study the effect of different modulators, we can inject the proteo-liposomes with different modulators. This methodology avoid problems associated with eukaryotic membrane proteins, such as protein folding, assembly, post-translational modification, and trafficking. We can easily study the membrane protein complex by simply reconstitution of membrane protein complex into liposome. For example, as shown in figure 4.20, bacterial ATPase SecA and SecYEG complex are reconstituted into liposome together to form proteo-liposomes with both protein inside. This method also provide such a good way to study lipid effect on channel activity.

Using this method, here we demonstrated the importance of lipids on Cx26 channel activity and identified several lipoid composition in which Cx26 channels showed much higher activity. Besides, this system was turned out to be an efficient way to study Cx26 channel activities in the presence of different regulators.

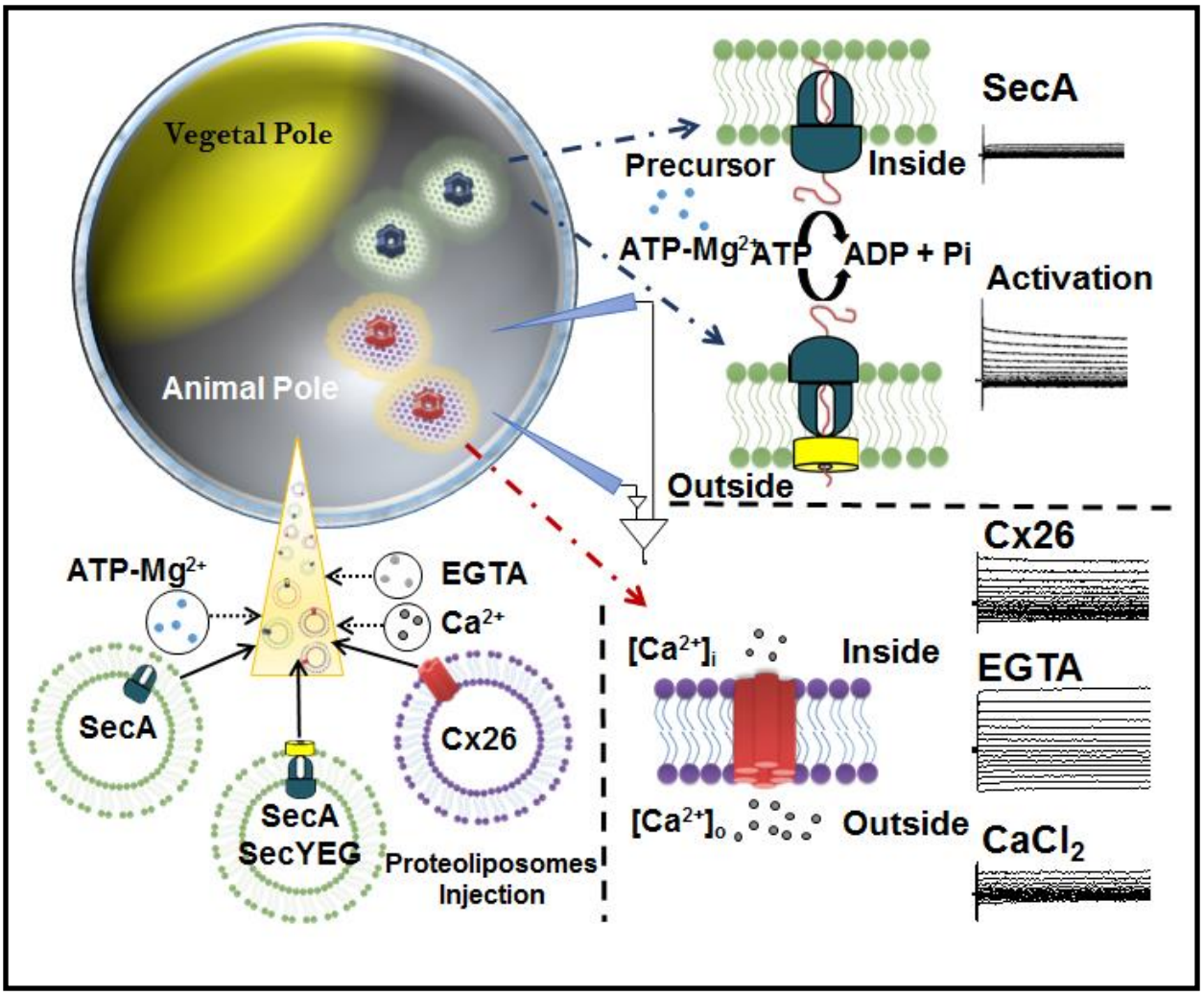

Figure 4.20 Working model: injection of proteo-liposomes in oocyte

Membrane protein or membrane protein complex were firstly reconstituted into liposome to form proteo-liposome. Proteo-liposomes were injected into oocytes at dark side animal pole for whole cell channel activity measurement. Cx26 proteo-liposome and SecA proteo-liposomes were used as two examples here to demonstrate how this system works.

To study the extracellular Ca^{2+} effects on Cx26, we inserted the reconstituted Cx26 liposomes into the oocytes, allowing the study of Cx26 channel activity with its regulatory

molecules. The interaction between membrane protein and membrane lipids play important role in the structure and function of membrane proteins (482-487). We first tested the effects of lipid composition on Cx26 channel activity. The endogenous phospholipids that tightly associated with hCx26 hemichannel or gap junction plaque were identified by Tandem electrospray-mass spectrometry and the proportion of them was analyzed, respectively, in earlier work (488). For our mCx26 purified from Sf9, different lipid combinations including PC, PS, PE, PG, 2PC/PS, 3PE/PG and E.coli total lipid were tested (**Fig. 4.21).** The channel activity was reflected by the channel current. It is surprised that Cx26 reconstituted in E.coli total lipids displayed the highest channel activity, as indicated by the channel current, followed by 2PC/PS and 3PE/PG. Single category of lipid like PC, PS, PE and PG only dramatically decreased the channel activity by more than 50 %. Thus, in the following experiments, we reconstituted Cx26 into the 2PC/PS liposome.

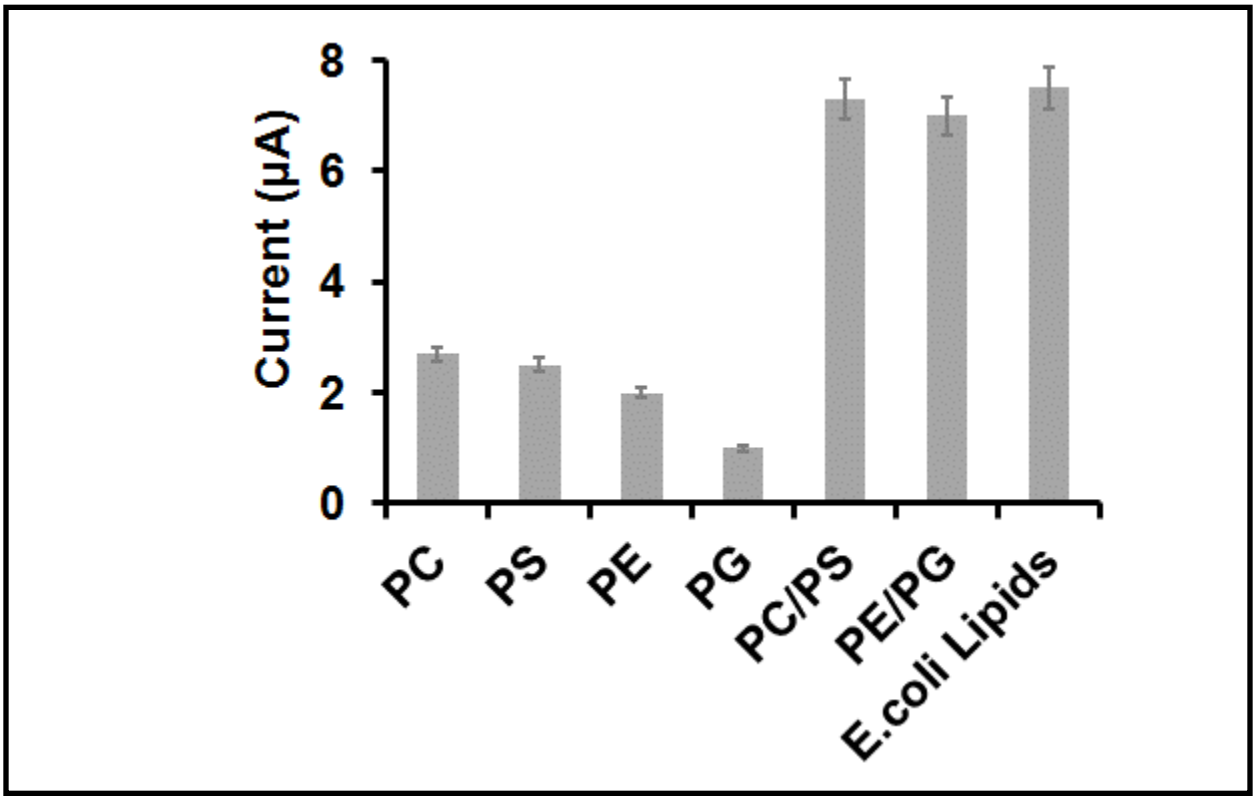

Figure 4.21 Effects of lipid compositions on Cx26 channel activity.

Cx26 purified from Sf9 were reconstituted into liposome and injected into the oocytes. The current of Cx26 inserted on the oocyte membrane were recorded. The ratios of PC/PS and PE/PG were 2:1 and 3:1, respectively.

The "expression" time course of Cx26-proteoliposome was firstly examined by measuring the channel currents at different time points after injection of Cx26-proteoliposome with 5 mM EGTA. The channel current reached its maximum after half hour post-injection (**Fig. 4.22a**). The low background current coming from the endogenous protein expressed in oocytes could be seen in oocytes without any liposome injection (**Fig. 4.22b**). Liposomes alone elicited very small background current, and EGTA slightly increased this current, indicating there was small endogenous channel activity (**Fig. 4.22b, lanes 2 and 3**), however this endogenous current was Ca^{2+}-independent (**Fig. 4.22b, lane 4**) since $CaCl_2$ did not make any changes regarding to the current. A small ionic channel activity around 2 μA was produced with the injection of Cx26-proteo-liposomes. This low activity may be caused by the inhibition of cytosolic Ca^{2+}. The activity of Cx26-proteoliposomes was slightly inhibited by co-injection with 2 mM $CaCl_2$ (**Fig. 4.22b, lanes 5 and 6**). In contrast, this activity was increased greatly to 7 μA by co-injection with 5 mM EGTA (**Fig. 4.22b, lane 7**); addition of $CaCl_2$ reduced the current back to less than 2 μA (**Fig.** 4.22**b, lane 8**).

Addition of 10 mM EGTA into the bath solution in which oocytes with injection of Cx26 proteo-liposome were immersed alone generated an increase of ion current from 2 to 7 μA within 2 minutes (**Fig.4.23a**). Further addition of 30 mM $CaCl_2$ immediately decreased this current from 7 back to 2 μA within 2 minutes (**Fig. 4.23a and b inset**). We also tested how much $CaCl_2$ is

needed to decrease the channel current after injection Cx26-proteo-liposomes with 10 mM EGTA. Various concentrations of $CaCl_2$ were added into the extracellular bath solution and channel currents were recorded. The channel activity dramatically dropped when 0.1 mM $CaCl_2$ was applied and 0.2 mM $CaCl_2$ addition allowed current decreased back to around 2 μA. We also tested liposome alone. The ion current change in oocytes injected with liposome was not $CaCl_2$ dependent, through EGTA could slightly evoked an increase of ion current. Taken together, the observation that Ca^{2+} regulates Cx26 channel activity are compatible with other earlier studies done by injection of cDNA into oocytes.

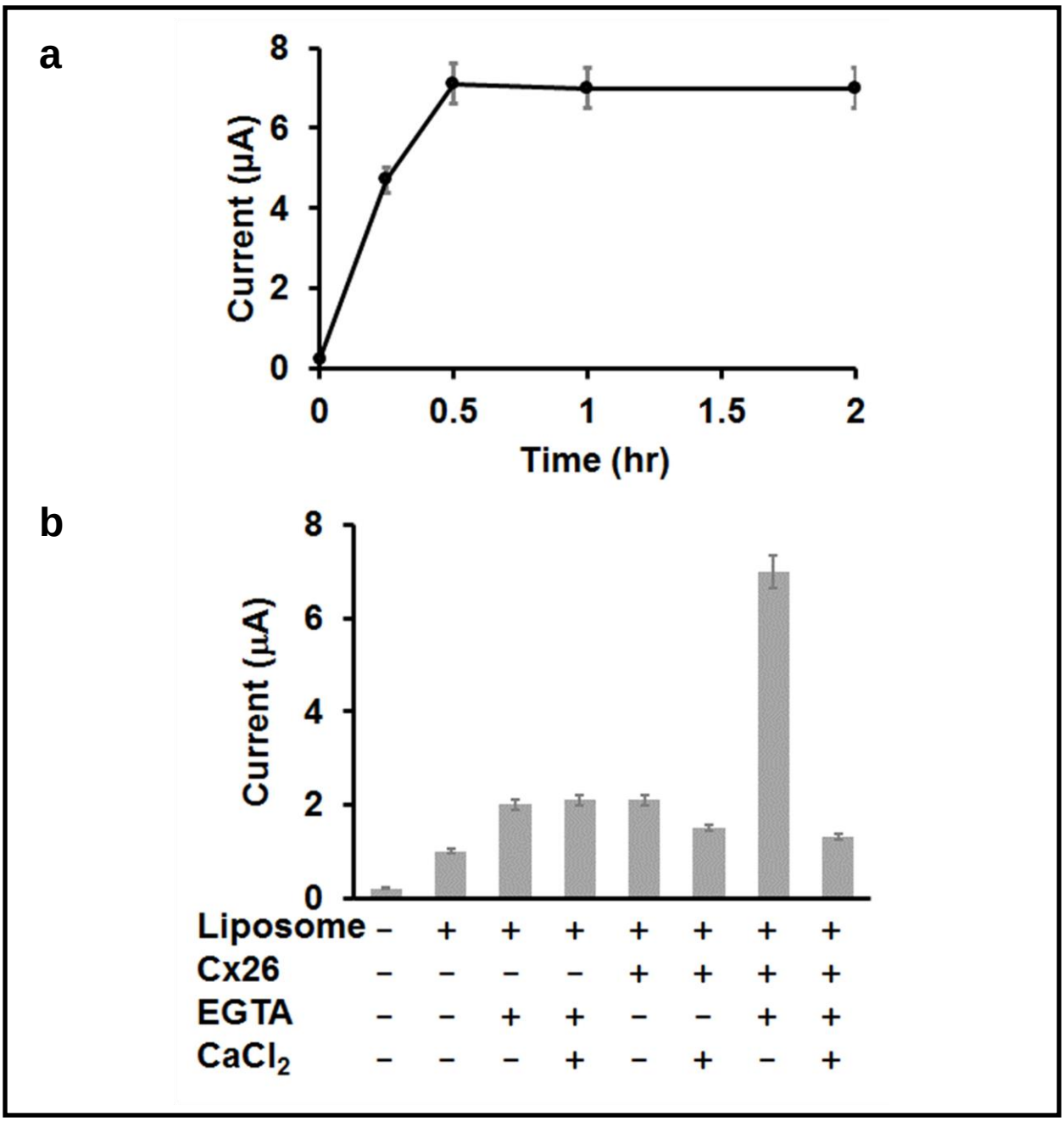

Figure 4.22 Channel activity of Cx26-liposomes in the oocytes.

(a) Time course of Cx26 channel expression injected with 5 mM EGTA. The current was checked every half hour post-injection and the recordings were for 1 min. Number of oocytes were around 15-20. (b)Liposome or Cx26-liposome were injected into oocytes with or without

co-injection of EGTA, and $CaCl_2$ as indicated. The lanes 4 and 6 were with 2 mM $CaCl_2$; lane 7 with 5 mM EGTA, and lane 8 was with 5 mM EGTA and 10 mM $CaCl_2$. Around 60 oocytes were examined for each condition.

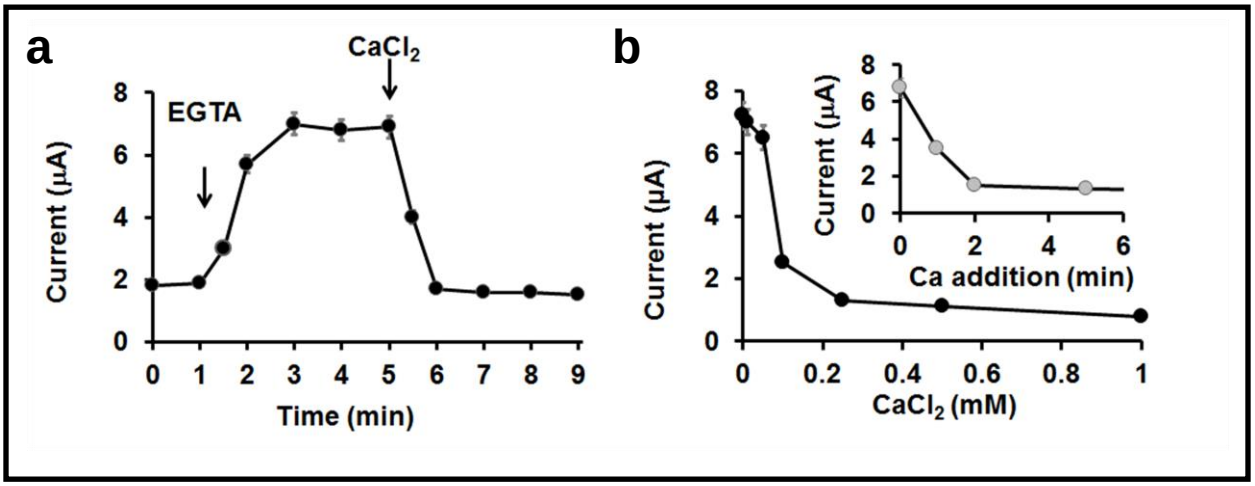

Figure 4.23 Cx26 channel activity regulated by $CaCl_2$.

(a) Cx26 proteo-liposomes were injected into oocytes. The ion current were monitored after 30 minutes. Then 10 mM EGTA was applied to the bath solution, followed by addition of 30 mM $CaCl_2$. Ion currents were monitored at different time points. (b) Cx26-proteo-liposomes were injected into oocyte with 10 mM EGTA. After 30 minutes, current recorded was around 7 μA. Then various concentration of $CaCl_2$ were added into bath solution before measuring currents. Number of oocytes was around 15-20.

4.3 Discussion

In this study, we predicted a putative Ca^{2+}-biding site residing at the mouth of extracellular side of Cx26 hemichannel channel using MUG^{SR}. MUG^{SR} is an updated based on our previous algorithm MUG which utilizes multiple geometries in the Ca^{2+}-binding pockets of holo-proteins

to identify possible Ca^{2+}-binding site. One of the drawback of MUG is that it does consider the possible conformational change induced by Ca^{2+}-binding. The new MUG^{SR} will first predict the Ca^{2+}-binding pocket as MUG does and then allow minor localized backbone conformation change or side chain rotation. Our prediction revealed that Ca^{2+} ion could be coordinated by oxygen atoms from residues E42, D46, E47, and E187. Among them, E47 is from adjacent Cx26 monomer. Thus, 6 possible Ca^{2+}-binding site exist in one hexamer (Hemichannel). Recently, a Ca^{2+}-bound Cx26 crystal structure was deposited in PDB with a refined resolution of 3.3 Å (88)(**Fig. 1.6)**. Ca^{2+} ion was coordinated by residues E42, G45, and E47. E42 is from monomer A and the rest two residues are from adjacent monomer B. By comparing the "apo-Cx26" structure with this bound form, they concluded that only little conformational change without physical closure of the channel upon Ca^{2+}-binding was observed as reviewed in the first chapter. By further investigating the electrostatic surface of the channel pore of Ca^{2+}-free and Ca^{2+}-bound Cx26, they believed that the strongly negative potential in the Ca^{2+}-binding pockets of Ca^{2+}-free Cx26 enables the rapid enter of positive ions like K^+, while Ca^{2+}-occupied Cx26 will exclude all those ions with positive charges. Finally they drew the conclusion that it is the electrostatic surface difference between Ca^{2+}-free and Ca^{2+}-bound Cx26 regulating the ion permeation. However, I have a few concerns about their conclusions. First, when they tried to obtain the Ca^{2+}-free Cx26 crystal, they did not use chelators like EGTA or EDTA in the buffer to completely remove Ca^{2+}, instead they just simply omitted $CaCl_2$. It is highly possible that the Ca^{2+}-free structure they believe is not the real free structure. It is hard to get rid of Ca^{2+} in the buffer since Ca^{2+} could exist in water used to prepare all buffers if chelator is not used. In this case, the comparison is of less meaning. Second, a very high concentration of Ca^{2+} (20 mM), far beyond the physiological level, was applied when they grew the Cx26 crystals. It is hard to believe the regulation mechanism they proposed here is

a physiologically relevant mechanism. It will be more persuasive if the Ca^{2+} concentration they used is more close to physiological extracellular Ca^{2+} concentration (around 1.8 mM). However, on the other side, this Ca^{2+}-bound crystal structure is almost overlapping with our predicted Ca^{2+}-binding pocket, indicating high accuracy of our computational algorithm

Due to the synthesis, trafficking, and translocation machinery difference between prokaryotic and eukaryotic organisms, high level expression of Cx26 in *E.coli* was not successful. This eukaryotic channel protein caused high toxicity to many E.coli stains as indicated by death of *E.coli* after transformation. Insect cell expression is a better candidate for Cx26 expression than *E.coli* in terms of yield, post-translational modification, trafficking, and translocation. Cx26 were located on insect cell surface and formed oligomers with proper shape under electron microscope. However, protein purified from Sf9 using detergent is not homogeneous and stable. Oligomers with different molecular size were detected by both SDS-Page gel, Western blotting, and native gel. This heterogeneity of Cx26 protein sample caused lots of problem when we tried to investigate the metal-binding property and Ca^{2+}-regulation characteristics. For example, the consistency for all experiment could not be maintained well. Cx26 wrapped by detergent is also not very stable. Gentle mixing or shaking when performing the titration experiment also caused signal inconsistency. The instability also brings lots of difficulty in storing the protein. We could not store Cx26 for over a week without precipitation. Moderate content of concentration also led to heavy precipitation. However, if we want to perform NMR experiment, we need homogeneous and high concentration of Cx26.

Tb^{3+} titration showed a two-phase binding status with different binding affinity and hill number. The first one binding state was well fit to 1 to 1 binding equation which assumes only one binding site exists. The second binding phase was fit to hill equation and yielded a hill number of

4.2, which indicates the existence of more than 4 binding site and cooperative binding property between them. This observation could be explained by the number of Tb^{3+}-binding site in Cx26 hexamer. Each Cx26 monomer harbors one Tb^{3+} binding site and there will be 6 of them in total in the hexamer. However, no significant change was detected in either Ca^{2+} titration experiment or Ca^{2+}-Tb^{3+} competition experiment. It seems the recent published Cx26 crystal structure with Ca^{2+} bound provides us with some clues. Upon Ca^{2+} binding, only very tiny conformation change was induced. Those localized changes occur in Ca^{2+}-binding ligand and residues inside of the Ca^{2+}-binding pocket. This result is consistent with our CD data and Ca^{2+} titration result in which no significant conformation changes were observed. The Ca^{2+}-binding affinity in Cx26 must be weak since Cx26 extracellular loops are exposed to $[Ca^{2+}]_o$ with a concentration in the mM range. This weak Ca^{2+}-binding may account for the unsuccessful Ca^{2+}-Tb^{3+} competition. The Ca^{2+}-binding site was also only observed in Cx26 crystals soaked in 20 mM $CaCl_2$.

Using mammalian cells, we proved that Cx26 hemi-channel permeability is regulated by $[Ca^{2+}]_o$. The expression pattern of Cx26 is not similar to other membrane proteins like cGPCRs. It presents on cell surface as punctate distribution. This phenomenon is associated with gap junction plaque. Gap junction plaques contains thousands of gap junction channels. Thus, Cx26 channels are not evenly distributed on cell surface, instead they gather together, showing as the punctate. When replacing the key residues inside of our predicted Ca^{2+}-binding pockets, most mutants led to cell apoptosis and death after transfection. This may be caused by the aberrant channel permeability and interrupted channel regulation by $[Ca^{2+}]_o$. Although D46 mutations did not led to lethal effect on HeLa cells, hemichannels formed by D46 mutants are not functional. Cx26 permeable dye PI could not enter the channel even in the absence of $[Ca^{2+}]_o$. Taken together, those

highly conserved residues inside of putative Ca^{2+}-binding site are of importance in structure and function.

5 ELUCIDATION OF A NOVEL EXTRACELLULAR CALCIUM-BINDING SITE ON METABOTROPIC GLUTAMATE RECEPTOR 5

5.1 Introduction

Metabotropic glutamate receptors, belonging to the family C G-protein coupled receptor (GPCR) family, can be categorized into three subgroups, group 1 (mGluR1 and mGluR5), group 2 (mGluR2 and mGluR3) and group 3 (mGluR4, 6, 7, and 8), based on sequence homology, G-protein coupling and ligand selectivity and the downstream signaling pathway (209,219,222,223,489). Sequence similarity can achieve as high as around 70% within each group, while between groups, this number decrease to 45% (209). They are well recognized as the targets of the major excitatory neurotransmitter L-Glu in mammalian central nervous system. Their involvements in numerous (patho)physiological processes by responding to extracellular stimuli are well documented (193,210,270,490,491). mGluR family members share a similar structural topology. They have a large extracellular domain (ECD) at the amino terminal, which is connected to seven classic alpha-helical transmembrane domains by the Cys-rich domain. The ECD is also referred as the Venus flytrap domain (VFD) due to its unique shape (163). Ligand binding to the VFD induces large conformation changes, resulting in the closure of the VFD and activation of mGluR (164). Two protomers form the functional dimer through the interaction between two VFDs (163). The carboxyl terminal facing the cytosol undergoes alternative splicing in several mGluRs, generating several variants (200,492-497), although the function of them still needs to be further elucidated. The widespread distribution of mGluRs in the central nervous system (CNS) and its extensive involvement in an array of signaling pathways attract considerable attention as drug targets for therapeutic remediation of a wide variety of CNS disorders.

Group I mGluRs (mGluR1 and mGluR5) are preferentially coupled to $G_{q/11}$, though in some cases Gi/o activation by group I mGluRs was observed (197,498) (**Fig. 5.1**). Activation of mGluR5 by extracellular stimuli subsequently stimulates phospholipase C, leading to the decomposition of PIP2 into IP3 and DAG. IP3 binds to IP3 receptors on the endoplasmic reticulum (ER), resulting in calcium release from intracellular calcium store. DAG on the cell membrane in turn activates protein kinase C, which has been proposed to be involved in activation of many enzymes by phosphorylation. In addition to this conventional pathway, alternative group I mGluRs-associated signaling pathways have also been identified (211).

Group I mGluRs share around 30% homology with calcium sensing receptor (CaSR) and 69 % homology with salmon bifunctional metabotropic (sBim) receptor. Belong to the same GPCR family, both CaSR and sBim receptor showed extracellular calcium $[Ca^{2+}]_o$ sensing capability(280,499,500). Therefore, the homology raised the question whether mGluR1 and mGluR5 can respond to $[Ca^{2+}]_o$ changes decades ago. Multitudes of studies using either heterologous systems or cells with native mGluRs suggested that extracellular Ca^{2+} directly activate or modulate the actions of agonist on some type of mGluRs, although there are some contrary results (287). By monitoring the activity of Ca^{2+}-Cl^- channels in oocytes expressed mGluR1 or mGluR5, Kubo et al., first reported that mGluR1/mGluR5 displayed similar response to CaSR with the application of extracellular Ca^{2+} (281). The ECD was identified as the key player for sensing extracellular Ca^{2+} by constructing chimeric molecules and S166 in the ECD of mGluR1 was proposed as the structural determinant for Ca^{2+} sensitivity. Purikinje cells from wild type mouse with predominant mGluR1 expression could sense $[Ca^{2+}]_o$, whereas the Ca^{2+}-sensing capability was lost in Purikinje cells derived from mGluR1 knockout mouse and regained in cells from mouse with mGluR1 re-introduced (286). In addition to direct activation, $[Ca^{2+}]_o$ also exerted

modulatory effect on various compounds which act on mGluRs. Sunders *et al*. reported that the [^{3}H]-InsP1 accumulation evoked by mGluR1 agonist was significantly facilitated by increasing $[Ca^{2+}]_o$ in baby hamster kidney cells (283). $[Ca^{2+}]_o$ also exerted marked broadening effect on the dynamic range of DHPG-evoked responses mediated through mGluR1 in Purikinje cells (286). Our lab also reported the modulatory effects of $[Ca^{2+}]_o$ on orthosteric or allosteric ligands observed in HEK293 cells expressing mGluR1 (501,502). The molecular elucidation of how $[Ca^{2+}]_o$ activate or modulate mGluRs remains controversial, although tremendous effort have been made to address this question since it was first raised. Advances in solving the crystal structure of mGluR have uncovered important structural characteristics of mGluRs, however, the invisibility of Ca^{2+}-binding site in solved mGluR crystal structures greatly hampered the study of Ca^{2+}'s role in modulating activity of mGluRs.

In the present study, we predicted a conserved Ca^{2+}-binding site in the hinge region of mGluR5 using our computational algorithm MUG. To investigate the connectivity between $[Ca^{2+}]_o$-binding site and function of mGluR5, and how $[Ca^{2+}]_o$ modulates the activity of mGluR5, we monitored the downstream intracellular signal changes in HEK293 cells expressing wild type and mutated mGluR5. We first demonstrated that mGluR5-ECD purified from insect cell Sf9 is able to bind with both Tb^{3+} and Ca^{2+} with μM and mM affinities, respectively. We further found that $[Ca^{2+}]_o$ could solely elicits mGluR5, leading to $[Ca^{2+}]_i$ oscillation and ERK1/2 phosphorylation. Higher $[Ca^{2+}]_o$ could induce broader dynamic changes in terms of oscillation frequency, amplitude of oscillation peaks, and amount of phosphorylated ERK1/2 accumulation. Mutating key residues in the predicted Ca^{2+}-binding pocket impaired the Ca^{2+}-sensing capability of mGluR5, though the surface expression level of mutants were maintained at similar level as wild type mGluR5, suggesting those putative residues are involved in Ca^{2+}-binding. In addition,

we examined the role of $[Ca^{2+}]_o$ in modulating the actions of L-Glu on mGluR5 in wild type or mutated mGluR5 transfected HEK293 cells, and also the effects of L-Glu on $[Ca^{2+}]_o$ in activating mGluR5.

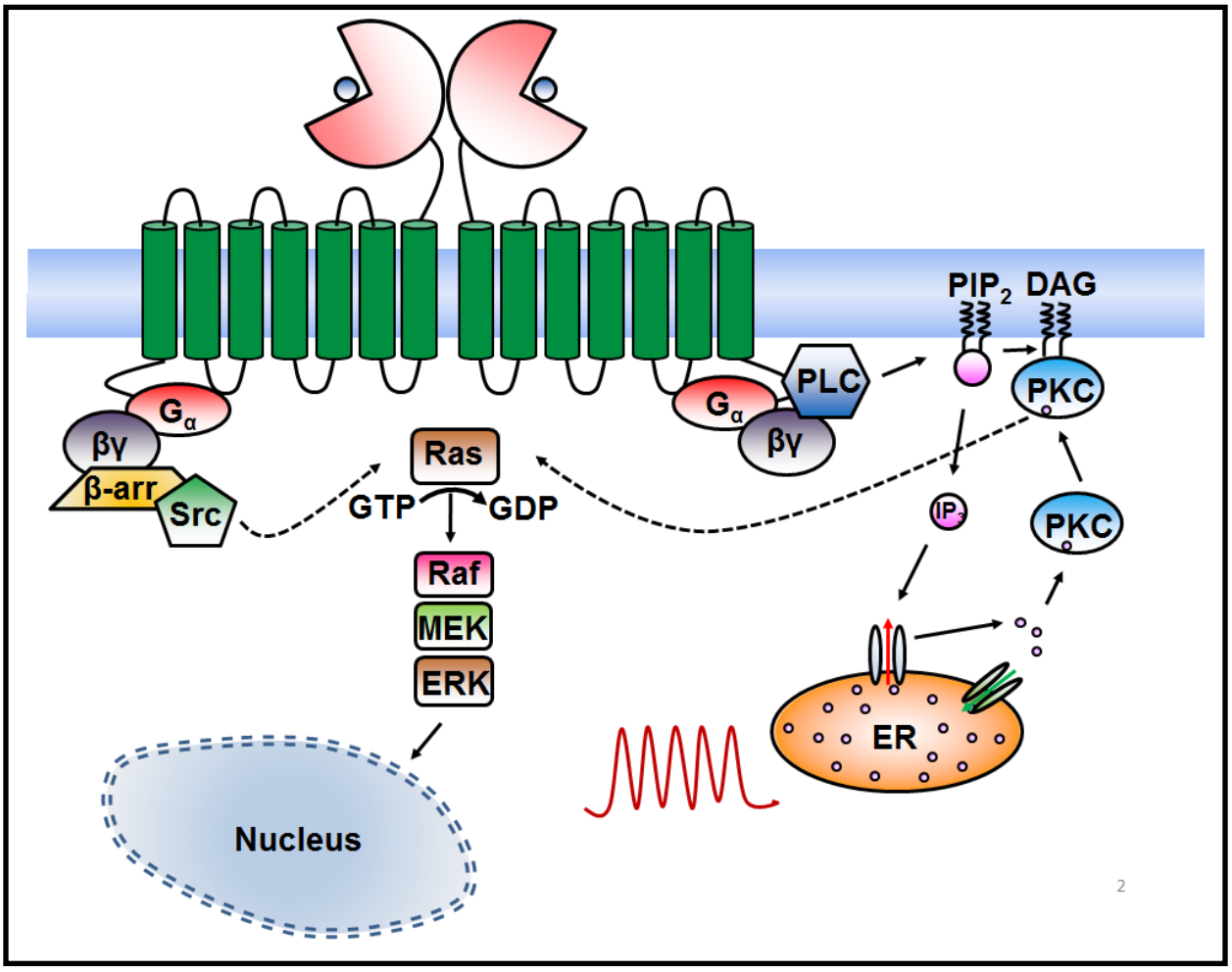

Figure 5.1 Signal transduction pathways activated by mGluR5 stimulation.

Agonist binding to mGluR5 activates G-protein signaling and downstream second messenger pathways including PKC, PLC and Ca^{2+} signaling. The conventional signal pathway mediated through mGluR5 is G-protein- and PLC- dependent. Activation of mGluR5 initiates Gα/q protein signaling that activates PLC. In turn, activation of PLC results in the

hydrolysis of phosphatidylinositol-4, 5-bisphosphate (PIP_2) to release the second messengers 1,2-Diacylglycerol (DAG) and IP_3. DAG is the physiological activator of PKC, which in turn plays important roles in various intracellular signaling cascades. IP_3 binds to intracellular IP_3 receptors on the ER membrane initiating Ca^{2+} release from the ER lumen into the cytoplasm, generating complex downstream Ca^{2+} signals and intracellular Ca^{2+} oscillation. The other signaling pathway will be monitored in my study is the Ras-Raf-MEK-ERK pathway. Activation of PKC will also activate Ras, initiating the PLC-dependent conventional Ras-Raf-MEK-ERK pathway. In addition to this conventional ERK signaling pathway, other novel PLC-independent pathway involving some small adapting proteins.

5.2 Result

5.2.1 Prediction of Ca^{2+}-binding site in the extracellular domain (ECD) of mGluR5

In the previous study, we identified a Ca^{2+}-binding site in the mGluR1 which is a group 1 mGluR using our graph theory-based algorithms MUG (501,503). The binding site is located in the hinge region of the ECD adjacent to the L-Glu binding site (**Fig. 5.2**). Residues D318, D322, D325 and the carboxyl group of the receptor's agonist Glu comprise the whole Ca^{2+}-binding site. D318 is shared by both the Ca^{2+}-binding and L-Glu binding site. When all the mGluRs are aligned together, it is notable that the putative Ca^{2+}-binding site we reported in mGluR1 is also very conserved in mGluR5, but not in the group II and III mGluRs. The conserved Ca^{2+}-binding site in mGluR5 constitutes residues D305, D309, D312 and the carboxyl group of agonist L-Glu. We hypothesize that Ca^{2+} binding to this region will activate mGluR5 and further induce the cytosolic Ca^{2+} concentration change.

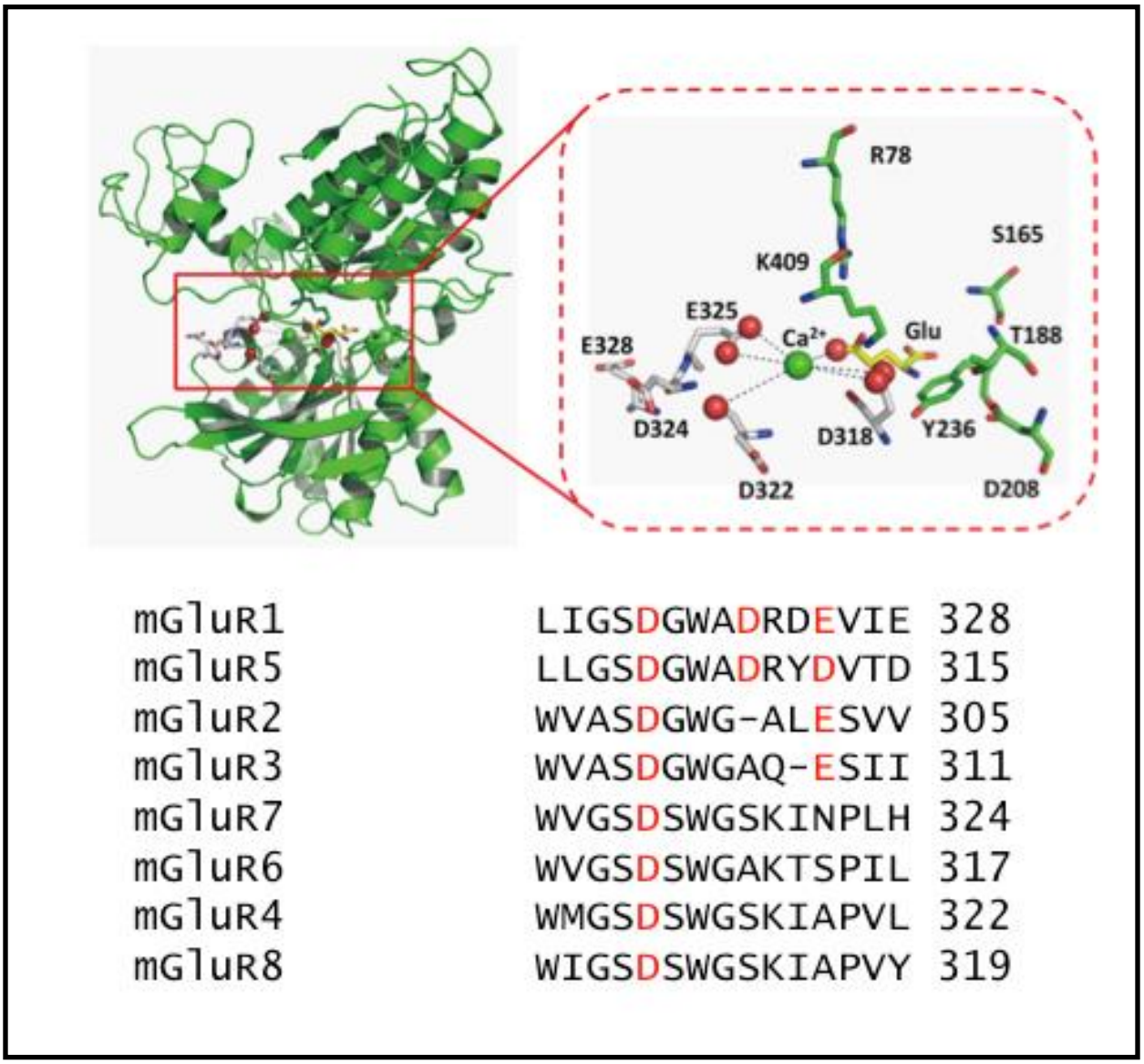

Figure 5.2 Putative Ca^{2+}-binding site in mGluR 1 and 5.

Our reported Ca^{2+}-binding site in mGluR1 is coordinated by amino acids D318, D322, D325 and adjacent agonist L-Glu. This site is located in the interface between lobe 1 and lobe 2 of mGluR1, adjacent to the L-Glu-binding site. Sequence alignment of all mGluRs shows that this pocket is highly conserved in group I mGluRs (mGluR1 and mGluR5), but not the rest

of mGluRs, although partial pockets exist in group II mGluRs (mGluR2 and mGluR3). The corresponding residues of the predicted binding site in mGluRs are highlighted in red.

5.2.2 Monitoring Ca^{2+} binding to mGluR5-ECD by fluorescence

We first evaluate the Ca^{2+} binding ability of mGluR5-ECD purified from the Sf9 culture. The purification of mGuR5-ECD from Sf9 culture is achieved through a special Ni sephorase beads, named as Ni sepharose Excel, which can tolerate high concentration of chelating ligand without Ni stripping even after incubation with10 mM EDTA for 24 hours. This beads allow direct medium loading without extensive and time-consuming pretreatment of medium containing chelating ligand, which is required to maintain well separated cells in suspension Sf9 culture. The purified mGluR5-ECD forms a dimer as indicated by the native gel (**Fig. 5.3**). The electrophoretic mobility in reducing SDS-Page and native gel are different. The band position in reducing SDS-Pages correlates well to the monomer (**Fig. 5.3a**), while the intermolecular disulfide bonds were not completed broken by the reducing reagent as indicated by the dimmer bands in western blot (**Fig. 5.3b**). Figure 4.2c shows that mGluR5-ECD exists as a dimer under native conditions (**Fig. 5.3c**).

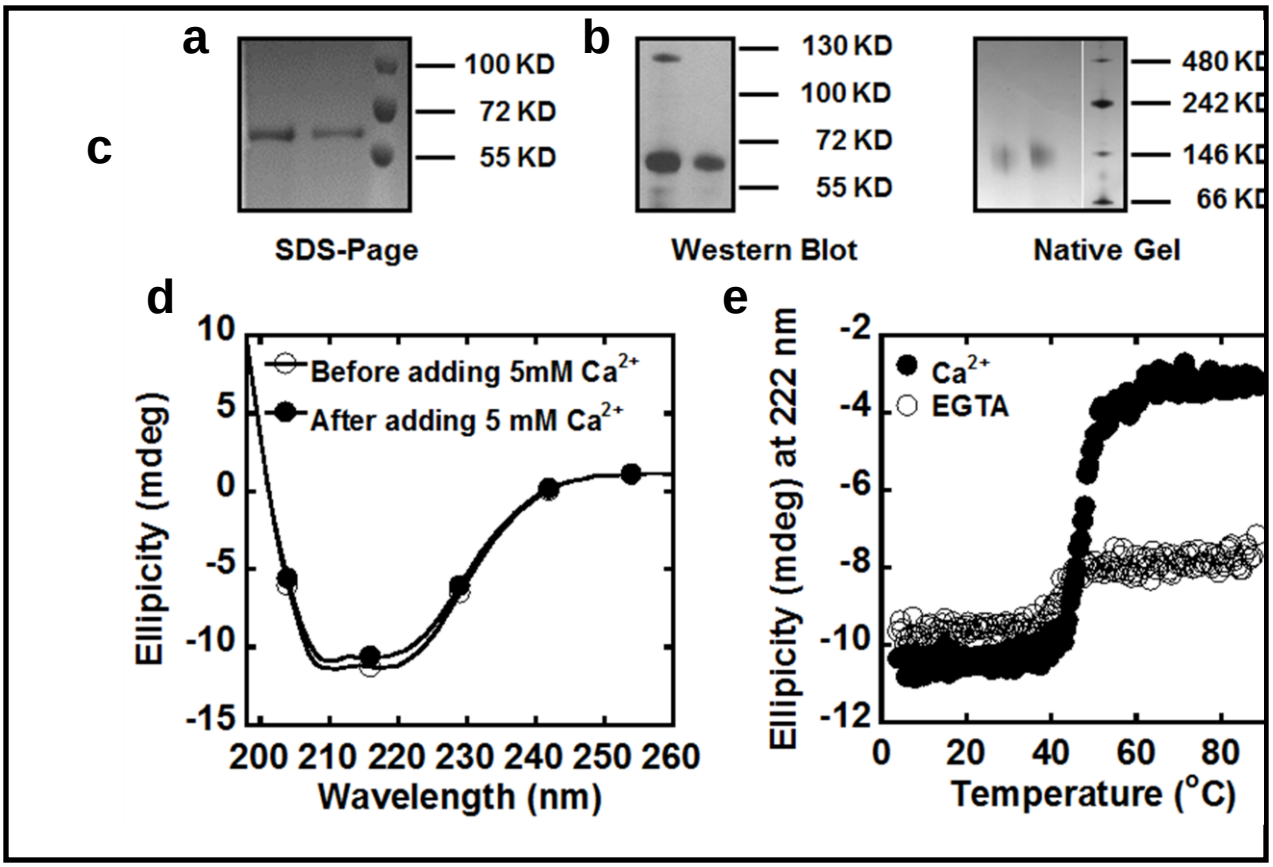

Figure 5.3 mGluR5-ECD forms a dimer.

(a) 5% β- mercaptoethanol was added in the SDS-PAGE sample buffer to break the disulfide bounds in mGluR5-ECD and the protein sample was subjected to SDS-PAGE. Monomer bands show between 55 and 72 kDa. (b) Anti-mGluR5 antibody was applied as mGluR5-ECD probe in western blot. In addition to the monomer as shown in SDS-PAGE gel, a weak dimmer band between 100 and 130 kDa also show up. (c) Under the native condition, mGluR5-ECD mobilize as a dimmer in the native gel. (d) Secondary structure of mGluR-ECD with or without the addition of 5 mM Ca^{2+} measured by CD. The peak at 208 and 222 nm confirms the helical structure of mGluR5-ECD purified from Sf9. Ca^{2+} did not induce significantly secondary structure change of mGluR5-ECD. Open circle: without addition of

5 mM Ca^{2+}; solid circle: with addition of 5 mM Ca^{2+}. (e) Thermal stability of mGluR-ECD in the presence or absence of Ca^{2+}. Signal at 222 nm was monitored while temperature was raised. Protein with Ca^{2+} was subjected heavy precipitation when temperature approached 45 °C, leading to inaccurate measurement of the thermo stability of mGluR-ECD. Open circle: with EGTA; solid circle: with Ca^{2+}.

The secondary structure of mGluR5-ECD was analyzed through circular dichroism (CD) measurement. The typical far UV CD spectrum of mGluR5-ECD was shown in Figure 4.2d. Analysis of the spectrum indicates mGluR5-ECD has a typical helical secondary structure, which is characterized by negative peaks at 222 and 208 nm. The addition of 5 mM Ca^{2+} to the protein sample produced minimal secondary structure change to the mGluR5-ECD. mGluR5-ECD was subjected to a stepwise increases in the temperature to measure the thermal stability in the presence of 5 mM EGTA or Ca^{2+}. The ellipticity signal was monitored from 4 to 90 °C at 222 nm (**Figure 5.3e**). During the experiment, protein with 5 mM Ca^{2+} started to form precipitation when temperature arrived above 45 degree. The reason behind this phenomenon is unclear to us.

Tb^{3+} is a common probe to study the Ca^{2+} binding to protein as a Ca^{2+} analog due to its high similarity with Ca^{2+} in radii and metal coordination chemistry. Sequence analysis of mGluR5-ECD revealed that a Trp residue is in the predicted Ca^{2+}-binding, therefore enabling the energy transfer between excited Trp and bound Tb^{3+}. As shown in Figure 5.4a, titration of Tb^{3+} into mGluR5-ECD induced an enhanced energy transfer between Trp and Tb^{3+}, consistent with Tb^{3+} binding to the predicted Ca^{2+}-binding pocket. In reverse, addition of Ca^{2+} to the Tb^{3+}-bound mGluR5-ECD led to the fluorescence intensity decrease, indicating competition between two metals (**Fig. 5.4c**). The normalized fluorescence change was plotted as a function of Tb^{3+}

concentration in Figure 5.4b. The Tb^{3+} binding affinity was yield by fitting the curve using a 1:1 binding equation. The well fitted titration curve suggests a 1:1 binding mode of the interaction between Tb^{3+} and mGluR5-ECD. The Ca^{2+}-Tb^{3+} competition experiment yielded the apparent dissociation constant from which the binding constant for Ca^{2+} was deduced (**Fig. 5.4d**). The Ca^{2+}-binding constant calculated from the Ca^{2+}-Tb^{3+} competition assay was 2.7 mM.

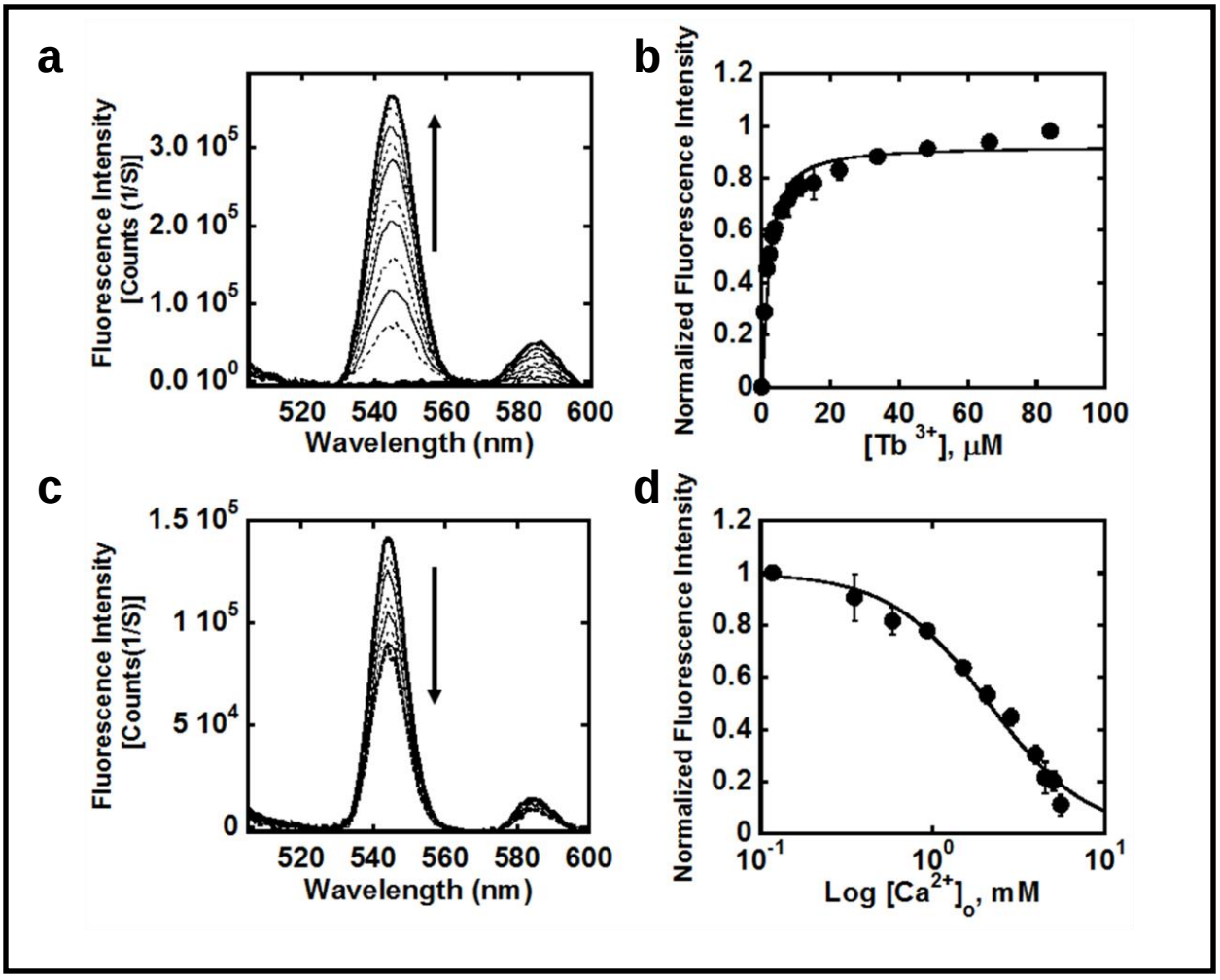

Figure 5.4 Determining Ca^{2+} binding capability using mGluR5-ECD purified from Sf9 culture. **(a) The calcium titration was performed in HEPES buffer (10 mM HEPES, 120 mM NaCl and 10 mM KCl, pH 7.2) with a protein concentration of 2.0 μM. The emission of internal**

Trp was monitored while titrating calcium. The arrow indicates the increase of Tb^{3+} fluorescence. (b) Magnesium titration curve of mGluR5-ECD. (c)Tb^{3+}-mGluR5-ECD fluorescence intensity change while titrating Ca^{2+}. The arrow indicates the decrease of Tb^{3+} fluorescence. (d) Ca^{2+}-Tb^{3+} competition curve of mGluR5-ECD.

5.2.3 Immunofluorescence analysis of surface expressed WT and its mutants in HEK293 cell

To evaluate the effects of mGluR5 mutations on cell surface expression in detail, HEK293 cells transfected with WT or mutated mGluR5 were fixed, stained with anti-FLAG antibody and examined by immunofluorescence microscopy. Without triton permeabilization, anti-FLAG antibody only detects the surface-expressed mGluR5. In cell that express the mGluR5 or mutants, anti-FLAG antibody detected similar intensity of signals on the cell surface (**Fig. 5.5a**). To further quantify the effect of these mutations on cell surface expression, cell surface protein isolation kit was used to isolate surface-expressed mGluR5 and compare the cell surface expression of WT mGluR5 and mutant mGluR5 (**Fig. 5.5b and 5.5c**). Cell surface proteins were labeled by a cell-impermeable, cleavable biotinylation reagent (Sulfo-NHS-SS-Biotin). After lysing the cells, all biotinylated surface proteins were isolated by streptavidin affinity chromatography. Using western blot with anti-FLAG antibody, we detected similar amount of biotinylated WT and mutated mGluR5, though D305A and D309A displayed a slightly lower amount of surface expression. Therefore, all mutants are properly expressed on the cell surface at similar levels.

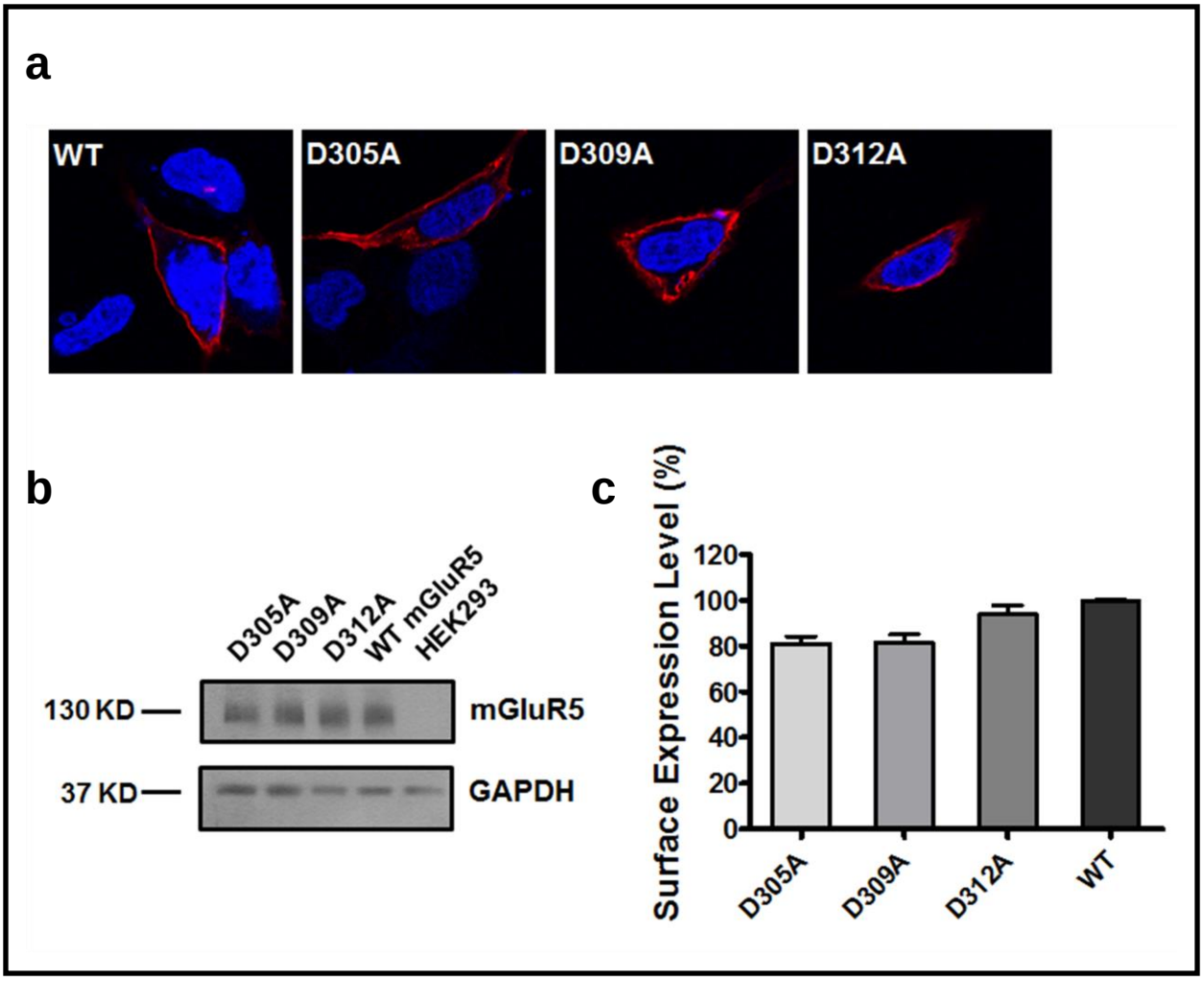

Figure 5.5 Analysis of cell surface expression of mGluR5 and its variants.

(a) Immunostaining of cell surface-expressed mGluR5 and its mutants. Immunostaining of non-permeabilized HEK293 cells expressing mGluR5 was done with monoclonal antibody, which recognizes the FLAG tag inserted in the ECD of mGluR5, and detection was carried out with Alexa Fluor conjugated, anti-mouse secondary antibody. Blue: DAPI staining cell nuclei. Green: mGluR5 immunoreactivity. (b) Cell surface protein biotinsylation and analysis. To specifically isolate and quantify mGluR5 on the cell surface, we labeled cell surface proteins with non-permeable but cleavable biotin first and isolated these tagged

proteins by streptavidin pull down. Then, the sample are subjected to SDS-PAGE separation, transferred to nitrocellulose membrane and probed with anti-FLAG antibody. GAPDH was used as an internal control. HEK293 cells without transfection was a negative control. (c) Quantification of cell surface expression was accomplished by densitometric measurement of the mGluR5 bands and subsequent normalization by GAPDH.

5.2.4 Extracellular Ca^{2+} solely elicits mGluR5-mediated $[Ca^{2+}]_i$ responses

We first examined whether $[Ca^{2+}]_o$ solely activates mGluR5 and elicits mGluR5-mediated $[Ca^{2+}]_i$ responses, monitoring the $[Ca^{2+}]_i$ concentration change by the ratiometric calcium dye Fura-2. Fura-2 is excited at 340 nm and 380 nm of light, and the ratio of the emissions at those wavelengths is directly related to the amount of intracellular calcium. mGluR5 transfected cells were loaded with Fura-2 before placed under the fluorescence microscope. Cells were bathed in 0 mM $[Ca^{2+}]_o$ solution, and then $[Ca^{2+}]_o$ was increased. As shown in Figure 5.6a, $[Ca^{2+}]_o$ stimulus induced $[Ca^{2+}]_i$ rise and oscillation similarly to the response of CaSR, as reflected by the emission ratio change of Fura-2, while no significant $[Ca^{2+}]_i$ responses could be detected in non-transfected HEK293 cells (**Fig. 5.6b**). In the single cell imaging experiment, three concentrations (0.5, 1.8 and 5.0 mM) of $[Ca^{2+}]_o$ were tested and applied to HEK293 cells transfected with mGluR5, respectively. All tested concentrations can elicits $[Ca^{2+}]_i$ responses in the manner of intracellular calcium oscillation, while the oscillation frequency varies (**Fig. 5.6c**). The centralized oscillation frequency range of cells exposed to 0.5 mM $[Ca^{2+}]_o$ stimuli was between 1 and 1.5 peak/min. The highest oscillation frequency that 0.5 mM $[Ca^{2+}]_o$ can achieve is 2.5-3 peak/min, while 5 mM $[Ca^{2+}]_o$ can even push this number to 3-3.5 peak/min. Higher concentrations of $[Ca^{2+}]_o$ further shifted the centralized oscillation distribution area to the right high oscillation frequency side in

addition to the decrease of percentages of cells oscillating at low frequency. To make a quantitative comparison of the mGluR5 responses to three $[Ca^{2+}]_o$ concentrations, we indirectly assayed the increment of $[Ca^{2+}]_i$ by measuring the F340/F380 ratio change. Figure 5.6d shows that the $[Ca^{2+}]_i$ rise in cells exposed to 5 mM $[Ca^{2+}]_o$ doubled when compared with cells stimulated by 0.5 mM $[Ca^{2+}]_o$. Cells elicited by 1.8 mM $[Ca^{2+}]_o$ show significantly higher $[Ca^{2+}]_i$ raise than 0.5 mM, but significantly lower than that of 5 mM $[Ca^{2+}]_o$. However, in HEK293 cells without mGluR5 transfection, $[Ca^{2+}]_o$ stimuli did not induce any significant $[Ca^{2+}]_i$ rise. Taken together, the result suggests $[Ca^{2+}]$ can solely activate mGluR5-mediated response and have $[Ca^{2+}]_o$ sensing capability to CaSR.

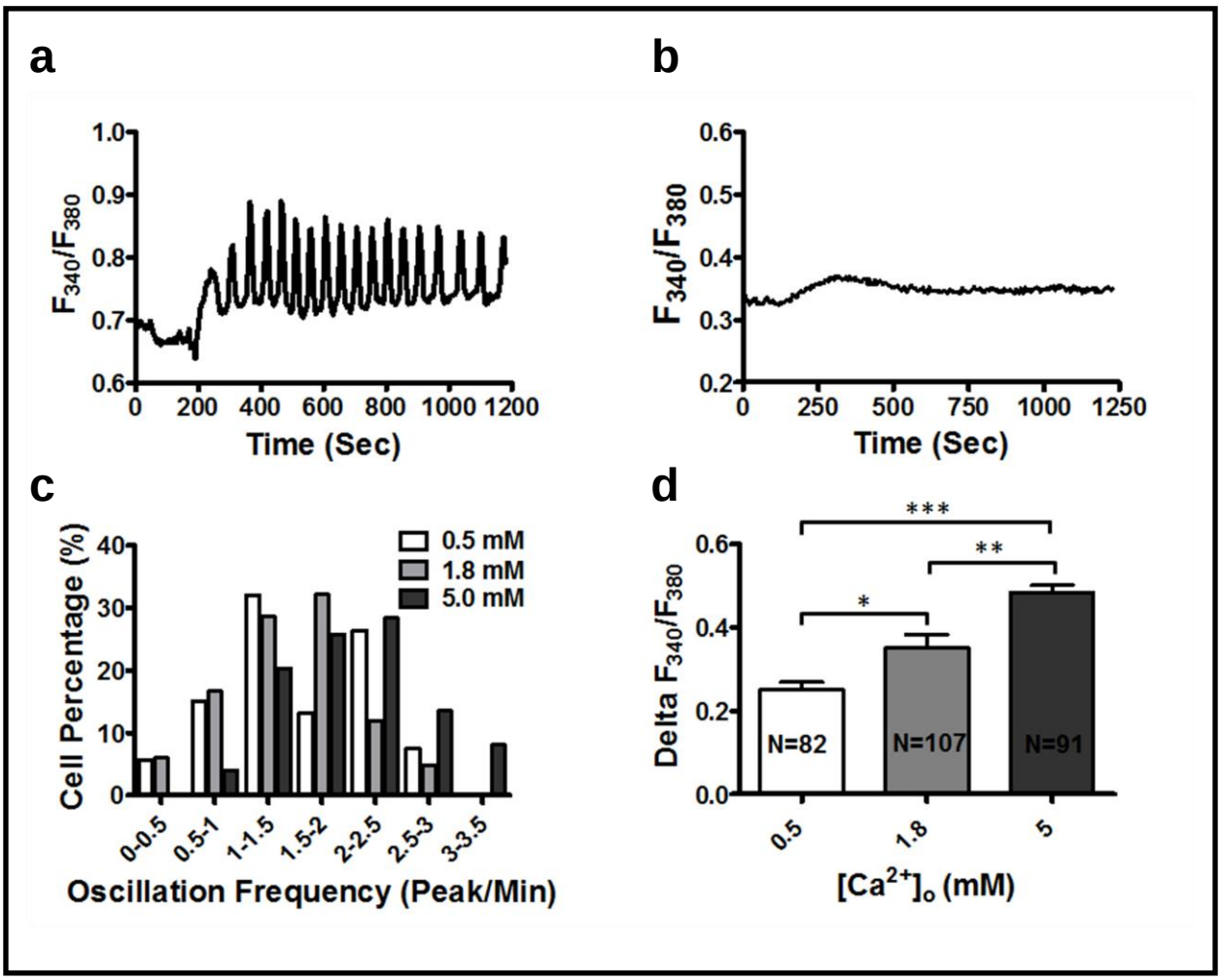

Figure 5.6 $[Ca^{2+}]_o$-sensing capability of mGluR5.

(a) $[Ca^{2+}]_i$ oscillation elicited by $[Ca^{2+}]_o$. mGluR5 transfected HEK293 cells were first loaded with 2 μM Fura-2 preceding the $[Ca^{2+}]_i$ measurement under fluorescence microscope. Cells were fist washed by 0 mM $[Ca^{2+}]_o$ bath solution before the application of 1.8 mM $[Ca^{2+}]_o$ at 200 sec (red arrow). (b) HEK293 cells without transfection has no significant $[Ca^{2+}]_i$ raise when 5 mM $[Ca^{2+}]_o$ was applied. (c) Oscillation frequency distribution of cells elicited by 0.5, 1.8 or 5 mM $[Ca^{2+}]_o$. Under each condition, total cell number is the sum of cells with oscillation. (d) Comparison of $[Ca^{2+}]i$ rise induced by 0.5, 1.8 or 5 mM $[Ca^{2+}]_o$. The $[Ca^{2+}]_i$

rise upon activation by different concentration of $[Ca^{2+}]_o$ was reflected by the increase of F340/F380. N stands for the number of cells we examined. *, $p < 0.05$; **, $p < 0.01$; and ***, $p < 0.001$.

5.2.5 Effects of mGluR5 mutating proposed Ca^{2+}-binding residues on $[Ca^{2+}]_o$ sensing capability

To identify the structural determinant of Ca^{2+} sensitivity within the ECD, we mutated three of our predicted Ca^{2+}-binding residues and compared their response to $[Ca^{2+}]_o$ with WT mGluR5(**Fig. 5.7a**). Figure 5.7b shows that substitution of Ala for Asp-305 abolished the $[Ca^{2+}]_o$ sensing capability in single cell imaging experiments. When 1.8 mM $[Ca^{2+}]_o$ was introduced to the bath chamber, no $[Ca^{2+}]_i$ oscillation was observed in cells transfected with D305A; instead a tiny transient peak was detected suggesting an insignificant $[Ca^{2+}]_i$ rise. The other two mutants (D309A and D305A) exhibited altered $[Ca^{2+}]_i$ responses with delayed oscillation and lower $[Ca^{2+}]_i$ increase. A 10-minute delay occurred in cells transfected with D309A (**Fig.5.7c**) and D312A (**Fig. 5.7d**), while WT mGluR5 started to oscillate immediately upon the addition of $[Ca^{2+}]_o$ (**Fig.5.7a**). The $[Ca^{2+}]_i$ enhancement elicited by $[Ca^{2+}]_o$ was strikingly reduced in D309A (about % decrease) and D312A (about % decrease) (**Fig.5.7f**) compared with WT, though D305A and D309A only displayed slightly lower cell surface expression as revealed above. Together, our results suggest that disturbance of the intact Ca^{2+}-binding pocket lead to impaired $[Ca^{2+}]_o$ sensing capability.

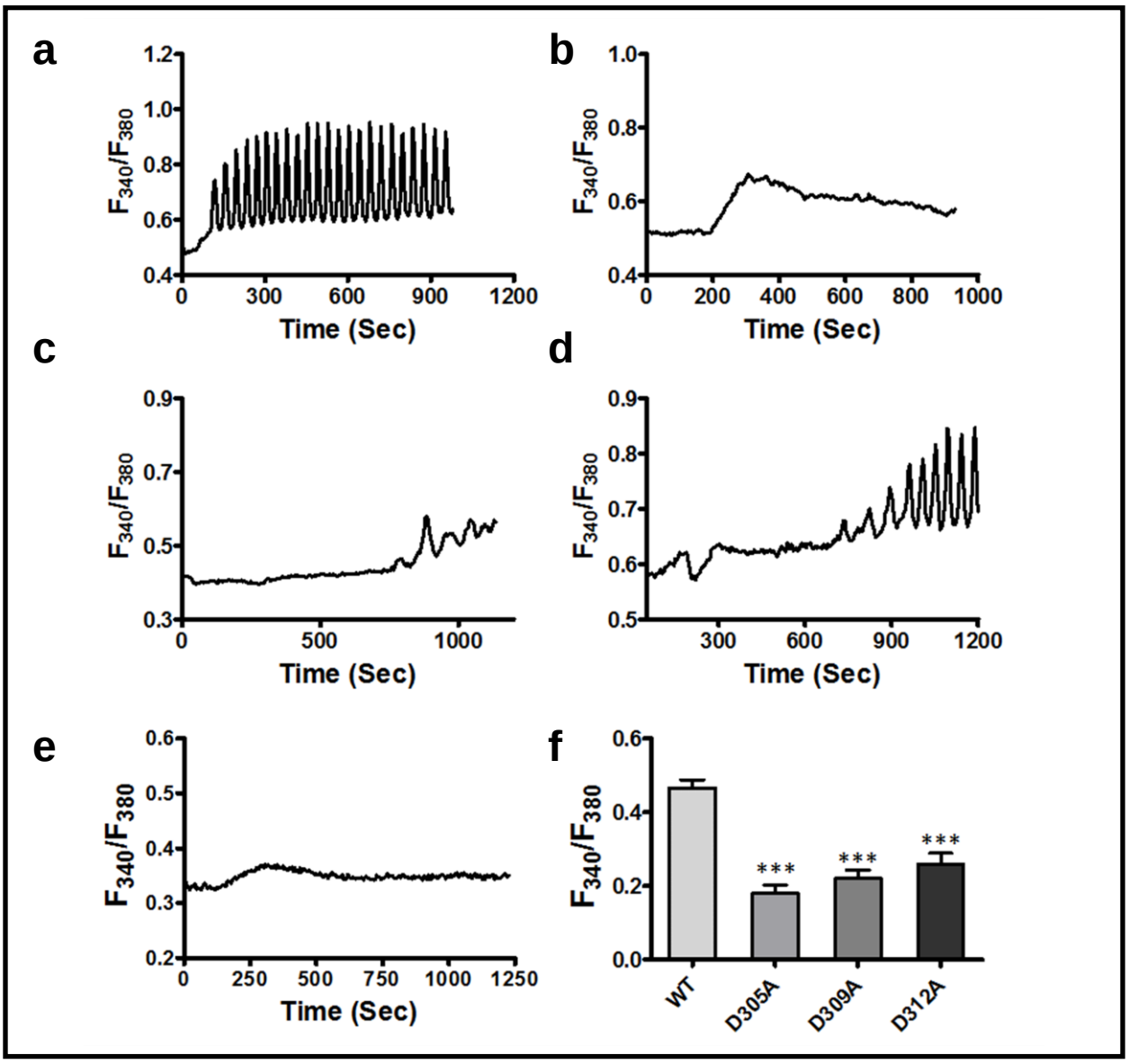

Figure 5.7 Disturbance of the intact Ca^{2+}-binding pocket lead to impaired $[Ca^{2+}]_o$ sensing capability.

(a) $[Ca^{2+}]_i$ oscillation evoked by 5 mM $[Ca^{2+}]_o$ in WT mGluR5-transfected HEK293 cells. (b) HEK293 cells transfected with D305A abolished the extracellular Ca^{2+}-elicited $[Ca^{2+}]_i$ oscillation. A small transient peak was observed in D305A mutant. (c) HEK293 cells transfected with D309A displayed delayed $[Ca^{2+}]_i$ oscillation when 5 mM Ca^{2+} was applied.

The amplitude of [Ca2+]i oscillation peaks were also significantly dropped. (d) HEK293 cells transfected with D312A also displayed impaired $[Ca^{2+}]_o$-sensing capability when compared with WT mGluR5. (e) No significant $[Ca^{2+}]_i$ response stimulated by extracellular Ca^{2+} were detected in non-transfected HEK293 cells. (f) $[Ca^{2+}]_i$ rise triggered by extracellular Ca^{2+} comparison between WT mGluR5 and three mutants. $[Ca^{2+}]_i$ increase in WT were dramatically higher than that in three mutants. ***, P < 0.001.

5.2.6 ERK1/2 phosphorylation in WT and point mutant of mGluR5 induced by $[Ca^{2+}]_o$

We further examined the effects of mutating proposed Ca^{2+}-binding residues on other signaling pathways, like the mitogen-activated protein kinases (MAPK) (ERK1/2) activation. Activation of group I mGluRs by various extracellular stimuli could result in phosphorylation of ERK1/2 (504-506). The conventional pathway transmitting signals from mGluR5 to ERK1/2 is linked with PIP_2 hydrolysis/Ca^{2+} release. However, it is reported that ERK1/2 phosphorylation involves the simultaneous participation of both PIP2 hydrolysis/Ca^{2+} and Homer pathways (506). In this study, the post-receptor signaling cascades on the signal pathway are not discussed. The activation of ERK1/2 mediated through mGluR5 is monitored to reflect the activation of mGluR5 by extracellular stimuli. Cells transfected with WT or mutated mGluR5 were exposed to increasing concentrations of Ca^{2+} (0-10 mM) for 5 minutes and the formation of phosphorylated ERK1/2 was detected by western blot as described in the methods. Exposure to WT mGluR5-transfected HEK293 cells to increasing concentrations of $[Ca^{2+}]_o$ in the range of 1.0-10.0 mM for 5 minutes resulted in significant accumulation of p44/42 ERK, reaching a response plateau at around 5 mM $[Ca^{2+}]_o$ (**Fig. 5.8**). The western blot result were further analyzed using Image J. The ration of phosphorylated ERK over total ERK were plotted as a function of $[Ca^{2+}]_o$ and fit to Hill equation,

yielding an EC_{50} of 2.8 mM. D305A dramatically impaired the $[Ca^{2+}]_o$-evoked ERK activation mediated through mGluR5. $[Ca^{2+}]_o$ in the range of 0.0-5.0 mM had little effect on the phosphorylation of p44/42 ERK. Mutants D309A and D312 A requires slightly higher (above 3 mM) $[Ca^{2+}]_o$ to trigger ERK phosphorylation. EC_{50} of $[Ca^{2+}]_o$ in three mutants were higher than WT, especially D305A (**Table 5.1**). In summary, mutating putative Ca^{2+}-binding ligands in mGluR5 impaired the ERK signaling mediated through mGluR5.

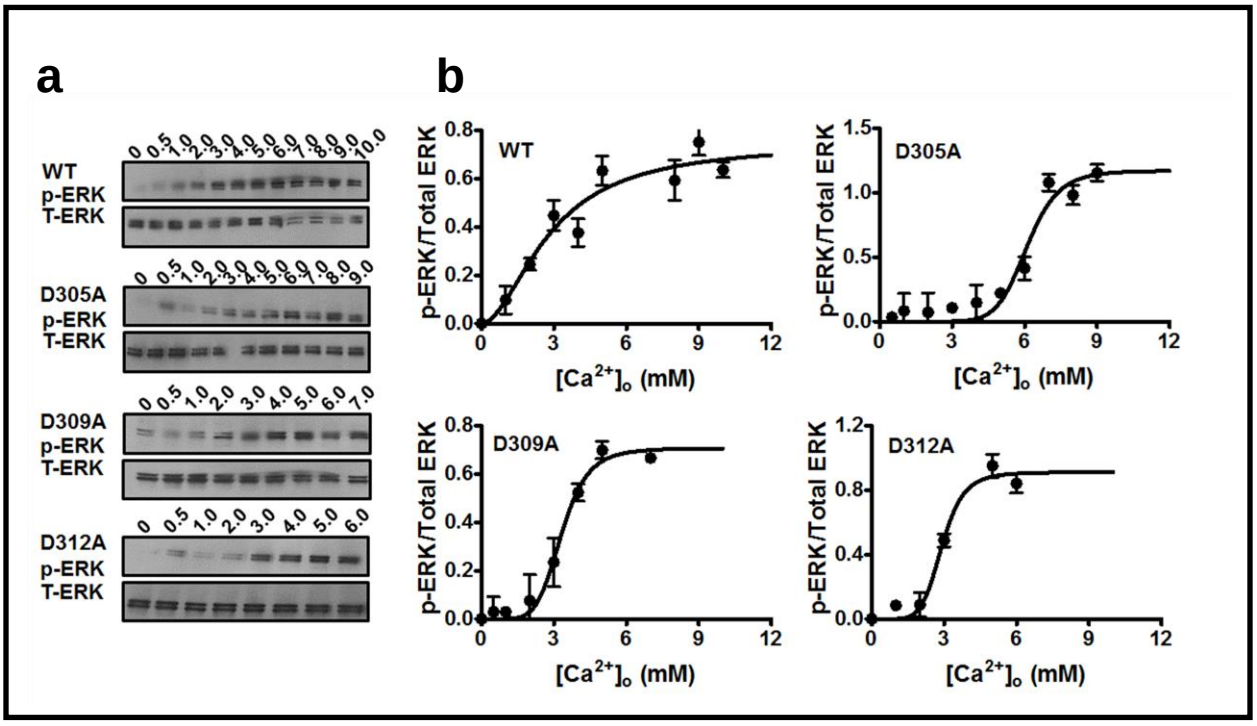

Figure 5.8 $[Ca^{2+}]_o$-activated ERK signaling in mGluR5-transfected HEK293 cells.

mGluR5- or its mutant-transfected HEK293 cells were starved in serum-free DMEM containing 0.2 % BSA overnight. Cells were treated with various Ca^{2+} concentrations (0.0 to 10 mM) for 5 minutes at 37 °C. The treatments were stopped by applying RIPA lysis buffer. The amount of phosphorylated ERK and total ERK were determined and analyzed using SDS-Page and western blot as described previously in the Methods section. (a)

Phosphorylated ERK and total ERK were probed by Anti-phospho-p44/42 ERK and Anti-p44/42 ERK polyclonal antibodies respectively during western blot. (b) The western blot resulted were further analyzed using Image J and the ration of phosphorylated ERK over total ERK were plotted against $[Ca^{2+}]_o$ and fit to Hill equation.

Table 5.1 Summary of EC50s from experiments measuring $[Ca^{2+}]_i$ response and ERK1/2 phosphorylation.

Mutants	EC_{50} (ERK1/2 activity)
WT	**2.8 ± 0.1 mM**
D305A	**6.1 ± 0.3 mM**
D309A	**3.3 ± 0.1 mM**
D312A	**3.0 ± 0.2 mM**

5.2.7 Enhancement of mGluR5 sensitivity and response to L-Glu by extracellular Ca^{2+}

Previous studies reported that $[Ca^{2+}]_o$ dramatically broaden the dynamic range of mGluR1-mediated responses to agonist DHPG (286) and $[Ca^{2+}]_o$ modulates the effects of many agonists and antagonists (280,281,283,502). We next examined the effects of $[Ca^{2+}]_o$ on the oscillation pattern of $[Ca^{2+}]_i$ induced by L-Glu in mGluR5-transfected HEK293 cells. An increasing concentrations of L-Glu were introduced to cells exposed to different concentrations of $[Ca^{2+}]_o$ and the $[Ca^{2+}]_o$ fluctuations were recorded by measuring the Fura-2 F340/F380 ratio through the fluorescence microscope. Cells with higher concentrations of $[Ca^{2+}]_o$ exposure exhibited faster frequency when the same concentration of L-Glu was applied (**Fig. 5.9**). Without the addition of $[Ca^{2+}]_o$, the oscillation frequency is always confined in the range of 0-0.5 peaks/min even when L-Glu concentration approached 10 μM. The centered oscillation frequency shifted from the left to the right side under the same concentration of L-Glu when comparison occurs between cells exposed to lower and higher $[Ca^{2+}]_o$. In addition, the sensitivity of mGluR5 to L-Glu also enhanced

by higher $[Ca^{2+}]_o$ as indicated by the oscillation starting point. In the absence of $[Ca^{2+}]_o$, 5 μM L-Glu is required to induce any response, while cells started to oscillate at lower concentration of L-Glu (1 μM) when $[Ca^{2+}]_o$ was present. These data suggest that increases in $[Ca^{2+}]_o$ raise both the potency and the efficacy of L-Glu, whereas reductions in $[Ca^{2+}]_o$ has the opposite modulation effect.

Next, we examined the modulatory effects of extracellular Ca^{2+} on L-Glu in HEK293 cells expressing mutated putative Ca^{2+}-binding residues. Cells transfected with mGluR5 mutants were placed in the same 1.8 mM $[Ca^{2+}]_o$ environment while stimulated with various concentrations of L-Glu. Replacing D305 with A completely abolished L-Glu-evoked intracellular responses of mGluR5 since D305 is one of the L-Glu coordinating ligand. In cells transfected with D305A, no intracellular Ca^{2+} mobilization was detected as shown in figure 5.10a. Mutation D309A and D312A responded similar to WT mGluR5 to L-Glu in addition to the oscillation starting point (**Fig. 5.10b**). In the presence of same concentration of $[Ca^{2+}]_o$, all cells with WT mGluR5 expression could respond to lower concentration of L-Glu (1 μM), while in contrast, less than 20 % of cells exprssing D309A and D312A showed responses to 1 μM L-Glu and majority of cells (70 %) oscillated at 3 μM L-Glu. The oscillation frequence of those two mutants were not significantly changed when compared with WT mGluR.

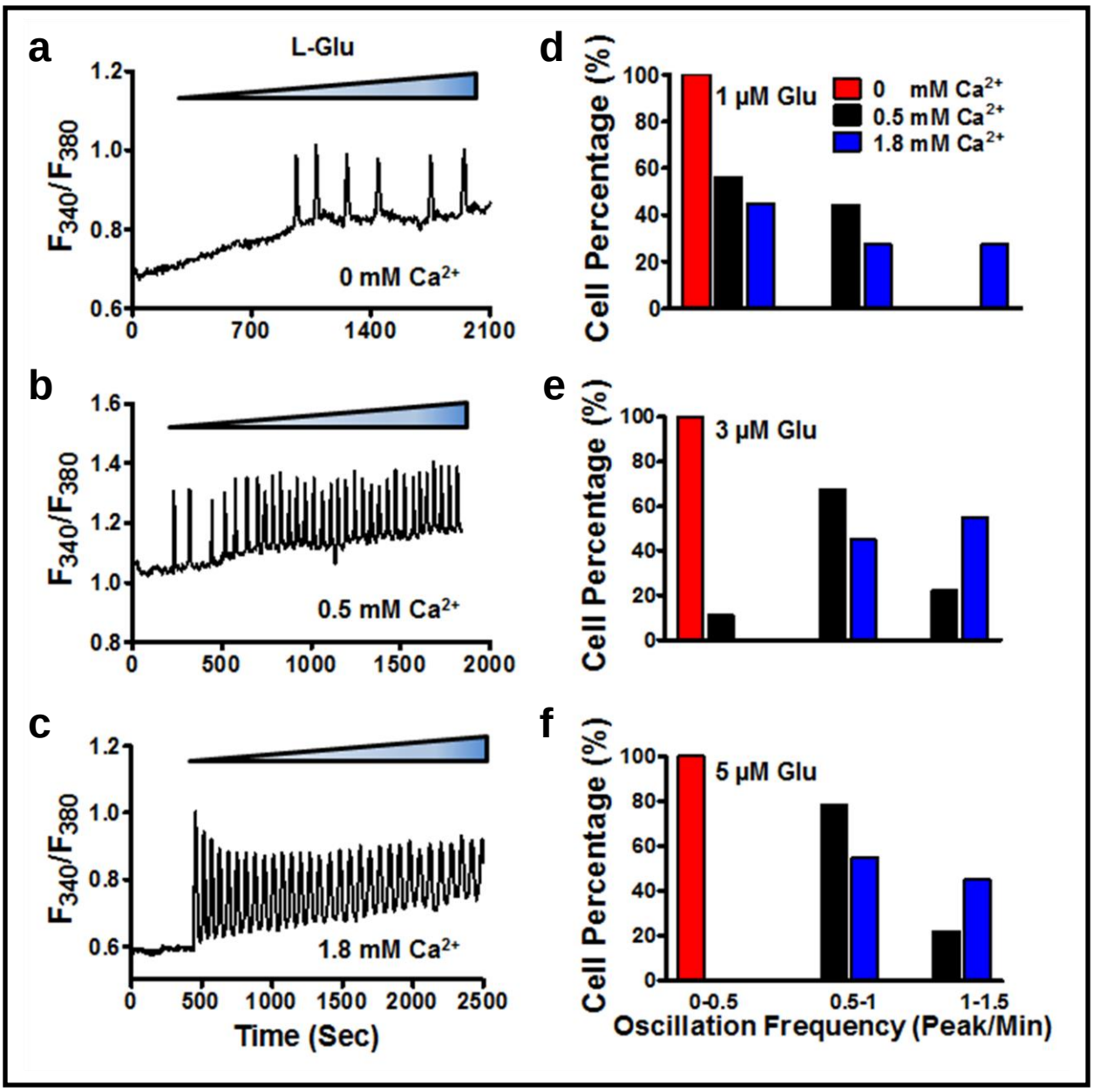

Figure 5.9 $[Ca^{2+}]_o$ potentiates L-Glu-activated $[Ca^{2+}]_i$ signaling in mGluR5-transfected HEK293 cells.

HEK293 cells transfected with mGluR5 were placed in bath solution containing 0 (a), 0.5 (b) or 1.8 (c) mM extracellular Ca^{2+} during the single cell imaging experiment. The $[Ca^{2+}]_i$ alternation were monitored by Fura-2 in single cells and recorded while applying various

concentration of L-Glu (1, 3, and 5 μM). For each extracellular Ca^{2+} concentration, the $[Ca^{2+}]_i$-oscillation pattern of one single cell were presented as an example and the oscillation frequency of over 100 cells were analyzed under each concentration of L-Glu and plotted as bar chart (d, e and f). Red, cells in 0 mM $[Ca^{2+}]_o$; black, cells in 0.5 mM $[Ca^{2+}]_o$; blue: cells in 1.8 mM $[Ca^{2+}]_o$. The color gradient of wedge block stands for L-Glu concentration, the darker the blue color, the higher the L-Glu applied.

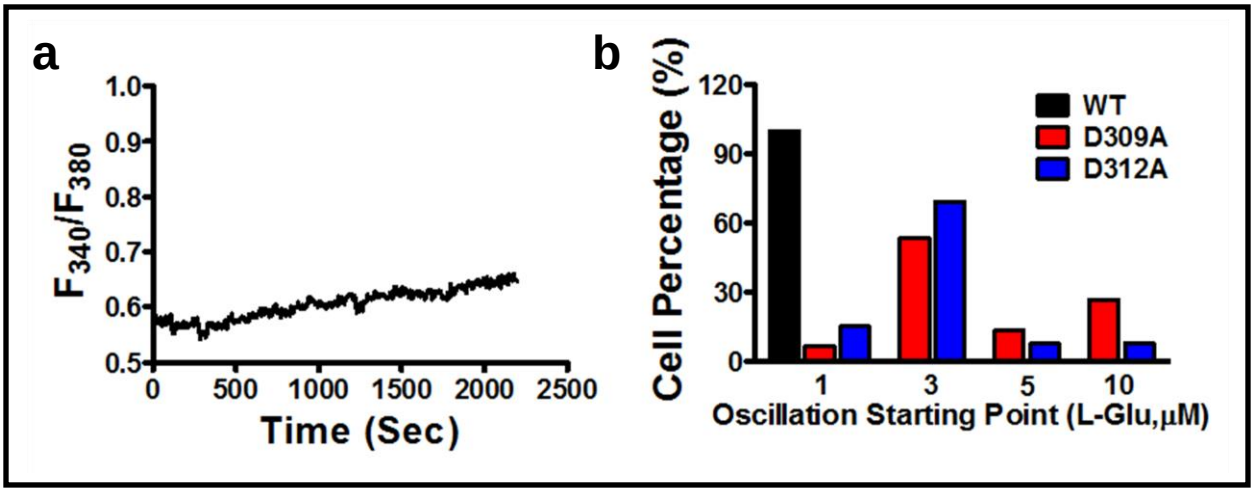

Figure 5.10 mGluR5 mutants' response to L-Glu in the presence of 1.8 mM Ca^{2+}.

(a) Cells expressing D305A lost its L-Glu sensitivity. (b) HEK293 cells transfected with WT and two mutants were stimulated with various concentrations of L-Glu in the presence of 1.8 mM $[Ca^{2+}]_o$. The oscillation starting point was analyzed for each cell. For WT and each mutated mGluR5, around 120 cells were analyzed.

5.3 Discussion

5.3.1 The putative Ca^{2+}-binding site is conserved in group I mGluRs

The predicted Ca^{2+} binding site we reported here, together with our earlier work, revealed the "invisible" binding pockets in the group I mGluRs. The ubiquitous actions of Ca^{2+} on cGPCRs have been extensively reported in the past; however, no Ca^{2+}-bound form of crystal structure was solved until now due to the challenges in membrane protein crystallization and the weak Ca^{2+}-binding property. The putative Ca^{2+}-binding pocket predicted by our computational algorithm, is sharing one ligand D305 with L-Glu-binding site. Replacement of D305 with A completely abolished both L-Glu- or Ca^{2+}-evoked intracellular Ca^{2+} response as suggested by our mutation data. D305 is corresponding to E297 of CaSR and D318 of mGluR5. E297 is one of the putative Ca^{2+}-binding ligand in the hinge region of CaSR and E297 mutations are associated with autosomal dominant hypocalcaemia and familial hypocalciuric hypercalcaemia which are two genetic diseases caused by disruption in Ca^{2+} homeostasis (322). Mutation E297I is reported significantly perturbed the Ca^{2+} sensitivity of CaSR (335,507) (322). D318I in mGluR1 showed similar surface expression as WT mGluR1, while abolished sensitivity to both L-Glu and $[Ca^{2+}]_o$ (501). The intracellular Ca^{2+} oscillation pattern and amplitude had been altered in other mutants D309A and D312A too. This site is highly conserved in both mGluR1 and mGluR5 (**Fig. 5.2**), suggesting those residues may play important role in structure or function. The equivalent surface expression of both WT and mutated mGluRs suggests that the difference between WT and mutants are due to the impaired receptor functions rather than the perturbation of receptor trafficking to the cell surface.

5.3.2 Ubiquitous actions of extracellular Ca^{2+} on mGluR5

The mGluR5-ECD we purified from insect cell stays as dimer in solution as suggested by native gel result. Though it cannot resemble the entire mGluR5 protein and the local environment is different from *in vitro*, the mGluR5-ECD allows us to obtain some information about metal binding. The Ca^{2+}-binding affinity of mGluR5-ECD determined by Ca^{2+}-Tb^{3+} competition experiment *in vitro* is around 2.1 mM, which is slightly higher than the physiological concentration of $[Ca^{2+}]_o$ in most tissues (1.8 mM); however, the $[Ca^{2+}]_o$ in the nervous system changes after periods of neuronal activities (288-297). This weak Ca^{2+}-binding property of mGluR5 can also avoid occupying the Ca^{2+}-binding site all the time, thus, the receptors are not always kept activated. We demonstrated that mGluR5 could be activated by either L-Glu or $[Ca^{2+}]_o$. The activation response of mGluR5 to $[Ca^{2+}]_o$ is as fast as to L-Glu, indicating that $[Ca^{2+}]_o$ is also an agonist of mGluR5. In our earlier report, L-Glu and $[Ca^{2+}]_o$ synergistically elicited mGluR1 to reach its maximum activity (501). Mutating either the residues in the L-Glu-binding or Ca^{2+}-binding pockets affected the sensing capability of mGluR5 to both L-Glu and Ca^{2+} in different extent. However, in the present study, no synergistic effect have been identified between L-Glu and $[Ca^{2+}]_o$, though $[Ca^{2+}]_o$ enhanced the L-Glu potential to mGluR5, in reverse, no such effect has shown (**Fig. 5.11**) when monitoring the intracellular Ca^{2+} responses evoked by $[Ca^{2+}]_o$ under different concentrations of $[Ca^{2+}]_o$. This phenomenon was also observed in another member of cGPCR, CaSR (349). A L-Phe-binding site adjacent to the predicted Ca^{2+}-binding site in CaSR was found to enhance the responses of CaSR to $[Ca^{2+}]_o$. L-Phe itself cannot solely elicits CaSR, but function as a co-agonist to further induce conformational change initiated by $[Ca^{2+}]_o$. In addition to the intracellular Ca^{2+} response, the accumulation of phosphorylated ERK1/2 also have been observed when treated with $[Ca^{2+}]_o$. Higher $[Ca^{2+}]_o$ were required to achieve the maximum

accumulation of phosphorylated ERK1/2 in three predicted Ca^{2+}-binding ligand mutations than in WT mGluR5 as indicated by the EC_{50} comparison table 5.1. Taken together, Ca^{2+} could function as both direct activator of mGluR5 or exhibit modulatory effect on other agonist as extensively reported in the past.

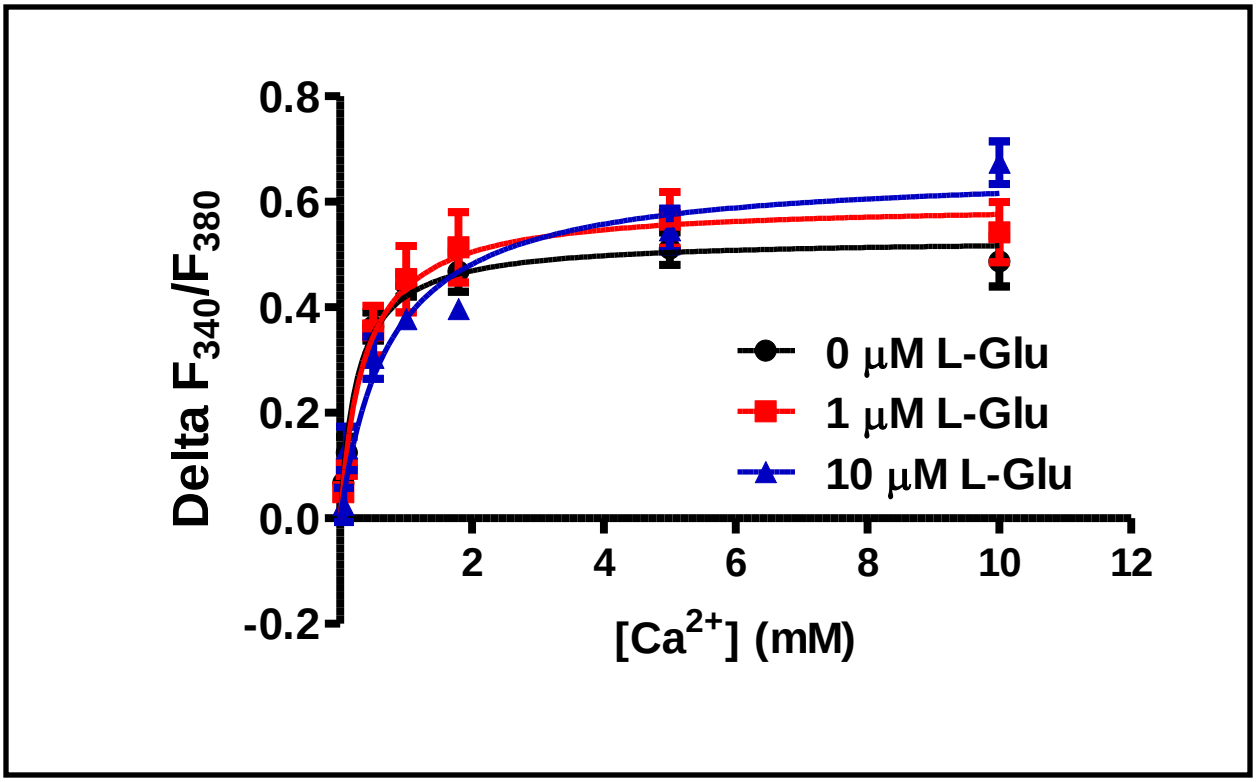

Figure 5.11 L-Glu did not influence the $[Ca^{2+}]_o$ sensitivity of mGluR5.

The $[Ca^{2+}]_i$ mobilization evoked by $[Ca^{2+}]_o$ in the presence of different concentrations of L-Glu were monitored using single cell imaging assay. No significant difference were observed when L-Glu were applied.

5.3.3 Possible physiological significance of $[Ca^{2+}]_o$ effects on mGluR5 in neuron system

Under physiological conditions, native mGluR5 receptors in mammalian neurons are exposure to a millimolar range of $[Ca^{2+}]_o$; thus, the function of mGluR5 may be modulated by $[Ca^{2+}]_o$ in several possible ways (**Fig. 5.12**)

Frist, the $[Ca^{2+}]_o$ fluctuations at where mGluR5 localized may activate this receptor. Though the data about $[Ca^{2+}]_o$ fluctuation in single synaptic clefts are not available due to the lack of experimental techniques which allows rapid Ca^{2+} measurement in synaptic cleft, there are some large spatiotemporal scale studies suggested that $[Ca^{2+}]_o$ in the synaptic cleft could change greatly as discussed in the first chapter. On the other hand, some studies at the mathematical and simulation level also indicated that large fluctuations in $[Ca^{2+}]_o$ in synaptic cleft may be part of normal neural activity (293). Thus, it is highly possible that mGluR5 can be activated by abrupt changes in $[Ca^{2+}]_o$ in the synaptic cleft during neural activities. The second possible way is through enhancing the sensitivity of other orthosteric ligand, such as L-Glu and L-Quis. Native group I mGluRs are rarely statured by L-Glu under physiological conditions, instead they are exposed to insufficient L-Glu as suggested by other studies (285,508). Therefore, $[Ca^{2+}]_o$ could exert modulatory effects on L-Glu and other orthosteric ligands by increasing mGluR5' sensitivity to them.

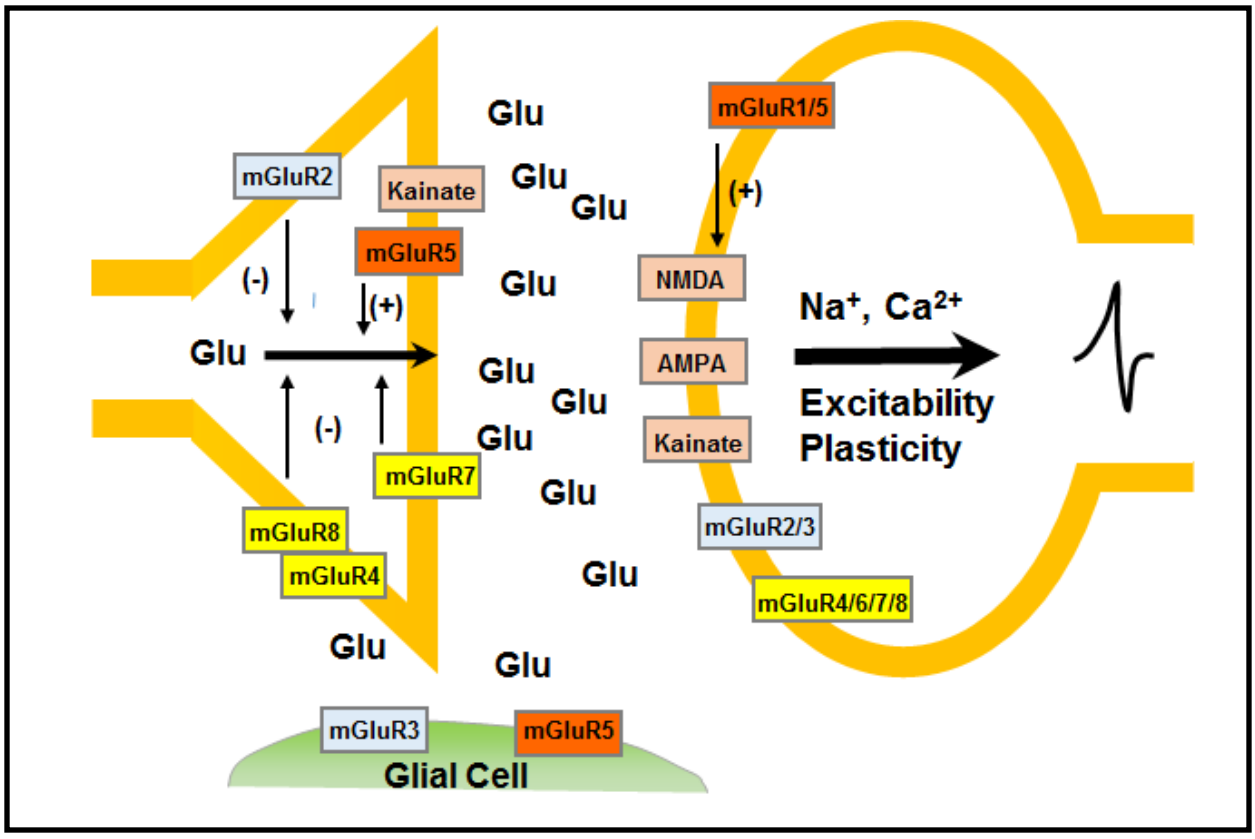

Figure 5.12 mGluR5 localization in neural system.

5.3.4 The response of mGluR5 to extracellular Ca^{2+} resemble CaSR more than mGLuR1

The intracellular Ca^{2+} response pattern of mGluR5 is similar to that of CaSR when activated. Both receptor activation accompany with intracellular Ca^{2+} oscillations (357-360,509,510); but not mGluR1 in which a simple transient peak occurs when evoked (511). The intracellular Ca^{2+} oscillation induced by activation of mGluR5 and CaSR arise from the dynamic phosphorylation and dephosphorylation of receptors by PKC, which is activated upon activation of receptors. Amino acids T840 and T888 in mGluR5 and CaSR (Fig, respectively, are the primary PKC phosphorylation sties (362-364,366,511); while this phosphorylation site in mGluR1 is substituted by D854 (511). Oscillation of $[Ca^{2+}]_o$ plays important role in signal transduction and

the regulation of gene expression. Different specific information can be decoded from the amplitude or frequency or duration of Ca^{2+} oscillation and transmitted into cells for various cell responses (512). Extracellular stimuli amount like the agonist concentration is proportional to the Ca^{2+} oscillation frequency or amplitude in most cases (513-516). Cells evoked by higher extracellular Ca^{2+} indeed displayed higher oscillation frequency and $[Ca^{2+}]_o$ rise than those exposed to lower extracellular Ca^{2+}. Besides, cells elicited by same concentration of L-Glu, but placed in various $[Ca^{2+}]_o$ showed different $[Ca^{2+}]_i$ oscillation frequency and sensitivity to L-Glu. The responses to L-Glu were altered in mutated mGluR5 with predicted Ca^{2+}-binding ligands replaced, showing lower sensitivity to L-Glu as suggested by the oscillation starting point (**Fig. 5.13).**

From the aspect of oscillation pattern, mGluR5 resembles CaSR more than mGluR1. More quantitative analysis such as monitoring the IP accumulation or EK1/2 phosphorylation using Cisbio kits need to be performed to compare the EC_{50} difference between mGluR1, wild type or mutated mGluR5 elicited by L-Glu in the presence of various $[Ca^{2+}]_o$.

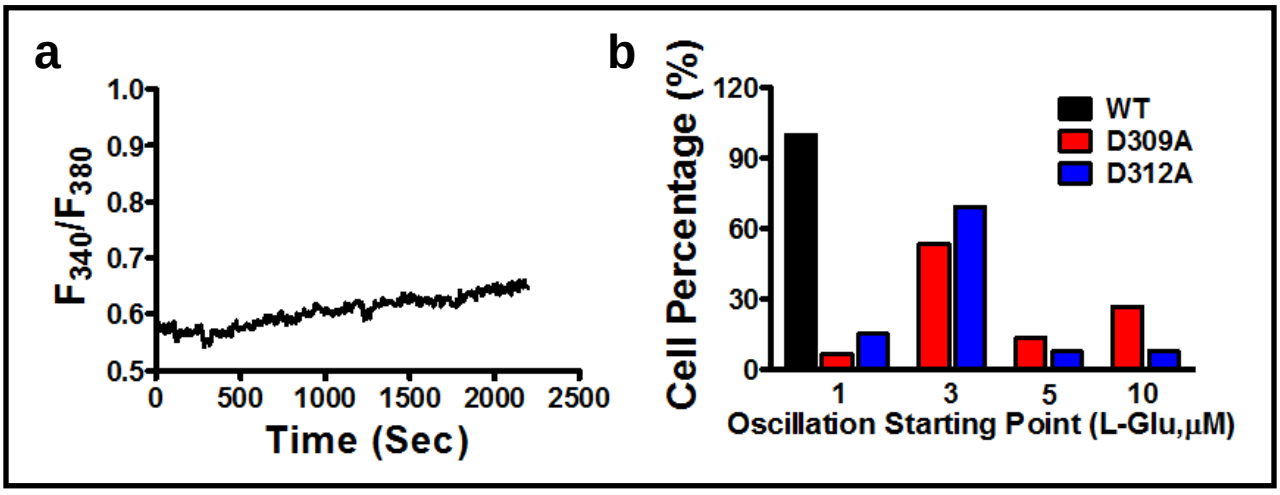

Figure 5.13 Impaired L-Glu sensitivity of mGluR5 variants.

(a) The $[Ca^{2+}]_i$ responses of D305A evoked by L-Glu in the presence of 1.8 mM $[Ca^{2+}]_o$. (b) The oscillation starting concentration of L-Glu at which mGluR5 wild type and mutants started to respond was plotted as bar chart. Total cells with responses were divided by number of cells which respond to each concentration of L-Glu and then plotted as y axis.

Taken together, we proved that $[Ca^{2+}]_o$ activates mGluR5 to induce $[Ca^{2+}]_i$ oscillation and ERK1/2 phosphorylation in the absence of Glu. A Ca^{2+}-binding site formed by residues D305, D309, and D312 at the hinge region of the extracellular domain of mGluR5 has been identified by site-directed mutagenesis. Our studies revealed an additional regulation of mGluR5-mediated signaling and provided a new avenue to design therapy with improved selectivity.

6 STRUCTURAL BASIS FOR REGULATION OF HUMAN CALCIUM-SENSING RECEPTOR BY MAGNESIUM IONS AND AN UNEXPECTED TRYPTOPHAN DERIVATIVE

6.1 Introduction

The discovery of the parathyroid Ca^{2+}-sensing receptor (CaSR) established a new paradigm that extracellular Ca^{2+} ($[Ca^{2+}]_o$) can act as a first messenger for regulation of diverse cellular processes, in addition to its well-known roles as a second messenger (279,517). Extracellular divalent cations, particularly $[Ca^{2+}]_o$ and magnesium $[Mg^{2+}]_o$, along with amino acids and neurotransmitters, regulate numerous cellular processes via CaSR and 14 other family C, G protein-coupled receptors (cGPCRs), including metabotropic glutamate (mGluRs) and γ aminobutyric acid (GABA)B receptors (518-522). CaSR have been reported to be present not only in the key tissues involved in extracellular Ca^{2+} and Mg^{2+} hemostasis (e.g., parathyroid, thyroid, kidney, bone) but also in diverse other non-homeostatic tissues (e.g., brain, skin, et.) (372,377,500,523-533). Small changes in $[Ca^{2+}]_o$ or $[Mg^{2+}]_o$ trigger CaSR-mediated intracellular Ca^{2+} signaling and activate ERK1/2 (534). CaSRs play a central role in regulating $[Ca^{2+}]_o$ and $[Mg^{2+}]_o$ homeostasis by activating intracellular Ca^{2+} signaling (535), in turn, inhibiting PTH release, stimulating calcitonin secretion and promoting renal Ca^{2+} excretion (536). L-amino acids, especially those with aromatic side chains, potentiate high $[Ca^{2+}]_o$–elicited activation of CaSR via positive heterotropic functional cooperativity (520). Like other cGPCRs, CaSR functions as a dimer (537,538) with a long (~600 amino acids) N-terminal ECD playing an important role in the receptor's cooperative responses to its agonists (522). Over 400 mutations in CaSR cause human disorders with abnormal $[Ca^{2+}]_o$ and $[Mg^{2+}]_o$ homeostasis, including familial hypocalciuric

hypercalcemia (FHH), neonatal severe hyperparathyroidism (NSHPT) and autosomal dominant hypocalcemia (ADH); 225 of the mutations map to the ECD, highlighting its critical role (539).

To date, how extracellular Ca^{2+}, Mg^{2+} and amino acids cooperatively modulate intracellular Ca^{2+} signaling is a long-standing unanswered question. Unfortunately, there are no determined CaSR structures reported thus far despite extensive effort. The ECD has been shown to play an important role in the cooperative responses of the receptor to changes of $[Ca^{2+}]_o$, amino acids, metabolites, and neurotransmitters (499,530,540-544). Determination of the X-ray structure of the ECD of CaSR is largely hampered by difficulty in crystallization due to heterogeneous and extensive glycosylation (11 N-glycosylation sites) as well as challenges associated with membrane proteins with large molecular size. Further, Ca^{2+} and ligand-binding sites with weak binding affinities and rapid off rates are often not occupied in determined X-ray structure. For example, no bound Ca^{2+} has been observed in all the reported X-ray structures of the ECD of mGluRs, despite the clear modulatory effect of $[Ca^{2+}]_o$ on this receptor.

To clarify the mechanism for cooperative activation of CaSR by $[Ca^{2+}]_o$, $[Mg^{2+}]_o$, and amino acids, we solved the first crystal structure of human CaSR-ECD bound with Mg^{2+} ions and a high-affinity tryptophan derivative at 2.1 Å using mammalian expressed dimer with reduced glycosylation. An unexpected Trp derivative bound at the putative ligand binding site is present in this crystal structure. The ligand shows an unusual high affinity and potentiates Mg^{2+} binding and activation of CaSR. We also identified Mg^{2+} binding sites at the hinge region and the lobe 2 dimerization interface. The structural information, together with structure-guided mutagenesis and cell-based functional assays, reveals the structure basis of agonist/co-agonist binding to CaSR and lays out a solid foundation for further clarification of the activation mechanism by ligands in a highly cooperatively way.

6.2 Results

6.2.1 Purified hCaSR-ECD from HEK293 cells forms a homodimer

Purified hCaSR-ECD was deglycosylated by Endo F1 incubation and the separation of hCaSR-ECD from Endo F1 was achieved by size exclusion chromatography. To roughly analyze the size of purified hCaSR-ECD, we mixed purified hCaSR-ECD with SEC standard proteins first and loaded the mixture to the SEC column. hCaSR-ECD was eluted out in the same position as the standard protein with a molecular weight of 158 kDa. This comparison of elution volumes of hCaSR-ECD and stand proteins suggests that the purified hCaSR-ECD forms a homodimer (Figure 5.1). Meanwhile, the SDS-Page gel of purified hCaSR-ECD in reducing and non-reducing conditions also clearly shows the electrophoretic mobility difference when reducing reagent was present or absent (**Figure 6.1 inset**). In the presence of reducing reagent, the hCaSR-ECD band showed between 50 and 75 kDa, while it appeared at 150 kDa when reducing reagent is absent. Taken together, those phenomena indicate that intermolecular disulfide bonds contribute to hCaSR-ECD dimerization. Structure-based sequence alignment of CaSRs and mGluRs showed that there are 6 highly invariant Cys residues in the ECD of both CaSRs and mGluRs.

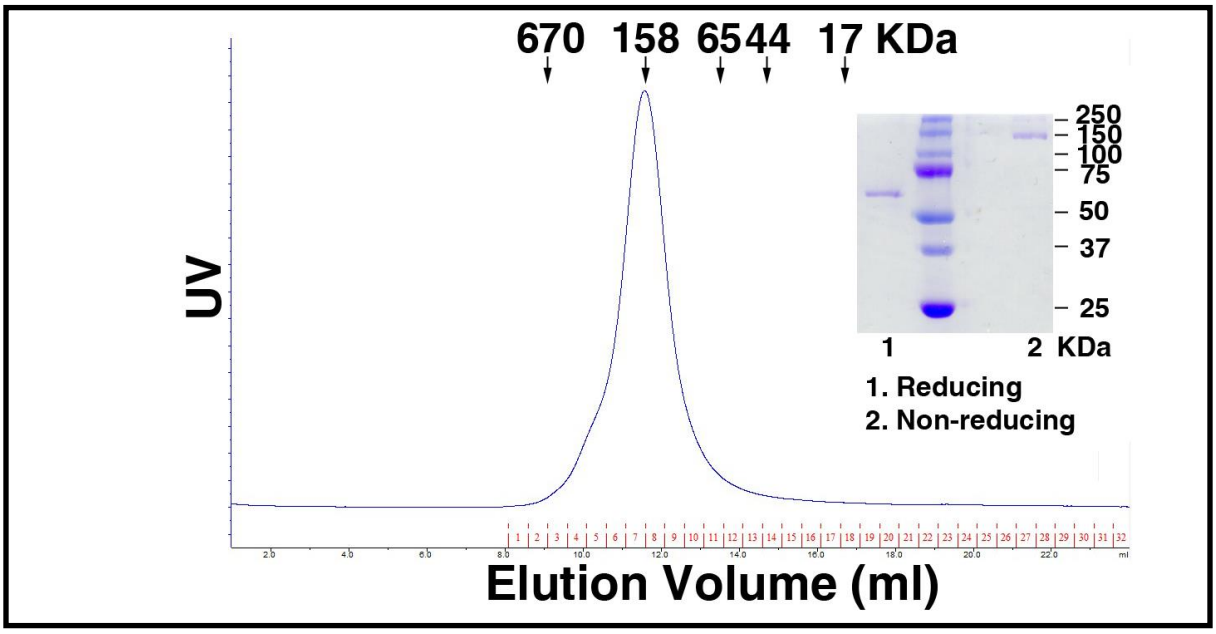

Figure 6.1 Size exclusion chromatography of purified hCaSR-ECD.

The elution volumes of the standard proteins are indicated by arrows. The inserted figure shows a SDS-PAGE of purified protein sample in reducing (lane 1) and non-reducing (lane 2) conditions, respectively. hCaSR-ECD forms a homodimer as determined by the elution volume observed in size exclusion chromatography and non-reducing SDS-PAGE. The intermolecular disulfide bonds contribute to dimerization.

6.2.2 Crystal structure of hCaSR-ECD

The Venus flytrap (VFT) domain of the human calcium-sensing receptor ECD (hCaSR-ECD, residues 20-541) was expressed in HEK293S (GnT1-) cells and purified by Ni^{2+}-NTA chromatography followed by treatment with EndoF1 and further purification by size exclusion chromatography. Only in 200 mM Mg^{2+} and 10 mM Ca^{2+}, we saw crystal formation that yields diffraction better than 4 Å. A mild dehydration significantly improved the resolution to 2.1 Å and

the structure was solved by molecular replacement using the structure of mGluR2 (PDB ID 4XAQ) as the search template **(Fig. 6.2 and Table. 6.1**).

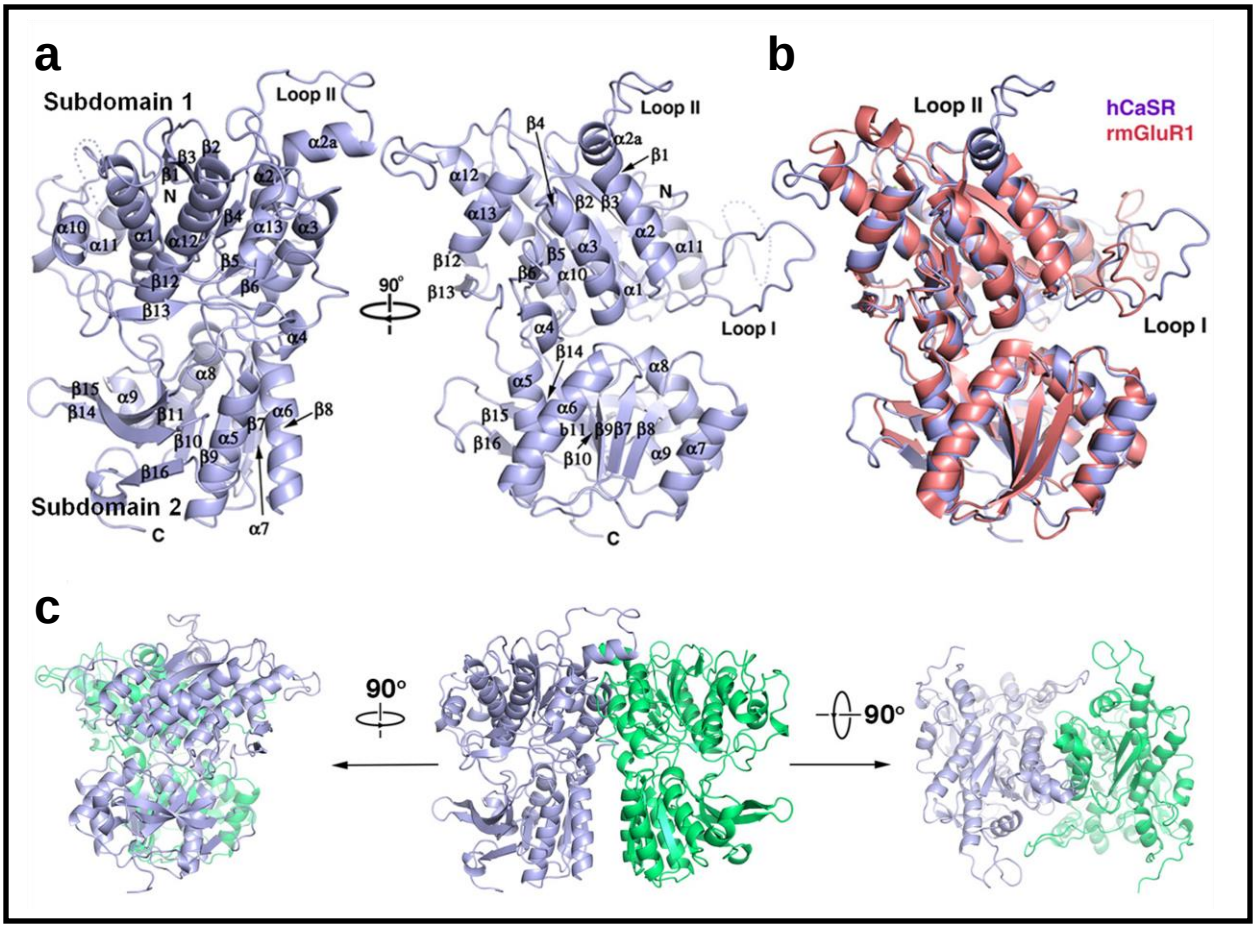

Figure 6.2 Crystal structure of hCaSR-ECD.

(a) Monomeric hCaSR-ECD with labeled secondary structural elements. (b) Structural overlap of hCaSR-ECD with rat mGluR1 in the closed conformation (PDB code: 1EWK). (c) Homodimer of hCaSR-ECD.

Table 6.1 Crystallographic statistics of hCaSR-ECD and hCaSR-ECD/Gd^{3+}.

Crystal	hCaSR-ECD	hCaSR-ECD/Gd^{3+}
Data Collection		
Wavelength (Å)	0.9785	1.6985
Space group	C2	C2
Cell Dimensions (Å)	a=170.9, b=82.9, c=94.3 α=γ=90°, β=105.1°	a=172.1, b=83.1, c=94.5 α=γ=90°, β=105.2°
*Resolution (Å)	40-2.1 (2.18-2.1)	40-2.7 (2.8-2.7)
*Redundancy	3.8 (3.8)	3.6 (3.6)
*Completeness (%)	100.0 (100.0)	98.9 (99.9)
*$I/\sigma I$	18.1 (1.5)	12.0 (2.8)
*,†R_{merge}	0.072 (0.913)	0.093 (0.772)
*,‡R_{pim}	0.043 (0.541)	0.058 (0.468)
§$CC_{1/2}$ of the highest resolution shell	0.631	0.645
Refinement		
Unique reflections	74,544	34,777
Number of Atoms		
Protein	7,449	7,264
CaSRL	32	32
Mg^{2+}	3	3
Gd^{3+}	-	2
Other ligands/ions	94	90
Water	323	17
‖R_{work}/R_{free}	0.190/0.223	0.188/0.245
Wilson B-factor (Å^2)	38.5	69.2
B-factors (Å^2)		
Protein	45.8	68.2
CaSRL	34.9	61.8
Mg^{2+}	53.1	74.5
Gd^{3+}	-	110.6
Other ligands/ions	62.9	108.3
Water	46.1	51.6
R.m.s. deviations		
Bond lengths (Å)	0.010	0.012
Bond angles (°)	1.39	1.52
Ramachandran plot (%)		
Favored	97.0	95.0
Allowed	3.0	4.6
Outliers	0.0	0.4

‡$R_{pim}=\sum_{hkl}[1/(N-1)]^{1/2}\sum_j|I_j(hkl)-\langle I(hkl)\rangle| / \sum_{hkl}\sum_j I_j(hkl)$, where N is the redundancy of the dataset.

§$CC_{1/2}$ is the correlation coefficient of the half datasets.

[||]$R_{work} = \sum_{hkl} | |F_{obs}| - |F_{calc}| | / \sum_{hkl} |F_{obs}|$, where F_{obs} and F_{calc} is the observed and the calculated structure factor, respectively, R_{free} is the cross-validation R factor for the test set of reflections (10% of the total) omitted in model refinement.

hCaSR-ECD contains two globular lobes with an overall structure similar to other cGPCR family members. Both the large lobe (subdomain 1) and the small lobe (subdomain 2) are typical α/β folds where the central parallel β-strands are sandwiched by α-helices (**Fig. 6.2**). In crystal packing, two hCaSR-ECD molecules associate with each other in one asymmetrical unit. Analysis of the dimerization interface shows that both dydrophobic residues and polar residues are involved in lobe 1 dimerization whereas the dimeric associations of lobe 2 are predominantly through hydrogen bonds, salt bridges and water molecules.

6.2.3 Identification of a tryptophan derivative tightly bound at the putative ligand binding site of hCaSR-ECD

Unexpectedly, a large, flatted and strong electron density was observed at the cleft between two lobes (**Fig. 6.3a**). Very interestingly, compared with the structure of mGluR with bound glutamate, this location of density largely overlaps with the Glu binding site of mGluR. We checked the size/shape of the known CaSR ligands, including Phe, Trp, GSH, as well as the reagents used in sample preparation and crystallization, but none of them fits the density well. Among these initial trials, Trp appears to be the best fit, but there is still unaccounted for density relative to the bound ligand observed here. Therefore, we suspected that this density corresponds to an unknown ligand of CaSR (denoted as CaSRL).

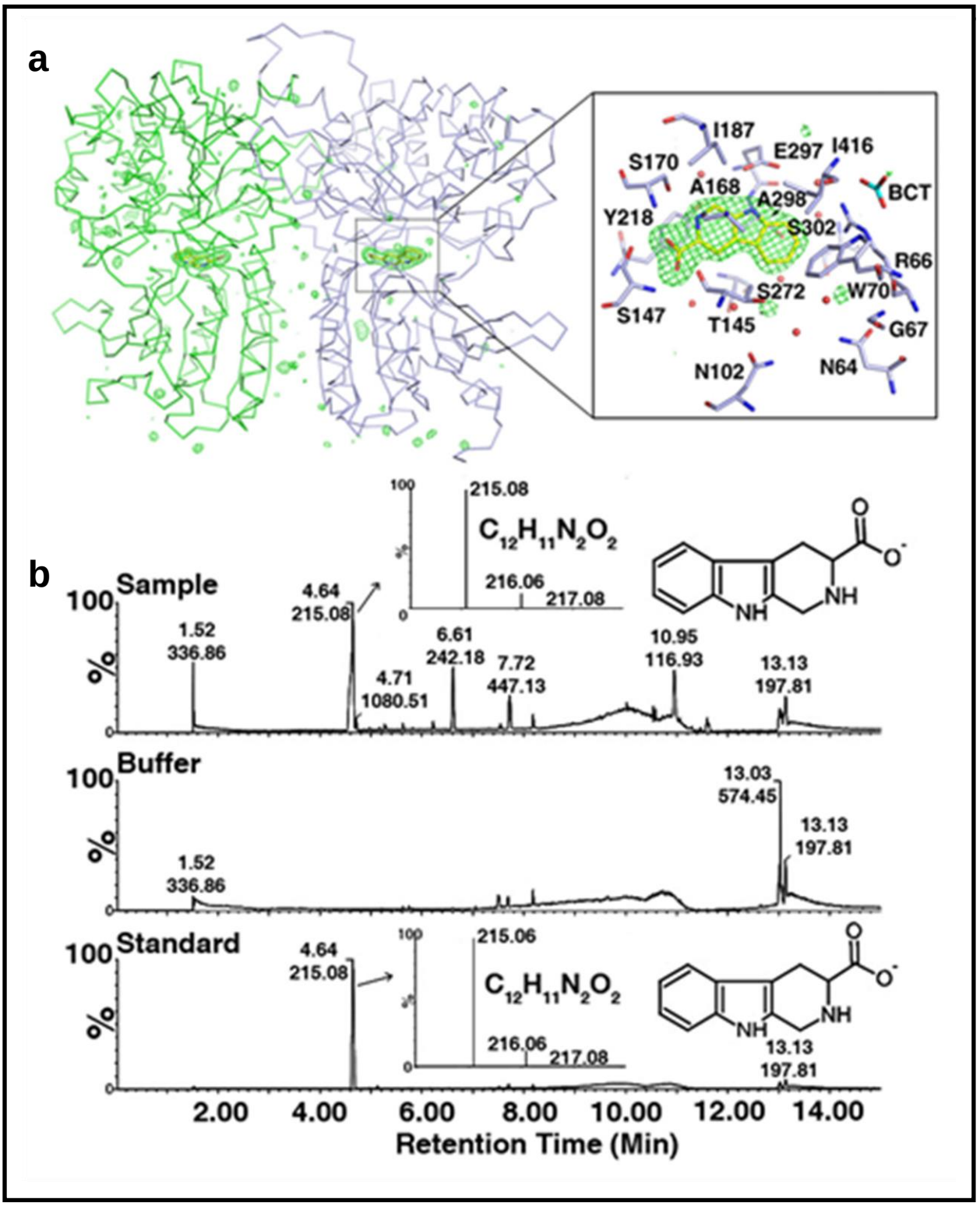
a
I187
E297
I416
S170
A168
A298
BCT
Y218
S302
R66
S272
W70
S147
T145
G67
N102
N64
b
Sample
100
%
0
1.52
336.86
4.64
215.08
4.71
1080.51
6.61
242.18
7.72
447.13
10.95
116.93
13.13
197.81
215.08
C12H11N2O2
216.06
217.08
NH
NH
O
O-
Buffer
13.03
574.45
13.13
197.81
1.52
336.86
Standard
4.64
215.08
215.06
C12H11N2O2
216.06
217.08
13.13
197.81
2.00
4.00
6.00
8.00
10.00
12.00
14.00
Retention Time (Min)

Figure 6.3 Identification and characterization of a tryptophan derivative bound to hCaSR-ECD. **(a) F_o-F_c omit map of CaSRL at σ=4.5. The protein is shown in ribbon mode and the ligand shown in stick mode. The residues around CaSRL are labeled in the zoomed-in figure. (b) LC-ESI-MS of protein sample (top), buffer (middle) and the standard compound (bottom) in negative-ion mode. The high resolution isotopic MS spectra of the indicated peaks are shown in the inserted figures.**

To identify this ligand, we conducted experiments using high resolution mass spectrometry. The size of the density suggests that this ligand contains 14-18 heavy atoms (C/N/O/S/P) and the absence of anomalous signal indicates that it does not contain S or P. Accordingly, the molecular weight of this ligand must be within the range of 180-250 Da. In mass experiments, we focused on the compounds within this range and looked for the candidates exclusively showing up in protein sample but not in the sample buffer. As shown in figure xx, LS-ESI-MS experiment identified a species eluting at ~ 4.65 min with a strong signal in negative mode. The high resolution isotopic MS data indicated that the molecular weight (M.W.) is 215.08 (m/z=215.08 and Z=-1). The formula best matching the M.W.is $C_{12}H_{11}N_2O_2$ (calculated mass = 215.0821, m = 1.4 ppm) (**Figs. 6.3b and 6.4**). A search of PubChem identified a tryptophan derivative, L-1,2,3,4-tetrahydronorharman-3-carboxylic acid (TNCA) with the predicted M_r and a shape of the observed density. When compared to tryptophan, TNCA contains one extra carbon atom linking the amine nitrogen atom and the C2 atom of the indole ring. TNCA can be detected in a various foods and biological systems likely due to tryptophan reacting with formaldehyde (545), and perhaps is generated during mammalian cell production of the recombinant protein. Elution time, molecular weight and MS fragmentation of synthetic TNCA matched those of CaSRL, confirming the identity of CaSRL (**Figs. 6.3b and 6.4**).

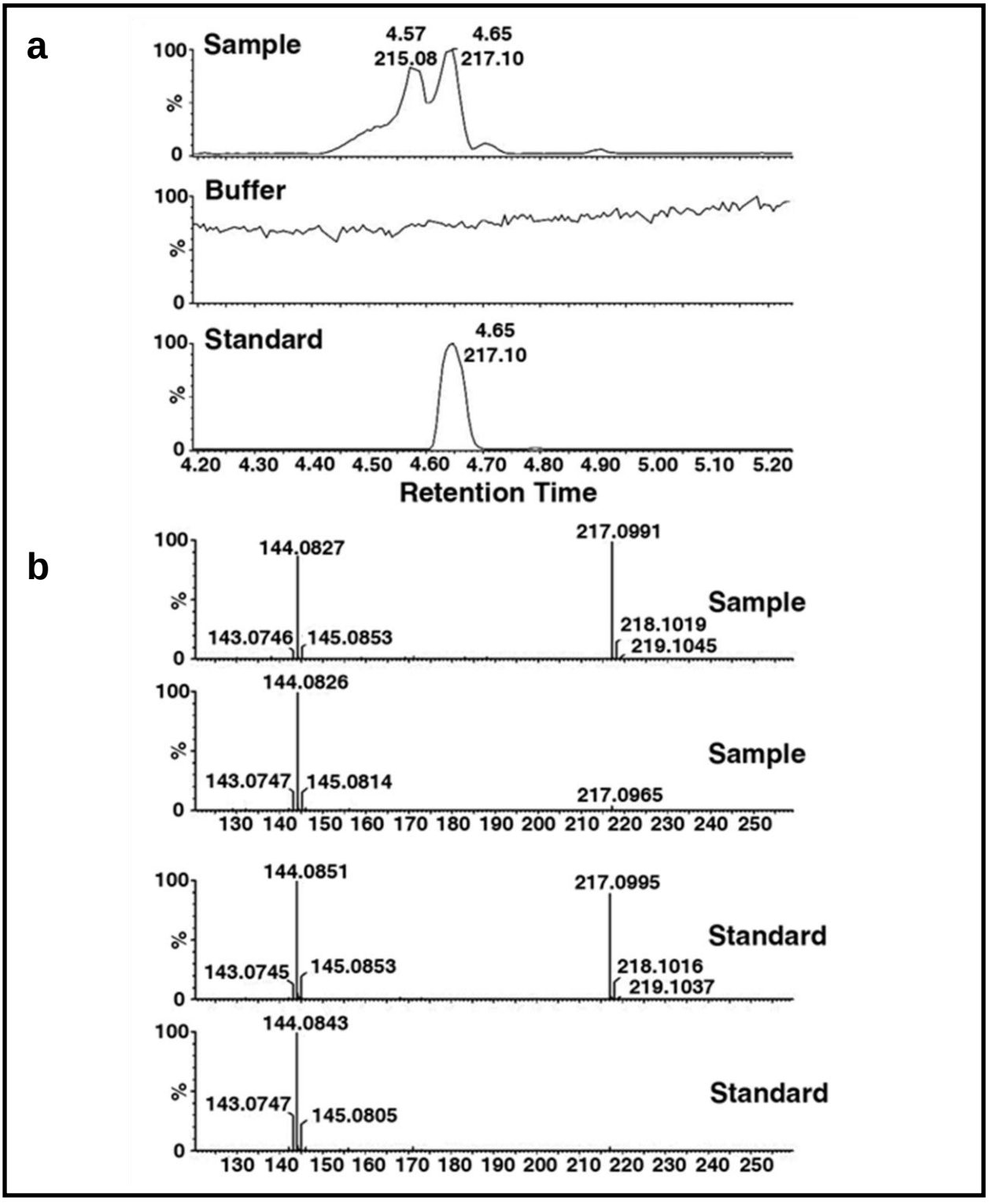

Figure 6.4 Identification of CaSRL.

(a) LC-ESI-MS in positive-ion mode. Only the zoomed-in regions are shown. The species eluted at 4.57 min with a M.W. of 215.08 in positive mode is an unidentified compound in the protein sample. A corresponding m/z 213.06 ion is not detected in negative-ion mode. (b) Fragmentation of CaSRL in positive-ion mode by application of increased collision energy in protein sample (upper two panels) and in standard sample (synthetic compound, lower two panels).

6.2.4 Mg^{2+} elicits CaSR-mediated $[Ca^{2+}]_i$ signaling pathways and ERK1/2 phosphorylation

Mg^{2+} homeostasis shares common regulatory hormones including parathyroid hormone and vitamin D to calcium homeostasis. Small changes in extracellular Ca^{2+} or Mg^{2+} in the presence of elevated concentrations of the other divalent cation are able to trigger CaSR mediated intracellular Ca^{2+} transients in mouse distal convoluted tubule cells (MDCT). There are relatively sparse functional data for the activation of the cloned CaSR by Mg^{2+}, to document that the receptor expressed in a heterologous expression system (HEK293 cells) could be activated by Mg^{2+}. We examined the effects of increasing Mg^{2+} concentrations on two commonly studied CaSR signaling pathways, changes in $[Ca^{2+}]_i$ and EKR1/2.

Activation of CaSR by extracellular stimuli leads to the activation of phospholipase C, resulting the decomposition of PIP2 into IP3 and DAG which is followed by Ca^{2+} release from intracellular Ca^{2+} store ER upon IP3 receptor activation by IP3. Here we used cell population assay to monitor changes in $[Ca^{2+}]_i$. Cell population assay is monitoring the average $[Ca^{2+}]_i$ change in a large cell population. Briefly, cells on coverslip were firstly loaded with Ca^{2+} indicator Fura-2 for 20 minutes before measuring the fluorescence intensity using the fluorometer. Fura-2 is a ratiometric dye which emits at 510 nm when excited at 340 or 380 nm. The emission ratio change

at 340 over 380 nm reflects the $[Ca^{2+}]i$ change as described in chapter 4. Figure 6.5 shows Mg^{2+} is able to mobilize intracellular Ca^{2+} by activating CaSR though the potency of Mg^{2+} (**Fig. 6.5a**) is much lower than that of extracellular Ca^{2+} (**Fig. 6.5b**). It is consistent with the earlier report that compared with Ca^{2+}, Mg^{2+} initiated a much weaker Ca^{2+}-activated Cl^- current in oocytes injected with CaSR RNA (279). The normalized intracellular Ca^{2+} responses were normalized and plotted against the concentration of extracellular Ca^{2+} or Mg^{2+} (**Fig. 6.5c**). In the presence of 0.5 mM or 1.5 mM extracellular Ca^{2+}, we further show that Mg^{2+} activation can be potentiated by Ca^{2+} since 1.5 mM Ca^{2+} largely reduced the EC50 for Mg^{2+} from 7.2 to 4.5 mM (**Fig. 6.5d**). This observation suggests that the two metals share a similar activation mechanism and two metals exhibit cooperativity in binding as reported earlier by other groups (336,341,546).

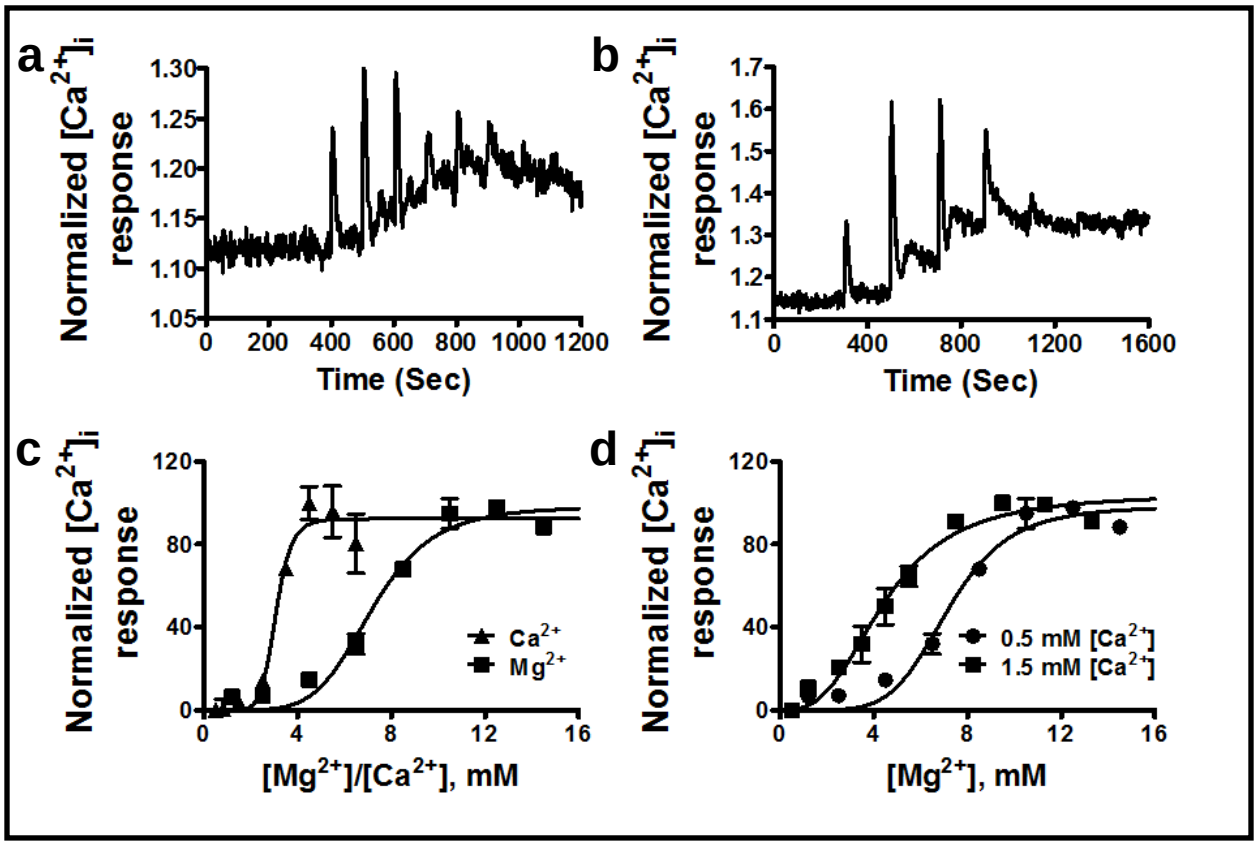

Figure 6.5 Mg^{2+} or Ca^{2+} elicited CaSR-mediated intracellular Ca^{2+} response.

(a) $[Ca^{2+}]_i$ was monitored using Fura-2 during cell population assay. The ratio of the intensity of light emitted at 510 nm upon excitation with 340 or 380 nm was normalized to its maximum response. $[Ca^{2+}]_i$ rise in cells stably expressing CaSR (5001) evoked by a step wise increase of extracellular Mg^{2+} was plotted aginist time. (b) $[Ca^{2+}]_i$ rise in 5001 cells elicited by a step wise increase of extracellular Mg^{2+} measured by cell population assay. (c) The normalized intracellular Ca^{2+} responses were plotted as a function of $[Mg^{2+}]_o$ or $[Ca^{2+}]_o$ and fit to the Hill equation. (d) In the presence of 0.5 mM (circles) or 1.5 mM (squares) $[Ca^{2+}]_o$, $[Ca^{2+}]_i$ was monitored using Fura-2 during stepwise increases of $[Mg^{2+}]_o$. The $[Mg^{2+}]_o$ concentration response curves were fitted using the Hill equation.

The downstream signaling pathways induced by CaSR are complicated (529,547), including Gq-mediated activation of phospholipase C (PLC) leading to production of IP_3 and DAG (317,318), Gi-mediated inhibition of AC (548), cytosolic phospholipase A2 ($cPLA_2$) activation leading to arachidonic acid (AA) release (549), phosphatidylinositol 3-kinase (PI_3 K)-mediated Akt activation, protein kinase C (PKC) activation, phosphatidylinositol 4-kinase (PI_4 K) activation leading to PIP_2 production, activation of the MAP kinases including p38 MAP kinase, Jun amino-terminal kinase (JNK) and extracellular signal-regulated kinase (ERK) and $G_{12/13}$-mediated phospholipase D (PLD) activation leading to phosphatidic acid (PA) production (550). In my study, in addition to the G_q pathway, I also examined another CaSR effector, ERK1/2. Typically, CaSR activation through extracellular stimuli lead to phosphorylation of ERK1/2 via Ras-dependent activation of MAP kinase kinase (MEK) (**Fig. 6.6**), inactivation of MEK by specific

inhibitors suppresses high extracellular Ca^{2+}-induced ERK1/2 activation in both bovine parathyroid and HEK-CaSR cells (551).

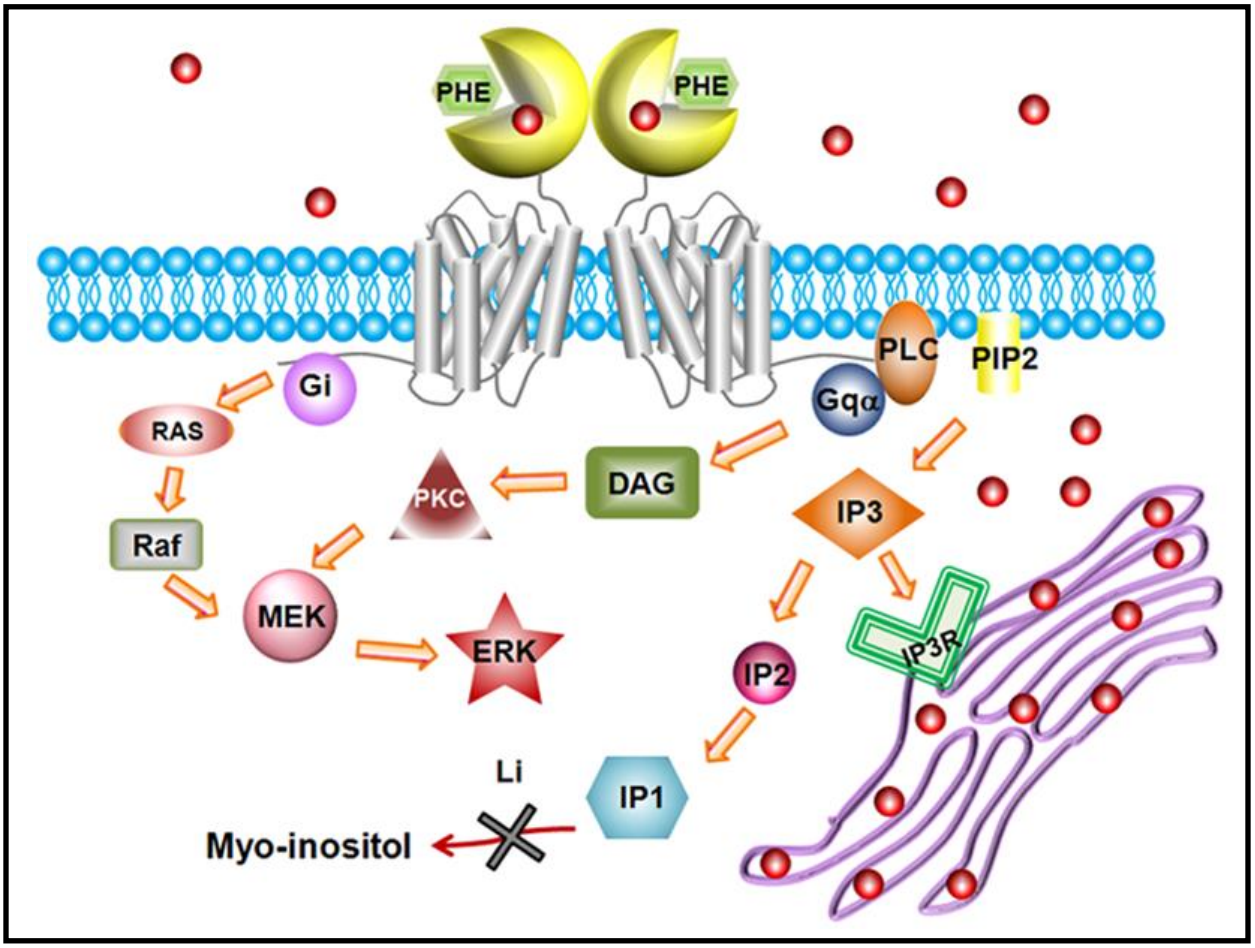

Figure 6.6 Schematic overview of CaSR effectors.

Extracellular stimuli (like Ca^{2+}, red dots; Phe) stimulates the activation of CaSR, leading to the downstream signaling changes (552). Gq-mediated activation of phospholipase C (PLC) leading to production of IP_3 and DAG, in turn, IP3 activates IP3 receptors to release Ca^{2+} from the intracellular Ca^{2+}-store. ERK1/2 can also be activated via Ras-dependent activation

of MEK. Thus, the $[Ca^{2+}]_i$ and amount of phosphorylated ERK1/2 could reflect the activity of CaSR.

5001 cells were treated with a series concentration of extracellular Mg^{2+} (0-30 mM) for 10 minutes before lysis. The amount of total ERK1/2 and phosphorylated ERK1/2 were measured by western blot and subsequently analyzed by Image J. Exposure to higher extracellular Mg^{2+} resulted in more accumulation of phosphorylated ERK1/2, which reached its maximum at round 30 mM Mg^{2+} (**Fig. 6.7a**). The percentage of phosphorylated ERK1/2 over total ERK1/2 were plotted as a function of extracellular Mg^{2+} and fit to Hill equation to obtain the EC50 for Mg^{2+}. A comparison between Mg^{2+} and Ca^{2+} was shown in Figure 6.7b. Ca^{2+} obviously displayed a much higher potency on CaSR than Mg^{2+} since the accumulation of phosphorylated ERK1/2 exhibited its maximum at around 8 mM Ca^{2+}, almost 3-fold lower than that of Mg^{2+}.

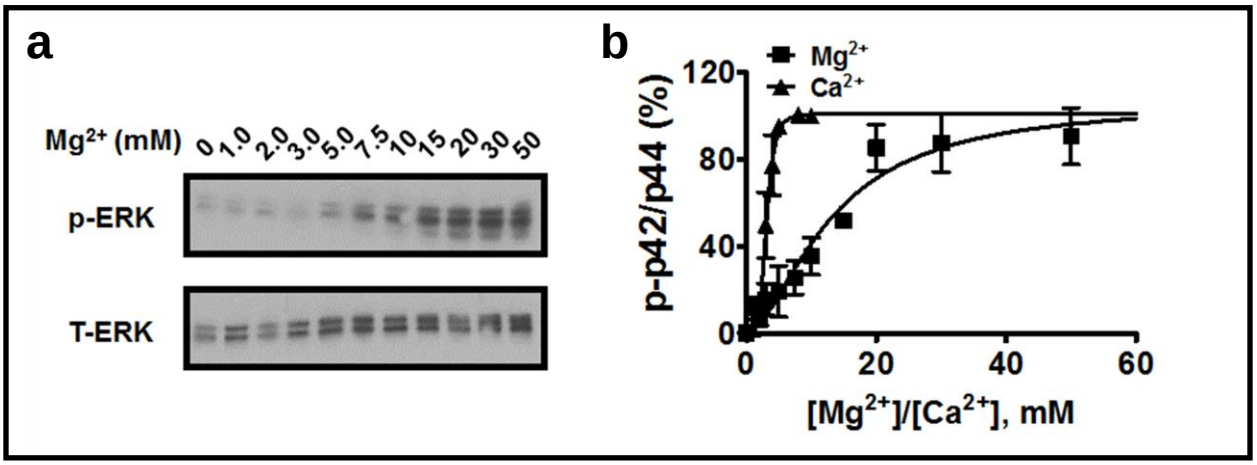

Figure 6.7 Extracellular Mg^{2+} evoked phosphorylation of ERK1/2.

(a) $[Mg^{2+}]_o$-activated ERK1/2 signaling in HEK293 cells stably transfected with CaSR. (b) ERK1/2 activities upon agonists' stimulation were detected using western blot and further

quantified using ImageJ. The measurements were plotted against different concentrations of $[Ca^{2+}]_o$ or $[Mg^{2+}]_o$ and fit to the Hill equation.

6.2.5 Identification of metal binding sites

In the crystal structure, two Mg^{2+}-binding sites were identified at positions designated site 1 and site 2 (**Fig. 6.8**). No bound Ca^{2+} ions were observed since concentration of Mg^{2+} is 20-fold higher than Ca^{2+} and Mg^{2+} is expected to displace Ca^{2+}. Site 1 is located at the dimerization interface of subdomain 2 and the bound Mg^{2+} coordinates with S240 and four water molecules with an ideal geometry for an Mg^{2+} ion. Notably, site 1 is surrounded by highly conserved residues (E228, E231 and E241*) ("*" means from the other protomer) within 5 Å from the "acidic patch" composed of negatively charged residues on subdomain 2 (**Fig. 6.9**). Site 2 is found on the periphery of subdomain 1 and an equivalent cation-binding site has been observed in mGluR (163) and likely plays a structural role. To locate additional high off-rate metal binding sites, we generated Gd^{3+}-derivatized crystals and identified another metal-binding site (site 3) on the "acidic patch" in the proximity of subdomain 2 dimerization interface (**Fig. 6.8b**) and adjacent to the Mg^{2+}-binding site 1. Site 3 largely overlaps with a previously predicted Ca^{2+}-binding site III (335).

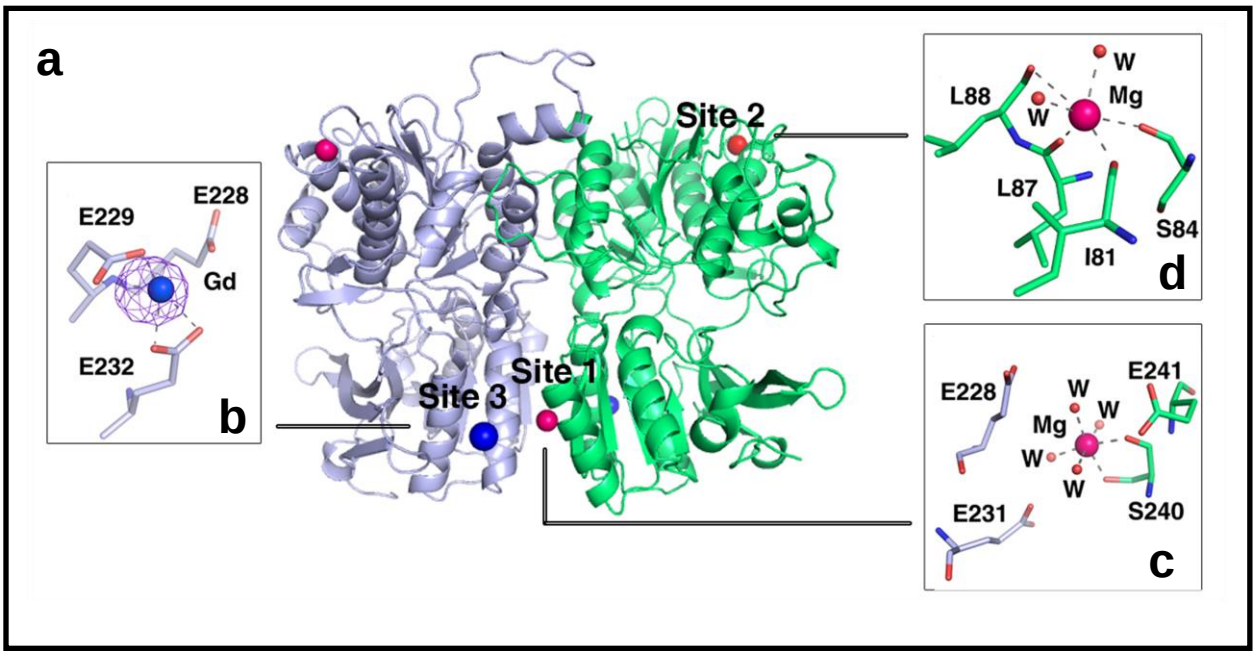

Figure 6.8 Structural Basis for Mg^{2+}/Ca^{2+} modulated CaSR activities.

(a) Identified metal binding sites in the structure of hCaSR-ECD homodimer. Mg^{2+} and Gd^{3+} are depicted as a hot pink and dark blue sphere, respectively. Anomalous difference map of Gd^{3+} ($\sigma = 8.0$) is shown in purple. W represents water molecules. Both site 1 (c) and site 3 (b) are on the "acidic patch" at the dimerization interface of subdomain 2 (Supplementary Fig. 7), whereas Mg^{2+} at site 2 in subdomain 1 (d) is primarily coordinated by the backbone carbonyl oxygen atoms.

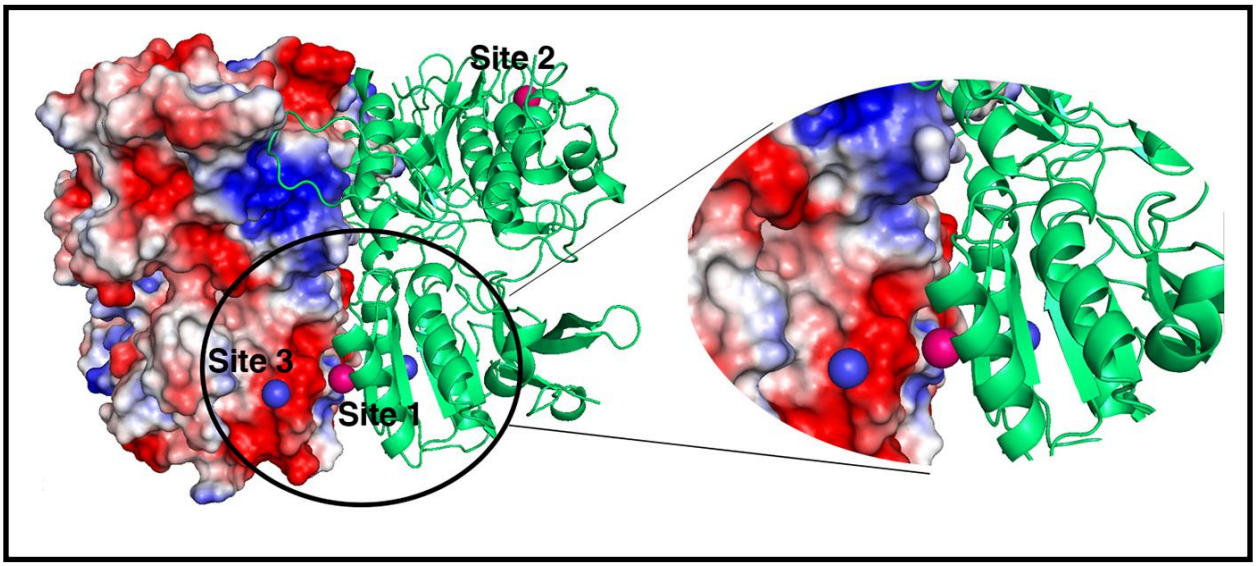

Figure 6.9 Metal binding at the "acidic patch".

The electrostatic potential map of hCaSR-ECD is colored in accordance to electrostatic potential- red indicates negative potential, and blue positive potential. Mg^{2+} is represented by hot pink spheres, while Gd^{3+} is shown as blue spheres. The large surface with negative potential at the dimerization interface of subdomain 2 is referred as to "acidic patch", where both Mg^{2+} and Gd^{3+} bind.

Mutation of site 3 coordinating residue (E228I or E228I/E229I double mutant) reduced Ca^{2+}/Mg^{2+}-sensing as well as Mg^{2+}-evoked intracellular Ca^{2+} mobilization. The EC50 for Mg^{2+} were remarkably increased when E228 and E229 were replaced by I. These results suggest the critical role of these metal-binding sites at the "acidic patch" in both metal-sensing (335) and in regulation of CaSR function (**Figs. 6.10, Table 6.2**).

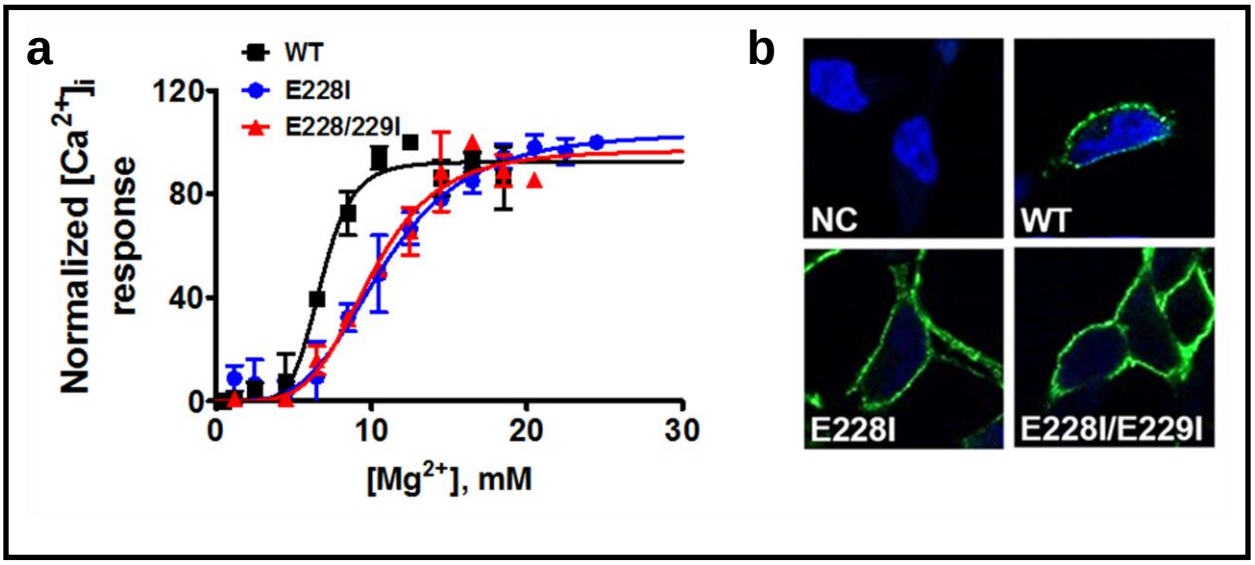

Figure 6.10 Mutations of site 3 coordinating residue (E228I or E228I/E229I double mutant) reduced Mg^{2+}-evoked intracellular Ca^{2+} mobilization.

(a) Single mutation of E228I and double mutation of E228/229I on the "acidic patch" significantly reduce CaSR mediated $[Ca^{2+}]_i$ responses in cell population assay. (b) Membrane expression of CaSR, mutant E228I and double mutant E228I/E229I. Blue: DAPI staining cell nuclei. Green: hCaSR immunoreactivity. NC is the non-transfected cell.

Table 6.2 EC50 of $[Mg^{2+}]_o$ for stimulation of $[Ca^{2+}]_i$ signaling in cell population assay.

(0.5 mM Ca^{2+})	EC_{50}	Hill number
WT	7.2 ± 0.4	4.0 ± 1.0
E228I	10.8 ± 0.3	3.9 ± 0.4
E228/229I	10.0 ± 0.5	4.6 ± 0.5

6.2.6 The unexpected Trp derivative function as a co-activator and potentiates the actions of extracellular divalent cations

To investigate the biophysiological function of CaSRL, we first want to address the question whether CaSRL solely acts on CaSR. The intracellular Ca^{2+} responses were examined in both single cell and cell population. Both of methods are monitoring the change of $[Ca^{2+}]_o$ by utilizing Fura-2. Fluorescence microscope allows us to measuring the $[Ca^{2+}]_o$ changes in single cell in the single cell image assay, while in cell population assay, the fluorometer measures the average $[Ca^{2+}]_o$ change in a large population of cell.

As shown in figure 6.11, in single cell image assay, addition of CaSRL up to 0.5 mM, which is the highest concentration we can achieve due to the poor solubility of this compound, to 5001 cells did not lead to any intracellular Ca^{2+} responses mediated through CaSR. Using the cell population assay, a step wise increase of CaSRL to the cuvette also did not evoke significant intracellular Ca^{2+} responses, which is consistent to the single cell image result (**Fig. 6.11**).

Figure 6.11 CaSRL does not function solely

The next question we asked is that whether CaSRL function in a similar way to the amino acids which can potentiate extracellular Ca^{2+}-elicited CaSR activation since it shares a very similar structure with Trp. It is reported that L-amino acids, especially aromatic amino acids (including L-Trp), enhance the sensitivity of CaSR to its agonist, like extracellular Ca^{2+} (347,349,553). We performed similar cell population assay. Cells were placed in bath solution containing basal CaSRL and elicited by either extracellular Ca^{2+} or Mg^{2+}. The control group were immersed in bath solution without any CaSRL. A comparison of EC50 of Ca^{2+} or Mg^{2+} for CaSR in the presence or absence of CaSRL shows that CaSR decreased the EC50 of both Ca^{2+} and Mg^{2+} significantly, suggesting CaSRL potentiated the actions of Ca^{2+} or Mg^{2+} on CaSR activation (**Fig. 6.12**). We also compare the potency of CaSRL and L-Phe. Though the structure of CaSRL is much closer to L-Trp than L-Phe, we have reported the EC50 of L-Phe in 2014 (349) and a comparison of EC50 between them will allow us to have a brief idea about how strong CaSRL is. In the presence of 10 mM L-Phe, the same concentrations of extracellular Mg^{2+} were applied. The response curves against the concentration of Mg^{2+} shifted to the right compared with that of CaSRL and the EC50 of Mg^{2+} for CaSR was higher when Phe instead of CaSRL was present. This result suggests that CaSRL is a more power and potent co-activator than L-Phe.

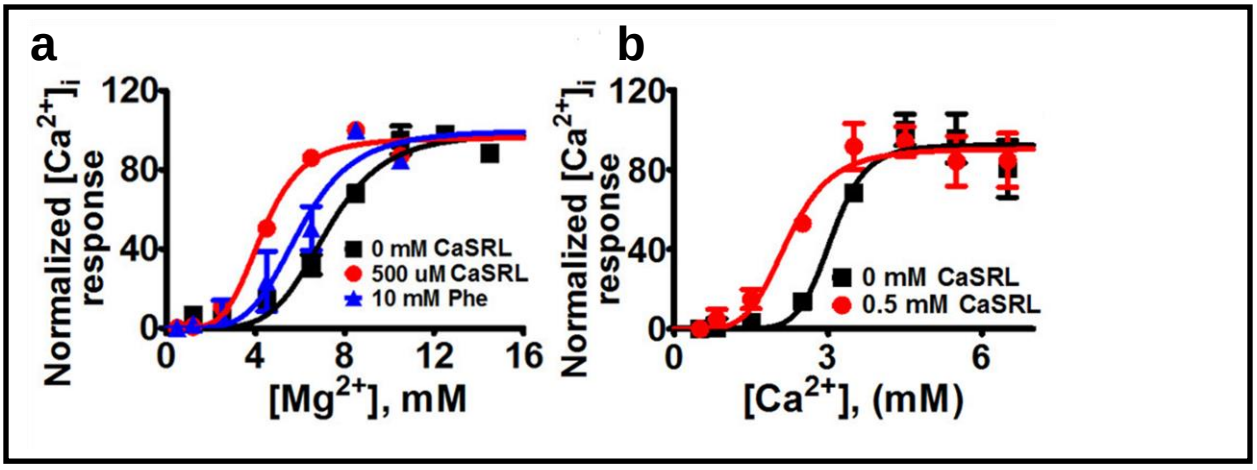

Figure 6.12 CaSRL function as a novel high-affinity co-agonist of CaSR.

(a) CaSRL potentiates $[Mg^{2+}]_o$ evoked $[Ca^{2+}]_i$ response in a population assay in 5001 cells measured by Fura-2 AM in the absence (black square) or presence of Phe (blue triangular) or CaSRL (red closed circle). (b) CaSRL potentiates $[Ca^{2+}]_o$ elicited $[Ca^{2+}]_i$ response in a population assay in 5001 cells measured by Fura-2 AM in the absence (black square) or presence of CaSRL (red closed circle).

In addition to potentiate divalent cations evoked $[Ca^{2+}]_i$ response, CaSRL also enhanced the phosphorylation of ERK1/2 elicited by extracellular Mg^{2+}. In the presence of CaSRL, more phosphorylated ERK1/2 accumulated at the same $[Mg^{2+}]_o$ (**Fig. 6.13**).

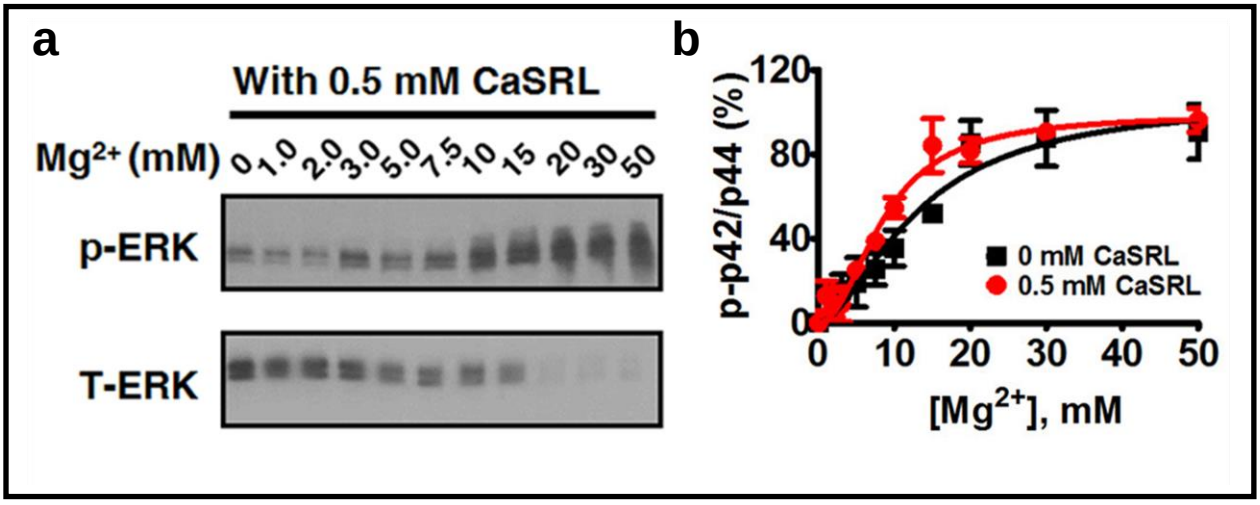

Figure 6.13 CaSRL potentiate CaSR mediated ERK1/2 activation.

(a) $[Mg^{2+}]_o$-activated ERK1/2 signaling in HEK293 cells stably transfected with CaSR in the presence of 0.5 mM CaSRL. (b) ERK1/2 activities upon stimulation by series concentrations of $[Mg^{2+}]_o$ in the absence or presence of CaSRL in CaSR stably expressed HEK293 cells (5001 cells) were plotted against $[Mg^{2+}]_o$ and fit with the Hill equation.

To measure the binding affinity of CaSRL to CaSR, we performed different experiments, including surface plasma resonance (SPR). However, none of the work well. The mechanism of SPR was described in detail in chapter 3. Basically we first immobilized hCaSR-ECD on the chip surface and then flow the CaSRL on the surface of chip. However, flowing CaSRL on the chip surface with hCaSR-ECD mobilized did not cause the response unit increase which indicated that no binding of CaSRL to the chip surface (**Fig. 6.14**). Several reasons accounted for the failure of this experiment. First, the hCaSR-ECD was fully occupied by CaSRL since this endogenous ligand was co-crystallized with hCaSR-ECD even after so many steps of purification or treatment. This suggested that it bond strongly. Second, CaSRL is very small compared with hCaSR-ECD. Binding of CaSRL to hCaSR-ECD may not cause any significant mass change and thickness alteration of the sensor chip. Therefore, we decided to briefly estimate the binding affinity or EC50 of CaSRL indirectly. During cell population assay, we elicited CaSR using a step wise increase of extracellular Mg^{2+} in the presence of different concentration of basal CaSRL. The EC50 of Mg^{2+} when co-applied with various concentrations of CaSRL were determined by fitting to Hill equation. The EC50 changes of Mg^{2+} were plotted agonist the CaSRL concentration and fit to Hill equation to estimate the EC50 of CaSRL. As shown in figure 6.15, higher concentration of CaSRL shifted the response curve of Mg^{2+} from right side to the left and decreased the EC50 of Mg^{2+} from 7.2 mM to 3.3 mM (**Table. 5.3**). The estimated EC50 of CaSRL indirectly obtained from response to Mg^{2+} was around 15 μM, thousand-time lower than that of L-Phe.

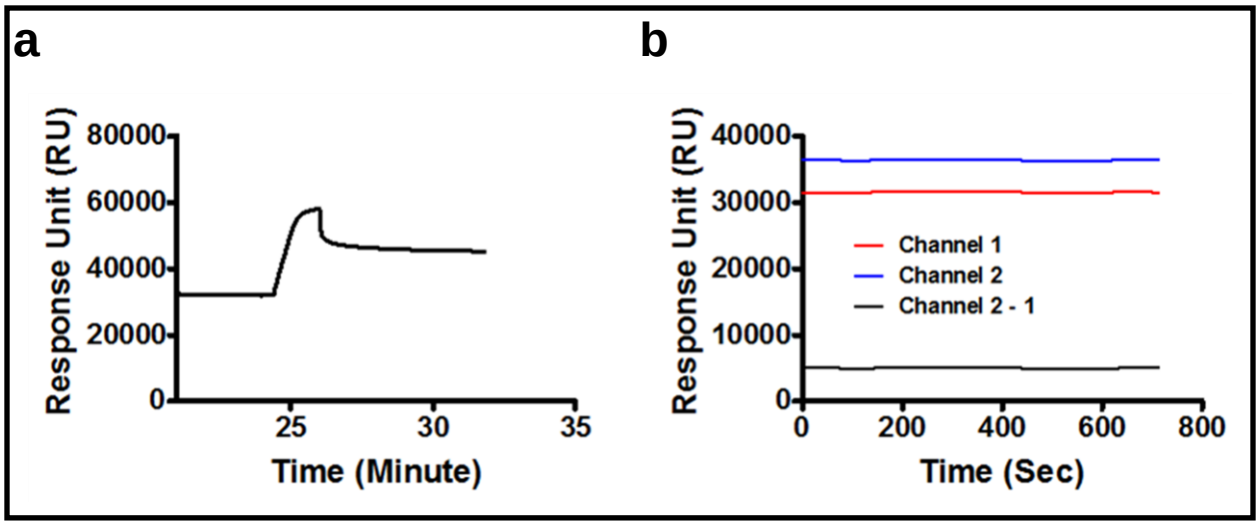

Figure 6.14 Monitoring CaSRL binding to hCaSR-ECD by SPR.

(a) Immobilization of hCaSR-ECD to CM5 chip surface. Injection of hCaSR-ECD resulted in response unit increase from 35000 to ~60000. (b) 0.5 mM CaSRL was injected for 300s and flowed on both channel 1 (control channel without hCaSR-ECD immobilization) and channel 2 (experimental channel with hCaSR-ECD immobilization). Red: control channel 1; Blue: experimental channel 2; Black: real response curve after background extraction.

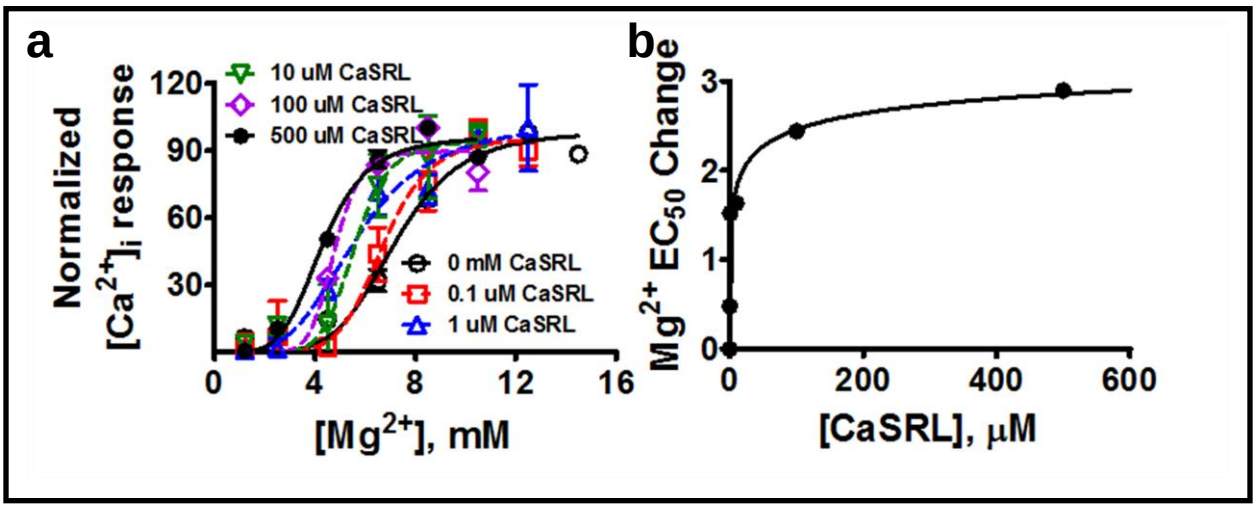

Figure 6.15 Indirectly measuring EC_{50} of CaSRL.

(a) $[Mg^{2+}]_o$-evoked $[Ca^{2+}]_i$ response in the presence of different concentrations of CaSRL in 5001 cells using cell population assay. (b) A maximally active concentration of 0.1 – 0.5 mM CaSRL dramatically reduces the EC_{50} for activation of $[Ca^{2+}]_i$ signaling by $[Mg^{2+}]_o$ in the presence of 0.5 mM $[Ca^{2+}]_o$. CaSRL displays an apparent K_d of 15 uM using whole curve fitting.

Table 6.3 EC_{50} of $[Mg^{2+}]_o$ for elicitation of $[Ca^{2+}]_i$ rise in cell population assay when different concentrations of CaSRL co-applied.

Co-activators	**EC_{50} of $[Mg^{2+}]_o$**
0.5 mM $[Ca^{2+}]_o$	7.2 ± 0.39
0.5 mM $[Ca^{2+}]_o$ + 0.0001 mM CaSRL	6.7 ± 0.25
0.5 mM $[Ca^{2+}]_o$ + 0.001 mM CaSRL	5.7 ± 0.47
0.5 mM $[Ca^{2+}]_o$ + 0.01 mM CaSRL	5.5 ± 0.27
0.5 mM $[Ca^{2+}]_o$ + 0.1 mM CaSRL	4.8 ± 0.24
0.5 mM $[Ca^{2+}]_o$ + 0.5 mM CaSRL	3.3 ± 0.70

The strong binding of CaSRL to CaSR was also proved by Phe replacement experiment. 150 mM Phe only partially replaced CaSRL in the purified hCaSR-ECD (**Fig. 6.16**). The peak of CaSRL in hCaSR-ECD detected by MS only decreased one fifth when 50 mM Phe were mixed with hCaSR-ECD overnight. The signal of CaSRL decreased half when 150 mM Phe was applied. The result suggest that Phe and CaSRL share the same binding site in hCaSR-ECD. Taken

together, CaSRL is a novel, high affinity co-agonist of CaSR in activation of both $[Ca^{2+}]_i$ signaling and ERK activity.

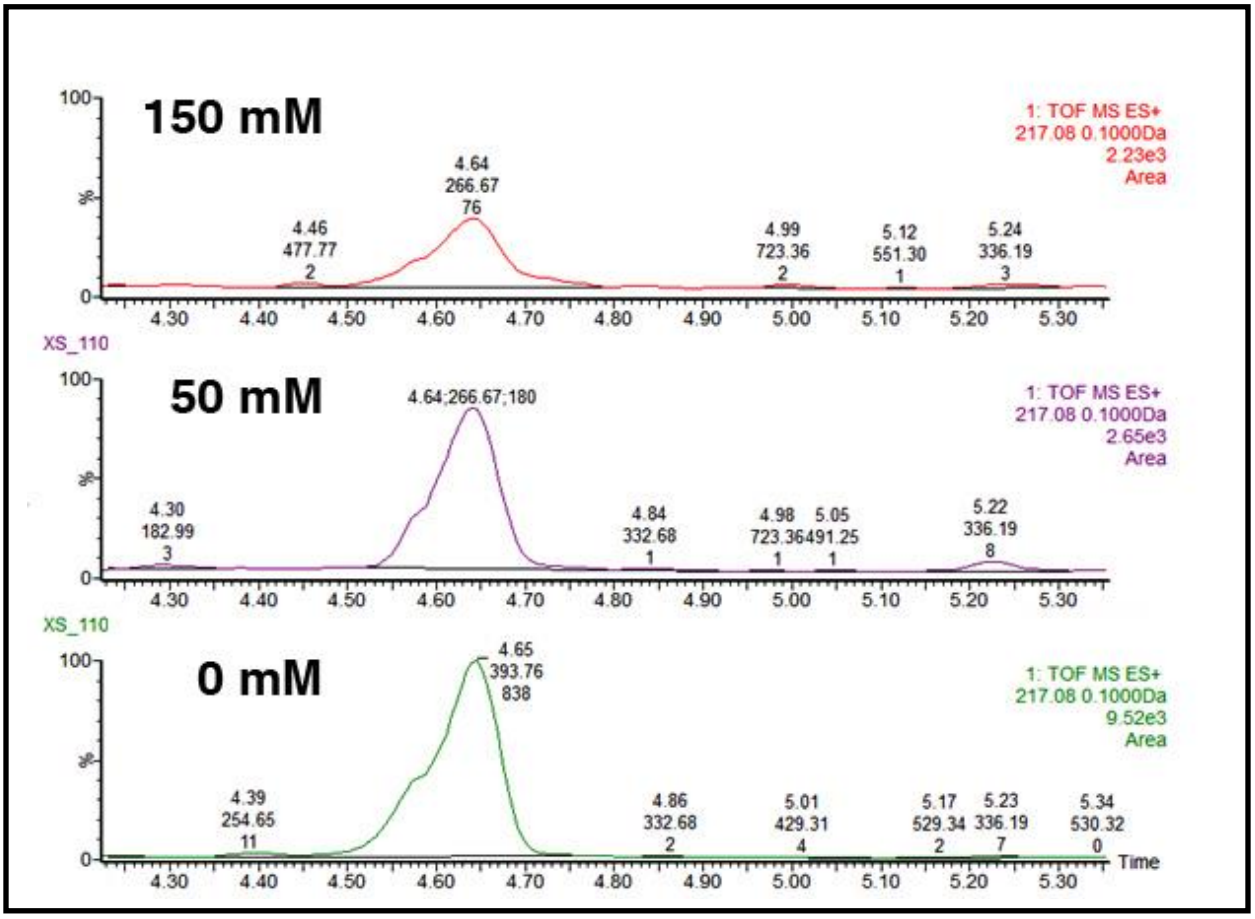

Figure 6.16 Replacement of CaSRL by phenylalanine.

With the increase of phenylalanine concentration (from 0 to 150 mM), the signal of CaSRL (the peak eluted at 4.64 min) detected by MS decreases correspondingly, indicating that the binding site of Phe and that of CaSRL are overlapping. The areas under the peaks are 838, 180 and 76, respectively.

6.2.7 Determining Mg^{2+} binding capability using hCaSR-ECD

To determine the Mg^{2+}-binding affinity to hCaSR-ECD, we performed Mg^{2+} titration experiment. The intrinsic Trp fluorescence emission was monitored using the fluorometer. Addition of Mg^{2+} into the curvet led to significant decrease of Trp fluorescence intensity until hCaSR-ECD was saturated at 24 mM Mg^{2+}. The fluorescence intensity changes were plotted against the concentration of Mg^{2+}, yielding a K_d of ~ 7 mM. We also performed Mg^{2+}-Tb^{3+} competition experiment to indirectly reflect the Mg^{2+}-binding capability to hCaSR-ECD. 30 µM Tb^{3+} was mixed with 2 µM hCaSR-ECD to allow Tb^{3+}-binding to hCaSR-ECD, followed by titrating high concentration of Mg^{2+} in to compete the pocket with Tb^{3+}. Tb^{3+} fluorescence intensity was decreased when the free Tb^{3+} concentration increased. As shown in figure 6.17, high concentration of Mg^{2+} was required to kick out the Tb^{3+} from the pocket, which suggests that Mg^{2+} binding is a weak binding.

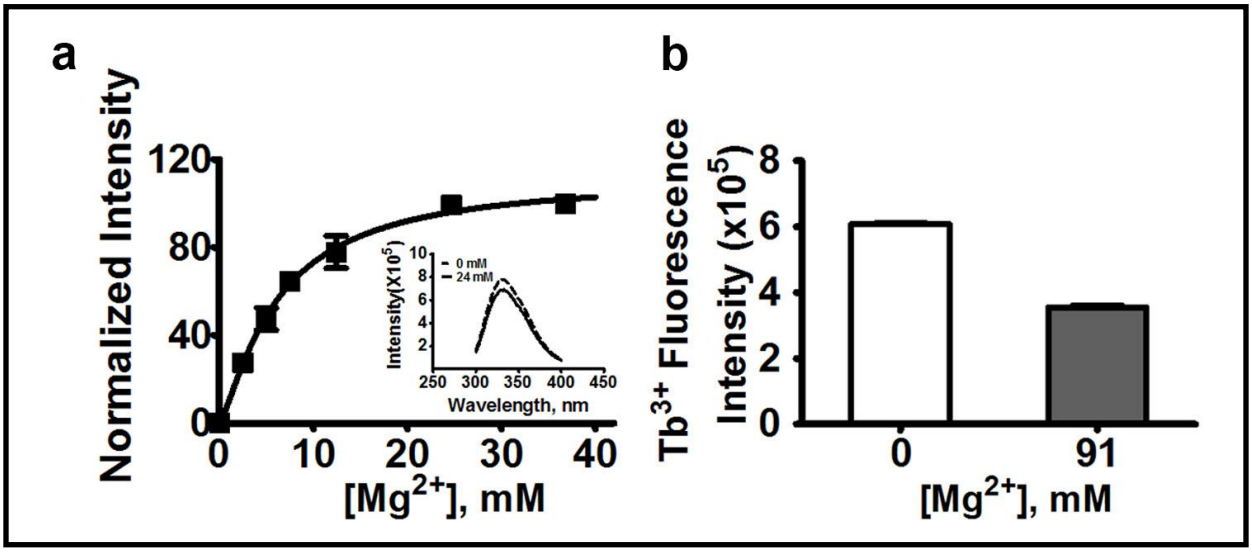

Figure 6.17 Determining Mg2+ binding capability using hCaSR-ECD.

The magnesium titration was performed in HEPES buffer (10 mM HEPES, 120 mM NaCl and 10 mM KCl, pH 7.2) with a protein concentration of 2.0 µM. (a) Magnesium titration curve of hCaSR-ECD (squares). Insert, Trp fluorescence spectra of hCaSR ECD in the presence of 0 (---) and 24 mM Mg^{2+} (—). (b) Tb^{3+}-hCaSR-ECD fluorescence intensity in the presence of 0 (white bar) or 91 mM Mg^{2+} (gray bar).

6.3 Discussion

The CaSR-ECD in the crystal structure is present as homodimer. This stable dimer structure of hCaSR-ECD is further supported by the elution volume observed in size exclusion chromatography and the molecular weight found in reducing/non-reducing page gel, which indicates that intermolecular disulfide bonds also contribute to dimerization (**Fig. 6.1**). In the crystal structure, both protomers in a closed conformation (**Fig. 6.2c**) similar to the equivalent closed conformation of mGluR1 bound with glutamate (r.m.s.d. of 1.24 Å for C (**Fig. 6.2b**) despite a low sequence similarity between members of family C (20-30%) (**Fig. 6.18)**(163). In addition, the direct and extensive homodimeric subdomain 2 interactions in the hCaSR-ECD are analogous to those observed in the mGluR2 dimer with a bound agonist (PDB code: 4XAQ), strongly suggesting that the hCaSR-ECD crystal structure represents an active conformation (**Fig. 6.19**) (391).

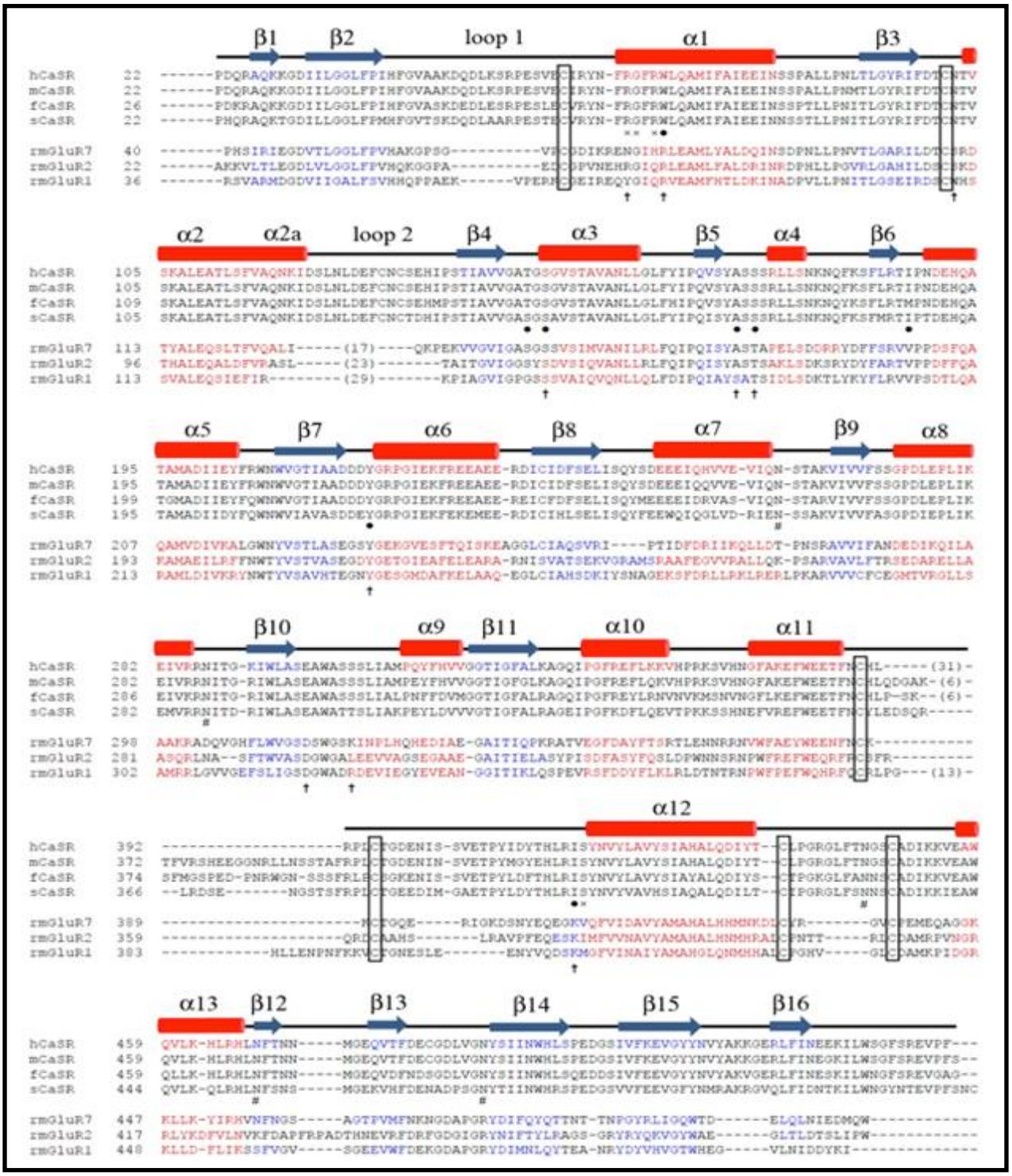
β1 β2 loop 1 α1 β3
α2 α2a loop 2 β4 α3 β5 α4 β6
α5 β7 α6 β8 α7 β9 α8
β10 α9 β11 α10 α11
α12
α13 β12 β13 β14 β15 β16
hCaSR
mCaSR
fCaSR
sCaSR
rmGluR7
rmGluR2
rmGluR1

Figure 6.18 Structure-based sequence alignment of CaSRs and mGluRs (by PROMALS3D) (439)).

α-helixes and β-strands are depicted as red cylinders and blue arrows, respectively. The invariant Cys residues are highlighted in black boxes. The following symbols indicate the residues involved in ligand/ion binding: ● CaSRL; † Glutamate; × Bicarbonate; # the site of glycosylation. hCaSR: Homo sapiens (AAI12237); mCaSR: Mus musculus (AAD28371); fCaSR: Xenopus (Silurana) tropicalis (XP_004919842); sCaSR: Salmo salar (NP_001119703); rmGlR7 (PDB code: 2E4Z); rmGluR2 (PDB code: 4XAQ); rmGluR1 (PDB code: 1EWK).

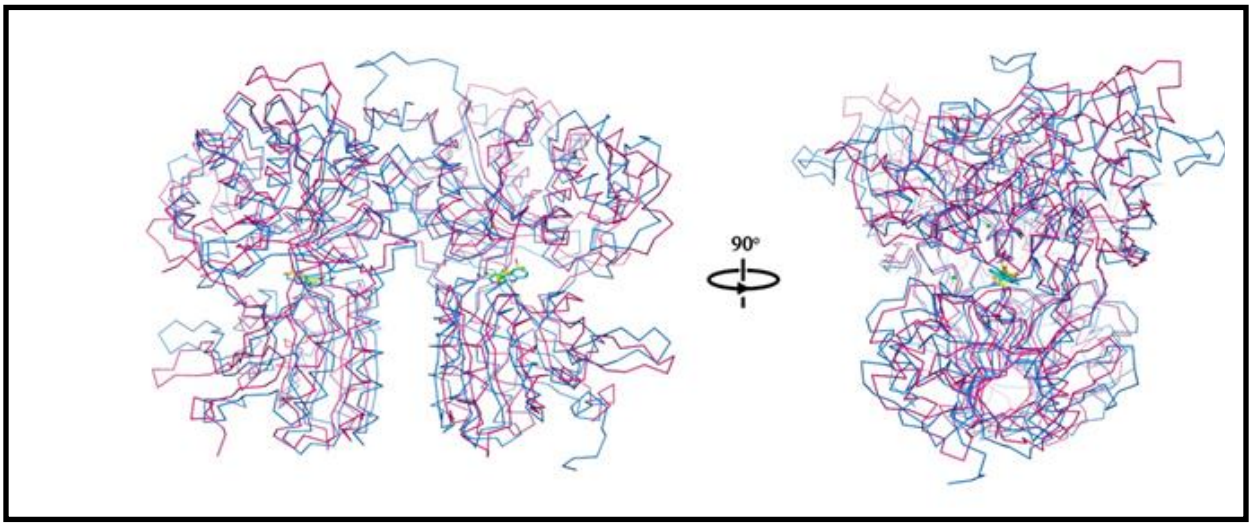

Figure 6.19 Comparison of CaSR and mGluR2 structures.

Structural overlapping of hCaSR-ECD dimer (blue) with mGluR2 dimer ECD (pink) with bound agonist (PDB code: 4XAQ) with a Cα r.m.s.d. of 2.8 Å. The proteins are depicted in ribbon mode, and CaSRL (cyan) and the mGluR agonist (yellow) are in stick mode.

A close inspection of the structure reveals two major differences between hCaSR-ECD and mGluR1-ECD. Firstly, loop 1 which connects β2 and α1, is significantly longer than those in mGluRs. Interestingly, loop 1 adopts a fairly extended conformation and forms a direct contact with α13*, the corresponding structural element from the other protomer. Importantly, Pro55, whose mutation to Lys leads to inactivation of CaSR in the human disorder Familial Hypocalciuric Hypercalcemia (FHH), is associated with Leu51 and Trp458* through hydrophobic interaction at the dimerization interface. As Leu51, Pro55 and Trp458 are highly conserved in CaSR across species. Loop 1-mediated contacts with α13 are presumed to be critical for the function of CaSR. Secondly, our structure reveals that loop 2, which link α2 and β4, also contributes to dimerization. Although disordered in one protomer, we can build the backbone structure of loop 2 in another protomer, which was not visible in mGluR structure due to high flexibility. The N-terminus of loop 2 is an alpha helix (α2a) extended from α2 with a 60^{o} kink at Asn118. The two α2a extensions, together with the two α2 helical segments embrace each other, likely stabilizing dimerization. Loop 2 contains two conserved Cys residues (Cys 129 and Cys131), and the approaching of the loop 2 from the two protomers provides a structural basis supporting the formation of the intermolecular disulfide bonds.

CaSR strongly prefers aromatic amino acid ligands, such as Phe and Trp, over negatively charged Glu, the ligand for mGluR. Structural comparison of the ligand-binding pocket in the hinge region between subdomains 1 and 2 of the hCaSR-ECD with that of mGluR1 reveals the structural basis of ligand selectivity (**Fig. 6.20**). Although the amino acid backbone of CaSRL adopts a similar conformation as Glu in mGluR1 through extensive interactions with S147, A168, S170, and Y218 (S156, S186, T188 and Y236 in mGluR1) (163). However, hCaSR and mGluR1 recognize the side chains of their preferred ligands differently: (1) Two positively charged residues

in mGluR1 (R78 and K409) that associate with the carboxylate group of the Glu ligand are replaced in hCaSR by W70 and I416 interacting with the indole ring of CaSRL. (2) Bulky residues (Y74, W110 and R323) limiting the mobility of the Glu side chain are replaced by smaller residues in hCaSR 9G67, N102 and S302). As a result, the size of the ligand binding pocket of hCaSR is significantly greater than that of mGluR1, consistent with the preference of CaSR for larger ligands.

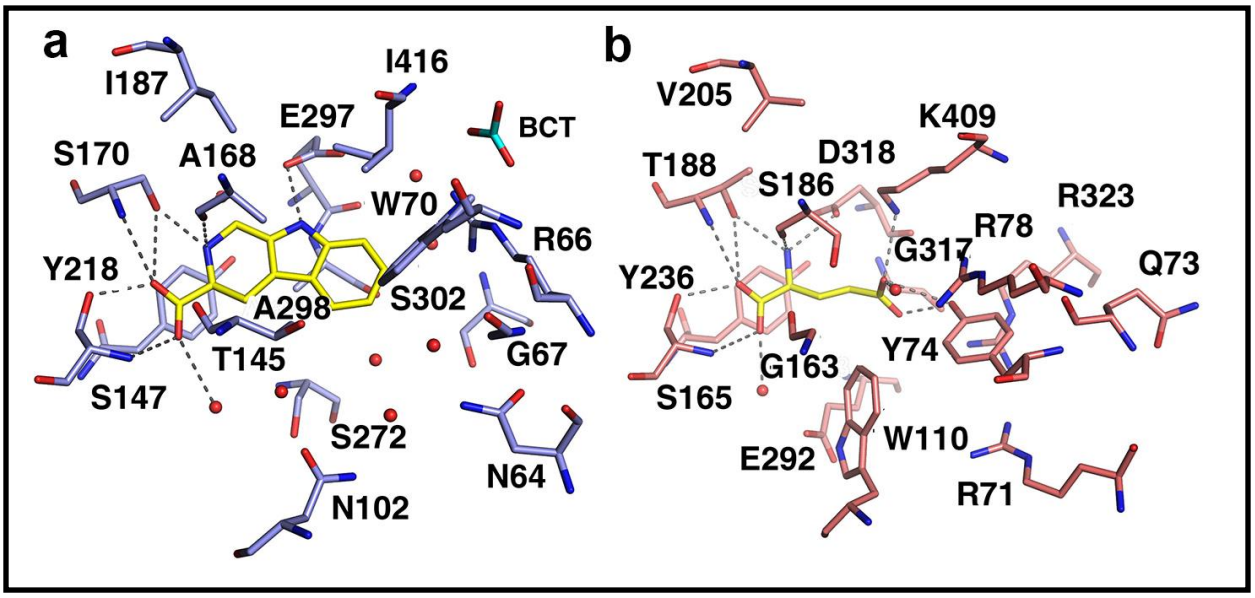

Figure 6.20 Structural comparison of CaSR ligand binding site with that of mGluR1.

The ligands (a) CaSRL in hCaSR-ECD and (b) Glu in mGluR1 are highlighted in yellow. The red balls represent water molecules. The hydrogen bonds are depicted by dashed lines. (B, PDB code: 1EWK).

Mapping of disease-associated mutations on the structure of hCaSR-ECD shows that the mutations are clustered in two regions: the hinge region between subdomains 1 and 2, and the dimerization interface (**Fig. 6.21**) (554,555). Indeed, our structural and functional data strongly

support the pivotal roles of these two regions in CaSR function. The hinge region between subdomains 1 and 2 harbors the binding site of TNCA supporting its role as a co-agonist of CaSR. Two other co-agonists of CaSR, Phe and Trp, likely bind in the same position (**Fig. 6.22**). We did not observe metal binding at the previously proposed "site 1" for Ca^{2+} (335,394,556). A close inspection of the structure reveals that the side chain of E297, a critical residue predicted for Ca^{2+} binding in the proposed "site 1", swings away from the other residues in "site 1" (S170, D190, Q193 and Y218), probably due to the extra carbon atom and the rigid structure of TNCA, ultimately resulting in its failure to capture the Ca^{2+} ion in combination with other "site 1" residues. (**Fig. 6.23**). Nevertheless, the essential role of E297 in Ca^{2+} sensing has been supported by previous mutational studies (335,522) and in the abrogated Mg^{2+} sensing of the E297I mutant (**Table 6.2**). Interestingly, a bicarbonate anion was also identified at the hinge region in the proximity of TNCA, coordinated by the side chains of R66, R69, W70, and S417 and the backbone amide nitrogen atoms of I416 and S417 (**Figs. 6.20 and 6.24**), potentially contributing to the known pH sensitivity of the CaSR (557).

Figure 6.21 Disease related mutations on CaSR ECD.

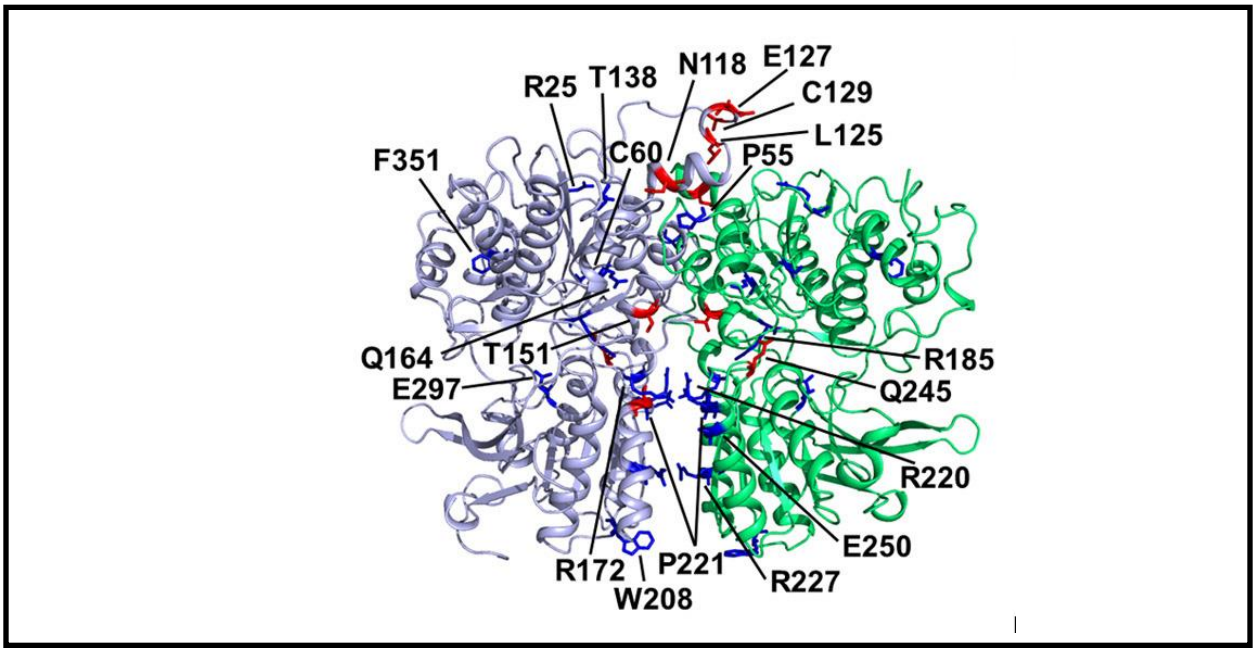

Blue: loss-of-function associated with familial hypocalciuric hypercalcemia (FHH). Red: gain-of-function mutations associated with autosomal dominant hypocalcemia (ADH).

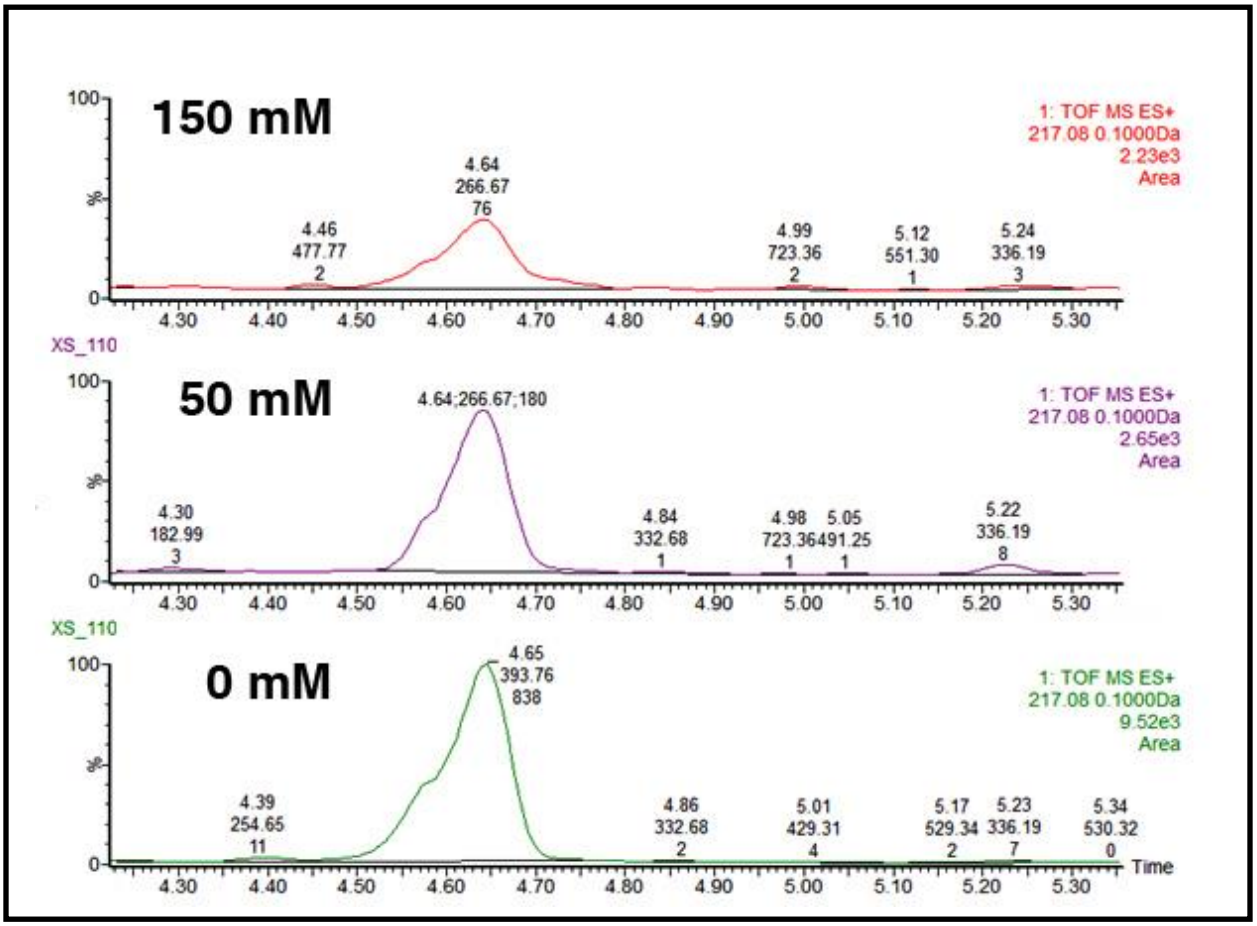

Figure 6.22 Replacement of TNCA by phenylalanine.

With the increase of phenylalanine concentration (from 0 to 150 mM), the signal of CaSRL (the peak eluted at 4.64 min) detected by MS decreases correspondingly, indicating that the binding site of Phe and that of CaSRL are overlapping. The areas under the peaks are 838, 180 and 76, respectively.

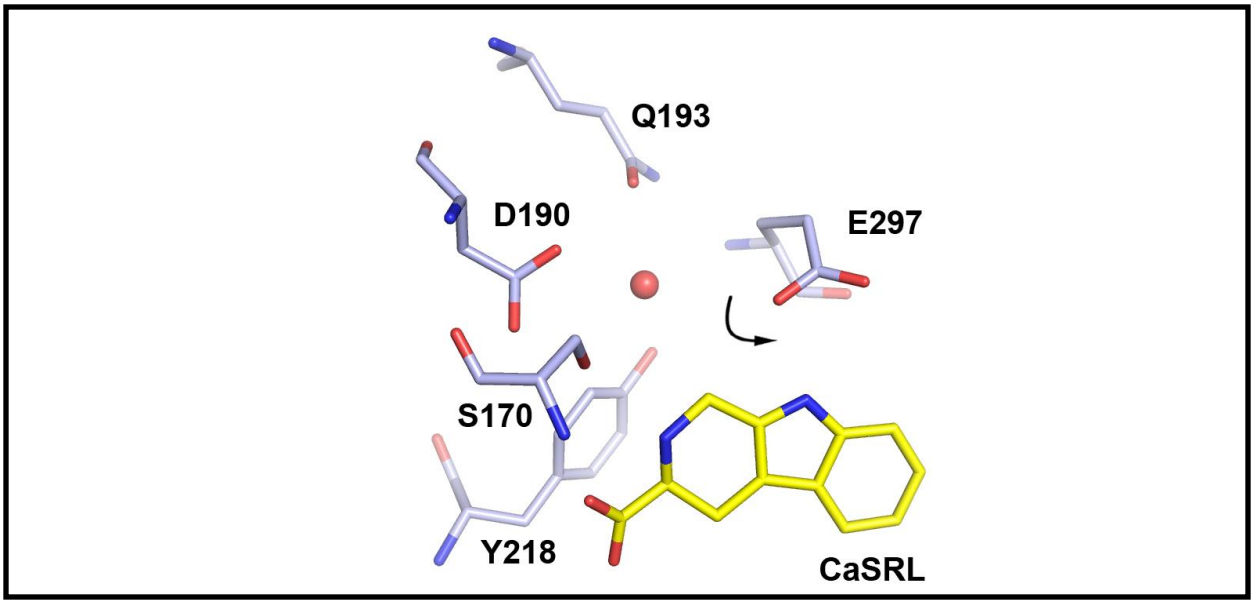

Figure 6.23 Structure of the proposed calcium binding "Site 1".

The residue of the proposed "site 1" and CaSRL are depicted in stick mode. The arrow indicates that the side chain of E297 swings away from the proposed calcium-binding site, due to steric hindrance imposed by CaSRL. As a result, E297 cannot join with other residues in "site 1" to capture the metal ion. Instead, E297 forms a hydrogen bond with the nitrogen atom on the indole ring of CaSRL. In the crystal structure, the proposed calcium-binding "site 1" is occupied by a water molecule (red sphere).

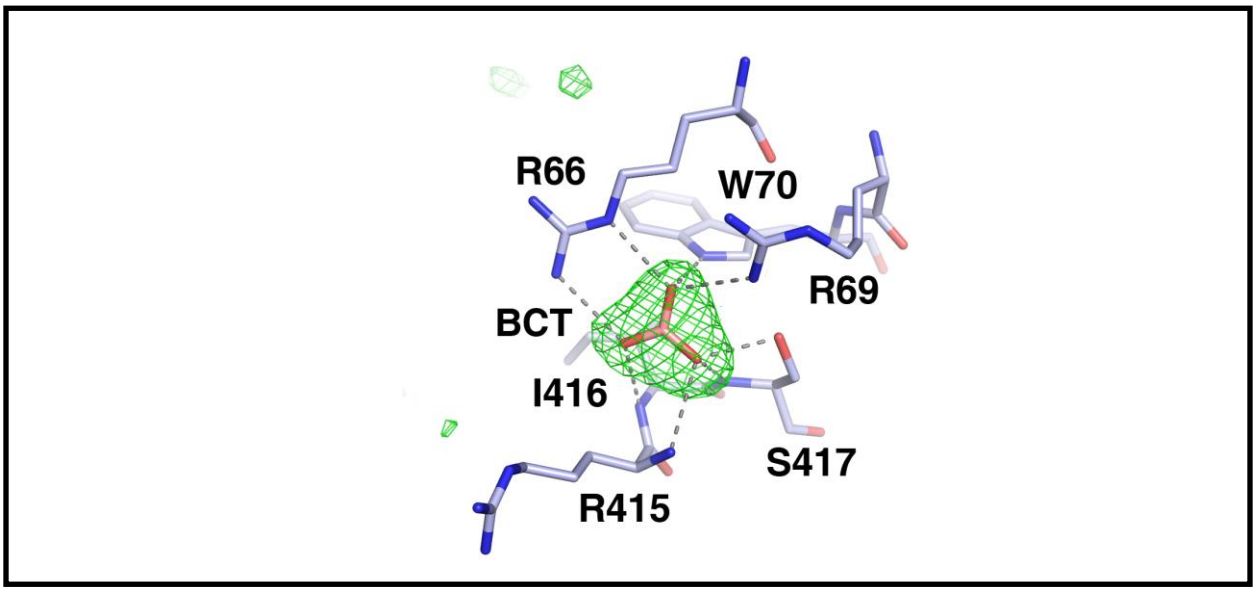

Figure 6.24 Identification of a bicarbonate anion near the ligand binding site.

The triangular planar-shaped electron density (Fo-Fc map at σ=4) is a bicarbonate anion, as there is no nitrate in the crystallization solution and the pH in the crystallization drop is 7.0. The bicarbonate anion is coordinated by the side chains of R66 (mutated in FHH and ovarian cancer), R69 (mutated in lung and endometrial cancer), W70 and S417, and the backbone amide nitrogen atoms of I416 and S417. Remarkably, R66, R69 and W70 are highly conserved in CaSR across species, but replaced by other residues in mGluRs. R66 and R69 are disease-related residues. Alterations in pH over the range of 5.5-6.0 to 9 are known to modulate the activity of the CaSR, and the bound bicarbonate identified here could potentially contribute to the pH sensitivity of the CaSR.

Evidence also suggested a potential Mg^{2+} binding site at the hinge region in the proximity of the bound TNCA (**Fig. 6.25**). Modeling a water molecule at this position led to a B factor (26-32 $Å^2$) substantially smaller than the coordinating atoms (35-40 $Å^2$), suggestive of a slightly

heavier atom occupying this position. Considering the negatively charged coordination sphere (A214, D216, Y218, S272, D275 and water), it was possible that this density corresponded to a bound Mg^{2+}. Mutations such as Y218K and D275I resulted in diminished intracellular calcium responses using both the cell population and single cell calcium imaging assays, although these mutations retained their surface expression (**Fig. 6.25b**). Alternatively, it may be a highly ordered water molecule trapped at the hinge region, as the distances to the coordinating oxygen atoms (2.5-2.8 Å) were significantly greater than typically observed Mg-O distance in biomolecules (2.1 Å) (558). Nevertheless, the low occupancy of Mg^{2+} due to its weak affinity may also cause a distorted geometry. At this stage, we have placed a water molecule in the model; however, given the importance of the hinge region in CaSR function and regulation, more functional and structural studies are warranted to further investigate this potential Mg^{2+} binding site identified here.

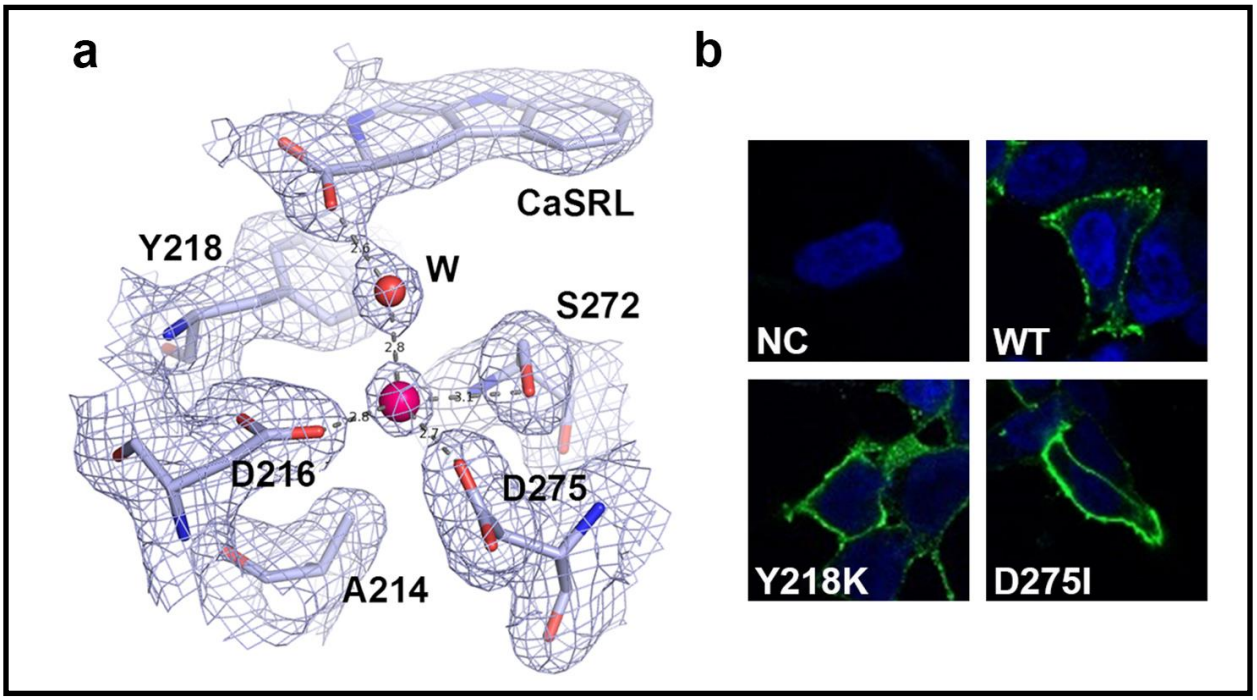

Figure 6.25 Identification of a potential Mg^{2+} binding site at the hinge region.

(a) Putative Mg^{2+} ion (large hot pink sphere) is coordinated by the side chains of D216, D275, S272 and a water molecule. The 2Fo-Fc electron density map (σ=1) is shown in light blue. W indicates the water molecule (small red sphere) bridging the putative Mg^{2+} and CaSRL. The dashed lines in grey indicate the potential Mg-O interaction, and the distances (in Å) between Mg^{2+} and oxygen atoms are shown on the dashed lines. (b) Membrane expression of CaSR and its variants. Immunostaining of non-permeabilized HEK293 cells expressing hCaSR was done with anti-FLAG monoclonal antibody, which recognizes the FLAG tag inserted in the CaSR ECD, and detection was carried out with Alexa Fluor 488-conjugated, goat anti-mouse secondary antibody. Blue: DAPI staining cell nuclei. Green: hCaSR immunoreactivity.

Several lines of evidence indicate a critical role of CaSR-ECD dimerization in CaSR function (**Figs. 6.2 and 6.27**). First, two metal binding sites (site 1 and site 3) are identified within the "acidic patch" at the dimerization interface of subdomain 2 **(Figs. 6.8 and 6.9).** A double mutant of CaSR (E228I/E229I) in site 3 showed a significantly decreased responsiveness to $[Ca^{2+}]_o$, and the E228I mutation also reduced activation of $[Ca^{2+}]_i$ oscillations induced by $[Mg^{2+}]_o$ as well as reduced Mg^{2+} binding, despite a similar level of membrane expression as WT CaSR (**Figs. 6.8, 6.10, Table 6.2**) (394). These data strongly suggest a role of metal binding at the "acidic patch" in metal sensing and signal transduction. Second, two loops (loop 1 and loop 2, **Fig. 6.2**) that mediate subdomain 1 dimerization, are functionally important (**Fig. 6.27a**). Loop 2, following α2, is largely disordered in mGluR structures, but is known to participate in two intermolecular disulfide bonds in CaSR through two conserved cysteine residues (C129 and C131) (537,559) (**Fig. 6.27b**). The N-terminal part of loop 2 forms a short α-helix (α2a) extended from α2 with a

kink at N118. The α2a segments from each protomer embrace each other, likely stabilizing dimerization (**Fig. 6.27a**). As several activating ADH mutations (L125P/F, E127G/A/K, C129Y/F/S/R, and N118K) and one inactivating FHH mutation are present on loop 2, subdomain 1 dimerization that is facilitated by loop 2 appears to be crucial in regulating the function of CaSR. Moreover, the highly conserved loop 1, which is significantly longer than the corresponding loop in mGluRs (**Fig. 6.26**), reaches across the dimerization interface to a hydrophobic surface on α13*. The hydrophobic interaction, primarily mediated by P55, L51 and W458*, stabilizes an extended conformation of loop 1, and a conserved positively charged patch also appears to contribute to dimerization of subdomain 1 (**Fig. 6.27a**). Notably, mutation of P55 causes FHH, indicative of a critical role of loop 1.

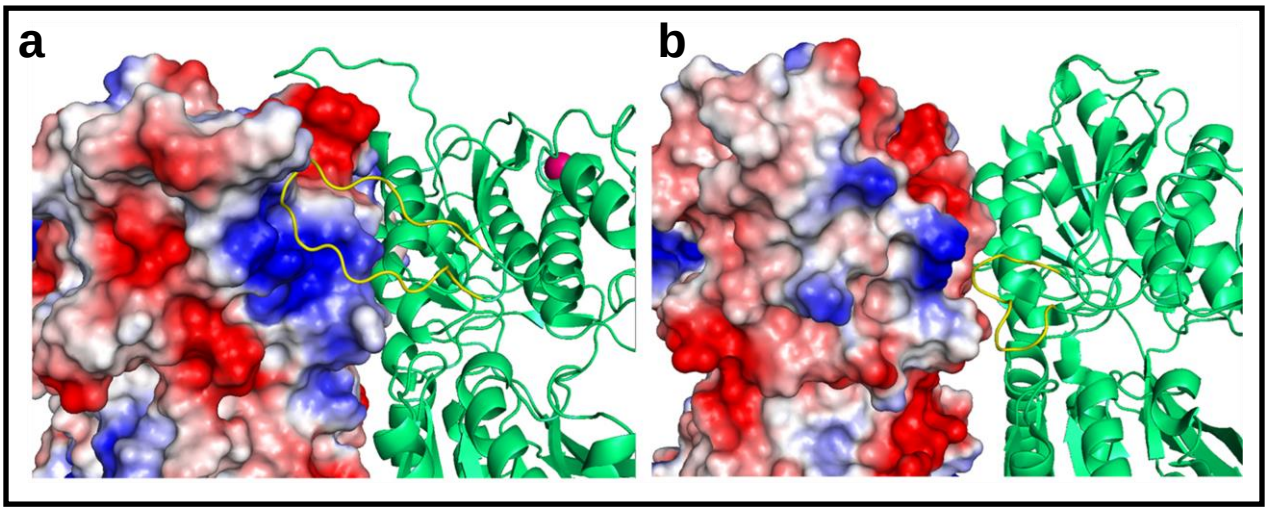

Figure 6.26 A positively charged pocket for loop 1 association.

Loop 1 for CaSR (a) and the corresponding loop in mGluR1 (b, PDB code 1EWK) are highlighed in yellow. The electrostatic potential map is colored in accordance to charge, with red representing negative potential, and blue positive potential. Loop 1 in CaSR is

significantly longer than the counterpart in mGluR1, reaching across the dimer interface to nestle into a positively charged pocket which is absent in mGluR1.

Where does this novel ligand come from puzzled us. We first checked fresh mammalian cell culture medium which was purchased from Invitrogen. We also checked medium when we purified hCaSR-ECD from cell culture and all purification buffer utilized in the purification procedure using mass spectrometry. However, we did not detect any TNCA in any of them. From the result, we could not draw conclusion that TNCA did not exist in culture medium since we did not enrich the medium. Human CaSR-ECD was firstly enriched by affinity column and then enriched again during crystallization. TNCA was tightly grabbed by hCaSR-ECD and was enriched simultaneously. However, when we checked cell culture medium, we did not enrich it. The TNCA amount in the culture medium may be below the limit of detection and resulted in the immeasurability. But it is also possible that TNCA is synthesized inside of cell during metabolism. It is likely produced by tryptophan reacting with formaldehyde in human. Next, we need to check the human blood sample and measure its concentration in blood since TNCA can be detected in various food and biological systems.

Figure 6.27 summarizes our present model for receptor activation and subsequent signal transduction that occurs via a conformational change induced by binding of ligand and calcium/magnesium at the cleft region between subdomains 1 and 2 as well as bridging interactions provided by metal ions binding at the “acidic patch” at the interface between the two subdomain 2 regions of the respective protomers. Initial dimerization of the CaSR ECD is facilitated by a unique “charged lock” between subdomains 1 of the two protomers orchestrated by conserved loop 1 and the charged pocket that embraces the two monomers and leads to a significantly greater

dimer interaction surface. Mutations at these key determinants in the ECD of CaSR cause human disorders with abnormal $[Ca^{2+}]_o$ and $[Mg^{2+}]_o$ homeostasis. The presumed conformational change induced by ligand/metal binding at the hinge region between subdomains 1 and 2, together with homodimerization of protomer subdomains 1 and 2 via loops 1 and 2, respectively, facilitates the approach of subdomains 1 and 2 from the two respective protomers. By neutralizing the repulsive effects of the negatively charged conserved "acidic patch", metal binding would stabilize subdomain 2 interactions. Dimerization of subdomain 2 is also critical for activation of mGluRs and GABAB receptors, and therefore it appears to be a common activation mechanism among cGPCRs that presumably leads to conformational changes of the transmembrane and intracellular domains, through which the intracellular signal cascades are initiated. Consistent with this model, mutations at these key determinants in hCaSR-ECD cause human disorders with abnormal $[Ca^{2+}]_o$ and $[Mg^{2+}]_o$ homeostasis. Thus, our proposed model, which is based on structural and associated biochemical and cellular studies on wild type and mutant proteins, reveals the structural basis of agonist/co-agonist binding to CaSR and provides a framework for further studies on the mechanism of receptor activation. The discovery of and unexpected tryptophan derivative ligand with unusually high affinity in potentiation of activation of CaSR by $[Ca^{2+}]_o$ and $[Mg^{2+}]_o$ also opens new avenues for development of agonists and antagonists as therapeutics for CaSR-related diseases.

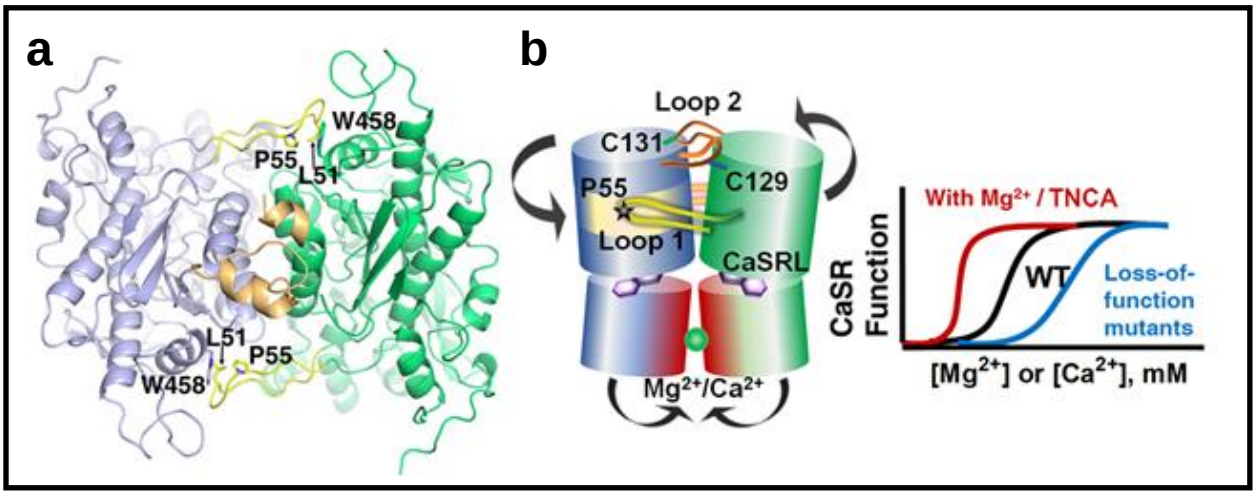

Figure 6.27 Key determinants for the molecular basis of disease-associated mutations and regulation.

(a) Involvement of loop 1 (Yellow) and loop 2 (Gold) in dimerization. (b) Working model for activation occurs via a conformational change induced by ligand binding at the hinge region between subdomains 1 and 2 as well as bridging interactions provided by metal ions binding at the "acidic patch" at the interface between the two subdomain 2 regions of the respective protomers. Mutations at these key determinants in the ECD of CaSR cause human disorders with abnormal $[Ca^{2+}]_o$ and $[Mg^{2+}]_o$ homeostasis.

7 MAJOR CONCLUSIONS AND SIGNIFICANCE

In summary, using different biophysical methods and cell-based assays, we performed a series of experiments elucidating the indispensable role of $[Ca^{2+}]_o$ in regulation of gap junction channel and mGluR5 activity, and revealing the structure of Ca^{2+}-sensing receptor with Mg^{2+} and unexpected ligand bound. The issue associated with large mammalian membrane protein expression and purification presented huge challenge in my studies, especially for the gap junction project. The codon preferred by eukaryotic hosts are quite different from the one used by *E.coli*. The low popularity of those tRNA matching the rare codons leads to the abortion of transcription and failure of protein expression. The large amount expression of exogenous proteins also caused huge toxicity for expression hosts. Exclusion bodies are usually formed to decrease this toxicity. However, this brings new problems associated with refolding the membrane proteins to the protein purification process. The purification of membrane protein usually starts with detergent extraction from membrane. The selection of detergent is crucial. The selection criteria is to extract as much protein as possible without destroy the membrane protein structure. Membrane protein are highly hydrophobic and tend to form aggregates following solubilization. Thus, the selected detergent needs to be efficient enough to warp the membrane protein and prevent the aggregation. I have struggled in the membrane protein expression and purification for a long time, from tissue isolation and *E.coli* expression to insect and mammalian cell expression. However, I am armed with rich membrane protein expression and purification experience after coming through all difficulties.

I am also so proud that we are the first group to provide more evidence for the debate in gap junction field. The role of CaM in regulation of gap junction has been came out for a long time and experienced spirited debate for a long time. However, so far no indecisive result came out to prove the direct interaction between gap junction protein and CaM. Using BRET assay, we

successfully detected the direct association between them. Different gap junction proteins distribution show tissue preference and the free $[Ca^{2+}]_i$ amount also varies in different tissue cells. Our finding that different connexins interact with CaM in different mode may relate with this $[Ca^{2+}]$i concentration variation and expression preference. $[Ca^{2+}]_i$ activates CaM to regulate cell-cell communication via gap junction proteins and differential interaction of CaM to vary connexins directly control their biological and physiological activities.

The first CaSR-ECD crystal structure provide the structure information for the whole CaSR field. The structure and function studies also revealed that Ca^{2+}/Mg^{2+} work cooperatively to active CaSR via ECD. The discovery of co-agonist TNCA with high affinity that potentiates the activation of CaSR by $[Ca^{2+}]_o$ and $[Mg^{2+}]_o$ opens new avenues for development of agonists and antagonists as therapeutics for CaSR-related diseases.

In summary, although the whole pass was covered with grass and thorns, we were able to achieve the following goals:

In Chapter 3, the studies on CaM and Cx45 association for the first time have revealed a Ca^{2+}-dependent interaction between them in living cells. Though previous studies reported that CaM was involved in Cx45 gap junction channel regulation, the evidence through CaM expression control were all indirect. No direct binding data are available. After successfully visualizing the interaction in living cell, we proceeded to identify the putative CaM binding site in Cx45. Using peptide mode, we proved that CaM binds with Cx45-derived peptide with a high affinity in the presence of Ca^{2+}. These finding advanced our understanding about Ca^{2+}/CaM gating of gap junction channels.

In Chapter 4, the studies on Cx26 regulation by $[Ca^{2+}]_o$ was hampered by lots of difficulties and challenges associated with this membrane protein and its mutants. We successfully predicted

a possible Ca^{2+}-binding pocket formed by extracellular loops of Cx26. This coordination ligand in Ca^{2+}-binding site is almost overlapping with the residues in the solved Ca^{2+}-bound Cx26 crystal structure published recently. To obtain enough Cx26 protein for biophysical studies, we successfully established baculovirus expression system which was also used for other membrane protein expression in our lab later. Besides, we also proved the gating effect of $[Ca^{2+}]_o$ on Cx26 hemichannels in HeLa cells using dye uptake assay. However, we could not successfully perform the same experiment in mutants which are predicted Ca^{2+}-binding ligand. Mutants in the putative Ca^{2+}-binding site caused cell death due to aberrant $[Ca^{2+}]_o$ regulation and some mutants formed non-functional hemichannels.

In Chapter 5, the studies on $[Ca^{2+}]_o$ modulation of mGluR5 further proved the conserved Ca^{2+}-binding site in group I mGluRs. This site was firstly reported by our group in mGluR1. Using the same computational algorithm and further sequence analysis, we reported a similar Ca^{2+}-binding site located in the hinge region of mGluR5. We further confirmed the regulatory function of this predicted Ca^{2+}-binding site through single cell imaging and mutagenesis studies. The response pattern of mGluR5 to $[Ca^{2+}]_o$ highly resemble Ca^{2+}-sensing receptor. On the other hand, $[Ca^{2+}]_o$ also found to enhance the action of orthosteric agonists (L-Glu and L-Quis) on mGluR5 by increasing their sensitivity and maximum responses. These discoveries may provide other opportunities for designing drugs with subtype selectivity.

In Chapter 6, the studies on Ca^{2+}-sensing receptor reported the first available crystal structure for CaSR, although this receptor have been identified more than 20 years ago. First, we successfully solved the crystal structure of hCaSR-ECD using crystals obtained in 200 mM Mg^{2+}. It was found that hCaSR-ECD formed dimer and both protomers were in open states. Besides, Mg^{2+} ions were identified in the hCaSR-ECD crystals. Using cell population assay and

mutagenesis studies, we further proved the function of those Mg^{2+}-binding sites in regulation of CaSR activity. In addition, we found an unexpected ligand in the hinge region of CaSR-ECD. It could function as co-agonist with Ca^{2+} or Mg^{2+} to decrease their EC_{50}. This ligand was identified as TNCA and was confirmed by MS. This ligand bound hCaSR-ECD very tight since 150 mM Phe could only replace partial of them from the pocket. The structure of hCaSR-ECD provided structural basis for Mg^{2+} regulation and drug development. Serving as a lead compound, the unexpected TCNA will facilitate the design of drugs targeting at CaSR.

PUBLICATIONS

(1) **Zou, J**., Samarian, M., Chen, Y., Veenstra, R., Louis, C. F., and Yang, J. J. (2014) Gap junction regulatio by calmodulin, *FEBS letters. 588(8),* 1430-1438.

(2) Chen, Y., Xu, **Zou, J**., Lopez, J., Yang, J. J., and Perez., Claudio. (2014) Myoplasmic resting Ca^{2+} regulation by ryanodine receptors is under the control of a novel Ca^{2+}-binding region of the receptor. *Biochem.J.460,*, 261-271.

(3) Hsieh, Y., **Zou, J**., Jin, J**.,** Yang, H., Chen, Y., Jiang, C., Yang, J. J., and Tai.P (2015) Monitoring channel activities of proteo-liposomes with SecAand Cx26 gap junction in single oocytes, *Analytical Biochemistry*, 480:58-66.

(4) Pu, F., Salarian, M., Xue, S., Qiao, J., Feng, J., Tan, S., Patel, A., Li, X., Mamouni, K., **Zou, J**., Wu, D., and Yang, J.J., (2016) Prostate-specific membrane antigen targeted protein contrast agents for molecular imaging of prostate cancer by MRI. *Nanoscale*

(5) Zhang, C., Zhang, Tuo., **Zou, J**., Miller, C., Gorkhali, R., Yang, J., Schilmiller, A., Wang, S., Huang, K., Brown, E., Moremen, K., Hu, J., and Yang, J.J. (2016) Structural basis for regulation of human calcium-sensing receptor by magnesium ions and an unexpected Tryptophan derivative co-agonist. *Science Advances*.

(6) Zhang, C., Miller, C., Gorkhali, R., **Zou, J**., Huang, K., Edward, B., and Yang, J.J. (2016) Molecular baiss of receptor-mediated cooperative extracellular Ca^{2+} signaling. *Frontiers in Physiology*.

MANUSCRIPT UNDER REVIEW OR IN PREPARATION

(1) Zhang, C., Miller, C., Gorkhali, R., **Zou, J**., Huang, K., Edward, B., and Yang, J.J. (2016) Molecular baiss of receptor-mediated cooperative extracellular Ca^{2+} signaling. *Frontiers in Physiology*, under review.

(2) **Zou, J**., Chen, Y., Brown, N., Helper, J., and Yang, J. J., "Direct visualization of interaction between Calmodulin and Connexin45". (2016) to be submitted to *Journal of Biological Chemistry*.

(3) **Zou, J**., Zhang, C., and Yang, J. J., (2016) "Extracellular Calcium modulates actions of orthosteric ligands on metabotropic glutamate receptor 5". To be submitted to *Journal of Biological Chemistry*.

(4) Jiang, J., Wong, H., Chen, Y., **Zou, J**., Blog, E., and Yang, J.J., "Structural bases for Ca^{2+} modulated CaM activation and inhibition of RyR1 via the multiple interaction sites with and without calcium". In preparation

REFERENCES

1. Harding, M. M. (1999) The geometry of metal-ligand interactions relevant to proteins. *Acta crystallographica. Section D, Biological crystallography* **55**, 1432-1443
2. Harding, M. M. (2000) The geometry of metal-ligand interactions relevant to proteins. II. Angles at the metal atom, additional weak metal-donor interactions. *Acta crystallographica. Section D, Biological crystallography* **56**, 857-867
3. Harding, M. M. (2001) Geometry of metal-ligand interactions in proteins. *Acta crystallographica. Section D, Biological crystallography* **57**, 401-411
4. Bagley, S. C., and Altman, R. B. (1995) Characterizing the microenvironment surrounding protein sites. *Protein science : a publication of the Protein Society* **4**, 622-635
5. Wei, L., and Altman, R. B. (1998) Recognizing protein binding sites using statistical descriptions of their 3D environments. *Pacific Symposium on Biocomputing. Pacific Symposium on Biocomputing*, 497-508
6. Kirberger, M., Wang, X., Deng, H., Yang, W., Chen, G., and Yang, J. J. (2008) Statistical analysis of structural characteristics of protein Ca2+-binding sites. *Journal of biological inorganic chemistry : JBIC : a publication of the Society of Biological Inorganic Chemistry* **13**, 1169-1181
7. Kirberger, M., Wang, X., Zhao, K., Tang, S., Chen, G., and Yang, J. J. (2010) Integration of Diverse Research Methods to Analyze and Engineer Ca-Binding Proteins: From Prediction to Production. *Current bioinformatics* **5**, 68-80
8. McPhalen, C. A., Strynadka, N. C., and James, M. N. (1991) Calcium-binding sites in proteins: a structural perspective. *Advances in protein chemistry* **42**, 77-144
9. Nayal, M., and Di Cera, E. (1994) Predicting Ca(2+)-binding sites in proteins. *Proceedings of the National Academy of Sciences of the United States of America* **91**, 817-821
10. Pidcock, E., and Moore, G. R. (2001) Structural characteristics of protein binding sites for calcium and lanthanide ions. *Journal of biological inorganic chemistry : JBIC : a publication of the Society of Biological Inorganic Chemistry* **6**, 479-489
11. Herzberg, O., Moult, J., and James, M. N. (1986) A model for the Ca2+-induced conformational transition of troponin C. A trigger for muscle contraction. *The Journal of biological chemistry* **261**, 2638-2644

12. Dudev, T., and Lim, C. (2003) Principles governing Mg, Ca, and Zn binding and selectivity in proteins. *Chemical reviews* **103**, 773-788
13. Hardingham, N. R., Bannister, N. J., Read, J. C., Fox, K. D., Hardingham, G. E., and Jack, J. J. (2006) Extracellular calcium regulates postsynaptic efficacy through group 1 metabotropic glutamate receptors. *The Journal of neuroscience : the official journal of the Society for Neuroscience* **26**, 6337-6345
14. Glusker, J. P. (1991) Structural aspects of metal liganding to functional groups in proteins. *Advances in protein chemistry* **42**, 1-76
15. Wang, X., Kirberger, M., Qiu, F., Chen, G., and Yang, J. J. (2009) Towards predicting Ca2+-binding sites with different coordination numbers in proteins with atomic resolution. *Proteins* **75**, 787-798
16. Maguire, M. E., and Cowan, J. A. (2002) Magnesium chemistry and biochemistry. *Biometals : an international journal on the role of metal ions in biology, biochemistry, and medicine* **15**, 203-210
17. Cowan, J. A. (1998) Metal Activation of Enzymes in Nucleic Acid Biochemistry. *Chemical reviews* **98**, 1067-1088
18. Dudev, T., Cowan, J. A., and Lim, C. (1999) Competitive binding in magnesium coordination chemistry: Water versus ligands of biological interest. *Journal of the American Chemical Society* **121**, 7665-7673
19. Palkina, K. K., Kuz'mina, N. E., Orlova, V. T., and Kondakova, I. V. (1999) Coordination Compounds of Some Transition Metal, Magnesium, and Calcium Nitrates with Dimethylcarbamide. *Russ J Inorg Chem+* **44**, 901-906
20. Cowan, J. A. (2002) Structural and catalytic chemistry of magnesium-dependent enzymes. *Biometals : an international journal on the role of metal ions in biology, biochemistry, and medicine* **15**, 225-235
21. Ringer, S. (1883) A further Contribution regarding the influence of the different Constituents of the Blood on the Contraction of the Heart. *The Journal of physiology* **4**, 29-42 23
22. Murphy, E. (2000) Mysteries of magnesium homeostasis. *Circulation research* **86**, 245-248
23. Bootman, M. D. (2012) Calcium signaling. *Cold Spring Harbor perspectives in biology* **4**, a011171
24. Kretsinger, R. H., and Nockolds, C. E. (1973) Carp muscle calcium-binding protein. II. Structure determination and general description. *The Journal of biological chemistry* **248**, 3313-3326
25. Valeyev, N. V., Bates, D. G., Heslop-Harrison, P., Postlethwaite, I., and Kotov, N. V. (2008) Elucidating the mechanisms of cooperative calcium-calmodulin interactions: a structural systems biology approach. *BMC systems biology* **2**, 48
26. Yanyi, C., Shenghui, X., Yubin, Z., and Jie, Y. J. (2010) Calciomics: prediction and analysis of EF-hand calcium binding proteins by protein engineering. *Science China. Chemistry* **53**, 52-60
27. O'Neil, K. T., and DeGrado, W. F. (1990) How calmodulin binds its targets: sequence independent recognition of amphiphilic alpha-helices. *Trends in biochemical sciences* **15**, 59-64

28. Rhoads, A. R., and Friedberg, F. (1997) Sequence motifs for calmodulin recognition. *FASEB journal : official publication of the Federation of American Societies for Experimental Biology* **11**, 331-340
29. Barbato, G., Ikura, M., Kay, L. E., Pastor, R. W., and Bax, A. (1992) Backbone dynamics of calmodulin studied by 15N relaxation using inverse detected two-dimensional NMR spectroscopy: the central helix is flexible. *Biochemistry* **31**, 5269-5278
30. Wall, M. E., Clarage, J. B., and Phillips, G. N. (1997) Motions of calmodulin characterized using both Bragg and diffuse X-ray scattering. *Structure* **5**, 1599-1612
31. Radivojac, P., Vucetic, S., O'Connor, T. R., Uversky, V. N., Obradovic, Z., and Dunker, A. K. (2006) Calmodulin signaling: analysis and prediction of a disorder-dependent molecular recognition. *Proteins* **63**, 398-410
32. Tidow, H., and Nissen, P. (2013) Structural diversity of calmodulin binding to its target sites. *The FEBS journal* **280**, 5551-5565
33. Hoeflich, K. P., and Ikura, M. (2002) Calmodulin in action: diversity in target recognition and activation mechanisms. *Cell* **108**, 739-742
34. Yap, K. L., Kim, J., Truong, K., Sherman, M., Yuan, T., and Ikura, M. (2000) Calmodulin target database. *Journal of structural and functional genomics* **1**, 8-14
35. Rellos, P., Pike, A. C., Niesen, F. H., Salah, E., Lee, W. H., von Delft, F., and Knapp, S. (2010) Structure of the CaMKIIdelta/calmodulin complex reveals the molecular mechanism of CaMKII kinase activation. *PLoS biology* **8**, e1000426
36. Meador, W. E., Means, A. R., and Quiocho, F. A. (1993) Modulation of calmodulin plasticity in molecular recognition on the basis of x-ray structures. *Science* **262**, 1718-1721
37. Evans, T. I., Hell, J. W., and Shea, M. A. (2011) Thermodynamic linkage between calmodulin domains binding calcium and contiguous sites in the C-terminal tail of Ca(V)1.2. *Biophysical chemistry* **159**, 172-187
38. Feldkamp, M. D., Yu, L., and Shea, M. A. (2011) Structural and energetic determinants of apo calmodulin binding to the IQ motif of the Na(V)1.2 voltage-dependent sodium channel. *Structure* **19**, 733-747
39. Bahler, M., and Rhoads, A. (2002) Calmodulin signaling via the IQ motif. *FEBS letters* **513**, 107-113
40. Neyton, J., and Trautmann, A. (1986) Physiological modulation of gap junction permeability. *The Journal of experimental biology* **124**, 993-114
41. Yeager, M., and Nicholson, B. J. (1996) Structure of gap junction intercellular channels. *Current opinion in structural biology* **6**, 183-192
42. Sohl, G., and Willecke, K. (2004) Gap junctions and the connexin protein family. *Cardiovascular research* **62**, 228-232
43. Bruzzone, R., White, T. W., and Paul, D. L. (1996) Connections with connexins: the molecular basis of direct intercellular signaling. *European journal of biochemistry / FEBS* **238**, 1-27
44. Kruger, O., Plum, A., Kim, J. S., Winterhager, E., Maxeiner, S., Hallas, G., Kirchhoff, S., Traub, O., Lamers, W. H., and Willecke, K. (2000) Defective vascular development in connexin 45-deficient mice. *Development* **127**, 4179-4193
45. Kumai, M., Nishii, K., Nakamura, K., Takeda, N., Suzuki, M., and Shibata, Y. (2000) Loss of connexin45 causes a cushion defect in early cardiogenesis. *Development* **127**, 3501-3512

46. Reaume, A. G., de Sousa, P. A., Kulkarni, S., Langille, B. L., Zhu, D., Davies, T. C., Juneja, S. C., Kidder, G. M., and Rossant, J. (1995) Cardiac malformation in neonatal mice lacking connexin43. *Science* **267**, 1831-1834
47. Lai-Cheong, J. E., Arita, K., and McGrath, J. A. (2007) Genetic diseases of junctions. *The Journal of investigative dermatology* **127**, 2713-2725
48. Henderson, D., Eibl, H., and Weber, K. (1979) Structure and biochemistry of mouse hepatic gap junctions. *J Mol Biol* **132**, 193-218
49. Hertzberg, E. L., and Gilula, N. B. (1979) Isolation and characterization of gap junctions from rat liver. *J Biol Chem* **254**, 2138-2147
50. Kistler, J., Kirkland, B., and Bullivant, S. (1985) Identification of a 70,000-D protein in lens membrane junctional domains. *J Cell Biol* **101**, 28-35
51. Manjunath, C. K., Goings, G. E., and Page, E. (1985) Proteolysis of cardiac gap junctions during their isolation from rat hearts. *J Membr Biol* **85**, 159-168
52. Beyer, E. C., Paul, D. L., and Goodenough, D. A. (1987) Connexin43: a protein from rat heart homologous to a gap junction protein from liver. *J Cell Biol* **105**, 2621-2629
53. Beyer, E. C., Paul, D. L., and Goodenough, D. A. (1990) Connexin family of gap junction proteins. *The Journal of membrane biology* **116**, 187-194
54. Bruzzone, R. (2001) Learning the language of cell-cell communication through connexin channels. *Genome biology* **2**, REPORTS4027
55. Das Sarma, J., Wang, F., and Koval, M. (2002) Targeted gap junction protein constructs reveal connexin-specific differences in oligomerization. *The Journal of biological chemistry* **277**, 20911-20918
56. Musil, L. S., and Goodenough, D. A. (1993) Multisubunit assembly of an integral plasma membrane channel protein, gap junction connexin43, occurs after exit from the ER. *Cell* **74**, 1065-1077
57. Koval, M., Harley, J. E., Hick, E., and Steinberg, T. H. (1997) Connexin46 is retained as monomers in a trans-Golgi compartment of osteoblastic cells. *The Journal of cell biology* **137**, 847-857
58. Ebihara, L., Beyer, E. C., Swenson, K. I., Paul, D. L., and Goodenough, D. A. (1989) Cloning and expression of a Xenopus embryonic gap junction protein. *Science* **243**, 1194-1195
59. Gimlich, R. L., Kumar, N. M., and Gilula, N. B. (1990) Differential regulation of the levels of three gap junction mRNAs in Xenopus embryos. *The Journal of cell biology* **110**, 597-605
60. Zhang, J. T., and Nicholson, B. J. (1994) The topological structure of connexin 26 and its distribution compared to connexin 32 in hepatic gap junctions. *The Journal of membrane biology* **139**, 15-29
61. Mese, G., Richard, G., and White, T. W. (2007) Gap junctions: basic structure and function. *The Journal of investigative dermatology* **127**, 2516-2524
62. Cottrell, G. T., and Burt, J. M. (2005) Functional consequences of heterogeneous gap junction channel formation and its influence in health and disease. *Biochimica et biophysica acta* **1711**, 126-141
63. Werner, R., Levine, E., Rabadan-Diehl, C., and Dahl, G. (1989) Formation of hybrid cell-cell channels. *Proceedings of the National Academy of Sciences of the United States of America* **86**, 5380-5384

64. Swenson, K. I., Jordan, J. R., Beyer, E. C., and Paul, D. L. (1989) Formation of gap junctions by expression of connexins in Xenopus oocyte pairs. *Cell* **57**, 145-155
65. Bruzzone, R., White, T. W., and Paul, D. L. (1994) Expression of chimeric connexins reveals new properties of the formation and gating behavior of gap junction channels. *Journal of cell science* **107 (Pt 4)**, 955-967
66. Trexler, E. B., Bennett, M. V., Bargiello, T. A., and Verselis, V. K. (1996) Voltage gating and permeation in a gap junction hemichannel. *Proceedings of the National Academy of Sciences of the United States of America* **93**, 5836-5841
67. Hu, X., Ma, M., and Dahl, G. (2006) Conductance of connexin hemichannels segregates with the first transmembrane segment. *Biophysical journal* **90**, 140-150
68. Bergoffen, J., Scherer, S. S., Wang, S., Scott, M. O., Bone, L. J., Paul, D. L., Chen, K., Lensch, M. W., Chance, P. F., and Fischbeck, K. H. (1993) Connexin mutations in X-linked Charcot-Marie-Tooth disease. *Science* **262**, 2039-2042
69. Kelsell, D. P., Dunlop, J., Stevens, H. P., Lench, N. J., Liang, J. N., Parry, G., Mueller, R. F., and Leigh, I. M. (1997) Connexin 26 mutations in hereditary non-syndromic sensorineural deafness. *Nature* **387**, 80-83
70. Mackay, D., Ionides, A., Kibar, Z., Rouleau, G., Berry, V., Moore, A., Shiels, A., and Bhattacharya, S. (1999) Connexin46 mutations in autosomal dominant congenital cataract. *American journal of human genetics* **64**, 1357-1364
71. Berry, V., Mackay, D., Khaliq, S., Francis, P. J., Hameed, A., Anwar, K., Mehdi, S. Q., Newbold, R. J., Ionides, A., Shiels, A., Moore, T., and Bhattacharya, S. S. (1999) Connexin 50 mutation in a family with congenital "zonular nuclear" pulverulent cataract of Pakistani origin. *Human genetics* **105**, 168-170
72. Deleze, J. (1967) [Effect of calcium ions on the demarcation of cardiac fibers following section in vitro]. *Helvetica physiologica et pharmacologica acta* **25**, CR177
73. de Mello, W. C., Motta, G. E., and Chapeau, M. (1969) A study on the healing-over of myocardial cells of toads. *Circulation research* **24**, 475-487
74. Deleze, J. (1970) The recovery of resting potential and input resistance in sheep heart injured by knife or laser. *The Journal of physiology* **208**, 547-562
75. De Mello, W. C. (1975) Effect of intracellular injection of calcium and strontium on cell communication in heart. *The Journal of physiology* **250**, 231-245
76. Nishiye, H. (1977) The mechanism of Ca2+ action on the healing-over process in mammalian cardiac muscles: a kinetic analysis. *The Japanese journal of physiology* **27**, 451-466
77. Deleze, J., and Loewenstein, W. R. (1976) Permeability of a cell junction during intracellular injection of divalent cations. *The Journal of membrane biology* **28**, 71-86
78. Loewenstein, W. R. (1966) Permeability of membrane junctions. *Annals of the New York Academy of Sciences* **137**, 441-472
79. Loewenstein, W. R. (1967) Cell surface membranes in close contact. Role of calcium and magnesium ions. *Journal of colloid and interface science* **25**, 34-46
80. Oliveira-Castro, G. M., and Loewenstein, W. R. (1971) Junctional membrane permeability : Effects of divalent cations. *The Journal of membrane biology* **5**, 51-77
81. Rose, B., and Loewenstein, W. R. (1975) Permeability of cell junction depends on local cytoplasmic calcium activity. *Nature* **254**, 250-252

82. Rose, B., and Loewenstein, W. R. (1976) Permeability of a cell junction and the local cytoplasmic free ionized calcium concentration: a study with aequorin. *The Journal of membrane biology* **28**, 87-119
83. De Mello, W. C. (1983) The influence of pH on the healing-over of mammalian cardiac muscle. *The Journal of physiology* **339**, 299-307
84. Peracchia, C., and Peracchia, L. L. (1980) Gap junction dynamics: reversible effects of divalent cations. *The Journal of cell biology* **87**, 708-718
85. Unwin, P. N., and Zampighi, G. (1980) Structure of the junction between communicating cells. *Nature* **283**, 545-549
86. Muller, D. J., Hand, G. M., Engel, A., and Sosinsky, G. E. (2002) Conformational changes in surface structures of isolated connexin 26 gap junctions. *The EMBO journal* **21**, 3598-3607
87. Thimm, J., Mechler, A., Lin, H., Rhee, S., and Lal, R. (2005) Calcium-dependent open/closed conformations and interfacial energy maps of reconstituted hemichannels. *The Journal of biological chemistry* **280**, 10646-10654
88. Bennett, B. C., Purdy, M. D., Baker, K. A., Acharya, C., McIntire, W. E., Stevens, R. C., Zhang, Q., Harris, A. L., Abagyan, R., and Yeager, M. (2016) An electrostatic mechanism for Ca(2+)-mediated regulation of gap junction channels. *Nature communications* **7**, 8770
89. Sjostrand, F. S., Andersson-Cedergren, E., and Dewey, M. M. (1958) The ultrastructure of the intercalated discs of frog, mouse and guinea pig cardiac muscle. *Journal of ultrastructure research* **1**, 271-287
90. Karrer, H. E. (1960) The striated musculature of blood vessels. II. Cell interconnections and cell surface. *The Journal of biophysical and biochemical cytology* **8**, 135-150
91. Dewey, M. M., and Barr, L. (1962) Intercellular Connection between Smooth Muscle Cells: the Nexus. *Science* **137**, 670-672
92. Robertson, J. D. (1961) Ultrastructure of excitable membranes and the crayfish median-giant synapse. *Annals of the New York Academy of Sciences* **94**, 339-389
93. Robertson, J. D. (1963) The Occurrence of a Subunit Pattern in the Unit Membranes of Club Endings in Mauthner Cell Synapses in Goldfish Brains. *The Journal of cell biology* **19**, 201-221
94. Stoeckenius, W. (1962) Some electron microscopical observations on liquid-crystalline phases in lipid-water systems. *The Journal of cell biology* **12**, 221-229
95. Revel, J. P., and Karnovsky, M. J. (1967) Hexagonal array of subunits in intercellular junctions of the mouse heart and liver. *The Journal of cell biology* **33**, C7-C12
96. Payton, B. W., Bennett, M. V., and Pappas, G. D. (1969) Permeability and structure of junctional membranes at an electrotonic synapse. *Science* **166**, 1641-1643
97. Goodenough, D. A. (1974) Bulk isolation of mouse hepatocyte gap junctions. Characterization of the principal protein, connexin. *The Journal of cell biology* **61**, 557-563
98. Caspar, D. L., Goodenough, D. A., Makowski, L., and Phillips, W. C. (1977) Gap junction structures. I. Correlated electron microscopy and x-ray diffraction. *The Journal of cell biology* **74**, 605-628
99. Nicholson, B. J., Gros, D. B., Kent, S. B., Hood, L. E., and Revel, J. P. (1985) The Mr 28,000 gap junction proteins from rat heart and liver are different but related. *The Journal of biological chemistry* **260**, 6514-6517

100. Kumar, N. M., and Gilula, N. B. (1986) Cloning and characterization of human and rat liver cDNAs coding for a gap junction protein. *The Journal of cell biology* **103**, 767-776
101. Unger, V. M., Kumar, N. M., Gilula, N. B., and Yeager, M. (1999) Three-dimensional structure of a recombinant gap junction membrane channel. *Science* **283**, 1176-1180
102. Yu, J., Bippes, C. A., Hand, G. M., Muller, D. J., and Sosinsky, G. E. (2007) Aminosulfonate modulated pH-induced conformational changes in connexin26 hemichannels. *The Journal of biological chemistry* **282**, 8895-8904
103. Oshima, A., Tani, K., Hiroaki, Y., Fujiyoshi, Y., and Sosinsky, G. E. (2007) Three-dimensional structure of a human connexin26 gap junction channel reveals a plug in the vestibule. *Proceedings of the National Academy of Sciences of the United States of America* **104**, 10034-10039
104. Oshima, A., Tani, K., Hiroaki, Y., Fujiyoshi, Y., and Sosinsky, G. E. (2008) Projection structure of a N-terminal deletion mutant of connexin 26 channel with decreased central pore density. *Cell communication & adhesion* **15**, 85-93
105. Oshima, A., Tani, K., Toloue, M. M., Hiroaki, Y., Smock, A., Inukai, S., Cone, A., Nicholson, B. J., Sosinsky, G. E., and Fujiyoshi, Y. (2011) Asymmetric configurations and N-terminal rearrangements in connexin26 gap junction channels. *Journal of molecular biology* **405**, 724-735
106. Maeda, S., Nakagawa, S., Suga, M., Yamashita, E., Oshima, A., Fujiyoshi, Y., and Tsukihara, T. (2009) Structure of the connexin 26 gap junction channel at 3.5 A resolution. *Nature* **458**, 597-602
107. Zhou, X. W., Pfahnl, A., Werner, R., Hudder, A., Llanes, A., Luebke, A., and Dahl, G. (1997) Identification of a pore lining segment in gap junction hemichannels. *Biophysical journal* **72**, 1946-1953
108. Kronengold, J., Trexler, E. B., Bukauskas, F. F., Bargiello, T. A., and Verselis, V. K. (2003) Single-channel SCAM identifies pore-lining residues in the first extracellular loop and first transmembrane domains of Cx46 hemichannels. *The Journal of general physiology* **122**, 389-405
109. Fleishman, S. J., Unger, V. M., Yeager, M., and Ben-Tal, N. (2004) A Calpha model for the transmembrane alpha helices of gap junction intercellular channels. *Molecular cell* **15**, 879-888
110. Skerrett, I. M., Aronowitz, J., Shin, J. H., Cymes, G., Kasperek, E., Cao, F. L., and Nicholson, B. J. (2002) Identification of amino acid residues lining the pore of a gap junction channel. *The Journal of cell biology* **159**, 349-360
111. Dahl, G., Levine, E., Rabadan-Diehl, C., and Werner, R. (1991) Cell/cell channel formation involves disulfide exchange. *European journal of biochemistry / FEBS* **197**, 141-144
112. Dahl, G., Werner, R., Levine, E., and Rabadan-Diehl, C. (1992) Mutational analysis of gap junction formation. *Biophys J* **62**, 172-180; discussion 180-172
113. Martin, P. E., Coleman, S. L., Casalotti, S. O., Forge, A., and Evans, W. H. (1999) Properties of connexin26 gap junctional proteins derived from mutations associated with non-syndromal heriditary deafness. *Human molecular genetics* **8**, 2369-2376
114. Thonnissen, E., Rabionet, R., Arbones, M. L., Estivill, X., Willecke, K., and Ott, T. (2002) Human connexin26 (GJB2) deafness mutations affect the function of gap junction channels at different levels of protein expression. *Human genetics* **111**, 190-197

115. Oshima, A., Doi, T., Mitsuoka, K., Maeda, S., and Fujiyoshi, Y. (2003) Roles of Met-34, Cys-64, and Arg-75 in the assembly of human connexin 26. Implication for key amino acid residues for channel formation and function. *The Journal of biological chemistry* **278**, 1807-1816
116. Zonta, F., Polles, G., Sanasi, M. F., Bortolozzi, M., and Mammano, F. (2013) The 3.5 angstrom X-ray structure of the human connexin26 gap junction channel is unlikely that of a fully open channel. *Cell communication and signaling : CCS* **11**, 15
117. Maeda, S., and Tsukihara, T. (2011) Structure of the gap junction channel and its implications for its biological functions. *Cellular and molecular life sciences : CMLS* **68**, 1115-1129
118. Yeager, M. (1998) Structure of cardiac gap junction intercellular channels. *Journal of structural biology* **121**, 231-245
119. Kumar, N. M., and Gilula, N. B. (1996) The gap junction communication channel. *Cell* **84**, 381-388
120. Hertzberg, E. L., Disher, R. M., Tiller, A. A., Zhou, Y., and Cook, R. G. (1988) Topology of the Mr 27,000 liver gap junction protein. Cytoplasmic localization of amino- and carboxyl termini and a hydrophilic domain which is protease-hypersensitive. *The Journal of biological chemistry* **263**, 19105-19111
121. Chen, Y., Zhou, Y., Lin, X., Wong, H. C., Xu, Q., Jiang, J., Wang, S., Lurtz, M. M., Louis, C. F., Veenstra, R. D., and Yang, J. J. (2011) Molecular interaction and functional regulation of connexin50 gap junctions by calmodulin. *The Biochemical journal* **435**, 711-722
122. Klevit, R. E., Dalgarno, D. C., Levine, B. A., and Williams, R. J. (1984) 1H-NMR studies of calmodulin. The nature of the Ca2+-dependent conformational change. *Eur J Biochem* **139**, 109-114
123. Wang, C. L. (1985) A note on Ca2+ binding to calmodulin. *Biochem Biophys Res Commun* **130**, 426-430
124. Bhattacharya, S., Bunick, C. G., and Chazin, W. J. (2004) Target selectivity in EF-hand calcium binding proteins. *Biochimica et biophysica acta* **1742**, 69-79
125. Kawasaki, H., and Kretsinger, R. H. (1995) Calcium-binding proteins 1: EF-hands. *Protein profile* **2**, 297-490
126. Ikura, M., and Ames, J. B. (2006) Genetic polymorphism and protein conformational plasticity in the calmodulin superfamily: two ways to promote multifunctionality. *Proceedings of the National Academy of Sciences of the United States of America* **103**, 1159-1164
127. Hsu, Y. T., and Molday, R. S. (1993) Modulation of the cGMP-gated channel of rod photoreceptor cells by calmodulin. *Nature* **361**, 76-79
128. Ehlers, M. D., Zhang, S., Bernhadt, J. P., and Huganir, R. L. (1996) Inactivation of NMDA receptors by direct interaction of calmodulin with the NR1 subunit. *Cell* **84**, 745-755
129. Rodney, G. G., Williams, B. Y., Strasburg, G. M., Beckingham, K., and Hamilton, S. L. (2000) Regulation of RYR1 activity by Ca(2+) and calmodulin. *Biochemistry* **39**, 7807-7812
130. Xia, X. M., Fakler, B., Rivard, A., Wayman, G., Johnson-Pais, T., Keen, J. E., Ishii, T., Hirschberg, B., Bond, C. T., Lutsenko, S., Maylie, J., and Adelman, J. P. (1998)

Mechanism of calcium gating in small-conductance calcium-activated potassium channels. *Nature* **395**, 503-507
131. Fanger, C. M., Ghanshani, S., Logsdon, N. J., Rauer, H., Kalman, K., Zhou, J., Beckingham, K., Chandy, K. G., Cahalan, M. D., and Aiyar, J. (1999) Calmodulin mediates calcium-dependent activation of the intermediate conductance KCa channel, IKCa1. *The Journal of biological chemistry* **274**, 5746-5754
132. Tang, J., Lin, Y., Zhang, Z., Tikunova, S., Birnbaumer, L., and Zhu, M. X. (2001) Identification of common binding sites for calmodulin and inositol 1,4,5-trisphosphate receptors on the carboxyl termini of trp channels. *The Journal of biological chemistry* **276**, 21303-21310
133. Zuhlke, R. D., and Reuter, H. (1998) Ca2+-sensitive inactivation of L-type Ca2+ channels depends on multiple cytoplasmic amino acid sequences of the alpha1C subunit. *Proceedings of the National Academy of Sciences of the United States of America* **95**, 3287-3294
134. Schonherr, R., Lober, K., and Heinemann, S. H. (2000) Inhibition of human ether a go-go potassium channels by Ca(2+)/calmodulin. *The EMBO journal* **19**, 3263-3271
135. Bers, D. M., and Grandi, E. (2009) Calcium/calmodulin-dependent kinase II regulation of cardiac ion channels. *Journal of cardiovascular pharmacology* **54**, 180-187
136. Dai, S., Hall, D. D., and Hell, J. W. (2009) Supramolecular assemblies and localized regulation of voltage-gated ion channels. *Physiological reviews* **89**, 411-452
137. Tadross, M. R., Dick, I. E., and Yue, D. T. (2008) Mechanism of local and global Ca2+ sensing by calmodulin in complex with a Ca2+ channel. *Cell* **133**, 1228-1240
138. Deleze, J. (1965) Electrophysiology of the Heart. in *Calcium ions and the healing-over in heart fibers*, Pergamon Press, Elmsford, New York. pp 147-148
139. Rose, B., Simpson, I., and Loewenstein, W. R. (1977) Calcium ion produces graded changes in permeability of membrane channels in cell junction. *Nature* **267**, 625-627
140. Cheung, W. Y. (1980) Calmodulin plays a pivotal role in cellular regulation. *Science* **207**, 19-27
141. Peracchia, C., Bernardini, G., and Peracchia, L. L. (1983) Is calmodulin involved in the regulation of gap junction permeability? *Pflugers Archiv : European journal of physiology* **399**, 152-154
142. Peracchia, C., and Bernardini, G. (1984) Gap junction structure and cell-to-cell coupling regulation: is there a calmodulin involvement? *Federation proceedings* **43**, 2681-2691
143. Peracchia, C. (1984) Communicating junctions and calmodulin: inhibition of electrical uncoupling in Xenopus embryo by calmidazolium. *The Journal of membrane biology* **81**, 49-58
144. Peracchia, C. (1987) Calmodulin-like proteins and communicating junctions. Electrical uncoupling of crayfish septate axons is inhibited by the calmodulin inhibitor W7 and is not affected by cyclic nucleotides. *Pflugers Archiv : European journal of physiology* **408**, 379-385
145. Hertzberg, E. L., and Gilula, N. B. (1982) Liver gap junctions and lens fiber junctions: comparative analysis and calmodulin interaction. *Cold Spring Harbor symposia on quantitative biology* **46 Pt 2**, 639-645
146. Van Eldik, L. J., Hertzberg, E. L., Berdan, R. C., and Gilula, N. B. (1985) Interaction of calmodulin and other calcium-modulated proteins with mammalian and arthropod junctional membrane proteins. *Biochem Biophys Res Commun* **126**, 825-832

147. Zimmer, D. B., Green, C. R., Evans, W. H., and Gilula, N. B. (1987) Topological analysis of the major protein in isolated intact rat liver gap junctions and gap junction-derived single membrane structures. *The Journal of biological chemistry* **262**, 7751-7763
148. Peracchia, C., Wang, X., Li, L., and Peracchia, L. L. (1996) Inhibition of calmodulin expression prevents low-pH-induced gap junction uncoupling in Xenopus oocytes. *Pflugers Archiv : European journal of physiology* **431**, 379-387
149. Sotkis, A., Wang, X. G., Yasumura, T., Peracchia, L. L., Persechini, A., Rash, J. E., and Peracchia, C. (2001) Calmodulin colocalizes with connexins and plays a direct role in gap junction channel gating. *Cell communication & adhesion* **8**, 277-281
150. Blodow, A., Ngezahayo, A., Ernst, A., and Kolb, H. A. (2003) Calmodulin antagonists suppress gap junction coupling in isolated Hensen cells of the guinea pig cochlea. *Pflugers Archiv : European journal of physiology* **446**, 36-41
151. Lurtz, M. M., and Louis, C. F. (2003) Calmodulin and protein kinase C regulate gap junctional coupling in lens epithelial cells. *American journal of physiology. Cell physiology* **285**, C1475-1482
152. Lurtz, M. M., and Louis, C. F. (2007) Intracellular calcium regulation of connexin43. *American journal of physiology. Cell physiology* **293**, C1806-1813
153. Churchill, G. C., Lurtz, M. M., and Louis, C. F. (2001) Ca(2+) regulation of gap junctional coupling in lens epithelial cells. *American journal of physiology. Cell physiology* **281**, C972-981
154. Zhou, Y., Yang, W., Lurtz, M. M., Ye, Y., Huang, Y., Lee, H. W., Chen, Y., Louis, C. F., and Yang, J. J. (2007) Identification of the calmodulin binding domain of connexin 43. *The Journal of biological chemistry* **282**, 35005-35017
155. Xu, Q., Kopp, R. F., Chen, Y., Yang, J. J., Roe, M. W., and Veenstra, R. D. (2012) Gating of connexin 43 gap junctions by a cytoplasmic loop calmodulin binding domain. *American journal of physiology. Cell physiology* **302**, C1548-1556
156. Zhou, Y., Yang, W., Lurtz, M. M., Chen, Y., Jiang, J., Huang, Y., Louis, C. F., and Yang, J. J. (2009) Calmodulin mediates the Ca2+-dependent regulation of Cx44 gap junctions. *Biophys. J.* **96**, 2832-2848
157. Zhang, X., and Qi, Y. (2005) Role of intramolecular interaction in connexin50: mediating the Ca2+-dependent binding of calmodulin to gap junction. *Archives of biochemistry and biophysics* **440**, 111-117
158. Peracchia, C., Young, K. C., Wang, X. G., and Peracchia, L. L. (2003) Is the voltage gate of connexins CO2-sensitive? Cx45 channels and inhibition of calmodulin expression. *The Journal of membrane biology* **195**, 53-62
159. O'Brien, J., Bruzzone, R., White, T. W., Al-Ubaidi, M. R., and Ripps, H. (1998) Cloning and expression of two related connexins from the perch retina define a distinct subgroup of the connexin family. *The Journal of neuroscience : the official journal of the Society for Neuroscience* **18**, 7625-7637
160. Burr, G. S., Mitchell, C. K., Keflemariam, Y. J., Heidelberger, R., and O'Brien, J. (2005) Calcium-dependent binding of calmodulin to neuronal gap junction proteins. *Biochem Biophys Res Commun* **335**, 1191-1198
161. Rondard, P., Goudet, C., Kniazeff, J., Pin, J. P., and Prezeau, L. (2011) The complexity of their activation mechanism opens new possibilities for the modulation of mGlu and GABAB class C G protein-coupled receptors. *Neuropharmacology* **60**, 82-92

162. Pin, J. P., Galvez, T., and Prezeau, L. (2003) Evolution, structure, and activation mechanism of family 3/C G-protein-coupled receptors. *Pharmacology & therapeutics* **98**, 325-354
163. Kunishima, N., Shimada, Y., Tsuji, Y., Sato, T., Yamamoto, M., Kumasaka, T., Nakanishi, S., Jingami, H., and Morikawa, K. (2000) Structural basis of glutamate recognition by a dimeric metabotropic glutamate receptor. *Nature* **407**, 971-977
164. Tsuchiya, D., Kunishima, N., Kamiya, N., Jingami, H., and Morikawa, K. (2002) Structural views of the ligand-binding cores of a metabotropic glutamate receptor complexed with an antagonist and both glutamate and Gd3+. *Proceedings of the National Academy of Sciences of the United States of America* **99**, 2660-2665
165. Muto, T., Tsuchiya, D., Morikawa, K., and Jingami, H. (2007) Structures of the extracellular regions of the group II/III metabotropic glutamate receptors. *Proceedings of the National Academy of Sciences of the United States of America* **104**, 3759-3764
166. Tsuji, Y., Shimada, Y., Takeshita, T., Kajimura, N., Nomura, S., Sekiyama, N., Otomo, J., Usukura, J., Nakanishi, S., and Jingami, H. (2000) Cryptic dimer interface and domain organization of the extracellular region of metabotropic glutamate receptor subtype 1. *The Journal of biological chemistry* **275**, 28144-28151
167. Ray, K., Hauschild, B. C., Steinbach, P. J., Goldsmith, P. K., Hauache, O., and Spiegel, A. M. (1999) Identification of the cysteine residues in the amino-terminal extracellular domain of the human Ca(2+) receptor critical for dimerization. Implications for function of monomeric Ca(2+) receptor. *The Journal of biological chemistry* **274**, 27642-27650
168. Ray, K., and Hauschild, B. C. (2000) Cys-140 is critical for metabotropic glutamate receptor-1 dimerization. *The Journal of biological chemistry* **275**, 34245-34251
169. Hu, J., Hauache, O., and Spiegel, A. M. (2000) Human Ca2+ receptor cysteine-rich domain. Analysis of function of mutant and chimeric receptors. *The Journal of biological chemistry* **275**, 16382-16389
170. Rondard, P., Liu, J., Huang, S., Malhaire, F., Vol, C., Pinault, A., Labesse, G., and Pin, J. P. (2006) Coupling of agonist binding to effector domain activation in metabotropic glutamate-like receptors. *The Journal of biological chemistry* **281**, 24653-24661
171. Conn, P. J., Christopoulos, A., and Lindsley, C. W. (2009) Allosteric modulators of GPCRs: a novel approach for the treatment of CNS disorders. *Nature reviews. Drug discovery* **8**, 41-54
172. Brauner-Osborne, H., Wellendorph, P., and Jensen, A. A. (2007) Structure, pharmacology and therapeutic prospects of family C G-protein coupled receptors. *Current drug targets* **8**, 169-184
173. Dore, A. S., Okrasa, K., Patel, J. C., Serrano-Vega, M., Bennett, K., Cooke, R. M., Errey, J. C., Jazayeri, A., Khan, S., Tehan, B., Weir, M., Wiggin, G. R., and Marshall, F. H. (2014) Structure of class C GPCR metabotropic glutamate receptor 5 transmembrane domain. *Nature* **511**, 557-562
174. Levenga, J., Hayashi, S., de Vrij, F. M., Koekkoek, S. K., van der Linde, H. C., Nieuwenhuizen, I., Song, C., Buijsen, R. A., Pop, A. S., Gomezmancilla, B., Nelson, D. L., Willemsen, R., Gasparini, F., and Oostra, B. A. (2011) AFQ056, a new mGluR5 antagonist for treatment of fragile X syndrome. *Neurobiology of disease* **42**, 311-317
175. Pin, J. P., Waeber, C., Prezeau, L., Bockaert, J., and Heinemann, S. F. (1992) Alternative splicing generates metabotropic glutamate receptors inducing different patterns of

calcium release in Xenopus oocytes. *Proceedings of the National Academy of Sciences of the United States of America* **89**, 10331-10335

176. Pickering, D. S., Thomsen, C., Suzdak, P. D., Fletcher, E. J., Robitaille, R., Salter, M. W., MacDonald, J. F., Huang, X. P., and Hampson, D. R. (1993) A comparison of two alternatively spliced forms of a metabotropic glutamate receptor coupled to phosphoinositide turnover. *Journal of neurochemistry* **61**, 85-92
177. Gabellini, N., Manev, R. M., Candeo, P., Favaron, M., and Manev, H. (1993) Carboxyl domain of glutamate receptor directs its coupling to metabolic pathways. *Neuroreport* **4**, 531-534
178. Prezeau, L., Gomeza, J., Ahern, S., Mary, S., Galvez, T., Bockaert, J., and Pin, J. P. (1996) Changes in the carboxyl-terminal domain of metabotropic glutamate receptor 1 by alternative splicing generate receptors with differing agonist-independent activity. *Molecular pharmacology* **49**, 422-429
179. Pin, J. P., Joly, C., Heinemann, S. F., and Bockaert, J. (1994) Domains involved in the specificity of G protein activation in phospholipase C-coupled metabotropic glutamate receptors. *The EMBO journal* **13**, 342-348
180. O'Connor, V., El Far, O., Bofill-Cardona, E., Nanoff, C., Freissmuth, M., Karschin, A., Airas, J. M., Betz, H., and Boehm, S. (1999) Calmodulin dependence of presynaptic metabotropic glutamate receptor signaling. *Science* **286**, 1180-1184
181. O'Hara, P. J., Sheppard, P. O., Thogersen, H., Venezia, D., Haldeman, B. A., McGrane, V., Houamed, K. M., Thomsen, C., Gilbert, T. L., and Mulvihill, E. R. (1993) The ligand-binding domain in metabotropic glutamate receptors is related to bacterial periplasmic binding proteins. *Neuron* **11**, 41-52
182. Pagano, A., Rovelli, G., Mosbacher, J., Lohmann, T., Duthey, B., Stauffer, D., Ristig, D., Schuler, V., Meigel, I., Lampert, C., Stein, T., Prezeau, L., Blahos, J., Pin, J., Froestl, W., Kuhn, R., Heid, J., Kaupmann, K., and Bettler, B. (2001) C-terminal interaction is essential for surface trafficking but not for heteromeric assembly of GABA(b) receptors. *The Journal of neuroscience : the official journal of the Society for Neuroscience* **21**, 1189-1202
183. Tu, J. C., Xiao, B., Yuan, J. P., Lanahan, A. A., Leoffert, K., Li, M., Linden, D. J., and Worley, P. F. (1998) Homer binds a novel proline-rich motif and links group 1 metabotropic glutamate receptors with IP3 receptors. *Neuron* **21**, 717-726
184. Ehrengruber, M. U., Kato, A., Inokuchi, K., and Hennou, S. (2004) Homer/Vesl proteins and their roles in CNS neurons. *Molecular neurobiology* **29**, 213-227
185. Boudin, H., Doan, A., Xia, J., Shigemoto, R., Huganir, R. L., Worley, P., and Craig, A. M. (2000) Presynaptic clustering of mGluR7a requires the PICK1 PDZ domain binding site. *Neuron* **28**, 485-497
186. El Far, O., Airas, J., Wischmeyer, E., Nehring, R. B., Karschin, A., and Betz, H. (2000) Interaction of the C-terminal tail region of the metabotropic glutamate receptor 7 with the protein kinase C substrate PICK1. *The European journal of neuroscience* **12**, 4215-4221
187. El Far, O., and Betz, H. (2002) G-protein-coupled receptors for neurotransmitter amino acids: C-terminal tails, crowded signalosomes. *The Biochemical journal* **365**, 329-336
188. Dev, K. K., Nakanishi, S., and Henley, J. M. (2001) Regulation of mglu(7) receptors by proteins that interact with the intracellular C-terminus. *Trends in pharmacological sciences* **22**, 355-361

189. Takahashi, K., Tsuchida, K., Tanabe, Y., Masu, M., and Nakanishi, S. (1993) Role of the large extracellular domain of metabotropic glutamate receptors in agonist selectivity determination. *The Journal of biological chemistry* **268**, 19341-19345
190. Okamoto, T., Sekiyama, N., Otsu, M., Shimada, Y., Sato, A., Nakanishi, S., and Jingami, H. (1998) Expression and purification of the extracellular ligand binding region of metabotropic glutamate receptor subtype 1. *The Journal of biological chemistry* **273**, 13089-13096
191. Han, G., and Hampson, D. R. (1999) Ligand binding to the amino-terminal domain of the mGluR4 subtype of metabotropic glutamate receptor. *The Journal of biological chemistry* **274**, 10008-10013
192. Hampson, D. R., Huang, X. P., Pekhletski, R., Peltekova, V., Hornby, G., Thomsen, C., and Thogersen, H. (1999) Probing the ligand-binding domain of the mGluR4 subtype of metabotropic glutamate receptor. *The Journal of biological chemistry* **274**, 33488-33495
193. Niswender, C. M., and Conn, P. J. (2010) Metabotropic glutamate receptors: physiology, pharmacology, and disease. *Annual review of pharmacology and toxicology* **50**, 295-322
194. Lee, J. H., Lee, J., Choi, K. Y., Hepp, R., Lee, J. Y., Lim, M. K., Chatani-Hinze, M., Roche, P. A., Kim, D. G., Ahn, Y. S., Kim, C. H., and Roche, K. W. (2008) Calmodulin dynamically regulates the trafficking of the metabotropic glutamate receptor mGluR5. *Proceedings of the National Academy of Sciences of the United States of America* **105**, 12575-12580
195. Aramori, I., and Nakanishi, S. (1992) Signal transduction and pharmacological characteristics of a metabotropic glutamate receptor, mGluR1, in transfected CHO cells. *Neuron* **8**, 757-765
196. Thomsen, C. (1996) Metabotropic glutamate receptor subtype 1A activates adenylate cyclase when expressed in baby hamster kidney cells. *Progress in neuro-psychopharmacology & biological psychiatry* **20**, 709-726
197. Hermans, E., Saunders, R., Selkirk, J. V., Mistry, R., Nahorski, S. R., and Challiss, R. A. (2000) Complex involvement of pertussis toxin-sensitive G proteins in the regulation of type 1alpha metabotropic glutamate receptor signaling in baby hamster kidney cells. *Molecular pharmacology* **58**, 352-360
198. Francesconi, A., and Duvoisin, R. M. (1998) Role of the second and third intracellular loops of metabotropic glutamate receptors in mediating dual signal transduction activation. *The Journal of biological chemistry* **273**, 5615-5624
199. Parmentier, M. L., Joly, C., Restituito, S., Bockaert, J., Grau, Y., and Pin, J. P. (1998) The G protein-coupling profile of metabotropic glutamate receptors, as determined with exogenous G proteins, is independent of their ligand recognition domain. *Molecular pharmacology* **53**, 778-786
200. Joly, C., Gomeza, J., Brabet, I., Curry, K., Bockaert, J., and Pin, J. P. (1995) Molecular, functional, and pharmacological characterization of the metabotropic glutamate receptor type 5 splice variants: comparison with mGluR1. *The Journal of neuroscience : the official journal of the Society for Neuroscience* **15**, 3970-3981
201. Knopfel, T., Kuhn, R., and Allgeier, H. (1995) Metabotropic glutamate receptors: novel targets for drug development. *Journal of medicinal chemistry* **38**, 1417-1426
202. Bedingfield, J. S., Kemp, M. C., Jane, D. E., Tse, H. W., Roberts, P. J., and Watkins, J. C. (1995) Structure-activity relationships for a series of phenylglycine derivatives acting at metabotropic glutamate receptors (mGluRs). *Br J Pharmacol* **116**, 3323-3329

203. Schoepp, D. D., Johnson, B. G., Salhoff, C. R., Valli, M. J., Desai, M. A., Burnett, J. P., Mayne, N. G., and Monn, J. A. (1995) Selective inhibition of forskolin-stimulated cyclic AMP formation in rat hippocampus by a novel mGluR agonist, 2R,4R-4-aminopyrrolidine-2,4- dicarboxylate. *Neuropharmacology* **34**, 843-850
204. Prezeau, L., Carrette, J., Helpap, B., Curry, K., Pin, J. P., and Bockaert, J. (1994) Pharmacological characterization of metabotropic glutamate receptors in several types of brain cells in primary cultures. *Molecular pharmacology* **45**, 570-577
205. Wright, R. A., and Schoepp, D. D. (1996) Differentiation of group 2 and group 3 metabotropic glutamate receptor cAMP responses in the rat hippocampus. *European journal of pharmacology* **297**, 275-282
206. Bruno, V., Battaglia, G., Copani, A., Giffard, R. G., Raciti, G., Raffaele, R., Shinozaki, H., and Nicoletti, F. (1995) Activation of class II or III metabotropic glutamate receptors protects cultured cortical neurons against excitotoxic degeneration. *The European journal of neuroscience* **7**, 1906-1913
207. Schoepp, D. D., Johnson, B. G., Salhoff, C. R., Wright, R. A., Goldsworthy, J. S., and Baker, S. R. (1995) Second-messenger responses in brain slices to elucidate novel glutamate receptors. *Journal of neuroscience methods* **59**, 105-110
208. Pin, J. P., and Acher, F. (2002) The metabotropic glutamate receptors: structure, activation mechanism and pharmacology. *Current drug targets. CNS and neurological disorders* **1**, 297-317
209. Willard, S. S., and Koochekpour, S. (2013) Glutamate, glutamate receptors, and downstream signaling pathways. *International journal of biological sciences* **9**, 948-959
210. Conn, P. J., and Pin, J. P. (1997) Pharmacology and functions of metabotropic glutamate receptors. *Annual review of pharmacology and toxicology* **37**, 205-237
211. Gerber, U., Gee, C. E., and Benquet, P. (2007) Metabotropic glutamate receptors: intracellular signaling pathways. *Current opinion in pharmacology* **7**, 56-61
212. Ribeiro, F. M., Paquet, M., Cregan, S. P., and Ferguson, S. S. (2010) Group I metabotropic glutamate receptor signalling and its implication in neurological disease. *CNS & neurological disorders drug targets* **9**, 574-595
213. Hall, R. A., Premont, R. T., and Lefkowitz, R. J. (1999) Heptahelical receptor signaling: beyond the G protein paradigm. *The Journal of cell biology* **145**, 927-932
214. Heuss, C., Scanziani, M., Gahwiler, B. H., and Gerber, U. (1999) G-protein-independent signaling mediated by metabotropic glutamate receptors. *Nature neuroscience* **2**, 1070-1077
215. Krause, M., Offermanns, S., Stocker, M., and Pedarzani, P. (2002) Functional specificity of G alpha q and G alpha 11 in the cholinergic and glutamatergic modulation of potassium currents and excitability in hippocampal neurons. *The Journal of neuroscience : the official journal of the Society for Neuroscience* **22**, 666-673
216. Gee, C. E., Benquet, P., and Gerber, U. (2003) Group I metabotropic glutamate receptors activate a calcium-sensitive transient receptor potential-like conductance in rat hippocampus. *The Journal of physiology* **546**, 655-664
217. Ferraguti, F., Baldani-Guerra, B., Corsi, M., Nakanishi, S., and Corti, C. (1999) Activation of the extracellular signal-regulated kinase 2 by metabotropic glutamate receptors. *The European journal of neuroscience* **11**, 2073-2082
218. Masu, M., Tanabe, Y., Tsuchida, K., Shigemoto, R., and Nakanishi, S. (1991) Sequence and expression of a metabotropic glutamate receptor. *Nature* **349**, 760-765

219. Houamed, K. M., Kuijper, J. L., Gilbert, T. L., Haldeman, B. A., O'Hara, P. J., Mulvihill, E. R., Almers, W., and Hagen, F. S. (1991) Cloning, expression, and gene structure of a G protein-coupled glutamate receptor from rat brain. *Science* **252**, 1318-1321
220. Sladeczek, F., Pin, J. P., Recasens, M., Bockaert, J., and Weiss, S. (1985) Glutamate stimulates inositol phosphate formation in striatal neurones. *Nature* **317**, 717-719
221. Nicoletti, F., Meek, J. L., Iadarola, M. J., Chuang, D. M., Roth, B. L., and Costa, E. (1986) Coupling of inositol phospholipid metabolism with excitatory amino acid recognition sites in rat hippocampus. *Journal of neurochemistry* **46**, 40-46
222. Tanabe, Y., Masu, M., Ishii, T., Shigemoto, R., and Nakanishi, S. (1992) A family of metabotropic glutamate receptors. *Neuron* **8**, 169-179
223. Abe, T., Sugihara, H., Nawa, H., Shigemoto, R., Mizuno, N., and Nakanishi, S. (1992) Molecular characterization of a novel metabotropic glutamate receptor mGluR5 coupled to inositol phosphate/Ca2+ signal transduction. *The Journal of biological chemistry* **267**, 13361-13368
224. Nakajima, Y., Iwakabe, H., Akazawa, C., Nawa, H., Shigemoto, R., Mizuno, N., and Nakanishi, S. (1993) Molecular characterization of a novel retinal metabotropic glutamate receptor mGluR6 with a high agonist selectivity for L-2-amino-4-phosphonobutyrate. *The Journal of biological chemistry* **268**, 11868-11873
225. Ohishi, H., Shigemoto, R., Nakanishi, S., and Mizuno, N. (1993) Distribution of the messenger RNA for a metabotropic glutamate receptor, mGluR2, in the central nervous system of the rat. *Neuroscience* **53**, 1009-1018
226. Okamoto, N., Hori, S., Akazawa, C., Hayashi, Y., Shigemoto, R., Mizuno, N., and Nakanishi, S. (1994) Molecular characterization of a new metabotropic glutamate receptor mGluR7 coupled to inhibitory cyclic AMP signal transduction. *The Journal of biological chemistry* **269**, 1231-1236
227. Tanabe, Y., Nomura, A., Masu, M., Shigemoto, R., Mizuno, N., and Nakanishi, S. (1993) Signal transduction, pharmacological properties, and expression patterns of two rat metabotropic glutamate receptors, mGluR3 and mGluR4. *The Journal of neuroscience : the official journal of the Society for Neuroscience* **13**, 1372-1378
228. Saugstad, J. A., Kinzie, J. M., Mulvihill, E. R., Segerson, T. P., and Westbrook, G. L. (1994) Cloning and expression of a new member of the L-2-amino-4-phosphonobutyric acid-sensitive class of metabotropic glutamate receptors. *Molecular pharmacology* **45**, 367-372
229. Duvoisin, R. M., Zhang, C., and Ramonell, K. (1995) A novel metabotropic glutamate receptor expressed in the retina and olfactory bulb. *The Journal of neuroscience : the official journal of the Society for Neuroscience* **15**, 3075-3083
230. Coutinho, V., and Knopfel, T. (2002) Metabotropic glutamate receptors: electrical and chemical signaling properties. *The Neuroscientist : a review journal bringing neurobiology, neurology and psychiatry* **8**, 551-561
231. Anwyl, R. (1999) Metabotropic glutamate receptors: electrophysiological properties and role in plasticity. *Brain research. Brain research reviews* **29**, 83-120
232. Valenti, O., Conn, P. J., and Marino, M. J. (2002) Distinct physiological roles of the Gq-coupled metabotropic glutamate receptors Co-expressed in the same neuronal populations. *Journal of cellular physiology* **191**, 125-137

233. Bellone, C., Luscher, C., and Mameli, M. (2008) Mechanisms of synaptic depression triggered by metabotropic glutamate receptors. *Cellular and molecular life sciences : CMLS* **65**, 2913-2923
234. Pinheiro, P. S., and Mulle, C. (2008) Presynaptic glutamate receptors: physiological functions and mechanisms of action. *Nature reviews. Neuroscience* **9**, 423-436
235. Staub, C., Vranesic, I., and Knopfel, T. (1992) Responses to Metabotropic Glutamate Receptor Activation in Cerebellar Purkinje Cells: Induction of an Inward Current. *The European journal of neuroscience* **4**, 832-839
236. Lingenhohl, K., Olpe, H. R., Bendali, N., and Knopfel, T. (1993) Phenylglycine derivatives antagonize the excitatory response to Purkinje cells to 1S,3R-ACPD: an in vivo and in vitro study. *Neuroscience research* **18**, 229-234
237. Vranesic, I., Staub, C., and Knopfel, T. (1993) Activation of metabotropic glutamate receptors induces an outward current which is potentiated by methylxanthines in rat cerebellar Purkinje cells. *Neuroscience research* **16**, 209-215
238. Ito, M., and Karachot, L. (1989) Long-term desensitization of quisqualate-specific glutamate receptors in Purkinje cells investigated with wedge recording from rat cerebellar slices. *Neuroscience research* **7**, 168-171
239. Shigemoto, R., Abe, T., Nomura, S., Nakanishi, S., and Hirano, T. (1994) Antibodies inactivating mGluR1 metabotropic glutamate receptor block long-term depression in cultured Purkinje cells. *Neuron* **12**, 1245-1255
240. Kullmann, D. M., and Lamsa, K. (2008) Roles of distinct glutamate receptors in induction of anti-Hebbian long-term potentiation. *The Journal of physiology* **586**, 1481-1486
241. Aiba, A., Chen, C., Herrup, K., Rosenmund, C., Stevens, C. F., and Tonegawa, S. (1994) Reduced hippocampal long-term potentiation and context-specific deficit in associative learning in mGluR1 mutant mice. *Cell* **79**, 365-375
242. Chiamulera, C., Epping-Jordan, M. P., Zocchi, A., Marcon, C., Cottiny, C., Tacconi, S., Corsi, M., Orzi, F., and Conquet, F. (2001) Reinforcing and locomotor stimulant effects of cocaine are absent in mGluR5 null mutant mice. *Nature neuroscience* **4**, 873-874
243. Brody, S. A., Conquet, F., and Geyer, M. A. (2003) Disruption of prepulse inhibition in mice lacking mGluR1. *The European journal of neuroscience* **18**, 3361-3366
244. Brody, S. A., Dulawa, S. C., Conquet, F., and Geyer, M. A. (2004) Assessment of a prepulse inhibition deficit in a mutant mouse lacking mGlu5 receptors. *Molecular psychiatry* **9**, 35-41
245. Bradbury, M. J., Campbell, U., Giracello, D., Chapman, D., King, C., Tehrani, L., Cosford, N. D., Anderson, J., Varney, M. A., and Strack, A. M. (2005) Metabotropic glutamate receptor mGlu5 is a mediator of appetite and energy balance in rats and mice. *The Journal of pharmacology and experimental therapeutics* **313**, 395-402
246. Masu, M., Iwakabe, H., Tagawa, Y., Miyoshi, T., Yamashita, M., Fukuda, Y., Sasaki, H., Hiroi, K., Nakamura, Y., Shigemoto, R., and et al. (1995) Specific deficit of the ON response in visual transmission by targeted disruption of the mGluR6 gene. *Cell* **80**, 757-765
247. Yokoi, M., Kobayashi, K., Manabe, T., Takahashi, T., Sakaguchi, I., Katsuura, G., Shigemoto, R., Ohishi, H., Nomura, S., Nakamura, K., Nakao, K., Katsuki, M., and Nakanishi, S. (1996) Impairment of hippocampal mossy fiber LTD in mice lacking mGluR2. *Science* **273**, 645-647

248. Higgins, G. A., Ballard, T. M., Kew, J. N., Richards, J. G., Kemp, J. A., Adam, G., Woltering, T., Nakanishi, S., and Mutel, V. (2004) Pharmacological manipulation of mGlu2 receptors influences cognitive performance in the rodent. *Neuropharmacology* **46**, 907-917
249. Morishima, Y., Miyakawa, T., Furuyashiki, T., Tanaka, Y., Mizuma, H., and Nakanishi, S. (2005) Enhanced cocaine responsiveness and impaired motor coordination in metabotropic glutamate receptor subtype 2 knockout mice. *Proceedings of the National Academy of Sciences of the United States of America* **102**, 4170-4175
250. Corti, C., Battaglia, G., Molinaro, G., Riozzi, B., Pittaluga, A., Corsi, M., Mugnaini, M., Nicoletti, F., and Bruno, V. (2007) The use of knock-out mice unravels distinct roles for mGlu2 and mGlu3 metabotropic glutamate receptors in mechanisms of neurodegeneration/neuroprotection. *The Journal of neuroscience : the official journal of the Society for Neuroscience* **27**, 8297-8308
251. Pekhletski, R., Gerlai, R., Overstreet, L. S., Huang, X. P., Agopyan, N., Slater, N. T., Abramow-Newerly, W., Roder, J. C., and Hampson, D. R. (1996) Impaired cerebellar synaptic plasticity and motor performance in mice lacking the mGluR4 subtype of metabotropic glutamate receptor. *The Journal of neuroscience : the official journal of the Society for Neuroscience* **16**, 6364-6373
252. Sugihara, H., Inoue, T., Nakanishi, S., and Fukuda, Y. (1997) A late ON response remains in visual response of the mGluR6-deficient mouse. *Neuroscience letters* **233**, 137-140
253. Gerlai, R., Roder, J. C., and Hampson, D. R. (1998) Altered spatial learning and memory in mice lacking the mGluR4 subtype of metabotropic glutamate receptor. *Behavioral neuroscience* **112**, 525-532
254. Masugi, M., Yokoi, M., Shigemoto, R., Muguruma, K., Watanabe, Y., Sansig, G., van der Putten, H., and Nakanishi, S. (1999) Metabotropic glutamate receptor subtype 7 ablation causes deficit in fear response and conditioned taste aversion. *The Journal of neuroscience : the official journal of the Society for Neuroscience* **19**, 955-963
255. Sansig, G., Bushell, T. J., Clarke, V. R., Rozov, A., Burnashev, N., Portet, C., Gasparini, F., Schmutz, M., Klebs, K., Shigemoto, R., Flor, P. J., Kuhn, R., Knoepfel, T., Schroeder, M., Hampson, D. R., Collett, V. J., Zhang, C., Duvoisin, R. M., Collingridge, G. L., and van Der Putten, H. (2001) Increased seizure susceptibility in mice lacking metabotropic glutamate receptor 7. *The Journal of neuroscience : the official journal of the Society for Neuroscience* **21**, 8734-8745
256. Bushell, T. J., Sansig, G., Collett, V. J., van der Putten, H., and Collingridge, G. L. (2002) Altered short-term synaptic plasticity in mice lacking the metabotropic glutamate receptor mGlu7. *TheScientificWorldJournal* **2**, 730-737
257. Cryan, J. F., Kelly, P. H., Neijt, H. C., Sansig, G., Flor, P. J., and van Der Putten, H. (2003) Antidepressant and anxiolytic-like effects in mice lacking the group III metabotropic glutamate receptor mGluR7. *The European journal of neuroscience* **17**, 2409-2417
258. Blednov, Y. A., Walker, D., Osterndorf-Kahanek, E., and Harris, R. A. (2004) Mice lacking metabotropic glutamate receptor 4 do not show the motor stimulatory effect of ethanol. *Alcohol* **34**, 251-259
259. Holscher, C., Schmid, S., Pilz, P. K., Sansig, G., van der Putten, H., and Plappert, C. F. (2004) Lack of the metabotropic glutamate receptor subtype 7 selectively impairs short-

term working memory but not long-term memory. *Behavioural brain research* **154**, 473-481

260. Holscher, C., Schmid, S., Pilz, P. K., Sansig, G., van der Putten, H., and Plappert, C. F. (2005) Lack of the metabotropic glutamate receptor subtype 7 selectively modulates Theta rhythm and working memory. *Learning & memory* **12**, 450-455
261. Callaerts-Vegh, Z., Beckers, T., Ball, S. M., Baeyens, F., Callaerts, P. F., Cryan, J. F., Molnar, E., and D'Hooge, R. (2006) Concomitant deficits in working memory and fear extinction are functionally dissociated from reduced anxiety in metabotropic glutamate receptor 7-deficient mice. *The Journal of neuroscience : the official journal of the Society for Neuroscience* **26**, 6573-6582
262. Goddyn, H., Callaerts-Vegh, Z., Stroobants, S., Dirikx, T., Vansteenwegen, D., Hermans, D., van der Putten, H., and D'Hooge, R. (2008) Deficits in acquisition and extinction of conditioned responses in mGluR7 knockout mice. *Neurobiology of learning and memory* **90**, 103-111
263. Stachowicz, K., Branski, P., Klak, K., van der Putten, H., Cryan, J. F., Flor, P. J., and Andrzej, P. (2008) Selective activation of metabotropic G-protein-coupled glutamate 7 receptor elicits anxiolytic-like effects in mice by modulating GABAergic neurotransmission. *Behavioural pharmacology* **19**, 597-603
264. Linden, A. M., Johnson, B. G., Peters, S. C., Shannon, H. E., Tian, M., Wang, Y., Yu, J. L., Koster, A., Baez, M., and Schoepp, D. D. (2002) Increased anxiety-related behavior in mice deficient for metabotropic glutamate 8 (mGlu8) receptor. *Neuropharmacology* **43**, 251-259
265. Duvoisin, R. M., Zhang, C., Pfankuch, T. F., O'Connor, H., Gayet-Primo, J., Quraishi, S., and Raber, J. (2005) Increased measures of anxiety and weight gain in mice lacking the group III metabotropic glutamate receptor mGluR8. *The European journal of neuroscience* **22**, 425-436
266. Robbins, M. J., Starr, K. R., Honey, A., Soffin, E. M., Rourke, C., Jones, G. A., Kelly, F. M., Strum, J., Melarange, R. A., Harris, A. J., Rocheville, M., Rupniak, T., Murdock, P. R., Jones, D. N., Kew, J. N., and Maycox, P. R. (2007) Evaluation of the mGlu8 receptor as a putative therapeutic target in schizophrenia. *Brain research* **1152**, 215-227
267. Bessis, A. S., Rondard, P., Gaven, F., Brabet, I., Triballeau, N., Prezeau, L., Acher, F., and Pin, J. P. (2002) Closure of the Venus flytrap module of mGlu8 receptor and the activation process: Insights from mutations converting antagonists into agonists. *Proceedings of the National Academy of Sciences of the United States of America* **99**, 11097-11102
268. Frauli, M., Hubert, N., Schann, S., Triballeau, N., Bertrand, H. O., Acher, F., Neuville, P., Pin, J. P., and Prezeau, L. (2007) Amino-pyrrolidine tricarboxylic acids give new insight into group III metabotropic glutamate receptor activation mechanism. *Molecular pharmacology* **71**, 704-712
269. Wu, S., Wright, R. A., Rockey, P. K., Burgett, S. G., Arnold, J. S., Rosteck, P. R., Jr., Johnson, B. G., Schoepp, D. D., and Belagaje, R. M. (1998) Group III human metabotropic glutamate receptors 4, 7 and 8: molecular cloning, functional expression, and comparison of pharmacological properties in RGT cells. *Brain research. Molecular brain research* **53**, 88-97
270. Schoepp, D. D., Jane, D. E., and Monn, J. A. (1999) Pharmacological agents acting at subtypes of metabotropic glutamate receptors. *Neuropharmacology* **38**, 1431-1476

271. Kew, J. N. (2004) Positive and negative allosteric modulation of metabotropic glutamate receptors: emerging therapeutic potential. *Pharmacology & therapeutics* **104**, 233-244
272. Ritzen, A., Mathiesen, J. M., and Thomsen, C. (2005) Molecular pharmacology and therapeutic prospects of metabotropic glutamate receptor allosteric modulators. *Basic & clinical pharmacology & toxicology* **97**, 202-213
273. Shipe, W. D., Wolkenberg, S. E., Williams, D. L., Jr., and Lindsley, C. W. (2005) Recent advances in positive allosteric modulators of metabotropic glutamate receptors. *Current opinion in drug discovery & development* **8**, 449-457
274. Hermans, E., Nahorski, S. R., and Challiss, R. A. (1998) Reversible and non-competitive antagonist profile of CPCCOEt at the human type 1alpha metabotropic glutamate receptor. *Neuropharmacology* **37**, 1645-1647
275. Brauner-Osborne, H., Jensen, A. A., and Krogsgaard-Larsen, P. (1999) Interaction of CPCCOEt with a chimeric mGlu1b and calcium sensing receptor. *Neuroreport* **10**, 3923-3925
276. Litschig, S., Gasparini, F., Rueegg, D., Stoehr, N., Flor, P. J., Vranesic, I., Prezeau, L., Pin, J. P., Thomsen, C., and Kuhn, R. (1999) CPCCOEt, a noncompetitive metabotropic glutamate receptor 1 antagonist, inhibits receptor signaling without affecting glutamate binding. *Molecular pharmacology* **55**, 453-461
277. Gasparini, F., Lingenhohl, K., Stoehr, N., Flor, P. J., Heinrich, M., Vranesic, I., Biollaz, M., Allgeier, H., Heckendorn, R., Urwyler, S., Varney, M. A., Johnson, E. C., Hess, S. D., Rao, S. P., Sacaan, A. I., Santori, E. M., Velicelebi, G., and Kuhn, R. (1999) 2-Methyl-6-(phenylethynyl)-pyridine (MPEP), a potent, selective and systemically active mGlu5 receptor antagonist. *Neuropharmacology* **38**, 1493-1503
278. Varney, M. A., Cosford, N. D., Jachec, C., Rao, S. P., Sacaan, A., Lin, F. F., Bleicher, L., Santori, E. M., Flor, P. J., Allgeier, H., Gasparini, F., Kuhn, R., Hess, S. D., Velicelebi, G., and Johnson, E. C. (1999) SIB-1757 and SIB-1893: selective, noncompetitive antagonists of metabotropic glutamate receptor type 5. *The Journal of pharmacology and experimental therapeutics* **290**, 170-181
279. Brown, E. M., Gamba, G., Riccardi, D., Lombardi, M., Butters, R., Kifor, O., Sun, A., Hediger, M. A., Lytton, J., and Hebert, S. C. (1993) Cloning and characterization of an extracellular Ca(2+)-sensing receptor from bovine parathyroid. *Nature* **366**, 575-580
280. Kubokawa, K., Miyashita, T., Nagasawa, H., and Kubo, Y. (1996) Cloning and characterization of a bifunctional metabotropic receptor activated by both extracellular calcium and glutamate. *FEBS letters* **392**, 71-76
281. Kubo, Y., Miyashita, T., and Murata, Y. (1998) Structural basis for a Ca2+-sensing function of the metabotropic glutamate receptors. *Science* **279**, 1722-1725
282. Abe, H., Tateyama, M., and Kubo, Y. (2003) Functional identification of Gd3+ binding site of metabotropic glutamate receptor 1alpha. *FEBS letters* **545**, 233-238
283. Saunders, R., Nahorski, S. R., and Challiss, R. A. (1998) A modulatory effect of extracellular Ca2+ on type 1alpha metabotropic glutamate receptor-mediated signalling. *Neuropharmacology* **37**, 273-276
284. Galvez, T., Urwyler, S., Prezeau, L., Mosbacher, J., Joly, C., Malitschek, B., Heid, J., Brabet, I., Froestl, W., Bettler, B., Kaupmann, K., and Pin, J. P. (2000) Ca(2+) requirement for high-affinity gamma-aminobutyric acid (GABA) binding at GABA(B) receptors: involvement of serine 269 of the GABA(B)R1 subunit. *Molecular pharmacology* **57**, 419-426

285. Tabata, T., and Kano, M. (2004) Calcium dependence of native metabotropic glutamate receptor signaling in central neurons. *Molecular neurobiology* **29**, 261-270
286. Tabata, T., Aiba, A., and Kano, M. (2002) Extracellular calcium controls the dynamic range of neuronal metabotropic glutamate receptor responses. *Molecular and cellular neurosciences* **20**, 56-68
287. Nash, M. S., Saunders, R., Young, K. W., Challiss, R. A., and Nahorski, S. R. (2001) Reassessment of the Ca2+ sensing property of a type I metabotropic glutamate receptor by simultaneous measurement of inositol 1,4,5-trisphosphate and Ca2+ in single cells. *The Journal of biological chemistry* **276**, 19286-19293
288. Nicholson, C., Bruggencate, G. T., Steinberg, R., and Stockle, H. (1977) Calcium modulation in brain extracellular microenvironment demonstrated with ion-selective micropipette. *Proceedings of the National Academy of Sciences of the United States of America* **74**, 1287-1290
289. Pumain, R., and Heinemann, U. (1985) Stimulus- and amino acid-induced calcium and potassium changes in rat neocortex. *Journal of neurophysiology* **53**, 1-16
290. Vassilev, P. M., Mitchel, J., Vassilev, M., Kanazirska, M., and Brown, E. M. (1997) Assessment of frequency-dependent alterations in the level of extracellular Ca2+ in the synaptic cleft. *Biophysical journal* **72**, 2103-2116
291. Egelman, D. M., and Montague, P. R. (1998) Computational properties of peri-dendritic calcium fluctuations. *The Journal of neuroscience : the official journal of the Society for Neuroscience* **18**, 8580-8589
292. Borst, J. G., and Sakmann, B. (1999) Depletion of calcium in the synaptic cleft of a calyx-type synapse in the rat brainstem. *The Journal of physiology* **521 Pt 1**, 123-133
293. Egelman, D. M., and Montague, P. R. (1999) Calcium dynamics in the extracellular space of mammalian neural tissue. *Biophysical journal* **76**, 1856-1867
294. Rusakov, D. A., Kullmann, D. M., and Stewart, M. G. (1999) Hippocampal synapses: do they talk to their neighbours? *Trends in neurosciences* **22**, 382-388
295. Wiest, M. C., Eagleman, D. M., King, R. D., and Montague, P. R. (2000) Dendritic spikes and their influence on extracellular calcium signaling. *Journal of neurophysiology* **83**, 1329-1337
296. Rusakov, D. A. (2001) The role of perisynaptic glial sheaths in glutamate spillover and extracellular Ca(2+) depletion. *Biophysical journal* **81**, 1947-1959
297. Rusakov, D. A., and Fine, A. (2003) Extracellular Ca2+ depletion contributes to fast activity-dependent modulation of synaptic transmission in the brain. *Neuron* **37**, 287-297
298. Gil-Sanz, C., Delgado-Garcia, J. M., Fairen, A., and Gruart, A. (2008) Involvement of the mGluR1 receptor in hippocampal synaptic plasticity and associative learning in behaving mice. *Cerebral cortex* **18**, 1653-1663
299. Menard, C., and Quirion, R. (2012) Group 1 metabotropic glutamate receptor function and its regulation of learning and memory in the aging brain. *Frontiers in pharmacology* **3**, 182
300. Riedel, G., Casabona, G., and Reymann, K. G. (1995) Inhibition of long-term potentiation in the dentate gyrus of freely moving rats by the metabotropic glutamate receptor antagonist MCPG. *The Journal of neuroscience : the official journal of the Society for Neuroscience* **15**, 87-98

301. Riedel, G., and Reymann, K. (1993) An antagonist of the metabotropic glutamate receptor prevents LTP in the dentate gyrus of freely moving rats. *Neuropharmacology* **32**, 929-931
302. Riedel, G., Wetzel, W., and Reymann, K. G. (1994) (R,S)-alpha-methyl-4-carboxyphenylglycine (MCPG) blocks spatial learning in rats and long-term potentiation in the dentate gyrus in vivo. *Neuroscience letters* **167**, 141-144
303. Martinez, J. L., Jr., and Derrick, B. E. (1996) Long-term potentiation and learning. *Annual review of psychology* **47**, 173-203
304. Richter-Levin, G., Errington, M. L., Maegawa, H., and Bliss, T. V. (1994) Activation of metabotropic glutamate receptors is necessary for long-term potentiation in the dentate gyrus and for spatial learning. *Neuropharmacology* **33**, 853-857
305. Balschun, D., and Wetzel, W. (1998) Inhibition of group I metabotropic glutamate receptors blocks spatial learning in rats. *Neuroscience letters* **249**, 41-44
306. Riedel, G., Manahan-Vaughan, D., Kozikowski, A. P., and Reymann, K. G. (1995) Metabotropic glutamate receptor agonist trans-azetidine-2,4-dicarboxylic acid facilitates maintenance of LTP in the dentate gyrus in vivo. *Neuropharmacology* **34**, 1107-1109
307. Chojnacka-Wojcik, E., Tatarczynska, E., and Pilc, A. (1997) The anxiolytic-like effect of metabotropic glutamate receptor antagonists after intrahippocampal injection in rats. *European journal of pharmacology* **319**, 153-156
308. Tatarczynska, E., Klodzinska, A., Kroczka, B., Chojnacka-Wojcik, E., and Pilc, A. (2001) The antianxiety-like effects of antagonists of group I and agonists of group II and III metabotropic glutamate receptors after intrahippocampal administration. *Psychopharmacology* **158**, 94-99
309. Varty, G. B., Grilli, M., Forlani, A., Fredduzzi, S., Grzelak, M. E., Guthrie, D. H., Hodgson, R. A., Lu, S. X., Nicolussi, E., Pond, A. J., Parker, E. M., Hunter, J. C., Higgins, G. A., Reggiani, A., and Bertorelli, R. (2005) The antinociceptive and anxiolytic-like effects of the metabotropic glutamate receptor 5 (mGluR5) antagonists, MPEP and MTEP, and the mGluR1 antagonist, LY456236, in rodents: a comparison of efficacy and side-effect profiles. *Psychopharmacology* **179**, 207-217
310. Pecknold, J. C., McClure, D. J., Appeltauer, L., Wrzesinski, L., and Allan, T. (1982) Treatment of anxiety using fenobam (a nonbenzodiazepine) in a double-blind standard (diazepam) placebo-controlled study. *Journal of clinical psychopharmacology* **2**, 129-133
311. Porter, R. H., Jaeschke, G., Spooren, W., Ballard, T. M., Buttelmann, B., Kolczewski, S., Peters, J. U., Prinssen, E., Wichmann, J., Vieira, E., Muhlemann, A., Gatti, S., Mutel, V., and Malherbe, P. (2005) Fenobam: a clinically validated nonbenzodiazepine anxiolytic is a potent, selective, and noncompetitive mGlu5 receptor antagonist with inverse agonist activity. *The Journal of pharmacology and experimental therapeutics* **315**, 711-721
312. Lima, V. C., Molchanov, M. L., Aguiar, D. C., Campos, A. C., and Guimaraes, F. S. (2008) Modulation of defensive responses and anxiety-like behaviors by group I metabotropic glutamate receptors located in the dorsolateral periaqueductal gray. *Progress in neuro-psychopharmacology & biological psychiatry* **32**, 178-185
313. Care, A. D., Sherwood, L. M., Potts, J. T., Jr., and Aurbach, G. D. (1966) Perfusion of the isolated parathyroid gland of the goat and sheep. *Nature* **209**, 55-57
314. Sherwood, L. M., Potts, J. T., Jr., Care, A. D., Mayer, G. P., and Aurbach, G. D. (1966) Evaluation by radioimmunoassay of factors controlling the secretion of parathyroid hormone. *Nature* **209**, 52-55

315. Lopez-Barneo, J., and Armstrong, C. M. (1983) Depolarizing response of rat parathyroid cells to divalent cations. *The Journal of general physiology* **82**, 269-294
316. Shoback, D., Thatcher, J., Leombruno, R., and Brown, E. (1983) Effects of extracellular Ca++ and Mg++ on cytosolic Ca++ and PTH release in dispersed bovine parathyroid cells. *Endocrinology* **113**, 424-426
317. Brown, E., Enyedi, P., LeBoff, M., Rotberg, J., Preston, J., and Chen, C. (1987) High extracellular Ca2+ and Mg2+ stimulate accumulation of inositol phosphates in bovine parathyroid cells. *FEBS letters* **218**, 113-118
318. Nemeth, E. F., and Scarpa, A. (1987) Rapid mobilization of cellular Ca2+ in bovine parathyroid cells evoked by extracellular divalent cations. Evidence for a cell surface calcium receptor. *The Journal of biological chemistry* **262**, 5188-5196
319. Kifor, O., and Brown, E. M. (1988) Relationship between diacylglycerol levels and extracellular Ca2+ in dispersed bovine parathyroid cells. *Endocrinology* **123**, 2723-2729
320. Shoback, D. M., Membreno, L. A., and McGhee, J. G. (1988) High calcium and other divalent cations increase inositol trisphosphate in bovine parathyroid cells. *Endocrinology* **123**, 382-389
321. Huang, Y., Zhou, Y. B., Yang, W., Butters, R., Lee, H. W., Li, S. Y., Castiblanco, A., Brown, E. M., and Yang, J. J. (2007) Identification and dissection of Ca2+-binding sites in the extracellular domain of Ca2+-sensing receptor. *Journal of Biological Chemistry* **282**, 19000-19010
322. Silve, C., Petrel, C., Leroy, C., Bruel, H., Mallet, E., Rognan, D., and Ruat, M. (2005) Delineating a Ca2+ binding pocket within the venus flytrap module of the human calcium-sensing receptor. *The Journal of biological chemistry* **280**, 37917-37923
323. Fan, G. F., Ray, K., Zhao, X. M., Goldsmith, P. K., and Spiegel, A. M. (1998) Mutational analysis of the cysteines in the extracellular domain of the human Ca2+ receptor: effects on cell surface expression, dimerization and signal transduction. *FEBS letters* **436**, 353-356
324. Zhao, X. M., Hauache, O., Goldsmith, P. K., Collins, R., and Spiegel, A. M. (1999) A missense mutation in the seventh transmembrane domain constitutively activates the human Ca2+ receptor. *FEBS letters* **448**, 180-184
325. Zhang, Z., Sun, S., Quinn, S. J., Brown, E. M., and Bai, M. (2001) The extracellular calcium-sensing receptor dimerizes through multiple types of intermolecular interactions. *The Journal of biological chemistry* **276**, 5316-5322
326. Petrel, C., Kessler, A., Dauban, P., Dodd, R. H., Rognan, D., and Ruat, M. (2004) Positive and negative allosteric modulators of the Ca2+-sensing receptor interact within overlapping but not identical binding sites in the transmembrane domain. *The Journal of biological chemistry* **279**, 18990-18997
327. Miedlich, S. U., Gama, L., Seuwen, K., Wolf, R. M., and Breitwieser, G. E. (2004) Homology modeling of the transmembrane domain of the human calcium sensing receptor and localization of an allosteric binding site. *The Journal of biological chemistry* **279**, 7254-7263
328. Petrel, C., Kessler, A., Maslah, F., Dauban, P., Dodd, R. H., Rognan, D., and Ruat, M. (2003) Modeling and mutagenesis of the binding site of Calhex 231, a novel negative allosteric modulator of the extracellular Ca(2+)-sensing receptor. *The Journal of biological chemistry* **278**, 49487-49494

329. Ray, K., Fan, G. F., Goldsmith, P. K., and Spiegel, A. M. (1997) The carboxyl terminus of the human calcium receptor. Requirements for cell-surface expression and signal transduction. *The Journal of biological chemistry* **272**, 31355-31361
330. Chang, W., Pratt, S., Chen, T. H., Bourguignon, L., and Shoback, D. (2001) Amino acids in the cytoplasmic C terminus of the parathyroid Ca2+-sensing receptor mediate efficient cell-surface expression and phospholipase C activation. *The Journal of biological chemistry* **276**, 44129-44136
331. Bai, M., Janicic, N., Trivedi, S., Quinn, S. J., Cole, D. E., Brown, E. M., and Hendy, G. N. (1997) Markedly reduced activity of mutant calcium-sensing receptor with an inserted Alu element from a kindred with familial hypocalciuric hypercalcemia and neonatal severe hyperparathyroidism. *The Journal of clinical investigation* **99**, 1917-1925
332. Gama, L., and Breitwieser, G. E. (1998) A carboxyl-terminal domain controls the cooperativity for extracellular Ca2+ activation of the human calcium sensing receptor. A study with receptor-green fluorescent protein fusions. *The Journal of biological chemistry* **273**, 29712-29718
333. Nemeth, E. F. (1990) Regulation of cytosolic calcium by extracellular divalent cations in C-cells and parathyroid cells. *Cell calcium* **11**, 323-327
334. McGehee, D. S., Aldersberg, M., Liu, K. P., Hsuing, S., Heath, M. J., and Tamir, H. (1997) Mechanism of extracellular Ca2+ receptor-stimulated hormone release from sheep thyroid parafollicular cells. *The Journal of physiology* **502 (Pt 1)**, 31-44
335. Huang, Y., Zhou, Y., Castiblanco, A., Yang, W., Brown, E. M., and Yang, J. J. (2009) Multiple Ca(2+)-binding sites in the extracellular domain of the Ca(2+)-sensing receptor corresponding to cooperative Ca(2+) response. *Biochemistry* **48**, 388-398
336. Bai, M., Quinn, S., Trivedi, S., Kifor, O., Pearce, S. H., Pollak, M. R., Krapcho, K., Hebert, S. C., and Brown, E. M. (1996) Expression and characterization of inactivating and activating mutations in the human Ca2+o-sensing receptor. *The Journal of biological chemistry* **271**, 19537-19545
337. Pearce, S. H., Bai, M., Quinn, S. J., Kifor, O., Brown, E. M., and Thakker, R. V. (1996) Functional characterization of calcium-sensing receptor mutations expressed in human embryonic kidney cells. *The Journal of clinical investigation* **98**, 1860-1866
338. Riccardi, D. (2002) Wellcome Prize Lecture. Cell surface, ion-sensing receptors. *Exp Physiol* **87**, 403-411
339. Navarro, J. F., Mora, C., Jimenez, A., Torres, A., Macia, M., and Garcia, J. (1999) Relationship between serum magnesium and parathyroid hormone levels in hemodialysis patients. *American journal of kidney diseases : the official journal of the National Kidney Foundation* **34**, 43-48
340. Brown, E. M. (1997) Mutations in the calcium-sensing receptor and their clinical implications. *Hormone research* **48**, 199-208
341. Ruat, M., Snowman, A. M., Hester, L. D., and Snyder, S. H. (1996) Cloned and expressed rat Ca2+-sensing receptor. *The Journal of biological chemistry* **271**, 5972-5975
342. Quinn, S. J., Ye, C. P., Diaz, R., Kifor, O., Bai, M., Vassilev, P., and Brown, E. (1997) The Ca2+-sensing receptor: a target for polyamines. *The American journal of physiology* **273**, C1315-1323
343. Brown, E. M., Katz, C., Butters, R., and Kifor, O. (1991) Polyarginine, polylysine, and protamine mimic the effects of high extracellular calcium concentrations on dispersed

bovine parathyroid cells. *Journal of bone and mineral research : the official journal of the American Society for Bone and Mineral Research* **6**, 1217-1225

344. Ye, C., Ho-Pao, C. L., Kanazirska, M., Quinn, S., Rogers, K., Seidman, C. E., Seidman, J. G., Brown, E. M., and Vassilev, P. M. (1997) Amyloid-beta proteins activate Ca(2+)-permeable channels through calcium-sensing receptors. *Journal of neuroscience research* **47**, 547-554
345. McLarnon, S., Holden, D., Ward, D., Jones, M., Elliott, A., and Riccardi, D. (2002) Aminoglycoside antibiotics induce pH-sensitive activation of the calcium-sensing receptor. *Biochem Biophys Res Commun* **297**, 71-77
346. May, L. T., Avlani, V. A., Sexton, P. M., and Christopoulos, A. (2004) Allosteric modulation of G protein-coupled receptors. *Current pharmaceutical design* **10**, 2003-2013
347. Conigrave, A. D., Quinn, S. J., and Brown, E. M. (2000) L-amino acid sensing by the extracellular Ca2+-sensing receptor. *Proceedings of the National Academy of Sciences of the United States of America* **97**, 4814-4819
348. Lee, H. J., Mun, H. C., Lewis, N. C., Crouch, M. F., Culverston, E. L., Mason, R. S., and Conigrave, A. D. (2007) Allosteric activation of the extracellular Ca2+-sensing receptor by L-amino acids enhances ERK1/2 phosphorylation. *The Biochemical journal* **404**, 141-149
349. Zhang, C., Huang, Y., Jiang, Y., Mulpuri, N., Wei, L., Hamelberg, D., Brown, E. M., and Yang, J. J. (2014) Identification of an L-phenylalanine binding site enhancing the cooperative responses of the calcium-sensing receptor to calcium. *The Journal of biological chemistry* **289**, 5296-5309
350. Nemeth, E. F., Steffey, M. E., Hammerland, L. G., Hung, B. C., Van Wagenen, B. C., DelMar, E. G., and Balandrin, M. F. (1998) Calcimimetics with potent and selective activity on the parathyroid calcium receptor. *Proceedings of the National Academy of Sciences of the United States of America* **95**, 4040-4045
351. Nemeth, E. F., Delmar, E. G., Heaton, W. L., Miller, M. A., Lambert, L. D., Conklin, R. L., Gowen, M., Gleason, J. G., Bhatnagar, P. K., and Fox, J. (2001) Calcilytic compounds: potent and selective Ca2+ receptor antagonists that stimulate secretion of parathyroid hormone. *The Journal of pharmacology and experimental therapeutics* **299**, 323-331
352. White, E., McKenna, J., Cavanaugh, A., and Breitwieser, G. E. (2009) Pharmacochaperone-mediated rescue of calcium-sensing receptor loss-of-function mutants. *Molecular endocrinology* **23**, 1115-1123
353. Huang, Y., and Breitwieser, G. E. (2007) Rescue of calcium-sensing receptor mutants by allosteric modulators reveals a conformational checkpoint in receptor biogenesis. *The Journal of biological chemistry* **282**, 9517-9525
354. Quinn, S. J., Bai, M., and Brown, E. M. (2004) pH Sensing by the calcium-sensing receptor. *The Journal of biological chemistry* **279**, 37241-37249
355. Quinn, S. J., Kifor, O., Trivedi, S., Diaz, R., Vassilev, P., and Brown, E. (1998) Sodium and ionic strength sensing by the calcium receptor. *The Journal of biological chemistry* **273**, 19579-19586
356. Wettschureck, N., Lee, E., Libutti, S. K., Offermanns, S., Robey, P. G., and Spiegel, A. M. (2007) Parathyroid-specific double knockout of Gq and G11 alpha-subunits leads to a

phenotype resembling germline knockout of the extracellular Ca2+ -sensing receptor. *Molecular endocrinology* **21**, 274-280
357. Breitwieser, G. E. (2006) Calcium sensing receptors and calcium oscillations: calcium as a first messenger. *Current topics in developmental biology* **73**, 85-114
358. Breitwieser, G. E., and Gama, L. (2001) Calcium-sensing receptor activation induces intracellular calcium oscillations. *American journal of physiology. Cell physiology* **280**, C1412-1421
359. Ridefelt, P., Bjorklund, E., Akerstrom, G., Olsson, M. J., Rastad, J., and Gylfe, E. (1995) Ca(2+)-induced Ca2+ oscillations in parathyroid cells. *Biochem Biophys Res Commun* **215**, 903-909
360. Miki, H., Maercklein, P. B., and Fitzpatrick, L. A. (1995) Spontaneous oscillations of intracellular calcium in single bovine parathyroid cells may be associated with the inhibition of parathyroid hormone secretion. *Endocrinology* **136**, 2954-2959
361. Rey, O., Young, S. H., Jacamo, R., Moyer, M. P., and Rozengurt, E. (2010) Extracellular calcium sensing receptor stimulation in human colonic epithelial cells induces intracellular calcium oscillations and proliferation inhibition. *Journal of cellular physiology* **225**, 73-83
362. McCormick, W. D., Atkinson-Dell, R., Campion, K. L., Mun, H. C., Conigrave, A. D., and Ward, D. T. (2010) Increased receptor stimulation elicits differential calcium-sensing receptor(T888) dephosphorylation. *The Journal of biological chemistry* **285**, 14170-14177
363. Davies, S. L., Ozawa, A., McCormick, W. D., Dvorak, M. M., and Ward, D. T. (2007) Protein kinase C-mediated phosphorylation of the calcium-sensing receptor is stimulated by receptor activation and attenuated by calyculin-sensitive phosphatase activity. *The Journal of biological chemistry* **282**, 15048-15056
364. Young, S. H., Wu, S. V., and Rozengurt, E. (2002) Ca2+-stimulated Ca2+ oscillations produced by the Ca2+-sensing receptor require negative feedback by protein kinase C. *The Journal of biological chemistry* **277**, 46871-46876
365. Jiang, Y. F., Zhang, Z., Kifor, O., Lane, C. R., Quinn, S. J., and Bai, M. (2002) Protein kinase C (PKC) phosphorylation of the Ca2+ o-sensing receptor (CaR) modulates functional interaction of G proteins with the CaR cytoplasmic tail. *The Journal of biological chemistry* **277**, 50543-50549
366. Bai, M., Trivedi, S., Lane, C. R., Yang, Y., Quinn, S. J., and Brown, E. M. (1998) Protein kinase C phosphorylation of threonine at position 888 in Ca2+o-sensing receptor (CaR) inhibits coupling to Ca2+ store release. *The Journal of biological chemistry* **273**, 21267-21275
367. Ritter, C. S., Pande, S., Krits, I., Slatopolsky, E., and Brown, A. J. (2008) Destabilization of parathyroid hormone mRNA by extracellular Ca2+ and the calcimimetic R-568 in parathyroid cells: role of cytosolic Ca and requirement for gene transcription. *Journal of molecular endocrinology* **40**, 13-21
368. Levi, R., Ben-Dov, I. Z., Lavi-Moshayoff, V., Dinur, M., Martin, D., Naveh-Many, T., and Silver, J. (2006) Increased parathyroid hormone gene expression in secondary hyperparathyroidism of experimental uremia is reversed by calcimimetics: correlation with posttranslational modification of the trans acting factor AUF1. *Journal of the American Society of Nephrology : JASN* **17**, 107-112

369. Colloton, M., Shatzen, E., Miller, G., Stehman-Breen, C., Wada, M., Lacey, D., and Martin, D. (2005) Cinacalcet HCl attenuates parathyroid hyperplasia in a rat model of secondary hyperparathyroidism. *Kidney international* **67**, 467-476
370. Chattopadhyay, N., Legradi, G., Bai, M., Kifor, O., Ye, C., Vassilev, P. M., Brown, E. M., and Lechan, R. M. (1997) Calcium-sensing receptor in the rat hippocampus: a developmental study. *Brain research. Developmental brain research* **100**, 13-21
371. Yano, S., Brown, E. M., and Chattopadhyay, N. (2004) Calcium-sensing receptor in the brain. *Cell calcium* **35**, 257-264
372. Cheng, I., Klingensmith, M. E., Chattopadhyay, N., Kifor, O., Butters, R. R., Soybel, D. I., and Brown, E. M. (1998) Identification and localization of the extracellular calcium-sensing receptor in human breast. *The Journal of clinical endocrinology and metabolism* **83**, 703-707
373. Wang, R., Xu, C., Zhao, W., Zhang, J., Cao, K., Yang, B., and Wu, L. (2003) Calcium and polyamine regulated calcium-sensing receptors in cardiac tissues. *European journal of biochemistry / FEBS* **270**, 2680-2688
374. Bikle, D. D., Ratnam, A., Mauro, T., Harris, J., and Pillai, S. (1996) Changes in calcium responsiveness and handling during keratinocyte differentiation. Potential role of the calcium receptor. *The Journal of clinical investigation* **97**, 1085-1093
375. Oda, Y., Tu, C. L., Pillai, S., and Bikle, D. D. (1998) The calcium sensing receptor and its alternatively spliced form in keratinocyte differentiation. *The Journal of biological chemistry* **273**, 23344-23352
376. Peiris, D., Pacheco, I., Spencer, C., and MacLeod, R. J. (2007) The extracellular calcium-sensing receptor reciprocally regulates the secretion of BMP-2 and the BMP antagonist Noggin in colonic myofibroblasts. *American journal of physiology. Gastrointestinal and liver physiology* **292**, G753-766
377. Buchan, A. M., Squires, P. E., Ring, M., and Meloche, R. M. (2001) Mechanism of action of the calcium-sensing receptor in human antral gastrin cells. *Gastroenterology* **120**, 1128-1139
378. Komuves, L., Oda, Y., Tu, C. L., Chang, W. H., Ho-Pao, C. L., Mauro, T., and Bikle, D. D. (2002) Epidermal expression of the full-length extracellular calcium-sensing receptor is required for normal keratinocyte differentiation. *Journal of cellular physiology* **192**, 45-54
379. Tu, C. L., Chang, W., Xie, Z., and Bikle, D. D. (2008) Inactivation of the calcium sensing receptor inhibits E-cadherin-mediated cell-cell adhesion and calcium-induced differentiation in human epidermal keratinocytes. *The Journal of biological chemistry* **283**, 3519-3528
380. Tennakoon, S., Aggarwal, A., and Kallay, E. (2016) The calcium-sensing receptor and the hallmarks of cancer. *Biochimica et biophysica acta* **1863**, 1398-1407
381. Wang, P., Wang, L., Wang, S., Li, S., Li, Y., and Zhang, L. (2015) Effects of calcium-sensing receptors on apoptosis in rat hippocampus during hypoxia/re-oxygenation through the ERK1/2 pathway. *International journal of clinical and experimental medicine* **8**, 12858-12865
382. Magno, A. L., Ward, B. K., and Ratajczak, T. (2011) The calcium-sensing receptor: a molecular perspective. *Endocrine reviews* **32**, 3-30

383. Riccardi, D., and Kemp, P. J. (2012) The calcium-sensing receptor beyond extracellular calcium homeostasis: conception, development, adult physiology, and disease. *Annual review of physiology* **74**, 271-297
384. Putkey, J. A., Slaughter, G. R., and Means, A. R. (1985) Bacterial expression and characterization of proteins derived from the chicken calmodulin cDNA and a calmodulin processed gene. *The Journal of biological chemistry* **260**, 4704-4712
385. Johnson, J. D., and Wittenauer, L. A. (1983) A fluorescent calmodulin that reports the binding of hydrophobic inhibitory ligands. *The Biochemical journal* **211**, 473-479
386. VanScyoc, W. S., and Shea, M. A. (2001) Phenylalanine fluorescence studies of calcium binding to N-domain fragments of Paramecium calmodulin mutants show increased calcium affinity correlates with increased disorder. *Protein science : a publication of the Protein Society* **10**, 1758-1768
387. Lee, H. W., Yang, W., Ye, Y., Liu, Z. R., Glushka, J., and Yang, J. J. (2002) Isolated EF-loop III of calmodulin in a scaffold protein remains unpaired in solution using pulsed-field-gradient NMR spectroscopy. *Biochimica et biophysica acta* **1598**, 80-87
388. Meng, L., Forouhar, F., Thieker, D., Gao, Z., Ramiah, A., Moniz, H., Xiang, Y., Seetharaman, J., Milaninia, S., Su, M., Bridger, R., Veillon, L., Azadi, P., Kornhaber, G., Wells, L., Montelione, G. T., Woods, R. J., Tong, L., and Moremen, K. W. (2013) Enzymatic basis for N-glycan sialylation: structure of rat alpha2,6-sialyltransferase (ST6GAL1) reveals conserved and unique features for glycan sialylation. *J. Biol. Chem.* **288**, 34680-34698
389. Otwinowski, Z., and Minor, W. (1997) Processing of X-ray diffraction data collected in the oscillation mode. *Methods Enzymol.* **276**, 307–326
390. Adams, P. D., Afonine, P. V., Bunkoczi, G., Chen, V. B., Davis, I. W., Echols, N., Headd, J. J., Hung, L. W., Kapral, G. J., Grosse-Kunstleve, R. W., McCoy, A. J., Moriarty, N. W., Oeffner, R., Read, R. J., Richardson, D. C., Richardson, J. S., Terwilliger, T. C., and Zwart, P. H. (2010) PHENIX: a comprehensive Python-based system for macromolecular structure solution. *Acta Crystallogr.* **66**, 213-221
391. Monn, J. A., Prieto, L., Taboada, L., Pedregal, C., Hao, J., Reinhard, M. R., Henry, S. S., Goldsmith, P. J., Beadle, C. D., Walton, L., Man, T., Rudyk, H., Clark, B., Tupper, D., Baker, S. R., Lamas, C., Montero, C., Marcos, A., Blanco, J., Bures, M., Clawson, D. K., Atwell, S., Lu, F., Wang, J., Russell, M., Heinz, B. A., Wang, X., Carter, J. H., Xiang, C., Catlow, J. T., Swanson, S., Sanger, H., Broad, L. M., Johnson, M. P., Knopp, K. L., Simmons, R. M., Johnson, B. G., Shaw, D. B., and McKinzie, D. L. (2015) Synthesis and pharmacological characterization of C4-disubstituted analogs of 1S,2S,5R,6S-2-aminobicyclo[3.1.0]hexane-2,6-dicarboxylate: identification of a potent, selective metabotropic glutamate receptor agonist and determination of agonist-bound human mGlu2 and mGlu3 amino terminal domain structures. *J. Med. Chem.* **58**, 1776-1794
392. Emsley, P., Lohkamp, B., Scott, W. G., and Cowtan, K. (2010) Features and development of Coot. *Acta Crystallogr.* **66**, 486-501
393. Winn, M. D., Ballard, C. C., Cowtan, K. D., Dodson, E. J., Emsley, P., Evans, P. R., Keegan, R. M., Krissinel, E. B., Leslie, A. G., McCoy, A., McNicholas, S. J., Murshudov, G. N., Pannu, N. S., Potterton, E. A., Powell, H. R., Read, R. J., Vagin, A., and Wilson, K. S. (2011) Overview of the CCP4 suite and current developments. *Acta Crystallogr.* **67**, 235-242

394. Huang, Y., Zhou, Y., Yang, W., Butters, R., Lee, H. W., Li, S., Castiblanco, A., Brown, E. M., and Yang, J. J. (2007) Identification and dissection of Ca(2+)-binding sites in the extracellular domain of Ca(2+)-sensing receptor. *J. Biol. Chem.* **282**, 19000-19010
395. Beyer, E. C. (1990) Molecular cloning and developmental expression of two chick embryo gap junction proteins. *The Journal of biological chemistry* **265**, 14439-14443
396. Coppen, S. R., Kodama, I., Boyett, M. R., Dobrzynski, H., Takagishi, Y., Honjo, H., Yeh, H. I., and Severs, N. J. (1999) Connexin45, a major connexin of the rabbit sinoatrial node, is co-expressed with connexin43 in a restricted zone at the nodal-crista terminalis border. *The journal of histochemistry and cytochemistry : official journal of the Histochemistry Society* **47**, 907-918
397. van Veen, T. A., van Rijen, H. V., van Kempen, M. J., Miquerol, L., Opthof, T., Gros, D., Vos, M. A., Jongsma, H. J., and de Bakker, J. M. (2005) Discontinuous conduction in mouse bundle branches is caused by bundle-branch architecture. *Circulation* **112**, 2235-2244
398. Verheijck, E. E., van Kempen, M. J., Veereschild, M., Lurvink, J., Jongsma, H. J., and Bouman, L. N. (2001) Electrophysiological features of the mouse sinoatrial node in relation to connexin distribution. *Cardiovasc Res* **52**, 40-50
399. Honjo, H., Boyett, M. R., Coppen, S. R., Takagishi, Y., Opthof, T., Severs, N. J., and Kodama, I. (2002) Heterogeneous expression of connexins in rabbit sinoatrial node cells: correlation between connexin isotype and cell size. *Cardiovasc Res* **53**, 89-96
400. Coppen, S. R., Dupont, E., Rothery, S., and Severs, N. J. (1998) Connexin45 expression is preferentially associated with the ventricular conduction system in mouse and rat heart. *Circ Res* **82**, 232-243
401. Maxeiner, S., Kruger, O., Schilling, K., Traub, O., Urschel, S., and Willecke, K. (2003) Spatiotemporal transcription of connexin45 during brain development results in neuronal expression in adult mice. *Neuroscience* **119**, 689-700
402. Willecke, K., Eiberger, J., Degen, J., Eckardt, D., Romualdi, A., Guldenagel, M., Deutsch, U., and Sohl, G. (2002) Structural and functional diversity of connexin genes in the mouse and human genome. *Biological chemistry* **383**, 725-737
403. Nakase, T., and Naus, C. C. (2004) Gap junctions and neurological disorders of the central nervous system. *Biochimica et biophysica acta* **1662**, 149-158
404. Hills, C. E., Price, G. W., and Squires, P. E. (2015) Mind the gap: connexins and cell-cell communication in the diabetic kidney. *Diabetologia* **58**, 233-241
405. D'Hondt, C., Iyyathurai, J., Himpens, B., Leybaert, L., and Bultynck, G. (2014) Cx43-hemichannel function and regulation in physiology and pathophysiology: insights from the bovine corneal endothelial cell system and beyond. *Frontiers in physiology* **5**, 348
406. Del Corsso, C., Iglesias, R., Zoidl, G., Dermietzel, R., and Spray, D. C. (2012) Calmodulin dependent protein kinase increases conductance at gap junctions formed by the neuronal gap junction protein connexin36. *Brain research* **1487**, 69-77
407. Bennett, M. V., Barrio, L. C., Bargiello, T. A., Spray, D. C., Hertzberg, E., and Saez, J. C. (1991) Gap junctions: new tools, new answers, new questions. *Neuron* **6**, 305-320
408. Johnson, C. K. (2006) Calmodulin, conformational states, and calcium signaling. A single-molecule perspective. *Biochemistry* **45**, 14233-14246
409. Kink, J. A., Maley, M. E., Preston, R. R., Ling, K. Y., Wallen-Friedman, M. A., Saimi, Y., and Kung, C. (1990) Mutations in paramecium calmodulin indicate functional differences between the C-terminal and N-terminal lobes in vivo. *Cell* **62**, 165-174

410. Budde, T., Meuth, S., and Pape, H. C. (2002) Calcium-dependent inactivation of neuronal calcium channels. *Nature reviews. Neuroscience* **3**, 873-883
411. Saimi, Y., and Kung, C. (2002) Calmodulin as an ion channel subunit. *Annual review of physiology* **64**, 289-311
412. Wei, F., Xia, X. M., Tang, J., Ao, H., Ko, S., Liauw, J., Qiu, C. S., and Zhuo, M. (2003) Calmodulin regulates synaptic plasticity in the anterior cingulate cortex and behavioral responses: a microelectroporation study in adult rodents. *The Journal of neuroscience : the official journal of the Society for Neuroscience* **23**, 8402-8409
413. Halling, D. B., Aracena-Parks, P., and Hamilton, S. L. (2006) Regulation of voltage-gated Ca2+ channels by calmodulin. *Science's STKE : signal transduction knowledge environment* **2006**, er1
414. Tan, B. Z., Jiang, F., Tan, M. Y., Yu, D., Huang, H., Shen, Y., and Soong, T. W. (2011) Functional characterization of alternative splicing in the C terminus of L-type CaV1.3 channels. *The Journal of biological chemistry* **286**, 42725-42735
415. Ben-Johny, M., and Yue, D. T. (2014) Calmodulin regulation (calmodulation) of voltage-gated calcium channels. *The Journal of general physiology* **143**, 679-692
416. Zou, J., Salarian, M., Chen, Y., Veenstra, R., Louis, C. F., and Yang, J. J. (2014) Gap junction regulation by calmodulin. *FEBS letters* **588**, 1430-1438
417. Peracchia, C. (2004) Chemical gating of gap junction channels; roles of calcium, pH and calmodulin. *Biochimica et biophysica acta* **1662**, 61-80
418. Pfleger, K. D., Seeber, R. M., and Eidne, K. A. (2006) Bioluminescence resonance energy transfer (BRET) for the real-time detection of protein-protein interactions. *Nature protocols* **1**, 337-345
419. Suga, M., Maeda, S., Nakagawa, S., Yamashita, E., and Tsukihara, T. (2009) A description of the structural determination procedures of a gap junction channel at 3.5 A resolution. *Acta Crystallogr D Biol Crystallogr* **65**, 758-766
420. Nagai, T., Ibata, K., Park, E. S., Kubota, M., Mikoshiba, K., and Miyawaki, A. (2002) A variant of yellow fluorescent protein with fast and efficient maturation for cell-biological applications. *Nature biotechnology* **20**, 87-90
421. Kumari, S. S., Varadaraj, K., Valiunas, V., Ramanan, S. V., Christensen, E. A., Beyer, E. C., and Brink, P. R. (2000) Functional expression and biophysical properties of polymorphic variants of the human gap junction protein connexin37. *Biochem Biophys Res Commun* **274**, 216-224
422. Contreras, J. E., Saez, J. C., Bukauskas, F. F., and Bennett, M. V. (2003) Gating and regulation of connexin 43 (Cx43) hemichannels. *Proceedings of the National Academy of Sciences of the United States of America* **100**, 11388-11393
423. Kalvelyte, A., Imbrasaite, A., Bukauskiene, A., Verselis, V. K., and Bukauskas, F. F. (2003) Connexins and apoptotic transformation. *Biochemical pharmacology* **66**, 1661-1672
424. Koreen, I. V., Elsayed, W. A., Liu, Y. J., and Harris, A. L. (2004) Tetracycline-regulated expression enables purification and functional analysis of recombinant connexin channels from mammalian cells. *The Biochemical journal* **383**, 111-119
425. Reddy Chichili, V. P., Xiao, Y., Seetharaman, J., Cummins, T. R., and Sivaraman, J. (2013) Structural basis for the modulation of the neuronal voltage-gated sodium channel NaV1.6 by calmodulin. *Scientific reports* **3**, 2435

426. Theoharis, N. T., Sorensen, B. R., Theisen-Toupal, J., and Shea, M. A. (2008) The neuronal voltage-dependent sodium channel type II IQ motif lowers the calcium affinity of the C-domain of calmodulin. *Biochemistry* **47**, 112-123
427. Klevit, R. E., Blumenthal, D. K., Wemmer, D. E., and Krebs, E. G. (1985) Interaction of calmodulin and a calmodulin-binding peptide from myosin light chain kinase: major spectral changes in both occur as the result of complex formation. *Biochemistry* **24**, 8152-8157
428. O'Neil, K. T., Erickson-Viitanen, S., and DeGrado, W. F. (1989) Photolabeling of calmodulin with basic, amphiphilic alpha-helical peptides containing p-benzoylphenylalanine. *The Journal of biological chemistry* **264**, 14571-14578
429. Ikura, M., Clore, G. M., Gronenborn, A. M., Zhu, G., Klee, C. B., and Bax, A. (1992) Solution structure of a calmodulin-target peptide complex by multidimensional NMR. *Science* **256**, 632-638
430. Seeholzer, S. H., and Wand, A. J. (1989) Structural characterization of the interactions between calmodulin and skeletal muscle myosin light chain kinase: effect of peptide (576-594)G binding on the Ca2+-binding domains. *Biochemistry* **28**, 4011-4020
431. Lehrman, S. R., Tuls, J. L., and Lund, M. (1990) Peptide alpha-helicity in aqueous trifluoroethanol: correlations with predicted alpha-helicity and the secondary structure of the corresponding regions of bovine growth hormone. *Biochemistry* **29**, 5590-5596
432. Luo, P., and Baldwin, R. L. (1997) Mechanism of helix induction by trifluoroethanol: a framework for extrapolating the helix-forming properties of peptides from trifluoroethanol/water mixtures back to water. *Biochemistry* **36**, 8413-8421
433. Luo, P., and Baldwin, R. L. (1999) Interaction between water and polar groups of the helix backbone: an important determinant of helix propensities. *Proceedings of the National Academy of Sciences of the United States of America* **96**, 4930-4935
434. Brokx, R. D., Scheek, R. M., Weljie, A. M., and Vogel, H. J. (2004) Backbone dynamic properties of the central linker region of calcium-calmodulin in 35% trifluoroethanol. *Journal of structural biology* **146**, 272-280
435. Kincaid, R. L., Vaughan, M., Osborne, J. C., Jr., and Tkachuk, V. A. (1982) Ca2+-dependent interaction of 5-dimethylaminonaphthalene-1-sulfonyl-calmodulin with cyclic nucleotide phosphodiesterase, calcineurin, and troponin I. *The Journal of biological chemistry* **257**, 10638-10643
436. Alaimo, A., Malo, C., Areso, P., Aloria, K., Millet, O., and Villarroel, A. (2013) The use of dansyl-calmodulin to study interactions with channels and other proteins. *Methods in molecular biology* **998**, 217-231
437. Fielding, L. (2003) NMR methods for the determination of protein-ligand dissociation constants. *Current topics in medicinal chemistry* **3**, 39-53
438. Weber, P. A., Chang, H. C., Spaeth, K. E., Nitsche, J. M., and Nicholson, B. J. (2004) The permeability of gap junction channels to probes of different size is dependent on connexin composition and permeant-pore affinities. *Biophysical journal* **87**, 958-973
439. Cao, F., Eckert, R., Elfgang, C., Nitsche, J. M., Snyder, S. A., DF, H. u., Willecke, K., and Nicholson, B. J. (1998) A quantitative analysis of connexin-specific permeability differences of gap junctions expressed in HeLa transfectants and Xenopus oocytes. *Journal of cell science* **111 (Pt 1)**, 31-43
440. Peracchia, C., Bernardini, G., and Peracchia, L. L. (1983) Is calmodulin involved in the regulation of gap junction permeability? *Pflugers Arch.* **399**, 152-154

441. Peracchia, C. (1984) Communicating junctions and calmodulin: inhibition of electrical uncoupling in Xenopus embryo by calmidazolium. *J. Membr. Biol.* **81**, 49-58
442. Peracchia, C. (1987) Calmodulin-like proteins and communicating junctions. Electrical uncoupling of crayfish septate axons is inhibited by the calmodulin inhibitor W7 and is not affected by cyclic nucleotides. *Pflugers Arch. Eur. J. Physiol.* **408**, 379-385
443. Eidne, K. A., Kroeger, K. M., and Hanyaloglu, A. C. (2002) Applications of novel resonance energy transfer techniques to study dynamic hormone receptor interactions in living cells. *Trends in endocrinology and metabolism: TEM* **13**, 415-421
444. Pfleger, K. D., and Eidne, K. A. (2005) Monitoring the formation of dynamic G-protein-coupled receptor-protein complexes in living cells. *The Biochemical journal* **385**, 625-637
445. Milligan, G., and Bouvier, M. (2005) Methods to monitor the quaternary structure of G protein-coupled receptors. *The FEBS journal* **272**, 2914-2925
446. Germain-Desprez, D., Bazinet, M., Bouvier, M., and Aubry, M. (2003) Oligomerization of transcriptional intermediary factor 1 regulators and interaction with ZNF74 nuclear matrix protein revealed by bioluminescence resonance energy transfer in living cells. *The Journal of biological chemistry* **278**, 22367-22373
447. Pfleger, K. D., and Eidne, K. A. (2006) Illuminating insights into protein-protein interactions using bioluminescence resonance energy transfer (BRET). *Nature methods* **3**, 165-174
448. Saul, J. P., Epstein, A. E., Silka, M. J., Berul, C. I., Dick, M., 2nd, Dimarco, J. P., Friedman, R. A., Rosenthal, E., Stephenson, E. A., Vetter, V. L., American College of, C., American Heart, A., Heart Rhythm, S., Pediatric, and Congenital Electrophysiology, S. (2008) Heart Rhythm Society/Pediatric and Congenital Electrophysiology Society Clinical Competency Statement: training pathways for implantation of cardioverter-defibrillators and cardiac resynchronization therapy devices in pediatric and congenital heart patients. *Heart Rhythm* **5**, 926-933
449. Black, D. J., Leonard, J., and Persechini, A. (2006) Biphasic Ca2+-dependent switching in a calmodulin-IQ domain complex. *Biochemistry* **45**, 6987-6995
450. Shah, V. N., Wingo, T. L., Weiss, K. L., Williams, C. K., Balser, J. R., and Chazin, W. J. (2006) Calcium-dependent regulation of the voltage-gated sodium channel hH1: intrinsic and extrinsic sensors use a common molecular switch. *Proceedings of the National Academy of Sciences of the United States of America* **103**, 3592-3597
451. Mori, M., Konno, T., Morii, T., Nagayama, K., and Imoto, K. (2003) Regulatory interaction of sodium channel IQ-motif with calmodulin C-terminal lobe. *Biochem Biophys Res Commun* **307**, 290-296
452. Houdusse, A., and Cohen, C. (1995) Target sequence recognition by the calmodulin superfamily: implications from light chain binding to the regulatory domain of scallop myosin. *Proceedings of the National Academy of Sciences of the United States of America* **92**, 10644-10647
453. Dodd, R., Peracchia, C., Stolady, D., and Torok, K. (2008) Calmodulin association with connexin32-derived peptides suggests trans-domain interaction in chemical gating of gap junction channels. *The Journal of biological chemistry* **283**, 26911-26920
454. Olwin, B. B., Edelman, A. M., Krebs, E. G., and Storm, D. R. (1984) Quantitation of energy coupling between Ca2+, calmodulin, skeletal muscle myosin light chain kinase, and kinase substrates. *The Journal of biological chemistry* **259**, 10949-10955

455. Olwin, B. B., and Storm, D. R. (1985) Calcium binding to complexes of calmodulin and calmodulin binding proteins. *Biochemistry* **24**, 8081-8086
456. Peersen, O. B., Madsen, T. S., and Falke, J. J. (1997) Intermolecular tuning of calmodulin by target peptides and proteins: differential effects on Ca2+ binding and implications for kinase activation. *Protein science : a publication of the Protein Society* **6**, 794-807
457. Kim, J., Ghosh, S., Liu, H., Tateyama, M., Kass, R. S., and Pitt, G. S. (2004) Calmodulin mediates Ca2+ sensitivity of sodium channels. *The Journal of biological chemistry* **279**, 45004-45012
458. Ahmad, S., Chen, S., Sun, J., and Lin, X. (2003) Connexins 26 and 30 are co-assembled to form gap junctions in the cochlea of mice. *Biochem Biophys Res Commun* **307**, 362-368
459. Kikuchi, T., Kimura, R. S., Paul, D. L., Takasaka, T., and Adams, J. C. (2000) Gap junction systems in the mammalian cochlea. *Brain research. Brain research reviews* **32**, 163-166
460. Stong, B. C., Chang, Q., Ahmad, S., and Lin, X. (2006) A novel mechanism for connexin 26 mutation linked deafness: cell death caused by leaky gap junction hemichannels. *The Laryngoscope* **116**, 2205-2210
461. Gerido, D. A., DeRosa, A. M., Richard, G., and White, T. W. (2007) Aberrant hemichannel properties of Cx26 mutations causing skin disease and deafness. *American journal of physiology. Cell physiology* **293**, C337-345
462. Sanchez, H. A., Mese, G., Srinivas, M., White, T. W., and Verselis, V. K. (2010) Differentially altered Ca2+ regulation and Ca2+ permeability in Cx26 hemichannels formed by the A40V and G45E mutations that cause keratitis ichthyosis deafness syndrome. *The Journal of general physiology* **136**, 47-62
463. Sanchez, H. A., Villone, K., Srinivas, M., and Verselis, V. K. (2013) The D50N mutation and syndromic deafness: altered Cx26 hemichannel properties caused by effects on the pore and intersubunit interactions. *The Journal of general physiology* **142**, 3-22
464. Wang, X., Zhao, K., Kirberger, M., Wong, H., Chen, G., and Yang, J. J. (2010) Analysis and prediction of calcium-binding pockets from apo-protein structures exhibiting calcium-induced localized conformational changes. *Protein science : a publication of the Protein Society* **19**, 1180-1190
465. Sievers, F., and Higgins, D. G. (2014) Clustal omega. *Current protocols in bioinformatics / editoral board, Andreas D. Baxevanis ... [et al.]* **48**, 3 13 11-16
466. Sievers, F., and Higgins, D. G. (2014) Clustal Omega, accurate alignment of very large numbers of sequences. *Methods in molecular biology* **1079**, 105-116
467. Ikemura, T. (1981) Correlation between the abundance of Escherichia coli transfer RNAs and the occurrence of the respective codons in its protein genes: a proposal for a synonymous codon choice that is optimal for the E. coli translational system. *Journal of molecular biology* **151**, 389-409
468. Dong, H., Nilsson, L., and Kurland, C. G. (1996) Co-variation of tRNA abundance and codon usage in Escherichia coli at different growth rates. *Journal of molecular biology* **260**, 649-663
469. Kurland, C., and Gallant, J. (1996) Errors of heterologous protein expression. *Current opinion in biotechnology* **7**, 489-493

470. Ghoshroy, S., Goodenough, D. A., and Sosinsky, G. E. (1995) Preparation, characterization, and structure of half gap junctional layers split with urea and EGTA. *The Journal of membrane biology* **146**, 15-28
471. Manjunath, C. K., Goings, G. E., and Page, E. (1984) Detergent sensitivity and splitting of isolated liver gap junctions. *The Journal of membrane biology* **78**, 147-155
472. Manthey, D., and Willecke, K. (2001) Transfection and expression of exogenous connexins in mammalian cells. *Methods in molecular biology* **154**, 187-199
473. Eckert, R., Dunina-Barkovskaya, A., and Hulser, D. F. (1993) Biophysical characterization of gap-junction channels in HeLa cells. *Pflugers Archiv : European journal of physiology* **424**, 335-342
474. Veenstra, R. D., Wang, H. Z., Westphale, E. M., and Beyer, E. C. (1992) Multiple connexins confer distinct regulatory and conductance properties of gap junctions in developing heart. *Circulation research* **71**, 1277-1283
475. Elfgang, C., Eckert, R., Lichtenberg-Frate, H., Butterweck, A., Traub, O., Klein, R. A., Hulser, D. F., and Willecke, K. (1995) Specific permeability and selective formation of gap junction channels in connexin-transfected HeLa cells. *The Journal of cell biology* **129**, 805-817
476. Lee, J. R., Derosa, A. M., and White, T. W. (2009) Connexin mutations causing skin disease and deafness increase hemichannel activity and cell death when expressed in Xenopus oocytes. *The Journal of investigative dermatology* **129**, 870-878
477. Valiunas, V. (2002) Biophysical properties of connexin-45 gap junction hemichannels studied in vertebrate cells. *The Journal of general physiology* **119**, 147-164
478. Li, H., Liu, T. F., Lazrak, A., Peracchia, C., Goldberg, G. S., Lampe, P. D., and Johnson, R. G. (1996) Properties and regulation of gap junctional hemichannels in the plasma membranes of cultured cells. *The Journal of cell biology* **134**, 1019-1030
479. Dascal, N. (1987) The use of Xenopus oocytes for the study of ion channels. *CRC critical reviews in biochemistry* **22**, 317-387
480. Weber, W. (1999) Ion currents of Xenopus laevis oocytes: state of the art. *Biochimica et biophysica acta* **1421**, 213-233
481. Weber, W. M. (1999) Endogenous ion channels in oocytes of xenopus laevis: recent developments. *The Journal of membrane biology* **170**, 1-12
482. Lee, A. G. (2003) Lipid-protein interactions in biological membranes: a structural perspective. *Biochimica et biophysica acta* **1612**, 1-40
483. Lee, A. G. (2004) How lipids affect the activities of integral membrane proteins. *Biochimica et biophysica acta* **1666**, 62-87
484. Palsdottir, H., and Hunte, C. (2004) Lipids in membrane protein structures. *Biochimica et biophysica acta* **1666**, 2-18
485. Sanderson, J. M. (2005) Peptide-lipid interactions: insights and perspectives. *Organic & biomolecular chemistry* **3**, 201-212
486. Hunte, C., and Richers, S. (2008) Lipids and membrane protein structures. *Current opinion in structural biology* **18**, 406-411
487. Marsh, D. (2008) Protein modulation of lipids, and vice-versa, in membranes. *Biochimica et biophysica acta* **1778**, 1545-1575
488. Locke, D., and Harris, A. L. (2009) Connexin channels and phospholipids: association and modulation. *BMC biology* **7**, 52

489. Nakanishi, S. (1992) Molecular diversity of glutamate receptors and implications for brain function. *Science* **258**, 597-603
490. Pin, J. P., De Colle, C., Bessis, A. S., and Acher, F. (1999) New perspectives for the development of selective metabotropic glutamate receptor ligands. *European journal of pharmacology* **375**, 277-294
491. Pellicciari, R., and Costantino, G. (1999) Metabotropic G-protein-coupled glutamate receptors as therapeutic targets. *Current opinion in chemical biology* **3**, 433-440
492. Hermans, E., and Challiss, R. A. (2001) Structural, signalling and regulatory properties of the group I metabotropic glutamate receptors: prototypic family C G-protein-coupled receptors. *The Biochemical journal* **359**, 465-484
493. Minakami, R., Katsuki, F., Yamamoto, T., Nakamura, K., and Sugiyama, H. (1994) Molecular cloning and the functional expression of two isoforms of human metabotropic glutamate receptor subtype 5. *Biochem Biophys Res Commun* **199**, 1136-1143
494. Sartorius, L. J., Nagappan, G., Lipska, B. K., Lu, B., Sei, Y., Ren-Patterson, R., Li, Z., Weinberger, D. R., and Harrison, P. J. (2006) Alternative splicing of human metabotropic glutamate receptor 3. *Journal of neurochemistry* **96**, 1139-1148
495. Valerio, A., Ferraboli, S., Paterlini, M., Spano, P., and Barlati, S. (2001) Identification of novel alternatively-spliced mRNA isoforms of metabotropic glutamate receptor 6 gene in rat and human retina. *Gene* **262**, 99-106
496. Malherbe, P., Kratzeisen, C., Lundstrom, K., Richards, J. G., Faull, R. L., and Mutel, V. (1999) Cloning and functional expression of alternative spliced variants of the human metabotropic glutamate receptor 8. *Brain research. Molecular brain research* **67**, 201-210
497. Corti, C., Restituito, S., Rimland, J. M., Brabet, I., Corsi, M., Pin, J. P., and Ferraguti, F. (1998) Cloning and characterization of alternative mRNA forms for the rat metabotropic glutamate receptors mGluR7 and mGluR8. *The European journal of neuroscience* **10**, 3629-3641
498. Selkirk, J. V., Price, G. W., Nahorski, S. R., and Challiss, R. A. (2001) Cell type-specific differences in the coupling of recombinant mGlu1alpha receptors to endogenous G protein sub-populations. *Neuropharmacology* **40**, 645-656
499. Bai, M. (1999) Structure and function of the extracellular calcium-sensing receptor (Review). *International journal of molecular medicine* **4**, 115-125
500. Brown, E. M., and MacLeod, R. J. (2001) Extracellular calcium sensing and extracellular calcium signaling. *Physiological reviews* **81**, 239-297
501. Jiang, Y., Huang, Y., Wong, H. C., Zhou, Y., Wang, X., Yang, J., Hall, R. A., Brown, E. M., and Yang, J. J. (2010) Elucidation of a novel extracellular calcium-binding site on metabotropic glutamate receptor 1{alpha} (mGluR1{alpha}) that controls receptor activation. *The Journal of biological chemistry* **285**, 33463-33474
502. Jiang, J. Y., Nagaraju, M., Meyer, R. C., Zhang, L., Hamelberg, D., Hall, R. A., Brown, E. M., Conn, P. J., and Yang, J. J. (2014) Extracellular calcium modulates actions of orthosteric and allosteric ligands on metabotropic glutamate receptor 1alpha. *The Journal of biological chemistry* **289**, 1649-1661
503. Deng, H., Chen, G., Yang, W., and Yang, J. J. (2006) Predicting calcium-binding sites in proteins - a graph theory and geometry approach. *Proteins* **64**, 34-42
504. Thandi, S., Blank, J. L., and Challiss, R. A. (2002) Group-I metabotropic glutamate receptors, mGlu1a and mGlu5a, couple to extracellular signal-regulated kinase (ERK)

activation via distinct, but overlapping, signalling pathways. *Journal of neurochemistry* **83**, 1139-1153
505. Wang, J. Q., Tang, Q., Parelkar, N. K., Liu, Z., Samdani, S., Choe, E. S., Yang, L., and Mao, L. (2004) Glutamate signaling to Ras-MAPK in striatal neurons: mechanisms for inducible gene expression and plasticity. *Molecular neurobiology* **29**, 1-14
506. Mao, L., Yang, L., Tang, Q., Samdani, S., Zhang, G., and Wang, J. Q. (2005) The scaffold protein Homer1b/c links metabotropic glutamate receptor 5 to extracellular signal-regulated protein kinase cascades in neurons. *The Journal of neuroscience : the official journal of the Society for Neuroscience* **25**, 2741-2752
507. Huang, Y., Zhou, Y., Yang, W., Butters, R., Lee, H. W., Li, S., Castiblanco, A., Brown, E. M., and Yang, J. J. (2007) Identification and dissection of Ca(2+)-binding sites in the extracellular domain of Ca(2+)-sensing receptor. *The Journal of biological chemistry* **282**, 19000-19010
508. Brasnjo, G., and Otis, T. S. (2001) Neuronal glutamate transporters control activation of postsynaptic metabotropic glutamate receptors and influence cerebellar long-term depression. *Neuron* **31**, 607-616
509. Nakahara, K., Okada, M., and Nakanishi, S. (1997) The metabotropic glutamate receptor mGluR5 induces calcium oscillations in cultured astrocytes via protein kinase C phosphorylation. *Journal of neurochemistry* **69**, 1467-1475
510. Flint, A. C., Dammerman, R. S., and Kriegstein, A. R. (1999) Endogenous activation of metabotropic glutamate receptors in neocortical development causes neuronal calcium oscillations. *Proceedings of the National Academy of Sciences of the United States of America* **96**, 12144-12149
511. Kawabata, S., Tsutsumi, R., Kohara, A., Yamaguchi, T., Nakanishi, S., and Okada, M. (1996) Control of calcium oscillations by phosphorylation of metabotropic glutamate receptors. *Nature* **383**, 89-92
512. Smedler, E., and Uhlen, P. (2014) Frequency decoding of calcium oscillations. *Biochimica et biophysica acta* **1840**, 964-969
513. Berridge, M. J. (1991) Cytoplasmic calcium oscillations: a two pool model. *Cell calcium* **12**, 63-72
514. Thomas, A. P., Bird, G. S., Hajnoczky, G., Robb-Gaspers, L. D., and Putney, J. W., Jr. (1996) Spatial and temporal aspects of cellular calcium signaling. *FASEB journal : official publication of the Federation of American Societies for Experimental Biology* **10**, 1505-1517
515. Dupont, G., Swillens, S., Clair, C., Tordjmann, T., and Combettes, L. (2000) Hierarchical organization of calcium signals in hepatocytes: from experiments to models. *Biochimica et biophysica acta* **1498**, 134-152
516. Schuster, S., Marhl, M., and Hofer, T. (2002) Modelling of simple and complex calcium oscillations. From single-cell responses to intercellular signalling. *European journal of biochemistry / FEBS* **269**, 1333-1355
517. Grant, M. P., Stepanchick, A., Cavanaugh, A., and Breitwieser, G. E. (2011) Agonist-driven maturation and plasma membrane insertion of calcium-sensing receptors dynamically control signal amplitude. *Science signaling* **4**, 78
518. Permyakov, E. A., and Kretsinger, R. H. (2009) Cell signaling, beyond cytosolic calcium in eukaryotes. *Journal of inorganic biochemistry* **103**, 77-86

519. Kubo, Y., Miyashita, T., and Murata, Y. (1998) Structural basis for a Ca^{2+}-sensing function of the metabotropic glutamate receptors. *Science.* **279**, 1722-1725
520. Conigrave, A. D., Quinn, S. J., and Brown, E. M. (2000) L-amino acid sensing by the extracellular Ca^{2+}-sensing receptor. *Proceedings of the National Academy of Sciences of the United States of America* **97**, 4814-4819
521. Huang, C., and Miller, R. T. (2007) The calcium-sensing receptor and its interacting proteins. *J Cell Mol Med.* **11**, 923-934
522. Zhang, C., Huang, Y., Jiang, Y., Mulpuri, N., Wei, L., Hamelberg, D., Brown, E. M., and Yang, J. J. (2014) Identification of an L-phenylalanine binding site enhancing the cooperative responses of the calcium-sensing receptor to calcium. *J. Biol. Chem.* **289**, 5296-5309
523. Lundgren, S., Hjalm, G., Hellman, P., Ek, B., Juhlin, C., Rastad, J., Klareskog, L., Akerstrom, G., and Rask, L. (1994) A protein involved in calcium sensing of the human parathyroid and placental cytotrophoblast cells belongs to the LDL-receptor protein superfamily. *Experimental cell research* **212**, 344-350
524. Cima, R. R., Cheng, I., Klingensmith, M. E., Chattopadhyay, N., Kifor, O., Hebert, S. C., Brown, E. M., and Soybel, D. I. (1997) Identification and functional assay of an extracellular calcium-sensing receptor in Necturus gastric mucosa. *The American journal of physiology* **273**, G1051-1060
525. Hinson, T. K., Damodaran, T. V., Chen, J., Zhang, X., Qumsiyeh, M. B., Seldin, M. F., and Quarles, L. D. (1997) Identification of putative transmembrane receptor sequences homologous to the calcium-sensing G-protein-coupled receptor. *Genomics* **45**, 279-289
526. Kovacs, C. S., Ho-Pao, C. L., Hunzelman, J. L., Lanske, B., Fox, J., Seidman, J. G., Seidman, C. E., and Kronenberg, H. M. (1998) Regulation of murine fetal-placental calcium metabolism by the calcium-sensing receptor. *The Journal of clinical investigation* **101**, 2812-2820
527. Chattopadhyay, N., Ye, C. P., Yamaguchi, T., Kerner, R., Vassilev, P. M., and Brown, E. M. (1999) Extracellular calcium-sensing receptor induces cellular proliferation and activation of a nonselective cation channel in U373 human astrocytoma cells. *Brain research* **851**, 116-124
528. Mathias, R. S., Mathews, C. H., Machule, C., Gao, D., Li, W., and Denbesten, P. K. (2001) Identification of the calcium-sensing receptor in the developing tooth organ. *Journal of bone and mineral research : the official journal of the American Society for Bone and Mineral Research* **16**, 2238-2244
529. Hofer, A. M., and Brown, E. M. (2003) Extracellular calcium sensing and signalling. *Nature reviews. Molecular cell biology* **4**, 530-538
530. Chang, W., and Shoback, D. (2004) Extracellular Ca2+-sensing receptors--an overview. *Cell calcium* **35**, 183-196
531. Fudge, N. J., and Kovacs, C. S. (2004) Physiological studies in heterozygous calcium sensing receptor (CaSR) gene-ablated mice confirm that the CaSR regulates calcitonin release in vivo. *BMC physiology* **4**, 5
532. Hofer, A. M., Gerbino, A., Caroppo, R., and Curci, S. (2004) The extracellular calcium-sensing receptor and cell-cell signaling in epithelia. *Cell calcium* **35**, 297-306
533. Hebert, S. C. (1996) Extracellular calcium-sensing receptor: implications for calcium and magnesium handling in the kidney. *Kidney international* **50**, 2129-2139

534. Bapty, B. W., Dai, L. J., Ritchie, G., Jirik, F., Canaff, L., Hendy, G. N., and Quamme, G. A. (1998) Extracellular $Mg^{2(+)}$- and $Ca^{2(+)}$-sensing in mouse distal convoluted tubule cells. *Kidney Int.* **53**, 583-592
535. Magno, A. L., Ward, B. K., and Ratajczak, T. (2011) The calcium-sensing receptor: a molecular perspective. *Endocrine reviews* **32**, 3-30
536. Hofer, A. M., and Brown, E. M. (2003) Extracellular calcium sensing and signalling. *Nat. Rev. Mol. Cell Biol.* **4**, 530-538
537. Ray, K., Hauschild, B. C., Steinbach, P. J., Goldsmith, P. K., Hauache, O., and Spiegel, A. M. (1999) Identification of the cysteine residues in the amino-terminal extracellular domain of the human $Ca^{(2+)}$ receptor critical for dimerization. Implications for function of monomeric $Ca^{(2+)}$ receptor. *J. Biol. Chem.* **274**, 27642-27650
538. Suzuki, Y., Moriyoshi, E., Tsuchiya, D., and Jingami, H. (2004) Negative cooperativity of glutamate binding in the dimeric metabotropic glutamate receptor subtype 1. *J. Biol. Chem.* **279**, 35526-35534
539. Pidasheva, S., D'Souza-Li, L., Canaff, L., Cole, D. E., and Hendy, G. N. (2004) CASRdb: calcium-sensing receptor locus-specific database for mutations causing familial (benign) hypocalciuric hypercalcemia, neonatal severe hyperparathyroidism, and autosomal dominant hypocalcemia. *Human mutation* **24**, 107-111
540. Conigrave, A. D., Franks, A. H., Brown, E. M., and Quinn, S. J. (2002) L-amino acid sensing by the calcium-sensing receptor: a general mechanism for coupling protein and calcium metabolism? *European journal of clinical nutrition* **56**, 1072-1080
541. Zhang, Z., Qiu, W., Quinn, S. J., Conigrave, A. D., Brown, E. M., and Bai, M. (2002) Three adjacent serines in the extracellular domains of the CaR are required for L-amino acid-mediated potentiation of receptor function. *The Journal of biological chemistry* **277**, 33727-33735
542. Bai, M. (2004) Structure-function relationship of the extracellular calcium-sensing receptor. *Cell calcium* **35**, 197-207
543. Conigrave, A. D., and Lok, H. C. (2004) Activation of renal calcium and water excretion by novel physiological and pharmacological activators of the calcium-sensing receptor. *Clinical and experimental pharmacology & physiology* **31**, 368-371
544. Mun, H. C., Franks, A. H., Culverston, E. L., Krapcho, K., Nemeth, E. F., and Conigrave, A. D. (2004) The Venus Fly Trap domain of the extracellular Ca2+ -sensing receptor is required for L-amino acid sensing. *The Journal of biological chemistry* **279**, 51739-51744
545. Herraiz, T., Galisteo, J., and Chamorro, C. (2003) L-tryptophan reacts with naturally occurring and food-occurring phenolic aldehydes to give phenolic tetrahydro-beta-carboline alkaloids: activity as antioxidants and free radical scavengers. *J. Agric. Food Chem.* **51**, 2168-2173
546. Brauner-Osborne, H., Jensen, A. A., Sheppard, P. O., O'Hara, P., and Krogsgaard-Larsen, P. (1999) The agonist-binding domain of the calcium-sensing receptor is located at the amino-terminal domain. *The Journal of biological chemistry* **274**, 18382-18386
547. Ward, D. T. (2004) Calcium receptor-mediated intracellular signalling. *Cell calcium* **35**, 217-228
548. Chen, C. J., Barnett, J. V., Congo, D. A., and Brown, E. M. (1989) Divalent cations suppress 3',5'-adenosine monophosphate accumulation by stimulating a pertussis toxin-

sensitive guanine nucleotide-binding protein in cultured bovine parathyroid cells. *Endocrinology* **124**, 233-239
549. Kifor, O., Diaz, R., Butters, R., and Brown, E. M. (1997) The Ca2+-sensing receptor (CaR) activates phospholipases C, A2, and D in bovine parathyroid and CaR-transfected, human embryonic kidney (HEK293) cells. *Journal of bone and mineral research : the official journal of the American Society for Bone and Mineral Research* **12**, 715-725
550. Huang, C., Hujer, K. M., Wu, Z., and Miller, R. T. (2004) The Ca2+-sensing receptor couples to Galpha12/13 to activate phospholipase D in Madin-Darby canine kidney cells. *American journal of physiology. Cell physiology* **286**, C22-30
551. Kifor, O., MacLeod, R. J., Diaz, R., Bai, M., Yamaguchi, T., Yao, T., Kifor, I., and Brown, E. M. (2001) Regulation of MAP kinase by calcium-sensing receptor in bovine parathyroid and CaR-transfected HEK293 cells. *American journal of physiology. Renal physiology* **280**, F291-302
552. Zhang, C., Mulpuri, N., Hannan, F. M., Nesbit, M. A., Thakker, R. V., Hamelberg, D., Brown, E. M., and Yang, J. J. (2014) Role of Ca2+ and L-Phe in regulating functional cooperativity of disease-associated "toggle" calcium-sensing receptor mutations. *PloS one* **9**, e113622
553. Wang, M., Yao, Y., Kuang, D., and Hampson, D. R. (2006) Activation of family C G-protein-coupled receptors by the tripeptide glutathione. *The Journal of biological chemistry* **281**, 8864-8870
554. Hannan, F. M., Nesbit, M. A., Zhang, C., Cranston, T., Curley, A. J., Harding, B., Fratter, C., Rust, N., Christie, P. T., Turner, J. J., Lemos, M. C., Bowl, M. R., Bouillon, R., Brain, C., Bridges, N., Burren, C., Connell, J. M., Jung, H., Marks, E., McCredie, D., Mughal, Z., Rodda, C., Tollefsen, S., Brown, E. M., Yang, J. J., and Thakker, R. V. (2012) Identification of 70 calcium-sensing receptor mutations in hyper- and hypo-calcaemic patients: evidence for clustering of extracellular domain mutations at calcium-binding sites. *Human molecular genetics* **21**, 2768-2778
555. Hannan, F. M., and Thakker, R. V. (2013) Calcium-sensing receptor (CaSR) mutations and disorders of calcium, electrolyte and water metabolism. *Best practice & research. Clinical endocrinology & metabolism* **27**, 359-371
556. Silve, C., Petrel, C., Leroy, C., Bruel, H., Mallet, E., Rognan, D., and Ruat, M. (2005) Delineating a Ca2+ binding pocket within the Venus Flytrap Module of the human calcium-sensing receptor. *J. Biol. Chem.* **280**, 37917-37923
557. Quinn, S. J., Bai, M., and Brown, E. M. (2004) pH Sensing by the calcium-sensing receptor. *J. Biol. Chem.* **279**, 37241-37249
558. Yang, W., Lee, H. W., Hellinga, H., and Yang, J. J. (2002) Structural analysis, identification, and design of calcium-binding sites in proteins. *Proteins* **47**, 344-356
559. Minami, H., Yoshida, T., Okutsu, K., Zhang, Q., Inoue, S., and Atsuya, I. (2001) Direct determination of silicon in powdered aluminium oxide by use of slurry sampling with in situ fusion graphite-furnace atomic-absorption spectrometry. *Fresenius J. Anal. Chem.* **370**, 855-859
560. Smith, G. E., Summers, M. D., and Fraser, M. J. (1983) Production of human beta interferon in insect cells infected with a baculovirus expression vector. *Molecular and cellular biology* **3**, 2156-2165
561. Jehle, J. A., Blissard, G. W., Bonning, B. C., Cory, J. S., Herniou, E. A., Rohrmann, G. F., Theilmann, D. A., Thiem, S. M., and Vlak, J. M. (2006) On the classification and

nomenclature of baculoviruses: a proposal for revision. *Archives of virology* **151**, 1257-1266

562. Blissard, G. W., and Rohrmann, G. F. (1990) Baculovirus diversity and molecular biology. *Annual review of entomology* **35**, 127-155

APPENDICES

Appendix A: Expression of mCx26 using Bac-to-Bac baculovirus expression system

Appendix A.1 Introduction

The baculovirus-insect cell expression system is widely used in and has proven successfully for production of many recombinant proteins, since when it was first described in the early 1980s (560). Baculovirus is a rod-shaped and enveloped virus, which can infect insect cells and replicate in the nucleus of insect cells (**Fig. A.1**). Two virion phenotypes have been found in most baculovirus. They are the budded virions and occlusion-derived virions (561). Occlusion-derived virions are occluded as occlusion body and ensure the survival of the virus in the external environment. In the alkaline environment, the protein matrix of occlusion body will be lysated and virus particles inside will initiate the infection of the insect host midgut cells. Virus will fulfill its replication in the host nucleus by taking control of the gene expression machinery. In the late infection stage, newborn virus are released from the cell via budding through the plasma membrane to infect other cells. In the very late stage, the coat protein polyhedron, a component of viral envelop to protect virus from dangerous environment, is the predominant protein that largely expressed-more than 50% virus protein are polyhedron. This polyhedron gene is non-essential gene. Without it, virus can still successfully infect the insect cells and finish the replication in the host cells. The Bac-to-Bac baculovirus expression system takes the advantage of this point and replaces the polyhedron gene with our target gene. Under the control of polyhedrin protomer, the foreign gene will be expressed in large scale. Besides, it has high potential of eukaryotic protein processing capability, like post-translational modifications, including folding, disulfide bond formation, oligomerization, glycosylation, acylation, and proteolytic cleavage and so on. In most cases, the recombinant protein is soluble. Inclusion body is hardly seen, while it frequently occurs

in the bacterial expression. In addition, expression of hetero-oligomeric protein complexes can be easily achieved by simultaneously infecting insect cell with two or more virus containing different target genes or with recombinant viruses containing two or more expression cassettes. Which is also appealing is that insect cell does not need CO_2 to grow, which is different from mammalian cells. They are also anchorage independent and can be readily adapted to high-density suspension culture for large-scale expression. Last, baculovirus have a restricted host range, limited to specific invertebrate species. They are safer to work with than most mammalian viruses since they are noninfectious to vertebrates. A comparison between baculovirus expression systems and others were compared in the following table (**Fig. A.2**). The combination of all these merits makes this expression system is popularly used to express more than 1000 eukaryotic, prokaryotic and viral recombinant proteins.

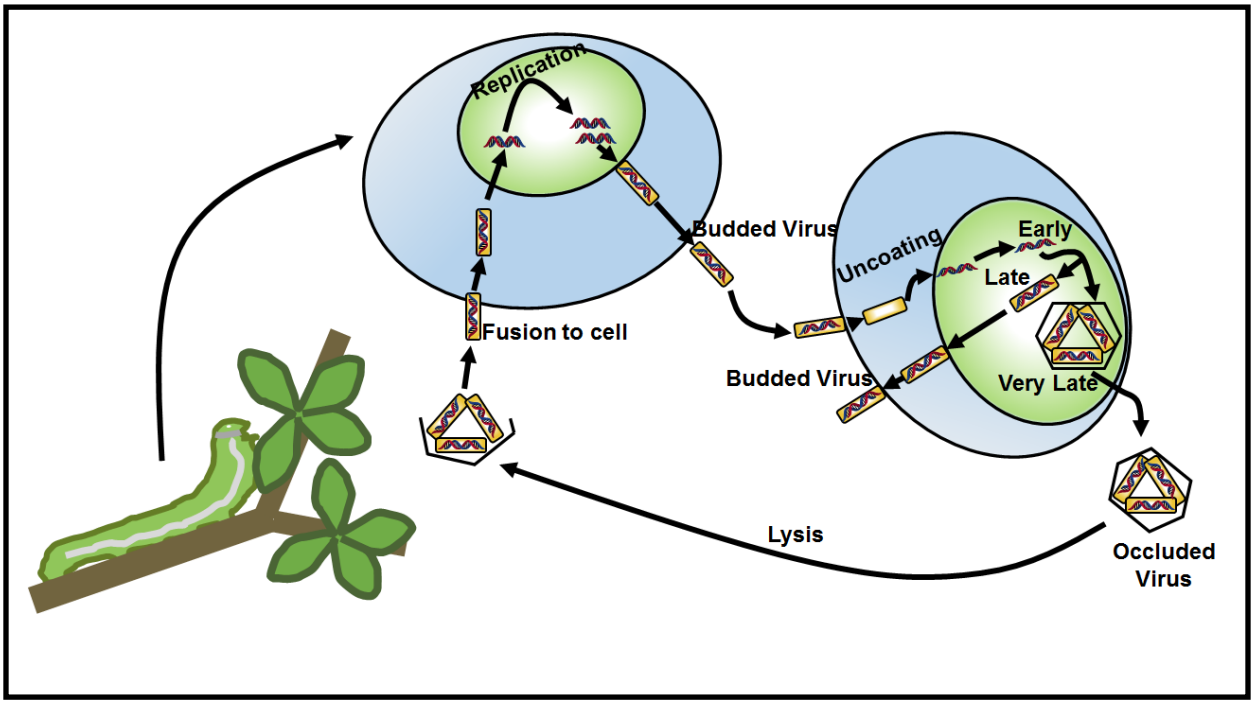

Figure A. 1 The replication cycle of baculovirus.

Occlusion bodies ingested by an insect dissolve in the midgut, and occlusion bodies are released which then infect midgut epithelial cells, in which baculovirus utilize the replication machinery of epithelial cells to generate copy of themselves. Those virus were budded out of the cell in a basal direction and initiate a systemic infection. In the early stage of infection, more rod virus were budded out, spreading the infection through surrounding insects. In the late stage of virus infection, occluded virus were produced, which cause the cell lysis and virus releases as occlusion bodies (562).

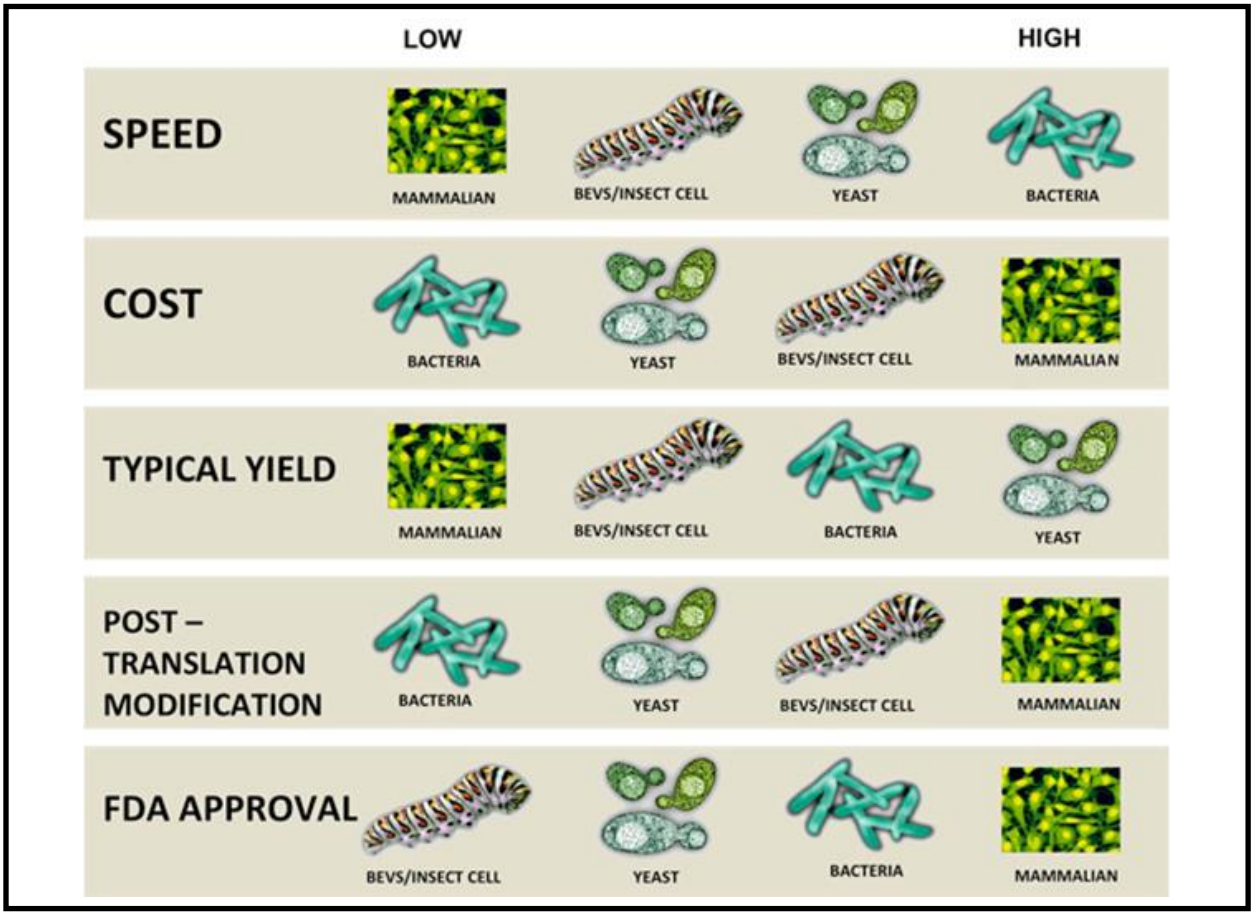

Figure A. 2 Expression system comparison.

Mammalian, insect cell, yeast and bacteria expression systems were compared in term of expression speed, cost, typical yield, post-translation medication and the chance of drug produced by those systems be approved by FDA.

Appendix A.2 Methods

Generating the recombinant pFastBac^{TM} vector

Mouse Cx26 gene was amplified by PCR using the mouse Cx26 DNA in pcDNA6/V5-His (A) vector (a gift from Dr. Eric Lin, Emory University, GA) as template with Bam H I and Hind III restriction sites added at the 5' and 3' ends and ligated into the modified Baculovirus donor plasmid pFastBac HT A vector (with C-terminal his tag). The mouse Cx26 gene was sequenced by GENEWIZ.

Generating the recombinant bacmid

The recombinant donor plasmid with inserted mouse Cx26 gene was transformed into DH10Bac competent cell. In brief, DH10Bac competent cells were gently mixed with around 1 ng of pFastBac HT A recombinant plasmid and placed on ice for 30 minutes before proceeding to 45-second heat shock at 42 ^{o}C. The mixture then was immediately transferred to ice and chilled for 2 minutes. Next, around 900 ml of room temperature S.O.C medium was added into the tube, which was subjected to 4-hour shaking at 37 ^{o}C with a speed of 225 rpm. The *E.coli* culture was diluted for 10, 100 and 1000 times, respectively. Around 100 μl dilutions were plated on LB agar plates containing 50 μg/ml kanamycin, 7 μg/ml gentamicin, 10 μg/ml tetracycline, 100 μg/ml X-gal, and 40 μg/ml IPTG. After 48-hour incubation at 37 ^{o}C, white colonies were picked up for further analysis.

Analyzing the recombinant bacmid

White colonies were picked up from the agar plate and inoculated into 5 ml of LB medium. Next day morning, recombinant bacmid extracted from *E.coli* were used as PCR template. pUC/M13 forward and reverse primers (forward: 5'-CCCAGTCACGACGTTGTAAAACG-3'; reverse: 5'-AGCGGATAACAATTTCACACAGG-3') which hybridize to sites flanking the mini-attTn7 site within the lacZ-complementation region is used to facilitate PCR analysis.

Cationic Liposome-Mediated Transfection Using Cellfectin II Reagent

Transfection of recombinant bacmid into insect cell Sf9 was achieved by following the instructions of Cellfectin II (Invitrogen). In general, to start with, Sf9 cells in Grace's medium with a density of 2x106 were seeded into 30 mm petri dish. Eight microliter Cellfectin II reagent was diluted in 100 µl unsupplemented Grace's medium without serum and antibiotics. Two micrograms of recombinant bacmid was diluted in 100 µl Grace's medium and then gently mixed with diluted Cellfectin. The mixture was incubated at room temperature for 20-30 minutes and added into Sf9 cells drop by drop. After 3-5 hours, the transfection mixture was removed and replaced with 2 ml of complete growth medium with 5% serum.

Virus plaque assay

To determine the infectious potency of the virus generated, virus plaque assay is performed to count the plaque formations in an immobilized monolayer culture to estimate the virus titer, which is a term used in virology to define the virus infectious efficiency (**Fig. A.3**). Firstly, Sf9 cells were seeded into 6-well plates with $1x10^6$ cells per 2 ml per well and allowed to attach for at least 1 hour. Overnight-seeding is also preferred. To remove the old medium from each well, the plate was tilted and medium was carefully sucked out along the side wall of dish. Serial dilutions (from 10^{-1} to 10^{-8}) of virus were diluted using culture medium containing 5% serum and 1 ml of

each dilutions were added into each well. One milliliter of culture medium instead of virus dilution was added to one well as a negative control. After 1-hour incubation, solution in each well was removed and replaced by 2 ml of 1% agarose overlay. Before adding 0.5 ml of fresh medium on top of the agarose, we allowed the agarose to solidify for 10-15 minutes in the incubator. After 4-5 days incubation in the 27 ^{o}C humidified incubator, 1 ml of 0.03% neutral red was applied to each well and incubated for 3 hours at room temperature. Then, the stain was removed from each well by suction and the plates which were covered by aluminum foil first and leaved upper side down for overnight at room temperature. Second day morning, we counted the plaques and calculated the titers using the following equation. The unit of titer is pfu/ml.

Number of Plaques / (Dilution factor x Volume of diluted virus/well) = pfu/ml

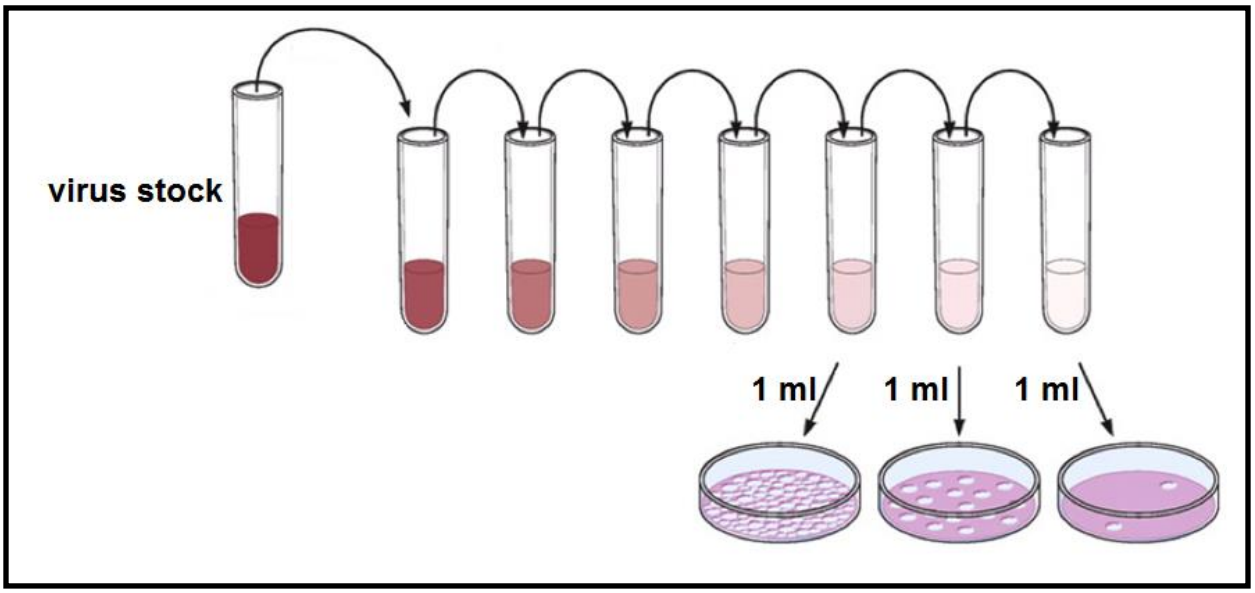

Figure A. 3 Plaque assay.

Series virus dilutions (10^{-1} to 10^{-8}) were prepared by mixing 0.1 ml of virus stock with 0.9 ml of fresh medium containing 5 % serum and applied to each dish to infect monolayer Sf9 cells. After 3-day infection, neutral red was applied to aid the visualization of plaque. Virus

plaques displayed as white dots on the red background. When count the plaques, dish with moderate amount of plaques was chose to gain more accurate titer.

Amplifying the baculovirus stock

To amplify the baculovirus, we used P1 viral stock to infect insect cell Sf9 twice to obtain baculovirus with higher titer. In brief, insect cells were seeded in 30 mm dish for 1 hour to allow attachment before infection. We inspected cells under an inverted microscope to verify attachment each time. Then appropriate amount of P1 viral stock was added to each dish to keep the multiplicity of infection value (MOI) between 0.1-0.5. MOI was calculated based on the following equation.

MOI = (volume of virus) (dilution) (number of plaques) / (total volume * cells / ml)

Optimizing heterologous protein production

To achieve the maximum expression of heterologous protein in Sf9, we optimized the infection time and MOI. We firstly performed a time course study to determine the point of maximum expression. Then different MOIs were used to determine which one could achieve the synchronous infection, which is defined as the infection of all cells in a culture at the same time point. The protein expression was compared using western blotting when different MOI or expression time were used.

Large scale recombinant protein expression

Suspension cells cultured in serum free Sf900 medium were first cultured to reach a density of $2x10^6$ and then infected by addition of proper amount of baculovirus. After 3-day infection, cells were sedimented down by centrifugation at 6x1000 rpm for 5 minutes at 4 ^oC. Pellet were frozen at -80 ^oC for further purification.

Appendix A.3 Results

Generation of recombinant bacmid

The recombinant pFastBac^{TM} H TA plasmid contains two arms of Tn7 transposon: Tn7L and Tn7R. When it is transformed into the competent cell DH10Bac^{TM} E.coli, which contains the virus bacmid with Tn7 target sequence miniattTn7, the DNA fragment between left arm and right Tn7 arm will be cleaved and integrated into the miniattTn7 sequence in the bacmid under the help of transposonase. This enzyme is coded by another relatively smaller plasmid in the competent cell. Once the transition is successful, the lac Z gene inside of the miniattTn7 sequence will be deleted. When we streak the transformed competent cell on the LB plates with antibiotics, IPTG and X-gal, colonies without lac Z gene will show white color, indicating successful recombinant bacmid generation. Twelve white colonies were picked up and re-streaked on 12 LB plates with antibiotics, IPTG and X-gal, no blue colonies show up again in all plates. To further verify the recombinant bacmid, 1 single colony from each plate were picked up and cultured in 5 ml LB medium overnight. Recombinant bacmid were extracted using of HiPure kits (Invitrogen). Target gene in recombinant bacmid was amplified by PCR. The bacmid contains M13 forward and M13 reverse priming sites flanking the min-attTn7 site within the lac Z complementation region to facilitate PCR analysis. The size of PCR product was around 3 kbp, which was the sum of target gene and the DNA fragment between two priming sites. The sequence of PCR product was also checked. As shown in figure A.3, PCR product sequence matched mCx26 gene well.

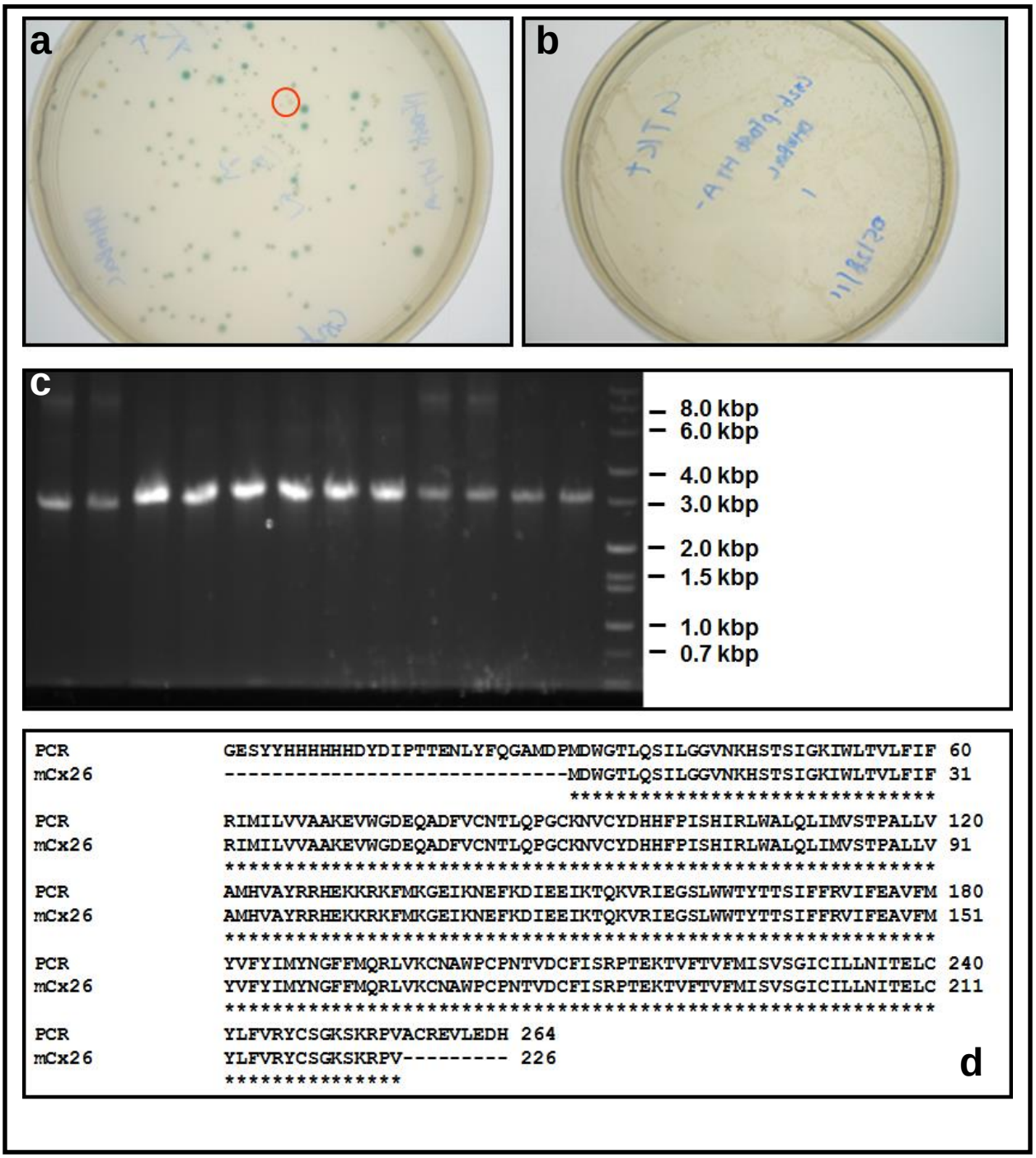

Figure A. 4 Generation of recombinant bacmid.

(a) Transformation of recombinant donor plasmid into DH10Bac competent cell. White color of colonies grown on LB plates with IPTG, antibiotics and X-gal indicated the successful insertion

of target gene into bacmid. On the contrary, blue colonies had the complete Lac Z gene without insertion. (b) White colonies were re-steaked on LB plates to avoid fake colony. (c) Target gene was amplified by PCR using the bacmid extracted from white colony as template, and M13 forward and reverse primers. The PCR product was separated by DNA gel. (d) PCR product was also sent for sequencing in GENEWIZ. The sequence result was aligned with DNA of mouse Cx26.

Generation of P1 baculovirus

Pure recombinant bacmid was transfected into Sf9 cells using CellFectin II reagent. Virus infected cells always display the following characteristics (Table A.1) as observed from virus inspection using an inverted microscope at 250-400 magnification. These characteristics at different time points provide us the criterion for determination the stages of virus generation. During the first two days, the difference between transfected cells and negative control cells were not very clear. Only when cells were checked under microscope with 40 times magnification, very few swollen cells, termed as “CPE”, could be distinguished in the transfected cells. On the third day of post-transfection, significant differences were revealed by the microscope in terms of cell number, cell size and shape (Fig. A.4). Negative control cells (Fig. A.4a) had regular round shape and uniform size. Compared with the transfected cells (Fig. A.4b), cell confluence is much higher, about 90%. The diameters of cells with transfection greatly increased, some even doubled, which was caused by generation of virus particles inside of Sf9 cells. Cells debris also spread in the dish with transfection and some small vesicles were around the surface of transfected cells. Those bubbles were filled with virus particles inside. Once the cell plasma membrane was liquefied by the virus lyase, these inclusion bodies were released. The adjacent cells would be infected by newborn virus to produce more virons. Once 70 % host cells detached the bottom of plates, viruses were harvested by centrifugation at 500 g for 5 minutes at 4 ^{o}C. Longer expression would lead to

loss of infection capability due to exposure of virus under the attacks of enzymes released from cells liquefied. Cx26 expression was examined by western blotting (Fig. A.4c).

Table A. 1 Characteristics of baculovirus infection.

Signs of Infection	Phenotype	Description
Early (first 24 hours)	Increased cell diameter	A 25-50% increase in cell diameter may be seen
	Increased size of cell nuclei	Nuclei may appear to "fill" the cells
Late (24-72 hours)	Cessation of cell growth	Cells appear to stop growing when compared to a cell-only control
	Granular appearance	Signs of viral budding, vesicular appearance to cells
	Detachment	Cells release from the plate or flask
Very late (> 72 hours)	Cell lysis	Cells appear lysed, and show signs of clearing in the monolayer

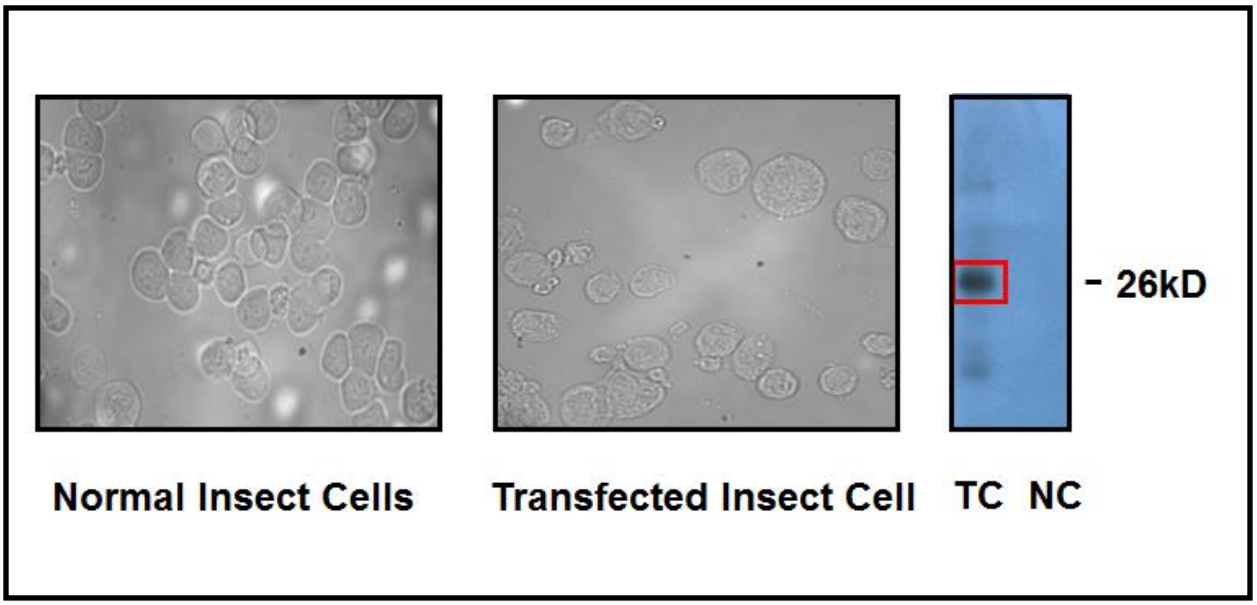

Figure A. 5 P1 virus generation.

(a) Non-transfected Sf9 cell were served as negative control. (b) Cells with bacmid transfection displayed large cell size, less cell confluence, and lots of cell debris. (c) Cx26 expression was detected in transfected cells using western blotting.

The dead cell was stained by 0.4% Trypan blue, which is a vital stain used to selectively color dead cells blue. Trypan blue is not cell membrane permeable and live cells won't absorb it, however, it can cross the plasma membrane in a dead cell. The cell death rate was calculated based on the dead cell number and total cell number. After 3-day post-transfection, the death rate was almost 3-fold higher than non-transfected cells (**Table A.2**).

Table A. 2 Cell death rate comparison between non-transfected and transfected cells.

	Total cell /ml	**Viable cell /ml**	**Dead cell /ml**	**Death rate**
Non-transfected cell	$3.1x10^6$	$2.4x10^6$	$7.4x10^5$	23.9%
Transfected cell	$1.2x10^6$	$1.0x10^5$	$1.1x10^6$	91.7%

Determination of viral titer by plaque assay

Before the viral stock is used to infect the insect cells, the viral plaque assay is recommended to determine the titer of baculovirus stock. Titer is a very important parameter to estimate the quality of virus. During the expression, the amount of virus added into the insect cell is a key factor that can influence the expression level. If there are too many virus particles per cell, the host cell cannot put up with them and will die immediately even without expression of the

virus proteins. While if the virus amount applied is too little, the yield of protein will be low. Thus appropriate amount of virus is indispensable for protein expression. Here the viral plaque assay can determine the viral infection efficiency and provides important data for following experiments.

A number of factors can influence the viral titer: 1) the size of your gene of interest. Generally titers will decrease as the size of the insert increases; 2) transfection efficiency. Higher transfection efficiency will dramatically increase the titer. For the highest efficiency, Cellfection reagent and unsupplemented Grace's insect medium are recommended. Since the unsupplemented medium does not contain antibiotics and serum which will interfere the transfection by interacting with transfection reagent; 3) the age of your baculoviral stock. Viral titer may decrease with long-term storage at 4 ^{o}C or -80 ^{o}C. If the baculoviral stock has been stored for 6 months to 1 year, re-titering is recommended prior to use in an expression experiment; 4) number of freeze/thaw cycle. If you are storing your virus at -80 ^{o}C, viral titer can decrease as much as 10% with each freeze/thaw cycle; 5) improper storage of your baculoviral stock. For routine use, baculoviral stocks should be aliquoted and stored at 4 ^{o}C, protected from light.

For the plaque assay experiment, there are some mistakes usually happening to beginners. The common one is using the wrong agarose, like agarose for DNA gel. Agarose for plaque assay is a kind of low melting gel, while agarose for DNA gel can harden quickly. When you placing the agarose layer over the cells, low melting gels can give you enough time to evenly put it on the cells. The second is that cell confluence is either too high or too low. For successful viral plaque assay, monolayer is required. In addition, the humidity of the incubator is of great importance. If there is no water bath inside the incubator, long-time incubation will lead to shrinking of the agarose layer. To avoid, an alternative way is to put 1 ml fresh medium above the agarose layer. But this way usually is more likely to cause contamination.

When infected by baculovirus, Sf9 was liquefied at the late stage, leading to empty area without cells on the Sf9 monolayer. Upon application of neutral red, those areas were not stained by this red dye, while the rest area with cells absorbed red dye and presented as red background (Fig. A.6). We amplified the P1 virus twice since the titer of P1 virus was not high enough (5 x 10^5) for recombinant protein expression. After amplification, P3 virus titer reached 10^8 range which could be used for efficient infection during protein expression.

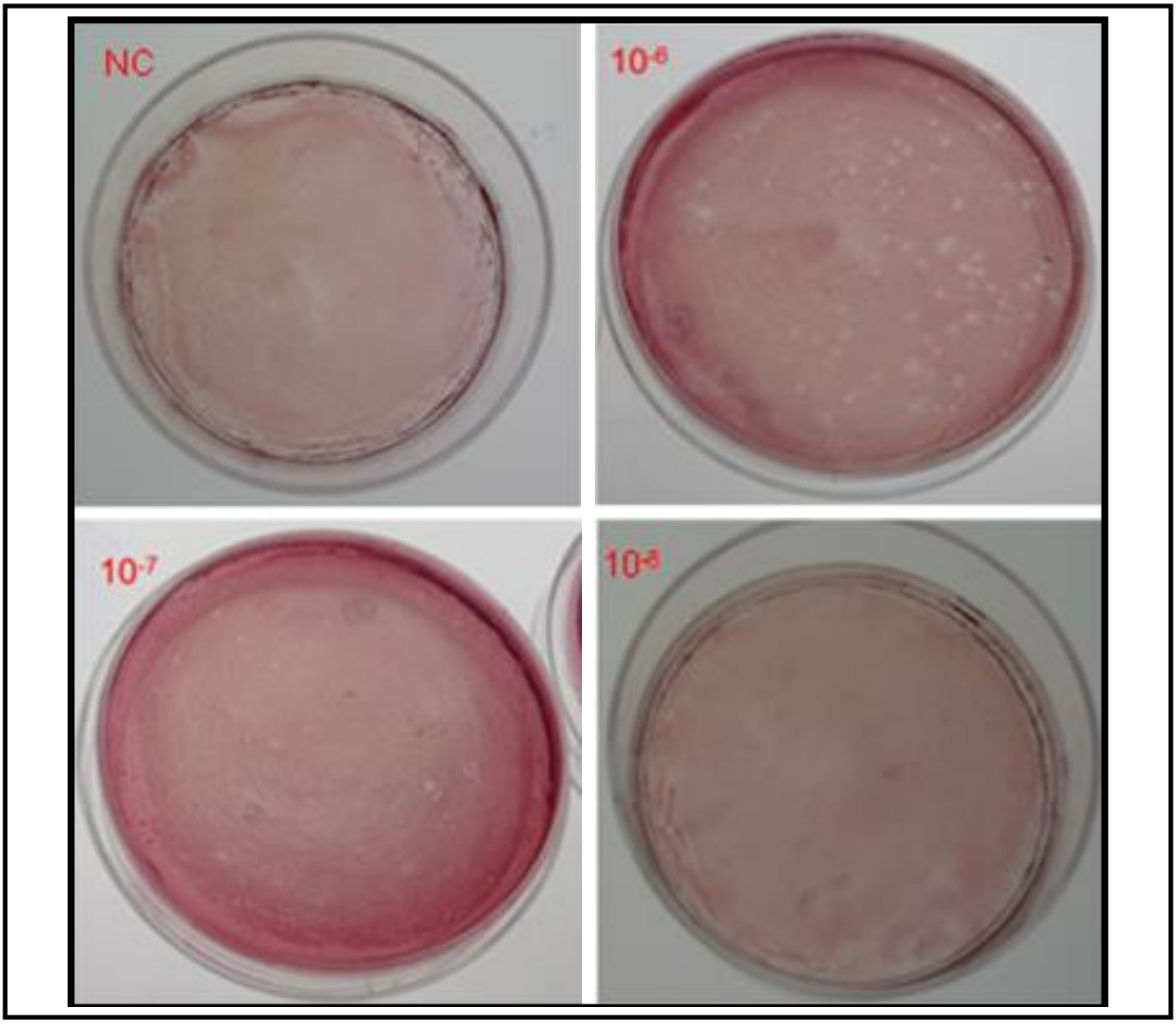

Figure A. 6 P1 virus titer determination by plaque assay.

Four dishes were presented here to illustrate what does plaques look like after neutral red staining. The first dish labeled as NC was negative control cells without addition of P1 virus. Second dish labeled with the dilution factor 10^{-6} was cells infected by virus with 10^{6} times dilution. This dish was chose for titer calculation since virus with 10^{7} times dilution did not generate enough plaques, while cells infected by virus with 10^{5} dilution produced excessive plaques which could not be distinguished clearly from each other.

Expression optimization

A number of factors can influence determination of optimal expression conditions including the cell line, MOI, application of interest, and the nature of gene of interest. Here we would perform the MOI and time course to determine the optimal conditions to use to express the recombinant protein of interest.

As discussed before, MOI is a key factor affecting protein expression. Different from generation of virus, in which 0.05-0.1 MOI is applied, a wide range of MOIs can be tested to determine which will induce the best kinetics of infection for maximum protein expression. An MOI of 1-20 is generally recommended for protein expression. Higher MOIs are preferable because they result in synchronous infection where all the cells become infected at time zero. As a result, theoretically all cells should be expressing protein at the same time so that the maximal amount of recombinant protein can be harvested at a given time point. Lower MOIs may result in only a small portion of the cell population being infected, while the rest of the cells continue to divide. These cells in turn become infected later on when the first group cells lyse. This results in a protein expression curve that is spread out over the time course, rather than peaking at a given

time point. Then the MOI that provides the optimal level of recombinant protein expression is used. Here I showed one example when I compared two different MOIs: 1 and 7 to have a rough estimation of the optimal MOI range. By analyzing the protein level in Sf9 cells by western blotting, we could concluded that 1 had a higher protein yield compared with 7 (**Fig. A.7**).

Time points taken at 24 hours intervals are recommended initially to get a general idea of when your protein is being expressed. Once we have determined a time frame where optimal protein expression occurs, we can perform a second time course with selected intermediate time points. This will allow us to further optimize our expression levels. In the initial phases of expression, when we are attempting to determine the optimal conditions for maximal expression, we should not rely only on SDS-PAGE analysis for detection of protein. Levels may be suboptimal and other more sensitive assays may be necessary. In my experiments, western blotting was used for determination of recombinant protein expression. I collected at different time points, 12, 24, 48, 72, and 84 hours and analyzed the yield of my protein by western blotting. As figure A.7 shows, the production at 72 hours is the most among all time points.

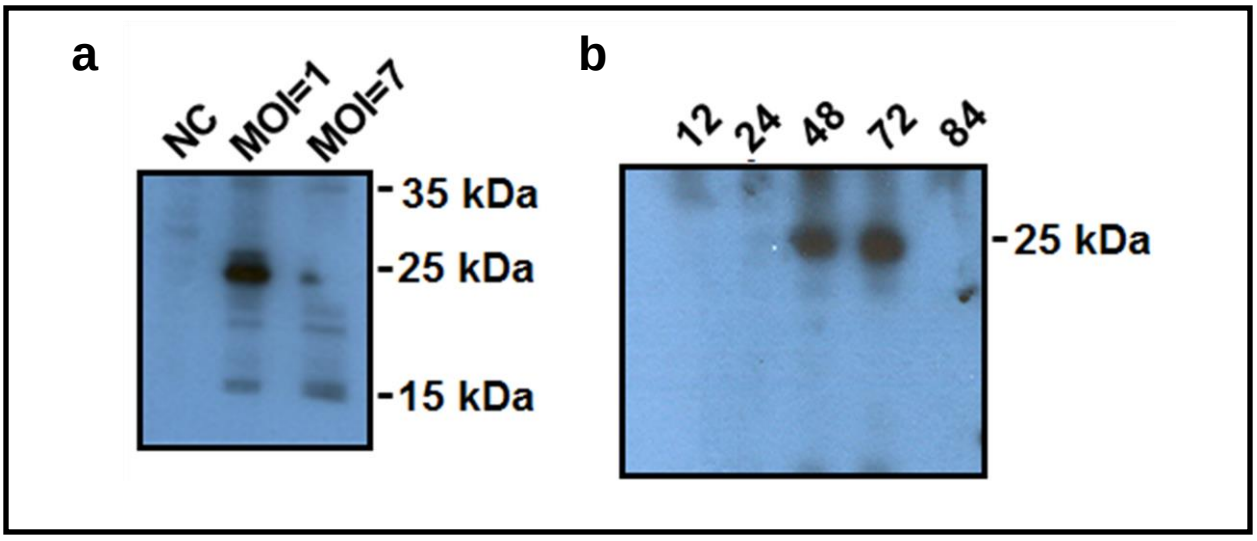

Figure A. 7 mCx26 expression optimization.

(a) Protein expression using MOI of 1 and 7. NC is the negative control cells. 1 and 7 stand for different MOIs. (b) Time course for expression of recombinant protein. In both experiment, western blotting was used to analyze the mCx26 expression level.

Large scale mCx26 expression in Sf9

Suspension Sf9 cell were infected by P3 virus for large scale expression of mCx26. Serum free medium was utilized for cell culture to simply purification work. The location of mCx26 expressed in Sf9 was checked by immunostaining (Fig. A.8). mCx26 were successfully translocated on the cell surface of Sf9.

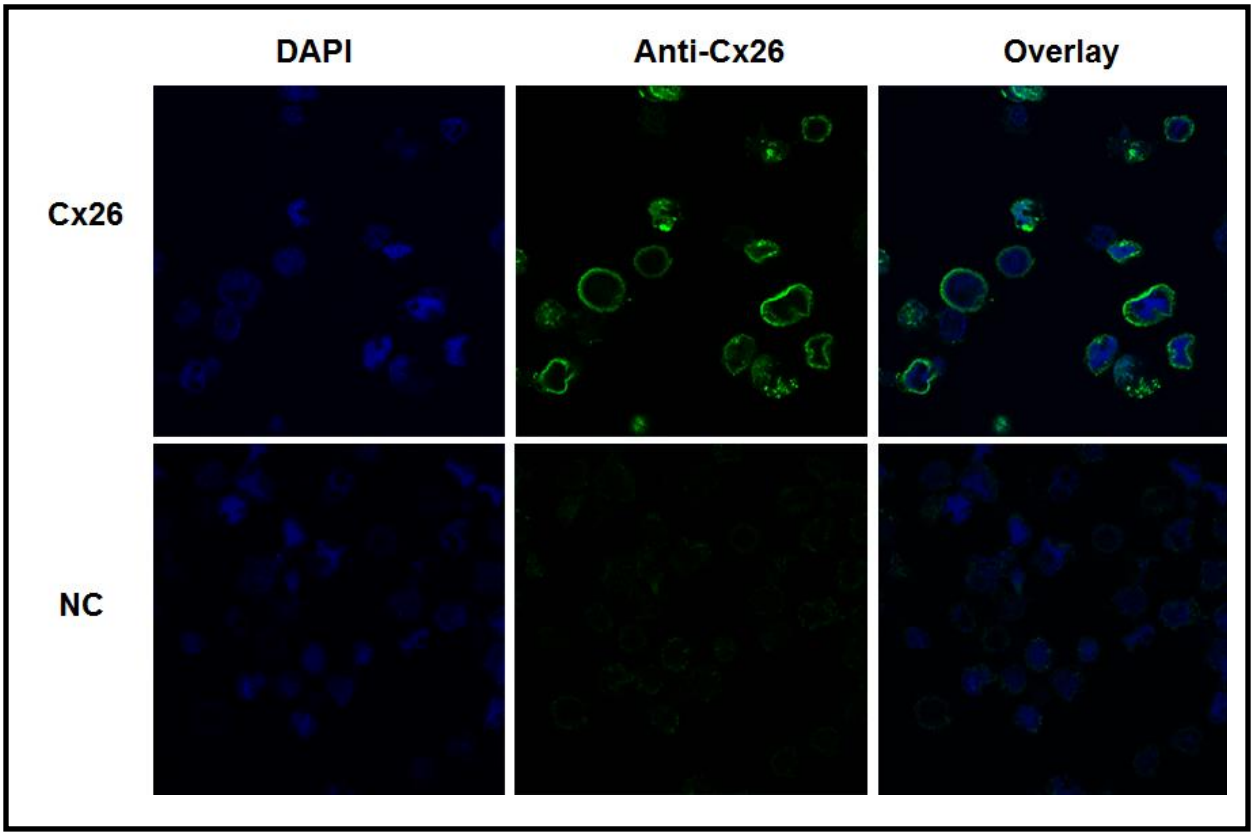

Figure A. 8 mCx26 is located on Sf9 surface.

Both transfected and non-transfected Sf9 cells were firstly fixed with 4% methanol-free formaldehyde, followed by 5% BSA blocking for 1 hour at room temperature. The primary antibody was further probed with goat anti-mouse IgG secondary antibody conjugated with Alexa Fluor 488. DAPI was applied to stain the nuclei. The fluorescence emission of Alexa Fluor 488 was captured under the confocal microscope.